Methods in Molecular Biology 1732

Springer Protocols

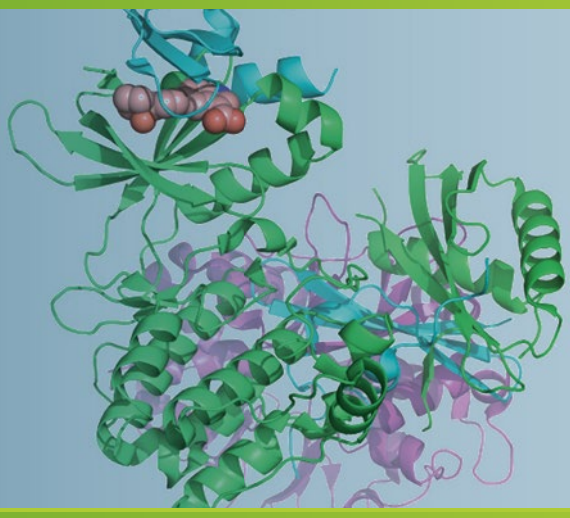

Dietbert Neumann
Benoit Viollet *Editors*

AMPK

Methods and Protocols

Humana Press

METHODS IN MOLECULAR BIOLOGY

Series Editor
John M. Walker
School of Life and Medical Sciences
University of Hertfordshire
Hatfield, Hertfordshire, AL10 9AB, UK

For further volumes:
http://www.springer.com/series/7651

AMPK

Methods and Protocols

Edited by

Dietbert Neumann

Department of Pathology, CARIM School for Cardiovascular Diseases, Maastricht University, Maastricht, The Netherlands

Benoit Viollet

Department EMD, Inserm, U1016, Institut Cochin, CNRS, UMR8104, Université Paris Descartes, Paris, France

Humana Press

Editors
Dietbert Neumann
Department of Pathology
CARIM School
for Cardiovascular Diseases
Maastricht University
Maastricht, The Netherlands

Benoit Viollet
Department EMD, Inserm, U1016
Institut Cochin, CNRS, UMR8104
Université Paris Descartes
Paris, France

ISSN 1064-3745 ISSN 1940-6029 (electronic)
Methods in Molecular Biology
ISBN 978-1-4939-7597-6 ISBN 978-1-4939-7598-3 (eBook)
https://doi.org/10.1007/978-1-4939-7598-3

Library of Congress Control Number: 2018931371

Cover Image: The overall topology of AMPK α1β1γ1 (colored green, cyan, pink) derived from 5KQ5.pdb. AMPK activator (PF-06409577) is bound at the ADaM site and shown in spheres. The image was prepared by Matthew Calabrese and is a courtesy of Pfizer Inc.

Printed on acid-free paper

This Humana Press imprint is published by Springer Nature
The registered company is Springer Science+Business Media, LLC
The registered company address is: 233 Spring Street, New York, NY 10013, U.S.A.

Preface

Since the discovery of AMPK in the early 1970s, this field garnered major interests among the scientists worldwide. Nowadays, the fundamental role of AMPK in integrating cellular and organismal energy metabolism is well recognized. In particular, the understanding of its upstream regulation and identification of novel downstream targets shed light on the broad cellular functions of AMPK. As a result, AMPK attracted widespread interest as a potential therapeutic target for the treatment of chronic metabolic diseases but also neurodegenerative diseases, inflammation, and cancer. Insights gained from animal and cellular genetic models and structure determination paved the way for the discovery of novel therapeutic avenues and the development of small molecule direct AMPK activators.

Recognizing the expanding size of the AMPK field, full coverage of the applied techniques would be truly a gigantic task. Therefore, this book provides a non-exhaustive overview of methods. We aimed at inclusion of a wide variety of protocols from various subdisciplines. Individual chapters are written by established experts, who developed and applied the described promising techniques in their lab. This volume is expected to be of use to graduate students, postdoctoral researchers, and established investigators with an interest in AMPK.

From the contents of the book, covering computational, biochemical, biophysical, cellular, ex vivo, and in vivo AMPK protocols and inclusion of various species plus a clinical perspective, a simple conclusion may be drawn: The AMPK field is extraordinarily rich in a diverse research expertise that is exemplified here in a series of lab-tested protocols.

We are extremely grateful to all of the authors for their contributions. We also thank Prof. John Walker, the MiMB series editor, for the regular guidance ultimately yielding this volume.

Maastricht, The Netherlands — *Dietbert Neumann*
Paris, France — *Benoit Viollet*

Contents

Contributors

Fabienne Andris • *Laboratoire d'Immunobiologie, Université Libre de Bruxelles—IBMM, Gosselies, Belgium*

Jean-Luc Balligand • *Pole of Pharmacology, Institut de Recherche Expérimentale et Clinique, Université catholique de Louvain, Brussels, Belgium*

Christophe Beauloye • *Pole of Cardiovascular Research, Institut de Recherche Expérimentale et Clinique, Université catholique de Louvain, Brussels, Belgium; Division of Cardiology, Cliniques Universitaires Saint-Luc, Brussels, Belgium*

Luc Bertrand • *Pole of Cardiovascular Research, Institut de Recherche Expérimentale et Clinique, Université catholique de Louvain, Brussels, Belgium*

Jesper B. Birk • *Section of Molecular Physiology, Department of Nutrition, Exercise and Sports, Faculty of Science, University of Copenhagen, Copenhagen, Denmark*

Kris A. Borzilleri • *Worldwide Research and Development, Pfizer Inc., Groton, CT, USA*

Luc Buée • *Univ. Lille, Inserm, CHU Lille, UMR-S 1172—JPArc—Centre de Recherche Jean-Pierre AUBERT, Lille, France*

Matthew F. Calabrese • *Worldwide Research and Development, Pfizer Inc., Groton, CT, USA*

Dipanjan Chanda • *Department of Molecular Genetics, CARIM School for Cardiovascular Diseases, Maastricht University, Maastricht, The Netherlands*

Anabela Cordeiro-da-Silva • *Parasite Disease Group, IBMC-Instituto de Biologia Molecular e Celular; Instituto de Investigação e Inovação em Saúde, and Departamento de Ciências Biológicas, Faculdade de Farmácia, Universidade do Porto, Porto, Portugal*

Will A. Coumans • *Department of Molecular Genetics, CARIM School for Cardiovascular Diseases, Maastricht University, Maastricht, The Netherlands*

Andreas Daiber • *Department of Cardiology 1, Center for Cardiology, Universitätsmedizin Mainz, Mainz, Germany*

Biplab Dasgupta • *Division of Oncology, Cincinnati Children's Hospital Medical Center, Cincinnati, OH, USA*

Emilie Demoinet • *Department of Biology, McGill University, Montreal, QC, Canada; Institute of Biology Valrose (iBV), CNRS, INSERM, University Côte d' Azur, Nice, France*

Sébastien Denanglaire • *Laboratoire d'Immunobiologie, Université Libre de Bruxelles—IBMM, Gosselies, Belgium*

Venkatasubramanian Dharmarajan • *Department of Molecular Medicine, The Scripps Research Institute, Jupiter, FL, USA*

Toby A. Dite • *Metabolic Signalling Laboratory, St. Vincent's Institute of Medical Research, Fitzroy, VIC, Australia*

Marc Dohmen • *Institute of Biochemistry and Molecular Biology, Medical School, RWTH Aachen University, Aachen, Germany*

Ingo Ebersberger • *Applied Bioinformatics Group, Institute of Cell Biology and Neuroscience, Goethe University Frankfurt, Frankfurt, Germany; Senckenberg Biodiversity and Climate Research Centre (BIK-F), Frankfurt, Germany*

Jérôme Estaquier • *CNRS FR 3636, Université Paris Descartes, Paris, France; Centre de Recherche du CHU de Québec, Université Laval, Laval, QC, Canada*

Marc Foretz • *U1016, Institut Cochin, Inserm, Paris, France; UMR8104, CNRS, Paris, France; Université Paris Descartes, Paris, France*
Morgan D. Fullerton • *Department of Biochemistry, Microbiology and Immunology, University of Ottawa, Ottawa, ON, Canada*
Fiona A. Fyffe • *Division of Cell Signalling and Immunology, School of Life Sciences, University of Dundee, Dundee, Scotland, UK*
Maria Adelaida Garcia-Gimeno • *Department of Biotecnología, Escuela Técnica Superior de Ingeniería Agronómica y del Medio Natural (ETSIAMN), University of Politécnica de Valencia, Valencia, Spain*
Noemí García-Tardón • *Department of Parasitology, Leiden University Medical Center, Leiden, The Netherlands*
Jan F. C. Glatz • *Department of Molecular Genetics, CARIM School for Cardiovascular Diseases, Maastricht University, Maastricht, The Netherlands*
Brendan Gongol • *Cardiopulmonary Sciences, Schools of Allied Health Professions and Medicine, Loma Linda University, Loma Linda, CA, USA*
Paul R. Gooley • *Department of Biochemistry and Molecular Biology, Bio21 Molecular Science and Biotechnology Institute, The University of Melbourne, Parkville, VIC, Australia*
Graeme J. Gowans • *Division of Cell Signalling and Immunology, School of Life Sciences, University of Dundee, Dundee, Scotland, UK*
Alexander Gray • *Division of Cell Signalling and Immunology, School of Life Sciences, University of Dundee, Dundee, Scotland, UK*
Adrien Grenier • *U1016, Institut Cochin, Inserm, Paris, France; UMR8104, CNRS, Paris, France; Université Paris Descartes, Paris, France; Equipe Labellisée Ligue Nationale Contre le Cancer (LNCC), Paris, France*
Patrick R. Griffin • *Department of Molecular Medicine, The Scripps Research Institute, Jupiter, FL, USA*
Silke Großе • *Institute of Molecular Cell Biology, Center for Molecular Biomedicine, Jena University Hospital, Jena, Germany*
Linda Gsaier • *Institut NeuroMyogène, CNRS UMR 5310, INSERM U1217, Université Claude Bernard Lyon 1, Villeurbanne, France*
Hélène Guermouche • *U1016, Institut Cochin, Inserm, Paris, France; UMR8104, CNRS, Paris, France; Université Paris Descartes, Paris, France; Equipe Labellisée Ligue Nationale Contre le Cancer (LNCC), Paris, France*
Bruno Guigas • *Department of Parasitology, Leiden University Medical Center, Leiden, The Netherlands; Department of Molecular Cell Biology, Leiden University Medical Center, Leiden, The Netherlands*
D. Grahame Hardie • *Division of Cell Signalling and Immunology, School of Life Sciences, University of Dundee, Dundee, Scotland, UK*
Simon A. Hawley • *Division of Cell Signalling and Immunology, School of Life Sciences, University of Dundee, Dundee, Scotland, UK*
Regine Heller • *Institute of Molecular Cell Biology, Center for Molecular Biomedicine, Jena University Hospital, Jena, Germany*
Sandrine Horman • *Pole of Cardiovascular Research, Institut de Recherche Expérimentale et Clinique, Université catholique de Louvain, Brussels, Belgium*
Julia A. Hubbard • *The Francis Crick Institute, London, UK*
Takanari Inoue • *Cell Biology and Biomedical Engineering, School of Medicine, Johns Hopkins University, Baltimore, MD, USA*

Arpit Jain • *Applied Bioinformatics Group, Institute of Cell Biology and Neuroscience, Goethe University Frankfurt, Frankfurt, Germany*
David A. Johnson • *Division of Biomedical Sciences, University of California, Riverside, Riverside, CA, USA*
Bruce E. Kemp • *Protein Chemistry and Metabolism Unit, St. Vincent's Institute of Medical Research, Fitzroy, VIC, Australia; Mary MacKillop Institute for Health Research, Australian Catholic University, Melbourne, VIC, Australia*
Allen Kim • *Cell Biology and Biomedical Engineering, School of Medicine, Johns Hopkins University, Baltimore, MD, USA*
Jérome Kluza • *Univ. Lille, Inserm, CHU Lille, UMR-S 1172—JPArc—Centre de Recherche Jean-Pierre AUBERT, Lille, France*
Anne Knierim • *Institute of Molecular Cell Biology, Center for Molecular Biomedicine, Jena University Hospital, Jena, Germany*
Ann Koay • *Department of Biochemistry and Molecular Biology, Bio21 Molecular Science and Biotechnology Institute, The University of Melbourne, Parkville, VIC, Australia; Experimental Therapeutics Centre, Agency for Science Technology and Research, Singapore, Singapore*
Olivier Kosmider • *U1016, Institut Cochin, Inserm, Paris, France; UMR8104, CNRS, Paris, France; Université Paris Descartes, Paris, France; Equipe Labellisée Ligue Nationale Contre le Cancer (LNCC), Paris, France*
Swenja Kröller-Schön • *Department of Cardiology 1, Center for Cardiology, Universitätsmedizin Mainz, Mainz, Germany*
Sarah Krieg • *Institute of Biochemistry and Molecular Biology, Medical School, RWTH Aachen University, Aachen, Germany*
Nderim Kryeziu • *Institute of Molecular Cell Biology, Center for Molecular Biomedicine, Jena University Hospital, Jena, Germany*
Ravi G. Kurumbail • *Worldwide Research and Development, Pfizer Inc., Groton, CT, USA*
Christopher G. Langendorf • *Protein Chemistry and Metabolism Unit, St. Vincent's Institute of Medical Research, Fitzroy, VIC, Australia*
Sabrina Ben Larbi • *Institut NeuroMyogène, CNRS UMR 5310, INSERM U1217, Université Claude Bernard Lyon 1, Villeurbanne, France*
Nicholas D. LeBlond • *Department of Biochemistry, Microbiology and Immunology, University of Ottawa, Ottawa, ON, Canada*
Isabelle Leclerc • *Section of Cell Biology and Functional Genomics, Division of Diabetes, Endocrinology and Metabolism, Imperial College London, London, UK*
Oberdan Leo • *Laboratoire d'Immunobiologie, Université Libre de Bruxelles—IBMM, Gosselies, Belgium*
Hui Li • *Division of Nephrology and Hypertension, Department of Medicine, USC/UKRO Kidney Research Center, Keck School of Medicine of USC, Los Angeles, CA, USA*
Mengqi Li • *State Key Laboratory of Cellular Stress Biology, Innovation Center for Cell Signaling Network, School of Life Sciences, Xiamen University, Xiamen, Fujian, China*
Sheng-Cai Lin • *State Key Laboratory of Cellular Stress Biology, Innovation Center for Cell Signaling Network, School of Life Sciences, Xiamen University, Xiamen, Fujian, China*
Joost J. F. P. Luiken • *Department of Molecular Genetics, CARIM School for Cardiovascular Diseases, Maastricht University, Maastricht, The Netherlands*
Miguel López • *NeurObesity Group, Department of Physiology, CIMUS, University of Santiago de Compostela-Instituto de Investigación Sanitaria, Santiago de*

Compostela, Spain; CIBER Fisiopatología de la Obesidad y Nutrición (CIBERobn), Santiago de Compostela, Spain

Bernhard Lüscher • *Institute of Biochemistry and Molecular Biology, Medical School, RWTH Aachen University, Aachen, Germany*

Florence Mailleux • *Pole of Cardiovascular Research, Institut de Recherche Expérimentale et Clinique, Université catholique de Louvain, Brussels, Belgium*

Sarah J. Mancini • *Institute of Cardiovascular and Medical Sciences, College of Medical, Veterinary and Life Sciences, University of Glasgow, Glasgow, UK*

Philippe Marchetti • *Univ. Lille, Inserm, CHU Lille, UMR-S 1172—JPArc—Centre de Recherche Jean-Pierre AUBERT, Lille, France*

Traci Marin • *Cardiopulmonary Sciences, Schools of Allied Health Professions and Medicine, Loma Linda University, Loma Linda, CA, USA*

Claudia Marinangeli • *Univ. Lille, Inserm, CHU Lille, UMR-S 1172—JPArc—Centre de Recherche Jean-Pierre AUBERT, Lille, France*

Aida Martinez-Sanchez • *Section of Cell Biology and Functional Genomics, Division of Diabetes, Endocrinology and Metabolism, Imperial College London, London, UK*

Takafumi Miyamoto • *Department of Internal Medicine (Endocrinology and Metabolism), Faculty of Medicine, University of Tsukuba, Ibaraki, Japan*

Jesse I. Mobbs • *Department of Biochemistry and Molecular Biology, Bio21 Molecular Science and Biotechnology Institute, The University of Melbourne, Parkville, VIC, Australia; Department of Biochemistry and Molecular Biology, School of Biomedical Sciences, Monash University, Clayton, VIC, Australia*

Johanna Mondésir • *U1016, Institut Cochin, Inserm, Paris, France; UMR8104, CNRS, Paris, France; Université Paris Descartes, Paris, France; Equipe Labellisée Ligue Nationale Contre le Cancer (LNCC), Paris, France*

Diana Moreira • *Parasite Disease Group, IBMC-Instituto de Biologia Molecular e Celular, Universidade do Porto, Porto, Portugal; Instituto de Investigação e Inovação em Saúde, Universidade do Porto, Porto, Portugal; Departamento de Ciências Biológicas, Faculdade de Farmácia, Universidade do Porto, Porto, Portugal; Life and Health Sciences Research Institute (ICVS), School of Medicine, University of Minho, Braga, Portugal; ICVS/3Bs-PT Government Associate Laboratory, Guimarães, Braga, Portugal*

Rémi Mounier • *Institut NeuroMyogène, CNRS UMR 5310, INSERM U1217, Université Claude Bernard Lyon 1, Villeurbanne, France*

Miranda Nabben • *Department of Molecular Genetics, CARIM School for Cardiovascular Diseases, Maastricht University, Maastricht, The Netherlands*

Dietbert Neumann • *Department of Pathology, CARIM School for Cardiovascular Diseases, Maastricht University, Maastricht, The Netherlands*

Marie-Sophie Nguyen-Tu • *Section of Cell Biology and Functional Genomics, Division of Diabetes, Endocrinology and Metabolism, Imperial College London, London, UK*

Jonathan S. Oakhill • *Metabolic Signalling Laboratory, St. Vincent's Institute of Medical Research, Fitzroy, VIC, Australia; Mary MacKillop Institute for Health Research, Australian Catholic University, Melbourne, VIC, Australia*

Séverine Olivier • *U1016, Institut Cochin, Inserm, Paris, France; UMR8104, CNRS, Paris, France; Université Paris Descartes, Paris, France*

Kazuhiro Omi • *Division of Nephrology and Hypertension, Department of Medicine, USC/UKRO Kidney Research Center, Keck School of Medicine of USC, Los Angeles, CA, USA*

Nuria M. Pastor-Soler • *Division of Nephrology and Hypertension, Department of Medicine, USC/UKRO Kidney Research Center, Keck School of Medicine of USC, Los Angeles, CA, USA*
Arnim Pause • *Goodman Cancer Research Centre, Biochemistry Department, McGill University, Montreal, Canada*
Tiphène Pirnay • *Laboratoire d'Immunobiologie, Université Libre de Bruxelles—IBMM, Gosselies, Belgium*
Elite Possik • *Goodman Cancer Research Centre, Biochemistry Department, McGill University, Montreal, Canada*
Francis Rajamohan • *Worldwide Research and Development, Pfizer Inc., Groton, CT, USA*
Roshan Rajani • *Division of Nephrology and Hypertension, Department of Medicine, USC/UKRO Kidney Research Center, Keck School of Medicine of USC, Los Angeles, CA, USA*
Renee Rao • *Division of Nephrology and Hypertension, Department of Medicine, USC/UKRO Kidney Research Center, Keck School of Medicine of USC, Los Angeles, CA, USA*
Allan R. Reyes • *Worldwide Research and Development, Pfizer Inc., Cambridge, MA, USA*
Elmer Rho • *Cell Biology and Biomedical Engineering, School of Medicine, Johns Hopkins University, Baltimore, MD, USA*
Valentin Roustan • *Department of Ecogenomics and Systems Biology, University of Vienna, Vienna, Austria*
Richard Roy • *Department of Biology, McGill University, Montreal, QC, Canada*
Fiona M. Russell • *Division of Cell Signalling and Immunology, School of Life Sciences, University of Dundee, Dundee, Scotland, UK*
Guy A. Rutter • *Section of Cell Biology and Functional Genomics, Division of Diabetes, Endocrinology and Metabolism, Imperial College London, London, UK*
Ian P. Salt • *Institute of Cardiovascular and Medical Sciences, College of Medical, Veterinary and Life Sciences, University of Glasgow, Glasgow, UK*
Pascual Sanz • *Instituto de Biomedicina de Valencia, CSIC and Centro de Investigación Biomédica en Red de Enfermedades Raras (CIBERER), Valencia, Spain*
Dhruv Sarma • *Division of Cardiovascular Medicine, Radcliffe Department of Medicine, University of Oxford, Oxford, UK; The Wellcome Centre for Human Genetics, University of Oxford, Oxford, UK*
Eberhard Schulz • *Department of Cardiology 1, Center for Cardiology, Universitätsmedizin Mainz, Mainz, Germany*
John W. Scott • *Mary MacKillop Institute for Health Research, Australian Catholic University, Melbourne, VIC, Australia; Protein Chemistry and Metabolism Unit, St. Vincent's Institute of Medical Research, Fitzroy, VIC, Australia*
William Seibel • *Division of Experimental Hematology and Cancer Biology, Cincinnati Children's Hospital Medical Center, Cincinnati, OH, USA*
Patricia Seoane-Collazo • *NeurObesity Group, Department of Physiology, CIMUS, University of Santiago de Compostela-Instituto de Investigación Sanitaria, Santiago de Compostela, Spain; CIBER Fisiopatología de la Obesidad y Nutrición (CIBERobn), Santiago de Compostela, Spain*
John Y.-J. Shyy • *Department of Medicine, University of California, San Diego, La Jolla, CA, USA*
Ricardo Silvestre • *Life and Health Sciences Research Institute (ICVS), School of Medicine, University of Minho, Braga, Portugal; ICVS/3Bs-PT Government Associate Laboratory, Guimarães, Braga, Portugal*

Katrin Spengler • *Institute of Molecular Cell Biology, Center for Molecular Biomedicine, Jena University Hospital, Jena, Germany*
Eduardo B. Sternick • *Instituto de Pós-Graduação, Faculdade de Ciências Médicas de Minas Gerais, Belo Horizonte, Brazil*
Pierre Sujobert • *Hospices Civils de Lyon, Centre Hospitalier Lyon Sud, Service d'Hématologie Biologique, Pierre-Bénite, France; Université Claude Bernard Lyon-1, Lyon, France; INSERM U1052, CNRS 5286, Université Claude Bernard, Faculté de Médecine Lyon-Sud Charles Mérieux, Université de Lyon, Lyon, France*
Jérôme Tamburini • *U1016, Institut Cochin, Inserm, Paris, France; UMR8104, CNRS, Paris, France; Université Paris Descartes, Paris, France; Equipe Labellisée Ligue Nationale Contre le Cancer (LNCC), Paris, France*
Marine Theret • *The Biomedical Research Centre, University of British Columbia, Vancouver, BC, Canada; Faculty of Medicine, The University of British Columbia, Vancouver, BC, Canada; Institut NeuroMyogène, CNRS UMR 5310, INSERM U1217, Université Claude Bernard Lyon 1, Villeurbanne, France*
Jörg Vervoorts • *Institute of Biochemistry and Molecular Biology, Medical School, RWTH Aachen University, Aachen, Germany*
Guillaume Vial • *INSERM U1042, Laboratoire Hypoxie-Physiopathologies cardiovasculaires et respiratoires HP2, Faculté de médecine et de pharmacie, Domaine de la merci, La Tronche, France; Université Grenoble-Alpes, Laboratoire Hypoxie-Physiopathologies cardiovasculaires et respiratoires HP2, Faculté de médecine et de pharmacie, Domaine de la merci, La Tronche, France*
Rosa Viana • *Instituto de Biomedicina de Valencia, CSIC and Centro de Investigación Biomédica en Red de Enfermedades Raras (CIBERER), Valencia, Spain*
Valérie Vingtdeux • *Univ. Lille, Inserm, CHU Lille, UMR-S 1172—JPArc—Centre de Recherche Jean-Pierre AUBERT, Lille, France*
Benoit Viollet • *U1016, Department EMD, Institut Cochin, Inserm, Paris, France; UMR8104, CNRS, Paris, France; Université Paris Descartes, Paris, France*
Qilong Wang • *Center for Molecular and Translational Medicine, Georgia State University, Atlanta, GA, USA*
Jessica Ward • *Worldwide Research and Development, Pfizer Inc., Cambridge, MA, USA*
Wolfram Weckwerth • *Department of Ecogenomics and Systems Biology, University of Vienna, Vienna, Austria; Vienna Metabolomics Center (VIME), University of Vienna, Vienna, Austria*
Michèle Weiss-Gayet • *Institut NeuroMyogène, CNRS UMR 5310, INSERM U1217, Université Claude Bernard Lyon 1, Villeurbanne, France*
Graham M. West • *Worldwide Research and Development, Pfizer Inc., Groton, CT, USA*
Jon R. Wilson • *The Francis Crick Institute, London, UK*
Jane M. Withka • *Worldwide Research and Development, Pfizer Inc., Groton, CT, USA*
Jørgen F. P. Wojtaszewski • *Section of Molecular Physiology, Department of Nutrition, Exercise and Sports, Faculty of Science, University of Copenhagen, Copenhagen, Denmark*
Bing Xiao • *The Francis Crick Institute, London, UK*
Arash Yavari • *Experimental Therapeutics, Radcliffe Department of Medicine, University of Oxford, Oxford, UK; Division of Cardiovascular Medicine, Radcliffe Department of Medicine, University of Oxford, Oxford, UK; The Wellcome Centre for Human Genetics, University of Oxford, Oxford, UK*

Chen-Song Zhang • *State Key Laboratory of Cellular Stress Biology, Innovation Center for Cell Signaling Network, School of Life Sciences, Xiamen University, Xiamen, Fujian, China*

Yue Zong • *State Key Laboratory of Cellular Stress Biology, Innovation Center for Cell Signaling Network, School of Life Sciences, Xiamen University, Xiamen, Fujian, China*

Ming-Hui Zou • *Center for Molecular and Translational Medicine, Georgia State University, Atlanta, GA, USA; Research Science Center Room 520, Center for Molecular and Translational Medicine, Georgia State University, Atlanta, GA, USA*

Chapter 1

Production and Crystallization of Full-Length Human AMP-Activated Protein Kinase (α1β1γ1)

Julia A. Hubbard, Bing Xiao, and Jon R. Wilson

Abstract

Determination of the crystal structure of AMP-activated protein kinase (AMPK) is fundamental to understanding its biological function and role in a number of diseases related to energy metabolism including type 2 diabetes, obesity, and cancer. We describe methods for the expression and purification of a human full-length active AMPK complex that is suitable for biochemical and structural analyses, followed by methods for its crystallization in complex with small molecule activators. Quality control of the purified protein by functional and biophysical analysis was an essential part of the process enabling the achievement of crystals of the full-length protein capable of being used for high-resolution structure determination by X-ray diffraction. X-ray structures have been determined of both phosphorylated and non-phosphorylated forms of full-length human AMPK α1β1γ1.

Key words AMPK, Crystallization, ADaM activator, Nucleotide binding, Kinase, Protein purification

1 Introduction

AMP-activated protein kinase (AMPK) has a key role in regulating metabolism and is therefore an important therapeutic target for metabolic disorders. Initial structural studies of AMPK, which focused on the structure of the regulatory sub-complex of AMPK (core domain: C-terminal domain of α-subunit, C-terminal domain of β-subunit, full-length γ-subunit) [1], facilitated an understanding of its activation by AMP, ADP, and ATP [2]. Detailed protocols for the crystallization of the core domain of AMPK can be obtained from these publications [1, 2] and from the thesis of Underwood, E [3].

Here we describe the purification and crystallization of the active full-length human AMPK (isoform α1β1γ1), which extended the work on the core domain and allowed for the first time an understanding of the protein's activation by potential drug molecules [4], the surprising feature of which was the identification and characterization of the binding site now referred to as the allosteric

Dietbert Neumann and Benoit Viollet (eds.), *AMPK: Methods and Protocols*, Methods in Molecular Biology, vol. 1732, https://doi.org/10.1007/978-1-4939-7598-3_1,

drug and metabolite (ADaM)-binding pocket. Ligand binding in the ADaM pocket occurs at the interface of the kinase and glycogen-binding domain (GBD).

Crystallization of full-length human AMPK α1β1γ1 took over a decade of iterative experimentation and was enabled by the close collaboration of protein chemists, structural biologists, protein biophysicists and biologists, as well as synthetic chemists and computational biochemists. This approach employed standard methods for the identification and removal of some disordered regions from the protein by limited proteolysis and structure prediction, mutation, optimization of construct design for expression and folding, optimization of growth conditions for yield of soluble protein and optimization of purification and protein storage, and crystal screening. An unusual but critical key feature that enabled crystallization of the full-length complex was the design of a suitable small molecule ligand, which had the properties of solubility and affinity required for stabilization of the full-length complex. Once the crystallization conditions were established, this enabled structure-activity relationships of a diverse set of chemistries to be explored with other small molecule ligands [5–7]. Recently crystal structures have been reported for full-length AMPK without small molecule activators in the ADaM site [8]; however, these are difficult to interpret in detail due to the lower resolution >4 Å obtained with this form of the protein.

In this way, direct knowledge of AMPK's structure has contributed to the development of new potential drug candidates. This is further evidenced by the identification of a new AMPK activator for treatment of lung cancer [9], which was based on the full-length human AMPK α1β1γ1 structure (Protein Data Bank, PDB ID: 4CFE). This chapter aims to enable the reader to rapidly progress to their own experimental biophysical and structural studies of full-length human AMPK α1β1γ1 protein.

2 Materials

2.1 Reagents and Equipment

Prepare all solutions using ultrapure water (prepared by purifying deionized water, to attain a sensitivity of 18 MΩ cm at 25 °C) and analytical grade reagents. Prepare and store all reagents at room temperature (unless indicated otherwise). Diligently follow local regulations when disposing waste materials.

1. Microbiological incubator.
2. Basic spectrophotometer to measure cell culture optical density.
3. NanoDrop spectrophotometer to measure protein concentration.

4. Variable-temperature shaking incubator with fittings for 12 × 2 L conical flasks.
5. Centrifuges and rotors, e.g., Beckman-Coulter J6 with JA-25.50 rotor and Beckman-Coulter J6-M1 with JS 4.2 rotor.
6. Sonicator fitted with microtip.
7. Syringe filters 0.45 μm.
8. Competent *E. coli* BL21 Star (DE3).
9. Stock solution of ampicillin (100 mg/mL).
10. 14 Luria-Bertani broth (LB) agar plates (with ampicillin 100 μg/mL).
11. 250 μL SOC media.
12. 10 L of Luria-Bertani broth (LB).
13. IPTG: 100 mM isopropyl β-D-galactosidase (IPTG) in water.
14. Lysis buffer: 50 mM Tris–HCl pH 8.0, 300 mM NaCl, 1 mM Tris(2-carboxyethyl)phosphine (TCEP), 20 mM imidazole, 1 mM $MgCl_2$, ×4 EDTA-free protease inhibitor tablets (Roche Products Ltd), and 12 μL benzonase.

    200 mL of lysis buffer is needed for washing pellets from 12 × 0.8 L growth flasks (*see* **Note 1**). Each 0.8 L culture typically yields 4–5 g of bacterial pellet.
15. Nickel A buffer: 50 mM Tris–HCl pH 8.0, 300 mM NaCl, 0.5 mM TCEP, and 20 mM imidazole.
16. Nickel B buffer: 50 mM Tris–HCl pH 8.0, 300 mM NaCl, 0.5 mM TCEP, and 400 mM imidazole.
17. Gel filtration buffer: 50 mM Tris–HCl pH 8.0, 300 mM NaCl, and 0.5 mM TCEP.

2.2 Crystallization Reagents and Equipment

1. 24- and 48-well crystallization plates (Hampton Research).
2. Crystallization solution: 13% (w/v) polyethylene glycol (PEG) 3350, 0.1 M $MgCl_2$, 1% (w/v) glucose, 0.15% (w/v) cocamidopropyl betaine (CAPB) in 100 mM imidazole at pH 6.2.
3. Crystallization solution: 12% (w/v) PEG 3350, 300 mM guanidine-HCl in 100 mM piperazine-*N*,*N*′-bis(2-ethanesulfonic acid) (PIPES) buffer at pH 7.2.
4. 10 mM staurosporine in DMSO and 10 mM AMP in water.
5. Ethylene glycol.
6. Low-power (magnification 40×) stereo microscope.
7. Range of sizes (0.1–0.4 mm) 18 mm mounted cryoloop (Hampton Research Ltd).
8. Liquid nitrogen for crystal freezing and storage.

2.3 Specialist Reagents and Equipment

1. The protein purification protocol used here makes use of the ÄKTA purification system (GE Healthcare). While these systems are widely available in many laboratories, an alternative chromatography system or stand-alone peristaltic pump could be substituted.
2. Chromatography columns. Size exclusion chromatography, Superdex HiLoad prep grade XK 16/600 (GE Healthcare). Nickel affinity chromatography, HisTrap FF Sepharose, 5 mL (GE Healthcare).
3. For gel analysis of protein samples. The NuPAGE mini-gel system (Thermo Fisher Scientific) was used with 4–12% acrylamide gradient Bis-Tris gels and the MES SDS gel running buffer system. The sample buffer was NuPAGE LDS sample buffer with 1 mM DTT. Mark12 markers (Thermo Fisher Scientific) were used to size the bands. InstantBlue (Expedeon) Coomassie protein stain was used to visualize the bands.
4. Protein was concentrated using Vivaspin protein concentrator columns (GE Healthcare).
5. The kinase CaMKKβ was prepared as described in Ref. [10].
6. The AMPK constructs were prepared in pET47 plasmid as described previously [4].
7. The benzimidazole derivative small molecule referred to as 991 is an AMPK activator that binds at the ADaM site. 991 is used in this protocol to stabilize full-length AMPK for crystallization. Its chemical name is 5-[6-chloro-5-(1-methylindol-5-yl)-1H-benzimidazol-2-yl]oxy-2-methyl-benzoic acid, and it can be purchased as a custom synthesis from specialist chemical supplies such as SpiroChem AG. As 991 is sparingly soluble in aqueous solvents, a 10 mM solution in 100% dimethyl sulfoxide (DMSO) needs to be prepared and stored at −20 °C.
8. As an alternative to 991, the commercially available small molecule ADaM-binding activator, A-769662 4-hydroxy-3-[4-(2-hydroxyphenyl)phenyl]-6-oxo-7H-thieno[2,3-b]pyridine-5-carbonitrile can be obtained from ApexBio Technology. Crystals obtained with this ligand diffract less well possibly due to the lower affinity of A-769662 compared to 991.

3 Methods

3.1 General Points

The first part of the protocol below describes optimized methods for expression and purification of crystallization-grade full-length AMPK α1β1γ1; however, the protocol can equally be used to produce the truncated core domain AMPK, which has also been crystallized [2]. Full-length protein is prone to aggregation during this process. This has been reduced by optimization of the process

into several distinct stages, each broadly consisting of 3–4 days of laboratory work. In terms of hours worked in the laboratory and scheduling of equipment, the most intensive is the purification of AMPK from a pellet of bacteria which have expressed the protein. The pellet can be frozen before use. However, the purification process after thawing the pellet is a 3-day process that in our hands has been most effectively carried out in a continuous process.

The protocol below is based on growth of 10 L of bacterial culture from 12 × 2 L flasks each containing 800 mL. This starting volume typically yields 50 mg of purified AMPK protein, which can be safely stored frozen at around 5–10 mg/mL in 10–20 μL aliquots at −80 °C until use for crystallization.

3.2 Expression and Production of AMPK in E. coli (4-Day Protocol)

Carry out all procedures at room temperature unless otherwise specified.

Day 1:

1. Make up LB agar plates containing 100 μg/mL ampicillin (two per transformation plus one for each flask of cells you wish to grow (in this example, for 12 flasks make 14 plates)).
2. Add 1 μL (50–1000 ng) of plasmid DNA (full-length AMPK, γ1[human, 1–331], AVI-tag-β1[human, 1–270], His-α1 [human, 1–552] in tricistronic vector) to one aliquot of BL21 Star (DE3) *E. coli* competent cells.
3. Incubate for 10 min on ice.
4. Transfer to a 42 °C heat block or water bath for 45 s to heat shock.
5. Immediately return the cells to ice for 2 min.
6. Allow cells to recover in 250 μL SOC media at 37 °C for 1 h.
7. Spread two different volumes (10 and 50 μL) of recovered cell mixture onto two LB-agar-ampicillin plates.
8. Incubate the plates overnight at 37 °C in a microbiological incubator.

Day 2:

9. First thing in the morning, pick a few colonies from the transformation plates and grow in 10 mL LB broth 100 μg/mL ampicillin in 50 mL plastic tubes at 37 °C with shaking at 200 rpm until the OD at 600 nm (1 cm path length cuvette) is between 2 and 3.
10. Take one culture that has grown (discard the rest). Plate out 200 μL of culture onto one LB-agar-ampicillin plate for every flask you wish to grow (e.g., if you are going to make 12 flasks, plate out 12 plates with 200 μL each). Use 10 μL inoculation loops for streaking out cultures and 1 μL inoculation loops for picking clones. Incubate plates overnight at 37 °C.

Day 3:

11. To prepare the inoculum for the 2 L flasks, add 5 mL of LB broth containing 100 μg/mL ampicillin to an agar plate that has grown visible colonies from **step 10**. Using a 10 μL loop, gently lift the cells off the plate. Pipette off the culture and transfer it to a conical flask labeled pooled inoculum. Repeat this procedure with a second 5 mL for the same plate. You should end up with just over 8 mL of inoculum from the plate.
12. Repeat for each plate. If you had, for example, 12 flasks, you should end up with around 96 mL of inoculum.
13. Make up the total volume of the inoculum from 12 using LB ampicillin according to the following equation: final volume of inoculum (mL) = ((no. flasks to be grown × 10) + 10). For example, for six flasks make up the final volume to 70 mL, or for 12 flasks make it up to 130 mL.
14. Grow cultures in 2 L flasks. Distribute 800 mL of LB ampicillin into each of 12 × 2 L flasks and then inoculate each with 10 mL of inoculum. Ideally the growth should be started at around 1–2 pm to allow cells to be induced and grown overnight.
15. Grow the bacterial cultures by incubating at 37 °C, 210–215 rpm, for 3–4 h or until the OD 600 is 1 (1 cm path length cuvette).
16. Induce protein expression in each flask by addition of 7.5 mL of 100 mM IPTG and incubate for 16–17 h (overnight) at 25 °C, shaking at 210–215 rpm.

Day 4:

17. Harvest the cells: pour cultures from each flask into 1 L centrifuge bottles and centrifuge at 4200 rpm (5000 × *g*) in a J6-MI centrifuge for 30 min at 4 °C.
18. Wash the cells by removing the supernatant and resuspend the cell pellet in 20–30 mL lysis buffer (Subheading 2.2 above). Ensure each cell pellet is well suspended by using a homogenizer and then transfer to 50 mL plastic centrifuge tubes. The supernatant must be carefully disposed of as it contains live bacteria. Destroy with whatever decontamination process is required in your laboratory.
19. Harvest the cell pellet again by centrifuging at 3000 rpm (1800 × *g*) for 30 min at 4 °C.
20. Discard the supernatant, weigh the cell pellets, and then freeze at −80 °C until required. Cell pellets are typically 4–5 g of bacterial pellet per flask.

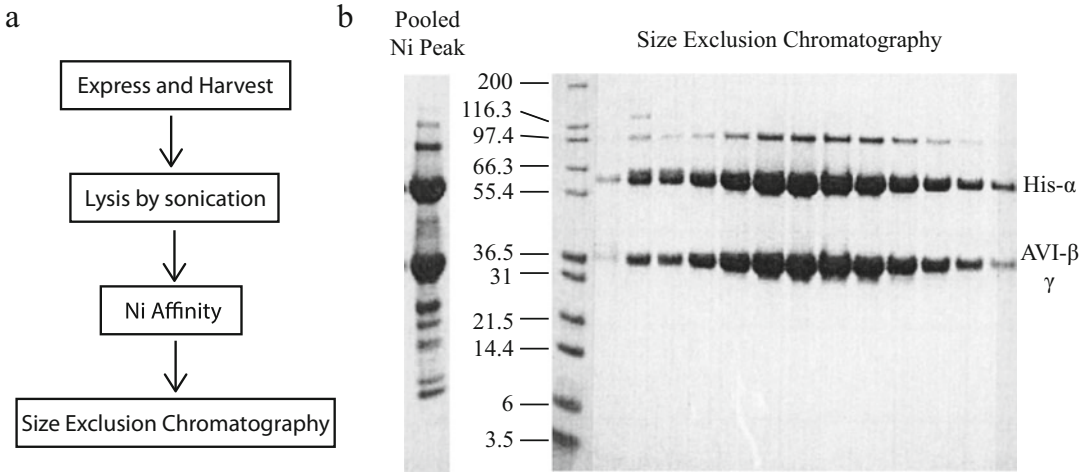

Fig. 1 Purification of AMPK α1β2γ3. (**a**) Purification scheme. (**b**) SDS-PAGE analysis of HisTrap purified AMPK complex and the analysis of size exclusion chromatography peak

3.3 Purification of AMPK Protein

This is a 3-day process including some longer 8–9 h days in the laboratory, assuming everything progresses smoothly (Fig. 1).

Day 1 AM:

1. Equilibrate the Superdex 200 size exclusion chromatography column with gel filtration buffer at flow rate of 1 mL/min. Ensure the pressure alarm is set. Equilibration is complete once a buffer volume greater than 120 mL has passed through the column.
2. Remove the column and seal it and keep for day 1 pm below.

Day 1 PM:

3. Break open the cell pellet and remove the cell debris from the solution fraction containing the AMPK protein. To do this first thaw the frozen cell pellets on ice and resuspend in lysis buffer. Use 4–5 mL of buffer per gram wet weight of cells.
4. Lyse the cells on ice using sonication in an appropriately sized beaker. Insert the sonicator probe about halfway down the depth of the lysate. In our hands cells are broken by sonicating on ice at (on 1 s, off 1 s) 40% power for a total time of 1 min and 30 s. However, these parameters will vary dependent on specific equipment, so it is critical to be certain that cells are broken but that material is not over-sonicated as this will heat and damage the sample. Two indicators of cell breakage are the change in the visible appearance of the suspension and the size of the remaining pellet after the next centrifugation step.
5. Pour the lysate into 50 mL centrifuge tubes and centrifuge at 20,000 rpm (33,000 × *g*) J-26 XP centrifuge for 45 min at 4 °C. The supernatant should be opaque, and the pellet which

now contains unbroken cells and cell debris should be significantly smaller. (*See* **Note 2**.)

6. Filter the supernatant on ice (or in the cold room) using 0.45 μm syringe filters. The lysate is ready for the purification procedure; store on ice. **Once lysate is ready for purification, proceed without delay to the nickel sepharose affinity purification.**
7. **Carry out all steps in a cold room at 4 °C.** Clean and prewash a 5 mL nickel sepharose column with five column volumes of elution buffer (nickel B buffer) and then five column volumes of binding buffer (nickel A buffer).
8. Apply the lysate to the nickel column at a rate of 2 mL/min using a stand-alone peristaltic pump or an ÄKTA purification system.
9. Collect the eluate as it passes through the column and label as unbound protein.
10. Wash the nickel column with lysis buffer (about 200 mL) at a rate of 2 mL/min. Collect the eluate as it passes through the column and label as wash.
11. If, as in this example, you are using an ÄKTA purification system, connect nickel buffer A to line A and nickel buffer B to line B. Run the buffers through the lines, B before A.
12. Attach the nickel sepharose column to the ÄKTA and run nickel A buffer through until the baseline absorbance has been reached, that is, a flat unchanging absorbance at 280 nm is observed. Then switch pumps off but leave the column attached. (*See* **Note 3**.)

Day 2:

13. Elute the protein from the column by running a linear gradient of nickel A and B buffers. First prepare the fraction collector (either 100 × 5 mL tubes or a 96 deep-well plate). Set the gradient to 0–100% nickel B buffer over 200 mL and start the gradient. If using ÄKTA set 0–100% nickel B, 100 min, at flow rate of 2 mL/min, end volume 200 mL and collect 2 mL fractions. Follow the absorbance at 280 nm. Normally, only one elution peak is observed, and corresponding fractions should be pooled. Typically select five 2 mL fractions on either side of the peak maximum.
14. Visualize an aliquot of each fraction on an SDS-PAGE gel to confirm the presence of the AMPK complex protein subunits: mix 5 μL of each fraction with 5 μL SDS-PAGE sample loading buffer, heat at 95 °C, and load onto a 4–12% gradient gel at 200 V for 35 min. 10 μL of pre-stained protein standards are run alongside. After running the gel, remove and stain the gel

with InstantBlue. After only a few minutes, bands demonstrating the presence of AMPK appear (*see* **Note 4**).

15. Concentrate fractions containing AMPK using 30 kDa cutoff spin filter concentrators. Typically this will be the peak fraction of around 2 mL and the best ten side fractions. The total volume will now be around 10–20 mL of eluate that will be concentrated down to around 5 mL. However depending on the amount of AMPK protein found and its purity (as determined from the gel), it may not be necessary (or feasible) to concentrate the pooled fractions, as if the protein sample is over 3 mg/mL the protein may precipitate upon concentration. In this case, separate gel filtration runs (below) are performed with the best fractions.
16. Size exclusion chromatography. If not prepared earlier (**step 1**), equilibrate a Superdex 200 XK 16/600 column with the gel filtration buffer.
17. Load the fractions containing AMPK from the nickel column that have been pooled and concentrated to 5 mL onto the Superdex 200 column using a flow rate of 1 mL/min.
18. Run the column and collect 1.5 mL fractions in 2 mL tubes or a 96 deep-well plate. Full-length AMPK protein elutes at an elution volume of approximately 70 mL (in the region of fraction 35–50).
19. Monitor the eluted protein by following the absorbance at 280 nm and run an SDS-PAGE gel as above of the peak fractions and side fractions (Fig. 1).
20. After gel filtration, the samples need to be handled very gently to prevent aggregation.
21. Pool the fractions containing AMPK. (*See* **Notes 5** and **6**.)
22. Measure the protein concentration of each sample using a NanoDrop spectrometer at absorbance at 280 nm.
23. **In vitro phosphorylation.** To prepare the phosphorylation reaction, add AMP and ATP to the protein separately to a final concentration of 500 μM, mixing gently by pipetting after each addition. Then add $MgCl_2$ to a final concentration of 2.5 mM. Add 1 mg of CaMKKβ for every 100 mg protein. Leave the sample overnight 16–17 h at 25 °C for phosphorylation to occur. There will normally be some protein precipitation after this stage, with loses of around 30% not unusual.

Day 3:

24. **Purification of the phosphorylated AMPK protein.** Clear the sample by filtration through a 0.45 μM syringe filter.
25. Then reapply the protein sample to a HisTrap FF 5 mL column, which has been pre-equilibrated with nickel A buffer,

using a peristaltic pump. This may take some time as the sample is now viscous. Once the entire sample has been applied, attach the column to the ÄKTA system and elute off the protein using 100% nickel B buffer at a speed of 1 mL/min and collect 1 mL factions.

26. The protein is eluted over a peak covering five 1 mL fractions.
27. The protein is now more stable and less sensitive to temperature.
28. Now run each fraction on a gel filtration column as described above, and recheck purity on an SDS-PAGE gel.
29. Pool the fractions containing AMPK and concentrate to between 7 and 9 mg/mL using a 30 kDa cutoff membrane spin concentrator.
30. Flash freeze the samples in liquid nitrogen and store at −80 °C.

3.4 Crystallization of Full-Length AMPK $\alpha 1\beta 1\gamma 1$

3.4.1 Crystallization of the Activator Complex of Phosphorylated Human AMPK Protein

The procedure that was used to generate the structure in the publication from the Gamblin lab [4] is described below. Prepare the AMPK complex stock solution using 7 mg/mL AMPK protein in 50 mM Tris, pH 8.0, 300 mM NaCl, and 1 mM TCEP, gently mixed with a threefold molar excess of AMP and onefold molar excess of staurosporine and 991 compounds (*see* **Note 7**).

1. Grow crystals by the vapor diffusion technique at 4 °C in hanging drops using the following optimized growth conditions by making the drops in the cold room or on ice.
2. Prepare drops by mixing equal volumes of AMPK complex stock solution with well reservoir solution containing 13% PEG3350, 0.1 M $MgCl_2$, 1% glucose, and 0.15% CAPB in 100 mM imidazole (pH 6.2). Typically, fill the reservoirs with 500 μL well solution, and then add 1 μL protein solution to a cover slip, followed rapidly by 1 μL of well solution to make 2 μL drops. **Quickly place the cover slip on the well to avoid dehydration of the drop.**
3. Look at the crystals with a microscope at low-power (×40) in the cold room every few days, and record the appearance of the drops, in terms of precipitate, clear, aggregate, or crystal (also size). Orthorhombic crystals typically appear in 3–5 days, and take at least a week to grow to usable sizes, typically 50 μm by 100 μm (Fig. 2).
4. For testing X-ray diffraction of the crystal and data collection, **first cryoprotect the crystal.**
5. Transfer crystals into a drop (2 μL) of well solution containing an additional 30% ethylene glycol. Mount the crystal in a suitably sized mounted cryoloop, then straight away plunge into liquid nitrogen and store for data collection (Fig. 2).

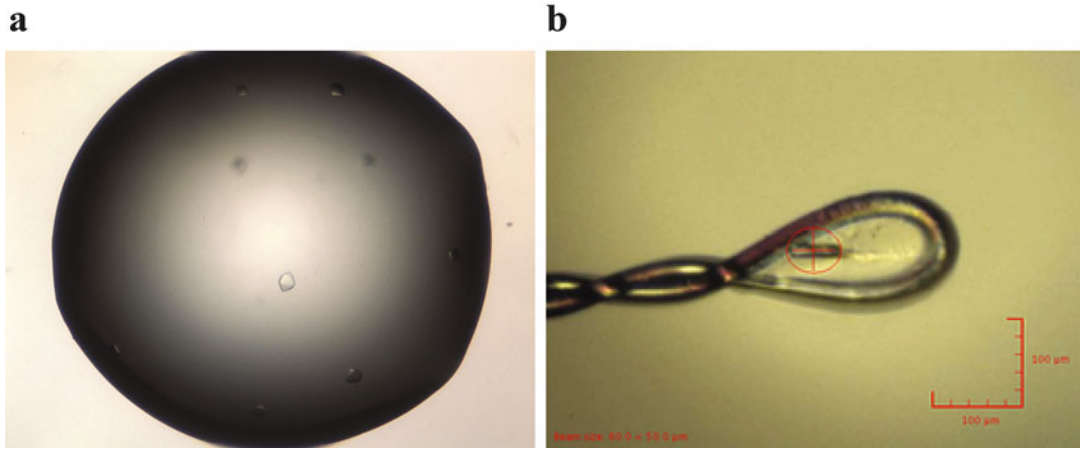

Fig. 2 Crystallization of AMPK. (**a**) Example of AMPK α1β1γ1 crystals growing in a crystallization well. (**b**) AMPK α1β1γ1 mounted in cryoloop

3.4.2 Re-Optimization of Crystallization Conditions for a New Batch of Protein

For a new batch of protein, slight re-optimization of growth conditions may be required.

1. Using the protein complex prepared as above, set up a grid of about 5 mL each of ten different well solutions. Use between 10% and 18% PEG3350 (in 2% steps), each at two pH values (6.2 and 6.5) while keeping other components constant.
2. Add 500 µL of each different well solution to a 24-well crystallization plate. Set up three crystallization trial drops, for example, 1 µL protein plus 1 µL well solution, 1.5 µL protein plus 0.5 µL well solution, and 0.5 µL protein plus 1.5 µL well solution. Monitor drops daily for the first week for precipitation and/or crystallization and then every few days subsequently.
3. Crystals that grow to at least 50 µm in width are best for data collection, but several different growth conditions (from the grid) and crystals from each drop may need to be tested for X-ray diffraction in order to obtain the optimal crystal growth conditions. Cryoprotect crystals with well solution with 30% ethylene glycol before freezing as before.
4. The crystals can now be tested for X-ray diffraction.

3.4.3 Crystallization of the Activator Complex of Unphosphorylated Human AMPK Protein

The procedure that was used to generate the structures [11] deposited in the PDB from the Gamblin lab is described below.

1. Grow crystals by vapor diffusion at 4 °C above (Subheading 3.4.1) but using AMPK protein that has not been subjected to in vitro phosphorylation to make the complex with. The best condition for crystallization was identified 12% PEG3350, 300 mM guanidine in 100 mM PIPES buffer at pH 7.2.

2. For a new batch of protein of unphosphorylated protein, the optimal condition for crystallization is likely to have also changed slightly so as set up a grid of different well solutions with a range of different PEG3350 concentrations and pH. Typically this would be 10–16% PEG3350, pH 7.0, 7.2, and 7.4. Also try varying the composition of the drops by changing the protein to well ratios; similarly try 1:1, 1.5:0.5, and 0.5:1.5.
3. Monitor the appearance of the drops as before using a microscope in the cold room. Crystals typically appear after around 3–10 days.
4. Cryoprotect by moving crystals into well solution with an additional 30% ethylene glycol, before plunging into liquid nitrogen and testing for diffraction of X-rays.

3.5 X-Ray Data Collection, Processing, and Model Building of AMPK

The instruments and procedures for collecting and processing X-ray data will vary dependent upon the access to and expertise of the individual scientist. For the scientist new to X-ray crystallography, this process requires specialist training and is outside the scope of this chapter.

Briefly, in our hands diffraction data were collected at 100K on a Pilatus 2 M detector (Dectris), Diamond Light Source, Oxford. The phosphorylated full-length AMPK activator complex crystals grown under these conditions were found to belong to the space group $P2_1$. For the unphosphorylated AMPK complex, the crystals belonged to the P1 2_1 1 space group.

Data were integrated using the program DENZO and scaled with SCALEPACK. The structure was solved by molecular replacement using PHASER, and standard refinement was carried out with PHENIX using 2Y94.pdb and 2F15.pdb as the search models, with manual model building with COOT. General crystallographic calculations were carried out using the CCP4 package. Figures were created with PyMOL.

4 Notes

1. The pH of Tris is temperature sensitive. Cool water in cold room before preparation of lysis buffer. Use buffer directly from cold room.
2. While this centrifugation step is ongoing, this is an opportunity to prepare the nickel column for the purification later in day 2.
3. Overnight the AMPK protein remains attached to the column at 4 °C in the cold room. Never elute the AMPK protein off the nickel column and leave overnight in imidazole as it is highly prone to aggregation at this stage.

4. The 30 kDa β-subunit has an anomalous electrophoretic mobility. This results in the β- and the γ-subunits (37 kDa) being difficult to resolve on a gel despite the difference in molecular weight. If in doubt, mass spectrometry can be used to validate the presence of both subunits accurately.
5. Do not concentrate the sample at this stage as if the protein concentration exceeds 3 mg/mL, it will precipitate during overnight phosphorylation.
6. Keep a sample of unphosphorylated protein for SDS-PAGE and mass spectrometry analysis.
7. In our hands, usable crystals of full-length human AMPK (α1β1γ1) could only be produced for protein that was complexed with nucleotides (AMP, ADP, or ATP) bound to the γ1 domain, a small molecule activator bound at the interface between α1 and β1, and with the kinase in an inhibited complex with staurosporine. Crystals could not be obtained in the absence of either staurosporine or a small molecule ADaM activator. However, crystals of rat α1, human β1, and human γ1 [5] were successfully produced in the absence of ADaM activators; however, the ADaM-binding site was partially occupied with SO_4^{2-} instead. Holocrystals of AMPK without activator bound but with cyclodextrin (as a mimic glycogen bound to a different region of the GBD domain instead) have been reported [8]. However, as they demonstrated a resolution of >4 Å, side chains and main chain can rarely be located with confidence.

Acknowledgments

This work was supported by the Francis Crick Institute, which receives its core funding from Cancer Research UK, the UK Medical Research Council and the Wellcome Trust. Julia Hubbard is a recipient of a Daphne Jackson Research Fellowship, which is funded by the Royal Society of Chemistry and the UK Medical Research Council. We greatly acknowledge Diamond Light Source for access to synchrotron time under proposal MX9826.

References

1. Xiao B, Heath R, Saiu P, Leiper FC, Leone P, Jing C, Walker PA, Haire L, Eccleston JF, Davis CT, Martin SR, Carling D, Gamblin SJ (2007) Structural basis for AMP binding to mammalian AMP-activated protein kinase. Nature 449:496–500
2. Xiao B, Sanders MJ, Underwood E, Heath R, Mayer FV, Carmena D, Jing C, Walker PA, Eccleston JF, Haire LF, Saiu P, Howell SA, Aasland R, Martin SR, Carling D, Gamblin SJ (2011) Structure of mammalian AMPK and its regulation by ADP. Nature 472:230–233
3. Underwood EA (2013) Nucleotide regulation of AMP-activated protein kinase. Doctoral thesis, University College London
4. Xiao B, Sanders MJ, Carmena D, Bright NJ, Haire LF, Underwood E, Patel BR, Heath RB, Walker PA, Hallen S, Giordanetto F, Martin

SR, Carling D, Gamblin SJ (2013) Structural basis of AMPK regulation by small molecule activators. Nat Commun 4:3017

5. Calabrese MF, Rajamohan F, Harris MS, Caspers NL, Magyar R, Withka JM, Wang H, Borzilleri KA, Sahasrabudhe PV, Hoth LR, Geoghegan KF, Han S, Brown J, Subashi TA, Reyes AR, Frisbie RK, Ward J, Miller RA, Landro JA, Londregan AT, Carpino PA, Cabral S, Smith AC, Conn EL, Cameron KO, Qiu X, Kurumbail RG (2014) Structural basis for AMPK activation: natural and synthetic ligands regulate kinase activity from opposite poles by different molecular mechanisms. Structure 22:1161–1172
6. Langendorf CG, Ngoei KR, Scott JW, Ling NX, Issa SM, Gorman MA, Parker MW, Sakamoto K, Oakhill JS, Kemp BE (2016) Structural basis of allosteric and synergistic activation of AMPK by furan-2-phosphonic derivative C2 binding. Nat Commun 7:10912
7. Salatto CT, Miller RA, Cameron KO, Cokorinos E, Reyes A, Ward J, Calabrese MF, Kurumbail RG, Rajamohan F, Kalgutkar AS, Tess DA, Shavnya A, Genung NE, Edmonds DJ, Jatkar A, Maciejewski BS, Amaro M, Gandhok H, Monetti M, Cialdea K, Bollinger E, Kreeger JM, Coskran TM, Opsahl AC, Boucher GG, Birnbaum MJ, DaSilva-Jardine P, Rolph T (2017) Selective activation of AMPK beta1-containing isoforms improves kidney function in a rat model of diabetic nephropathy. J Pharmacol Exp Ther 361:303–311
8. Li X, Wang L, Zhou XE, Ke J, de Waal PW, Gu X, Tan MH, Wang D, Wu D, Xu HE, Melcher K (2015) Structural basis of AMPK regulation by adenine nucleotides and glycogen. Cell Res 25:50–66
9. Leung L-H, Yao X-J, Wong KW, Liu L, Chen X (2016) Identification of a new AMPK activator for treatment of lung cancer. US Patent US9364469(B1)
10. Woods A, Dickerson K, Heath R, Hong SP, Momcilovic M, Johnstone SR, Carlson M, Carling D (2005) Ca2+/calmodulin-dependent protein kinase kinase-beta acts upstream of AMP-activated protein kinase in mammalian cells. Cell Metab 2:21–33
11. Xiao B, Hubbard JA, Gamblin SJ (2017) Structure of full length human AMPK (non-phosphorylated at t-loop) in complex with a small molecule activator, a benzimidazole derivative (991). Protein Database: 5ISO

Chapter 2

Visualizing AMPK Drug Binding Sites Through Crystallization of Full-Length Phosphorylated α2β1γ1 Heterotrimer

Christopher G. Langendorf, Jonathan S. Oakhill, and Bruce E. Kemp

Abstract

Here, we describe the crystallization protocol for AMPK, including protein production and purification. AMPK can be readily crystallized in the presence of PEG to give diffracting crystals to a resolution of between 2.5 and 3.5 Å using synchrotron radiation. This method allows for visualization of drugs or small molecules that bind to the ADaM site, CBS sites, ATP binding site, and the newly identified C2 binding sites in the γ-subunit via co-crystallization with phosphorylated AMPK (pT172) α2β1γ1 isoform or α2/1β1γ1 chimera. Drugs with binding affinities above 500 nM fail to co-crystallize with AMPK using these parameters.

Key words AMPK heterotrimer, Protein crystallization, Allosteric activation, Recombinant protein, Expression and purification

1 Introduction

AMP-activated protein kinase (AMPK) has become an attractive drug target for therapeutics aimed at type 2 diabetes, obesity, nonalcoholic fatty liver disease (NAFLD), cardiovascular disease, and some cancers. The AMPK complex is an αβγ heterotrimer containing a catalytic α-subunit and regulatory β- and γ-subunits. Multiple isoforms of each subunit exist in mammals (α1/2, β1/2, γ1/2/3) with each displaying cell/tissue-specific variation in expression. The potential importance of AMPK in metabolic disease treatment is well illustrated by the discovery that the glucose-lowering drug metformin, used to treat over 120 million people globally with type 2 diabetes, is an indirect activator of AMPK [1].

The first direct allosteric activator of AMPK, A-769662, was identified by Cool and colleagues in 2006 [2]. The discovery of a direct allosteric activator increased the urgency for AMPK structural information, which at this stage was limited to an isolated

Dietbert Neumann and Benoit Viollet (eds.), *AMPK: Methods and Protocols*, Methods in Molecular Biology, vol. 1732, https://doi.org/10.1007/978-1-4939-7598-3_2,

fragment of the β-subunit [3], the carbohydrate binding module (CBM), and a truncated kinase domain from the orthologous yeast kinase, SNF1 [4]. The fission yeast core αβγ structure comprising fragments of the α- and β-subunits associated with γ was the first to reveal the nucleotide binding architecture [5]. From this point on there was incremental increase in our AMPK structural knowledge until the landmark report from the Gamblin laboratory of the full-length α2β1γ1 heterotrimer [6]. This structure was followed quickly by the full-length structures of α1β1γ1 and α1β2γ1 [7] heterotrimers (for a comprehensive review of the structural history of AMPK, *see* Kurumbail and Calabrese [8]). It should be noted that while full-length proteins were crystallized, the resulting structures lacked density for the first ~70 residues of the β-subunit and approximately 80 residues from two flexible loops in the C-terminus of the α-subunit. The initial α2β1γ1 crystallization conditions were identified and optimized using the second-generation high-affinity drug 991 [6], which were then used to obtain the co-crystal structure of A-769662 bound to AMPK at 3.92 Å resolution. The three full-length AMPK heterotrimer structures all have a different α-/β-subunit combination in complex with γ1.

The full-length AMPK structures revealed the A-769662 allosteric binding site, later termed the allosteric drug and metabolite (ADaM) binding site (Fig. 1) [9]. The ADaM site is a hydrophobic pocket formed between the α-N-lobe of the kinase domain and the β-CBM (Fig. 1) [6, 10]. The allosteric activation by ADaM site drugs is thought to occur through stabilization of the α-C-helix by the β-C-interacting helix, which is directly C-terminal to the β-CBM [6]. The X-ray crystal structures of AMPK have been critical for identifying and understanding the allosteric binding sites. Recently we used X-ray crystallography to discover novel allosteric sites in the γ-subunit, distinct from the AMP sites [10]. We solved the structure of AMPK, co-crystallized in the presence of the AMP-mimetic C2 (5-(5-hydroxyl-isoxazol-3-yl)-furan-2-phosphonic acid); the resulting structure revealed two molecules of C2 bound to the solvent accessible core of the γ-subunit (Fig. 1). Here in we described the techniques that will allow for visualization of compounds targeted to all of the known AMPK allosteric sites via X-ray crystallography.

1.1 Expression and Purification of AMPK for X-Ray Crystallography

The heterotrimeric constructs utilized here are full-length α2β1γ1 (UniProt: P54646, Q9Y478, and P54619, respectively) and a chimeric enzyme with the α-regulatory interacting motif (α-RIM, Fig. 1) from α1 interchanged with α2 (α2(1–347)/α1 (349–401)/α2(397–end) β1γ1; α1 UniProt: Q13131) [10].

We use dual AMPK expression vectors, cloning α2/γ1 into pETDuet™-1 and β1 into pRSFDuet™-1, resulting in incorporation of an N-terminal hexa-histidine tag onto α2 [10]. Most

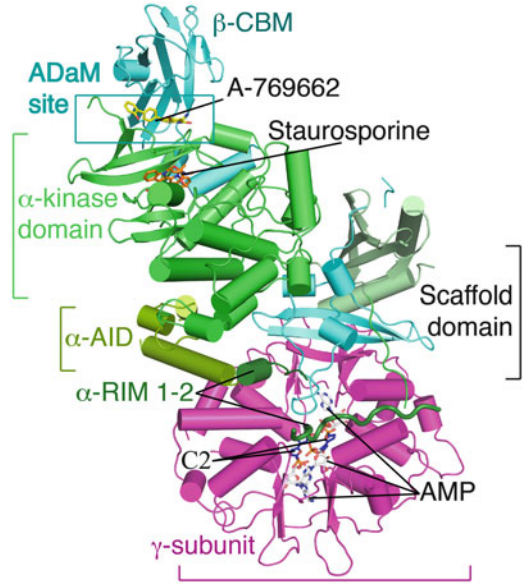

Fig. 1 Cartoon representation of AMPK heterotrimer. α2β1γ1 (PDB/4CFE [6]) showing the α-subunit (*green*), β-subunit (*cyan*), and γ-subunit (*magenta*). Key structural features have been labeled as follows: α-kinase domain, α-auto-inhibitory domain (α-AID), α-regulatory interacting motif (α-RIM) 1 and 2, β-carbohydrate binding module (β-CBM), allosteric drug and metabolite (ADaM) binding site, and the αβγ-scaffold domain. Allosteric modulators have been labeled, including staurosporine, AMP, A-769662, and C2, the latter overlaid from PDB 4ZHX [10]

laboratories have utilized tricistronic expression vectors to produce recombinant enzyme for full-length AMPK crystallization [6, 7, 11].

Full-length active AMPK is purified via a two-step method involving NiNTA IMAC affinity resin and size-exclusion chromatography. CaMKK2 purified from insect cells is then used to activate AMPK by phosphorylation of Thr172 in the activation loop. This is one of the most critical steps as over-phosphorylation can inhibit crystallization (*see* **Note 1**). Before crystallization experiments, the protein is further purified with another size-exclusion step.

1.2 AMPK Crystallization

The structure of full-length α2β1γ1 bound to C2 revealed the α2-RIM was disengaged. The added flexibility of the α2-RIM inhibited C2-α2β1γ1 co-crystallization; therefore, we employed two methods to reduce the impact of the α-RIM on crystallization. (1) AMP bound to the γ-subunit strengthens the α2-RIM/γ-subunit interaction; therefore, we used a combination of AMP-bound and C2-bound AMPK heterotrimer for crystal formation. In this system we are using the AMP-bound molecule to add structural integrity to the crystal, which allows for the more flexible

C2-bound AMPK to co-crystallize [10]. (2) Structural analysis of the α1-RIM reveals it forms a stronger interaction with the γ-subunit than the α2-RIM; therefore, we utilized a α1/2-RIM swap chimera for crystallization studies [10]. We have optimized conditions for the two crystallization constructs based on the previously published method by Xiao and colleagues [6].

1.3 Cryoprotection of AMPK Crystals

Cryoprotection is the most important step in producing high-quality diffracting AMPK crystals but also the most variable. Cryoprotectants are used to protect the protein crystals against freezing damage by ice formation during flash cooling. Xiao and colleagues reported that the reservoir solution supplemented with 30% ethylene glycol sufficiently protects AMPK crystals during flash cooling [6]; however, in our hands we find the diffractive quality of crystals cooled in this way differs greatly between samples. We prefer to use a combination of cryoprotectants mixed in with the reservoir solution in a stepwise manner.

X-ray crystallographic studies of full-length AMPK are valuable for the development of therapeutic activators and inhibitors for AMPK, whether they bind to the ADaM site, α-kinase domain, or γ-CBS motifs. Here we describe detailed, optimized protocols from our laboratory for the crystallization of full-length α2β1γ1 AMPK, including protein production and purification and cryoprotection of the crystals. The techniques described will allow for visualization of compounds targeted at all of the known AMPK allosteric sites.

2 Materials

2.1 Expression and Purification of AMPK for Crystallization

1. AMPK α2β1γ1 dual expression constructs: cDNAs for α2/γ1 cloned into pETDuet™-1 multiple cloning sites (MCS) 1 (BamH1/Not1) and 2 (MfeI/XhoI), respectively, and β1 cDNA cloned into pRSFDuet™-1 MCS1 (NcoI/BamHI).
2. AMPK α2/α1 RIM chimera dual expression constructs: cDNAs for α2/1 (α2(1–347)/α1(349–401)/α2(397-end))/γ1 cloned into pETDuet™-1 multiple cloning sites (MCS) 1 (BamHI/Not1) and 2 (MfeI/XhoI), respectively, and cDNA for β1 into pCOLADuet™-1 MCS1 (NcoI/BamHI) (*see* **Note 2**).
3. LB (lysogeny broth): 10 g/L tryptone, 5 g/L yeast extract, and 10 g/L NaCl.
4. LB agar: 1.5% (w/v) agar in LB media and then autoclave.
5. Ampicillin 1000× stock: 50 mg/ml ampicillin in water.
6. Kanamycin 1000× stock: 50 mg/ml kanamycin in water.
7. Autoclaved glycerol.
8. Expression flask: 2 L baffled Erlenmeyer flask.

9. Heating/cooling shaking incubator.
10. IPTG 1000× stock: 500 mM isopropyl β-D-1-thiogalactopyranoside (IPTG) in water.
11. Spectrophotometer that can measure wavelengths of 600 nm.
12. Plastic cuvettes suitable for spectrophotometer.
13. Centrifuge.
14. Protease inhibitor stock: 10 mM leupeptin, 1 M benzamidine-HCl, and 100 mM AEBSF, all solubilized in water.
15. Cell disruptor or homogenizer or sonicator.
16. Nickel column: Prepacked 5 ml nickel Sepharose IMAC (immobilized metal affinity column) resin.
17. Peristaltic pump.
18. Lysis buffer: 50 mM Tris–HCl, pH 7.6, 500 mM NaCl, 5% glycerol, 50 mM imidazole, 2 mM β-mercaptoethanol.
19. Elution buffer: 50 mM Tris–HCl, pH 7.6, 150 mM NaCl, 10% glycerol, 2 mM β-mercaptoethanol, 400 mM imidazole.
20. SEC column: S200 size-exclusion chromatography column, 120 ml bed volume.
21. Storage buffer: 50 mM Tris–HCl, pH 8.0, 150 mM NaCl, 2 mM Tris (2-carboxyethyl) phosphine (TCEP).
22. 15 ml concentrator, 30 kDa cutoff.
23. AMP: 100 mM stock (solubilized in 50 mM Tris–HCl, pH 7.4) for CaMKK2 treatment.
24. ATP: 100 mM stock (solubilized in 50 mM Tris–HCl, pH 7.4) for CaMKK2 treatment.
25. $MgCl_2$: 1.0 M magnesium chloride (dissolved in water) for CaMKK2 treatment.
26. CaMKK2 (*see* Subheadings 2.2 and 3.2).

2.2 Production and Purification of CaMKK2 for AMPK Phosphorylation

1. CaMKK2 expression vector: CaMKK2 cDNA (UniProt: Q96RR4-1) in pFASTBAC1-FLAG-N-TEV.
2. Sf21 insect cells.
3. Sf-900 II media.
4. Heating/cooling shaking incubator.
5. PBS (phosphate-buffered saline): 137 mM NaCl, 2.7 mM KCl, 10 mM Na_2HPO_4, 1.8 mM KH_2PO_4.
6. Insect lysis buffer: 50 mM Tris–HCl, pH 7.4, 200 mM NaCl, and 1 mM EDTA.
7. FLAG monoclonal antibody-coupled affinity resin.
8. Insect elution buffer: Insect lysis buffer with FLAG peptide (DYKDDDDK) added (0.25 mg/ml).
9. Liquid nitrogen.

2.3 Crystallization for ADaM Site Activators

1. AMP: 9 mM adenosine monophosphate (AMP) solubilized in 50 mM Tris–HCl, pH 7.4.
2. A769662: 3 mM A769662 solubilized in DMSO.
3. Staurosporine: 3 mM staurosporine solubilized in DMSO.
4. S108tide: 600 μM S108 synthetic peptide (corresponding to β1(102–114) $Arg^{112–114}$) (NH_2-KLPLTRSHNNFVARRR-COOH), solubilized in 50 mM Tris–HCl, pH 7.4.
5. SAMS peptide: 600 μM SAMS peptide (NH_2-HMRSAMSGLHLVKRR-COOH), solubilized in 50 mM Tris–HCl, pH 7.4.
6. 24-Well crystallization plate.
7. Reservoir solution: 7–8.5% polyethylene glycol (PEG) 3350, 0.1 M $MgCl_2$, 1.0% glucose, 0.0005–0.003% cocamidopropyl betaine, and 0.1 M imidazole HCl (pH 6.2).

2.4 Crystallization for C2-Site Activators

1. C2: 9 mM C2 (5-(5-hydroxyl-isoxazol-3-yl)-furan-2-phosphonic acid) solubilized in DMSO.

2.5 Cryoprotection of AMPK Crystals

1. 1% cryo-solution: 7–8.5% polyethylene glycol (PEG) 3350, 0.1 M $MgCl_2$, 1.0% glucose, 0.0005–0.003% cocamidopropyl betaine and 0.1 M imidazole (pH 6.2), 1.0% glycerol, 1.0% PEG 400, 1.0% (±)-2-methyl-2,4-pentanediol (MPD), 1.0% sucrose, 1.0% sorbitol, and 1.0% ethylene glycol.
2. 2% cryo-solution: 7–8.5% polyethylene glycol (PEG) 3350, 0.1 M $MgCl_2$, 1.0% glucose, 0.0005–0.003% cocamidopropyl betaine and 0.1 M imidazole (pH 6.2), 2.0% glycerol, 2.0% PEG 400, 2.0% (±)-2-methyl-2,4-pentanediol (MPD), 2.0% sucrose, 2.0% sorbitol, and 2.0% ethylene glycol.
3. 3% cryo-solution: 7–8.5% polyethylene glycol (PEG) 3350, 0.1 M $MgCl_2$, 1.0% glucose, 0.0005–0.003% cocamidopropyl betaine and 0.1 M imidazole (pH 6.2), 3.0% glycerol, 3.0% PEG 400, 3.0% (±)-2-methyl-2,4-pentanediol (MPD), 3.0% sucrose, 3.0% sorbitol, and 3.0% ethylene glycol.
4. 4% cryo-solution: 7–8.5% polyethylene glycol (PEG) 3350, 0.1 M $MgCl_2$, 1.0% glucose, 0.0005–0.003% cocamidopropyl betaine and 0.1 M imidazole (pH 6.2), 4.0% glycerol, 4.0% PEG 400, 4.0% (±)-2-methyl-2,4-pentanediol (MPD), 4.0% sucrose, 4.0% sorbitol, and 4.0% ethylene glycol.
5. 5% cryo-solution: 7–8.5% polyethylene glycol (PEG) 3350, 0.1 M $MgCl_2$, 1.0% glucose, 0.0005–0.003% cocamidopropyl betaine and 0.1 M imidazole (pH 6.2), 5.0% glycerol, 5.0% PEG 400, 5.0% (±)-2-methyl-2,4-pentanediol (MPD), 5.0% sucrose, 5.0% sorbitol, and 5.0% ethylene glycol.
6. Liquid nitrogen.

3 Methods

3.1 Expression and Purification of AMPK for Crystallization

1. Transformation of expression vectors: Add 50 ng of either AMPK α2β1γ1 or AMPK α1/α2 RIM chimera dual expression constructs into 20 μl of Rosetta™ 2 (DE3) *E. coli* competent cells, and incubate on ice for 30 min.
2. Heat shock cells by incubating at 42 °C for 45 s, then rest on ice for 5 min.
3. Add 0.1 ml of LB to the transformation mixture and incubate at 37 °C for 1 h.
4. Plate the transformation mixture onto LB agar plates containing 1/1000 ampicillin 1000× stock and 1/1000 kanamycin 1000× stock, and incubate at 37 °C overnight.
5. Transfer a single colony into 3 ml of LB with 3 μl of ampicillin 1000× stock and 3 μl kanamycin 1000× stock, and incubate at 37 °C overnight.
6. Make a glycerol stock from the overnight culture. Add 100 μl of autoclaved glycerol to 900 μl of LB and store at −80 °C (*see* **Note 3**).
7. Starter culture: In the expression flask, add 100 ml LB, 50 μl of AMPK glycerol stock, 100 μl ampicillin 1000× stock, and 100 μl kanamycin 1000× stock. Incubate the starter culture overnight in a shaking incubator at 37 °C with shaking at 120 rpm.
8. Expression culture: Add 900 ml of LB (supplemented with 900 μl ampicillin 1000× stock and 900 μl kanamycin 1000× stock) directly to the starter culture, and incubate in a shaking incubator at 37 °C with shaking at 120 rpm until OD_{600} reaches 3.0 (*see* **Notes 4** and **5**).
9. Induce protein expression by adding 1.0 ml IPTG 1000× stock to the culture, and incubate in a shaking incubator at 16 °C with shaking at 120 rpm overnight (approximately 20 h).
10. Pellet cultured cells by centrifugation at 3000 × *g* for 20 min at 4 °C and remove supernatant.
11. Resuspend pelleted cells in chilled lysis buffer (with 1000× protease inhibitor stock added), and maintain at 4 °C at all times.
12. Lyse cells via cell disruption and then clarify lysate by centrifugation at 44,000 × *g* for 30 min at 4 °C; transfer supernatant to a fresh tube.
13. Equilibrate the nickel column with lysis buffer. Ensure to wash with at least 10 column volumes (CV) of buffer (CV = 5 ml bed volume).

14. Pass clarified lysate over the nickel column using a peristaltic pump at 1 ml/min.
15. Wash the nickel column with lysis buffer until the concentration of protein eluting is low, approximately 10 CV.
16. Elute AMPK by passing 1–2 CV of elution buffer over the nickel column, pool the protein peak, and concentrate to 5 ml if necessary.
17. Apply the protein peak to a SEC column, pre-equilibrated in storage buffer.
18. Concentrate the AMPK containing fractions to ~5.0 ml for CaMKK2 phosphorylation.
19. Phosphorylate AMPK by incubation with CaMKK2 at a ratio of 1:2400 (w/w) (CaMKK2/AMPK) in the presence of 2.5 mM $MgCl_2$, 0.5 mM ATP, and 0.5 mM AMP. Incubate the phosphorylation reaction mixture at 22 °C for 1 h with gentle rolling.
20. Terminate the reaction by applying the phosphorylation reaction mixture to a SEC column (repeat **step 17**).
21. Concentrate the pure AMPK containing fractions to ~10 mg/ml, and flash freeze in liquid nitrogen. Store the purified enzyme at −80 °C. The yield from typical protein purification is between 10 and 15 mg/L of culture.

3.2 Production and Purification of CaMKK2 for AMPK Phosphorylation

1. Culture the Sf21 insect cells in Sf-900 II media, incubating in a shaking incubator at 26 °C with shaking at 150 rpm.
2. Infect the Sf21 cells at a multiplicity of infection of 10 and continue incubation for 72 h post-infection.
3. Harvest the Sf21 cells by centrifugation at 1,000 × *g* for 15 min at 4 °C; discard the supernatant.
4. Wash the pellet with PBS and store at −80 °C.
5. Thaw and resuspend the Sf21 cells in 0.05× culture volume of ice-cold insect lysis buffer with protease inhibitors. Maintain at 4 °C at all times.
6. Lyse Sf21 cells and clarify the lysate by centrifugation at 40,000 × *g* for 60 min at 4 °C; transfer supernatant to a fresh tube.
7. Equilibrate FLAG monoclonal antibody-coupled affinity resin in 10× volumes of insect lysis buffer.
8. Add equilibrated FLAG monoclonal antibody-coupled affinity resin to the Sf21 lysate, and mix on a rotating wheel at 4 °C for 1 h.

9. Wash FLAG monoclonal antibody-coupled affinity resin extensively in insect lysis buffer (5 × 10 volumes).
10. Elute CaMKK2 in insect elution buffer. Aliquot and flash freeze eluted protein in liquid nitrogen and store at −80 °C.

3.3 Crystallization for ADaM Site Activators

1. Dilute full-length phosphorylated α2β1γ1 to 4 mg/ml (30 μM) in storage buffer containing a threefold molar excess of AMP (90 μM), an equimolar (30 μM) of staurosporine and A-769662 (*see* **Note 6**), and two- to fivefold molar excess (60–150 μM) of synthetic peptide S108tide or SAMS (*see* **Note 7**), and incubate on ice for 30 min.
2. Set up hanging drop crystallization experiments in a 24-well crystallization plate by adding 500 μl of reservoir solution to the crystallization plate. We suggest altering the concentration of both cocamidopropyl betaine (*see* **Note 8**) and PEG 3350 in a grid screen.
3. Add 1.0 μl of the AMPK/compound mixture to the reservoir solution at a 1:1 ratio, and incubate the crystallization plate at 4 °C. Crystallization experiments can be set at room temperature or at 4 °C. Crystals should appear after 2–4 days, growing to their full size within 2 weeks (Fig. 2).
4. Crystal size can be increased by one of two methods, either protein feeding (*see* **Note 9**) or macro-seeding (*see* **Note 10**).

3.4 Crystallization for C2-Site Activators

It is possible to use different protein constructs to visualize the γ1-subunit activator C2, full-length phosphorylated α2β1γ1, and full-length phosphorylated AMPK α1/α2 RIM chimera (*see* **Note 11**).

1. Dilute full-length phosphorylated α2β1γ1 as described in **step 1** in Subheading 3.3 with the following exceptions: make two separate AMPK protein stocks at 4 mg/ml, one containing twofold molar excess of AMP (60 μM) and the other containing twofold molar excess of C2 (60 μM), without AMP. Incubate the protein/compound mixture at 4 °C for 30 min, and then combine prior to setting the hanging drop experiment described in **steps 2** and **3** in Subheading 3.3.
2. Dilute full-length phosphorylated AMPK α1/α2 RIM chimera [12] (4 mg/ml, 30 μM) as described in **step 1** in Subheading 3.3 with the following exception exchange AMP for a sixfold molar excess of C2 (180 μM).
3. Hanging drop crystallization experiments were set up as described in **steps 2** and **3** in Subheading 3.3.

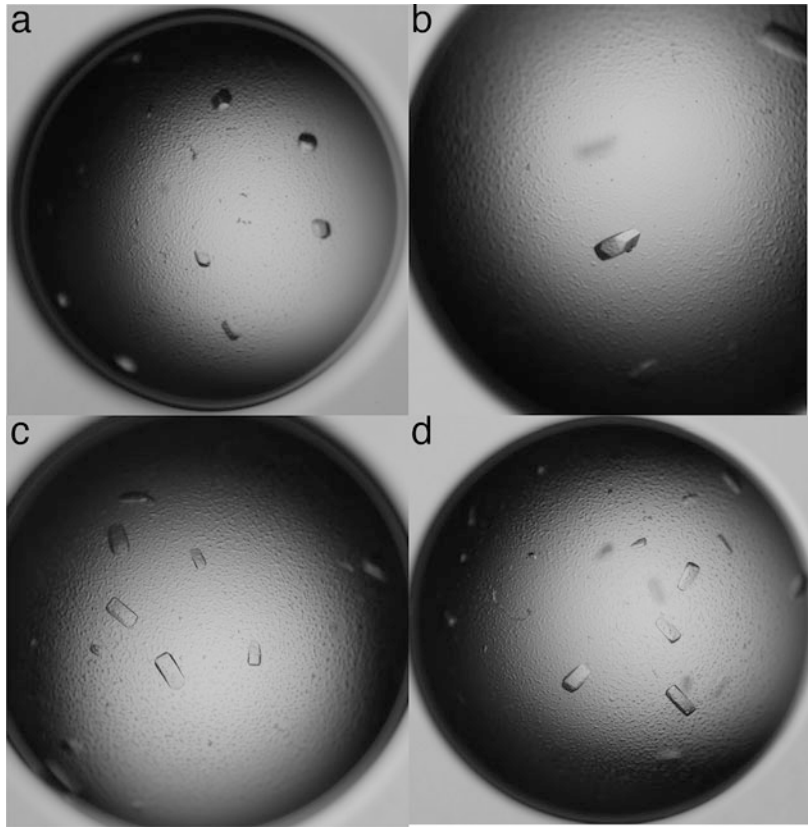

Fig. 2 Full-length phosphorylated α2β1γ1 AMPK crystals. Examples of crystals grown in 7–8.5% PEG 3350, 0.1 M $MgCl_2$, 1.0% glucose, 0.0005–0.003% cocamidopropyl betaine and 0.1 M imidazole (pH 6.2), co-crystallized with 3× AMP, 1× A-769662, 1× staurosporine, 5× S108tide after incubation at 4 °C for 3 weeks. (**a**, **b**) The hexagonal ends of the crystal are clearly visible, (**c**, **d**) while from the side the crystals appear rectangular

3.5 Cryoprotection of AMPK Crystals

Perform the following steps in a 4 °C cold room.

1. Quickly transfer a single crystal into a 2–3 μl drop of 1% cryo-solution; incubate for 10–20 s.
2. Repeat **step 1**, transferring the crystal incrementally into 2%, 3%, 4%, and 5% cryo-solution. Incubate the crystals for 60–120 s in 5% cryo-solution.
3. After the final incubation, quickly flash cool the crystal in liquid nitrogen for storage/transport. Typically crystals should diffract to a resolution between 2.5 and 3.5 Å.

4 Notes

1. Levels of AMPK phosphorylation induced by CaMKK2 are critical for producing protein that will crystallize; high levels of phosphorylation on the β1-subunit will inhibit crystallization. Analyzing protein phosphorylation using protein TOF mass spectrometry, we see between one and two individual phosphorylation events on the β1-subunit of protein that readily crystallizes. Inhibition of crystallization occurs when there is between three and six separate phosphorylation events on the β1-subunit of AMPK.
2. Once the glycerol stock has been made, **steps 1–6** can be skipped for future preparations.
3. We see increased yields of AMPK using the pCOLADuet™-1/pETDuet™-1 system over the pRSFDuet™-1/pETDuet™-1. A number of crystallization studies have successfully used tricistronic vectors for AMPK heterotrimer expression [6, 7, 11].
4. Check the optical density of the expression culture in a 1 ml disposable plastic cuvette hourly by spectrophotometry at a wavelength of 600 nm using LB as a blank.
5. We see increased yields of AMPK when inducing protein expression during stationary phase ($OD_{600} = 3.0$), compared to inducing during exponential growth phase ($OD_{600} = 0.6–1.0$).
6. The ratio of A-769662 to AMPK is crucial for co-crystallization, and concentrations of A-769662 above twofold of AMPK inhibit crystallization. In addition we have found that co-crystallization of different ADaM site compounds is more likely to be successful when their affinity for AMPK is <500 nM.
7. The synthetic peptides have not been resolved in the X-ray crystal structures. Only very weak density has been obtained for a few residues of the peptide.
8. The cocamidopropyl betaine concentration we use, 0.0005–0.003%, is quite different to the concentration used by other researchers, 0.15% [6, 10]. This could be due to concentration discrepancies between the suppliers. We recommend using a broad concentration range of cocamidopropyl betaine for initial screening.
9. Protein feeding experiments involve adding more protein directly to a crystallization drop containing crystals. Prepare the protein sample at 4 mg/ml, diluted with storage buffer and aforementioned compounds.

10. Macro-seeding is a common crystallographic technique used to improve crystal size. Transfer a crystal into a fresh drop containing protein/compounds and reservoir solution. Reduce the concentration of the precipitant (PEG 3350) in the reservoir solution until no new crystals form (typically between 3% and 5% PEG 3350), but high enough that crystal growth can be observed over 7–10 days.
11. Depending on the chemistry of the compounds binding to the γ-subunit, the RIM may or may not interact. In the case of C2, we would recommend using the AMPK α1/α2 RIM chimera for crystallization trials. The advantage of using the AMP/C2 combined approach with α2β1γ1 is the binding of the two molecules can be directly compared within the one crystal structure.

Acknowledgments

These authors are supported by grants from the National Health and Medical Research Council, the Australian Research Council, the Victorian Government Operational Infrastructure Support Scheme, and the Jack Brockhoff Foundation (JBF-4206, 2016), and C.G.L. is an E.H. Flack Research fellow. B.E.K. and J.S.O. are NHMRC and ARC Research fellows, respectively.

References

1. Zhou G, Myers R, Li Y, Chen Y, Shen X, Fenyk-Melody J, Wu M, Ventre J, Doebber T, Fujii N, Musi N, Hirshman MF, Goodyear LJ, Moller DE (2001) Role of AMP-activated protein kinase in mechanism of metformin action. J Clin Invest 108(8):1167–1174. https://doi.org/10.1172/JCI13505
2. Cool B, Zinker B, Chiou W, Kifle L, Cao N, Perham M, Dickinson R, Adler A, Gagne G, Iyengar R, Zhao G, Marsh K, Kym P, Jung P, Camp HS, Frevert E (2006) Identification and characterization of a small molecule AMPK activator that treats key components of type 2 diabetes and the metabolic syndrome. Cell Metab 3(6):403–416. https://doi.org/10.1016/j.cmet.2006.05.005
3. Polekhina G, Gupta A, van Denderen BJ, Feil SC, Kemp BE, Stapleton D, Parker MW (2005) Structural basis for glycogen recognition by AMP-activated protein kinase. Structure 13(10):1453–1462. https://doi.org/10.1016/j.str.2005.07.008
4. Nayak V, Zhao K, Wyce A, Schwartz MF, Lo WS, Berger SL, Marmorstein R (2006) Structure and dimerization of the kinase domain from yeast Snf1, a member of the Snf1/AMPK protein family. Structure 14 (3):477–485. https://doi.org/10.1016/j.str.2005.12.008
5. Townley R, Shapiro L (2007) Crystal structures of the adenylate sensor from fission yeast AMP-activated protein kinase. Science 315 (5819):1726–1729. https://doi.org/10.1126/science.1137503
6. Xiao B, Sanders MJ, Carmena D, Bright NJ, Haire LF, Underwood E, Patel BR, Heath RB, Walker PA, Hallen S, Giordanetto F, Martin SR, Carling D, Gamblin SJ (2013) Structural basis of AMPK regulation by small molecule activators. Nat Commun 4:3017. https://doi.org/10.1038/ncomms4017
7. Li X, Wang L, Zhou XE, Ke J, de Waal PW, Gu X, Tan MHE, Wang D, Wu D, Xu HE, Melcher K (2015) Structural basis of AMPK regulation by adenine nucleotides and glycogen. Cell Res 25(3):398. https://doi.org/10.1038/cr.2015.27

8. Kurumbail RG, Calabrese MF (2016) Structure and regulation of AMPK. EXS 107:3–22. https://doi.org/10.1007/978-3-319-43589-3_1
9. Langendorf CG, Kemp BE (2015) Choreography of AMPK activation. Cell Res 25(1):5–6. https://doi.org/10.1038/cr.2014.163
10. Langendorf CG, Ngoei KR, Scott JW, Ling NX, Issa SM, Gorman MA, Parker MW, Sakamoto K, Oakhill JS, Kemp BE (2016) Structural basis of allosteric and synergistic activation of AMPK by furan-2-phosphonic derivative C2 binding. Nat Commun 7:10912. https://doi.org/10.1038/ncomms10912
11. Calabrese MF, Rajamohan F, Harris MS, Caspers NL, Magyar R, Withka JM, Wang H, Borzilleri KA, Sahasrabudhe PV, Hoth LR, Geoghegan KF, Han S, Brown J, Subashi TA, Reyes AR, Frisbie RK, Ward J, Miller RA, Landro JA, Londregan AT, Carpino PA, Cabral S, Smith AC, Conn EL, Cameron KO, Qiu X, Kurumbail RG (2014) Structural basis for AMPK activation: natural and synthetic ligands regulate kinase activity from opposite poles by different molecular mechanisms. Structure 22(8):1161–1172. https://doi.org/10.1016/j.str.2014.06.009
12. Hunter RW, Foretz M, Bultot L, Fullerton MD, Deak M, Ross FA, Hawley SA, Shpiro N, Viollet B, Barron D, Kemp BE, Steinberg GR, Hardie DG, Sakamoto K (2014) Mechanism of action of compound-13: an alpha1-selective small molecule activator of AMPK. Chem Biol 21(7):866–879. https://doi.org/10.1016/j.chembiol.2014.05.014

Chapter 3

Biophysical Interactions of Direct AMPK Activators

Ravi G. Kurumbail, Graham M. West, Venkatasubramanian Dharmarajan, Kris A. Borzilleri, Jane M. Withka, Jessica Ward, Allan R. Reyes, Francis Rajamohan, Patrick R. Griffin, and Matthew F. Calabrese

Abstract

Protein-ligand interactions can be evaluated by a number of different biophysical methods. Here we describe some of the experimental methods that we have used to generate AMPK protein reagents and characterize its interactions with direct synthetic activators. Recombinant heterotrimeric AMPK complexes were generated using standard molecular biology methods by expression either in insect cells via infection with three different viruses or more routinely in *Escherichia coli* with a tricistronic expression vector. Hydrogen/deuterium exchange (HDX) coupled with mass spectrometry was used to probe protein conformational changes and potential binding sites of activators on AMPK. X-ray crystallographic studies were carried out on crystals of AMPK with bound ligands to reveal detailed molecular interactions formed by AMPK activators at near-atomic resolution. In order to gain insights into the mechanism of enzyme activation and to probe the effects of AMPK activators on kinetic parameters such as Michaelis-Menten constant (K_m) or maximal reaction velocity (V_{max}), we performed classical enzyme kinetic studies using radioactive ^{33}P–ATP-based filter assay. Equilibrium dissociation constants (K_D) and on and off rates of ligand binding were obtained by application of surface plasmon resonance (SPR) technique.

Key words X-ray, Crystallography, HDX, Hydrogen/deuterium exchange, SPR, Enzymology, Kinetics, AMPK, Activation, Baculovirus, Tricistronic

1 Introduction

Molecular interactions of small molecules with proteins define the fundamental processes involved in recognition and discrimination of substrates, cofactors, and products in endogenous systems. It is often the ligand-induced conformational changes that are responsible for modulation of functional activity of proteins. Quantifying and carefully evaluating these biophysical interactions are critical for the discovery and development of novel therapeutics. Methods based on NMR, X-ray crystallography, cryo-electron microscopy, and mass spectrometry have evolved over the years to characterize binding sites and interactions between protein and ligands.

Dietbert Neumann and Benoit Viollet (eds.), *AMPK: Methods and Protocols*, Methods in Molecular Biology, vol. 1732, https://doi.org/10.1007/978-1-4939-7598-3_3,

Modulation of enzymatic activity of proteins by small molecules can be probed by classical enzymology methods which reveal insights into effects on the Michaelis-Menten constant (K_m) or the maximal reaction rate (V_{max}). Interactions of small molecule synthetic activators of AMP-activated protein kinase (AMPK) have been probed by the application of these biochemical and biophysical methods.

AMPK is a heterotrimeric serine/threonine protein kinase that regulates cellular and whole-body energy homeostasis in response to metabolic stress. It consists of a catalytic α subunit, which contains the kinase module, and two regulatory subunits, β and γ. In vivo, it is regulated by reversible phosphorylation as well as by binding of nucleotides to its γ subunit [1–4]. Activation of AMPK by small molecule synthetic activators has been pursued as a viable strategy for the development of novel therapeutics for insulin resistance and metabolic syndrome [5–8]. We have probed the interactions of AMPK with small molecules using a number of methods including X-ray crystallography, SPR, HDX, and enzymatic assays which are briefly described below [9–11]. Also included is a brief description of two molecular biology methods that we have used to generate recombinant AMPK protein reagents.

1.1 Recombinant Protein Production

All biophysical techniques described below rely on the availability of highly pure and homogenous recombinant AMPK. As expression of individual subunits (either in *E. coli* or insect cells) did not yield sufficient quantities of soluble protein (in-house unpublished data), we pursued simultaneous expression of AMPK subunits. As reported by Neumann et al., a single plasmid carrying all three subunits of AMPK α1β1γ1 driven by T7 RNA polymerase as a single tricistronic messenger in *E. coli* allows spontaneous formation of the heterotrimeric complex in the bacterial cytosol [12]. Using this method we generated multiple combinations of full-length and truncated mammalian AMPK complexes in *E. coli* [9, 11, 13, 14]. In addition, we have also produced recombinant AMPK in insect cells by co-transfection with three viruses that contain individual AMPK α, β, or γ subunits (*see* **Note 1**).

1.2 Hydrogen/Deuterium Exchange Coupled to Mass Spectrometry

Hydrogen/deuterium exchange (HDX) coupled to mass spectrometry is a powerful technique to investigate protein structure and conformational dynamics as it reports on changes in solvent deuterium uptake on the backbone amides in response to chemical and posttranslational modifications (PTMs), mutations, and ligand binding events [15, 16]. High-resolution structural tools such as X-ray crystallography and NMR provide a detailed picture of a protein's structure and ligand binding mode. However, crystal structures can only provide a single snapshot of a protein's conformation ensemble, and protein dynamics studies using NMR are often limited to small molecular weight protein systems that are

complicated by the need for labeled protein reagents. Protein function is governed by local and global structural fluctuations that can be quite complex for large protein complexes such as AMPK heterotrimers that contain multiple binding pockets within all three subunits [17–20]. HDX is a reliable tool to examine such conformational fluctuations. This technique can reveal the nuances of allosteric communication within and between subunits and provide insights into mechanism of enzyme activation [11, 16, 21].

1.3 X-Ray Crystallography

X-ray crystallography is the most widely used method to study three-dimensional structures of proteins. Structure-based drug design critically depends on insights into the binding modes of ligands in druggable binding sites on proteins, usually revealed by crystallography [22]. Well-ordered crystals are produced from homogenous protein derived from recombinant methods or from natural sources. Methods such as hanging drop or sitting drop vapor diffusion are typically used to produce protein crystals [23, 24]. These are then flash frozen in liquid nitrogen or liquid ethane in the presence of suitable cryoprotectants prior to X-ray diffraction experiments. At present, most diffraction measurements are made at dedicated high-energy synchrotron laboratories around the world. Sophisticated computational algorithms that employ Fourier mathematics of the measured X-ray diffraction data reveal the distribution of electron density at near-atomic resolution. Ligands are either soaked into preexisting crystals of proteins, or crystals are generated after forming the protein-ligand complex in solution in order to gain information on binding of ligands.

1.4 Enzymatic Assays

The rate of catalysis of enzymes varies as a function of substrate concentration in a hyperbolic fashion. At low substrate concentration (S), the reaction velocity is a linear function of (S), but it is independent of (S) at saturating concentrations. By following the rate of product formation at different substrate and enzyme concentrations, we can derive the V_{max} (the maximum velocity) or K_m (Michaelis-Menten constant, concentration of substrate required to reach ½ V_{max}) assuming steady-state kinetics. Enzyme activators can bring about allosteric changes on proteins through effects on either V_{max} or K_m or both. As is true for all protein kinases, AMPK has two substrates: ATP/Mg^{2+} and a peptide or protein substrate. We have used a 15 amino acid peptide fragment known as SAMS peptide derived from one of the well-studied AMPK substrates, ACC1 (acetyl-CoA carboxylase 1), for our biochemical assays and mechanistic studies [25]. By varying the concentration of one substrate while keeping the other fixed at tenfold its K_m value, we have determined the effects of small molecule enzyme activators on the kinetic parameters of AMPK [13, 26].

The biochemical assay method we have employed to monitor the enzyme kinetics of AMPK is a ^{33}P-ATP-based filter assay. In our

experience this assay is preferred for enzyme kinetic experiments since it can be easily adapted for testing at a range of peptide or ATP concentrations [9, 10, 13]. Once the phosphorylation reaction is completed, it is quenched with phosphoric acid at desired time points. Under these conditions, the kinase is inactivated, the SAMS peptide becomes protonated allowing for retention on the phosphocellulose membrane via a charge interaction, and the ^{33}P-ATP is removed by filtration. The method below describes a discontinuous assay format where a reaction progress curve is generated by measuring the amount of phosphorylated SAMS peptide product produced over time. The linear range of each time course can be used to determine the rate at each reaction condition. The rates determined at different substrate concentrations can then be plotted as a function of (S) to elucidate the K_m and V_{max} parameters [9].

1.5 Surface Plasmon Resonance

Surface plasmon resonance (SPR) is the biophysical technique of choice in pharmaceutical research to determine equilibrium binding affinities (K_D) and binding kinetics (k_{on}, k_{off}) of small molecules to protein targets [27]. In this method, protein reagents, referred to as the ligand in SPR, are immobilized onto a sensor chip using direct immobilization protocols such as amine coupling of surface lysines or by an interaction of an engineered protein tag to a specific chip surface. For example, this type of immobilization could include coupling of a His-tagged protein onto a Ni-NTA surface or capture of a biotin-tagged protein on a streptavidin surface, as is described below for AMPK. In SPR, binding affinities and kinetics are determined by injecting the small molecule, referred to as the analyte, over the sensor surface containing immobilized protein. The analyte is usually prepared in aqueous sample buffer. Binding of an analyte to the immobilized protein causes a change in the refractive index at the sensor surface, which is captured by a sensitive detector.

2 Materials

2.1 Recombinant Protein Production

1. Vector for expression in bacterial cells: pET14b expression vector.
2. Host cells for bacterial expression: *E. coli* BL21-CodonPlus™ (DE3)-RIPL strain.
3. AMPK plasmid for expression in *E. coli*: Tricistronic construct that contains open reading frames of human α, β, and γ subunits codon-optimized for expression in *E. coli* with *NcoI* and *XhoI* sites for ligation to pET14b vector (*see* **Note 2**).
4. AMPK plasmids for expression in insect cells: Genes for human AMPK α, β, and γ subunits custom-synthesized with codon

optimization for expression in *Spodoptera frugiperda* (Sf-9) insect cells (*see* **Note 3**).

5. Expression media and reagents: LB broth, LB agar plates, 100 mg/ml ampicillin, and 100 mM isopropyl β-D-thiogalactopyranoside (IPTG).
6. DH10BAC cells: *E. coli* cells that contain bacmid DNA.
7. Host insect cells: *Spodoptera frugiperda* (Sf-9) insect cells.
8. Recombinant virus: Virus generated by transfecting insect cells with recombinant bacmid DNA that contains the gene of interest integrated into viral DNA.
9. Cell lysis buffer: 50 mM Tris–HCl, pH 8.0, 150 mM NaCl, 5% (v/v) glycerol, 2 mM tris-2-carboxyethyl phosphine (TCEP), 20 mM imidazole, 0.001% (v/v) Triton X-100.
10. Cell sonicator: e.g., Branson ultrasonic disintegrator.
11. Nickel affinity chromatography column: e.g., 5 ml HisTrap™ HP column.
12. Elution buffer: 50 mM Tris–HCl, pH 8.0, 150 mM NaCl, 5% (v/v) glycerol, 2 mM TCEP, 20 mM imidazole, 0.001% (v/v) Triton X-100, 300 mM imidazole.
13. Dialysis buffer: 50 mM Tris–HCl, pH 8.0, 150 mM NaCl, 5% (v/v) glycerol, 2 mM TCEP, 0.001% (v/v) Triton X-100.
14. Size exclusion chromatography column: e.g., Superdex 200 HiLoad 16/60 column.
15. Size exclusion chromatography (SEC) buffer: 50 mM Tris–HCl, pH 8.0, 150 mM NaCl, 5% (v/v) glycerol, 2 mM TCEP, and 0.001% (v/v) Triton X-100.
16. Vector for expression in insect cells: e.g., pFastBac-1 insect cell expression vector.
17. Serum-free insect cell medium: e.g., Sf-900 III SFM.

2.2 Hydrogen/Deuterium Exchange Coupled to Mass Spectrometry

1. Protein storage buffer: 50 mM Tris–HCl, pH 8.0, 150 mM NaCl, 10% (v/v) glycerol, 2 mM TCEP, and 0.001% (v/v) Triton X-100 (*see* **Note 4**).
2. H_2O HDX buffer: 50 mM Tris–HCl, pH 8.0, 150 mM NaCl, 10% (v/v) glycerol, 2 mM TCEP in H_2O (*see* **Note 5**).
3. D_2O HDX or labeling buffer: 50 mM Tris–HCl, pH 8.0, 150 mM NaCl, 10% (v/v) glycerol, 2 mM TCEP in D_2O (*see* **Notes 5** and **6**).
4. Quench buffer: 3 M urea, 1% (v/v) trifluoroacetic acid (TFA) in H_2O, pH 2.4 (*see* **Notes 7** and **8**). Add fresh reducing agent (2 mM TCEP).
5. HDX Mobile phase A: 0.3% (v/v) formic acid in H_2O.

6. HDX Mobile phase B: 0.3% (v/v) formic acid in acetonitrile: H_2O (ratio of 4:1).
7. HDX Mobile phase C (protease column buffer): 0.1% (v/v) TFA in H_2O.
8. Protease column: Pepsin immobilized on resin (1 mm× 20 mm).
9. Chromatography columns: 1 mm × 10 mm C8 trap and 1 mm × 50 mm C18 analytical columns.
10. Acetonitrile: Stock solution of 100% (v/v) acetonitrile (ACN).
11. Formic acid: 0.3% (v/v) formic acid (FA).
12. Mass spectrometer for peptide identification experiments: LTQ XL™ linear ion trap mass spectrometer or a similar instrument (*see* **Note 9**).
13. Instrumentation for differential HDX experiments: Ideally use a fully automated system, e.g., LEAP Technologies Twin HTS PAL liquid handling robot interfaced to a high-resolution (70,000 at m/z 400) Exactive Orbitrap mass spectrometer (*see* **Note 10**).
14. Software for analysis of mass spectrometric data: e.g., Mascot (Matrix Science, London, UK) for peptide identification and HDX Workbench or similar for differential HDX data processing.

2.3 X-Ray Crystallography

1. X-ray size exclusion chromatography (SEC) buffer: 25 mM Tris–HCl, pH 7.5, 150 mM NaCl, 10% (v/v) glycerol, 2 mM TCEP.
2. Protein crystallization buffers and precipitation agents: 1.6 M trisodium citrate tribasic dihydrate, 2 M lithium sulfate, 3.5 M ammonium sulfate, 100% (v/v) ethylene glycol.
3. Crystallization ligands: 21 mM staurosporine and 10 mM AMP.
4. 96–3 shallow well Intelliplates for sitting drop vapor diffusion crystallization.
5. Crystallization instrument: e.g., mosquito nanoliter-scale crystallization robot.
6. Crystal mounting: e.g., CrystalCap SPINE-style cryo-crystal mounts.
7. PF-06409577 (available from Sigma [aka PZ0319]).

2.4 Enzymatic Assays

1. Kinase assay buffer: 50 mM HEPES-NaOH pH 7.4, 1 mM EGTA, 10 mM $MgCl_2$, 0.25 mM dithiothreitol (DTT), 0.01% (v/v) Tween 20, 0.01% (w/v) bovine serum albumin (BSA).

2. Wash buffer: 50 mM HEPES-NaOH pH 7.4, 1 mM EGTA, 10 mM $MgCl_2$, 0.1% (v/v) Tween 20, 0.01% (w/v) BSA.
3. Kinase assay reagents: 100 mM ATP, 3000 Ci/mmol (10 mCi/ml) ^{33}P–ATP, 2% (v/v) phosphoric acid, and 20 mM SAMS peptide.
4. AMPK activators: 50 mM PF-06409577, a proprietary Pfizer AMPK activator.
5. Negatively-charged phosphocellulose (PH) filter plate.

2.5 Surface Plasmon Resonance

1. SPR buffer A: 25 mM Tris–HCl pH 7.5, 150 mM NaCl, 250 μM TCEP, 0.01% (v/v) P20 surfactant, 0.2 mg/ml BSA, 150 μM AMP (*see* **Notes 11** and **12**).
2. SPR buffer B: Buffer A + 2% (v/v) DMSO.
3. HBS-P buffer: 10 mM HEPES-NaOH, pH 7.5, 150 mM NaCl, 0.01% (v/v) P20.
4. SPR instrument: e.g., Biacore™ 3000.
5. Chips for immobilization of protein: Streptavidin-based sensor chips.
6. Conditioning solution: 1 M NaCl + 50 mM NaOH.
7. Software for SPR data analysis: e.g., Scrubber2 and BIAeval.

3 Methods

Carry out all procedures at room temperature unless otherwise specified.

3.1 Recombinant Protein Production

For bacterial expression of AMPK and purification, follow ***steps 1–14*** *below.*

1. For bacterial expression of AMPK, design a tricistronic AMPK expression plasmid (*see* **Note 2**) (Fig. 1a).
2. Synthesize the above-described gene with codon optimization for bacterial expression.
3. Subclone the tricistronic gene into the *NcoI* and *XhoI* sites of bacterial expression vector (pET14b) under the control of T7 promoter using standard molecular biology techniques (*see* **Note 13**).
4. Transform the construct into *E. coli* cells and select transformants on LB agar plates containing ampicillin (100 μg/ml).
5. For large-scale expression and purification, inoculate an Erlenmeyer flask containing 1 l of LB broth supplemented with 100 μg/ml ampicillin with 25 ml of overnight culture and grow in a shaker incubator at 37 °C to an OD_{600} of 0.8.

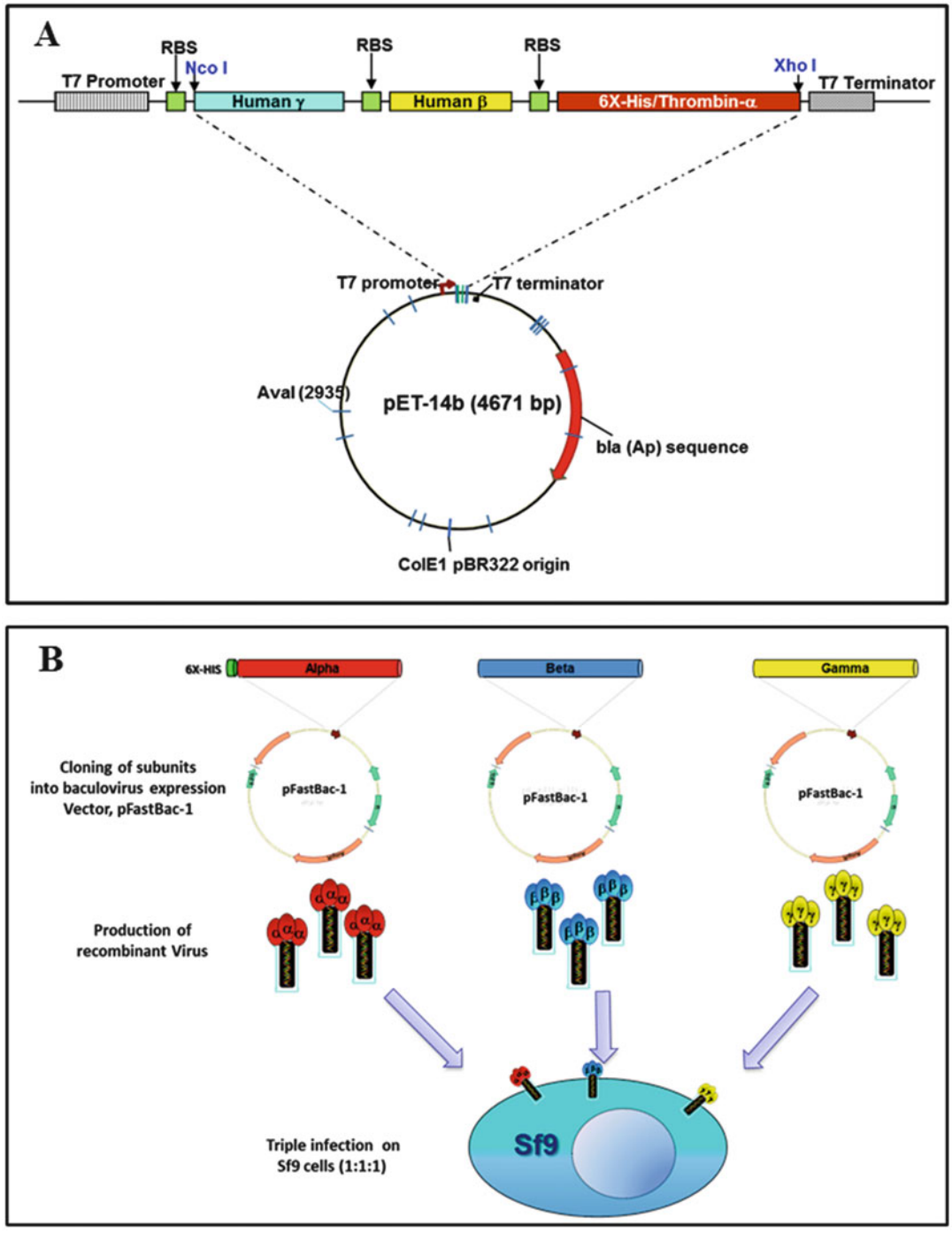

Fig. 1 AMPK expression constructs in bacteria and insect cells. (**a**) Diagram of recombinant human AMPK heterotrimeric construct inserted between *NcoI* and *XhoI* sites of pET14b *E. coli* expression vector. (**b**) Schematic representation of heterotrimer expression strategy in Sf-9 eukaryotic cells

6. Induce protein expression with 100 μM (final concentration) of isopropyl β-D-thiogalactopyranoside (IPTG), reduce the temperature to 18 °C, and grow the cells for an additional 18 h.
7. Harvest the cells and re-suspend them in 50 ml of cell lysis buffer.
8. Sonicate the cell suspension on ice for 2–4 min at 50% of duty cycle.
9. Remove the insoluble material by centrifugation at 29,000 × *g* in a centrifuge for 30 min at 4 °C.
10. Load the supernatant onto a nickel affinity chromatography column and wash with 10 column volumes of cell lysis buffer.
11. Elute the bound proteins using a linear gradient (10 column volume) with elution buffer.
12. Pool fractions containing the AMPK subunits based on 10% SDS-PAGE analysis and dialyze overnight in dialysis buffer.
13. For further purification, load the AMPK protein on a size exclusion chromatography column.
14. Isolate the appropriate fractions corresponding to AMPK heterotrimer (~135 kDa MW), which occur at approximately 70 ml of elution volume (if using the Superdex 200 HiLoad 16/60 column) depending on injection volume and column connections.

For expression of AMPK in insect cells, follow ***steps 15–21*** *below.*

15. Custom synthesize the genes for human AMPK subunits for expression in insect cells (*see* **Note 3**).
16. Subclone them individually into the *BamHI* and *XhoI* sites insect cell expression vector (pFastBac1) under the control of polyhedrin promoter using standard molecular biology techniques.
17. Generate recombinant viruses and amplify them (*see* **Note 14**).
18. For expression of the heterotrimeric complex, infect 1 l of Sf-9 cells at a cell density of 2×10^6 viable cells/ml and an MOI of 0.5 at 1:1:1 ratio of α, β, and γ subunit containing viruses in a serum-free insect cell medium (Fig. 1b).
19. Grow the cells for 48–72 h after infection and harvest them when their viability reaches 80–88%.
20. Store the harvested cells at −80 °C until further use.
21. For purification of AMPK, follow **steps 7–14** above.

3.2 Hydrogen/Deuterium Exchange Coupled to Mass Spectrometry

Buffer exchange all recombinantly purified human AMPK heterotrimeric proteins (full-length or truncated) into protein storage buffer and dilute to a final working concentration of 10 μM in H_2O HDX buffer [11] (*see* **Note 15**).

1. Prepare fresh H_2O and D_2O HDX buffers to match the AMPK protein storage buffer (*see* **Notes 15** and **16**).
2. Prepare 125 μl of each sample (Apo protein or ligand complex) at a final working concentration of 10 μM in H_2O HDX buffer. Initiate complex formation by incubating the AMPK protein sample with tenfold molar excess (100 μM final concentration) of ligand(s) from DMSO stock solutions or equal volume of 100% DMSO (Apo) and incubate for 1 h on ice (or desired temperature) before subjecting to HDX analysis.
3. Before running a HDX experiment (MS^1 data) to measure deuterium uptake kinetics, it is a prerequisite to generate a list of peptic peptides (generated by treatment with pepsin) covering all three AMPK subunits using tandem MS (MS/MS or MS^2) under identical sample, chromatographic, and MS conditions needed for HDX. Scan this peptide set against HDX datasets (see below) to estimate the deuteration profiles for each peptide based on its monoisotopic mass and deuterium uptake over time. For AMPK heterotrimers (134 kDa), we followed over 500 peptides.

For peptide identification and tandem MS, follow ***steps 4–17*** *below.*

4. Perform the MS/MS experiments on a high-resolution-capable LTQ XL™ linear ion trap mass spectrometer or a similar instrument (*see* **Note 9**).
5. Prepare a 10 μM solution of AMPK in H_2O HDX buffers. For protein-protein complex studies, it is advisable to prepare the AMPK sample in the presence of other interacting partners to optimize pepsin digestion efficiency and sequence coverage in the context of complex (*see* **Note 17**).
6. Dilute 4 μl of 10 μM AMPK solution with 16 μl of AMPK HDX H_2O buffer and then mix with 30 μl of quench solution (*see* **Note 18**). Inject 50 μl into the LC/MS for protease digestion, peptide trapping, and gradient elution.
7. Pass the mixture across an in-house packed pepsin column (1 mm × 20 mm) at 50 μl/min. We usually place the pepsin column inside a temperature control chamber held at 15 °C to allow for optimal pepsin digestion activity (*see* **Notes 19** and **20**).
8. Capture the digested peptides onto a 1 mm × 10 mm C8 trap column and desalt them (total time for digestion and desalting is 2.5 min).
9. Separate the peptides across a 1 mm × 50 mm C18 analytical column with a 75- min linear gradient (5–50% ACN and 0.3% FA over 60 min initially; and then increased to 100% ACN, 0.3% FA for 15 min, and finally reduced to 5% ACN, 0.3% FA within 1 min).

10. Electrospray ionization parameters are set as follows: sheath gas 30 au, auxiliary gas 15 au, spray voltage 3.7 V, capillary temperature 225 °C, capillary voltage 25 V, tube lens 95 V, skimmer 16 V.
11. Acquire mass spectrometric data with a resolving power of 70,000 at m/z 400.
12. Acquire product ion spectra in a data-dependent mode and then select the five most abundant ions for the product ion analysis.
13. Convert the MS/MS *.raw data files to *.mgf files. For peptide identification, submit the MS/MS data to Mascot (*see* **Note 21**).
14. We usually consider only those peptides that had a Mascot score of 20 or greater for the HDX analysis. We recommend running an MS/MS Mascot search against a decoy (reverse) sequence to rule out ambiguous identifications (*see* **Note 22**).
15. Inspect the MS/MS spectra of all the peptide ions from the Mascot hits for verifiable fragmentation pattern and pepsin cleavage preferences [28]. Use only those verifiable peptides for estimating the sequence coverage.
16. Map the unambiguously identified peptides onto the AMPK heterotrimer sequence to estimate the protein sequence coverage across all three subunits.
17. Repeat MS/MS experiments with varying AMPK protein concentration and quench conditions to optimize sequence coverage if necessary (*see* **Note 23**).

    For hydrogen/deuterium exchange experiments, follow ***steps 18–29*** *below.*

18. Prepare a 125 μl of 10 μM solution of Apo AMPK in H_2O HDX buffers and dispense in position A1 of 96-well sample plate. For each AMPK-ligand complex pairwise comparison, prepare 125 μl of 10 μM AMPK solution containing each individual ligand at 10× final concentration and dispense it in position A2. Aliquot 100 μl of H_2O HDX buffer in A3 for blank measurements (*see* **Notes 24** and **25**).
19. Place an empty 96-well tray inside the robotic station assigned for sample mixing.
20. Aliquot 30 μl of ice-cold quench solution in wells for rows A–C and E of the 96-well quench tray.
21. Allow the samples to equilibrate inside the HDX system for 1 h. This incubation time can be adjusted for ligands that bind with weak affinity to AMPK based on SPR data or reduced for protein systems that are less stable over long experiment times (12–14 h) needed for the automated HDX-MS analysis.

22. Initiate each exchange reaction by incubating 4 μl of AMPK protein (with or without ligand) with 16 μl of AMPK D_2O buffer for a predetermined time (10 s, 30 s, 60 s, 300 s, 900 s, and 3600 s in a randomized order) on a 96-well plate setup. Sample and D_2O buffer volume can be adjusted using concentrated protein samples, and incubation times can be varied to get maximum deuterium incorporation (*see* **Notes 26–29**).
23. Slow the exchange reaction rate by mixing the protein solution with 30 μl of ice-cold quench solution (*see* **Note 16**).
24. For peptide identification, collect three replicates of control undeuterated AMPK sample mixed with H_2O HDX buffer for time 0 s and quenched similar to D_2O-containing samples.
25. Pass the quenched reaction mixture (50 μl) through the immobilized pepsin column at 50 μl/min, and capture the digested peptides onto a C8 trap column and desalt (total time for digestion and desalting is 2.5 min).
26. Separate the peptides using a C18 analytical column with a short 8-min linear gradient (5–40% ACN and 0.3% formic acid over 5 min, then increased to 100% ACN for 2 min, and finally reduced to 5% ACN over 1 min).
27. Protein digestion and peptide separation steps utilized for HDX-MS experiments are identical to MS/MS except for the use of a time-compressed gradient used in HDX-MS runs to reduce D/H back exchange with chromatography solvents and preserve exchanged deuterium (*see* **Note 16**).
28. Electrospray ionization and MS data acquisition parameters are set similar to the tandem MS experiments described above.
29. Perform three technical replicates for each on-exchange time point to allow statistical analysis of the data.

    For HDX data analysis, follow ***steps 30–34*** *below.*

30. Load data from mass spectrometer into HDX Workbench [29] (previous versions include Deuterator [30] and HD Desktop [31]) or similar software. Other software packages can be used, but they should be capable of handling high-resolution HDX-MS data that are often large and should also support ligand comparisons (*see* **Note 30**).
31. Check that sufficient sequence coverage and unambiguous peptide identification (mass accuracy <3 ppm for precursor monoisotopic mass) are obtained in the initial peptide detection step using undeuterated control samples before proceeding to estimate percent deuterium incorporation. Sequence coverage on HDX datasets is comparatively lower than the MS/MS run due to peptide loss in shorter HDX gradient, ion suppression by complex samples, and multiple injections

required for the complete HDX-MS profile analysis of AMPK (42 total injections for a single pairwise comparison for Apo AMPK vs. Ligand one encompassing seven time points and three replicates).

32. Manually inspect data from each peptide to ensure accurate analysis parameters are used in deuterium level measurements (e.g., retention time, S/N intensity, and absence of interfering ion signals from overlapping peptides in m/z bars).
33. To identify significant differences between individual peptides across the two protein states (Apo AMPK vs. AMPK-AMP ligand complex), statistical analysis based on p-values ($p < 0.05$ for any two time points or <0.01 for a single time point) from a simple Student's t test between the replicates from the bound and free states is used to differentiate true statistically significant differences in perturbation from experimental noise distribution.
34. Present the HDX-MS data in an user-desired format such as time-dependent deuterium uptake plots; sequence coverage differential perturbation heat map view, overlaid on a 3D structure or model using PyMOL; experiment comparison view comparing multiple ligands in a table format; and residue-level perturbation data extrapolated from overlapping peptides or a Bayesian approach [11, 32] (*see* **Note 31**) (Fig. 2).

3.3 X-Ray Crystallography

Follow ***steps 1–5*** *for crystallization of AMPK.*

1. Design a construct suitable for crystallographic studies of AMPK [9] (*see* **Note 32**).
2. After purification of recombinant $AMPK^{xtal}$ (*see* **steps 2–14** in Subheading 3.1), confirm protein purity by mass spectrometry and SDS-PAGE analysis. Pool peak fractions and concentrate to 10–15 mg/ml. Aliquot into 30 μl single-use tubes and flash freeze in liquid nitrogen. Store at −80 °C until use.
3. Prepare a 96-well crystallization grid based on the following condition: 100 mM trisodium citrate, 750 mM ammonium sulfate, 500 mM lithium sulfate, and 1% (v/v) ethylene glycol. Vary concentration of ammonium sulfate and lithium sulfate systematically (from ~250 mM to ~1 M), and screen for wells that give largest/best crystals (*see* **Note 33**). If dispensing directly into 96-well trays (Intelliplates), prepare 70–75 μl of each condition. If mixing manually, prepare 500–1000 μl of each condition and dispense into 24-well plates.
4. Thaw an aliquot of AMPK on ice. Then add 400 μM of staurosporine and 400 μM of AMP. Incubate on ice ~10 min.

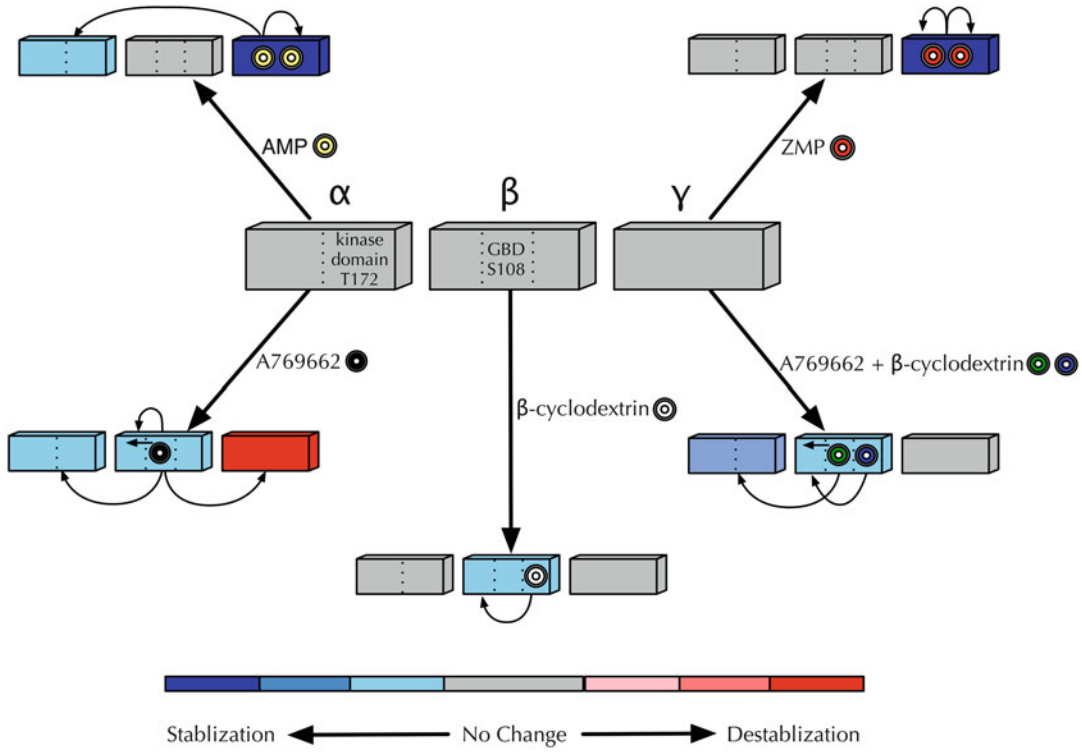

Fig. 2 Schematic of differential HDX profile obtained with human AMPK α1β1γ1 and AMPK activators. Protein stabilization caused by ligand binding (as measured by differential HDX) is shown in blue, while destabilization is shown in red. Changes in stabilization are a result of altered conformation of the protein. Known or putative ligand binding sites on AMPK subunits are shown by yellow circles (AMP), red circle (ZMP), black circle (A769662), and gray circle (β-cyclodextrin). This is a schematic representation of the general observations from the HDX experiments with different ligands showing that AMP binding results in enhanced protection or stabilization of the γ subunit and the activation loop in the kinase module of the α subunit. Binding of ZMP, an AMP analogue and a cellular metabolite of AICAR, primarily alters the HDX profile in the γ subunit. The synthetic activator A769662 displays strong stabilization of the β subunit and portions of the α subunit involved in substrate binding and catalysis. Also, A769662 causes destabilization of the γ subunit, the reasons for which are not completely understood. The effect of the glycogen mimetic, β-cyclodextrin, is mostly restricted to the β subunit. Combination of A769662 and β-cyclodextrin (green and blue circle) elicits a profile that is a combination of the individual profiles obtained by each of the ligands. These results also suggest that A769662 and β-cyclodextrin bind at nonoverlapping sites on the glycogen binding module of the β subunit. The HDX data strongly suggest two fundamentally different modes of AMPK activation by A769662 and the nucleotides

Sample may begin to show slight precipitate. Spin in a bench-top microcentrifuge ~15,000 × *g* for 10 min at 4 °C.

5. Set crystal tray using a mosquito robot at room temperature dispensing 200 nL of protein + 200 nL of reservoir solution into Intelliplate 96–3 shallow well sitting drop plates. Seal crystal tray with clear film or tape and incubate near room temperature (~22 °C). Crystals may begin to appear in

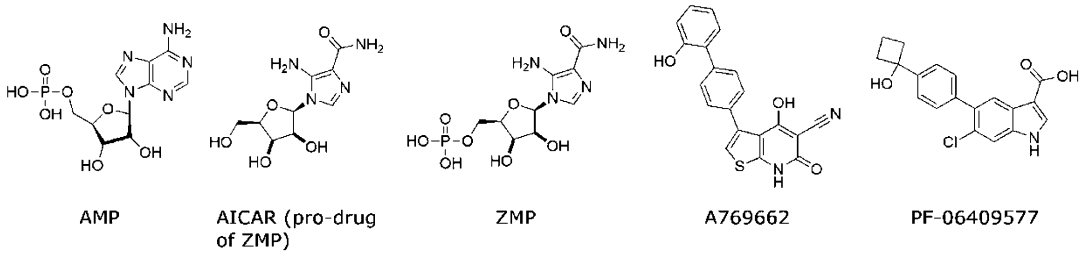

Fig. 3 Chemical structures of some of the known AMPK direct activators and their prodrugs. AICAR is not a direct activator by itself but becomes phosphorylated in vivo to generate ZMP which functions as an AMP mimetic

1–3 days and typically reach full size by 7–10 days. Wells often become a bit gummy beyond 2 weeks, and crystals beyond this age may yield poorer diffraction (*see* **Note 34**).

Follow ***steps 6–9*** *below for crystal harvesting and X-ray data collection.*

6. For structural analysis with bound ligands, mix 50 μl of soak solution and 50 μl of cryo-solution. Solutions are matched to the composition of the reservoir in which the crystal is growing with the addition of 10% (v/v) glycerol (soak solution) or 28% (v/v) glycerol (cryo-solution). To both cryo- and soak solution, also add 200 μM of staurosporine, 400 μM of AMP, and 500 μM of ligand of interest (Fig. 3). Centrifuge these samples for 10 min at 19,000 × *g* at room temperature.
7. For crystal soaking, break film or tape on top of crystal well and add 0.5 μl of soak solution directly onto crystal drop. Reseal well with tape and incubate overnight at room temperature (*see* **Note 35**).
8. Harvest the crystals the next day (Fig. 4a). Transfer single crystal by pipette from the soak reservoir well into ~10 μl of fresh soak solution (with compounds) on a glass coverslip under microscope. Using a mounted loop (*see* Subheading 2.3, **item 6**) attached to a magnetic crystal wand, transfer a single crystal into 10 μl of fresh cryo-solution (with compounds). Allow crystal to soak for at least a few seconds, then loop again with litholoop and plunge into liquid nitrogen to freeze (*see* **Note 36**). Transfer to cryo-vial or puck to enable storage and shipment in cryo-dewars.
9. Mail dry shipping dewars containing frozen crystals to a synchrotron light source for exposure to X-rays and diffraction data collection.

For structure solution and analysis, follow ***steps 10–13*** *below.*

10. Process the diffraction images using the software HKL2000 [33].

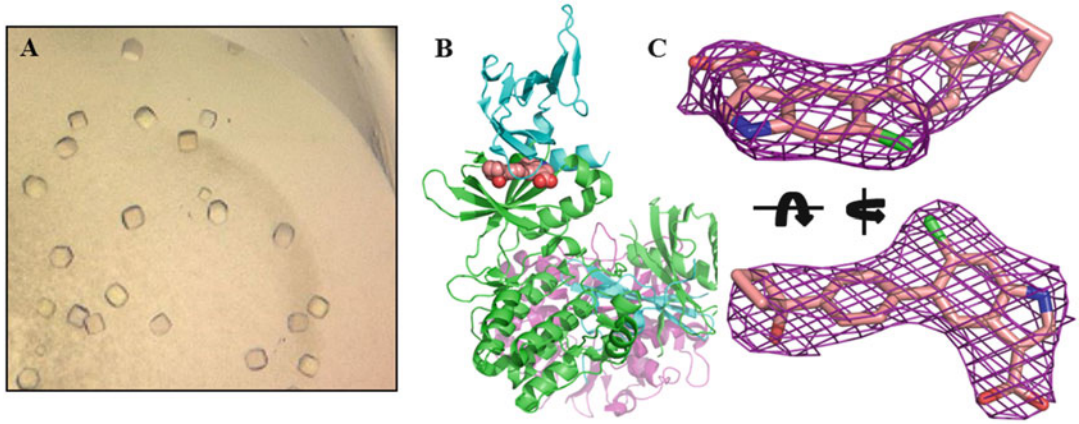

Fig. 4 X-ray crystallography of AMPK α1β1γ1 complexes with ligands. (**a**) Image of crystals of AMPK α1β1γ1 ($AMPK^{xtal}$) growing in sitting drop well. Crystals shown are approximately 50–100 μm in size. (**b**) Overall topology of AMPK α1β1γ1 (colored green, cyan, pink) derived from 5KQ5.pdb (10). Activator (PF-06409577) is bound at the ADaM site and shown in spheres. (**c**) Electron density is shown (2Fo-Fc map, contoured at 1 σ) with modeled conformation of ligand

11. Solve the crystal structure of $AMPK^{xtal}$ by molecular replacement using known structures of different AMPK fragments using the Phaser application in the CCP4 suite of crystallography programs [34].
12. Refine the structure using autoBUSTER [35] and Coot [36] (Fig. 4b).
13. In order to avoid crystallographic bias, it is important to first refine the "Apo" protein structure and calculate an electron density map prior to inclusion of the ligand of interest. This allows interrogation of an "unbiased" difference density map illustrating regions of mismatch between map and model. Modeling into this map using ligand-fitting protocols such as RHOFIT [37] generates an initial docking pose which is subsequently refined to improve the goodness of fit (*see* **Notes 37** and **38**) (Fig. 4c).

3.4 Enzymatic Assays

The method below is for a 384-well assay plate; however, volume adjustments can be made for other plate densities.

1. Prepare working solution mixtures: *Activator mixture*—Dilute compound to 4× the desired final compound concentration in 1× kinase buffer. *AMPK enzyme mixture*—Prepare a 4× AMPK enzyme solution by diluting AMPK in 1× kinase buffer to desired concentration. The selected AMPK concentration should be optimized so the reaction is linear with good assay window over a reasonable period of time (*see* **Note 39**). *4× ATP mixture*—Prepare ATP solution by diluting ATP in 1× kinase buffer to a concentration equal to 40× the reported

K_m value for the specific isoform and to a suggested final ^{33}P-ATP specific activity of 0.25 μCi/nmol (*see* **Note 40**). Since this solution will be diluted 4× when added to the reaction, the final (ATP) in the reaction will be 10× the ATP K_m value. *4× SAMS peptide substrate mixture*—Prepare SAMS peptide solution by diluting SAMS peptide in 1× kinase buffer to a concentration equal to 40× the reported K_m value for the specific isoform. Serially dilute the SAMS mix to cover a concentration range of 0.1 to 10-fold the expected K_m value in the final reaction mixture.

2. Add 10 μl of the activator mixture and 10 μl of the AMPK enzyme mixture to a 384-well polypropylene plate. Incubate the plate at room temperature for 15 min to allow enzyme and compound to come to equilibrium.
3. Add 10 μl of the ATP mixture.
4. Add 10 μl of the SAMS peptide substrate mixture to initiate the kinase reaction (*see* **Note 41**). Reaction time courses can be performed by initiating reactions in specific wells at different times and terminating all reactions simultaneously with the addition of 20 μl of 2% (v/v) phosphoric acid.
5. Pre-wet the phosphocellulose filter plate by adding ~50 μl of 2% (v/v) phosphoric acid and filter by applying vacuum using the vacuum manifold (*see* **Note 42**).
6. Transfer the quenched AMPK reaction mixture to the filter plate and filter by applying vacuum. Wash the wells six times with 75 μl of wash buffer.
7. Allow filter plate to dry. Seal the bottom of the plate using a plate seal and add 25 μl of scintillation fluid.
8. Seal the top of the plate and count the radioactivity on an instrument such as a PerkinElmer MicroBeta Trilux. The signal in each well (CPM) is directly proportional to the amount of phosphorylated peptide produced (*see* **Note 43**).
9. Plot the signal from each well as a function of time to generate a reaction progress curve. The slope of the initial linear portion of this time course is used to determine the rate of each reaction.
10. Plot the reaction rates at different concentration of peptide as a function of the concentration of peptide. Fit the data in this hyperbolic plot to the Michaelis-Menten equation using GraphPad Prism or a similar software to determine the V_{max} and K_m. Compare these kinetic parameters with and without compound treatment to determine the direct effects of the allosteric activators on V_{max} and K_m [9, 10] (*see* **Note 44**).

3.5 Surface Plasmon Resonance (SPR)

Design a suitable SPR construct for the immobilization of AMPK on streptavidin chips (*see* **Note 45**).

Follow ***steps 1–6*** *below for capturing AMPK onto streptavidin-based SPR chips.*

1. Dock the streptavidin sensor chip in the Biacore™ 3000 instrument and prime the system 3× with HBS-P buffer.
2. Condition all four flow cells on the chip surface. Set the flow rate to 100 μl/min and inject 50 μl of conditioning solution three consecutive times using the Quickinject with Extraclean option for the injections.
3. Normalize all four flow cells on the chip surface: Run the normalize procedure found under the Tools tab of the Biacore software.
4. Switch the buffer system to SPR Buffer B by priming 1× and put instrument in sensorgram mode (found under the Run tab).
5. Dilute the protein to 1.25 μg/ml in Buffer B and inject onto flow cells 2 and 3 at a rate of 5 μl/min in order to achieve ~4000–6000 RU of binding to the chip surface.
6. Flow Buffer B over all four flow cells of the chip surface to equilibrate the chip surface at a flow rate of 5 μl/min for approximately 4 h before collecting compound binding data.
7. Prepare compound solutions with starting compound concentrations of at least 20-fold over the known EC_{50} value while still maintaining 2% DMSO in the solutions. The final compound solution is then diluted serially in either 3× or 2× dilutions. Use the equation $C_1V_1 = C_2V_2$. where C_1 is the concentration of compound stock in DMSO, V_1 volume of DMSO, C_2 starting concentration of compound for serial dilution, and V_2 final volume of compound solution. Solve for C_1 to determine the compound stock concentration in DMSO. Example: Compound X is made up in DMSO stock solutions of 50 μM, 16.7 μM, 5.55 μM, and 1.85 μM. Add 4 μl of each compound concentration to 196 μl of Buffer A, resulting in a final DMSO concentration of 2% (v/v) and final compound concentrations of 1 μM, 333 nM, 111 nM, and 37 nM.
8. Prepare a DMSO sample curve by adding 5, 10, 20, 30, and 40 μl of DMSO to 1 ml of assay Buffer A, resulting in final concentrations of 0.5, 1, 2, 3, and 4% DMSO.

Follow ***steps 9–15*** *below for acquisition of SPR data of compounds and their analysis.*

9. Assemble a 96-well sample Greiner Bio-One Plate to include the following samples: the DMSO standard curve samples, buffer blanks consisting of Buffer B alone, and each

concentration series of compounds. Total volume for each well is 200 μl. The DMSO standards and the compound samples are set up from the lowest to highest concentrations. The total number of compound concentrations is based on whether you expect to observe binding kinetics (use four compound concentrations) or equilibrium binding (use six compound concentrations).

10. Add four buffer blanks to the beginning of the plate, followed by the DMSO standards.
11. Add two blanks between the DMSO standards and the compound samples, while also including two buffer blanks between each compound concentration series.
12. Using the Biacore software, create a method such that all samples are injected at a flow rate of 50 μl/min and 120 s contact time. DMSO standards and buffer blanks should have a short dissociation time of 10 s. Compound samples will have longer dissociation times (generally 300–600 s) based on anticipated off rates (k_{off}). Compounds need to be fully dissociated before the start of the subsequent injection.
13. Process the binding responses using Scrubber2 to zero, x-align, double reference, and correct for excluded volume effects (DMSO) in the data.
14. If the association and dissociation phases of compound binding are observable on the time scale of detection, data is fit to a simple 1:1 kinetic model using BIAeval to obtain the rate parameters (k_{on}, k_{off}) and corresponding affinity constant ($K_D = k_{off}/k_{on}$) (Fig. 5).
15. If the association and dissociation phases of compound binding are too fast to measure, K_D is determined by fitting the data to a steady-state affinity algorithm for single site binding, available within the Scrubber2 software [9, 10, 13].

4 Notes

1. Recombinant proteins can be produced by heterologous expression in several host systems such as *E. coli*, insect cells, yeast, or mammalian cells. Biophysical studies require highly pure and homogenous protein in large amounts. Expression in *E. coli* or insect cells in general allows one to generate recombinant proteins at reasonable costs while meeting the stringent purity demands of biophysical studies of AMPK that exists as a heterotrimer of α, β, and γ subunits. All of crystallographic and HDX studies of AMPK that have been reported hitherto date have utilized protein reagents produced in bacterial or insect cells.

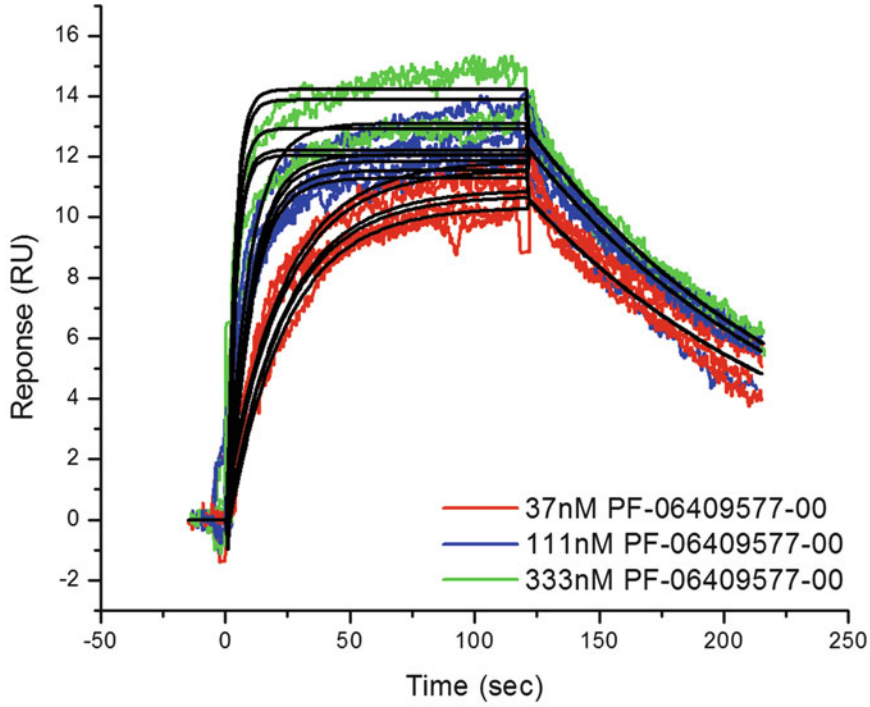

Fig. 5 SPR ligand binding profile of PF-06409577 to AMPK α1β1γ1. Raw data (colored traces) are displayed for PF-06409577 injections against immobilized AMPK at the concentrations indicated. Superimposed are the kinetic fits (black lines) permitting determination of k_{on}, k_{off}, and K_D

2. The AMPK expression plasmid includes open reading frames of full-length α, β, and γ subunits of human AMPK with a ribosome-binding site (RBS) upstream of each coding region followed by three stop codons at the end of each coding region. It also includes a 22-residue tag which contains six histidine residues and a cleavage site for thrombin (MGSSHHHHHHSSGLVPRGSMGT) at the N-terminal end of the α subunit to aid purification. In addition, the tricistronic expression plasmid contains *NcoI* and *XhoI* sites for ligation to pET14b expression vector.
3. Synthesize codon-optimized genes corresponding to human α, β, and γ subunits for expression in Sf-9 cells. To aid purification, insert an additional 16-residue tag that includes six histidine residues and a cleavable site for thrombin (MHHHHHHSSGLVPRGS) at the N-terminal end of the α subunit.
4. Buffers can be stored at −20 or −80 °C until further use.
5. HDX reaction is highly pH dependent (tenfold change in exchange rate for every unit change in pH), and small variations in buffer and sample pH can lead to ambiguous and

irreproducible results. Buffer pH should be adjusted and verified using standard commercial pH meters and also double-checked with pH strips for accuracy.

6. Correct for pH of D_2O buffers by adjusting the actual reading from the pH meter to take in to account electrode differences between reading protons and deuterons. pD = actual pH meter reading + 0.4.
7. Confirm that pH of quenched samples is 2.5 or below after mixing with protein sample buffer. These pH tests can be made in solutions of the buffer that do not contain protein.
8. Store quench solution at 4 °C while in use (~1 week) or at −80 °C for long-term storage (>1 week).
9. Modern-day mass spectrometers capable of high-resolution data acquisition (minimum resolving power of 60,000 at m/z 400) are needed for accurately assigning peptide peaks and reliable percent deuterium calculations for high MW (>80 kDa) proteins and protein complexes. An Exactive Orbitrap instrument capable of a resolving power of 100,000 at m/z 400 was used for the HDX experiments reported in Landgraf et al. [11].
10. A typical setup for running of HDX experiments requires HPLC columns, robotics, and protease columns integrated with a high-resolution mass spectrometer. We have described the instrumentation setup in our lab, but other combinations of the individual components are also possible.
11. It is critical that the amount of DMSO is matched between samples and running buffer (Buffer B). Making up the samples using the original buffer solutions will help to eliminate refractive index jumps that could otherwise be observed if the buffer and samples are not matched.
12. When making Buffers A and B, it is important to use degassed water to help eliminate bubbles in the samples and the possibility of injecting air.
13. Although the pET14b expression vector contains built-in DNA for a His-tag and a thrombin cleavage site, we incorporated the coding sequence for a His-tag into our synthetic tricistronic expression plasmid for increased flexibility in positioning the His-tag at the appropriate location of AMPK subunits. Cleaving the vector with *NcoI* and *XhoI* restriction enzymes removes the His-tag and thrombin site from the vector.
14. Generate P0 viruses containing individual recombinant AMPK α, β, and γ subunits. Amplify the viruses by infecting Sf-9 cells with P0 viruses and thus generate P1, P2, etc., viruses.

Determine the viral titer of the amplified viruses for each of the AMPK subunits.

15. Any buffer that is free from high concentrations of salts (>500 mM) and ionic detergents, which are not MS friendly in later steps of the protocol, will work. We have had success with HEPES, TRIS, and phosphate buffer systems. (Note: Tris buffer changes pH with temperature, and it is important to use cold solvents when making Tris buffers for HDX.)
16. Utmost care should be taken to minimize deuterium back exchange (D/H) reaction with chromatography solvents. All HPLC buffers are maintained in acidic (~pH 2.5) and refrigerated conditions, and short gradients are employed ($t_{1/2}$ of D/H is ~30–45 min at pH 2.5 and 0 °C).
17. MS/MS sequence coverage is a function of protein concentration and is further complicated by short protease digestion times when studying large protein systems like AMPK. Higher protein concentration and alternative quench conditions are often required to study large protein complexes.
18. While this could be done manually, use of a robot such as the Twin PAL liquid handling robot minimizes pipetting errors and improves data reproducibility.
19. The pepsin column is housed inside a temperature controlled box held at 15 °C to improve digestion efficiency while sacrificing minimally on back exchange using short digestion times (~1 min).
20. Immobilized protease columns provide significant advantages over pepsin solutions in terms of digestion reproducibility and efficiency.
21. Mascot is a software search engine used to identify proteins and peptides based on mass spectrometric data. It uses a probabilistic scoring algorithm to identify peptides. While the software is freely available to use on the website of Matrix Science, a license will be required for in-house use.
22. Stringent quality threshold criteria should be applied to MS/MS spectra (e.g., Mascot score, manual inspection, and pepsin preferred and forbidden cleavage rule [21] for accurate peptide identification).
23. Other denaturants such as guanidine hydrochloride and use of strong reducing agents like TCEP have proven to be effective for the analysis of large proteins like antibodies and membrane proteins that contain multiple disulfide bonds.
24. HDX data reproducibility is affected by batch to batch variability in AMPK protein preparations. Comparison of D_2O exchange kinetics of Apo AMPK across various batches is recommended for testing sample heterogeneity. Avoid

multiple freeze/thaw cycles from the same stock to maintain protein stability.

25. Solubility of AMPK ligands at high concentrations in aqueous HDX buffers needs to be tested and liganded samples should be devoid of protein aggregation inducers.
26. Columns and connector tubings need to be replaced if the pressure rises above normal operating ranges. Clogged pepsin columns can lead to significant peptide carry-over between experiments.
27. Blank injections with buffer (no protein) are included in between sample injections in the macros for HDX methods to estimate peptide carry-over between experiments.
28. The LC system, but not the protease column, is washed (3×) using a 2-propanol:ACN (2:1 ratio), 0.3% FA gradient between HDX experiments to ensure that all columns and lines are clean and free of material from prior injections.
29. Repeated injections can likely clog the pepsin column, and blank HDX runs (a full empty run) with buffer only are required as a monthly routine procedure to maintain the lifetime of pepsin columns. Never expose the pepsin column to pH above 8.0 as pepsin will be irreversibly inactivated.
30. Sophisticated software and significant computational power is necessary to handle processing of hundreds of peptides with multiple replicates over multiple time points.
31. While localization of perturbation HDX differences are often limited to peptide level changes, single amide level resolution can be achieved using overlapping peptides, a newly devised Bayesian approach [21], or through alternative fragmentation techniques such as electron transfer dissociation (ETD) and electron capture dissociation (ECD) available in many state-of-the art mass spectrometers.
32. To enable crystallographic studies of activators bound to AMPK at the allosteric drug and metabolite (ADaM) site, generate a slightly modified form of rat AMPK (called $AMPK^{xtal}$) that contains full-length γ subunit but incorporates the following changes on the α and β subunits [9] A flexible segment of the α subunit (470–524) is replaced with an 8 amino acid linker (ASGGPGGS) while the first 67 amino acids of the β subunit are eliminated. Follow **steps 2–14** in Subheading 3.1 for expression and purification of the crystallographic construct. In the last step of the purification, elute the $AMPK^{xtal}$ protein from the sizing column with the crystallographic SEC buffer (*see* **item 1** in Subheading 2.3).
33. Once initial crystallization conditions are identified, further optimization is usually done by systematic screening around

the observed conditions. While keeping the buffer (trisodium citrate at 100 mM) and ethylene glycol (1% (v/v)) concentrations fixed, a two-dimensional screening is done by systematically varying ammonium sulfate and lithium sulfate concentrations between 250 mM and 1 M. Such a broad crystallization range helps to ensure that crystals are obtained from different batches of proteins which could be slightly different from each other.

34. AMPK crystals cannot be stored indefinitely. In our experience, after ~14 days, crystals are less amenable to handling, often associated with a film or precipitate, and yield poorer diffraction data.
35. Minimize the time involved in looping or manipulating crystals. As the crystallization drop is exposed to air, salt crystals will begin to form and complicate harvesting.
36. Ensure AMP is maintained throughout soaks and cryoprotection. Removal of AMP during crystal manipulation has yielded poorer diffraction.
37. To confirm ligand binding pose in the 3–3.5 Å resolution regime, we have found it helpful to determine the structure with halogenated analogs of ligands (e.g., Br-containing) to enable collection of anomalous diffraction data to uniquely identify the location of electron-dense bromine atom [9].
38. The direct output of X-ray diffraction from protein crystals is not an automated molecular structure. Rather, the observed diffraction data is used to compose electron density distribution within the crystals which a crystallographer interprets in the form of an atomic model. As such, a "crystal structure" is a crystallographer's interpretation of experimental electron density which best explains the observed diffraction data while conforming to physical and chemical restraints. Given the dynamic nature of AMPK, the resolution range for full-length AMPK structures is approximately 3–3.5 Å, a threshold that is slightly low for typical structure-based drug design. As such, particular care must be taken in both modeling and interpreting ligand pose.
39. The final AMPK enzyme concentration used in the assay should be predetermined to ensure the reaction is in the linear phase during the selected time course. It is recommended to perform a time course of the reaction at various enzyme concentrations to select a final condition where approximately less than 10% of the substrate has been converted to product.
40. The SAMS peptide and ATP K_m values vary depending on the AMPK isoform. Use the reported K_m for the desired AMPK isoform in choosing the range of substrate concentrations. For initial experiments, we typically use just a few substrate

concentrations to get an initial estimate, and then repeat the experiment with at least eight concentrations ranging from 0.1 to 10-fold the expected K_m.

41. Traditionally, kinase reactions are initiated with the addition of the ATP mixture. However, since AMP is generally used as a positive control for AMPK and ATP and AMP can compete for binding sites within the protein, we initiate the reaction with SAMS peptide to allow nucleotides to achieve equilibrium prior to the reaction.
42. Pre-wetting the filter membranes and the simultaneous transfer and filtering of samples are essential for data consistency. The amount of product retained in the membrane will increase over time; therefore, it is important for reactions to be transferred simultaneously to the plate.
43. Raw CPM counts can be normalized to product (pM of phosphorylated SAMS) by including a standard curve in each assay. A phosphorylated SAMS peptide standard can be produced by setting up a reaction at a fixed peptide concentration with a single high concentration of AMPK and allowing the kinase reaction to go to completion so that nearly 100% of the SAMS peptide is phosphorylated. Dilute the mixture and spot onto the filter plates to generate the standard curve and convert the raw CPM values into concentration units of product.
44. The conditions described above are for determining the K_m and V_{max} for the SAMS peptide. If the ATP substrate is of interest, repeat the experiment above but with varying ATP concentrations at saturating SAMS peptide (10× SAMS peptide K_m).
45. Generate a modified form of full-length human AMPK α1β1γ1 to enable biophysical studies by surface plasmon resonance technique. Incorporate an AviTag™ (GLNDIFEAQKIEWHE) at the N-terminal of the γ subunit and co-express with biotin ligase (BirA) in the presence of 50 μM biotin (final concentration) [9]. Follow **items 2–14** in Subheading 2.3 for expression and purification of the SPR construct.

Disclosure of Competing Interests:

R.G.K., G.M.W., K.A.B., J.M.W., J.W., A.R.R. and F.R. are employees of Pfizer Inc., a for-profit global healthcare company. V.D. and P.R.G declare no competing financial interests.

References

1. Carling D (2017) AMPK signaling in health and disease. Curr Opin Cell Biol 45:31–37
2. Hardie DG, Schaffer BE, Brunet A (2016) AMPK: an energy-sensing pathway with multiple inputs and outputs. Trends Cell Biol 26 (3):190–201
3. Oakhill JS, Scott JW, Kemp BE (2012) AMPK functions as an adenylate charge-regulated protein kinase. Trends Endocrinol Metab 23 (3):125–132
4. Steinberg GR, Kemp BE (2009) AMPK in health and disease. Physiol Rev 89 (3):1025–1078
5. Cameron KO, Kurumbail RG (2016) Recent progress in the identification of adenosine monophosphate-activated protein kinase (AMPK) activators. Bioorg Med Chem Lett 26(21):5139–5148
6. Kim J, Yang G, Kim Y, Kim J, Ha J (2016) AMPK activators: mechanisms of action and physiological activities. Exp Mol Med 48(4): e224
7. Miglianico M, Nicolaes GAF, Neumann D (2016) Pharmacological targeting of AMP-activated protein kinase and opportunities for computer-aided drug design: miniperspective. J Med Chem 59(7):2879–2893
8. Viollet B, Mounier R, Leclerc J, Yazigi A, Foretz M, Andreelli F (2007) Targeting AMP-activated protein kinase as a novel therapeutic approach for the treatment of metabolic disorders. Diabetes Metab 33(6):395–402
9. Calabrese MF, Rajamohan F, Harris MS, Caspers NL, Magyar R, Withka JM, Wang H, Borzilleri KA, Sahasrabudhe PV, Hoth LR, Geoghegan KF, Han S, Brown J, Subashi TA, Reyes AR, Frisbie RK, Ward J, Miller RA, Landro JA, Londregan AT, Carpino PA, Cabral S, Smith AC, Conn EL, Cameron KO, Qiu X, Kurumbail RG (2014) Structural basis for AMPK activation: natural and synthetic ligands regulate kinase activity from opposite poles by different molecular mechanisms. Structure 22(8):1161–1172
10. Cameron KO, Kung DW, Kalgutkar AS, Kurumbail RG, Miller R, Salatto CT, Ward J, Withka JM, Bhattacharya SK, Boehm M, Borzilleri KA, Brown JA, Calabrese M, Caspers NL, Cokorinos E, Conn EL, Dowling MS, Edmonds DJ, Eng H, Fernando DP, Frisbie R, Hepworth D, Landro J, Mao Y, Rajamohan F, Reyes AR, Rose CR, Ryder T, Shavnya A, Smith AC, Tu M, Wolford AC, Xiao J (2016) Discovery and preclinical characterization of 6-Chloro-5-[4-(1-hydroxycyclobutyl)phenyl]-1H-indole-3-carboxylic acid (PF-06409577), a direct activator of adenosine monophosphate-activated protein kinase (AMPK), for the potential treatment of diabetic nephropathy. J Med Chem 59 (17):8068–8081
11. Landgraf RR, Goswami D, Rajamohan F, Harris MS, Calabrese MF, Hoth LR, Magyar R, Pascal BD, Chalmers MJ, Busby SA, Kurumbail RG, Griffin PR (2013) Activation of AMP-activated protein kinase revealed by hydrogen/deuterium exchange mass spectrometry. Structure 21(11):1942–1953
12. Neumann D, Woods A, Carling D, Wallimann T, Schlattner U (2003) Mammalian AMP-activated protein kinase: functional, heterotrimeric complexes by co-expression of subunits in *Escherichia coli*. Protein Expr Purif 30:230–237
13. Rajamohan F, Reyes AR, Frisbie RK, Hoth LR, Sahasrabudhe P, Magyar R, Landro JA, Withka JM, Caspers NL, Calabrese MF, Ward J, Kurumbail RG (2016) Probing the enzyme kinetics, allosteric modulation and activation of 1- and 2-subunit-containing AMP-activated protein kinase (AMPK) heterotrimeric complexes by pharmacological and physiological activators. Biochem J 473(5):581–592
14. Ramanathan L, Sheth PR, Ogas P, Le HV, Xiao L (2010) Purification and characterization of truncated human AMPK $\alpha 2\beta 2\gamma 3$ heterotrimer from baculovirus-infected insect cells. Protein Expr Purif 70(1):13–22
15. Chalmers MJ, Busby SA, Pascal BD, He Y, Hendrickson CL, Marshall AG, Griffin PR (2006) Probing protein ligand interactions by automated hydrogen/deuterium exchange mass spectrometry. Anal Chem 78 (4):1005–1014
16. Marciano DP, Dharmarajan V, Griffin PR (2014) HDX-MS guided drug discovery: small molecules and biopharmaceuticals. Curr Opin Struct Biol 28:105–111
17. Chen L, Wang J, Zhang YY, Yan SF, Neumann D, Schlattner U, Wang ZX, Wu JW (2012) AMP-activated protein kinase undergoes nucleotide-dependent conformational changes. Nat Struct Mol Biol 19(7):716–718
18. Chen L, Xin FJ, Wang J, Hu J, Zhang YY, Wan S, Cao LS, Lu C, Li P, Yan SF, Neumann D, Schlattner U, Xia B, Wang ZX, Wu JW (2013) Conserved regulatory elements in AMPK. Nature 498(7453):E8–10

19. Li X, Wang L, Zhou XE, Ke J, de Waal PW, Gu X, Tan MH, Wang D, Wu D, Xu HE, Melcher K (2015) Structural basis of AMPK regulation by adenine nucleotides and glycogen. Cell Res 25(1):50–66
20. Xiao B, Sanders MJ, Underwood E, Heath R, Mayer FV, Carmena D, Jing C, Walker PA, Eccleston JF, Haire LF, Saiu P, Howell SA, Aasland R, Martin SR, Carling D, Gamblin SJ (2011) Structure of mammalian AMPK and its regulation by ADP. Nature 472 (7342):230–233
21. Pirrone GF, Iacob RE, Engen JR (2015) Applications of hydrogen/deuterium exchange MS from 2012 to 2014. Anal Chem 87(1):99–118
22. Noe MC, Kurumbail RG (2015) Fifty years of structural biology: a perspective on how biophysics has influenced medicinal chemistry. In: Desai MC (ed) Medicinal chemistry reviews, vol 50. Medicinal Chemistry Division of American Chemical Society, Washington, D.C., USA, pp 299–346
23. Ducruix A, Giegé R (1992) Crystallization of nucleic acids and proteins: a practical approach. IRL Press at Oxford University Press, England
24. McPherson A (2004) Introduction to protein crystallization. Methods 34(3):254–265
25. Davies SP, Carling D, Hardie DG (1989) Tissue distribution of the AMP-activated protein kinase, and lack of activation by cyclic-AMP-dependent protein kinase, studied using a specific and sensitive peptide assay. Eur J Biochem 186(1–2):123–128
26. Ward J, Reyes AR, Kurumbail RG (2017) Allosteric modulation of AMPK enzymatic activity: in vitro characterization. Methods Enzymol 587:481–509
27. Nguyen H, Park J, Kang S, Kim M (2015) Surface plasmon resonance: a versatile technique for biosensor applications. Sensors 15 (5):10481–10510
28. Hamuro Y, Coales SJ, Molnar KS, Tuske SJ, Morrow JA (2008) Specificity of immobilized porcine pepsin in H/D exchange compatible conditions. Rapid Commun Mass Spectrom 22 (7):1041–1046
29. Pascal B, Willis S, Lauer J, Landgraf R, West G, Marciano D, Novick S, Goswami D, Chalmers M, Griffin P (2012) HDX workbench: software for the analysis of H/D exchange MS data. J Am Soc Mass Spectrom 23(9):1512–1521
30. Pascal BD, Chalmers MJ, Busby SA, Mader CC, Southern MR, Tsinoremas NF, Griffin PR (2007) The Deuterator: software for the determination of backbone amide deuterium levels from H/D exchange MS data. BMC Bioinformatics 8(1):156
31. Pascal B, Chalmers M, Busby S, Griffin P (2009) HD desktop: an integrated platform for the analysis and visualization of H/D exchange data. J Am Soc Mass Spectrom 20 (4):601–610
32. Saltzberg DJ, Broughton HB, Pellarin R, Chalmers MJ, Espada A, Dodge JA, Pascal BD, Griffin PR, Humblet C, Sali A (2017) A residue-resolved bayesian approach to quantitative interpretation of hydrogen-deuterium exchange from mass spectrometry: application to characterizing protein-ligand interactions. J Phys Chem B 121(15):3493–3501
33. Otwinowski Z, Minor W (1997) Processing of X-ray diffraction data collected in oscillation mode. Methods Enzymol 276:307–326
34. McCoy AJ, Grosse-Kunstleve RW, Adams PD, Winn MD, Storoni LC, Read RJ (2007) Phaser crystallographic software. J Appl Crystallogr 40:658–674
35. Blanc E, Roversi P, Vonrhein C, Flensburg C, Lea SM, Bricogne G (2004) Refinement of severely incomplete structures with maximum likelihood in BUSTER-TNT. Acta Crystallogr D Biol Crystallogr 60:2210–2221
36. Emsley P, Cowtan K (2004) Coot: model-building tools for molecular graphics. Acta Crystallogr D Biol Crystallogr 60:2126–2132
37. Smart OS, Womack TO, Shariff A, Flensburg C, Keller P, Paciorek W, Vonrhein C, Bricogne G (2014) RHOFIT. Version 1.2.4. Global Phasing Ltd., Cambridge, United Kingdom

Chapter 4

Biochemical Measurement of Glycogen: Method to Investigate the AMPK-Glycogen Relationship

Elite Possik and Arnim Pause

Abstract

Glycogen is a main carbohydrate energy storage primarily found in fungi and animals. It is a glucose polymer that comprises α(1-4) glycosidic linkages attaching UDP-glucose molecules linearly and α(1-6) linkages branching glucose chains every 8-10 molecules to the main backbone chain. Glycogen synthase, branching enzyme, and glycogen phosphorylase are key enzymes involved in glycogen synthesis and degradation. These enzymes are tightly regulated by upstream kinases and phosphatases that respond to hormonal cues in order to coordinate storage and degradation and meet the cellular and organismal metabolic needs. The 5'AMP-activated protein kinase (AMPK) is one of the main regulators of glycogen metabolism. Despite extensive research, the role of AMPK in glycogen synthesis and degradation remains controversial. Specifically, the level and duration of AMPK activity highly influence the outcome on glycogen reserves. Here, we describe a rapid and robust protocol to efficiently measure the levels of glycogen in vitro. We use the commercially available glycogen determination kit to hydrolyze glycogen into glucose, which is oxidized to form D-gluconic acid and hydrogen peroxide that react with the OxiRed/Amplex Red probe generating a product that could be detected either in a colorimetric or fluorimetric plate format. This method is quantitative and could be used to address the role of AMPK in glycogen metabolism in cells and tissues.

Summary

This chapter provides a quick and reliable biochemical quantitative method to measure glycogen in cells and tissues. Briefly, this method is based on the degradation of glycogen to glucose, which is then specifically oxidized to generate a product that reacts with the OxiRed probe with maximum absorbance at 570 nm. This method is very accurate and highly sensitive. In the notes of this chapter, we shed the light on important actions that should be followed to get reliable results. We also state advantages and disadvantages of this method in comparison to other glycogen measurement techniques.

Key words Glycogen, Glucose, Colorimetric assay, Hydrolysis enzyme mix, Development enzyme mix, Oxiprobe, Biochemical titration, Fluorimetric, Colorimetric

1 Introduction

Glycogen is a complex carbohydrate that serves as a major energy storage readily used to meet cellular and organismal metabolic requirement. It is a multibranched glucose polymer that exists in fungi and in invertebrate and vertebrate animals [1]. Glucosyl

Dietbert Neumann and Benoit Viollet (eds.), *AMPK: Methods and Protocols*, Methods in Molecular Biology, vol. 1732, https://doi.org/10.1007/978-1-4939-7598-3_4,

residues are linked linearly with each other via α(1-4) glycosidic bonds, and branching chains form every 8–12 residues via α(1-6) glycosidic bonds. Glycogen synthase is the enzyme responsible for attaching UDP-glucose molecules linearly, while branching enzyme is the one responsible for starting branching chains of glucosyl residues [2, 3]. The branches and chains of glucose are attached to a central protein complex called glycogenin.

In humans, glycogen is stored primarily in the liver and muscle tissues [2]. Normally, glycogen degradation occurs upon acute metabolic stress situations to sustain energy levels and promote survival. For instance, starvation and exercise trigger glycogen degradation in muscle and liver tissues to maintain blood glucose levels. Upon the need of glucose or glucose-derived metabolites including glucose-6-phosphate, glycogen is degraded by glycogen phosphorylase through a phosphorolysis reaction. Both glycogen synthase and glycogen phosphorylase are regulated by hormonal cues [2, 3]. When the body needs glucose, epinephrine and glucagon are released to activate glycogen degradation leading to glucose-6-phosphate, an important intermediate that could be used for different purposes according to the cellular needs [1]. However, when the body has an excess of glucose that needs to be stored, insulin is secreted and glucose molecules are stored in the form of glycogen [3–5]. Glycogen synthase and glycogen phosphorylase are regulated via phosphorylation and dephosphorylation events by upstream kinases and phosphatases, respectively. In general, phosphorylation events activate glycogen phosphorylase and inhibit the activity of glycogen synthase [4]. Accordingly, dephosphorylation events activate glycogen synthase and inactivate glycogen phosphorylase. Glycogen synthase and glycogen phosphatase are also allosterically regulated by the level of metabolites including adenosine phosphate molecules and glucose-6-phosphate [3, 5, 6].

The 5'AMP-activated protein kinase (AMPK) is a heterotrimeric protein complex that orchestrates important signaling cascades to regulate cellular energy metabolism [7–9]. In general, upon stress that could be caused by starvation or exercise, AMPK is activated which induces energy-producing catabolic pathways including glycogen breakdown. However, when nutrients are plentiful, AMPK is inhibited, inducing energy-consuming anabolic pathways including glycogen synthesis [7–9]. Specifically, acute AMPK activation leads to phosphorylation and inactivation of glycogen synthase and a decrease in glycogen content [10–13]. While this role of AMPK in glycogen metabolism has been widely accepted, increasing evidence suggest that the chronic activation of AMPK leads to glycogen accumulation instead of glycogen degradation [14–16]. AMPK is chronically activated during endurance exercise, which promotes glycogen accumulation in muscles with training. Accordingly, the constitutive activation of AMPK via mutations in the γ2 and γ3 subunits leads to the accumulation of

glycogen in the skeletal and cardiac muscles of pigs and mice [16–22]. Hunter et al. [14] demonstrated that the chronic AMPK activation heightens glucose uptake and increases glucose-6-phosphate cellular levels, which allosterically activate glycogen synthase, bypassing the inhibitory effects of its phosphorylation by AMPK [14]. This has been reported in multiple systems and organisms. In *C. elegans*, we have shown that AMPK mutant animals display decreased levels of glycogen [23, 24], similarly to what has been previously observed in yeast [25]. However, loss of *flcn-1*, the worm homolog of the BHD gene responsible for the Birt-Hogg-Dubé neoplastic syndrome in humans, constitutively activates AMPK and leads to glycogen accumulation [23, 24].

The role of AMPK in the regulation of glycogen metabolism is a long paradox that needs to be resolved. Glycogen determination in cells and tissues is therefore an important method that could be utilized to address this aspect. Here, we describe a quantitative in vitro glycogen determination biochemical technique using a colorimetric or fluorimetric method that involves glycogen extraction from cells and hydrolysis into glucose monomers using amyloglucosidase enzyme. Glucose is then oxidized by glucose oxidase to produce D-gluconic acid and hydrogen peroxide, which interacts with the kit's probe leading to a product that could be detected either in a colorimetric plate format or in fluorimetric plate format. These kits are widespread and are based on the same strategy. They are sold at a reasonable price by several commercial companies worldwide. In Subheading 4, we compare this method to other alternative techniques that could be used for this purpose. We provide a list of advantages and disadvantages of this method in comparison to other biochemical titration methods. We also describe extensively tricks and cautions that should be taken into consideration while performing this method.

2 Materials

2.1 Cell Lysis and Glycogen Extraction

1. Phosphate buffer solution (PBS): 10 mM phosphate, 137 mM NaCl, and 2.7 mM KCl. To prepare 1× PBS, use 8 g of NaCl, 0.2 g of KCl, 0.2 g of KH_2PO_4, 1.15 g of Na_2HPO_4, and add Milli-Q H_2O up to 1 l. Adjust the pH to 7.4.
2. 30% potassium hydroxide buffer.
3. 95% ethanol.
4. Cooled high-speed centrifuge.
5. Milli-Q H_2O.

2.2 Hydrolysis and Development Reagent Preparation

In this section we provide the components that are utilized by most commercial glycogen detection kits, with their composition, and method of action.

1. Hydrolysis enzyme mix: Lyophilized mixture encompassing the amyloglucosidase enzyme.
2. Hydrolysis buffer: This is an acetate buffer. Most kits use between 25 mM and 50 mM sodium acetate at pH 4.5.
3. Development enzyme mix: It is a lyophilized mixture that encompasses the glucose oxidase enzyme. This enzyme oxidizes glucose molecules to produce gluconic acid and hydrogen peroxide.
4. Development buffer: This is a concentrated phosphate buffer at pH 7.4. Most kits utilize between 0.1 M and 0.5 M K_2HPO_4.
5. OxiRed probe also called Amplex Red: It is a lyophilized powder of 10-acetyl-3.7-dihydroxyphenoxazine (ADHP). It is a highly sensitive and stable substrate for horseradish peroxidase (HRP) that specifically reacts with hydrogen peroxide to produce resorufin that could be detected by colorimetric (lmax = 570 nm) or fluorimetric (Ex/Em = 535/587 nm) detection methods.

2.3 Glycogen Determination in Standard Curve and Samples

1. Black flat bottom 96-well plate (if performing the fluorimetric assay).
2. Clear flat bottom 96-well plate (if performing the colorimetric assay).
3. Glycogen standard (2 mg/ml, provided in the commercial glycogen determination kit).
4. ELISA microplate reader.

3 Methods

All procedures should be carried out at room temperature unless specified otherwise.

3.1 Cell Lysis and Glycogen Extraction

1. Grow the cells in 100 mm diameter dish (*see* **Note 1**) at 37 °C. Harvest the cells when they reach ~80% confluence. Place the plates on ice.
2. Wash the cells three times with PBS buffer to remove the remaining glucose molecules from culture medium.
3. On ice, add 300 μl of 30% potassium hydroxide and scrape the cells (*see* **Note 2**).
4. Transfer the samples to Eppendorf tubes and boil at 95 °C for 10 min to inactivate the enzymes (*see* **Note 3**).

5. After boiling, take a 100 µl aliquot for protein measurement (*see* **Note 4**).
6. Transfer the rest to a prechilled 15 ml conical tubes and add three volumes of 95% ethanol to precipitate the glycogen. Vortex and keep the tubes on ice for 10 min.
7. Centrifuge the lysate for 10 min at 12,000 × *g* at 4 °C.
8. Discard supernatant and wash twice with cold 70% ethanol.
9. Discard the supernatant and remove all traces of ethanol. Dry the pellet and resuspend with 50 µl of Milli-Q H_2O.
10. Determine glycogen content using commercially available glycogen determination kit (*see* **Notes 5** and **6**).
11. Make sure to dilute the samples to meet the detection range (*see* **Note 7**).

3.2 Glycogen Hydrolysis Enzyme Mix, Development Enzyme Mix, and Probe Preparations

1. Dissolve the hydrolysis enzyme mix with 220 µl of the glycogen hydrolysis buffer by gentle pipetting up and down (*see* **Notes 8** and **9**). This mix encompasses the amyloglucosidase enzyme responsible for glycogen degradation (*see* **Note 10**). Bring to room temperature before use and avoid light exposure.
2. Dissolve the development enzyme mix with 220 µl of Milli-Q H_2O by gentle pipetting up and down. Bring to room temperature before use and avoid light exposure (*see* **Note 11**).
3. Dissolve the probe powder with 220 µl of Milli-Q H_2O by gentle pipetting up and down. Bring to room temperature before use and avoid exposure to light.

3.3 Samples and Standard Curve Hydrolysis Reaction

1. To start the reactions, use a clear flat bottom 96-well plate for colorimetric assays and black flat bottom plates for fluorimetric assays (*see* **Note 12**). For every experiment, include a background control, a standard curve, and your samples to measure both glycogen and glucose levels (*see* **Note 13** and Table 1).
2. Use the glycogen standard (2 mg/ml) to prepare the standard curve. Start by preparing a 0.2 mg/ml of glycogen standard solution by diluting 10 µl of the provided standard with 90 µl of Milli-Q H_2O (*see* **Note 14**). For the fluorimetric assay, dilute the 10 µl of the glycogen standard in 990 µl of Milli-Q H_2O.
3. Add a series of 0, 2, 4, 6, 8, and 10 µl of the diluted glycogen standard (0.2 mg/ml for colorimetric and 0.02 mg/ml for fluorimetric) in the 96-well plates, and complement with 50, 48, 46, 44, 42, and 40 µl of glycogen hydrolysis buffer, respectively (*see* Table 1).
4. In other wells, add 1–50 µl samples prepared in Subheading 3.1 (in triplicates) and complete the volume to 50 µl with the glycogen hydrolysis buffer (*see* **Note 14**).

Table 1
Glycogen standard curve and sample preparation

Glycogen standard volume (μl)	Hydrolysis enzyme buffer (μl)	Hydrolysis enzyme mix (μl)	Development buffer (μl)
0	50	2	50
2	48	2	50
4	46	2	50
6	44	2	50
8	42	2	50
10	40	2	50
Sample volume (μl)	Hydrolysis enzyme buffer (μl)	Hydrolysis enzyme mix (μl)	Development buffer (μl)
1–50	Up to 50	2	50
1–50	Up to 50	0	50

5. For every sample include a sample background control. Add the same amount of samples used in **step 3** and complete the volume up to 50 μl with the glycogen hydrolysis buffer. To these samples, do *NOT* add the hydrolysis enzyme mix. Readings of these wells will reveal the amount of glucose contamination in your samples prior to glycogen hydrolysis (*see* Table 1).
6. Add 2 μl of the hydrolysis enzyme mix to the standard curve and sample wells for the colorimetric assay. For the fluorimetric assay, add only 1 μl of the hydrolysis enzyme mix. The "0" well is the background control. Readings of these wells will measure the amount of glucose resultant from the hydrolysis of glycogen in the standard glycogen solution and in your samples (*see* **Note 15**).
7. Wrap your plate with aluminum foil to protect from light and incubate with gentle shaking for 30 min.

3.4 Development and Output Measurement

1. During the 30 min incubation, prepare a master mix of the development mix solution. Depending on the number of reactions used, prepare enough reagents to cover all samples and controls. For every reaction, consider 46 μl of development buffer, 2 μl of Oxiprobe, and 2 μl of development enzyme mix for the colorimetric assay. For the fluorimetric assay, for every reaction, add 48.7 μl of the development buffer, 1 μl of the development enzyme mix, and 0.3 μl of OxiRed.
2. Add 50 μl of the development enzyme mix to every well and mix well by gentle up and down pipetting. Avoid bubbles and

Table 2
Development reagents in colorimetric and fluorimetric assays

	Colorimetric assay (volume in μl)	Fluorimetric assay (volume in μl)
Development enzyme mix	2	1
Development enzyme buffer	46	48.7
OxiRed	2	0.3

foam. Cover plate with aluminum foil to protect from light, and incubate 30 min at room temperature with gentle shaking (*see* Table 2).

3. Read the plate using an ELISA microplate reader immediately after incubation at OD570 nm for colorimetric assays or at Ex535/Em587 for fluorimetric assays (*see* **Note 16**).

3.5 Analysis and Calculations

1. Subtract the background from all the readings. Also subtract the free glucose background levels from corresponding samples. Apply the corrected reading to the standard curve to get the amount of glycogen in the samples (μg). *See* Fig. 1 for a representative standard curve graph.
2. Apply the following formula to calculate the concentration of glycogen in your samples:

   C = (μg glycogen in standard curve/samples volume) × dilution factor = μg/μl (*see* **Note 17**).

4 Notes

1. Cellular density highly influences glycogen content. Higher amounts of glycogen are found when cells are confluent. To have accurate measurements, cells need to be evenly spread in the dish.
2. Working on ice is important to slow down the activity of the enzymes that could break down glycogen. Proceed quickly during this step to limit glycogen hydrolysis events.
3. Boiling the samples inactivates the enzymes that could hydrolyze glycogen in your samples.
4. Protein levels could be determined using the Bradford assay. Other protein assays can also be used if they are compatible with the used concentration of potassium hydroxide.
5. Commercially available kits for glycogen determination are similar in context and content. They are widespread and easily available at a reasonable price. Because in this assay multiple enzymes are needed to lead to the end product, we find that

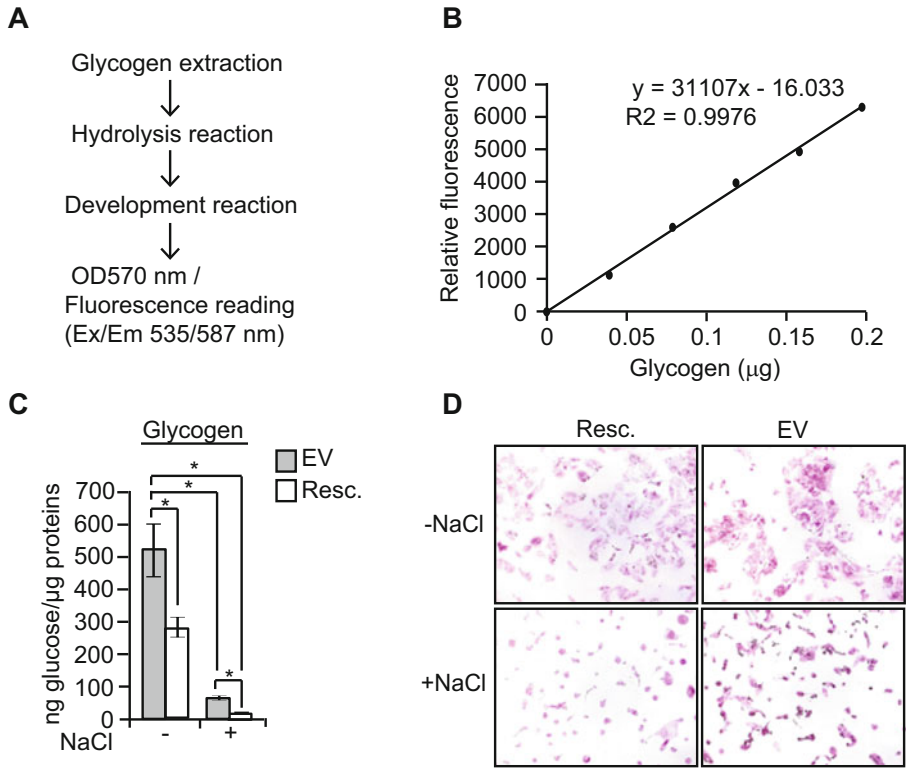

Fig. 1 Protocol demonstration using UOK257 EV and FLCN rescued cells. (**a**) Representative scheme of the protocol summary. (**b**) Glycogen standard curve example. (**c**) Glycogen determination using this protocol in UOK 257 cells lacking or rescued for folliculin expression at basal level or after exposure to 250 mM NaCl for 24 h. (**d**) Periodic acid-Schiff staining in UOK 257 cells lacking or rescued for folliculin expression at basal level or after exposure to 250 mM NaCl for 24 h

ready-made kits where conditions are already optimized are important. However, based on the content of this chapter, where we describe the content of every component, it is possible to extrapolate an easy protocol that serves the same purpose. Such kits are sold in BioVision, Sigma, Abcam, Cayman Chemical, Bio-labs, and many other companies. Figure 1 of this chapter has been generated using BioVision.

6. This procedure can be slightly modified to extract glycogen from tissues (livers and muscles). Briefly, use 50–100 mg of tissues. Wash twice with cold 1× PBS and incubate with 300 µl of 30% KOH at 70 °C for 2 h. For a faster procedure, homogenize the tissues in 300 µl of 30% KOH with a homogenizer and boil for 10 min. Centrifuge at 12,000 × *g* at 4 °C for 10 min to remove cellular debris. Transfer the supernatant to prechilled conical tubes, and add four volumes of 95% cold ethanol to precipitate the glycogen. Wash pellets with 70% ethanol twice

and let it dry. Resuspend with Milli-Q H_2O. Dilute the samples to be within the detection range.

7. Dilution of the samples to meet the detection range is essential. When the samples contain high amounts of glycogen, the hydrolysis reaction leads to high amounts of glucose, which could interfere with the OxiRed probe. With concentrated samples, it is very common to see the pink and brown colors develop and then disappear. Dilute the samples to have accurate measurements.
8. Avoid foaming or bubbles while reconstituting this mix since they could interfere with the readings later on.
9. The reconstituted hydrolysis enzyme mix is stable for 2 months at −20 °C. To avoid repetitive freeze/thaw cycles, aliquot the reconstituted hydrolysis enzyme mix and store in the dark at −20 °C. When using frozen aliquots, make sure to equilibrate it to room temperature before use because cold temperatures lower the enzyme activity, which would slow down the glycogen hydrolysis process.
10. In several organisms and tissues, the presence of acid-insoluble pools of glycogen has been reported. These pools differ structurally from the acid-soluble glycogen. In this case, the degradation efficiency of glycogen by glucoamylase enzyme is different between samples, and the results obtained with this kit may not reflect the "real" glycogen concentration in the samples. In this situation, the determination of glycogen levels using other techniques such as periodic acid-Schiff or iodine staining of tissues/organisms is recommended.
11. Similar to *see* **Notes 8** and **9**, mix gently by pipetting up and down the development enzyme mix. This mix could be stored at −20 °C in the dark for 2 months. Frozen aliquots are recommended to avoid repetitive freeze and thaw cycles. Bring to room temperature frozen aliquots before experimental use.
12. These kits could be used as fluorimetric kits. In this case, the volume of hydrolysis enzyme mix used is lower. Consult Table 1 for information. Black flat bottom 96-well plates should be used for the fluorimetric assay, and readings should be taken at Ex = 535 nm/Em = 587 nm.
13. The sample volume depends on the glycogen concentration in these samples. It is recommended to test several dilutions of samples to make sure that the readings are within the standard curve range. For highly glycogen-rich samples, dilute your samples with the glycogen hydrolysis buffer.
14. Accurate pipetting is important to get good results. Bubbles could lead to pipetting errors and interfere with the reading.

15. Be careful while adding the hydrolysis enzyme mix. Make sure to add the 2 μl inside the solution and not on the side and mix well. Quick plate centrifugation is recommended to bring down the solution inside the wells. Proceed quickly at this step to avoid long exposure to light.
16. Prepare the reading parameters during the 30 min development. Be careful with the choice of the plate on the ELISA reader machine. It is recommended to take two consecutive readings and average both results.
17. Normalizing to accurate protein measurements is very important. Error in the levels of protein content highly influences the results.

Acknowledgments

We acknowledge salary support to E.P. from the Rolande and Marcel Gosselin Graduate Studentship and the CIHR/FRSQ training grant in cancer research of the McGill Integrated Cancer Research Training Program (MICRTP). The work was supported by grants to A.P. from the Myrovlytis Trust, the Terry Fox Research Foundation, and the Kidney Foundation of Canada.

References

1. Braeckman BP (2009) Intermediary metabolism. 16 February 2009 edn., wormbook. doi:10.1895
2. Adeva-Andany MM, Gonzalez-Lucan M, Donapetry-Garcia C et al (2016) Glycogen metabolism in humans. BBA Clin 5:85–100
3. Roach PJ, Depaoli-Roach AA, Hurley TD, Tagliabracci VS (2012) Glycogen and its metabolism: some new developments and old themes. Biochem J 441:763–787
4. Jensen J, Lai YC (2009) Regulation of muscle glycogen synthase phosphorylation and kinetic properties by insulin, exercise, adrenaline and role in insulin resistance. Arch Physiol Biochem 115:13–21
5. Roach PJ (2002) Glycogen and its metabolism. Curr Mol Med 2:101–120
6. Jensen TE, Richter EA (2012) Regulation of glucose and glycogen metabolism during and after exercise. J Physiol 590:1069–1076
7. Gowans GJ, Hardie DG (2014) AMPK: a cellular energy sensor primarily regulated by AMP. Biochem Soc Trans 42:71–75
8. Hardie DG (2014) AMPK: positive and negative regulation, and its role in whole-body energy homeostasis. Curr Opin Cell Biol 33C:1–7
9. Hardie DG, Ashford ML (2014) AMPK: regulating energy balance at the cellular and whole body levels. Physiology (Bethesda) 29:99–107
10. Carling D, Hardie DG (1989) The substrate and sequence specificity of the AMP-activated protein kinase. Phosphorylation of glycogen synthase and phosphorylase kinase. Biochim Biophys Acta 1012:81–86
11. Jorgensen SB, Nielsen JN, Birk JB et al (2004) The alpha2-5′AMP-activated protein kinase is a site 2 glycogen synthase kinase in skeletal muscle and is responsive to glucose loading. Diabetes 53:3074–3081
12. Wojtaszewski JF, Jorgensen SB, Hellsten Y et al (2002) Glycogen-dependent effects of 5-aminoimidazole-4-carboxamide (AICA)-riboside on AMP-activated protein kinase and glycogen synthase activities in rat skeletal muscle. Diabetes 51:284–292
13. Miyamoto L, Toyoda T, Hayashi T et al (2007) Effect of acute activation of 5′-AMP-activated protein kinase on glycogen regulation in isolated rat skeletal muscle. J Appl Physiol (1985) 102:1007–1013

14. Hunter RW, Treebak JT, Wojtaszewski JF, Sakamoto K (2011) Molecular mechanism by which AMP-activated protein kinase activation promotes glycogen accumulation in muscle. Diabetes 60:766–774
15. Aschenbach WG, Hirshman MF, Fujii N et al (2002) Effect of AICAR treatment on glycogen metabolism in skeletal muscle. Diabetes 51:567–573
16. Luptak I, Shen M, He H et al (2007) Aberrant activation of AMP-activated protein kinase remodels metabolic network in favor of cardiac glycogen storage. J Clin Invest 117:1432–1439
17. Arad M, Benson DW, Perez-Atayde AR et al (2002) Constitutively active AMP kinase mutations cause glycogen storage disease mimicking hypertrophic cardiomyopathy. J Clin Invest 109:357–362
18. Ahmad F, Arad M, Musi N et al (2005) Increased alpha2 subunit-associated AMPK activity and PRKAG2 cardiomyopathy. Circulation 112:3140–3148
19. Zou L, Shen M, Arad M et al (2005) N488I mutation of the gamma2-subunit results in bidirectional changes in AMP-activated protein kinase activity. Circ Res 97:323–328
20. Milan D, Jeon JT, Looft C et al (2000) A mutation in PRKAG3 associated with excess glycogen content in pig skeletal muscle. Science 288:1248–1251
21. Barnes K, Ingram JC, Porras OH et al (2002) Activation of GLUT1 by metabolic and osmotic stress: potential involvement of AMP-activated protein kinase (AMPK). J Cell Sci 115:2433–2442
22. Yu H, Hirshman MF, Fujii N et al (2006) Muscle-specific overexpression of wild type and R225Q mutant AMP-activated protein kinase gamma3-subunit differentially regulates glycogen accumulation. Am J Physiol Endocrinol Metab 291:E557–E565
23. Possik E, Ajisebutu A, Manteghi S et al (2015) FLCN and AMPK confer resistance to hyperosmotic stress via remodeling of glycogen stores. PLoS Genet 11(10):e1005520
24. Possik E, Pause A (2016) Glycogen: a must have storage to survive stressful emergencies. WormBook 5(2):e1156831
25. Wang Z, Wilson WA, Fujino MA, Roach PJ (2001) Antagonistic controls of autophagy and glycogen accumulation by Snf1p, the yeast homolog of AMP-activated protein kinase, and the cyclin-dependent kinase Pho85p. Mol Cell Biol 21:5742–5752

Chapter 5

Cell-Free Assays to Measure Effects of Regulatory Ligands on AMPK

Fiona A. Fyffe, Simon A. Hawley, Alexander Gray, and D. Grahame Hardie

Abstract

AMP-activated protein kinase (AMPK) is an energy sensor that is activated by increases in the cellular AMP/ATP and ADP/ATP ratios by three mechanisms: (1) allosteric activation, (2) promotion of phosphorylation at Thr172 on the α subunit by upstream kinases, and (3) inhibition of dephosphorylation of Thr172 by protein phosphatases. All of these effects are triggered by the binding of AMP or ADP at one or more of three sites on the γ subunit, where they displace ATP. AMPK is also activated by ligands that bind in the ADaM site, which is located between the α and β subunits. In this chapter we describe cell-free assays that can be used to study these varied activation mechanisms.

Key words AMP-activated protein kinase, AMPK, Kinase assay, Allosteric activation, Phosphorylation, Dephosphorylation

1 Introduction

AMP-activated protein kinase (AMPK) is a protein kinase that exists universally as heterotrimeric complexes containing catalytic α subunits and regulatory β and γ subunits [1]. Each subunit is encoded by at least two genes (*PRKAA1/PRKAA2* encoding α1 and α2, *PRKAB1/PRKAB2* encoding β1 and β2, and *PRKAG1/PRKAG2/PRKAG3* encoding γ1, γ2, and γ3), generating at least 12 heterotrimeric combinations [2]. The regulatory nucleotides AMP, ADP, and ATP bind to two or three sites located between the two pairs of CBS repeat motifs on the γ subunit, with one site (involving CBS2) remaining unoccupied [3–6]. AMPK is normally only active when phosphorylated at a conserved threonine residue (usually termed Thr172 [7]) located in the activation loop of the kinase domain on the α subunit, which is phosphorylated by the upstream kinases LKB1 and CaMKK2. AMPK acts as a sensor of cellular energy status, being activated by increases in cellular AMP/ATP or ADP/ATP ratio by three complementary mechanisms: (1) allosteric activation, caused by binding of AMP only,

Dietbert Neumann and Benoit Viollet (eds.), *AMPK: Methods and Protocols*, Methods in Molecular Biology, vol. 1732, https://doi.org/10.1007/978-1-4939-7598-3_5,

(2) promotion of phosphorylation at Thr172 by upstream kinase (s) via binding of either AMP or ADP, and (3) inhibition of dephosphorylation of Thr172 by protein phosphatases via binding of either AMP or ADP; all three effects are antagonized by binding of ATP [8–10]. AMPK can also be activated by synthetic activators such as A-769662 [11] or 991 [3] and natural products such as salicylate [12], which bind in the so-called allosteric drug and metabolite (ADaM) site [13] located between the carbohydrate-binding module (CBM) on the β subunit and the small lobe of the kinase domain on the α subunit [3, 14, 15]. Most activators binding this site cause a large allosteric activation of AMPK, even with enzyme that is not phosphorylated on Thr172, although this allosteric effect may require prior phosphorylation at Ser108 on the β subunit, a site subject to autophosphorylation [16]. However, compounds that bind at the ADaM site also protect Thr172 from dephosphorylation [17, 18].

When assaying AMPK, the choice of method is dependent on the starting material to be used. AMPK heterotrimers can be expressed in an inactive form in bacteria using a polycistronic expression vector [19], and these can be used in cell-free in-solution kinase assays either in their unphosphorylated "naïve" state or after phosphorylation and activation by an upstream kinase. Using bacterially expressed AMPK, one can use solution-phase assays to examine effects of ligands that bind at the nucleotide and ADaM sites, particularly their effects on allosteric activation, promotion of Thr172 phosphorylation, and protection against Thr172 dephosphorylation. However, if the AMPK complexes are derived from cultured mammalian cells or tissues without prior purification, in-solution assays are not recommended. While the synthetic peptide(s) used in AMPK assays are relatively specific, other kinases present in cell lysates may be able to phosphorylate them. Also, different subunit isoforms of AMPK phosphorylate these peptides equally well and therefore cannot be distinguished by in-solution kinase assays. To circumvent both problems, AMPK is first immunoprecipitated using isoform-specific antibodies and then assayed in resuspended immunoprecipitates (referred to below as IP kinase assays). There are a number of commercially available immunoprecipitating antibodies that recognize AMPK subunits and do not affect the kinase activity (although carrying out large numbers of IP kinase assays using commercial antibodies can be expensive, in which case it may be cheaper to get them custom-made).

Whether using bacterially expressed AMPK in in-solution assays, or IP kinase assays using AMPK derived from cell lysates, it is essential to ensure that the appropriate amount of enzyme is used so that the assay operates within the linear range. Thus, pilot experiments titrating the quantity of AMPK, or the quantity of lysate immunoprecipitated, are essential.

In this chapter, we will discuss how cell-free assays can be used to test the effects of ligands and drugs on the three mechanisms: (1) allosteric activation, (2) promotion of Thr172 phosphorylation, and (3) inhibition of Thr172 dephosphorylation, by which AMPK is regulated.

In the description below, we describe kinase assays using [γ-^{32}P]ATP, which our laboratory prefers due to their great sensitivity, flexibility, and reproducibility. However, the protocols can be adapted for nonradioactive kinase assays.

2 Materials

Prepare all solutions with ultrapure water. Reagents are stored at room temperature unless indicated otherwise.

2.1 Kinase Assays: Making Up ATP and Determining Specific Radioactivity

1. Unlabeled ATP: 100 mM ATP.
2. [γ-^{32}P]ATP: Around 6000 Ci/mmol.
3. Kinase assay buffer: 50 mM Na HEPES, pH 7.4, 150 mM NaCl, 1 mM DTT, 0.02% (v/v) Brij-35. Store at room temperature, but do not add Brij-35 and DTT until immediately prior to use; otherwise, store in aliquots at −20 °C.
4. NaOH (1 mol.L^{-1}).
5. pH electrode and meter.
6. UV/visible spectrophotometer.

2.2 Expression and Purification of AMPK from Bacterial Cells

1. Polycistronic bacterial plasmid expressing all three subunits of AMPK (e.g., [19]).
2. BL21-CodonPlus (DE3)-RIL bacterial cells.
3. SOC medium: Dissolve to 1 L deionized water, 20 g of tryptone, 5 g of yeast extract, 2 mL of 5 M NaCl, 2.5 mL of 1 M KCl, 10 mL of 1 M $MgCl_2$, and 10 mL of 1 M $MgSO_4$. Autoclave at 121 °C for 15 min and add 20 mL filter sterilized 1 M glucose.
4. Lysogeny Broth (LB) medium with appropriate antibiotic: Dissolve to 1 L deionized water, 10 g tryptone, 10 g NaCl, 5 g yeast extract, and autoclave at 121 °C for 15 min. Add antibiotic when cooled.
5. LB plates with appropriate antibiotic: LB as above with the addition of 12 g of Select agar. When cooled but still fluid, add antibiotic and pour into plates.
6. Auto-induction medium with appropriate antibiotic: Dissolve 10 g tryptone and 5 g yeast extract in 929 mL deionized water and autoclave at 121 °C for 15 min. Once cooled, add appropriate antibiotic, 1 mL of 1 M $MgSO_4$, 20 mL of 50 × 5052

(weigh 250 g glycerol, 25 g glucose, 100 g α-lactose, gently heated and dissolved in 730 mL deionized water and autoclaved at 110 °C for 10 min), 50 mL of 20 × NPS (weigh 66 g NH_4SO_4, 136 g KH_2PO_4, 142 g Na_2HPO_4 gently heated and dissolved in 900 mL deionized water and autoclaved at 121 °C for 15 min).

7. Isopropyl β-D-1-thiogalactopyranoside (IPTG): 1 M IPTG.
8. Bacterial culture flasks.
9. Centrifuge and centrifuge pots.
10. Pestle, mortar, and liquid nitrogen.
11. Lysis buffer for AMPK: 50 mM Tris–HCl, pH 8.0, 500 mM NaCl, 20 mM imidazole, with EDTA-free protease inhibitor tablets dissolved according to manufacturers' instructions.
12. Elution buffer for AMPK: 50 mM Tris–HCl, pH 8.0, 500 mM NaCl, 500 mM imidazole.
13. Dialysis buffer for unphosphorylated AMPK: 50 mM Na HEPES, pH 8.0, 200 mM NaCl.
14. Bacterial plasmid expressing CaMKK2 (e.g., [20].)
15. Lysis buffer for CaMKK2: 50 mM Tris–HCl, 500 mM NaCl, 1 mM DTT, 1 mM EGTA, 1 mM EDTA, with EDTA-free protease inhibitor tablets dissolved according to manufacturers' instructions.
16. Elution buffer for CaMKK2: 50 mM Na HEPES, pH 8.0, 200 mM NaCl, 20 mM glutathione.
17. Protein purification system (e.g., GE Healthcare ÄKTA).
18. HisTrap FF and GSTrap FF columns.

2.3 Phosphorylation of Bacterially Expressed AMPK at Thr172 Using CaMKK2

1. Gel filtration equilibration buffer: 50 mM Na HEPES, pH 8.0, 200 mM NaCl.
2. Dialysis buffer for phosphorylated, active AMPK: 50 mM Na HEPES, pH 8.0, 200 mM NaCl, 50% (v/v) glycerol.
3. Protein purification system (e.g., GE Healthcare ÄKTA).
4. GSTrap FF and HiLoad 16/600 Superdex 200 pg columns.
5. Dialysis tubing or cassettes.
6. Unlabeled Mg.ATP: 10 mM $MgCl_2$, 400 μM unlabeled ATP.

2.4 In-Solution Kinase Assay

1. Phosphocellulose (P81) paper cut into 1 cm squares, numbered with a hard pencil (if one corner is folded over, this makes the squares easier to pick up using forceps).
2. Kinase assay buffer: 50 mM Na HEPES, pH 7.4, 150 mM NaCl, 1 mM DTT, 0.02% (v/v) Brij-35. Store at room temperature, but do not add Brij-35 and DTT until immediately prior to use; otherwise, store in aliquots at −20 °C.

3. Synthetic peptide substrate [either SAMS (*HMRSAMSGLHLVKRR* [21]) or AMARA (*AMARAA-SAAALARRR* [22])], 1 mM in kinase assay buffer.
4. AMP: 1 mM AMP in kinase assay buffer.
5. Radioactive Mg.ATP: [γ-^{32}P]ATP 150–300 cpm/pmol, 1 mM ATP, 25 mM $MgCl_2$.
6. Phosphoric acid: 1% (v/v) phosphoric acid.
7. Scintillation counter and nonaqueous scintillation fluid.
8. AMPK, diluted appropriately in kinase assay buffer.

2.5 Immuno-precipitate (IP) Kinase Assay

1. Benchtop refrigerated centrifuge.
2. Roller mixer.
3. Benchtop air incubator suitable to hold small orbital shaker.
4. IP buffer: 50 mM Tris–HCl, pH 7.4 at 4 °C, 150 mM NaCl, 50 mM NaF, 5 mM Na pyrophosphate, 1 mM EDTA, 1 mM EGTA, 1 mM DTT, 0.1 mM benzamidine, 0.1 mM PMSF, 5 μg/mL soybean trypsin inhibitor, 1% (v/v) Triton-X100. Immediately prior to use add 1 mM DTT, 0.1 mM benzamidine, 0.1 mM PMSF, 5 μg/mL soybean trypsin inhibitor, and 1% (v/v) Triton-X100.
5. Assay mix "plus peptide": peptide substrate (440 μL, 200 μM final concentration in assay); AMP (440 μL, 200 μM final concentration in assay); $MgCl_2$/[γ-^{32}P]ATP (440 μL, 5 mM/200 μM final concentration in assay).
6. Assay mix "minus peptide": assay buffer (220 μL); AMP (220 μL, 200 μM final concentration in assay); $MgCl_2$/[γ-^{32}P]ATP (220 μL, 5 mM/200 μM final concentration in assay).
7. Small orbital shaker (set at about 1000 rpm).
8. Protein G-Sepharose.
9. Anti-AMPK antibody (any immunoprecipitating antibody against target subunit or complex can be used; our standard protocol uses an equal mixture of anti-α1 and anti-α2 antibodies to precipitate total AMPK from cell lysates).
10. Other reagents as for in-solution kinase assays as in Subheading 2.4.
11. Cell or tissue lysates containing AMPK.

2.6 Allosteric Activation by Ligands Binding the Nucleotide or ADaM Sites

1. Reagents as Subheadings 2.4 or 2.5.

2.7 Promotion of Thr172 Phosphorylation

1. AMPK, either immunoprecipitated from mammalian cells or purified from bacterial cells in kinase assay buffer (*see* **Note 1**).
2. Purified and active LKB1 complex (*see* **Note 2**).
3. SDS sample buffer and equipment to run and analyze Western blots.
4. Phosphospecific (anti-pT172) and total AMPK antibodies.
5. Other reagents as for in-solution kinase assays as Subheading 2.4.

2.8 Protection Against Thr172 Dephosphorylation

1. AMPK, either immunoprecipitated from mammalian cells or purified from bacterial cells (*see* **Note 3**).
2. Assay buffer (as for in-solution assays above).
3. IP buffer containing phosphatase inhibitors: 50 mM Tris–HCl, pH 7.4 at 4 °C, 150 mM NaCl, 50 mM NaF, 5 mM Na pyrophosphate, 1 mM EDTA, 1 mM EGTA, 1 mM DTT, 0.1 mM benzamidine, 0.1 mM PMSF, 5 μg/mL soybean trypsin inhibitor, 1% v/v Triton-X100. Immediately prior to use add 1 mM DTT, 0.1 mM benzamidine, 0.1 mM PMSF, 5 μg/mL soybean trypsin inhibitor, 1% v/v Triton-X100.
4. AMP or ADaM site activator: 1 mM AMP or ADAM site activator dissolved in assay buffer (*see* **Note 4**).
5. $MgCl_2$: 50 mM $MgCl_2$.
6. Protein phosphatase: PP1 catalytic subunit (*see* **Note 5**).
7. SDS sample buffer and equipment to run and analyze Western blots.
8. Phospho-Thr172 and total AMPK antibodies.

3 Methods

3.1 Kinase Assays: Making Up ATP

To accurately determine the degree of allosteric activation by AMP, it is essential that the unlabeled ATP used as substrate is free from contaminating AMP. We recommend preparing a stock solution of unlabeled ATP at a concentration of approximately 100 mM (which is stable at −80 °C in frozen aliquots for 1–2 years). The purity of this stock preparation can be monitored using liquid chromatography or capillary electrophoresis (*see* Chapters 15 and 16).

1. Weigh out sufficient ATP to give 20 mL of 100 mM solution.
2. Place 17 mL of kinase assay buffer in a small beaker, and place this in a large beaker partially filled with ice (this keeps the buffer chilled). Set this stirring, with a clean pH electrode in the buffer.

3. Add small amounts of the ATP to the buffer, allowing each addition to fully dissolve before adding more. Maintain the pH between 7 and 8 using 1 mol.L^{-1} NaOH, to prevent any breakdown of ATP to ADP and AMP.
4. After dissolving all the ATP, make the final volume up to 20 mL using kinase assay buffer.
5. The exact concentration of ATP should be calculated, based on a molar extinction coefficient for ATP of 15,000 at 260 nm. Dilute a sample of the putative 100 mM ATP solution 5000-fold in water (serial dilution of 1:100, then 1:50) and monitor its absorbance at 260 nm, which should be 0.3.
6. Store unlabeled ATP at −20 °C in frozen aliquots; add radioactive ATP as required, to give a final specific radioactivity of 50–300 cpm/pmol or more if using ATP at higher concentrations in the assay (e.g., final concentrations of 1 or 5 mM, rather than 200 μM, *see* Subheading 3.6). For a tip regarding safe handling of radioactive ATP solutions, *see* **Note 6**.

3.2 Expression and Purification of AMPK and CaMKK2 from Bacterial Cells

A polycistronic expression plasmid [19] allows expression of all three subunits within the same bacterial cell, facilitating the formation and stabilization of the complex. Our AMPK polycistronic plasmids encoding AMPK [12, 23] produce His-tagged proteins, while our CaMKK2 plasmids [20] produce GST-tagged proteins; other tags may also be used.

1. Transform both plasmids by incubating 0.1–1 μg DNA with 25 μL BL21-CodonPlus (DE3)-RIL bacterial cells and incubate on ice for 30 min. Heat shock the cells at 42 °C for 1 min followed by a further 5 min on ice. Add 200 μL of SOC medium and incubate cells at 37 °C for 1 h and then spread cells onto LB plates containing appropriate antibiotic. Select individual clones, inoculate into 100 mL of LB media, and incubate overnight at 37 °C.
2. For AMPK expression, inoculate 1 L of auto-induction medium with 10 mL of overnight culture, and incubate at 37 °C with shaking at 180 rpm, until absorbance at 600 nm is ≈0.4. Reduce temperature of incubator to 25 °C and incubate for a further 18 h (*see* **Note 7**). Larger cultures may also be used, depending on protein recovery and other requirements. Recover cells by centrifugation at 7000 × *g* for 30 min at 4 °C, and freeze the pellets in liquid nitrogen.
3. For CaMKK2 expression, inoculate 1 L of LB media with 10 mL of overnight culture, and incubate at 37 °C, shaking at 180 rpm, until absorbance at 600 nm is ≈0.5. Remove culture flask, store at 4 °C for 10 min, add IPTG to a final concentration of 1 mmol.L^{-1}, and then reduce temperature to 18 °C and incubate flask for a further 18 h. Larger cultures may

also be used, depending on protein recovery and other requirements. Recover cells by centrifugation at 7000 × *g* for 30 min at 4 °C, and freeze the pellets in liquid nitrogen.

4. Lyse cell pellets using a mortar and pestle under liquid nitrogen, transfer powdered cells to 50 mL Falcon tubes, and resuspend in lysis buffer. Typically 1 L of bacterial culture requires 10 mL of lysis buffer. Clarify the lysate by centrifugation at 100,000 × *g* for 30 min at 4 °C and apply supernatant to an affinity-based chromatography column at a flow rate of 1 mL/min.
5. Wash the column in ten column volumes and carry out elution. GST-tagged proteins are eluted in buffer containing 20 mM glutathione at a flow rate of 1 mL/min, while His-tagged proteins are eluted using an imidazole gradient. Typically the gradient (20–500 mM imidazole) is performed at 1 mL/min over 30 min. On elution of protein (based on UV absorbance), the gradient is stopped until absorbance at 280 nm has returned to baseline, and the gradient is then resumed.
6. Fractions containing the desired protein (usually detected by SDS-PAGE) are pooled, concentrated, and flash frozen in liquid nitrogen. AMPK protein is first dialyzed (4 × 1 L of dialysis buffer for 30 min) before being flash frozen.

3.3 Phosphorylation of Bacterially Expressed AMPK Using CaMKK2

AMPK expressed in bacteria is not phosphorylated on Thr172 and has a very low basal activity. This "naïve" unphosphorylated protein can be used to study allosteric activation or promotion of phosphorylation. However, if the user requires AMPK protein phosphorylated on Thr172, then this will have to be carried out using either LKB1 or CaMKK2. LKB1 is a heterotrimeric complex and for full activity must be expressed in complex with STRAD and MO25; for this reason CaMKK2 is easier to use. Pilot studies are first performed to determine how much CaMKK2 is required to phosphorylate a given amount of AMPK.

1. Mix 5 μL of AMPK (0.1 μg/μL) and 5 μL of CaMKK2 (various amounts) and store on ice. Start the reaction at 15 s intervals by adding 10 μL of unlabeled Mg.ATP, vortexing, and incubating at 30 °C for 10 min. Blanks lacking AMPK should be performed to ensure CaMKK2 is unable to phosphorylate the AMPK substrate peptide.
2. At 15 s intervals, remove 5 μL from the first assay and add to 20 μL of kinase assay mix (*see* Subheading 3.4) pre-dispensed into 1.5 mL microcentrifuge tubes, vortex, and incubate at 30 °C for 10 min.
3. Complete the kinase assays of this pilot as in Subheading 3.4.

4. Having decided how much CaMKK2 to use to obtain maximal Thr172 phosphorylation, scale up the activation assay with the required amount of CaMKK2—typically 5 mg of purified AMPK is phosphorylated. After the scaled-up assay, the mixture is applied to a HiLoad 16/600 Superdex 200 pg gel filtration column with an in-line 5 mL glutathione-Sepharose FF column, both pre-equilibrated in gel filtration equilibration buffer run at 1 mL/min (*see* **Note 8**).
5. Fractions containing the desired protein (usually monitored by SDS-PAGE) are pooled, concentrated using centrifugal concentrators (following manufacturers' instructions) to ≈3 mL, dialyzed against 4 × 1 L of phosphorylated AMPK dialysis buffer for 30 min each (*see* **Note 9**), and stored at −20 °C.

3.4 Standard In-Solution Kinase Assay

This protocol refers to our standard final assay volume of 25 μL.

1. Mix the following components in 1.5 mL microcentrifuge tubes: (1) 5 μL of peptide substrate (*SAMS* or *AMARA*, final concentration 200 μM); (2) 5 μL of AMP (final concentration 200 μM); (3) 5 μL of AMPK (appropriately diluted to ensure activity is proportional to amount added); (4) 5 μL of kinase assay buffer.
2. Start the reaction (typically at 15 s intervals) by adding 5 μL of $MgCl_2$/[γ-^{32}P]ATP (final concentration 5 mM/200 μM), vortex, and incubate at 30 °C for 10 min. Also perform blanks where the peptide is omitted. It is also possible to prepare master mixes that include $MgCl_2$/[γ-^{32}P]ATP, in which case the reaction is initiated by addition of AMPK instead. AMP can also be replaced in the master mix with assay buffer to determine AMPK activity in the absence of allosteric activator or replaced by another allosteric activator such as A769662.
3. Stop the reactions at 15 s intervals by removing 15 μL and pipetting onto a P81 paper square held with forceps. As soon as the fluid has soaked in (about 1 s), drop the square into a large beaker containing 500 mL of 1% phosphoric acid.
4. Once all the reactions have been stopped, stir the beaker containing the paper squares gently on a magnetic stirrer for 5 min at room temperature.
5. Pour off the phosphoric acid to radioactive waste. Add 500 mL of 1% phosphoric acid and again stir the beaker containing the paper squares gently on a magnetic stirrer for 5 min at room temperature. Pour off the phosphoric acid to radioactive waste and repeat this washing step once more.
6. Lay filters out on absorbent paper on a radioactive spill tray and allow to dry in the air.

7. Place each square into a scintillation vial containing 3 mL of scintillation fluid and count them using a suitable ^{32}P program.
8. Also count duplicate or triplicate samples of the labeled ATP used in the assays. To do this, make a 1:50 dilution of the labeled ATP and pipette 10 μL onto one or more P81 paper squares. Air-dry these paper squares without washing with phosphoric acid. Knowing the amount of ATP in each 10 μL aliquot (if you diluted your 1 mM stock by 50-fold this will be 200 pmol), it is then easy to calculate the specific radioactivity in cpm/nmol. If these paper squares are counted whenever a set of assays is performed using that batch of radioactive ATP and the specific radioactivity recalculated, there is no need to correct for decay of ^{32}P radioactivity.
9. Subtract the values obtained in blanks without peptide substrate, divide by the specific radioactivity of the ATP in cpm/nmol to obtain the nmol phosphate incorporated, and then divide by the incubation time in minutes to obtain the enzyme activity in nmol/min. It is also possible to divide by the weight (mg) of kinase added to obtain the enzyme activity in nmol/min/mg protein. Remember to correct for the fact that only 15 μL (assuming that was indeed the volume sampled) of the 25 μL assay had been pipetted onto the P81 paper square.

3.5 Standard Immunoprecipitate Kinase Assay

Prior to the assay itself, all steps should be carried out on ice or at 4 °C. **Steps 1–4** relate to the binding of the antibody to protein G-Sepharose and can be carried out in advance of the assay. It is possible to prepare sufficient antibody bound to protein G-Sepharose for a large number of experiments (*see* **Note 10**). The protocol below relates to 20 immunoprecipitates (60 assays, 2 duplicates assayed with substrate peptide, and 1 blank assayed without peptide for each immunoprecipitate) but can be scaled up or down according to need. This assay is also applicable when immunoprecipitating tagged proteins expressed in mammalian cells (*see* **Note 11**). In this case substitute anti-AMPK antibody by the appropriate anti-epitope antibody (*see* Chapter 10).

1. Wash 120 μL (packed volume) of protein G-Sepharose with 3 × 1 mL of IP buffer. Resuspend in 1 mL of IP buffer. This will be sufficient for 20 immunoprecipitation reactions (*see* **Note 12**).
2. Add 120 μg of anti-AMPK antibody (1 μg of antibody per μL of packed protein G-Sepharose beads). Adjust the volume of the protein G-Sepharose solution with IP buffer, such that the beads constitute 20% of the total volume, to ensure adequate mixing. Mix on a roller mixer for 1 h at 4 °C.
3. Centrifuge the slurry at 17,000 × *g* for 2 min at 4 °C, and wash the pellet with 3 × 1 mL of IP buffer containing 0.5 M NaCl,

followed by 2 × 1 mL of IP buffer. Resuspend the final pellet in 1 mL total volume of IP buffer and divide into 20 × 50 μL aliquots.

4. To each 50 μL aliquot of protein G-Sepharose, add an appropriate amount of cell lysate (as determined by titration in a pilot experiment: 100–300 μg is a good starting range for most cell types). Add 500–700 μL of IP buffer to ensure adequate mixing and then mix for 2 h at 4 °C on a roller mixer.
5. Centrifuge the mixture at 17,000 × *g* for 3 min at 4 °C and wash the pellet with 1 × 1 mL ice-cold IP buffer containing 0.5 M NaCl, then 1 × 1 mL ice-cold IP buffer, and then 1 × 1 mL ice-cold assay buffer. Resuspend in a final volume of 320 μL assay buffer.
6. Divide the mixture into 3 × 100 μL aliquots in 3 pre-labeled microcentrifuge tubes. Centrifuge the mixture at 17,000 × *g* for 3 min at 4 °C, remove 80 μL of supernatant, and retain the pellets on ice for assay.
7. Start the assay reactions at 15 s intervals by adding 30 μL of the appropriate assay mix (either "+ peptide" or "– peptide") to the 20 μL of immunoprecipitate. After each addition, cap the tube and insert it into an orbital shaker (operating at about ≈1000 rpm, which keeps the Sepharose beads suspended) within a benchtop air incubator maintained at 30 °C.
8. Continue incubations for 15 min at 30 °C.
9. Stop the reactions at 15 s intervals and wash and count the filters as described in **steps 4–10** Subheading 3.4.
10. Activities may be presented as phosphate incorporated in nmol/min/mg, where "mg" is the amount of protein in the original lysate immunoprecipitated. Remember to correct for the fact that only 30 μL (assuming that was indeed the volume sampled) of the 50 μL assay had been analyzed.

3.6 Allosteric Activation by Ligand Binding the Nucleotide or ADaM Sites

For allosteric activation assays using AMP, a greater degree of activation is obtained if assays are carried out in 5 mM ATP compared to the standard conditions of 200 μM, possibly because this concentration of ATP depresses the basal activity [8]. If the concentration of ATP utilized is increased, we keep $MgCl_2$ at a concentration 4.8 mM above the concentration of ATP, because with that protocol the concentration of the Mg.ATP complex varies as a constant proportion of the total ATP [24] (do not vary $MgCl_2$ and ATP in a fixed ratio). If using a higher final ATP concentration, it may also be necessary to increase the specific radioactivity by adding more labeled ATP. Since ATP slowly breaks down non-enzymatically to ADP and/or AMP during the assay, keep the incubation times short (5–10 min). It is also recommended to use the *SAMS* peptide rather than the *AMARA* peptide as

substrate, because (for reasons that remain unclear) a higher AMP dependence is always obtained using the former. With any new assay format, pilot experiments should be performed to ensure that the counts obtained are proportional to the amount of kinase added.

1. Carry out either in-solution kinase assays or IP kinase assays as described in Subheadings 3.4 or 3.5, but varying the concentration of AMP or other allosteric activator. The range of concentrations used should be determined by pilot experiments—try plotting the results as a semilog plot, i.e., $\log_{10}$ [activator] concentration versus activity. Defining EC_{50} as the concentration giving half-maximal activation, the range of concentrations should cover from one to two orders of magnitude below to one to two orders of magnitude above the EC_{50}.
2. Calculate the results as described in Subheading 3.4 or 3.5. The activities can be expressed either as nmol/min/mg or relative to activities obtained in the absence of allosteric activator.
3. At concentrations higher than those that cause activation by binding to the γ subunit, AMP begins to inhibit AMPK due to competitive binding with ATP at the catalytic site on the α subunit [8]. Using suitable software such as GraphPad Prism, the data can be fitted to the equation:

$$\Upsilon = \text{Basal} + \frac{(((Activation \times Basal) - Basal) \times X)}{(EC_{50} + X)} - \frac{((Activation \times Basal) \times X)}{(IC_{50} + X).}$$

where Υ is activity, *Basal* is the activity in the absence of activator, *Activation* is the maximal degree of activation relative to *Basal*, *X* is the AMP concentration, EC_{50} is the concentration of AMP giving half-maximal activation due to binding to the γ subunit, and IC_{50} is the concentration of AMP giving half-maximal inactivation due to binding at the catalytic site. If the activities were expressed relative to those obtained in the absence of allosteric activator, then *Basal* should be set to a fixed value of 1. Using activators that do not inhibit at high concentrations, including most of those binding at the ADaM site, a simpler equation, which omits the inactivation term, may be used instead:

$$\Upsilon = Basal + \frac{(((Activation \times Basal) - Basal) \times X)}{(EC_{50} + X)}$$

3.7 Promotion of Thr172 Phosphorylation

Note that AMPK used for promotion of phosphorylation assays must be dephosphorylated and inactive (*see* **Note 13**). It is essential that pilot experiments are performed to ensure that activation in the assay is proportional to the amount of upstream kinase added. The user should aim for an increase in basal AMPK activity of three- to fivefold. In-solution assays are typically performed in 25 μL reactions using 0.1 μg of bacterially expressed heterotrimer. IP kinase assays are usually performed in 50 μL reactions, with the generation of starting material essentially as in Subheading 3.5. **Steps 1–2** and

3–4 below refer to in-solution and IP kinase assays, respectively. **Step 5** is common to both methods.

1. For in-solution assays, mix the following components in 1.5 mL microcentrifuge tubes: (1) 5 μL of AMPK, (2) 5 μL of 1 mM AMP or assay buffer, (3) 5 μL of upstream kinase (LKB1 or CaMKK2), (4) 5 μL of kinase assay buffer (Subheading 2.4).
2. Start the reaction at 15 s intervals by adding 5 μL of $MgCl_2$/ATP (25 mM/1 mM), vortex, and incubate at 30 °C for 10 min. Also perform blanks where upstream kinase is omitted.
3. For immunoprecipitation assays, mix the following components in 1.5 mL microcentrifuge tubes: (1) 20 μL of AMPK immunoprecipitate, (2) 10 μL of AMP (1 mM) or kinase assay buffer, (3) 10 μL of upstream kinase (LKB1 or CaMKK2).
4. Start the reaction at 15 s intervals by adding 10 μL of $MgCl_2$/ATP (25 mM/1 mM) and incubate in shaking incubator at 30 °C for 10 min. Also perform blanks where upstream kinase is omitted.
5. Terminate the reactions at 15 s intervals by the addition of SDS sample buffer and run a predetermined quantity of protein on the gel to obtain quantitative signals for Thr172 phosphorylation by Western blotting. Alternatively, Thr172 phosphorylation can be monitored by kinase assays (*see* **Note 14**).

3.8 Protection Against Thr172 Dephosphorylation

AMPK used in dephosphorylation protection assays must be phosphorylated on Thr172 and thus active (*see* **Note 15**). Pilot experiments should be performed to ensure that the amount of phosphatase used in the assay gives around 70–80% dephosphorylation/inactivation, so that any inhibition of dephosphorylation will be evident. In-solution assays are typically performed in 25 μL reactions with 0.1 μg of phosphorylated bacterially expressed protein. Immunoprecipitation assays are usually performed in 50 μL reactions with the generation of starting material essentially as in Subheading 3.5. **Steps 1–2** and **3–4** refer to in-solution and IP kinase assays, respectively. **Step 5** refers to terminating the reaction and analyzing the results.

1. For in-solution assays mix the following components in 1.5 mL microcentrifuge tubes (if the phosphatase is cation-dependent, e.g., PP2Cα, Mg^{2+} must also be included in the dephosphorylation mixture): (1) 5 μL of AMPK; (2) 5 μL of 1 mM AMP or assay buffer; (3) 10 μL of kinase assay buffer.
2. Start the reactions at 15 s intervals by adding 5 μL of phosphatase, vortex, and incubate at 30 °C for 10 min. Also perform blanks where the phosphatase is omitted.

3. For immunoprecipitation assays mix the following components in 1.5 mL microcentrifuge tubes: (1) 20 μL of AMPK immunoprecipitate; (2) 10 μL of 1 mM AMP, ADaM site activator or assay buffer; (3) 10 μL of kinase assay buffer.
4. Start the reaction at 15 s intervals by adding 10 μL of phosphatase and incubate in shaking incubator at 30 °C for 10 min. Also perform blanks where the phosphatase is omitted.
5. Terminate the reactions at 15 s intervals by the addition of SDS sample buffer and run a predetermined quantity of protein on the gel to obtain good signal by Western blot.
6. While the above method uses Western blotting as a readout, it is possible to substitute or supplement this with the AMPK activity assay, although special consideration should be given to inhibition of the phosphatase. If kinase assays are to be carried out, we recommend using an okadaic acid-sensitive phosphatase such as PP1γ and then using okadaic acid to inhibit the phosphatase. We have found that washing and dilution may be insufficient to remove the protein phosphatase (*see also* **Note 1**).

4 Notes

1. AMPK for promotion of phosphorylation assays must be unphosphorylated. Use either naïve, unphosphorylated, bacterially expressed AMPK or kinase immunoprecipitated from a cell line that does not express LKB1 (e.g., Hela, G361, or A549 cells). If the AMPK is phosphorylated on Thr172, the user must first dephosphorylate it, but it is essential that the protein phosphatase is then completely removed and/or inhibited prior to the promotion assay. For this reason, we recommend using an okadaic acid-sensitive protein phosphatase such as PP1γ [10], rather than PP2Cα. If the AMPK is immunoprecipitated, the phosphatase can be removed by extensive washing of the immunoprecipitate in either case, but to ensure there is no remaining contamination with phosphatase, when using PP1γ you can add okadaic acid (25 μM final) to inhibit any residual phosphatase. Okadaic acid completely blocks PP1 action without inhibiting LKB1 or AMPK, but there are no suitable specific inhibitors of PP2Cα.
2. We use His-tagged LKB1/STRADα/MO25α complex expressed in, and purified from, insect (Sf9) cells [25].
3. AMPK for protection against dephosphorylation assays must be phosphorylated at Thr172 and active. The user may either use bacterially expressed kinase that has been phosphorylated by an upstream kinase (ensuring that the upstream kinase has been subsequently completely removed) or kinase

immunoprecipitated from a cell line that expresses LKB1 (HEK293, COS7). Before lysis, the user may treat the cells with an activator of AMPK (e.g., phenformin, berberine) to ensure maximal Thr172 phosphorylation.

4. Some activators may initially need to be dissolved in dimethyl sulfoxide.
5. Commercially available from the MRC-PPU at Dundee: *See* mrcppureagents.dundee.ac.uk/reagents-view-proteins/609955).
6. If screw cap or flip-top microcentrifuge tubes containing radioactive ATP are always spun in a microcentrifuge for a few seconds before opening, this avoids getting radioactive contamination on your gloves (which would then be spread elsewhere) when the tubes are opened.
7. We find that expression of AMPK is greatly increased when bacterial cells are incubated in auto-induction medium compared with LB medium. Expression at 25 °C allows phosphorylation of Ser108 on the AMPK-β subunit. We find this essential for allosteric activation, protection against dephosphorylation, and promotion of phosphorylation assays by AMP.
8. The in-line glutathione-containing column is to remove CaMKK2, while the gel filtration column exchanges the buffer and removes small molecules such as Mg.ATP.
9. Dialysis into buffer containing 50% glycerol reduces the volume and thus further concentrates the protein. Also, buffer containing 50% glycerol does not freeze at −20 °C, and this enhances the stability of the protein while allowing easy dispensing.
10. In our experience, antibodies bound to protein G-Sepharose are stable for several months when stored in the fridge at 4 °C.
11. N- and C-terminal tags work well for both the α and γ subunits; such tagged proteins form active complexes with no obvious detriment to activity or regulation. However, N-terminal tagging of β subunits prevents N-terminal myristoylation, while C-terminal tags appear to hinder complex formation.
12. **Important**: Before pipetting protein G-Sepharose, cut approximately 5 mm off pipette tips with scissors. This prevents the Sepharose beads from getting damaged or from blocking the pipette tip.
13. AMPK used for promotion of phosphorylation assays must be inactive. The user may use either naïve, unphosphorylated, bacterially expressed kinase or kinase immunoprecipitated from a cell line that does not express LKB1 (Hela, G361,

A549). If material is active, the user must dephosphorylate the starting material; we recommend using PP1γ and then using okadaic acid to inhibit the phosphatase in the subsequent assays. We have found that washing the immunoprecipitate alone to be insufficient to completely remove PP1γ.

14. Thr172 phosphorylation can also be monitored by performing secondary in-solution or IP kinase assays, as in Subheading 3.4 or 3.5. This is more quantitative than Western blots, but the experiments require careful design. If the AMPK is attached to protein G-Sepharose beads, ensure that the beads are well washed with assay buffer to remove upstream kinases prior to the secondary kinase assay. If the AMPK is in-solution, it must be diluted sufficiently in assay buffer to ensure that the carry-over of upstream kinase into the secondary assay is negligible.
15. Protein for dephosphorylation protection assays must be phosphorylated on Thr172 and thus active. Either use bacterially expressed AMPK that has been phosphorylated by an upstream kinase (Subheading 3.3) ensuring that the upstream kinase has subsequently been removed, or use AMPK immunoprecipitated from a cell line expressing LKB1 (e.g., HEK293, COS7 cells). Before cell lysis, the user may treat the cells with an AMPK activator such as phenformin or berberine to cause maximal Thr172 phosphorylation and then immunoprecipitate in the presence of NaF (50 mM) to prevent dephosphorylation.

Acknowledgment

Studies in the Hardie Laboratory were supported by a Senior Investigator Award (097726) from the Wellcome Trust and by a Programme Grant (C37030/A15101) from Cancer Research UK.

References

1. Hardie DG, Schaffer BE, Brunet A (2016) AMPK: an energy-sensing pathway with multiple inputs and outputs. Trends Cell Biol 26 (3):190–201. https://doi.org/10.1016/j.tcb.2015.10.013
2. Ross FA, MacKintosh C, Hardie DG (2016) AMP-activated protein kinase: a cellular energy sensor that comes in 12 flavours. FEBS J 283 (16):2987–3001. https://doi.org/10.1111/febs.13698
3. Xiao B, Sanders MJ, Carmena D, Bright NJ, Haire LF, Underwood E, Patel BR, Heath RB, Walker PA, Hallen S, Giordanetto F, Martin SR, Carling D, Gamblin SJ (2013) Structural basis of AMPK regulation by small molecule activators. Nat Commun 4:3017. https://doi.org/10.1038/ncomms4017
4. Xiao B, Sanders MJ, Underwood E, Heath R, Mayer FV, Carmena D, Jing C, Walker PA, Eccleston JF, Haire LF, Saiu P, Howell SA, Aasland R, Martin SR, Carling D, Gamblin SJ (2011) Structure of mammalian AMPK and its regulation by ADP. Nature 472 (7342):230–233. https://doi.org/10.1038/nature09932. nature09932 [pii]
5. Xiao B, Heath R, Saiu P, Leiper FC, Leone P, Jing C, Walker PA, Haire L, Eccleston JF, Davis CT, Martin SR, Carling D, Gamblin SJ (2007)

Structural basis for AMP binding to mammalian AMP-activated protein kinase. Nature 449 (7161):496–500

6. Chen L, Wang J, Zhang YY, Yan SF, Neumann D, Schlattner U, Wang ZX, JW W (2012) AMP-activated protein kinase undergoes nucleotide-dependent conformational changes. Nat Struct Mol Biol 19(7):716–718. https://doi.org/10.1038/nsmb.2319
7. Hawley SA, Davison M, Woods A, Davies SP, Beri RK, Carling D, Hardie DG (1996) Characterization of the AMP-activated protein kinase kinase from rat liver and identification of threonine 172 as the major site at which it phosphorylates AMP-activated protein kinase. J Biol Chem 271(44):27879–27887
8. Gowans GJ, Hawley SA, Ross FA, Hardie DG (2013) AMP is a true physiological regulator of AMP-activated protein kinase by both allosteric activation and enhancing net phosphorylation. Cell Metab 18(4):556–566. https://doi.org/10.1016/j.cmet.2013.08.019
9. Oakhill JS, Chen ZP, Scott JW, Steel R, Castelli LA, Ling N, Macaulay SL, Kemp BE (2010) beta-Subunit myristoylation is the gatekeeper for initiating metabolic stress sensing by AMP-activated protein kinase (AMPK). Proc Natl Acad Sci U S A 107(45):19237–19241. https://doi.org/10.1073/pnas.1009705107. 1009705107 [pii]
10. Ross FA, Jensen TE, Hardie DG (2016) Differential regulation by AMP and ADP of AMPK complexes containing different gamma subunit isoforms. Biochem J 473(2):189–199. https://doi.org/10.1042/BJ20150910
11. Cool B, Zinker B, Chiou W, Kifle L, Cao N, Perham M, Dickinson R, Adler A, Gagne G, Iyengar R, Zhao G, Marsh K, Kym P, Jung P, Camp HS, Frevert E (2006) Identification and characterization of a small molecule AMPK activator that treats key components of type 2 diabetes and the metabolic syndrome. Cell Metab 3(6):403–416
12. Hawley SA, Fullerton MD, Ross FA, Schertzer JD, Chevtzoff C, Walker KJ, Peggie MW, Zibrova D, Green KA, Mustard KJ, Kemp BE, Sakamoto K, Steinberg GR, Hardie DG (2012) The ancient drug salicylate directly activates AMP-activated protein kinase. Science 336 (6083):918–922. https://doi.org/10.1126/science.1215327
13. Langendorf CG, Kemp BE (2015) Choreography of AMPK activation. Cell Res 25(1):5–6. https://doi.org/10.1038/cr.2014.163
14. Calabrese MF, Rajamohan F, Harris MS, Caspers NL, Magyar R, Withka JM, Wang H, Borzilleri KA, Sahasrabudhe PV, Hoth LR, Geoghegan KF, Han S, Brown J, Subashi TA, Reyes AR, Frisbie RK, Ward J, Miller RA, Landro JA, Londregan AT, Carpino PA, Cabral S, Smith AC, Conn EL, Cameron KO, Qiu X, Kurumbail RG (2014) Structural basis for AMPK activation: natural and synthetic ligands regulate kinase activity from opposite poles by different molecular mechanisms. Structure 22(8):1161–1172. https://doi.org/10.1016/j.str.2014.06.009
15. Li X, Wang L, Zhou XE, Ke J, de Waal PW, Gu X, Tan MH, Wang D, Wu D, Xu HE, Melcher K (2015) Structural basis of AMPK regulation by adenine nucleotides and glycogen. Cell Res 25(1):50–66. https://doi.org/10.1038/cr.2014.150
16. Scott JW, Ling N, Issa SM, Dite TA, O'Brien MT, Chen ZP, Galic S, Langendorf CG, Steinberg GR, Kemp BE, Oakhill JS (2014) Small molecule drug A-769662 and AMP synergistically activate naive AMPK independent of upstream kinase signaling. Chem Biol 21 (5):619–627. https://doi.org/10.1016/j.chembiol.2014.03.006
17. Goransson O, McBride A, Hawley SA, Ross FA, Shpiro N, Foretz M, Viollet B, Hardie DG, Sakamoto K (2007) Mechanism of action of A-769662, a valuable tool for activation of AMP-activated protein kinase. J Biol Chem 282(45):32549–32560
18. Sanders MJ, Ali ZS, Hegarty BD, Heath R, Snowden MA, Carling D (2007) Defining the mechanism of activation of AMP-activated protein kinase by the small molecule A-769662, a member of the thienopyridone family. J Biol Chem 282(45):32539–32548
19. Neumann D, Woods A, Carling D, Wallimann T, Schlattner U (2003) Mammalian AMP-activated protein kinase: functional, heterotrimeric complexes by co-expression of subunits in Escherichia Coli. Protein Expr Purif 30 (2):230–237
20. Hawley SA, Pan DA, Mustard KJ, Ross L, Bain J, Edelman AM, Frenguelli BG, Hardie DG (2005) Calmodulin-dependent protein kinase kinase-beta is an alternative upstream kinase for AMP-activated protein kinase. Cell Metab 2(1):9–19
21. Davies SP, Carling D, Hardie DG (1989) Tissue distribution of the AMP-activated protein kinase, and lack of activation by cyclic-AMP-dependent protein kinase, studied using a specific and sensitive peptide assay. Eur J Biochem 186(1-2):123–128
22. Dale S, Wilson WA, Edelman AM, Hardie DG (1995) Similar substrate recognition motifs for mammalian AMP-activated protein kinase, higher plant HMG-CoA reductase kinase-A, yeast SNF1, and mammalian calmodulin-

dependent protein kinase I. FEBS Lett 361:191–195

23. Ross FA, Rafferty JN, Dallas ML, Ogunbayo O, Ikematsu N, McClafferty H, Tian L, Widmer H, Rowe IC, Wyatt CN, Shipston MJ, Peers C, Hardie DG, Evans AM (2011) Selective expression in carotid body type I cells of a single splice variant of the large conductance calcium- and voltage-activated potassium channel confers regulation by AMP-activated protein kinase. J Biol Chem 286(14):11929–11936. https://doi.org/10.1074/jbc.M110.189779. M110.189779 [pii]
24. Storer AC, Cornish-Bowden A (1976) Concentration of MgATP2- and other ions in solution. Calculation of the true concentrations of species present in mixtures of associating ions. Biochem J 159(1):1–5
25. Zeqiraj E, Filippi BM, Deak M, Alessi DR, van Aalten DM (2009) Structure of the LKB1-STRAD-MO25 complex reveals an allosteric mechanism of kinase activation. Science 326 (5960):1707–1711. https://doi.org/10.1126/science.1178377. 1178377 [pii]

Chapter 6

Applications of NMR and ITC for the Study of the Kinetics of Carbohydrate Binding by AMPK β-Subunit Carbohydrate-Binding Modules

Paul R. Gooley, Ann Koay, and Jesse I. Mobbs

Abstract

Understanding the kinetics of proteins interacting with their ligands is important for characterizing molecular mechanism. However, it can be difficult to determine the extent and nature of these interactions for weakly formed protein-ligand complexes that have lifetimes of micro- to milliseconds. Nuclear magnetic resonance (NMR) spectroscopy is a powerful solution-based method for the atomic-level analysis of molecular interactions on a wide range of timescales, including micro- to milliseconds. Recently the combination of thermodynamic experiments using isothermal titration calorimetry (ITC) with kinetic measurements using ZZ-exchange and CPMG relaxation dispersion NMR spectroscopy have been used to determine the kinetics of weakly interacting protein systems. This chapter describes the application of ITC and NMR to understand the differences in the kinetics of carbohydrate binding by the β1- and β2-carbohydrate-binding modules of AMP-activated protein kinase.

Key words Carbohydrate, CPMG relaxation dispersion, Isothermal titration calorimetry, Ligand binding, Nuclear magnetic resonance, ZZ-exchange

1 Introduction

AMPK, composed of different β-isoform subunits, binds carbohydrates with varying affinities due to the carbohydrate-binding modules (β1- or β2-CBM) that they carry [1–3]. The β2-CBM binds carbohydrate with greater affinity than those with the β1-CBM. To gain a better understanding of this difference, the thermodynamics and kinetics of binding can be characterized by a variety of analytical methods. Initial characterization of the affinities by fluorescence spectrophotometry and NMR spectroscopy showed dissociation constants (K_d) of 0.5–10 μM for various carbohydrates [2]. Further tests suggested the molecular mass of the CBMs (~10 kDa), small ligand size (~1 kDa), and these affinities were not suitable for using surface plasmon resonance (SPR), an excellent method for obtaining kinetics and thermodynamic data [4]. On the other hand, as

Dietbert Neumann and Benoit Viollet (eds.), *AMPK: Methods and Protocols*, Methods in Molecular Biology, vol. 1732, https://doi.org/10.1007/978-1-4939-7598-3_6,

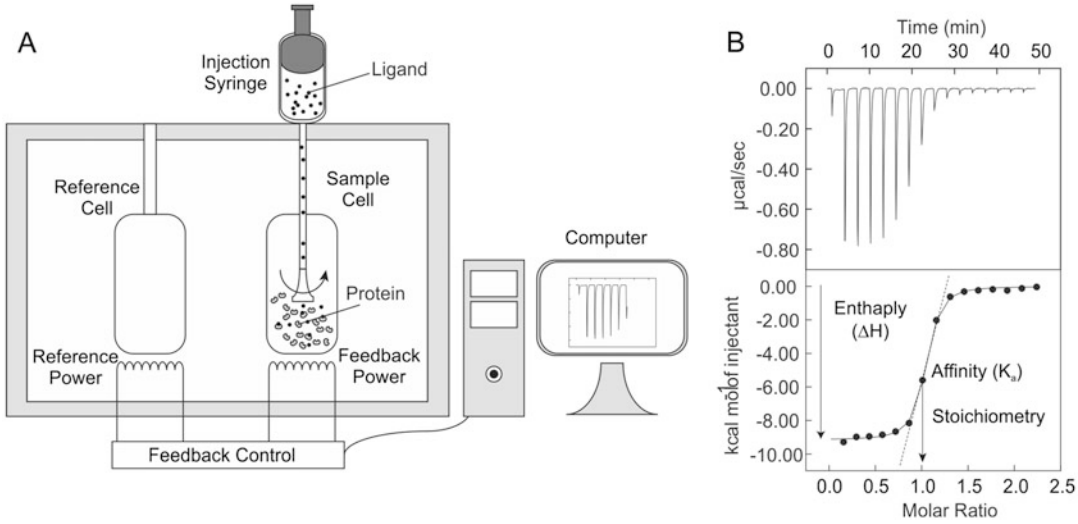

Fig. 1 Isothermal titration calorimetry—(**a**) Schematic of an isothermal titration calorimetry (ITC) instrument. An ITC is composed of two cells (sample and reference) surrounded by a heat jacket, an injection syringe that also stirs the sample, and a computer controlled thermostat. (**b**) Example of an ITC experiment. The additional power needed to keep the sample cell at the same temperature as the reference cell is the monitored signal. This is plotted as a function of time in the top graph as a series of downward peaks. The area under each peak is plotted in the bottom graph as a function of molar ratio. This plot can be fitted with an appropriate model, and the binding affinity (K_a), stoichiometry (n), and enthalpy (ΔH) can be obtained

shown for other proteins [5], combining isothermal titration calorimetry (ITC) and various nuclear magnetic resonance (NMR) spectroscopy experiments, especially Carr-Purcell-Meiboom-Gill (CPMG) relaxation dispersion and ZZ-exchange spectroscopy, allowed the elucidation of both thermodynamic and kinetic data of binding [3]. In this chapter we outline the application of these latter experiments.

An ITC instrument works via a computer controlled thermal feedback system. It consists of a reference cell and a sample cell with a syringe that can titrate into the sample (Fig. 1a). The sample, usually the protein of interest, is placed in the sample cell, and the ligand, in this case carbohydrate, is titrated in. As each injection occurs, a protein-carbohydrate complex is formed, and heat is released (exothermic) or absorbed (endothermic) upon the interaction. The feedback system then needs to increase or decrease the temperature to keep the sample and reference cells at the same temperature. This thermal power is then recorded as a series of peaks (Fig. 1b), and the area under each peak can be determined to find the heat of each injection [6]. The heat of each injection can then be plotted against protein-carbohydrate molar ratio and be fit to the appropriate nonlinear binding equation (single-site, multisite, sequential, or competitive) in order to obtain the enthalpy (ΔH), stoichiometry (n) and affinity (the association constant, K_a). From the affinity and enthalpy,

it is then straightforward to calculate Gibbs free energy (ΔG) and the entropy (ΔS). The following relationships are required to determine these parameters. For a single binding site, the binding constant, K_a, is given by:

$$K_a = \frac{\Theta}{(1-\Theta)[X]} \tag{1}$$

where Θ is the fraction of sites occupied by ligand X and $[X]$ is the free concentration of ligand. The total concentration of ligand X_t is represented by:

$$X_t = [X] + n\Theta P_t \tag{2}$$

where P_t is the total concentration of protein in the cell. The total heat content (Q) of the volume of solution contained in the cell (V_0) at fractional saturation is defined by the following equation:

$$Q = n\Theta P_t \Delta H V_0 \tag{3}$$

Combining eqs. (1) and (2) results in a quadratic equation that can be solved and substituted into eq. (3) to give the following:

$$Q = \frac{nP_t\Delta H V_0}{2}\left[1 + \frac{X_t}{nP_t} + \frac{1}{nK_aP_t} - \sqrt{\frac{\left(1 + \frac{X_t}{nP_t} + \frac{1}{nK_aP_t}\right)^2 - 4X_t}{nP_t}}\right] \tag{4}$$

The value of Q can now be calculated as a function of K_a, n, and ΔH as the other parameters are all known. However, this value of Q only applies for V_0 (initial volume), and therefore a correction (V_i) must be made after each injection. The change in heat after each injection is now defined as:

$$\Delta Q(i) = Q(i) + \frac{dV_i}{V_o}\left[\frac{Q(i) + Q(i-1)}{2} - Q(i-1)\right] \tag{5}$$

Equation (5) can now be used to obtain best fit values for K_a, n, and ΔH by standard Marquardt methods, using the commercial software of the instrument, until no further improvement of fit occurs. The dissociation constant, K_d, is obtained from the inverse of K_a. The Gibbs free energy (ΔG^0) can be obtained from the following thermodynamic equation:

$$\Delta G^0 = \Delta H^0 - T\Delta S^0 = -RT \ln K_d \tag{6}$$

where R is the gas constant (1.987 cal.K^{-1}.mol^{-1}) and T is temperature.

A range of NMR experiments are available for monitoring protein conformational change on a range of timescales [7]. Such experiments can also probe the kinetics of ligand binding. Usually

these experiments are conducted on isotope (^{15}N or ^{13}C)-enriched molecules, and for that reason protein, rather than ligand, resonances are most often monitored. Importantly, the resonances will be those sensitive to the ligand and are most often in or near the ligand binding site. Which experiment can be applied is dependent on the rate of exchange of the ligand from the free to the bound state under equilibrium conditions. It is expected that a resonance that is sensitive to the presence of the ligand experiences chemical exchange. At its essence chemical exchange is a rate measurement between two states such as free protein (A) to ligand bound protein (B) and can determine the appearance of an NMR spectrum. The below equation describes this exchange:

$$A \underset{k_{\text{off}}}{\overset{k_{\text{on}}[X]}{\rightleftharpoons}} BX \tag{7}$$

where k_{off} (s^{-1}) is the first-order dissociation rate constant, k_{on} (M^{-1} s^{-1}) is the second-order association rate constant, and $[X]$ is the concentration of unbound ligand in solution. Typically exchange rate is categorized into three broad exchange regimes which are determined by comparing exchange rate ($k_{\text{ex}} = k_{\text{on}} + k_{\text{off}}$) to the change in chemical shift ($\Delta\omega = \omega_A - \omega_B$), both measures in per second. In the slow exchange regime ($k_{\text{ex}} < \Delta\omega$), two distinct peaks are observed for the two states (A and B) since there is little interconversion between states ($A \rightleftharpoons B$) during the experiment. The population of each state (p_A and p_B) can be obtained from the intensity of each peak. In the intermediate ($k_{\text{ex}} \approx \Delta\omega$) and fast exchange regimes, a single population averaged peak is observed. For fast exchange the rapid exchange between states ($A \rightleftharpoons B$) results in a well-defined peak, whereas an exchange broadened peak is observed in intermediate exchange due to the interference from the interconversion between states [8, 9]. Two experiments that are conducted at sub-stoichiometric concentrations of ligand to protein can provide kinetic data of binding: ZZ-exchange spectroscopy is suited to slow exchange and can measure rates in the millisecond to seconds, while CPMG relaxation dispersion is more suited to intermediate to fast exchange and can measure rates in the microsecond to millisecond timescale [7]. From these experiments k_{off} can be determined and then k_{on} from K_d that is measured by ITC [5].

$$k_{\text{on}} = \frac{k_{\text{off}}}{K_d} \tag{8}$$

In ZZ-exchange spectroscopy [10], for a typical experiment, a sample is made such that approximately half the protein population is in the free state A and the other half is in the bound state B. A series of 2D spectra are recorded in which the magnetization is

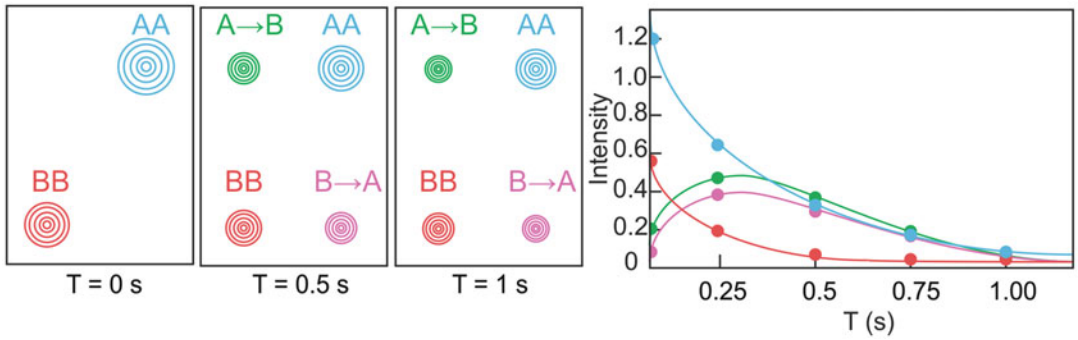

Fig. 2 Schematic of ZZ-exchange NMR spectroscopy—In an exchange spectroscopy experiment, two auto-peaks are observed (*AA* and *BB*) corresponding to the *A* and *B* states, and two exchange cross peaks are observed ($A \rightarrow B$ and $B \rightarrow A$). Note *AA* and *BB* are resolved in both dimensions of the 2D spectrum. The intensity of these peaks can be fit to a binding model to obtain rate constants

transferred into the z-axis (along B_0) with varying mixing times (T_{mix}) at which point interconversion between states is allowed to occur. Two auto-peaks are observed for states A and B, and two cross peaks are observed for the exchange between states ($A \rightarrow B$ and $B \rightarrow A$) (Fig. 2). The integral of each peak can be taken and fit to a binding model in order to obtain kinetic rates [5, 7]:

$$\begin{bmatrix} I_{AA} & I_{BA} \\ I_{AB} & I_{BB} \end{bmatrix} = \begin{bmatrix} 1 & y_{BA} \\ y_{AB} & y_{BB} \end{bmatrix} \cdot \exp\left(T_{\text{mix}} \begin{bmatrix} -k'_{\text{on}} - R_1^A & k_{\text{off}} \\ k'_{\text{on}} & -k_{\text{off}} - R_1^B \end{bmatrix} \right) \cdot \begin{bmatrix} I_0^A & 0 \\ 0 & I_0^B \end{bmatrix} \tag{9}$$

$$k'_{\text{on}} = k_{\text{on}}[X] = k_{\text{off}} \frac{p_B}{1 - p_B} \tag{10}$$

where I_{AA} and I_{BB} are the measured peak volumes of the auto-peaks, I_{AB} and I_{BA} of the cross peaks, and I_0^A and I_0^B in the absence of mixing, R_1^A and R_1^B are the ^{15}N longitudinal relaxation times, and y_{AB}, y_{BA}, and y_{BB} account for differential relaxation after the mixing time.

CPMG relaxation dispersion experiments contain a spin-echo pulse that has two fixed time delay periods (τ) with a 180° pulse in-between (τ-180°-τ) and is applied as a repeated train of pulses (τ-180°-τ)$_n$ to refocus transverse magnetization [11]. In a typical experiment, a series of 2D spectra are obtained with differing length of spin-echo pulses which are conveniently denoted as a frequency ($\nu_{\text{CPMG}} = 1/4\tau$). As ν_{CPMG} frequency increases, the dephasing of spins is decreased, which leads to increased intensity and reduced relaxation rates (R_2^{obs}). Usually a series of 2D spectra are recorded with varying ν_{CPMG} frequency (between 50 and

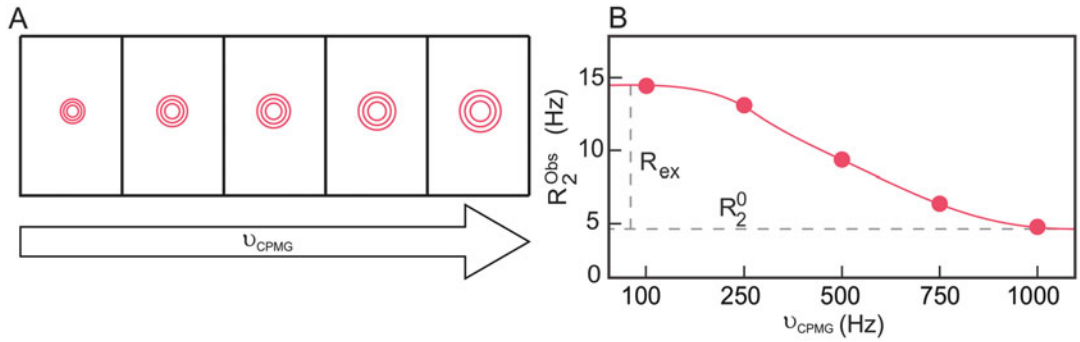

Fig. 3 Schematic of CPMG relaxation dispersion NMR spectroscopy—(**a**) Peaks of a 2D spectra intensify with increasing ν_{CPMG} and are used to create a R_2 relaxation profile. (**b**) R_2 relaxation profile is obtained by plotting the observed relaxation rate ($\boldsymbol{R_2^{obs}}$) against the ν_{CPMG} frequency. These plots can then be fit to appropriate models in order to obtain exchange rates (k_{ex}, k_{on}, k_{off}), populations of states (p_A and p_B), and chemical shifts ($\Delta\omega = \omega_A$ - ω_B)

1200 Hz) where the R_2^{obs} is dependent on ν_{CPMG} (Fig. 3). The intensity of the peaks can be taken and converted to plots of R_2^{obs} vs ν_{CPMG} by the following expression:

$$R_2^{obs} = -\ln\left(\frac{I_{vCPMG}}{I_0}\right)/T_{CPMG} \tag{11}$$

where $I_{\nu CPMG}$ is the intensity of the peak and I_0 is the intensity of the peak in a reference spectrum where $\nu_{CPMG} = 0$. These R_2^{obs} profiles can be fit to an appropriate exchange model in order to obtain structural (chemical shift $\Delta\omega = \omega_A + \omega_B$), kinetic (exchange rate k_{ex}), and population (p_A and p_B) parameters [5, 7, 12]. For a two-state binding model, CPMG data can be fitted to [12]:

$$R_2^{calc} = -\ln\left(\frac{M_B(4n\delta)}{M_B(0)}\right) \tag{12}$$

where $\boldsymbol{M}(4n\delta) = \left(\exp(\boldsymbol{A}\delta)\exp\left(\tilde{\boldsymbol{A}}\delta\right)\exp\left(\tilde{\boldsymbol{A}}\delta\right)\exp(\boldsymbol{A}\delta)\right)n\boldsymbol{M}(0)$, $T_{CPMG} = 4n\delta$ with $2n$ the number of 180° pulses within the T_{CPMG} period, $\boldsymbol{M}(t)$ is the magnetization vector given by $(M_B(t)$, and $M_A(t))T$ for two-site binding between states A and B, and $\boldsymbol{A}$ and $\tilde{\boldsymbol{A}}$ by:

$$\boldsymbol{A} = \begin{pmatrix} -R_2^A - k'_{on} + i\Delta\omega & k_{off} \\ k'_{on} & -k_{off} - R_2^B \end{pmatrix} \tag{13}$$

$$\tilde{\boldsymbol{A}} = \begin{pmatrix} -R_2^A - k'_{on} - i\Delta\omega & k_{off} \\ k'_{on} & -k_{off} - R_2^B \end{pmatrix} \tag{14}$$

where k'_{on} is defined in eq. (10), $\Delta\omega$ (s^{-1}) is the chemical shift difference of the free (A) and bound (B) states, and R_2^A and R_2^B are the transverse relaxation rates of the free and bound states.

The combination of ITC and NMR is a proven method and has been used previously for studying protein interactions when conventional methods fail [5, 13]. However, care needs to be taken to appropriately apply the experiments. β1- and β2-CBM have differences in protein motion [14]. When studied by CPMG relaxation dispersion, β1-CBM appears to have no μs-ms motion in the free or bound state, whereas β2-CBM has significant dynamics in both states. In order to study carbohydrate-binding kinetics of β1-CBM, CPMG relaxation dispersion experiments, in the presence of sub-stoichiometric amounts of carbohydrate, were applied, thus monitoring μs-ms motion. On the other hand, this method could not be used for β2-CBM as microsecond motion observed in the free state could confound results obtained in the presence of sub-stoichiometric amounts of ligand. As carbohydrate binding to β2-CBM appears to result in slow exchange, ZZ-exchange spectroscopy was used to study the dynamics of β2-CBM binding carbohydrate. These NMR methods were used to obtain dissociation rates (k_{off}) of carbohydrate binding which could be used in conjunction with ITC-derived affinity values (K_d) to obtain association rates (k_{on}) [3].

2 Materials

1. Purified β1 and β2 CBMs, Q75 to K156 (using β2 numbering) of the β-subunit of *Rattus norvegicus* AMPK cloned into pGEX-6P-3 (*see* **Note 1**).
2. β-cyclodextrin (BCD) (Sigma Aldrich), glucosyl-β-cyclodextrin (gBCD) (Wako Pure Chemical Industries Ltd.).
3. Sodium phosphate buffer: 100 mM Na_2HPO_4/NaH_2PO_4, pH 6.8, degassed (*see* **Note 2**).
4. Mini dialysis kit, 1 kDa cutoff.
5. Calorimeter: e.g., MicroCal iTC200 (Malvern).
6. NMR spectrometers of two or more field strengths, e.g., Bruker 600–800 MHz of the Avance II or more recent models, equipped with triple resonance cryoprobes (^1H, ^{13}C, ^{15}N) (TXI or TCI).
7. Spectrophotometer: e.g., Bio-Rad Smart Spec 3000 or similar device.
8. Hamilton syringe 200 μl.

3 Methods

3.1 Sample Preparation for ITC and NMR Spectroscopy

1. Before ITC experiments, unlabelled β1- and β2-CBM protein samples are dialyzed overnight in 100 mM sodium phosphate buffer (pH 6.8). Similarly before NMR experiments, ^{15}N–labelled β1- and β2-CBM protein samples are dialyzed in the same buffer system. In all cases, the dialysate is used to prepare solutions of glucosyl-β-cyclodextrin (gBCD) and β-cyclodextrin (BCD) of known concentrations.
2. Protein concentration measurements are based on the absorbance at 280 nm. The theoretical extinction coefficient for the β-CBMs was calculated by ProtParam (http://www.expasy.ch/tools/protparam.html) based on [15].

3.2 Isothermal Titration Calorimetry Measurements

1. A 200 μl sample of 30 μM protein is loaded into the sample cell using a Hamilton syringe; extra care must be taken to avoid introducing air bubbles. Samples can be degassed if needed.
2. More than 40 μl of 300 μM ligand can be added to a PCR tube and loaded into the syringe following the instructions from the ITC software (*see* **Note 3**).
3. With stirring a titration is performed with 16 injections of 2.5 μl of carbohydrate with the sample cell set to a desired temperature. Each injection is done over a 5 s period with a 180 s delay between injections.
4. A blank sample of injecting carbohydrate into buffer is performed identically and subtracted from each result so that at saturation the binding curves should approach zero kcal.mol^{-1}.
5. The data is fitted using the Origin MicroCal software assuming a single-site binding model. However, the values for stoichiometry are also fitted, along with the binding affinity ($K_a = 1/K_d$) and enthalpy (ΔH).

3.3 ZZ-Exchange NMR Spectroscopy Measurements

1. A 500 μM sample of ^{15}N–labelled β2-CBM is mixed with a sub-stoichiometric amount (250 μM) of carbohydrate. The binding of carbohydrate must fit to a slow exchange condition such that two signals are observed in the 2D ^{1}H, ^{15}N HSQC (heteronuclear single quantum correlated) spectrum, one reflecting the free state and another the bound state. This may require trial and error until the signals are approximately equal. Also to see exchange the resonances of the free and bound are ideally resolved in both the ^{1}H and ^{15}N dimensions of a 2D ^{1}H, ^{15}N HSQC spectrum (Fig. 2).
2. Once placed in the spectrometer, samples are equilibrated at 25 °C or the desired temperature, and ^{1}H and ^{15}N channels are optimally tuned.

3. The sample is gradient-shimmed, optimally using a round of three-dimensional shimming and then one-dimensional shimming until no further improvement.
4. The ^{1}H 90° pulse is experimentally optimized (pulse program zg, with O1 offset from the water) for individual samples by observing a 360° null.
5. The ^{1}H 90° pulse is copied forward into experiments with the ZZ-exchange pulse sequence (hsqcexf3gpwgph). Normally the ^{15}N pulse does not need optimization, and the default pulse is used.
6. A series of 2D experiments are separately set up and acquired sequentially with a varying mixing time delay (d7) for exchange. For example, for here delays of 0.03, 0.05, 0.09, 0.13, 0.15, 0.35, 0.55, 0.75, and 0.95 s are used and collected in random order. The experiments are then performed with 2048 t_2 and 128 t_1 points with 64 scans per t_1 point (*see* **Note 4**).
7. Spectra are processed using NMRPipe [16] or similar software (*see* **Note 5**).
8. For resolved resonances, peak volumes are measured with SPARKY (DG Kneller, I. K. UCSF Sparky-an NMR display, annotation and assignment tool. *University of California, San Francisco,* (1993)) or similar software.
9. Peak volumes could then be analyzed with MATLAB scripts provided by Dr. Demers and Dr. Mittermaier [5]. Values of k_{off} are obtained by a global fit of all the data and k_{on} values determined with the use of ITC-derived K_d values. The initial round of data fitting occurs on a per residue basis. At this stage each residue will have its own plot and fit allowing the user to identify residues with weak data or regions of overlapping intensities. These "poor residues" can then be excluded from further analysis. In the final step, a global analysis is performed where all residues are fitted together and Monte Carlo simulations are performed to obtain k_{off} and NMR derived k_{on} values as well as their errors (*see* **Note 6**).

3.4 CPMG Relaxation Dispersion NMR Spectroscopy Measurements

1. A 500 μM sample of β1-CBM is mixed with a sub-stoichiometric amount (20 μM) of carbohydrate. For other CBMs and carbohydrates, the optimal amount requires trial and error until a suitable dispersion signal is obtained.
2. The sample is transferred into a 5 mm NMR tube and included 5% $^{2}H_2O$ for locking.
3. The pulse sequence for CPMG relaxation dispersion used on the Bruker spectrometer is encoded in the library as hsqcrexetf3gpsi3d as a pseudo 3D experiment with single scan interleaving.

4. As for the ZZ-exchange experiment, the sample is tuned and shimmed, and the ^{1}H 90° pulse is determined.
5. A list of pulse frequencies (vdlist) is prepared (0, 50, 2x75, 100, 2x150, 200, 300, 500, 2x700, 800, 900, 1000, 1500 Hz). The list is prepared with the frequencies in a random manner. It is important to set *TD1* and *NBL* to the number of entries in the vdlist (here 16). The length of mixing time per CPMG block (d21) is typically set to 40 ms, so that T_{CPMG} is 80 ms. Individual 2D data sets are acquired with 2048 t_2 (^{1}H) and 256 t_1 (^{15} N) points and 24 scans for each t_1 point (*see* **Note 7**).
6. Trial experiments are conducted at a single field varying ligand concentrations until optimal and significant R_2^{obs} are observed (Fig. 3) [17]. Full data collection is then conducted on the same sample at two magnetic fields.
7. Data can be processed using various software packages. We use NMRPipe to process our data (*see* **Note 8**).
8. The processed NMR data is read into software such as SPARKY or similar software and peak intensities (heights) measured. For specific peaks these intensities are fitted to the model using software packages kindly provided by Dr. Korzhnev [12]. From these data k_{off} is determined and k_{on} from ITC-derived K_d values (eqs. 8 and 10). CPMG dispersion profiles are initially fit with all parameters calculated on a per residue basis. Initial fits are observed to determine if reasonable chemical exchange occurred and residues could be excluded from further analysis if poor or no chemical shift is observed. In the final round residues are fit in a global manner where a single k_{off} value can be obtained. If chemical shifts for the unbound and saturated states are known, chemical shift differences can be supplied to calculations (*see* **Note 9**).

4 Notes

1. Overexpression of the AMPK β-CBMs in *Escherichia coli* is straightforward. For ITC, protein is expressed in *E. coli* BL21 (DE3) in rich media (2xYT) to produce milligram quantities of protein. Protein is purified to homogeneity [3]. As the NMR experiments described here require ^{15}N–labelling of the protein, expression in *E. coli* BL21(DE3) is more demanding, requiring minimal media with ^{15}N–ammonium chloride the sole nitrogen source and glucose as the sole carbon source. Our favored protocols for obtaining large milligram quantities for NMR experiments are found in these publications [18, 19]. Over the course of our work, the β1- and β2-CBM ^{1}H, ^{13}C, ^{15}N NMR spectra

have been assigned. For any ligand binding study, it is desirable to assign at least the backbone (^{1}HN, ^{15}N, ^{13}Cα, ^{13}Cβ) resonances. Once assigned, titrations of ^{15}N–labelled protein monitored by ^{1}H, ^{15}N HSQC usually reveal the number of binding sites and K_d, complementing ITC experiments. Further these experiments will inform whether ligand binding fits the slow or fast exchanging regime. However, to conduct the experiments, we have described in this article one does not absolutely require assignments to obtain information from ZZ-exchange or CPMG relaxation dispersion NMR spectroscopy. Nevertheless, we note for proteins up to about 15 kDa software and technical improvements have made assignment of backbone resonances straightforward and we encourage this approach as considerable ligand binding and protein behavior information are gained.

2. As NMR experiments are conducted with relative high concentrations of protein and ligand, it is important that buffers are of a reasonable concentration, as pH may change. We suggest at least 50 mM and to avoid buffers such as PBS (phosphate buffer saline).
3. Appropriate protein and ligand concentrations are determined by trial and error as the quality of the signal is dependent on K_d and ΔH.
4. Number of t_1 points and spectral widths are experimentally determined. Also to improve resolution (in F1), isolated peaks can be folded into the spectrum and the spectral width in that dimension reduced.
5. NMRPipe scripts for processing ZZ-exchange are simple scripts for 2D data and follow the same processing as applied to a ^{1}H, ^{15}N HSQC spectrum.
6. For estimation of errors of the nonlinear fits of ZZ-exchange spectroscopy, *see* [5].
7. Number of t_1 points and spectral widths are experimentally determined. Also to improve resolution (in F1), isolated peaks can be folded into the spectrum. In deciding the number of data sets to collect, it is typical to repeat three frequency points in the CPMG to determine significance of data.
8. NMRPipe script for separating the pseudo 3D CPMG relaxation dispersion data into single 2D files. These single files can then be processed similarly to a 2D ^{1}H, ^{15}N HSQC spectrum.

```
bruk2pipe -in ./ser \
  -bad 0.0 -aswap -DMX -decim 2218.66666666667 -dspfvs
20 -grpdly 67.9862518310547 \
 -xN 2048 -yN 16 -zN 256 \
 -xT 1024 -yT 16 -zT 128 \
 -xMODE DQD -yMODE real -zMODE Echo-AntiEcho \
```

```
-xSW 10416.667 -zSW 2351.499 \
-xOBS 800.133 -zOBS 81.086 \
-xCAR 4.703 -zCAR 119.000 \
-xLAB HN -zLAB 15N \
-ndim 3 -aq2D States \
| nmrPipe -fn TP \
| nmrPipe -fn ZTP \
| nmrPipe -fn TP -hyper \
| pipe2xyz -x -out ./fid/test_%03d.fid -verb -ov
```

9. For estimation of errors of the nonlinear fits of CPMG relaxation dispersion data, *see* [5, 12].

References

1. Koay A, Rimmer KA, Mertens HD et al (2007) Oligosaccharide recognition and binding to the carbohydrate binding module of AMP-activated protein kinase. FEBS Lett 581:5055–5059
2. Koay A, Woodcroft B, Petrie EJ et al (2010) AMPK beta subunits display isoform specific affinities for carbohydrates. FEBS Lett 584:3499–3503
3. Mobbs JI, Koay A, Di Paolo A et al (2015) Determinants of oligosaccharide specificity of the carbohydrate-binding modules of AMP-activated protein kinase. Biochem J 468:245–257
4. Navratilova I, Papalia GA, Rich RL et al (2007) Thermodynamic benchmark study using Biacore technology. Anal Biochem 364:67–77
5. Demers JP, Mittermaier A (2009) Binding mechanism of an SH3 domain studied by NMR and ITC. J Am Chem Soc 131:4355–4367
6. Velazquez-Campoy A, Ohtaka H, Nezami A et al. (2004) Isothermal titration calorimetry. Curr Protoc Cell Biol. Chapter 17:Unit 17 18
7. Kleckner IR, Foster MP (2011) An introduction to NMR-based approaches for measuring protein dynamics. Biochim Biophys Acta 1814:942–968
8. Henzler-Wildman K, Kern D (2007) Dynamic personalities of proteins. Nature 450:964–972
9. Vafabakhsh R, Levitz J, Isacoff EY (2015) Conformational dynamics of a class C G-protein-coupled receptor. Nature 524:497–501
10. Farrow NA, Zhang O, Forman-Kay JD et al (1994) A heteronuclear correlation experiment for simultaneous determination of 15N longitudinal decay and chemical exchange rates of systems in slow equilibrium. J Biomol NMR 4:727–734
11. Loria JP, Rance M, Palmer AG (1999) A relaxation-compensated carr-purcell-meiboom-gill sequence for characterizing chemical exchange by NMR spectroscopy. J Am Chem Soc 121:2331–2332
12. Korzhnev DM, Salvatella X, Vendruscolo M et al (2004) Low-populated folding intermediates of Fyn SH3 characterized by relaxation dispersion NMR. Nature 430:586–590
13. Meneses E, Mittermaier A (2014) Electrostatic interactions in the binding pathway of a transient protein complex studied by NMR and isothermal titration calorimetry. J Biol Chem 289:27911–27923
14. Bieri M, Mobbs JI, Koay A et al (2012) AMP-activated protein kinase beta-subunit requires internal motion for optimal carbohydrate binding. Biophys J 102:305–314
15. Gill SC, Von Hippel PH (1989) Calculation of protein extinction coefficients from amino acid sequence data. Anal Biochem 182:319–326
16. Delaglio F, Grzesiek S, Vuister GW et al (1995) NMRPipe: a multidimensional spectral processing system based on UNIX pipes. J Biomol NMR 6:277–293
17. Sugase K, Lansing JC, Dyson HJ et al (2007) Tailoring relaxation dispersion experiments for fast-associating protein complexes. J Am Chem Soc 129:13406–13407
18. Cai M, Huang Y, Sakaguchi K et al (1998) An efficient and cost-effective isotope labeling protocol for proteins expressed in Escherichia Coli. J Biomol NMR 11:97–102
19. Marley J, Lu M, Bracken C (2001) A method for efficient isotopic labeling of recombinant proteins. J Biomol NMR 20:71–75

Chapter 7

Bioinformatics Approach to Identify Novel AMPK Targets

Brendan Gongol, Traci Marin, David A. Johnson, and John Y.-J. Shyy

Abstract

In silico analysis of Big Data is a useful tool to identify putative kinase targets as well as nodes of signaling cascades that are difficult to discover by traditional single molecule experimentation. System approaches that use a multi-tiered investigational methodology have been instrumental in advancing our understanding of cellular mechanisms that result in phenotypic changes. Here, we present a bioinformatics approach to identify AMP-activated protein kinase (AMPK) target proteins on a proteome-wide scale and an in vitro method for preliminary validation of these targets. This approach offers an initial screening for the identification of AMPK targets that can be further validated using mutagenesis and molecular biology techniques.

Key words AMPK target validation, AMPK kinase assay, Consensus sequence mapping, R programming, Bioinformatics, Systems biology

1 Introduction

In silico bioinformatics provides powerful tools and methods to delineate novel insights from complex biological datasets (Big Data) such as signaling cascades emanating from posttranslational modifying enzymes including kinases [1, 2]. AMP-activated protein kinase (AMPK), a master regulator of cellular stress response and energy status, is a serine/threonine kinase that is a potential actionable clinical target [1, 2]. However, because knowledge of its target spectrum is incomplete, consensus sequence mapping can be utilized to reveal unrecognized targets. The most stringent phosphorylation consensus sequence (PCS) of AMPK is βφβXXXS/TXXXφ, where hydrophobic, φ = M, L, I, F, or V; basic, β = R, K, or H; X = any amino acid; and S/T = phosphorylation site [3, 4]. However, AMPK phosphorylation sites have been identified that lack the basic residues [1]. Several databases have been established that predict putative AMPK targets including Scansite [5]. A major hurdle in the identification of AMPK targets is the structural variations due to Brownian motion that occur between

Dietbert Neumann and Benoit Viollet (eds.), *AMPK: Methods and Protocols*, Methods in Molecular Biology, vol. 1732, https://doi.org/10.1007/978-1-4939-7598-3_7,

the kinase and substrate. Other pattern matching algorithms, including Scansite, utilize position weight matrices to create a probability score for the identified site. In this method, the stringency for the AMPK target identified depends on the construction of logical operators within the pattern matching function itself. An advantage of this strategy is the integration of identified putative targets into an R script that allows customizable integration with resources listed on Bioconductor (https://www.bioconductor.org/) for further categorization. Here, we present a two-step protocol to identify and to preliminarily validate unrecognized AMPK targets. The first step utilizes the open-source R software platform and specific coding required for the mapping of the PCS to a proteome in search for proteins that contain the AMPK PCS [6]. The coding includes annotation of peptide sequences with peptide IDs and known gene symbols that are imported into an Excel workbook. The second step of the protocol involves preliminary target validation and describes the use of radiolabeled ATP ([γ-^{32}P] ATP) in conjunction with autoradiography to assess the susceptibility of putative target phosphorylation by AMPK.

2 Materials

All reagents should be molecular biology grade prepared with ultrapure double deionized water with a sensitivity of 18 MΩ-cm at 25 °C and should be stored at room temperature unless otherwise indicated. Proper protective equipment should be worn at all times including gloves, a lab coat, and an eye protection. Additionally, all preparations using [γ-^{32}P]ATP should be performed behind appropriate radiation shields in an environmental health and safety (EH&S)-approved area. It is also necessary to follow appropriate decontamination procedures and dispose all waste materials via EH&S-approved methods.

2.1 Materials for In Silico Analyses

A Windows-, Mac-, or Linux OS-based computer with a minimum of 8 gigabytes (gb) of random access memory (ram), 250 gigabytes of storage, and connected to the Internet.

2.2 Materials for AMPK Kinase Assay

Kinase Assay

1. Aluminum foil.
2. Purified activated recombinant AMPKαβγ heterotrimer. Recombinant AMPK complexes can be purified from bacterial, insect, or mammalian cell lysates (*see* Chapters 1–3, 5, and 10) or purchased commercially [1, 2]. Store at −80 °C or according to the manufacturer's instructions, and thaw on ice prior to use (*see* **Note 1**).

3. Purified recombinant target protein. Target protein can be purified from cell lysate or purchased commercially. Store at −80 °C or according to the manufacturer's instructions, and thaw on ice prior to use (*see* **Note 1**).
4. [γ-^{32}P] ATP: 250 μCi (3000 Ci/mmol) diluted to 10 mCi/ml and shielded in lead [1] (*see* **Note 2**).
5. Adenosine 5′-monophosphate (AMP) solution: 10 mM AMP in distilled water. Store at −80 °C and thaw on ice prior to use [1].
6. Magnesium chloride ($MgCl_2$) solution: 250 mM $MgCl_2$ in distilled water. Store on ice.
7. Heating block: must be capable of holding a constant temperature between 37 °C and 100 °C.
8. Centrifuge tubes: must hold at least 50 μl total volume.
9. Buffer A: 50 mM HEPES, pH 7.4 (*see* **Notes 3** and **4**).

Protein Separation

10. SDS-PAGE gels: commercially available.
11. Tris-glycine running buffer: 0.025 M Tris, 0.192 M glycine, 0.1% (w/v) SDS prepared in distilled water or obtained commercially.
12. 4× Laemmli sample buffer: 200 mM Tris–HCl, pH 6.8, 8% (w/v) SDS, 40% (v/v) glycerol, 4% (v/v) β-mercaptoethanol, 0.05 M EDTA, 0.08% (w/v) bromophenol blue prepared in distilled water or obtained commercially.
13. Vertical SDS-PAGE electrophoresis system: commercially available.
14. Orbital shaker or rocker: commercially available.
15. SDS-PAGE molecular weight markers: commercially available.
16. Coomassie R-250 stain: 0.1% (w/v) Coomassie Brilliant Blue R-250, 5% (v/v) methanol prepared in 10% (v/v) glacial acetic acid and filtered through Whatman filter paper with a minimum grade of one to remove any aggregated stain. It is also commercially available.
17. Destaining solution: 5% (v/v) methanol, 10% (v/v) acetic acid diluted in distilled water or commercially available.

Film Development

18. Whatman paper: grade one or equivalent wide enough to cover the entire gel.
19. Transparency sheets: commercially available.
20. Laboratory tape: commercially available.
21. Autoradiograph cassette: commercially available.

22. Autoradiography film: commercially available.
23. Film fixative and developer: commercially available.
24. Automated film developer (optional) or two plastic trays: must be large enough to accommodate the autoradiography film.

3 Methods

3.1 Identification of Proteins Containing AMPK Consensus Sequence

1. Install R statistical software from the comprehensive R archive network (CRAN) (https://cran.r-project.org/).
2. Once R is installed, install and open RStudio (https://www.rstudio.com/).
3. Operating within RStudio, the following packages should be installed by entering the following lines of code at the console (*see* **Notes 5** and **6**):

```
source("http://bioconductor.org/biocLite.R");
biocLite("Biostrings");
source("https://bioconductor.org/biocLite.R");
biocLite("biomaRt");
install.packages("data.table");
install.packages("stringr")
```

4. Load required libraries by running the following code at the console in RStudio (*see* **Note 7**):

```
library(Biostrings); library(data.table); library(stringr); library(biomaRt)
```

5. Download proteomes from ensemble:

Files downloaded from http://uswest.ensembl.org/info/data/ftp/index.html. Other proteome sources can be used; however, the files need to be organized in FASTA format. Alternatively, the human GRCh38 proteome can be downloaded by running the following code at the console in RStudio (*see* **Note 8**):

```
URL <- "ftp://ftp.ensembl.org/pub/release
 87/fasta/homo_sapiens/pep/Homo_sapiens.GRCh38.pep.all.fa.gz";
 download.file(URL, destfile = "enter file path here/Human_Proteome.fa.gz")
```

6. Load downloaded proteomes into R by running the following code at the console in RStudio (*see* **Notes 9** and **10**):

```
 proteomehuman <- readAAStringSet ("Human_Proteome.fa.gz ","fasta")
```

7. Identify protein sequences containing at least one variation of the AMPK consensus sequence by running the following code at the console in RStudio [1]:

```
 myhitshuman <- proteomehuman[grepl("(K|R|H)(L|V|M|I|A|F)....(S|T)...(I|L|V|M|A|F)|
 (L|V|M|I|A|F)(K|R|H)...(S|T)...(I|L|V|M|A|F)|
```

```
(K|R|H)(L|V|M|I|A|F)(K|R|H)...(S|T)...(I|L|V|M|A|F)", proteomehuman)]
```

8. Remove any duplicated hits by running the following code at the console in RStudio:

```
humanduprm <- myhitshuman[!duplicated(myhitshuman),]
```

9. Compile the protein sequences containing an AMPK consensus sequence to individual strings by running the following code at the console in RStudio:

```
seq <- NULL;
for (z in 1:length(humanduprm)){;
seq[z] <- toString(humanduprm[z])};
Sequence <- data.table(sequence=seq)
```

10. Compile protein IDs by running the following code at the console in RStudio:

```
accession <- data.table(longname=humanduprm@ranges@NAMES);
accession[,ensembl_peptide_id:= word(longname)];
accession$longname <- NULL;
accession$ensembl_peptide_id <- sub("\cr..*", "", accession$ensembl_peptide_id)
```

11. Download gene symbols IDs by running the following code at the console in RStudio:

```
Keys <- accession$ensembl_peptide_id
mymarthuman <- useMart("ENSEMBL_MART_ENSEMBL",
  host="www.ensembl.org");
mymarthuman
useMart("ENSEMBL_MART_ENSEMBL",dataset="hsapiens_gene_ensembl",
host="www.ensembl.org");
myhitshuman_genename <- getBM(attributes=c("ensembl_peptide_id",
"external_gene_name"), values = Keys, mart = mymarthuman)
```

12. Create a data table by running the following code at the console in RStudio:

```
myhitshuman <- cbind(Sequence, accession);
myhitshuman <- merge(myhitshuman, myhitshuman_genename, by =
    "ensembl_peptide_id")
```

13. The data table can then be written out to an Excel workbook by running the following code at the console in RStudio (*see* **Notes 11** and **12**):

```
write.table(myhitshuman, file = "AMPK consensus sequence containing proteins.xls",
    sep = "\t", quote = FALSE, row.names = FALSE)
```

3.2 Validation of Putative AMPK Targets

All procedures are to be performed at room temperature unless otherwise specified.

1. Prepare a fresh SDS-PAGE gel for each putative target (*see* **Note 13**). For each target protein of interest, prepare two reaction tubes: one with and one without AMPK. For reactions containing AMPK, prepare Buffer B by adding 1 μl of recombinant AMPK to 3 μl of Buffer A (*see* **Note 4**).
2. In a clean centrifuge tube, prepare Buffer C by adding 1 μl of 250 mM $MgCl_2$, 0.4 μl of [γ-^{32}P] ATP, 5 μl of 10 mM AMP, and 3.6 μl of Buffer A (*see* **Note 4**).
3. On ice, add 10 μl of Buffer C to each reaction tube, 1 μg of target substrate, 4 μl of Buffer B for reactions containing AMPK, and bring the reaction volume to 50 μl with Buffer A (*see* **Notes 14–16**).
4. Incubate reactions at 37 °C for 1 h (*see* **Note 17**).
5. Stop reactions with the addition of 16.7 μl of 4× Laemmli buffer, and place in the heating block set at 100 °C for 15 min.
6. While the reactions are incubated, set up SDS-PAGE electrophoresis equipment per the manufacturer's instructions, and fill the inner and outer buffer chambers with Tris-glycine running buffer [7, 8].
7. Load equal volumes of each sample into individual wells, set the power supply to 100 volts, and operate until the bromophenol reaches the bottom of the gel.
8. Remove the gel from the electrophoresis cassette, immerse it in Coomassie stain, and gently agitate with the orbital shaker or rocker for 15 min or until the Coomassie stain has completely penetrated the gel.
9. Place the gel in destaining solution and gently agitate. Periodically change the destaining solution until the gel regains its transparent appearance and the target protein bands are clearly visible. Note that under the reaction conditions present in this protocol, AMPK subunit concentrations are below the detectable limit of Coomassie stain. At this point, a Geiger counter can be used to assess the level of radiation in the gel. Be sure the gel is not submerged in destaining solution while assessing the radioactivity, because water will shield radiation causing a false reading (Fig. 1).
10. Lay a clean transparency sheet on a bench or flat surface. Dampen a piece of Whatman filter paper with water and lay it on top of the transparency sheet. Gently remove the gel from destaining solution and place it on top of the Whatman paper. Once the gel is in place and flat on the Whatman paper, lay a

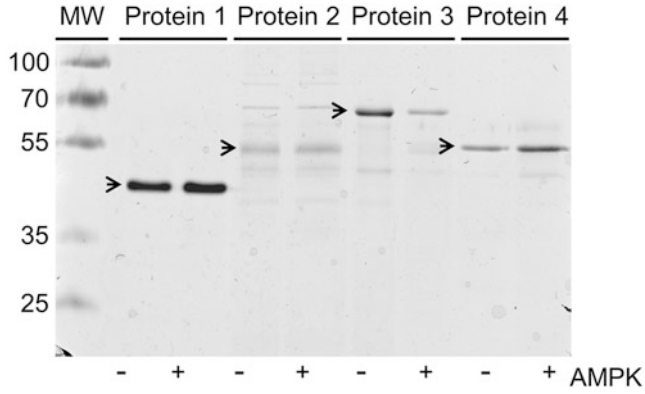

Fig. 1 Analysis of kinase assay loading. Coomassie stained gel containing AMPK and target protein substrates. MW indicates the lane containing the molecular weight markers. Molecular weights corresponding to each band are listed to the left of the figure. Protein bands corresponding to purified targets are indicated with arrows. Lanes containing AMPK in the reaction are indicated with a "+" at the bottom of the gel, while those without AMPK are indicated by a "−"

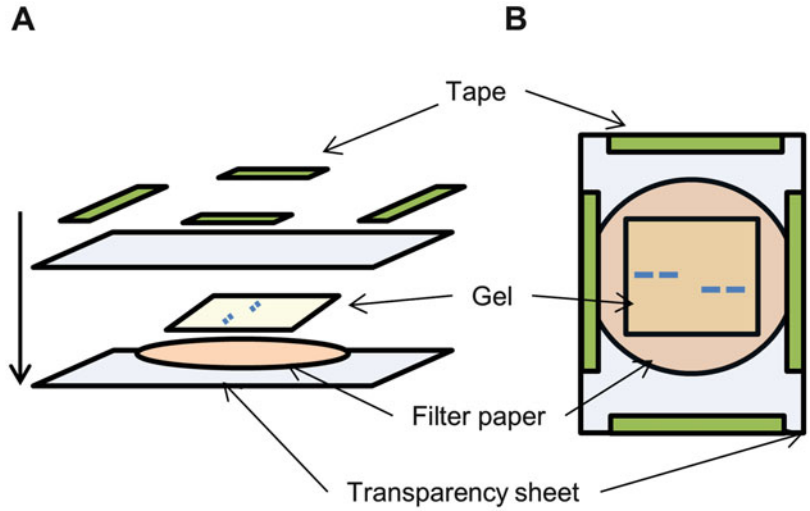

Fig. 2 Coomassie gel set up for autoradiography. (**a**) Side view and (**b**) top-down view of gel set up for autoradiography. Individual components are labeled accordingly

second piece of transparency sheet over the gel and then secure with laboratory tape (Fig. 2).

11. (Optional) Use gel drying equipment to dry the gel. This may increase the radiation signal but is not always necessary (*see* **Note 18**).
12. Place the gel with transparency sheet into an autoradiography cassette. In a dark room, position three to five autoradiography films over the gel and allow exposure to occur from 1 h to

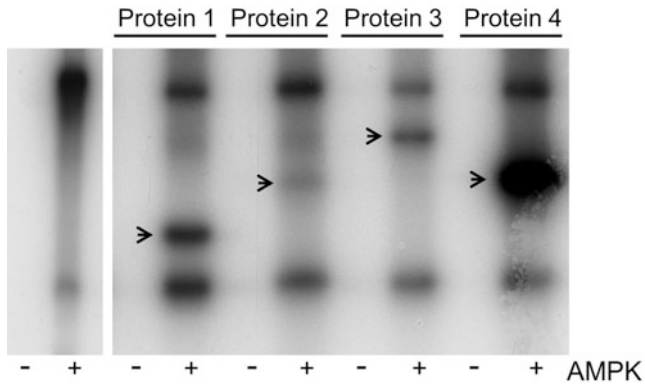

Fig. 3 Final autoradiography results. Autoradiograph of AMPK alone (left panel) or in the presence of target substrates (right panel). Autoradiograph bands resulting from γ-^{32}P incorporation into target proteins are indicated with arrows. Lanes containing AMPK in the reaction are indicated with a "+" at the bottom of the gel, while those without AMPK are indicated by a "−". These data indicate that AMPK can phosphorylate the target substrates in vitro and that phosphorylation of these targets is dependent on AMPK since the target substrate incubated without AMPK does not illustrate an autoradiograph band

2 weeks depending on the radiant intensity of the sample (*see* **Note 19**).

13. Following exposure, the films can be developed in a dark room one at a time by running through an automated developer. If an automated developer is unavailable, develop one film at a time by submerging in a tray containing developer with gentile agitation for 1–5 min prior to placing it in the fixative solution with gentle agitation for 1–5 min. Wash with water and hang to dry. Positive results will appear as a third band on the autoradiograph (Fig. 3).

4 Notes

1. Due to the sensitivity of recombinant proteins to degradation by freezing and thawing, it is best to aliquot recombinant proteins into single-use aliquots to minimize the loss of AMPK activity.
2. Because [γ-^{32}P] ATP has a half-life of 2 weeks, it should be used soon after arrival for optimal results.
3. It is recommended to prepare fresh HEPES buffer prior to use, and the pH should be adjusted to 7.4.
4. Buffer A, B, and C should be kept on ice.
5. For each step, the codes should be entered as single lines at the console in RStudio.
6. Refer to Entrosolve.com for programming assistance if necessary.

7. The error "Error in library() : there is no package called "" indicates that the package is not installed. Rerun the code listed in the materials section of the protocol.
8. The user must enter their working directory file path name where the R code prompts "enter file path here."
9. The error "Error: could not find function" indicates that the library has not been installed or loaded. Rerun the code listed in the materials section of the protocol or the first step of the methods to install and load the package.
10. The error "Error in .Call2("new_input_filexp", filepath, PACKAGE = "XVector") : cannot open file 'Human_Proteome.fa.gz '" indicates that the Human_Proteome.fa.gz file is not located in your working directory. Change your working directory to the location of the file.
11. The final Excel sheet produced by the R script is saved in the user's working directory. This can be found by typing "getwd ()" at the console in RStudio. To list the files in your working directory from R, type "dir()" at the console in RStudio. To change the user's working directory, navigate in the header in RStudio to Session → Set Working Directory → Choose Directory, and then select the desired location of the working directory. Alternatively, enter the following code at the console in RStudio: setwd("Path to directory").
12. This protocol results in the identification of 44,762 proteins. Putative target selection is dependent on the interest of the researcher. Further stratification can be accomplished by assessing species conservation. This can be accomplished by rerunning the script using a FASTA file containing protein sequences from a different species. Additionally, conducting gene ontology analysis (GO) may be used to further characterize putative targets. To accomplish this, the investigator may download additional annotation information such as Gene Ontology from biomaRT (https://www.bioconductor.org/packages/release/bioc/html/biomaRt.html). To list available annotation information and download GO identifiers, the researcher may replace the following code in **step 11** of Subheading 3.1:

```
Keys <- accession$ensembl_peptide_id
mymarthuman <- useMart("ENSEMBL_MART_ENSEMBL", host="www.ensembl.org")
mymarthuman <-
useMart("ENSEMBL_MART_ENSEMBL",dataset="hsapiens_gene_ensembl",
host="www.ensembl.org")
listAttributes(mymarthuman)
myhitshuman_genename <- getBM(attributes=c("ensembl_peptide_id", "external_gene_name",
"go_id", "definition_1006"), values = Keys, mart = mymarthuman)
```

13. SDS-PAGE gel percentage must be optimized to ensure maximum separation between AMPK subunits and target proteins of interest. The molecular weight of AMPK according to each subunit is as follows: α (64 kDa), β (30 kDa), and γ (38 kDa) subunits of AMPK.
14. It is recommended to use both positive and negative controls. Negative controls can also be used to identify proteins that contain autophosphorylation activity under the experimental conditions.
15. The ratio of kinase to target protein in the kinase reaction assay may be adjusted, but be aware that nonspecific phosphorylation is more likely to occur as the concentration of AMPK and target substrates are increased.
16. As AMPK has autophosphorylation activity, reactions containing AMPK alone can be used as a control [1]. However, it may also be necessary to use reactions containing a known substrate of AMPK such as acetyl-coA carboxylase (ACC) as a positive control [9].
17. Reaction incubation time may be adjusted; however, 1 h for kinase reactions is usually sufficient to obtain positive autoradiographs.
18. Gels that are not dried prior to developing the autoradiograph film may have some radiation shielded. If no autoradioactivity is detected, drying the gel may intensify the signal.
19. The autoradiograph exposure time depends on the level of radiant intensity of each sample. If no radiation is detected with short exposure times, increasing the exposure time to 12 h or even several days may be beneficial [10].

Acknowledgments

This work was supported in part by NIH research grants R01 HL89940 and R01 HL108735 (JS) and Loma Linda University GRASP 699349 (BG), GRASP 699330 (TM), and GRASP 699336 (TM).

References

1. Marin TL, Gongol B, Martin M, King SJ, Smith L, Johnson DA, Subramaniam S, Chien S, Shyy JY (2016) Identification of AMP-activated protein kinase targets by a consensus sequence search of the proteome. BMC Syst Biol 11:9–13
2. Marin TL, Gongol B, Zhang F, Martin M, Johnson DA, Xiao H, Wang Y, Subramaniam S, Chien S, Shyy JY (2017) AMPK promotes mitochondrial biogenesis and function by phosphorylating the epigenetic factors DNMT1, RBBP7, and HAT1. Sci Signal 10(464):eaaf7478

3. Towler MC, Hardie DG (2007) AMP-activated protein kinase in metabolic control and insulin signaling. Circ Res 100:328–341
4. Leff T (2003) AMP-activated protein kinase regulates gene expression by direct phosphorylation of nuclear proteins. Biochem Soc Trans 31:224–227
5. Schaffer BE, Levin RS, Hertz NT, Maures TJ, Schoof ML, Hollstein PE, Benayoun BA, Banko MR, Shaw RJ, Shokat KM, Brunet A (2015) Identification of AMPK phosphorylation sites reveals a network of proteins involved in cell invasion and facilitates large-scale substrate prediction. Cell Metab 22:907–921
6. Eglen SJ (2009) A quick guide to teaching R programming to computational biology students. PLoS Comput Biol 5(8):e1000482
7. Brunelle JL, Green R (2014) One-dimensional SDS-polyacrylamide gel electrophoresis (1D - SDS-PAGE). Methods Enzymol 541:151–159
8. Hwang AC, Grey PH, Cuddy K, Oppenheimer DG (2012) Pouring and running a protein gel by reusing commercial cassettes. J Vis Exp 60:3465
9. Park SH, Gammon SR, Knippers JD, Paulsen SR, Rubink DS, Winder WW (1985) Phosphorylation-activity relationships of AMPK and acetyl-CoA carboxylase in muscle. J Appl Physiol 92:2475–2482
10. Huebner VD, Matthews HR (1985) Autoradiography of gels containing (32)p. Methods Mol Biol 2:51–53

Chapter 8

Studying AMPK in an Evolutionary Context

Arpit Jain, Valentin Roustan, Wolfram Weckwerth, and Ingo Ebersberger

Abstract

The AMPK protein kinase forms the heart of a complex network controlling the metabolic activities in a eukaryotic cell. Unraveling the steps by which this pathway evolved from its primordial roots in the last eukaryotic common ancestor to its present status in contemporary species has the potential to shed light on the evolution of eukaryotes. A homolog search for the proteins interacting in this pathway is considerably straightforward. However, interpreting the results, when reconstructing the evolutionary history of the pathway over larger evolutionary distances, bears a number of pitfalls. With this in mind, we present a protocol to trace a metabolic pathway across contemporary species and backward in evolutionary time. Alongside the individual analysis steps, we provide guidelines for data interpretation generalizing beyond the analysis of AMPK.

Key words AMPK evolution, Targeted ortholog search, Feature architecture, Functional equivalence, Phylogenetic profiles

1 Introduction

Technological advances and continuing drop in prices [1] have rendered genome sequencing a routine task in biological research. The ultimate goal of any sequencing project is to characterize structural and functional components in a genome shedding light on the metabolic characteristics of the corresponding species. Comprehensive experimental characterization of protein function is however limited to only few model organisms. In the case of "non-model" organisms, for which protocols for experimental research are often not established, or which are even uncultivable under lab conditions, analyses rely on bioinformatics approaches to transfer annotations of protein functions from model organisms. Phylogenetic profiling is the current state-of-the-art bioinformatics technique to reconstruct the evolutionary history of genes and pathways [2], to predict protein–protein interactions [3], and to infer functional similarities between proteins [4]. The phylogenetic profile for a gene is constructed as a {1,0} vector representing the presence (1) or absence (0) of homologs in contemporary species.

Dietbert Neumann and Benoit Viollet (eds.), *AMPK: Methods and Protocols*, Methods in Molecular Biology, vol. 1732, https://doi.org/10.1007/978-1-4939-7598-3_8,

To increase the precision of evolutionary conclusions that can be drawn from phylogenetic profiles, it is common to use the subset of homologs, which descended from a common ancestor through a speciation event, so-called orthologs [5]. Orthologs serve as an indispensable resource to reconstruct the evolutionary relationships of species [6]. At the same time two orthologs represent the mutually closest related sequences in the genomes of two species. It is thus that orthologs are considered as the best guess when aiming at the identification of functional equivalents in the genome of newly sequenced species [7–9]. However, also orthologs can diverge in their function, and this change becomes more likely the more time has passed since their separation from a shared ancestral sequence. As a consequence, the function a protein exerts in a pathway might be younger than the protein itself. This makes a careful curation necessary before one can assume a functional equivalence between two orthologous sequences [9–11].

In the light of the above, we present a comprehensive workflow to study the evolution of a functional pathway that has been described in a given model species. This elucidates the progressive construction of this pathway over evolutionary time and, at the same time, facilitates the identification of the corresponding pathways—or of parts of it—in the genomes of non-model organisms. We illustrate our approach by tracing the AMPK pathway across the three domains of life [12]. We collect the AMPK pathway components (121 proteins) from the KEGG database [13] and perform a targeted ortholog search using each of the 121 proteins to seed its phylogenetic profile. We then infer for each of the detected orthologs the extent of protein feature architecture similarity to the seed protein. Precisely, we calculate a feature architecture similarity score ranging between 0 (no similarity) and 1 (ortholog displays all features of the seed), and assess whether the ortholog is likely to share the same function with the the seed. Lastly, we provide a novel R/Shiny-based application to dynamically visualize multilayered phylogenetic profiles.

2 Materials

The following collection provides all relevant data sources and bioinformatics tools for analyzing proteins in a functional and evolutionary context. We assume basic knowledge in bioinformatics sequence data processing and management. Prior experiences with working in a Unix shell, such as the *bash*, will be helpful; however, it is considerably straightforward to acquire this knowledge in the course of the analysis. To keep the protocol concise, we do not list all alternative software choices for the individual analysis steps. Instead, we have exemplarily selected those tools that we have successfully applied in our daily routine. If the reader prefers one

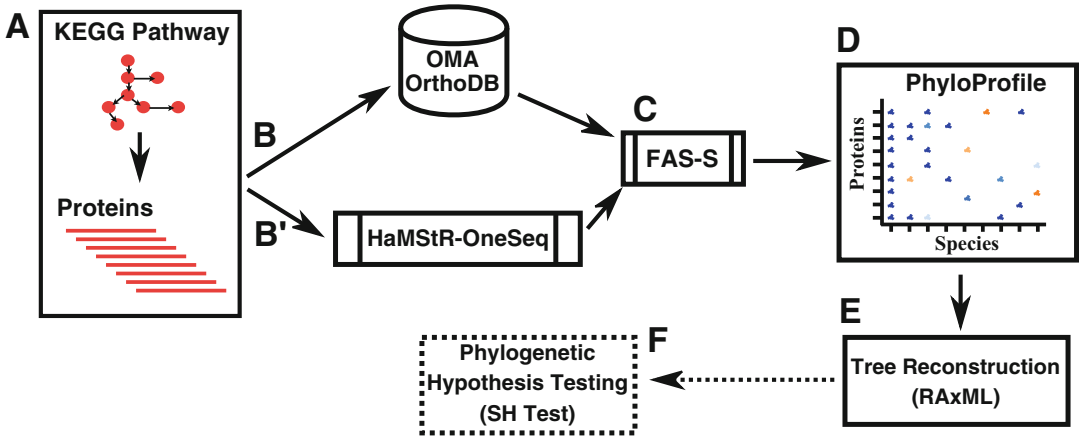

Fig. 1 Example workflow for tracing the evolutionary history of a metabolic pathway. (**a**) Identify the pathway of interest and retrieve the protein sequences for the individual pathways components from the KEGG database. (**b**) For every protein, retrieve orthologs in a selection of target taxa from public databases. (**b′**) Alternatively identify orthologs using a targeted ortholog search with HaMStR-OneSeq. (**c**) Compute for each ortholog its pairwise feature architecture similarity (FAS) to the seed protein. Note that this step is already integrated into the HaMStR-OneSeq search. (**d**) Create a phylogenetic profile displaying orthologs and FAS information for all pathway components with PhyloProfile. (**e**) Reconstruct the evolutionary relationships for individual or collections of seed proteins with RAxML. (**f**) Optionally, test the resulting sequence tree against an expected phylogeny, e.g., the species tree

particular tool over the one that we have listed, it is easy to substitute it in the analysis workflow (Fig. 1). All analyses can be run on a typical desktop computer with at least 8 GB RAM and 500 GB disk space. We suggest any Linux distribution or alternatively Mac OSX as operating systems. Make sure that Perl (≥v5.22.1), Python (v2.7), JAVA (≥v1.7), and R (≥v3.3.3) are installed.

2.1 Protein Sequence Databases

You can generate a data collection optimized for your analysis from a plethora of different public web pages and data repositories. Note that almost all data is generated from draft genome sequences. Thus, a fraction of the genome is not represented in the assembly, and the annotation of genes is likely to be incomplete. Therefore, a fraction of genes that are encoded in a species' genome might not be represented in the reconstructed gene set.

2.1.1 Joint Genome Institute (JGI) Genome Portal [14]

The JGI genome portal (http://genome.jgi.doe.gov) provides access to all JGI genome databases. The complete gene sets for individual species from all areas of the tree of life are available for download through an ftp server (*see* **Note 1**). The JGI **G**enome **O**n**L**ine **D**atabase (https://gold.jgi.doe.gov/) provides an excellent start for compiling a data set.

2.1.2 National Center for Biotechnology Information (NCBI)

NCBI (https://www.ncbi.nlm.nih.gov/) provides an open-source web server for searching and retrieving protein and nucleotide

sequences. An FTP server (ftp://ftp.ncbi.nlm.nih.gov/genomes) facilitates the bulk download even of larger selections of genomes.

2.1.3 Universal Protein Resource (UniProt) [15]

UniProt has a dedicated database for providing access to the gene sets (here called "proteomes") of organisms with a genome sequence available. Visit the site http://www.uniprot.org/proteomes to access the protein sequences and their annotations.

2.1.4 Ensembl [16]

Ensembl (http://www.ensembl.org/) is a comprehensive genome browser for high-quality vertebrate genomes. Ensembl provides access to the annotated gene sets in the individual genomes via the data mining tool, BioMart. Ensembl Genomes (http://ensemblgenomes.org/) extends the genome information of Ensembl across the taxonomic space and provides access to non-vertebrate genome resources. Currently, five projects are maintained dedicated to the genomes of bacteria, plants, protists, metazoa, and fungi, respectively.

2.1.5 Quest for Orthologs Reference Proteomes [17]

The Quest For Orthologs (QfO) Reference Proteomes (http://www.ebi.ac.uk/reference_proteomes) is a collection of complete nonredundant gene sets for a curated compilation of species representing the three domains of life. Each gene is represented here by one protein.

2.1.6 Others

There are several other genome databases that provide access to potentially relevant sequence data. Among these are the Baylor College (https://www.hgsc.bcm.edu/), the Saccharomyces Genome Database (http://www.yeastgenome.org/), the CryptoDB (http://cryptodb.org/cryptodb/), and the Candida Genome Database (http://www.candidagenome.org/).

2.2 Pathway Databases

2.2.1 KEGG Pathways [13]

KEGG pathways (http://www.genome.jp/kegg/pathway.html) are a collection of manually curated molecular interaction and reaction networks based on the experimental analysis of well-studied model organisms.

2.2.2 WikiPathways Database [18]

The WikiPathways database (http://www.wikipathways.org/index.php/WikiPathways) is an open collaborative project to complement pathway information available from ongoing efforts, such as KEGG [13], Reactome [19], or Pathway Commons [20].

2.3 Software for Ortholog Search

2.3.1 InParanoid [21]

InParanoid is a software for identifying orthologs in pairs of species. According to a recent benchmark [22], the tool provides a good balance between accuracy and sensitivity. An online database is available at http://inparanoid.sbc.su.se/cgi-bin/index.cgi, and the InParanoid software can be downloaded for stand-alone ortholog searches.

2.3.2 OMA [23]

OMA (http://omabrowser.org/oma/home/) is a comprehensive database providing access to precomputed orthologs on different levels of inclusiveness. Orthologs between pairs of species—similar to the InParanoid orthologs—are the most inclusive level. They are complemented by hierarchical orthologous groups (HOGs) comprising sequences from more than two species. OMA groups, the most stringent level, represent cliques of orthologs for which the algorithm confirmed orthology between any pair of proteins in the group. A stand-alone version for OMA is available at http://omabrowser.org/standalone/.

2.3.3 OrthoDB [24]

OrthoDB is a comprehensive catalog of orthologous sequences across the tree of life. OrthoDB provides hierarchal orthologs for each major clade of the taxonomy. OrthoDB provides ready-to-download, precomputed orthologs for extant protein sequences (http://www.orthodb.org/). The stand-alone version for the software is available at http://www.orthodb.org/?page=software.

2.3.4 HaMStR [25]

The HaMStR package is a collection of tools to identify and annotate orthologs in collections of protein or transcript sequences. HaMStR [25] is a profile hidden Markov model (pHMM)-based method to extend predefined orthologous groups with sequences from further species. HaMStR-OneSeq [26] is an extension of the HaMStR algorithm for a targeted ortholog search starting with single seed sequences. FAS-S is a software for annotating and scoring feature architecture similarity between pairs of sequences. The HaMStR package is available at https://github.com/BIONF/HaMStR.

2.4 Software for Domain Architecture Analysis and Comparison

InterProScan annotates a query protein for the presence of protein domains, protein family classification, and other features. InterProScan is available both as a web server (http://www.ebi.ac.uk/Tools/pfa/iprscan5/) and as a stand-alone tool (ftp://ftp.ebi.ac.uk/pub/software/unix/iprscan/5/).

2.4.1 InterProScan [27]

2.4.2 Pfam Database [28]

Pfam (http://pfam.xfam.org/) is a large database comprising multiple sequence alignments (MSAs) and hidden Markov models (HMMs) of protein domains and families. The Pfam web server facilitates an online annotation of protein domains. Alternatively, the Pfam database can be downloaded for stand-alone usage, e.g., in combination with the HMMER package (*see* Subheading 2.5).

2.4.3 FAS-S

The Feature Architecture Similarity Score, FAS-S, is a stand-alone program to compare feature architecture between two protein sequences. Features here refer to protein domains, secondary structure elements, and low-complexity regions. The similarity scoring is based on an algorithm originally implemented into FACT

[29]. The tool is integrated into the HaMStR package (https://github.com/BIONF/HaMStR).

2.4.4 DoMosaics [30]

DoMosaics (http://www.domosaics.net/) is a tool to annotate and visualize protein domain architectures in protein sequences. The resulting architectures can be displayed on a user-provided phylogeny of the analyzed sequences to reconstruct domain architecture evolution over time.

2.5 Evolutionary Sequence Analysis

The HMMER package (http://hmmer.org/) is a collection of tools for the analysis of biological sequences using profile hidden Markov models. HMMER is often used together with a profile database, such as Pfam or many of the databases that participate in InterPro (http://www.ebi.ac.uk/interpro/).

2.5.1 HMMER [31]

2.5.2 MUSCLE [32]

MUSCLE is a multiple sequence alignment tool that is available both as a web server (http://www.ebi.ac.uk/Tools/msa/muscle/) and as a stand-alone tool (http://www.drive5.com/muscle/downloads.htm).

2.5.3 MAFFT [33]

The web server for the multiple sequence alignment tool MAFFT is available at http://mafft.cbrc.jp/alignment/server/ and as a stand-alone tool for download at http://mafft.cbrc.jp/alignment/software/.

2.5.4 ProtTest [34]

ProtTest (http://darwin.uvigo.es/software/prottest_server.html) facilitates the selection of best-fitting amino acid substitution model for protein sequence evolution.

2.5.5 RAxML [35]

RAxML (http://sco.h-its.org/exelixis/web/software/raxml/index.html) is a maximum likelihood tree reconstruction method.

2.6 Visualization of Phylogenetic Trees

FigTree (http://tree.bio.ed.ac.uk/software/figtree/) is a graphical tree visualization software and provides tools to output high-resolution publication-ready tree images.

2.6.1 FigTree [36]

2.6.2 Baobab

Baobab (http://kimura.univ-montp2.fr/~jdutheil/Baobab/Baobab.html) is a JAVA-based tree visualization software and allows interactive tree manipulation.

2.7 Visualization of Phylogenetic Profiles

The PhyloProfile application (https://github.com/BIONF/PhyloProfile) is a R/Shiny package to dynamically visualize and explore phylogenetic profiles.

2.8 Taxonomic Databases

The NCBI taxonomy (https://www.ncbi.nlm.nih.gov/taxonomy) is a curated classification and nomenclature for all of the organisms in the public sequence databases.

3 Methods

3.1 Collecting the Pathway Components

Identify the pathway of interest and download the involved protein sequences in FASTA format. End with a nonredundant list of proteins for downstream analysis (*see* **Note 2**).

1. Visit the KEGG pathway web site at http://www.genome.jp/kegg/pathway.html. Specify *Homo sapiens* as the species of interest by setting the "select prefix" to *hsa*, and enter the term "AMPK" into the keyword field. Run the search and select the AMPK pathway (hsa04152) from the result list (Fig. 2). This will lead you to the web page describing the human AMPK pathway in greater detail.
2. From the link list in the top right corner of the AMPK pathway web page, follow the link "KEGG GENES." This will result in a list of genes associated with this pathway (Fig. 3a). For the human AMPK pathway, the list contains 121 proteins of which each is briefly described.
3. To retrieve further information about individual genes of interest, follow the corresponding link. You will be guided to a new web page, at the bottom of which you will find the amino acid sequence of the human protein together with the coding sequence. Click on the tab "AA seq" and save the protein sequence in FASTA format (Fig. 3b).
4. A bulk download of all genes is a bit more complex, because KEGG currently provides no option for this. **Steps 5–11** can be used as a quick work-around.
5. Open a text editor and copy the list of all genes and their description into a text file.
6. To access the individual fields in the gene list, you can use the bash function *cut*. Alternatively, import the text file into a spreadsheet, e.g., Microsoft Excel. Choose "Delimited" as field separator and specify the delimiter as "space." This will place the KEGG gene identifier into the first column of your spreadsheet and protein KO identifiers in second column.
7. Copy the contents of the first column, open the UniProt [15] cross-referenced databases (http://www.uniprot.org/database/), and click on "Retrieve/ID mapping" in the menu bar.
8. Paste the KEGG identifier list in the search field. Select KEGG as database from where you have obtained the sequence identifier and UniProtKB as the database to which you want to convert your identifier. Upon hitting the "Go" button, a results page opens providing the cross-references (Fig. 3c).
9. Activate the "Filter by Reviewed" to reduce the output to the 120 Swiss-Prot entries (*see* **Note 3**). This step will get rid of

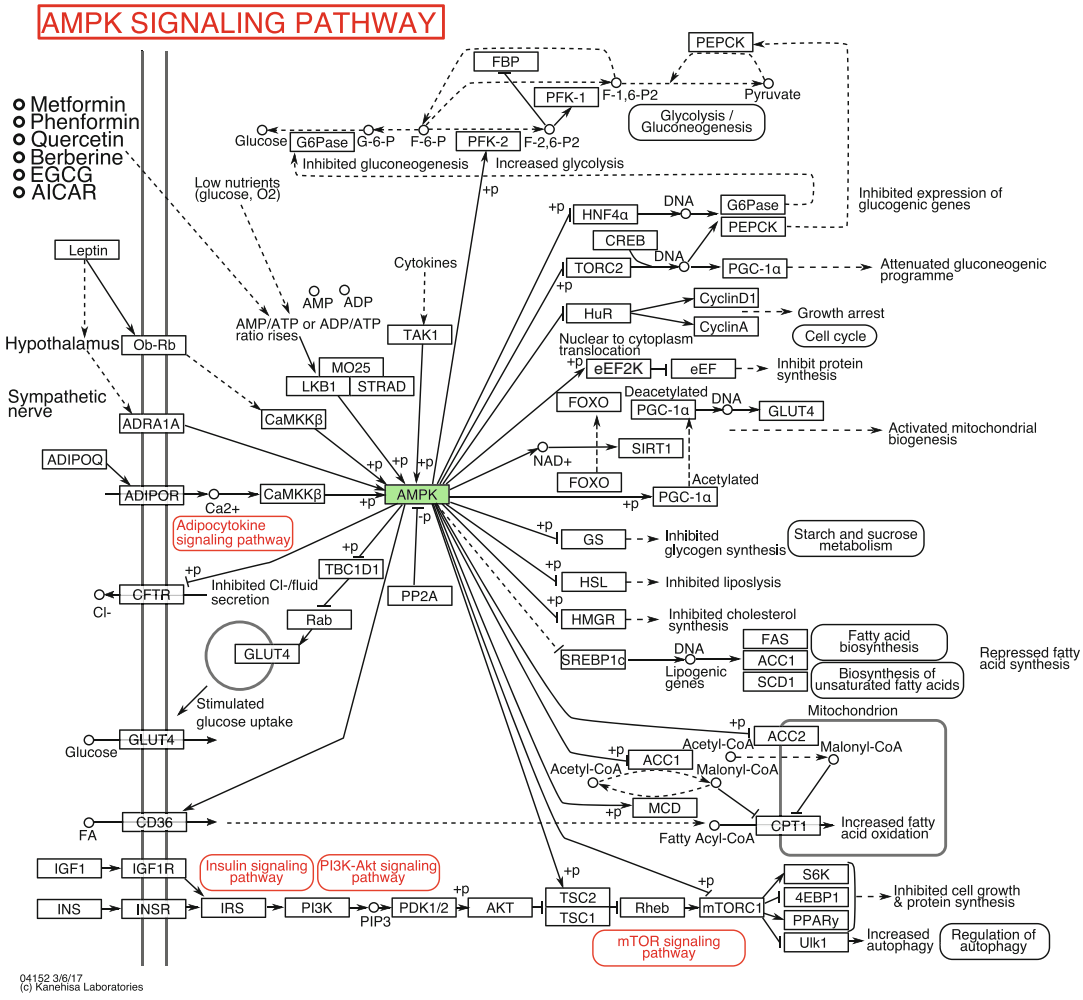

Fig. 2 Structure of the human AMPK pathway in the KEGG pathways database [13]. The AMPK is highlighted in green, connected pathways are represented in red color

redundancies due to proteins being represented both in Swiss-Prot and TrEMBL.

10. Choose "Download" from the menu and select "Fasta (canonical)" as sequence format. Download the data also as tab-separated text that can be imported into a spreadsheet for later use. Add KO identifier (*see* **step 6** in Subheading 3.1) corresponding to every protein in the cross-reference file.
11. Rename the downloaded files to something meaningful, e.g., *AMPK-hsa.fa* and *AMPK-hsa-xref.txt*.

3.2 Compiling a Set of Target Species

Select a representative set of target species for your analysis. If you consider a custom search for orthologs, end with a collection of protein sets each representing the gene set of an individual species.

(A)

Mode: Single Entry to Database
From: KEGG PATHWAY hsa04152
To: KEGG GENES
Hits: 121 from 1 database

ID	Definition
hsa:10000	K04456 RAC serine/threonine-protein kin
hsa:101930123	K08292 elongation factor 2 kinase [EC:2
hsa:10488	K09048 cyclic AMP-responsive element-bi
hsa:10645	K07359 calcium/calmodulin-dependent pro
hsa:1080	K05031 cystic fibrosis transmembrane co
hsa:10890	K07903 Ras-related protein Rab-10 | (Re
hsa:10891	K07202 alpha peroxisome proliferator-act

(B)

```
>hsa:10000 K04456 RAC serine/threonine-protein kinase [EC:2.7.11.1]
MSDVTIVKEGWVQKRGEYIKNWRPRYFLLKTDGSFIGYKEKPQDVDLPYPLNNFSVAKCQ
LMKTERPKPNTFIIRCLQWTTVIERTFHVDTPEEREEWTEAIQAVADRLQRQEEERMNCS
PTSQIDNIGEEEMDASTTHHKRKTMNDFDYLKLLGKGTFGKVILVREKASGKYYAMKILK
KEVIIAKDEVAHTLTESRVLKNTRHPFLTSLKYSFQTKDRLCFVMEYVNGGELFFHLSRE
RVFSEDRTRFYGAEIVSALDYLHSGKIVYRDLKLENLMLDKDGHIKITDFGLCKEGITDA
ATMKTFCGTPEYLAPEVLEDNDYGRAVDWWGLGVVMYEMMCGRLPFYNQDHEKLFELILM
EDIKFPRTLSSDAKSLLSGLLIKDPNKRLGGGPDDAKEIMRHSFFSGVNWQDVYDKKLVP
PFKPQVTSETDTRYFDEEFTAQTITITPPEKYDEDGMDCMDNERRPHFPQFSYSASGRE
```

(C)

Entry	Entry name	Protein names	Gene names	Organism	Length
Q96RR4	KKCC2_HUMAN	**Calcium/calmodulin-dependent protei...**	**CAMKK2** CAMKKB, KIAA0787	Homo sapiens (Human)	588
P50416	CPT1A_HUMAN	**Carnitine O-palmitoyltransferase 1,...**	**CPT1A** CPT1	Homo sapiens (Human)	773
O43889	CREB3_HUMAN	**Cyclic AMP-responsive element-bindi...**	**CREB3** LZIP	Homo sapiens (Human)	395
P13569	CFTR_HUMAN	**Cystic fibrosis transmembrane condu...**	**CFTR** ABCC7	Homo sapiens (Human)	1,480
Q9Y243	AKT3_HUMAN	**RAC-gamma serine/threonine-protein ...**	**AKT3** PKBG	Homo sapiens (Human)	479

Fig. 3 Retrieving annotated pathway components from KEGG pathways database. (**a**) An example output from clicking "KEGG GENES" link for the AMPK pathway. (**b**) Amino acid sequence for gene id "hsa:10000" obtained from the KEGG database in FASTA format. The first line starting with ">" is the sequence identifier. (**c**) Tab-delimited cross-reference table resulting from the online conversion of KEGG gene ids to UniProt ids

Compiling the sequence databases for your study is a critical task, but analysis scenarios are too diverse to give an all-embracing recipe. In the following we provide some general guidelines.

1. Make sure that your data collection is not a black box. You should always know exactly which species are represented and how they are related. Moreover, the assumption that the entire gene set of a species is represented in the database should—at least approximately—hold. Don't forget in this context that the non-detection of a pathway component in a particular species might have a relevant functional implication (*see* **Note 4**).
2. Select species such that they cover the full phylogenetic range you are interested in. For example, if you are focusing on pathway evolution in fungi, use a representative set of fungal species plus a couple of close outgroup species, e.g., animals. Plant or bacterial genomes are probably only adding to the complexity of the analysis and are likely to provide no further insights.
3. Sub-select species/strains such that you arrive at a desired level of resolution in your analysis. For example, it does make little sense to consider data from 25 different yeast strains if you are interested in evolutionary events that happened a long time before yeast existed as a species. However, at the same time,

don't be too sparse in your taxon sampling, as otherwise evolutionary conclusions depend too heavily on individual species and the quality of their genome reconstruction (*see* **Note 5**).

4. For a start, you can use the collection of currently 78 species represented in the Quest for Orthologs (QfO) reference proteome collection that is provided with the HaMStR package. These species cover the full diversity of the tree of life. However, due to the considerably low number of species, the resolution of individual phylogenetic lineages is not great.

3.3 Phylogenetic Profiling

Search for orthologs to your pathway components. End with a phylogenetic profile for every gene informing about the presence/absence of orthologs across your collection of target species. Retrieve orthologs directly from an online database such as OMA [23] or OrthoDB [24]. This provides a quick access to precomputed results and reduces computations to a minimum. In **steps 1–5**, we explain the ortholog retrieval for individual seed sequences via the web interfaces of the OMA database. For the use of OrthoDB, directly jump to **step 6**.

If you prefer OMA over OrthoDB, proceed as follows:

1. Go to the OMA homepage (http://omabrowser.org/oma/home/).
2. Query for orthologs providing one of the following information as input into the search field: (1) OMA sequence identifier, (2) the protein sequence, (3) the OMA group identifier, or (4) a keyword. The sequence identifiers in OMA have a specific format. For example, human PRKAA1 protein has the OMA identifier HUMAN23295, where "HUMAN" is the species identifier for *Homo sapiens* and "23295" corresponds to sequence identifier in the OMA human gene set database.
3. When the search was performed with an OMA identifier, an output page is obtained providing detailed information about the seed protein. Alternatively, when the search was initiated with a protein sequence, you may have to follow the "Entry" link representing your query organism ("*Homo sapiens*" in this case). This will result in a page with all information related to the seed protein.
4. Follow the link "Orthologs." This will show all the orthologs to the seed protein. Download the sequences in FASTA format. Provide this file some meaningful name. For example, if you search for orthologs to PRKAA1, choose *AMPK_PRKAA1_Orthologs.fa* as file name.
5. Filter the orthologs file and retain only the sequences from your target species. Save this modified file with a new name like *AMPK_PRKAA1_Orthologs_Filtered.fa*.

If you prefer OrthoDB over OMA, proceed as follows:

6. Open the URL http://www.orthodb.org/.
7. You can query the database for ortholog of your seed protein using (1) the protein sequence, (2) the gene name, or (3) protein annotations. Select the species to display, i.e., the set of taxa of interest, and click "Submit." This will result in hierarchal orthologous groups at each major taxonomic level of the selected species.
8. Download all orthologous groups for PRKAA1 as FASTA files. Filter for sequences from your target taxa and save into a new file, *AMPK_PRKAA1_Orthologs_Filtered.fa*.

*Optional **steps 9–18**. See **steps 19–21** for an alternative approach.*

You can use HaMStR [25] for extending precompiled orthologous groups retrieved in the previous steps with sequences from species not represented in the online ortholog collections (*see* **Note 6**). HaMStR lets you identify orthologs both in protein sequence data and in transcript collections.

9. Download and install HaMStR. We will refer in the following to the HaMStR directory on your file systems as *pathToHaMStR*.
10. Follow the guidelines of the HaMStR package to set the stage for your search. Per default, HaMStR comes with a ready-to-use collection of protein sets from the Quest for Orthologs Reference Species collection (http://www.ebi.ac.uk/reference_proteomes). If your analysis requires protein sets from further species, the HaMStR documentation provides the necessary details for their addition.
11. For every protein, create a directory inside *pathToHaMStR/core_orthologs*. For example, for the protein PRKAA1, create a directory *pathToHaMStR/core_orthologs/PRKAA1*. Copy the prepared ortholog file *AMPK_PRKAA1_Orthologs_Filtered.fa* (*see* **step 8** in Subheading 3.3) and rename the file as *PRKAA1.fa*. Please note that the name of the file should be the same as the name of the directory (PRKAA1 in this case). HaMStR is a bit picky concerning the format of sequence headers. In brief, it expects the following structure: proteinName|taxonName|sequenceId. For example, if PRKAA1 has the sequence identifier "Q13131" in the human gene set provided to HaMStR, the sequence header should read as ">PRKAA1|HUMAN@9606|Q13131" where *HUMAN@9606* is the file name of the human gene set (*see* **Note 7**). Take into account that HaMStR assumes that a sequence in a FASTA file is not interrupted by line breaks.
12. Generate a multiple sequence alignment for ortholog sequences in *pathToHaMStR/core_orthologs/PRKAA1/PRKAA1.fa* using MUSCLE [32]: *muscle -in PRKAA1.fa -out PRKAA1.aln*.

13. Train a profile hidden Markov model using *hmmbuild* from the HMMER package [31]: *hmmbuild PRKAA1.hmm PRKAA1.aln*.
14. Create two directories, *hmm_dir* and *aln_dir* inside *pathToHaMStR/core_orthologs/PRKAA1/*. Place *PRKAA1.aln* inside *aln_dir* and *PRKAA1.hmm* inside *hmm_dir*.
15. Run the HaMStR search. For every target species, perform its own HaMStR search. An example command for a HaMStR search would look like the following: *pathToHaMStR/bin/hamstr -sequence_file=pathToInfile/inFile.fa -taxon=yourTaxonName -hmmset=PRKAA1 –refspec=HUMAN@9606 -checkCoorthologsRef -representative* (*see* **Note 8**).
16. Information about the orthologs identified by HaMStR are stored in a file with the extension "*.out*." Upon opening the file, you will find the results reported in the following format: "proteinName|queryTaxonName|targetTaxonName|targetProteinId|representative|targetProteinSequence." The field "representative" takes either 1 or 0 as value. If HaMStR identifies more than one ortholog (co-orthologs), it will identify the one being most similar to the seed sequence. This will be considered the "representative ortholog" and obtains a 1. All other co-orthologs will be flagged with a 0. If you choose the parameter "-representative" in the HaMStR call, the output of co-orthologs will be suppressed, and only the "representative" ortholog will be reported.
17. Collect the orthologs across all species and add them to the file *AMPK_PRKAA1_Orthologs_Filtered.fa*. To keep track of the changes in the file, you may want to rename it to *AMPK_PRKAA1_Orthologs_Filtered_extended.fa*.
18. We recommend deleting the HaMStR output files, especially when working with large collections of seed proteins and many species.

    *Phylogenetic profiling using a targeted ortholog search (**steps 19–21**).*

    You can optionally bypass the use of precomputed ortholog sets and directly perform a targeted search for orthologs with HaMStR-OneSeq [26] using a single seed sequence.
19. HaMStR-OneSeq is part of the HaMStR package. If you have not already installed HaMStR, download and install the package (*see* **step 9** in Subheading 3.3).
20. Save the seed protein sequence in FASTA format and save it under *pathToHaMStR/data*. Use this file for initiating the ortholog search with HaMStR-OneSeq. A standard search command looks like the following: *pathToHaMStR/bin/oneSeq.pl -sequence_file=seedFileName.fa -seqname=seedName*

-refspec=seedSpecies -coreOrth=4 -minDist=genus -maxDist=kingdom -strict -checkCoorthologsRef -representative -cleanup. "minDist" and "maxDist" control the phylogenetic diversity of the core ortholog set. In the example call, no two sequences from the same genus will be considered for training the pHMM, and no sequences from a different kingdom than your seed species. "coreOrth" takes the maximum number of orthologs added to the seed sequence for the final pHMM training. "cleanup" removes the temporary files created during HaMStR-OneSeq run. Refer to the HaMStR-OneSeq-help for the meaning of the other options. HaMStR-OneSeq will by default search for orthologs in all species listed in the directory *pathToHaMStR/genome_dir*.

21. After a successful HaMStR-OneSeq run, a file with an extension "*.extended.fa*" will be generated. This file contains all orthologs for the query protein with each sequence header having the following format: "proteinName|targetTaxaName|targetProteinId|number" (*see* **step 16** in Subheading 3.3). As a last step, combine the contents of all files ending with "*.extended.fa*" obtained from all seed proteins into a single file. Name this file *AMPK.extended.fa*.

    Building the phylogenetic profile.

22. Once you have compiled the orthologs for every gene in your pathway of interest, the next step is to build a phylogenetic profile. In a nutshell, a phylogenetic profile is basically a tab-delimited text file where the first row specifies the species names and the first column specifies the gene names. The remaining cells in the phylogenetic profile matrix are then filled with either "1" denoting presence or "0" denoting the absence of an ortholog, respectively (Fig. 4a). For the dynamic visualization and analysis of phylogenetic profiles using the Phylo-Profile application (*see* Subheading 3.5), we recommend the format displayed in Fig. 4b. Here, you provide the NCBI taxon id instead of the species name. For example, "*Homo sapiens*" will be replaced by ncbi9606. In the cell corresponding to the seed protein, we note the presence of an ortholog in the format "targetProteinId#FAS_score," where "targetProteinId" is the sequence identifier of the ortholog. We will discuss the FAS score in detail in **step 2** of Subheading 3.4. If no ortholog was found in a given species, fill the corresponding cell with "NA." Repeat this for all species–gene combinations and save the phylogenetic profile matrix file as *AMPK_phylogenetic_profile_matrix*. Obviously, the generation of a phylogenetic profile requires quite some text processing. However, if you identified orthologs with HaMStR-OneSeq, you are already in possession of a ready-to-use phylogenetic profile. It is stored in the file ending with "*.matrix*."

(A)

geneID	*H. sapiens*	*M. musculus*	*D. melanogaster*	*S. cerevisiae*	*A. thaliana*	*M. jannaschhii*	*C. aurantiacus*
PRKAA1	1	1	1	1	1	0	1
PRKAA2	1	1	1	1	1	0	1
PRKAB1	1	1	1	1	1	0	0
PRKAB2	1	1	1	1	1	0	0
PRKAG1	1	1	0	1	1	0	1
PRKAG2	1	1	0	0	0	0	1
PRKAG3	1	1	0	0	1	1	1

(B)

geneID	ncbi9606	ncbi10090	ncbi7227	ncbi559292	ncbi3702	ncbi243232	ncbi324602
PRKAA1	Q13131#1.0	Q5EG47#0.9992	O18645#0.9760	P06782#0.9754	Q38997#0.9939	NA	A9WD85#0.1306
PRKAA2	P54646#1.0	Q8BRK8#0.9984	O18645#0.9760	P06782#0.9750	Q38997#0.9934	NA	A9WD85#0.1315
PRKAB1	Q9Y478#1.0	Q9R078#1.0	A1Z7Q8#0.9758	Q04739#0.9865	Q9SCY5#0.9950	NA	NA
PRKAB2	O43741#1.0	Q6PAM0#0.9996	A1Z7Q8#0.9758	P34164#0.9875	Q9SCY5#0.9944	NA	NA
PRKAG1	P54619#1.0	O54950#0.9999	NA	P12904#0.9997	Q944A6#0.9868	NA	A9WBL7#0.9919
PRKAG2	Q9UGJ0#1.0	Q91WG5#0.9996	NA	NA	NA	NA	A9WHY8#0.4073
PRKAG3	Q9UGI9#1.0	Q8BGM7#0.9998	NA	NA	Q8LBB2#0.9902	Q58799#0.9367	A9WGZ6#0.7253

Fig. 4 Different types of phylogenetic profile. (**a**) General format of a phylogenetic profile. The first row and first column represent taxa and gene ids, respectively. The "1" and "0" in the cells represent the presence and absence of orthologs, respectively. (**b**) Phylogenetic profile in the PhyloProfile format. The first row and first column correspond to taxa and proteins, respectively. The cells have values in the format "OrthologId#FAS," where OrthologId is the protein sequence identifier, and FAS is the Feature Architecture Similarity score between the seed and the ortholog. "NA" indicates that no ortholog was found

3.4 Assessing the Feature Architecture Similarity (FAS) Between Proteins

This protocol allows analyzing and comparing feature architectures between the identified orthologs and the corresponding seed protein. The procedure ends with a similarity measure aiding in the conclusion whether or not an identified ortholog is likely to have diverged in function from the seed (*see* **Note 9**). One can manually compare feature architectures between proteins using InterProScan, as explained in **step 1**. For an automated comparison of feature architectures, use FAS-S, a software to assess and score the feature architecture similarity (FAS) between two proteins. FAS scores range from 0, i.e., two architectures share no features, to 1, when all features of the seed protein are represented in the ortholog. The generation of FAS scores in combination with a phyletic profiling with HaMStR_OneSeq is described in **steps 2–5**. The later FAS scoring of existing orthologous protein pairs is outlined in **steps 6–11**.

Manual comparison of feature architectures between proteins.

1. For the analysis of individual seed–ortholog pairs by eye, annotate the feature architectures with InterProScan [27]. Open the web interface of InterProScan, paste the protein sequence into the search field, and submit. You can always analyze only a single sequence at a time. Compare the resulting architectures by eye. Look out for a conspicuous absence of seed protein features in the ortholog and for features of the ortholog that are missing in the seed protein. Figures 5 and 6 display the InterProScan annotation for PRKAA1 protein from human (Q13131) and of its ortholog in the fruit fly, *D. melanogaster*, (O18645), respectively. All features of the human protein are present in the drosophila ortholog as well. Thus, there is no

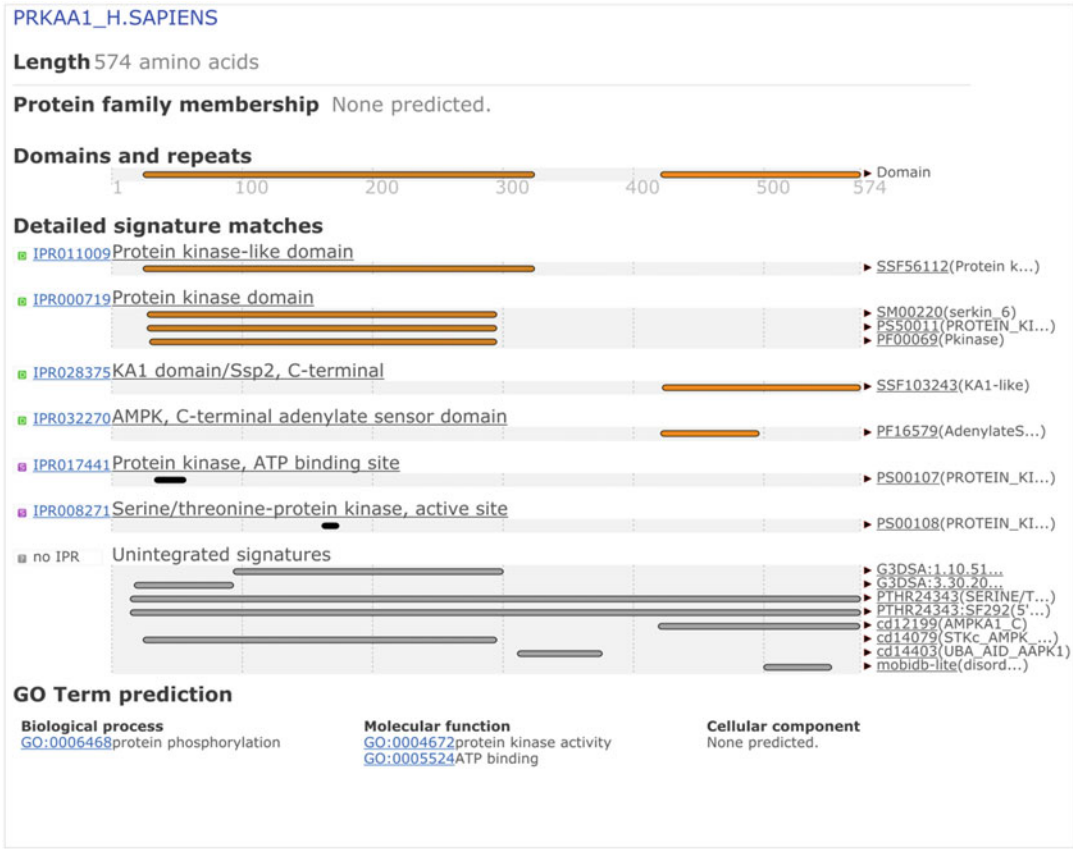

Fig. 5 Feature architecture of human PRKAA. The plot displays the results of an InterProScan [27] analysis of human PRKKA1 (AMP-activated protein kinase alpha subunit, UniProt ID Q13131)

reason at this level to assume that the two proteins have diverged in their functionality.

Feature Architecture Similarity (FAS) score calculation integrated into HaMStR-OneSeq.

2. The FAS scoring is natively implemented in the HaMStR-OneSeq workflow (*see* **steps 19–21** in Subheading 3.3). For orthologs predicted with this tool, no further steps are required. The relevant results are stored in three files whose contents can later be visualized with the PhyloProfile application (*see* Subheading 3.5): (1) *seedProteinName_1.matrix*, this file is the phylogenetic profile vector for the query protein; (2) *seedProteinName.extended.profile*, this file provides the ortholog ids along with their FAS score; (3) *seedProteinName_1.domains*, this file contains information about the domain architectures of the seed protein and of the corresponding orthologs.

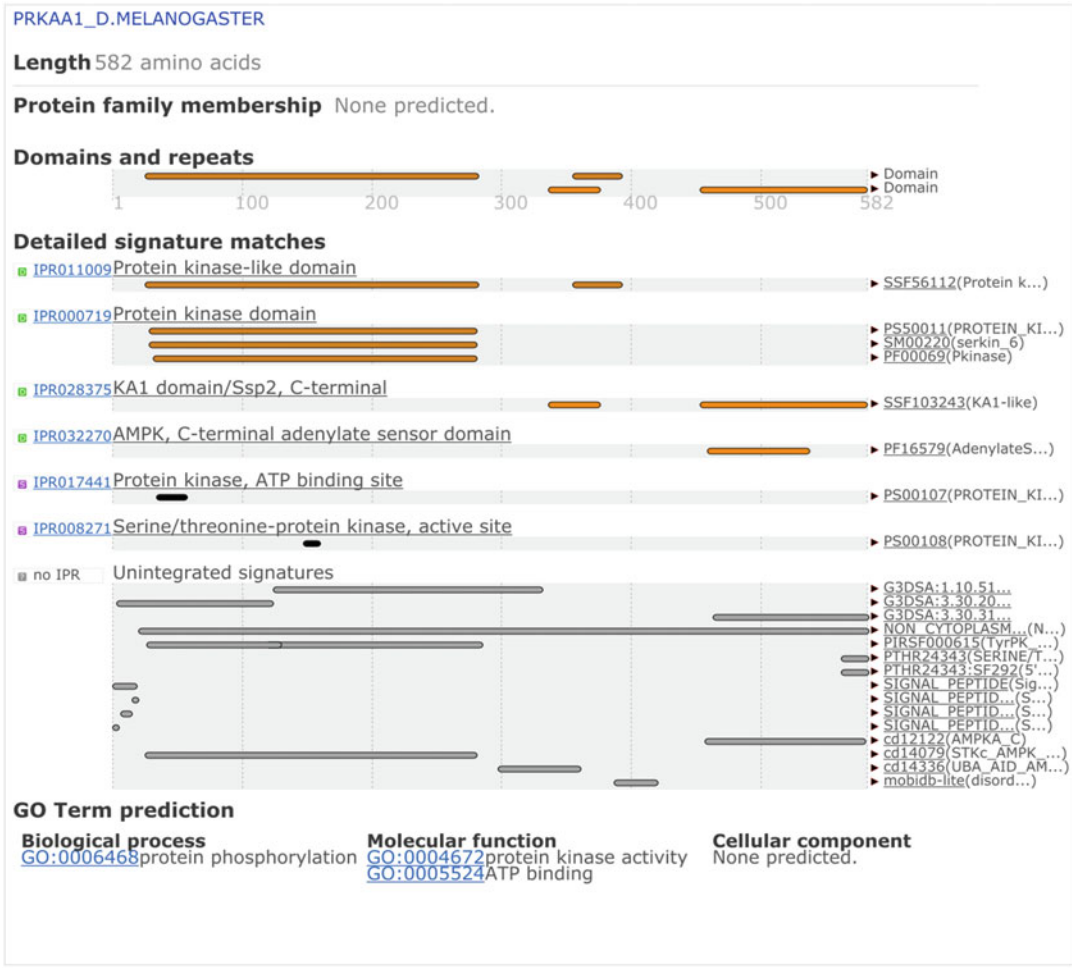

Fig. 6 Feature architecture of the human PRKAA1 ortholog in *D. melanogaster*. The plot displays the results of an InterProScan using the *D. melanogaster* protein with the UniProt ID O18645 as query

3. To later visualize the information for all pathway proteins in one go, you need to combine the contents of the files ending in "*.domains*" for all proteins and store it in a file named *AMPK.domains*.
4. Combine the contents of all files ending in "*.extended.profile*" and store the information in the file *AMPK.extended.profile*.
5. Recreate the "*.matrix*" file by running the command *pathToHaMStR/bin/visuals/parseOneSeq.pl –i* AMPK.*extended.profile –o AMPK*.

Feature Architecture Similarity (FAS) score calculation for pre-existing ortholog pairs.

A post hoc FAS scoring of orthologs downloaded from public repositories is possible, yet it is a bit more complex. We

outline the routine for species represented in the QfO reference proteome collection, as the sequences in these sets are available pre-annotated from the HaMStR project page. Per default, this information is stored in *pathToHaMStR/weight_dir* where each species has its own directory.

6. Create a directory to store the output of the annotation procedure. Give this directory a meaningful name like *pathToHaMStR/data/AMPK_annoDir*.
7. For every seed–ortholog pair, extract the precomputed feature annotations. Run the script *pathToHaMStR/bin/fas/annotation.pl* script for this purpose. Create a new directory *pathToHaMStR/data/AMPK_annoDir/singleProteins*.
8. Extract now the feature architecture information for PRKAA1 from human. Note that the species names used here might deviate from the ones in the actual distribution: *pathToHaMStR/bin/fas/annotation.pl -path=pathToHaMStR/weight_dir/HUMAN@9606 -name=Q13131 -extract=pathToHaMStR/data/AMPK_annoDir/singleProteins/homsa_PRKAA1*.
9. Rerun the above command for the yeast ortholog of PRKAA1. To do so, simply replace *YEAST@559292* for *HUMAN@9606*, set *–name* to *P06782*, and modify the "extract" path accordingly.
10. Use the feature architectures extracted in the previous steps as input for the script greedyFAS.py to calculate the FAS score between the two proteins. *pathToHaMStR/bin/fas/greedyFAS.py -s pathToHaMStR/data/AMPK_annoDir/singleProteins/homsa_PRKAA1 -p pathToHaMStR/data/AMPK_annoDir/singleProteins/sacce_PRKAA1 -o 1 –r pathToHaMStR/weight_dir/HUMAN@9606 -j prkaa1_homsa_sacce_FAS_Result.xml*. The parameters *–r* and *–j* specify the species used for feature weighting and the output file name, respectively.
11. To extract the corresponding feature architectures for a later visualization, run the script pathToHaMStR*/bin/visuals/parseArchitecture.pl: pathToHaMStR/bin/visuals/parseArchitecture.pl -i prkaa1_homsa_sacce_FAS_Result.xml -g PRKAA*. Upon completion, the script will create an output file named *prkaa1_homsa_sacce_FAS_Result.xml.domains*.

3.5 Visualizing FAS-Enhanced Phylogenetic Profile

Visualize and explore the FAS-enhanced phylogenetic profile with the PhyloProfile application. This will result in a comprehensive overview of the phyletic distribution of the pathway components.

1. Install the PhyloProfile application. A simple way to do it is using the git tools [37]: *git clone https://github.com/BIONF/PhyloProfile*. You will need an up-to-date R installation to run the PhyloProfile application.

2. Run the application and upload the customized phylogenetic profile matrix (*AMPK_1.matrix*) as input file (*see* **Note 10**). Upload further the *AMPK.domains* file as "Additional annotation." Optionally, when hitting the "FASTA config" button, you can provide a file, *AMPK.extended.fa*, with all ortholog sequences for display within the application.
3. Set the taxonomic rank on which you want to group your species. For a start, "species" is a good choice.
4. Choose your "taxon of interest". Typically, one selects here the seed species with which you started the phyletic profiling. In the case of the AMPK pathway analysis, use *Homo sapiens*. Note, you can change your choice at a later time point.
5. Upon clicking the "PLOT" button, the "Main profile" tab will open, and the graphic representation of the phylogenetic profile will be displayed. An example is shown in Fig. 7a.
6. Adjust the display of the phylogenetic profile. In particular, height and width of the plotting area and of the number of genes displayed might require adjustment.
7. Take a look at the presence–absence pattern of orthologs to your seed proteins and start exploring the data (*see* **Note 11**).
8. The tab "Customized profile" allows you to sub-select genes and species for display. Choose "PRKAA1" from the gene list to see only the representation of orthologs for this gene. Multiple selections are possible (Fig. 7b).
9. Click on individual dots in the phylogenetic profile matrix to obtain detailed information, such as the FAS score, sequence identifier of the ortholog, and, if provided, the sequence of the ortholog and the graphical display of its feature architecture in comparison to the seed (Fig. 7c).
10. PhyloProfile offers you the option to dynamically explore the phylogenetic profile.
11. Go back to the "Input & settings" tab, select "Phylum" as taxonomic rank, and choose "Chordata" as "taxon of interest." After clicking the "PLOT" button, the updated profile will be displayed.
12. In the "Main profile," tab you can now apply a cutoff for the minimal fraction of species in a phylum for which an ortholog to a seed gene was detected (default is 0). This considers that spurious orthology assignments will typically lead to only few species in a systematic group displaying an ortholog candidate. The more stringent the cutoff is, the sparser your phylogenetic profile becomes. A reasonable cutoff helps reducing the impact of spurious ortholog assignments.

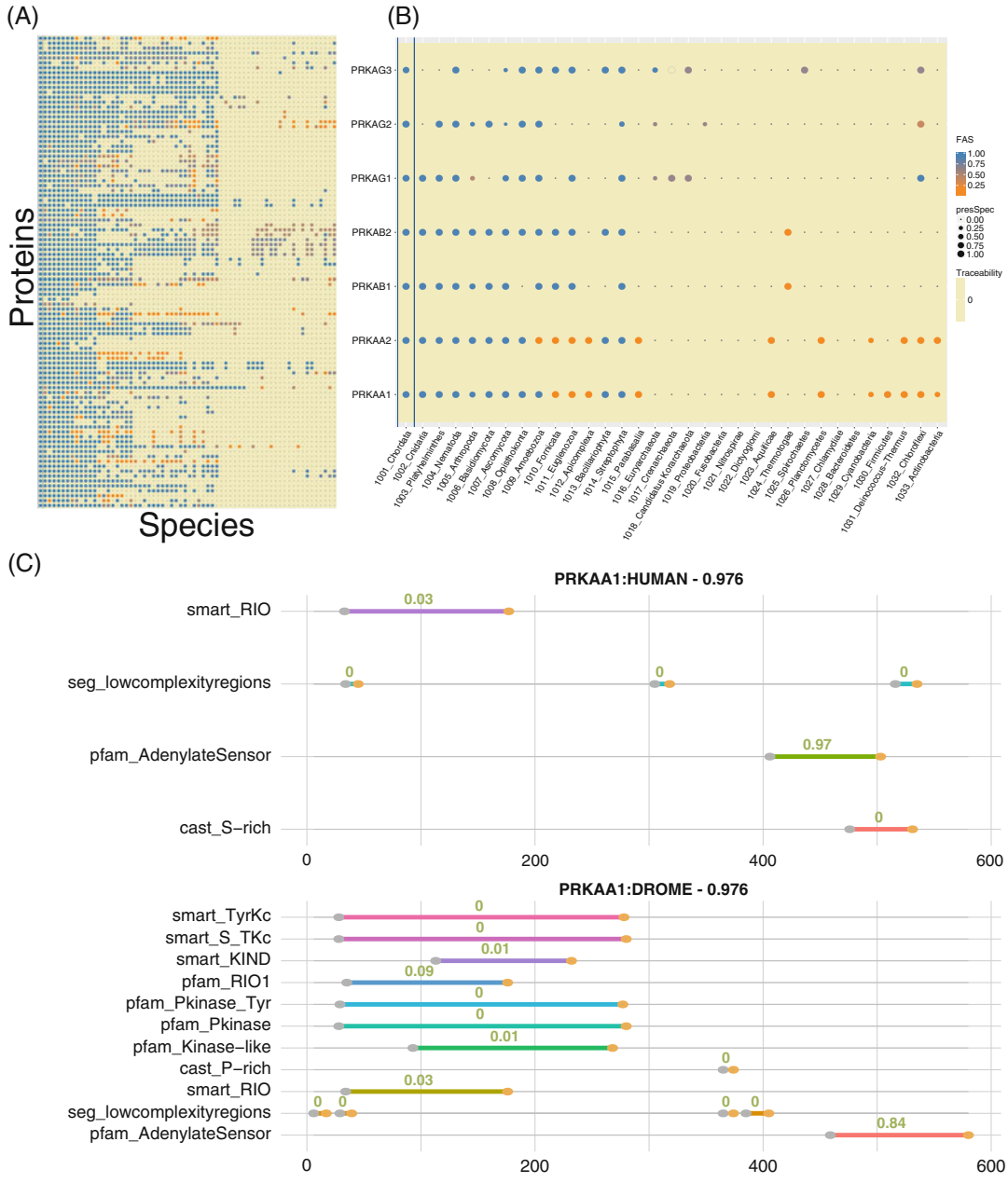

Fig. 7 Visualization of phylogenetic profiles using PhyloProfile. (**a**) Phylogenetic profile of the human AMPK pathway. The color code represents the FAS score. (**b**) Customized phylogenetic profile for seven AMPK proteins: PRKAA1, PRKAA2, PRKAB1, PRKAB2, PRKAG1, PRKAG2, and PRKAG3. Species are summarized on the phylum level. The size of the dots indicates the fraction of species in a phylum with an ortholog present. (**c**) Domain architecture comparison between human PRKAA1 (above) and its ortholog in yeast (below). Note that the FAS-S algorithm ignores the accumulation of redundant features annotated in the N-terminal half of the yeast ortholog. All main features of the human protein are observed also in the yeast sequence, and hence we have no reason to assume functional divergence of the two proteins

13. Likewise, you can also apply a cutoff for the minimal FAS score (default is 0). This option serves to reduce the impact of orthologs displaying deviating feature architectures and might be helpful in tracing functionality rather than only orthology.

3.6 Integration of Phylogenetic Profiles and KEGG Pathway Maps

The following steps will result in a graphical pathway representation where proteins are labeled if an ortholog was identified in a (set of) species.

1. Decide on a set of species for which you want to display the information. For a start, use *Mus musculus*, *Drosophila melanogaster*, *Saccharomyces cerevisiae*, *Arabidopsis thaliana*, *Methanocaldococcus jannaschii*, and *Chloroflexus aurantiacus*.
2. Transfer the KO identifier of the seed protein to its orthologs in the species selected in the previous step. Use the earlier generated cross-reference file *AMPK-hsa-xref.txt* (*see* **step 11** in Subheading 3.3) to obtain the KO identifiers.
3. Create an input file for the KEGG Mapper (http://www.genome.jp/kegg/tool/map_pathway.html). You will find details about the file format on the KEGG web page (http://www.genome.jp/kegg/tool/example/genelist2.txt).
4. Open the KEGG Mapper web page, upload the input file, and execute the mapping.
5. The KEGG Mapper will present you with a list of pathways to which your KO identifiers match. Choose the appropriate one (AMPK) for display. Figure 8 shows the representation of the human AMPK-TOR pathways in four eukaryotes, one archaeon, and one bacterium.

3.7 Phylogenetic Analysis to Explore the Evolutionary History of Individual Pathway Components

The aim of the following steps is the assignment of either a speciation event or a gene duplication event to each split in the reconstructed phylogeny. Given the plethora of different tools that can be used in the workflow of phylogeny reconstructions, we refrain from providing a tool-specific step-by-step guide where we trust that the tool use is self-explanatory. We put more emphasis on the interpretation of the phylogenies.

1. For phylogenetic tree reconstruction, assemble the orthologous sequences for one protein—or several related proteins—of interest into a single text file. The FASTA format is most widely used as a format to store sequence information and is accepted by almost all sequence analysis tools.
2. As all files generated in the course of this analysis contain human-readable text, it comes in handy to use file endings that inform about the file format, such as *yourname.fa* for sequence files in FASTA format or *yourname.phy* for the Phylip format.

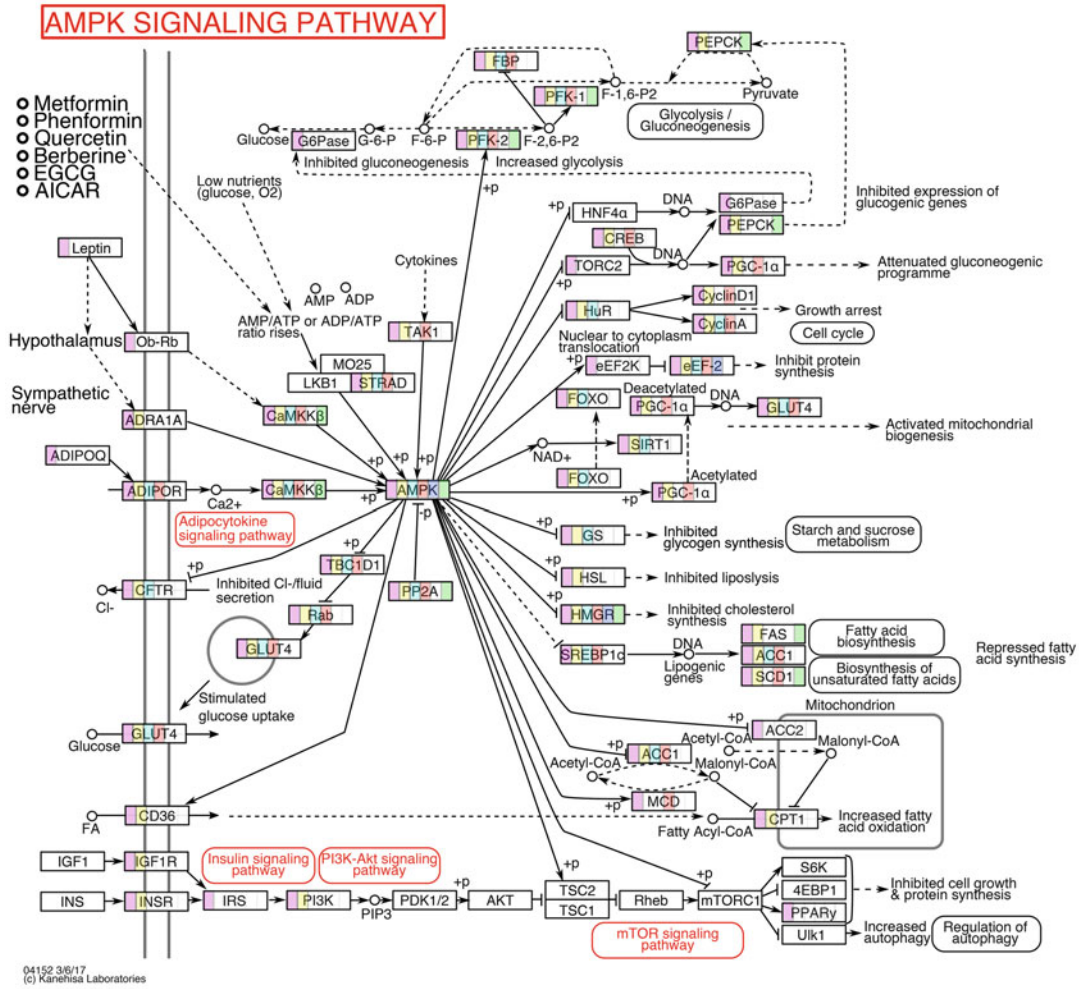

Fig. 8 Mapping identified orthologs on the reference pathway. Tracing representation of human AMPK pathway components in *Mus musculus*, *Drosophila melanogaster*, *Saccharomyces cerevisiae*, *Arabidopsis thaliana*, *Methanocaldococcus jannaschii* (archaea), and *Chloroflexus aurantiacus* (bacteria). Each protein is represented as a box, and every box is divided into six columns, and each column represents the presence/absence of the protein in corresponding species. If an ortholog to a pathway component is represented in a species, the corresponding column is colored. The columns represent from left to right the order of the species list above

3. Align the orthologous sequences with MUSCLE [32] (*see* **Note 12**) and store the alignment in the appropriate file format. Most tree reconstruction software accept the FASTA and Phylip formats as input (Fig. 9; *see* **Notes 13** and **14**). For file format conversion at a later step in the analysis, you can use online tools such as ALTER [38], the format converter available at http://phylogeny.lirmm.fr/phylo_cgi/data_converter.cgi, or the sequence alignment tool ClustalW [39] with the option *–reformat*.

(A) FASTA format

```
>A1_YEAST
MSSNNNTNT-------------APANANSQRDKMSEQE-ARRFFQQIISAVEY-------
CHRHKIVHRDLKPENLLLDEHLNVKIADFGLSNIMTDGNFLKTSCGSPNYAAPEVISGKL
YAGPEVDVWSCGVIL----------------------
>PRKAA1_SORCE
MARCL-----------------VCNAENPGSARFCVAC-GASLTAKEAGAGAATSAPPAP
GPRTTVPGQPLLGALVPEDPAHRASL------SALAAGGANGPAANV---HAPHIVPAPL
AGSLPRRA--PGGHLP----------------------
>A1_ENTHI
-----------------------------MSQCYRV-GQFIIGKKLGEGMC-------
G-KVYLAFHEKTGVKVAIKIVDKTKL----MRKPEMKRKVEREIAFLKIINHRNVMQLYT
VYETTRYLFLVMELLEGGELFDYISSKGKLEIEEVLV
>A1_ARATH
MFKRVDEFNLVSSTIDHRIFKSRMDGSGTGSRSGVESILPNYKLGRTLGIGSF-------
G-RVKIAEHALTGHKVAIKILNRRKI-----KNMEMEEKVRREIKILRLFMHPHIIRLYE
VIETPTDIY-----------------------------
>PRKAA1_HUMAN
-MRRLSSWR-------------KMATAEKQKHDGRVKI-GHYILGDTLGVGTF-------
G-KVKVGKHELTGHKVAVKILNRQKI-----RSLDVVGKIRREIQNLKLFRHPHIIKLYQ
VISTPSDIFMVMEYVSRAR------------------
>PRKAA1_MOUSE
-MRRLSSWR-------------KMATAEKQKHDGRVKI-GHYILGDTLGVGTF-------
G-KVKVGKHELTGHKVAVKILNRQKI-----RSLDVVGKIRREIQNLKLFRHPHIIKLYQ
VISTPSDI-----------------------------
```

(B) Phylip format

```
      6    157
A1_YEAST   MSSNNNTNT- ---------- --APANANSQ RDKMSEQE-A RRFFQQIISA
PRKAA1_SOR MARCL----- ---------- --VCNAENPG SARFCVAC-G ASLTAKEAGA
A1_ENTHI   ---------- ---------- ---------- -MSQCYRV-G QFIIGKKLGE
A1_ARATH   MFKRVDEFNL VSSTIDHRIF KSRMDGSGTG SRSGVESILP NYKLGRTLGI
PRKAA1_HUM -MRRLSSWR- ---------- --KMATAEKQ KHDGRVKI-G HYILGDTLGV
PRKAA1_MOU -MRRLSSWR- ---------- --KMATAEKQ KHDGRVKI-G HYILGDTLGV

           VEY------- CHRHKIVHRD LKPENLLLDE HLNVKIADFG LSNIMTDGNF
           GAATSAPPAP GPRTTVPGQP LLGALVPEDP AHRASL---- --SALAAGGA
           GMC------- G-KVYLAFHE KTGVKVAIKI VDKTKL---- MRKPEMKRKV
           GSF------- G-RVKIAEHA LTGHKVAIKI LNRRKI---- -KNMEMEEKV
           GTF------- G-KVKVGKHE LTGHKVAVKI LNRQKI---- -RSLDVVGKI
           GTF------- G-KVKVGKHE LTGHKVAVKI LNRQKI---- -RSLDVVGKI

           LKTSCGSPNY AAPEVISGKL YAGPEVDVWS CGVIL----- ----------
           NGPAANV--- HAPHIVPAPL AGSLPRRA-- PGGHLP---- ----------
           EREIAFLKII NHRNVMQLYT VYETTRYLFL VMELLEGGEL FDYISSKGKL
           RREIKILRLF MHPHIIRLYE VIETPTDIY- ---------- ----------
           RREIQNLKLF RHPHIIKLYQ VISTPSDIFM VMEYVSRAR- ----------
           RREIQNLKLF RHPHIIKLYQ VISTPSDI-- ---------- ----------

           -------
           -------
           EIEEVLV
           -------
           -------
           -------
```

Fig. 9 Commonly used multiple sequence alignment formats. (**a**) FASTA and (**b**) Phylip. Please note that the sequence identifiers in Phylip format are typically limited to a maximum of ten characters. Format converters will therefore shorten longer identifier in the FASTA format (e.g., "PRKAA1_SORCE") to the maximum length of ten characters ("PRKAA1_SOR") in Phylip format. You should therefore pay particular attention that the identifiers are still unique after the conversion

4. In cases where the alignment contains lots of gaps, you can add an optional post-processing step with Guidance [40] or TCS [41]. This serves to reduce noise in the data due to incorrectly aligned residues. Alternatively, you can remove alignment columns where the number of sequences represented by an amino acid does not exceed a certain threshold. A limit of 50% is common; however, you can increase this value if a more stringent analysis is desired.
5. Maximum likelihood tree reconstruction requires the *a priori* definition of a protein sequence evolution model. Use the (post-processed) alignment as input for a ProtTest run (v3.4.1) [34]. Let ProtTest define its own tree for the analysis and choose AIC as a model selection criterion. Make sure to enable the testing for modeling substitution rate heterogeneity across sites (option *G*), invariant sites (option *I*), and for using empirical amino acid frequencies (option *F*). The top-ranked model according to the AIC is the one that provides the best fit to your data and should be used for downstream maximum likelihood tree reconstruction (*see* **Note 15**).
6. Use the multiple sequence alignment and the model for sequence evolution as input for the maximum likelihood (ML) tree reconstruction with RAxML [35]. When you add the option *–f A*, RAxML will compute the maximum likelihood tree together with a rapid bootstrap support. Specify the number of bootstrap replicates with the option *–N*. A complete program call could read something like this: *raxml –n outputFileName –s alignmentFileName –m PROTGAMMAILGF*

–f A –N 100 –p 77 –x 933. Here, we use the LG model of protein sequence evolution [42] with empirical equilibrium frequencies for the 20 amino acids. We model substitution rate heterogeneity across sites with a Γ-distribution and allow a fraction of invariant sites. The uneven numbers provided with the options *–p* and *–x* specify random seeds for initializing the parsimony stepwise addition and the rapid bootstrapping procedure, respectively. Once RAxML has completed successfully, it will have generated a number of output files. The one ending with "*bipartitionsBranchLabels.bs*" contains the maximum likelihood tree together with the branch support labels in *Newick* format.

7. For tree visualization, open the ML tree with FigTree [36]. The program gives you a broad variety of options to adjust the tree display. A maximum likelihood tree reconstruction results in an unrooted tree, and thus the direction of time in the tree remains unknown. To make tree interpretation more intuitive, we recommend to root the tree. If possible, place the root on a branch leading to a known outgroup. If you have no a priori knowledge about a possible outgroup in your data set, you can still use a midpoint root. The root is then placed such that it is approximately equidistant to all leaves (*see* **Note 16**).
8. Interpret the evolutionary history of your protein on the basis of the rooted tree. Again, we can give only very general guidelines. The conceptual principles are outlined in Fig. 10, and a real-world example—the evolutionary relationships of human AMPKγ with particular focus on its homologs in plants, AMPKβγ and KING1—is shown in Fig. 11. As a start, make yourself familiar with the evolutionary relationships of the species whose sequences you are analyzing, i.e., the species tree. When you are investigating the evolutionary history of orthologs, the gene tree should be congruent to the species tree (Fig. 10a). Incongruences between the gene tree and the species tree indicate the presence of non-orthologous sequences, problems during tree reconstruction, or both (*see* **Note 17**; Fig. 10b). If you have combined orthologs for more than one seed protein in the analysis, then you should see the species tree reflected in the individual subtrees corresponding to the orthologous groups (Fig. 10c). The node connecting the orthologs from the two evolutionarily most distantly related species informs about the minimal age of the protein. Any species that can be traced back to this ancestral node must have the protein present unless it was secondarily lost. Gene duplications are indicated by a duplicated subtree in the phylogeny. These subtrees generally represent sequences from at least overlapping species sets. If a species is represented only in one of the two subtrees, it must have lost one copy of the

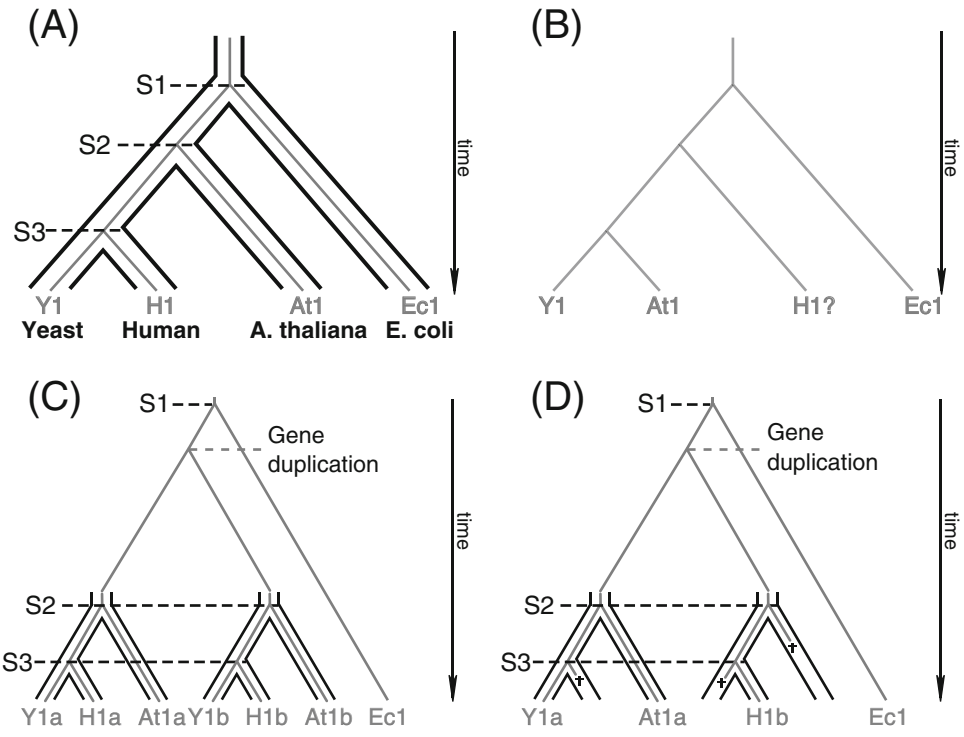

Fig. 10 The evolution of species and of their genes. (**a**) The outer tree in black represents the evolutionary relationships of the species, and we refer to it as the *species tree*. S1–S3 denote speciation events. The *sequence tree* (syn. *Gene tree*) connecting the four proteins Y1, H1, At1, and Ec1 is shown in gray. As the evolutionary lineages of the four proteins were separated by a speciation event rather than by a gene duplication, we call them *orthologs.* The sequence tree connecting the four proteins is, thus, congruent to the species tree. (**b**) Quite often, the reconstructed sequence tree deviates from the species tree. This can indicate tree reconstruction artifacts resulting in sequence tree not accurately reflecting the phylogenetic signal in the data. Alternatively, the sequences placed at unexpected positions might not be orthologous (denoted here by the "?" that is appended to H1). (**c**) An idealized sequence tree of proteins which evolutionary histories include a gene duplication (paralogs). Note that the sequence subtrees originating at the gene duplication event each reflect the evolutionary relationships of the species that diversified after the gene duplication event (black subtrees). (**d**) The minimal evolutionary scenario required to explain the gene tree in (**b**). It invokes one gene duplication and three independent gene losses

duplicated gene (Fig. 10d). If gene loss appears prevalent in one subtree, it is worthwhile considering a tree reconstruction artifact rather than a gene duplication (Fig. 11; *see* **Note 18**).

9. When a sequence tree does not follow your expectation (Fig. 10), you can test whether it explains the data significantly better than the tree you were expecting [43]. For example, the ML tree in Fig. 11 places the fungal sequences at positions that disagree with the commonly accepted eukaryote phylogeny.
10. To test whether this discrepancy is indeed significantly supported by the data, modify a copy of the maximum likelihood tree such that it reflects the expected tree (*see* **Note 19**).

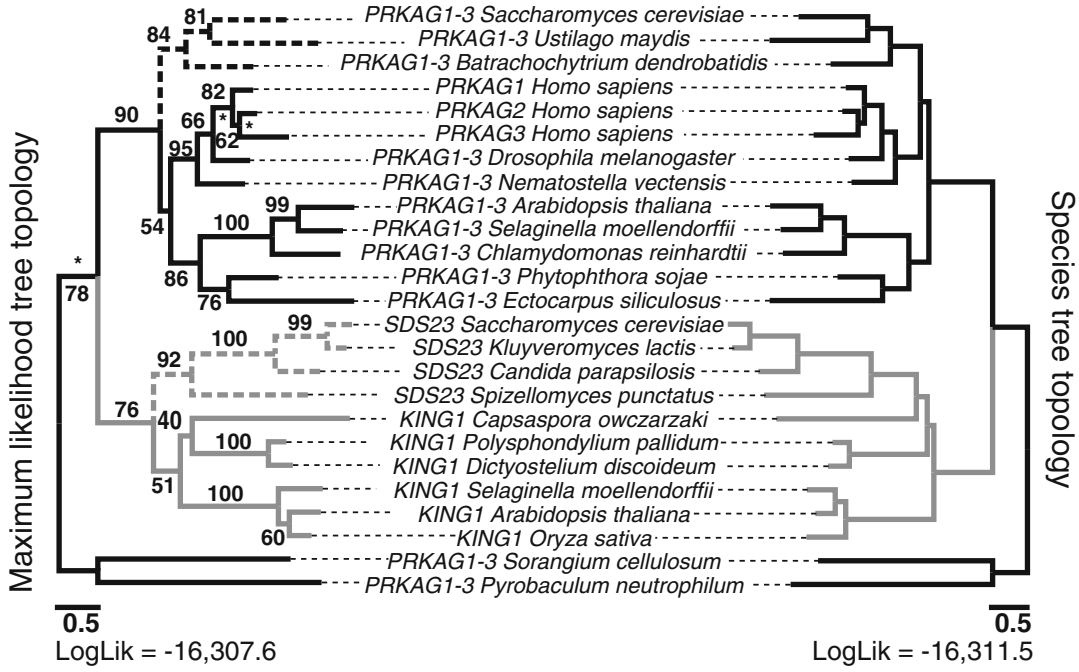

Fig. 11 The evolutionary histories of the human AMPKγ subunit and of its homologs in plants, AMPKβγ and KING1. The tree to the left represents the maximum likelihood (ML) topology computed with RAxML (substitution model: LG [42] + I + G). Branch labels denote percent bootstrap support. Asterisks indicate gene duplication events. The subtree harboring AMPKγ of animals together with its fungal and plant orthologs is shown in black. A gene duplication event in the last common ancestor of the eukaryotes gave rise to the gray subtree, which harbors KING1 and its orthologs. This rejects the hypothesis that KING1 is the plant counterpart to animal AMPKγ (*see* [12] for details). The positioning of the fungal sequences in both trees (hatched clades) is at odds with the placement of fungi in the eukaryote species phylogeny (right tree). The log likelihoods of the data given the ML tree and given a tree placing the fungal sequences at the expected position are given below the respective trees. *See* the main text on tree topology testing for further details

11. Use then the Shimodaira–Hasegawa test [44] implemented into RAxML to test whether the ML tree explains the data significantly better than the alternative tree, in which the fungi are placed such that they agree with the species phylogeny. To do so run *raxml –n outputFileName –s alignmentFilename –m modelOfChoice –f h –t mlTreeFilename –z alternativeTreeFilename*. The program will then tell you whether or not the ML tree is significantly better than the alternative tree. In the example of Fig. 11, the sequence tree modified to reflect the evolutionary relationships of the species is only 3.9 log likelihood units worse than the ML tree. According to the SH test, this difference is not significant ($p < 0.01$), and thus both trees explain the data equally well. It is therefore unnecessary to invoke complex evolutionary scenarios (*see* Fig. 10d) to explain the deviations of the ML tree from the species tree topology.

3.8 Integration of Sequence Phylogeny and Domain Architecture

You will obtain a phylogenetic tree resembling the evolutionary history of the analyzed sequences. The Pfam domain annotation of the analyzed proteins will be displayed at the leaves of the tree. This provides an initial impression of how the domain architectures and thus the molecular functions of the sequences have evolved.

1. Upload the set of sequences used for tree reconstruction into DoMosaics [30]. Annotate Pfam-A domains [28] in the input sequences by running a *hmmscan* analysis [31] within DoMosaics. Once the Pfam annotation has completed, DoMosaics will provide you with a graphical representation of the domain architectures.
2. Upload a phylogenetic tree, and DoMosaic will let you integrate the phylogenetic information with the Pfam domain architecture of the sequences that were used for tree reconstruction (*see* **Note 20**). This serves then as an excellent basis to formulate more comprehensive hypotheses concerning the evolution of protein families and of their functionality. An example is shown in Fig. 12.

4 Notes

1. Pay attention that many of the provided genome sequences are unpublished. While this has no effect for analyzing the data, you may require permissions to publish the results.
2. When working with gene sets from two or more pathways, it is a good idea to analyze a single combined nonredundant gene set. This avoids repeated calls of the same programs, and it ensures that you use the same set of parameters for all proteins. You can divide the proteins and the newly generated metadata at a later point in the analysis. Note that individual proteins might be represented in more than pathway.
3. It happens now and then that the number of sequence identifiers, for which you have obtained cross-references, differs from the original number of sequences. The reason is that the optimal case of a one-to-one relationship between identifiers in different databases is not always accomplished. Make sure to track and explain any difference in the number of sequences before and after the cross-referencing step to avoid information loss or the accumulation of redundancies.
4. Pan-species databases, such as the nonredundant protein database of NCBI, are not a particularly good choice for such analyses. It is almost impossible to assess which species are represented by what sequences, and thus the database is simply a huge black box.

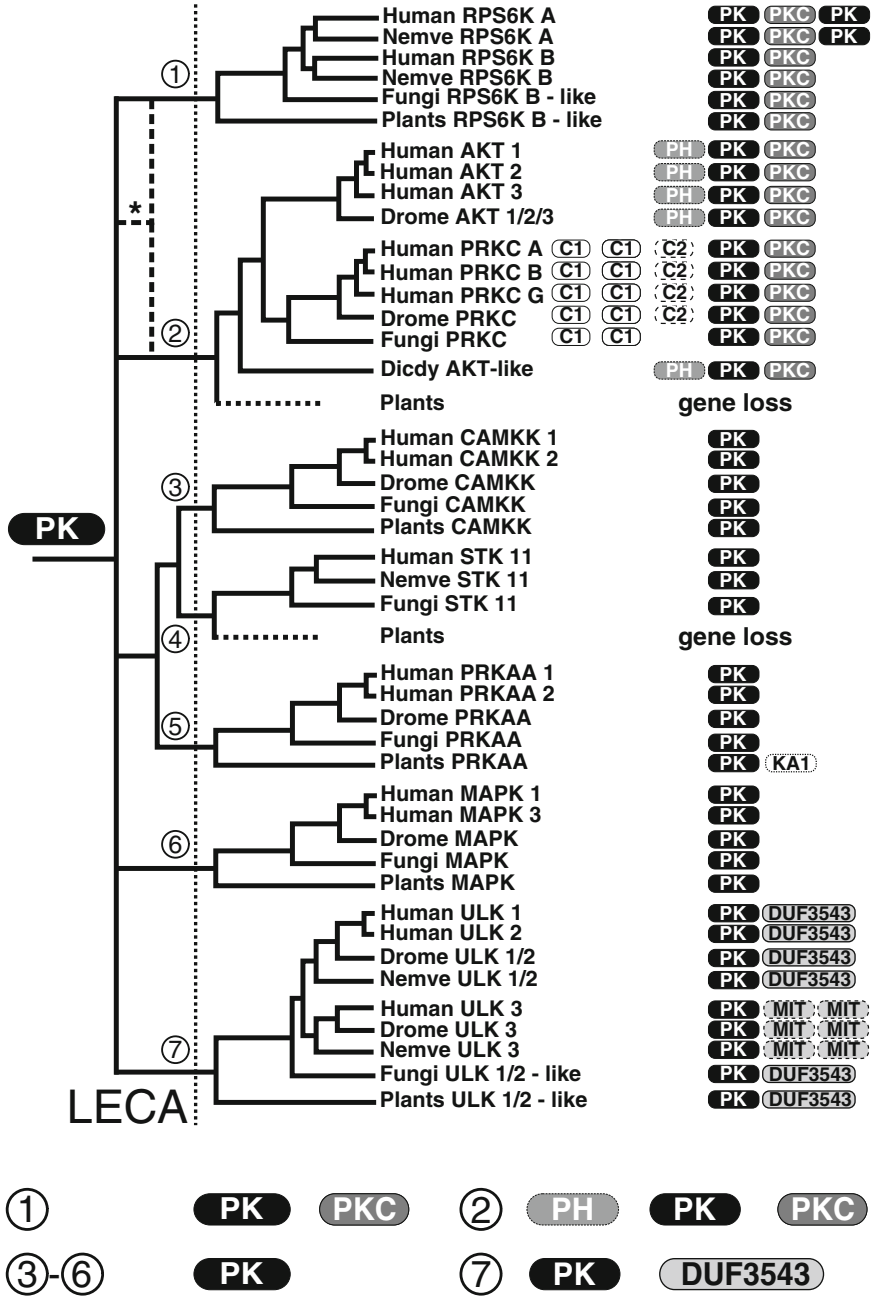

Fig. 12 A hypothetical evolutionary scenario of eukaryotic kinase evolution. The figure integrates the results from phylogenetic tree reconstruction and Pfam domain architecture analysis. The phylogenetic relationships of contemporary kinases imply the existence of seven proto-kinases in the last eukaryotic common ancestor (LECA). A parsimony criterion was used to infer the Pfam domain architecture of these ancestral proteins (numbers 1–7 below the tree). *See* [12] for details

5. In a nutshell, a gene missed in the annotation of a draft genome does little harm to the analysis, if there is a second genome from a species in the same clade where the gene has been correctly identified.
6. The extension of precompiled orthologous groups with HaMStR [25] is in principle straightforward. However, the naming conventions of sequences in this package are very strict, and it might be not too simple for an uninitiated user to meet all requirements. We therefore recommend for the start the use of HaMStR_OneSeq instead.
7. Please be aware that file names used here are only examples and may differ in the actual version of the program you are using.
8. For a more stringent ortholog identification, replace the *–refspec* option with *-strict* and omit any specification of a reference species. The "*-strict*" option in HaMStR tells the program to confirm orthology of a candidate sequence from the target species for each sequence and species represented in the core ortholog set. Refer to the HaMStR manual for further details.
9. Remember that orthology specifies only the evolutionary relationships of two sequences. However, it does not inform about whether or not two sequences also exert the same function.
10. If you run the PhyloProfile application for the first time, it may perform some preprocessing on your data, such as mapping the NCBI taxonomy ids to species names. Simply follow the guidelines of the tool. Once the preprocessing is completed, a restart of the application might be required.
11. Exploring phylogenetic profiles for the first time is not easy. It requires to have the evolutionary relationships of the analyzed species in mind, together with all possible evolutionary events explaining the presence/absence pattern of proteins in these species. Only then will the phylogenetic profile start making sense. As an example, imagine you find orthologs to a particular protein in all mammals except say the dog. It is then safe to assume that the corresponding protein was present in the last common ancestor of all mammals. From this follows that the corresponding gene was either lost on the dog lineage or it was erroneously missed in the annotation of the dog genome. You would need to look into the genome assembly of the dog to differentiate between the two possibilities. If, however, a second species that is more closely related to dogs than to any other species in your collection also lacks the protein, the "loss hypothesis" gains weight, as it might appear less likely that twice the same gene has been missed in two independent genome reconstructions. Of course, you could ask to what extent the reconstructions are indeed independent. Imagine

now further that for the same protein, you then don't find any orthologs in nonmammalian eukaryotes, but there are few bacterial species predicted to have an ortholog present. Now the situation becomes complex as you then need to choose between at least three alternative explanations: First, the corresponding gene is as old as the last common ancestor of bacteria and eukaryotes and was independently lost multiple times on the eukaryotic lineage such that it is nowadays represented only in mammals. Second, you are facing the result of a horizontal gene transfer from bacteria into the mammalian lineage. Third, the orthology assignment is wrong. Further analyses are then required to solve this issue. Among others, a look at the feature architecture similarity of the proteins might provide some indications about how to explain the observation best.

12. There is no gold standard for a sequence alignment program. We suggest MUSCLE [32], because it facilitates the alignment of large data collections containing hundreds to thousands of sequences. To rule out any influence of the alignment program on the outcome of the phylogenetic analysis, you may consider repeating the analysis with different aligners and to monitor any changes.
13. It is always advisable to keep sequence headers concise, making sure that the first ten characters identify the sequence uniquely. Moreover, white spaces should be avoided.
14. Sequence header should be designed such that the information provided is consistent across all sequences and taxa. It might be helpful to think about the header as a row in a spread sheet, where each cell contains a particular kind of information.
15. ProtTest [34] comes with other selection criteria (BIC, AICc, and LnL). The criteria penalize model complexity slightly differently, and thus the favored model might differ between the criteria. If you are unsure which selection criterion should be used, and if the highest ranked model differs between them, you can compute trees using alternative models and check for differences in the branching order.
16. Midpoint rooting makes perfect sense when sequences evolve approximately clocklike, i.e., accumulate similar amounts of sequence change per unit of time on all branches. However, quickly evolving sequences represented by long branches in the tree tend to attract the midpoint root placement leaving the root without evolutionary meaning. You can identify such instances when the root placement renders a known monophyletic group (single evolutionary origin) such as animals, plants, or fungi as paraphyletic (multiple evolutionary origins).

17. Reconstructing the evolutionary history of old proteins that extends easily over a billion years or more is tricky, as the phylogenetic signal in the data generally does not suffice. In particular, old events are frequently not accurately reconstructed. While in some instances such problems are indicated by low branch support values, this is not always the case. There is unfortunately no easy way out of this problem, because the truth is unknown. As a rule of thumb, misplaced sequences in a tree typically require the assumption of a plethora of additional evolutionary events, mostly independent gene losses, to explain the present-day data. Although such complex scenarios cannot a priori be ruled out, they should at least raise attention about a possible tree reconstruction artifact.
18. It will rather often happen that you fail to fully explain the evolutionary history of all sequences. Typically, individual sequences end up in places in the tree where it simply does not make sense. There are several possibilities to explain this, among which methodological artefacts at all levels of the analysis-from the gene prediction in the genome to the phylogeny reconstruction-prevail.
19. For those who are not familiar with trees in Newick format—but for more experienced people as well—modifying Newick trees is painful, especially when trees become larger. One way to do it is with the help of Baobab, a tree visualization and modification software. You can modify the tree graphically and then export the modified tree in Newick format.
20. Make sure that the identifiers of the sequences you upload into DoMosaics [30] are identical to the leaf labels of the tree. Only then can the tool link the information.

Acknowledgment

This work was supported by the Marie Curie ITN project CALIPSO (GA ITN-2013 607 607), and by the Deutsche Forschungsgesellschaft (EB 285/2-1).

References

1. Wetterstrand KA (2016) DNA sequencing costs: data from the NHGRI large-scale genome sequencing program. www.genome.gov/sequencingcostsdata. Accessed 4 Sept. 2016
2. Vitulo N, Vezzi A, Romualdi C et al (2007) A global gene evolution analysis on Vibrionaceae family using phylogenetic profile. BMC Bioinformatics 8(Suppl 1):S23. https://doi.org/10.1186/1471-2105-8-S1-S23
3. Sun J, Xu J, Liu Z et al (2005) Refined phylogenetic profiles method for predicting protein-protein interactions. Bioinformatics 21:3409–3415. https://doi.org/10.1093/bioinformatics/bti532
4. Pellegrini M, Marcotte EM, Thompson MJ et al (1999) Assigning protein functions by comparative genome analysis: protein phylogenetic profiles. Proc Natl Acad Sci U S A 96:4285–4288. https://doi.org/10.1073/pnas.96.8.4285

5. Jensen RA (2001) Orthologs and paralogs - we need to get it right. Genome Biol 2(8):interactions1002.1–interactions1002.3. https://doi.org/10.1186/gb-2001-2-8-interactions1002
6. Baldauf SL (2003) Phylogeny for the faint of heart: a tutorial. Trends Genet 19:345–351. https://doi.org/10.1016/S0168-9525(03)00112-4
7. Koonin EV (2005) Orthologs, paralogs, and evolutionary genomics. Annu Rev Genet 39:309–338. https://doi.org/10.1146/annurev.genet.39.073003.114725
8. Dolinski K, Botstein D (2007) Orthology and functional conservation in eukaryotes. Annu Rev Genet 41:465–507. https://doi.org/10.1146/annurev.genet.40.110405.090439
9. Studer RA, Robinson-Rechavi M (2009) How confident can we be that orthologs are similar, but paralogs differ? Trends Genet 25:210–216. https://doi.org/10.1016/j.tig.2009.03.004
10. Nehrt NL, Clark WT, Radivojac P, Hahn MW (2011) Testing the ortholog conjecture with comparative functional genomic data from mammals. PLoS Comput Biol 7(6):e1002073. https://doi.org/10.1371/journal.pcbi.1002073
11. Gabaldón T, Koonin EV (2013) Functional and evolutionary implications of gene orthology. Nat Rev Genet 14:360–366. https://doi.org/10.1038/nrg3456
12. Roustan V, Jain A, Teige M et al (2016) An evolutionary perspective of AMPK-TOR signaling in the three domains of life. J Exp Bot 67:3897–3907. https://doi.org/10.1093/jxb/erw211
13. Kanehisa M, Goto S (2000) KEGG: kyoto encyclopaedia of genes and genomes. Nucleic Acids Res 28:27–30. https://doi.org/10.1093/nar/28.1.27
14. Nordberg H, Cantor M, Dusheyko S et al (2014) The genome portal of the department of energy joint genome institute: 2014 updates. Nucleic Acids Res 42(Database issue):D26–D31. https://doi.org/10.1093/nar/gkt1069
15. Bateman A, Martin MJ, O'Donovan C et al (2015) UniProt: a hub for protein information. Nucleic Acids Res 43:D204–D212. https://doi.org/10.1093/nar/gku989
16. Herrero J, Muffato M, Beal K et al (2016) Ensembl comparative genomics resources. Database 2016:baw053. https://doi.org/10.1093/database/bav096
17. Sonnhammer ELL, Gabaldon T, Sousa Da Silva AW et al (2014) Big data and other challenges in the quest for orthologs. Bioinformatics 30:2993–2998. https://doi.org/10.1093/bioinformatics/btu492
18. Kelder T, Van Iersel MP, Hanspers K et al (2012) WikiPathways: building research communities on biological pathways. Nucleic Acids Res 40(Database issue):D1301–D1307. https://doi.org/10.1093/nar/gkr1074
19. Fabregat A, Sidiropoulos K, Garapati P et al (2016) The reactome pathway knowledgebase. Nucleic Acids Res 44:D481–D487. https://doi.org/10.1093/nar/gkv1351
20. Cerami EG, Gross BE, Demir E et al (2011) Pathway commons, a web resource for biological pathway data. Nucleic Acids Res 39(Database):D685–D690. https://doi.org/10.1093/nar/gkq1039
21. Sonnhammer ELL, Östlund G (2015) InParanoid 8: orthology analysis between 273 proteomes, mostly eukaryotic. Nucleic Acids Res 43:D234–D239. https://doi.org/10.1093/nar/gku1203
22. Altenhoff AM, Boeckmann B, Capella-Gutierrez S et al (2016) Standardized benchmarking in the quest for orthologs. Nat Methods 13:425–430. https://doi.org/10.1038/nmeth.3830
23. Altenhoff AM, Šunca N, Glover N et al (2015) The OMA orthology database in 2015: function predictions, better plant support, synteny view and other improvements. Nucleic Acids Res 43:D240–D249. https://doi.org/10.1093/nar/gku1158
24. Zdobnov EM, Tegenfeldt F, Kuznetsov D et al (2016) OrthoDB v9.1: cataloging evolutionary and functional annotations for animal, fungal, plant, archaeal, bacterial and viral orthologs. Nucleic Acids Res 45(D1):D744–D749. https://doi.org/10.1093/nar/gkw1119
25. Ebersberger I, Strauss S, von Haeseler A (2009) HaMStR: profile hidden markov model based search for orthologs in ESTs. BMC Evol Biol 9:157. https://doi.org/10.1186/1471-2148-9-157
26. Ebersberger I, Simm S, Leisegang MS et al (2014) The evolution of the ribosome biogenesis pathway from a yeast perspective. Nucleic Acids Res 42:1509–1523. https://doi.org/10.1093/nar/gkt1137
27. Jones P, Binns D, Chang HY et al (2014) InterProScan 5: genome-scale protein function classification. Bioinformatics 30:1236–1240. https://doi.org/10.1093/bioinformatics/btu031
28. Finn RD, Mistry J, Tate J et al (2010) The Pfam protein families database. Nucleic Acids Res 38:D211–D222. https://doi.org/10.1093/nar/gkm960

29. Koestler T, von Haeseler A, Ebersberger I (2010) FACT: functional annotation transfer between proteins with similar feature architectures. BMC Bioinformatics 11:417. https://doi.org/10.1186/1471-2105-11-417
30. Moore AD, Heldy A, Terrapon N et al (2014) DoMosaics: software for domain arrangement visualization and domain-centric analysis of proteins. Bioinformatics 30:282–283. https://doi.org/10.1093/bioinformatics/btt640
31. Finn RD, Clements J, Arndt W et al (2015) HMMER web server: 2015 update. Nucleic Acids Res 43:W30–W38. https://doi.org/10.1093/nar/gkv397
32. Edgar RC (2004) MUSCLE: multiple sequence alignment with high accuracy and high throughput. Nucleic Acids Res 32:1792–1797. https://doi.org/10.1093/nar/gkh340
33. Katoh K, Standley DM (2013) MAFFT multiple sequence alignment software version 7: improvements in performance and usability. Mol Biol Evol 30:772–780. https://doi.org/10.1093/molbev/mst010
34. Darriba D, Taboada GL, Doallo R, Posada D (2011) ProtTest-HPC: fast selection of best-fit models of protein evolution. In: Lect. Notes Comput. Sci. (including Subser. Lect. Notes Artif. Intell. Lect. Notes Bioinformatics). pp 177–184
35. Stamatakis A (2014) RAxML version 8: a tool for phylogenetic analysis and post-analysis of large phylogenies. Bioinformatics 30:1312–1313. https://doi.org/10.1093/bioinformatics/btu033
36. Rambaut A (2009) FigTree v1.3.1. 2006–2009. Program package available at http://tree.bio.ed.ac. Accessed 29 Nov. 2012
37. Pipinellis A (2015) GitHub essentials. Packt Publishing Ltd., Birmingham
38. Glez-Peña D, Gómez-Blanco D, Reboiro-Jato M et al (2010) ALTER: program-oriented conversion of DNA and protein alignments. Nucleic Acids Res 38(Web Server issue): W14–W18. https://doi.org/10.1093/nar/gkq321
39. Larkin MA, Blackshields G, Brown NP et al (2007) ClustalW and ClustalX version 2.0. Bioinformatics 23:2947–2948. https://doi.org/10.1093/bioinformatics/btm404
40. Penn O, Privman E, Ashkenazy H et al (2010) GUIDANCE: a web server for assessing alignment confidence scores. Nucleic Acids Res 38 (Web Server issue):W23–W28. https://doi.org/10.1093/nar/gkq443
41. Chang JM, Di Tommaso P, Notredame C (2014) TCS: a new multiple sequence alignment reliability measure to estimate alignment accuracy and improve phylogenetic tree reconstruction. Mol Biol Evol 31:1625–1637. https://doi.org/10.1093/molbev/msu117
42. Le SQ, Gascuel O (2008) An improved general amino acid replacement matrix. Mol Biol Evol 25:1307–1320. https://doi.org/10.1093/molbev/msn067
43. Goldman N, Anderson JP, Rodrigo a G (2000) Likelihood-based tests of topologies in phylogenetics. Syst Biol 49:652–670. https://doi.org/10.1080/106351500750049752
44. Shimodaira H, Hasegawa M (1999) Multiple comparisons of log-likelihoods with applications to phylogenetic inference. Mol Biol Evol 16:1114–1116. https://doi.org/10.1177/0148607109348061

Chapter 9

AMPK Protein Interaction Analyses by Yeast Two-Hybrid

Pascual Sanz, Rosa Viana, and Maria Adelaida Garcia-Gimeno

Abstract

Mammalian AMP-activated protein kinase (AMPK) is a Ser/Thr protein kinase that acts as a crucial energy sensor in the cell. Since AMPK plays a key role in a multitude of different pathways in the cell, major efforts have been concentrated to elucidate its signaling network, mainly by the identification of AMPK downstream targets. In this chapter we describe a yeast two-hybrid method for the direct evaluation of the interaction between an AMPK subunit and putative substrates.

Key words AMPK, Bait plasmid, Prey plasmid, β-Galactosidase, Yeast two-hybrid

1 Introduction

Mammalian AMP-activated protein kinase (AMPK) is a Ser/Thr protein kinase that acts as a crucial energy sensor in the cell. It is activated by nutritional and other kind of stress conditions and once activated it stimulates metabolic pathways that produce energy (catabolic pathways) whereas inhibits those that consume energy (anabolic pathways) in order to maintain energy status. In mammalian cells, AMPK is a heterotrimer composed of three different subunits: a catalytic subunit which harbors the Ser/Thr protein kinase activity (AMPKα, with two isoforms α1 and α2), a nucleotide binding regulatory subunit (AMPKγ, with three isoforms γ1, γ2 and γ3, which differ in the N-terminal extension) and a scaffolding subunit where both AMPKα and AMPKγ subunits interact (AMPKβ, with two isoforms β1 and β2) [1–3].

AMPK function has been implicated in multiple metabolic pathways. It interacts with a great variety of different substrates leading to short-term (i.e. regulation of the activity of defined enzymes by direct phosphorylation) and long-term effects (i.e. regulation of the transcriptional activity of several transcription factors) [1–3]. Since AMPK plays a key role in a multitude of different pathways in the cell, major efforts have been concentrated to elucidate its signaling network, mainly by the identification of

Dietbert Neumann and Benoit Viollet (eds.), *AMPK: Methods and Protocols*, Methods in Molecular Biology, vol. 1732, https://doi.org/10.1007/978-1-4939-7598-3_9,

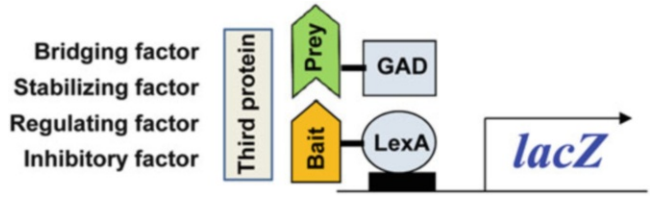

Fig. 1 Schematic drawing of the yeast two-hybrid system. The technique is based on the reconstitution of a transcription factor [a DNA binding module (LexA) and a transcription factor activating domain (GAD)] when a bait protein (i.e. AMPK subunit) interacts with a prey protein (putative AMPK interactor). This leads to the expression of a reporter gene (i.e. *lacZ*, encoding the β-galactosidase enzyme). The interaction between the bait and the prey proteins can be modulated by the expression of a third protein, which could be necessary for the interaction, could improve it by stabilizing the interaction, could regulate it (by i.e. by introducing post-translational modifications) or could inhibit the interaction

AMPK downstream targets. Several physical protein-protein interaction techniques (multidimensional substrate-screen, affinity purification, etc.) have been reported in the literature [4–8]. Alternatively, genetic techniques such as yeast two-hybrid have also been used to identify putative AMPK interactors [9–12]. In this chapter we will describe a yeast two-hybrid method for the direct evaluation of the interaction between an AMPK subunit and putative substrates [13–16], and the possibility to express a third component in the assay (yeast triple-hybrid) that could modify the initial interaction between AMPK subunit and its putative substrate [11] (Fig. 1). The effect of this third component could allow, stabilize, regulate or even inhibit the interaction between the bait and the prey proteins.

2 Materials

2.1 Plasmids

The ORFs corresponding to any of the AMPK subunits have to be cloned into appropriate bait yeast two-hybrid vectors containing a DNA-binding domain, such as pBTM116 [17], which carries a *TRP1* selection marker and produces a fusion protein with LexA at the N-terminus of the AMPK subunit (LexA-AMPK subunit; bait plasmid) (*see* **Notes 1** and **2**). The ORF corresponding to the putative AMPK interactor has to be cloned into Gal4-Activating-Domain containing plasmids, such as pACT2 [18] or pGADT7 (Clontech), which carry a *LEU2* selection marker and produce a fusion protein with GAD at the N-terminus of the protein (GAD-protein; prey plasmid) (*see* **Note 3**). If a third protein needs to be present in the two-hybrid system to regulate the interaction between the bait and the prey, the corresponding ORF has to be cloned into compatible yeast plasmids such as pWS93 [19], which carries an *URA3* selection marker and produces a fusion protein with an HA epitope at the N-terminus of the third protein. In this case,

the additional plasmid has to be introduced into the cells containing already the bait and prey plasmids, and the new transformants selected on SC + 2% glucose medium lacking tryptophan, leucine and uracil. As control, the same transformation should be conducted using an empty plasmid (*see* **Note 4**).

2.2 Yeast and Bacterial Strains

1. When the bait plasmid contains a LexA module, a yeast strain carrying *lexA* operators regulating the expression of reporter genes has to be used in the two-hybrid assay. We use the *Saccharomyces cerevisiae* THY-AP4 strain (*MATa, ura3, leu2, lexA::lacZ::trp1, lexA::HIS3, lexA::ADE2*) [20]. This strain requires the complementation of the culture medium with uracil, leucine, tryptophan, histidine and adenine, for growth (*see* **Note 5**). An advantage of this strain is that it carries the yeast biosynthetic gene *HIS3* under the control of the *lexA* operator, so that the interaction between AMPK subunits and putative partners can be carried out both by nutritional selection for histidine prototrophy and by an assay for β-galactosidase activity (which results from the expression of the *lacZ* gene under the control of *lexA* operator). To maintain the strain, cells are grown in complete YPD medium (*see* below).
2. Bacterial Strain: *Escherichia coli* KC8 (pyrF::Tn5, leuB600, trpC-9830, hisB463).

2.3 Culture Media

1. Complete YPD medium plates [21]: 2% (w/v) glucose, 2% (w/v) peptone, 1% (w/v) yeast extract, 2% (w/v) agar, adjusted to pH 6.0.
2. Synthetic complete (SC) + 2% glucose medium plates [21]: To prepare 400 ml of medium, autoclave 340 ml of water containing 8 g agar. Cool down the medium to 55 °C, and add 20 ml of 40% (w/v) glucose solution and 40 ml of a 10× solution of YNB + amino acid mix [6.7 g of yeast nitrogen base without amino acids plus 0.95 g of an amino acid mix (1.25 g arginine, 1.25 g methionine, 1.88 g tyrosine, 1.88 g isoleucine, 1.88 g lysine, 3.13 g phenylalanine, 6.25 g glutamic acid, 6.25 g aspartic acid, 9.38 g valine, 25 g serine and 25 g threonine) in 100 ml]. When necessary, 4 ml of each of the following stock solutions should be added to 400 ml of SC medium: 10 mg/ml leucine, 10 mg/ml tryptophan, 10 mg/ml histidine, 2.5 mg/ml uracil, 2.5 mg/ml adenine.
3. M9 minimal medium plates for *E. coli KC8* cells: To prepare 400 ml of medium, autoclave 315 ml of water containing 8 g agar. Cool down the medium to 55 °C, and add 40 ml of a 10× solution of M9 salts (sterile filtered 128 g/l $Na_2HPO_4.12H_2O$, 30 g/l KH_2PO_4, 5 g/l NaCl, 10 g/l NH_4Cl), 5.5 ml of 1 M NaOH, 4 ml of 40% (w/v) glucose, 40 ml of 10× amino

acid mix (9.5 g/l amino acid mix, as above), 400 μl of 100 mg/ml ampicillin, 400 μl of 1 M thiamine-HCl, 800 μl of 1 M $MgSO_4$ and 40 μl of 1 M $CaCl_2$. Then add 4 ml each of sterile filtered 10 mg/ml histidine, 10 mg/ml tryptophan and 2.5 mg/ml uracil.

4. LB + Amp plates: 1% (w/v) NaCl, 1% (w/v) peptone, 0.5% (w/v) yeast extract, 2% (w/v) agar, adjusted to pH: 7.5. Autoclave and cool down the medium to 55 °C, and add 1 ml/l of 100 mg/ml ampicillin.

2.4 Yeast Transformation Materials

1. TE-LiAc solution: sterile 0.1 M lithium acetate in Tris-EDTA buffer (TE, 10 mM Tris–HCl, pH 8.0, 1 mM EDTA).
2. PEG-TE-LiAc solution: sterile 40% (w/v) polyethylene glycol 3350 in TE-LiAc solution.
3. Salmon sperm DNA: sterile denaturized 10 mg/ml salmon sperm DNA.
4. Extraction buffer for plasmid recovery: 10 mM Tris–HCl, pH 8.0, 100 mM NaCl, 1 mM EDTA, 2% (v/v) Triton X-100, 1% (w/v) SDS.
5. Acid-washed glass beads 425–600 μm diameter.
6. Phenol-Chloroform solution: 50% (v/v) phenol, 48% (v/v) chloroform, 2% (v/v) isoamyl alcohol.

2.5 Qualitative β-Galactosidase Assay

1. Z-Buffer: 60 mM Na_2HPO_4, 40 mM NaH_2PO_4, 10 mM KCl, 1 mM $MgSO_4$, 50 mM 2-mercaptoethanol. Weigh 16.1 g of $Na_2HPO_4{\cdot}7H_2O$, 5.5 g of $NaH_2PO_4{\cdot}H_2O$, 0.75 g of KCl, 0.25 g of $MgSO_4{\cdot}7H_2O$, in water up to 1 l of solution. Adjust pH to 7.0. Add then 2.7 ml 2-mercaptoethanol; this product should be added extemporaneously.
2. X-Gal stock solution: 100 mg/ml 5-bromo-4-chloro-3-indolyl-β-D-galactopyranoside (X-Gal) in dimethylformamide.

2.6 Quantitative β-Galactosidase Assay

1. SDS: 0.1% (w/v) sodium dodecyl sulfate (SDS).
2. Chloroform.
3. ONPG: 4 mg/ml o-nitrophenylgalactopyranoside (ONPG).
4. Na_2CO_3: 1 M Na_2CO_3.

2.7 Other Materials

1. Sterile flat tooth-picks.
2. Glass rod 0.3 cm diameter.
3. 90 mm wide nitrocellulose (0.45 μm) circular filters.
4. Regular filter paper.
5. 90 mm wide circular 3MM chromatography paper.

3 Methods

3.1 Transformation of Yeast Cells with Bait and Prey Plasmids and Selection of Putative Positive Transformants

1. THY-AP4 yeast cells are transformed with a combination of bait and prey plasmids using the lithium acetate method [22]. Remove 50 ml of yeast cells growing exponentially in YPD liquid medium (A_{600} 0.5) and spin them down at 4000 × *g* for 5 min.
2. Resuspend the pellet in 5 ml of sterile TE-LiAc solution and spin down the samples again at 4000 × *g* for 5 min. Then, resuspend the cells in 0.5 ml of TE-LiAc solution.
3. To 50 μl of cell suspension, add 2 μl of carrier DNA (denaturized 10 mg/ml salmon sperm DNA), 2–3 μl of each plasmid (containing 100 ng each) and 300 μl of PEG-TE-LiAc solution. Mix carefully and incubate the mixture at 30 °C for 30 min.
4. Then, incubate the samples at 42 °C for 15 min.
5. Spin down the samples at 4000 × *g* for 5 min and resuspend the cell pellet in 1 ml of water (by pipetting up and down with a blue tip). Spin down the cells at 4000 × *g* for 5 min and resuspend them in 200 μl of water.
6. Spread 100 μl of each transformation onto SC + 2% glucose plates lacking tryptophan and leucine.
7. Individual colonies should appear around 36–48 h of growth at 30 °C. With the help of a sterile tooth-pick, recover the cells from a single colony and spread them in a line (0.5 cm long) of two consecutive plates of SC + 2% glucose lacking tryptophan and leucine. For each combination of bait and prey plasmids around 8–10 colonies should be analyzed. As sometimes colonies of different size appear in the plates, we normally make lines of colonies of different sizes to conduct qualitative β-galactosidase assays. Placing a form with marked squares (grid form) at the bottom of the plate helps identifying the position of the different lines (Fig. 2a). Allow the cells to grow for 36–48 h at 30 °C (Fig. 2b). One set of plates will be used in the qualitative β-galactosidase assay whereas the second one will be used as master plate to inoculate cells in the quantitative β-galactosidase assay.

   As controls, combinations of bait with an empty prey plasmid and of empty bait with the corresponding prey plasmid are also introduced into the yeast cells. In addition we recommend carrying out an additional transformation with plasmids that give a positive interaction as control.

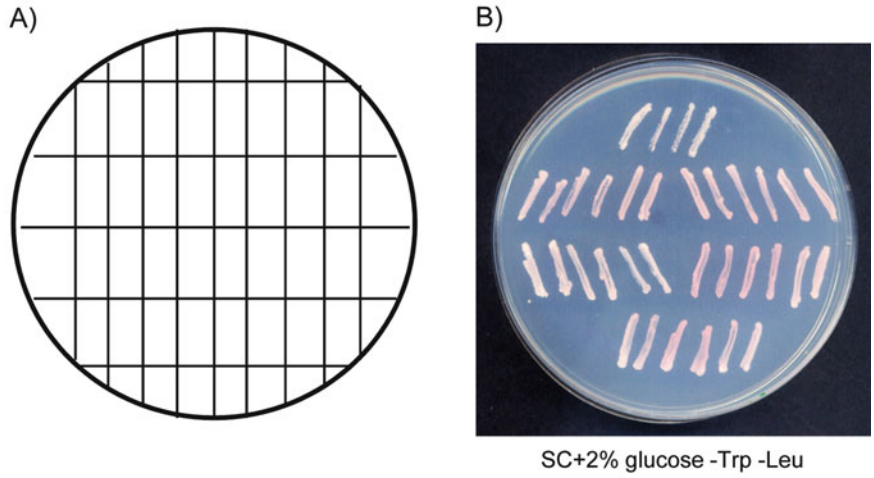

Fig. 2 Growth of the selected transformants on SC + 2% glucose plates lacking tryptophan and leucine. (**a**) Example of a grid form that can be used to identify the position of the different lines of growth. (**b**) Example of a plate after growing the transformants at 30 °C for 48 h

3.2 Qualitative β-Galactosidase Assay

The technique consists basically in transferring colonies to a nitrocellulose membrane and then carrying a β-galactosidase assay in the colonies that are on the membrane [23]. It has several steps:

1. Lay a 90 mm wide nitrocellulose circular filter onto one of the plates with the yeast growth lines and allow it to wet completely. With a glass rod press the filter to make sure it contacts with the cell cultures of the plate. With a needle, drill holes in the membrane and plate medium in order to orientate the culture lines.
2. Lift the nitrocellulose filter off of the plate carefully to avoid smearing the colonies and place it with the colonies side up on top of a regular filter paper. Place the filters at −80 °C for at least 2 h.
3. Remove the nitrocellulose filters from the freezer and, in a fume hood, place them with the cells side up in a petri dish containing a 90 mm wide circular 3MM chromatography paper, soaked with 3 ml of Z buffer containing 1 mg/ml X-Gal. Seal the plates with parafilm to avoid the nasty odor of 2-mercaptoethanol and incubate the filters at 30 °C for no more than 2 h. If there is an interaction between the bait and prey fusion proteins, the expression of the *lacZ* gene will be activated, resulting in the synthesis of β-galactosidase. This enzyme will act on the X-gal substrate releasing a blue color that will remain in the cells (Fig. 3a). The time at which the blue color appears and its intensity is a qualitative reflection of the intensity of the interaction between the bait and prey proteins. For this reason we recommend checking the color

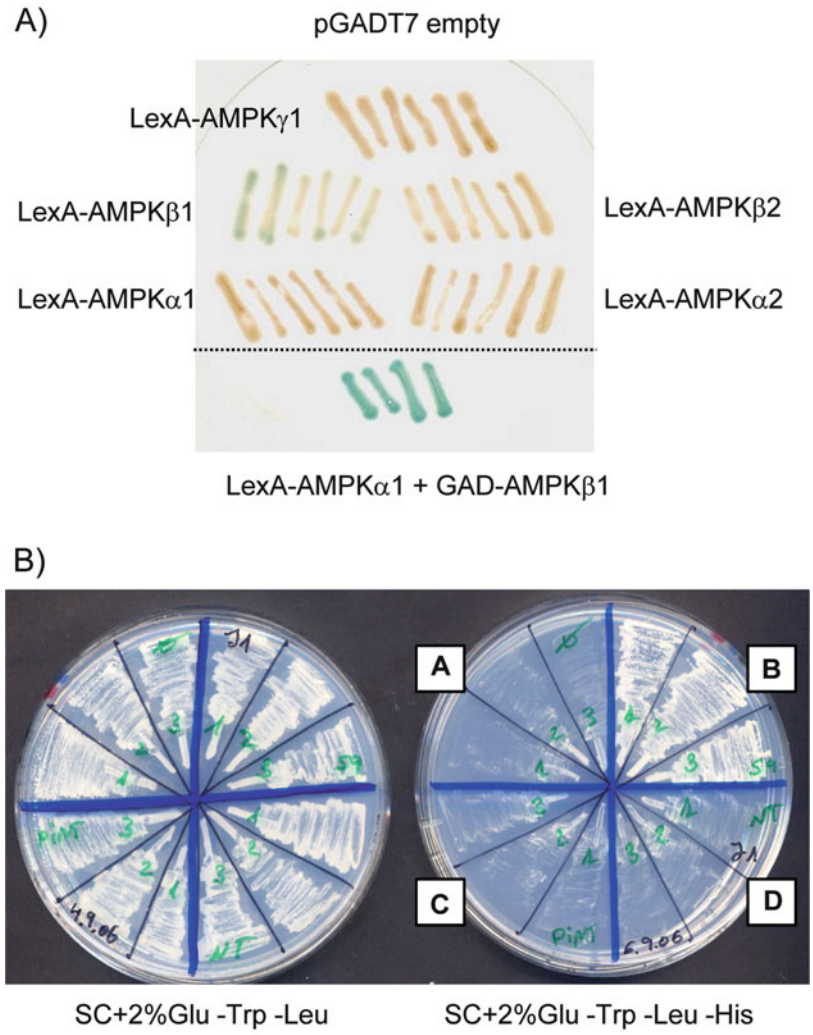

Fig. 3 Qualitative assays for two-hybrid interaction. (**a**) Qualitative β-galactosidase assay. Transformants containing different combinations of plasmids were grown in SC + 2% glucose plates lacking tryptophan and leucine. When the growth in the form of lines was evident, plates were subjected to the qualitative β-galactosidase assay described in Methods. Blue colonies are indicative of a two-hybrid interaction. This filter shows the assay of transformants containing an empty prey plasmid (pGADT7) and either LexA-AMPKα1, LexA-AMPKα2, LexA-AMPKβ1, LexA-AMPKβ2 or LexA-AMPKγ1. As it can be observed, the expression of LexA-AMPKβ1 has weak self-activating properties (pale blue color of the corresponding colonies in comparison to the pale brown color present in cells containing LexA-AMPKβ2). The bottom row shows the assay of transformants containing LexA-AMPKα2 and GAD-AMPKβ1, which shows a clear two-hybrid interaction (blue colonies). (**b**) Qualitative growth assay in plates lacking histidine. Selected transformants were grown in SC + 2% glucose medium lacking tryptophan and leucine and in SC + 2% glucose medium lacking tryptophan, leucine and histidine. Only transformants showing an interaction between the bait and the prey proteins will allow the transcription of the *HIS3* gene resulting in allowing the growth of the transformants in the selective medium lacking histidine. Three colonies of independent transformants containing different combination of plasmids were grown in the culture media indicated above: (**a**) pBTM116 (empty) and pGADT7-PSMD11; (**b**) pBTM-AMPKα2 and pGADT7-PSMD11; (**c**) pBTM-AMPKα2 and pGADT7 (empty); pBTM-AMPKγ1 and pGADT7-PSMD11. Only AMPKα2 but not AMPKγ1 is able to interact with PSMD11, a non-ATPase subunit of the proteasome [11]

of the colonies after periods of 30 min. By comparison with the positive and negative control, one can estimate qualitatively the strength of the interaction (Fig. 3a) (*see* **Note 6**). After 2 h of incubation at 30 °C, remove the nitrocellulose filters and let them dry in the fume hood, to keep them as records of the experiment.

3.3 Qualitative Growth Assay in Plates Lacking Histidine

An alternative method to assess qualitatively the interaction is by growing the transformants in a culture medium lacking tryptophan (to maintain the bait plasmid), leucine (to maintain the prey plasmid) and histidine (to select for two-hybrid interaction). If there is an interaction between AMPK subunit and the putative interactor, the transcription of the *HIS3* gene will be activated resulting in allowing the growth of the transformants in this selective medium. Colonies of the corresponding transformants are spread on SC + 2% glucose plates lacking tryptophan, leucine and histidine and incubated at 30 °C for 24–48 h (Fig. 3b).

3.4 Quantitative β-Galactosidase Assay

1. From the master plate with the yeast growth lines, inoculate cells in 5 ml of liquid SC + 2% glucose medium lacking tryptophan and leucine. Inoculate at least six individual colonies from each combination of bait and prey plasmids. When they are growing at the exponential phase (A_{600} between 0.3 and 0.8) collect 0.5 OD of cells (i.e., 1 ml of a culture at A_{600} 0.5) in a small glass tube. Spin down the cells for 5 min at 4000 × *g* and discard the supernatant.
2. Resuspend the cell pellet in 1 ml of Z buffer. In parallel carry one tube with 1 ml of Z buffer alone (negative control). Add 25 μl of 0.1% SDS and 25 μl of chloroform. Vortex the tubes for 15 s and leave them warming at 30 °C in a water bath. This treatment opens some holes in the yeast surface and allows the contact of the β-galactosidase enzyme with its substrate.
3. In a time dependent way, add 0.2 ml of ONPG solution and incubate at 30 °C in a water bath. If the transformants express the *lacZ* gene, the β-galactosidase will act on the ONPG substrate releasing o-nitrophenol which gives a yellow color. As soon as a yellow color appears in the tubes, we recommend stopping the reaction and annotating the time.
4. Stop the reaction at a defined period of time (max. 2 h) with 0.5 ml of 1 M Na_2CO_3. Spin down for 5 min to remove cell debris. Transfer the supernatant to a clean tube and measure the yellow absorbance at 420 nm. In our hands, the color is only stable during the first 15 min after stopping the reaction, so the measurement of the absorbance should be performed during this period of time.

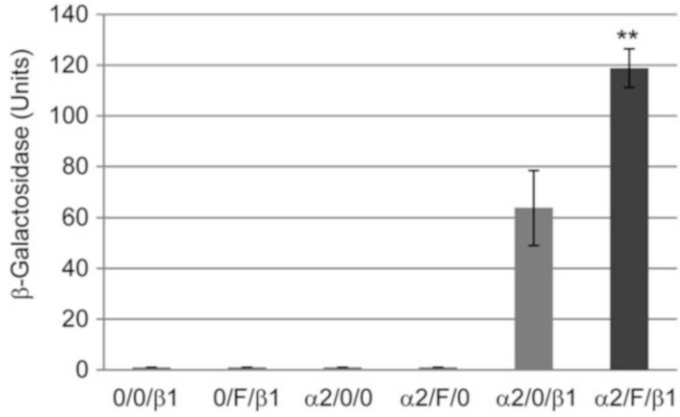

Fig. 4 Quantitative β-galactosidase assay of the interaction between LexA-AMPKα2 and GAD-AMPKβ1. In the nomenclature (i.e., α2/F/β1), the first position corresponds to transformants expressing the bait (0, means empty pBTM116 vector; α2, means LexA-AMPKα2), the second position corresponds to a third protein being expressed (0, means empty pWS93 vector; F, means pWS93-F) and the third position corresponds to the prey (0, means empty pGADT7 vector; β1, means pGADT7-AMPKβ1). The strength of the interaction is a direct correlation of the levels of β-galactosidase activity (values are means of at least six transformants per condition; bars indicate standard deviation). As observed, the expression of protein F improves the interaction between LexA-AMPKα2 and GADT7-AMPKβ1 (**$p < 0.01$)

5. The units of β-galactosidase activity (Miller Units) are defined as value of $A_{420} \times 2000$/time of the reaction in minutes [24]. A regular two-hybrid assay should contain the values of the controls with the empty plasmids and the values of the interaction between the AMPK subunit and the putative interactor (Fig. 4) (*see* **Note 7**).
6. In order to validate the results of the two-hybrid analysis it is necessary to check the correct expression of the fusion proteins (Fig. 5) (*see* **Note 8**).

3.5 Screening of Yeast Two-Hybrid Libraries for New Interactors

The yeast two-hybrid system allows the screening of a cDNA library using a LexA-AMPK subunit as bait. Different cDNA libraries from different tissues exist in the market and distinct protocols can be used to perform the screening, but we still carry out the one based on the co-transformation of the yeast TAT7 or THY-AP4 strains with a pBTM116-AMPK subunit plasmid and a commercial cDNA library in a pGAD-based vector (Clontech) [10, 11]. We carry out the following steps:

1. Transform the yeast strain (i.e., THY-AP4) with the bait plasmid (i.e., pBTM-AMPKα2) and different amounts of the selected cDNA library (based in pACT2; prey plasmid). Follow the steps described in Subheading 2.3 (**steps 1–6**). In this way we will determine the best ratio between bait and prey plasmids to obtain the highest number of transformants.

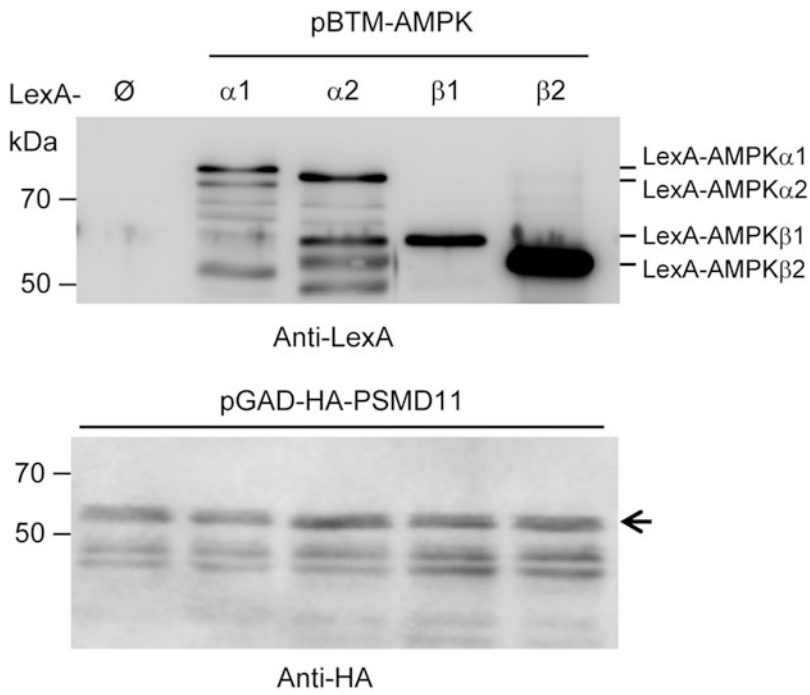

Fig. 5 Western blot analysis of selected transformants. Transformants containing different combination of plasmids were analyzed by SDS-PAGE and immunoblotting using anti-LexA and anti-HA antibodies. In this case, all transformants contained the prey plasmid pGADT7-PSMD11 (expressing a non-ATPase subunit of the proteasome [11]) and different bait plasmids expressing LexA-AMPKα1, LexA-AMPKα2, LexA-AMPKβ1, LexA-AMPKβ2 or the empty plasmid pBTM116 (ϕ). Molecular size markers are indicated. The empty pBTM116 plasmid produces LexA protein (27 kDa) but it is not shown in the picture. The protein bands of lower molecular size in the lanes of LexA-AMPKα1 and LexA-AMPKα2 are probably due to degradation products of the full length forms. The position of the full length GAD-HA-PSMD11 protein is indicated with an arrow

2. Once the best ratio of the combination of bait and cDNA library plasmid is determined, repeat the transformation under these conditions, but select the transformants in SC + 2% glucose plates lacking tryptophan, leucine and histidine. Only transformants that are able to activate the expression of the *HIS3* gene will be recovered (*see* **Note 9**). Spread also one aliquot of the transformed cells in SC + 2% glucose plates lacking only tryptophan and leucine to assess the total number of transformants. Repeat this step as many times as necessary to cover at least a total of 500,000 independent transformants.
3. Pick up the putative positive colonies that have grown up in the absence of tryptophan, leucine and histidine and screen them for β-galactosidase activity using the qualitative method described in Subheading 2.4.
4. Recover the corresponding library plasmid in those transformants that give a clear positive β-galactosidase reaction. To do this, grow the corresponding transformants in SC + 2% glucose

medium lacking only leucine, since the prey plasmid contains a *LEU2* selection marker. At the exponential phase (A_{600} 0.5) remove 5 ml of culture and spin it down at 4000 × *g* for 5 min. Resuspend the pellet in 1 ml of Tris-EDTA (TE) buffer and spin the cells down again. Resuspend the pellet in 200 μl of extraction buffer. Add 0.3 g of acid-washed glass beads and 200 μl of phenol-chloroform solution. Vortex at full speed for 2 min and spin down the suspension at 4000 x *g* for 5 min. Finally, transfer the aqueous phase to a clean tube.

5. Transform the *Escherichia coli KC8* strain with 10 μl of samples obtained above. Plate the bacteria first on LB + Amp plates. Colonies will appear after 24–48 h of incubation at 37 °C. This step improves the recovery of colonies carrying the prey plasmid. Transfer colonies to M9 minimal medium plates lacking leucine. Incubate bacteria at 37 °C for 24–48 h until colonies appear. Obtain the prey plasmid from cultures of these colonies by standard bacterial miniprep methods. Make sure that the recovered plasmids are prey plasmids, i.e., by enzyme restriction digestion.
6. These putative positive plasmids are rechecked for two-hybrid interaction with empty pBTM116 and the LexA-AMPK subunit plasmids. Only those plasmids that do not have self-activating properties and maintain the interaction with the corresponding AMPK subunit are sequenced, and the sequences characterized by BLAST analysis [25]. The strength of the interaction is quantified by measuring the β-galactosidase activity in these selected transformants (*see* above). In this way, a collection of putative AMPK interactors is defined (*see* **Note 10**) [10, 11].

4 Notes

1. The yeast two-hybrid is based on the reconstruction of a transcription factor that has to go to the nucleus to exert its function (Fig. 1). Therefore the yeast two-hybrid system only works for soluble proteins that must be transported to the nucleus. Thus, the assay is not valid for membrane proteins or for proteins that aggregate in the cytosol. The original method was based on the reconstruction of the Gal4 transcription factor, placing the Gal4-DNA Binding Domain (GBD) in the bait plasmid and the Gal4-Activating Domain (GAD) in the prey plasmid [26]. Later on, the Gal4-GBD was substituted by the bacterial LexA repressor [17, 27]. In our hands, the use of LexA-based system has some advantages on the GBD-based one: i.e., it produces less false positives since LexA is an heterologous protein that does not interact with yeast proteins, the

strength of the interaction is normally higher when using a LexA-based bait plasmid in comparison to the GBD-based one and, in addition, there are good anti-LexA antibodies in the market that can be used to test the production and quality of the bait fusion protein (unfortunately no good commercial antibody for Gal4-GBD is in the market yet).

2. There are alternative vectors in the market that produce LexA-fusion proteins both with LexA at the N-terminus or as a C-terminal fusion. The choice depends on the stability of the fusion protein and on the preservation of the function of the AMPK subunit. In our hands, N-terminal fusions of LexA give better results than C-terminal fusion proteins.
3. The main difference between the available GAD-based plasmids is the type of multicloning site present in them. Both pACT2 and pGADT7 contain an HA-epitope between the GAD and the corresponding ORF which can be used to detect the production and quality of the prey fusion proteins (GAD-HA-prey fusion protein). AMPK subunits should be also subcloned into these plasmids to confirm the interaction with the putative substrate. In this way both directions of the two-hybrid assay are covered [(1) bait-AMPK subunit and prey-interactor; (2) bait-interactor and prey-AMPK subunit], since sometimes one direction gives stronger results that the other. The GAD-based constructs become completely necessary when a particular AMPK subunit shows signs of self-activating properties when fused to LexA (*see* **Note 9**).
4. Since the yeast strain contains four usable different auxotrophies (*trp1*, *leu2*, *ura3* and *his3*), up to two additional plasmids carrying the selection markers *URA3* and *HIS3* can be introduced in the cells to regulate the interaction mediated by the bait (*TRP1*) and prey (*LEU2*) plasmids. In Fig. 4, it is shown that the expression of a third protein (protein F) improves the interaction between AMPKα2 and AMPKβ1.
5. Alternative yeast strain can be used in the yeast two-hybrid assay. For example CTY10.5d *(MATa ade2 his3 leu2 trp1 ga 4 gal80 URA3::lexAop-lacZ)* or TAT7 *(MATa ade2 his3 leu2 trp1 ga4 gal80 LYS2::lexAop-HIS3 URA3::lexAop-lacZ)* [11, 28]. However, in our hands the THY-AP4 strain gives better performance that the other ones.
6. In the yeast two-hybrid assay it is essential to analyze if the bait construct by itself has self-activating properties. In other words, if the bait plasmid by itself is able to activate the transcription of the reporter genes. In the case of AMPK, bait plasmids such as LexA-AMPKα1, LexA-AMPKα2, LexA-AMPKβ2, LexA-AMPKγ1 and LexA-AMPKγ2 give negative results on self-activation (Fig. 3a). However, LexA-AMPKβ1 has a weak self-activating performance (Fig. 3a) and LexA-

AMPKγ3 has a strong self-activating profile [13]. In the case of weak self-activating properties, the regular measurement of the β-galactosidase activity is still a good way to measure the interaction with a prey, provided this interaction gives higher enzymatic activity than the bait alone. In the case of strong self-activating properties, probably the amount of β-galactosidase is too high to allow the detection of differences in the activity when a prey protein is present. In these cases, moving the ORF of the AMPK subunit into the prey plasmid and placing the protein of interest into the bait plasmid may help. Alternatively, the ORF of the self-activating subunit can be shortened either from the N- or the C-terminus to obtain a construct devoid of self-activating properties [11].

7. The yeast two-hybrid system is very versatile and allows checking whether the interaction between two components changes depending on the growth environmental conditions. For example, by growing the cells in high glucose (4%) and shifting them to low glucose (0.05%), the two-hybrid system allows knowing whether the interaction changes under glucose starvation conditions. The effect of alternative changes in growth media conditions or the effect of the presence of different kind of stress conditions (i.e., heat shock, salt stress, etc.) on the strength of the interaction can easily be detected by this technique.
8. It is essential to check the expression of the bait and prey proteins to understand the results of the two-hybrid technique. With this aim, we obtain yeast extracts and analyze them by SDS-PAGE and immunoblotting [11, 28]. To check the expression of the bait fusion proteins, we normally use either commercial anti-LexA antibodies or the corresponding anti-AMPK subunit antibodies. Sometimes there is no detectable two-hybrid interaction but this is due to poor expression of the proteins being involved. In this case, we recommend repeating the two-hybrid with proteins with different tags or with truncated forms of the proteins, if the full length protein is unstable.
9. In the case of weak self-activating properties of the bait or to enhance the stringency of the screening, the enzymatic activity encoded by the *HIS3* reporter gene may be partially inhibited by increasing concentrations of 3-aminotriazole (3-ATZ) (from 5 mM to 10 mM) in the culture medium. In this way, only transformants with a strong interaction between the bait and the prey will grow in the selective medium (SC + 2%glucose -Trp, -Leu, -His +3-ATZ).
10. Several proteins appear continuously in unrelated two-hybrid screenings. Golemis and co-workers created a list of false positive proteins for classic yeast two-hybrid analysis [27]. In brief,

they are heat shock, ribosomal and mitochondria proteins; proteasome subunits, elongation factors, etc. The collection of positive interactors obtained after the AMPK-based two-hybrid screening should be compared with this list to validate the possible candidates.

Acknowledgements

This study was supported by grants from the Spanish Ministry of Education and Science (SAF2014-54604-C3-1-R) and Generalitat Valenciana (PrometeoII/2014/029) to P.S.

References

1. Carling D, Thornton C, Woods A, Sanders MJ (2012) AMP-activated protein kinase: new regulation, new roles? Biochem J 445(1):11–27
2. Hardie DG (2014) AMP-activated protein kinase: maintaining energy homeostasis at the cellular and whole-body levels. Ann Rev Nutr 34:31–55
3. Hardie DG, Ashford ML (2014) AMPK: regulating energy balance at the cellular and whole body levels. Physiology (Bethesda) 29 (2):99–107
4. Tuerk RD, Thali RF, Auchli Y, Rechsteiner H, Brunisholz RA, Schlattner U, Wallimann T, Neumann D (2007) New candidate targets of AMP-activated protein kinase in murine brain revealed by a novel multidimensional substrate-screen for protein kinases. J Proteome Res 6 (8):3266–3277
5. Thali RF, Tuerk RD, Scholz R, Yoho-Auchli Y, Brunisholz RA, Neumann D (2010) Novel candidate substrates of AMP-activated protein kinase identified in red blood cell lysates. Biochem Biophys Res Commun 398(2):296–301
6. Behrends C, Sowa ME, Gygi SP, Harper JW (2010) Network organization of the human autophagy system. Nature 466(7302):68–76
7. Ewing RM, Chu P, Elisma F, Li H, Taylor P, Climie S, McBroom-Cerajewski L, Robinson MD, O'Connor L, Li M, Taylor R, Dharsee M, Ho Y, Heilbut A, Moore L, Zhang S, Ornatsky O, Bukhman YV, Ethier M, Sheng Y, Vasilescu J, Abu-Farha M, Lambert JP, Duewel HS, Stewart II, Kuehl B, Hogue K, Colwill K, Gladwish K, Muskat B, Kinach R, Adams SL, Moran MF, Morin GB, Topaloglou T, Figeys D (2007) Large-scale mapping of human protein-protein interactions by mass spectrometry. Mol Sys Biol 3:89
8. Qi J, Gong J, Zhao T, Zhao J, Lam P, Ye J, Li JZ, Wu J, Zhou HM, Li P (2008) Downregulation of AMP-activated protein kinase by Cidea-mediated ubiquitination and degradation in brown adipose tissue. EMBO J 27 (11):1537–1548
9. Bruckner A, Polge C, Lentze N, Auerbach D, Schlattner U (2009) Yeast two-hybrid, a powerful tool for systems biology. Int J Mol Sci 10 (6):2763–2788
10. Solaz-Fuster MC, Gimeno-Alcaniz JV, Casado M, Sanz P (2006) TRIP6 transcriptional co-activator is a novel substrate of AMP-activated protein kinase. Cell Signal 18 (10):1702–1712
11. Moreno D, Viana R, Sanz P (2009) Two-hybrid analysis identifies PSMD11, a non-ATPase subunit of the proteasome, as a novel interaction partner of AMP-activated protein kinase. Int J Biochem Cell Biol 41 (12):2431–2439
12. Rolland T, Tasan M, Charloteaux B, Pevzner SJ, Zhong Q, Sahni N, Yi S, Lemmens I, Fontanillo C, Mosca R, Kamburov A, Ghiassian SD, Yang X, Ghamsari L, Balcha D, Begg BE, Braun P, Brehme M, Broly MP, Carvunis AR, Convery-Zupan D, Corominas R, Coulombe-Huntington J, Dann E, Dreze M, Dricot A, Fan C, Franzosa E, Gebreab F, Gutierrez BJ, Hardy MF, Jin M, Kang S, Kiros R, Lin GN, Luck K, MacWilliams A, Menche J, Murray RR, Palagi A, Poulin MM, Rambout X, Rasla J, Reichert P, Romero V, Ruyssinck E, Sahalie JM, Scholz A, Shah AA, Sharma A, Shen Y, Spirohn K, Tam S, Tejeda AO, Trigg SA, Twizere JC, Vega K, Walsh J, Cusick ME, Xia Y, Barabasi AL, Iakoucheva LM, Aloy P, De Las Rivas J, Tavernier J, Calderwood MA, Hill DE, Hao T, Roth FP, Vidal

M (2014) A proteome-scale map of the human interactome network. Cell 159(5):1212–1226

13. Viana R, Towler MC, Pan DA, Carling D, Viollet B, Hardie DG, Sanz P (2007) A conserved sequence immediately N-terminal to the Bateman domains in AMP-activated protein kinase gamma subunits is required for the interaction with the beta subunits. J Biol Chem 282(22):16117–16125
14. Solaz-Fuster MC, Gimeno-Alcaniz JV, Ros S, Fernandez-Sanchez ME, Garcia-Fojeda B, Criado Garcia O, Vilchez D, Dominguez J, Garcia-Rocha M, Sanchez-Piris M, Aguado C, Knecht E, Serratosa J, Guinovart JJ, Sanz P, Rodriguez de Cordoba S (2008) Regulation of glycogen synthesis by the laforin-malin complex is modulated by the AMP-activated protein kinase pathway. Hum Mol Genet 17 (5):667–678
15. Vernia S, Solaz-Fuster MC, Gimeno-Alcaniz JV, Rubio T, Garcia-Haro L, Foretz M, de Cordoba SR, Sanz P (2009) AMP-activated protein kinase phosphorylates R5/PTG, the glycogen targeting subunit of the R5/PTG-protein phosphatase 1 holoenzyme, and accelerates its down-regulation by the laforin-malin complex. J Biol Chem 284(13):8247–8255
16. Oligschlaeger Y, Miglianico M, Dahlmans V, Rubio-Villena C, Chanda D, Garcia-Gimeno MA, Coumans WA, Liu Y, Voncken JW, Luiken JJ, Glatz JF, Sanz P, Neumann D (2016) The interaction between AMPKbeta2 and the PP1-targeting subunit R6 is dynamically regulated by intracellular glycogen content. Biochem J 473(7):937–947
17. Vojtek AB, Cooper JA, Hollenberg SM (1997) Searching for interacting proteins with the two-hybrid system II. In: Bartel PL, Fields S (eds) The yeast two-hybrid system. Oxford University Press, Oxford, pp 29–42
18. Legrain P, Dokhelar M-C, Transy C (1994) Detection of protein-protein interactions using different vectors in the two-hybrid system. Nucleic Acids Res 22:3241–3242
19. Sanz P, Alms GR, Haystead TA, Carlson M (2000) Regulatory interactions between the Reg1-Glc7 protein phosphatase and the Snf1 protein kinase. Mol Cell Biol 20 (4):1321–1328
20. Paumi CM, Menendez J, Arnoldo A, Engels K, Iyer KR, Thaminy S, Georgiev O, Barral Y, Michaelis S, Stagljar I (2007) Mapping protein-protein interactions for the yeast ABC transporter Ycf1p by integrated split-ubiquitin membrane yeast two-hybrid analysis. Mol Cell 26(1):15–25
21. Rose MD, Winston F, Hieter P (1990) Methods in yeast genetics, a laboratory course manual. Cold Spring Harbor laboratory press. Cold Spring Harbor, New York
22. Ito H, Fukuda Y, Murata K, Kimura A (1983) Transformation of intact yeast cells treated with alkali cations. J Bacteriol 153:163–168
23. Yang X, Hubbard EJ, Carlson M (1992) A protein kinase substrate identified by the two-hybrid system. Science 257 (5070):680–682
24. Ludin K, Jiang R, Carlson M (1998) Glucose-regulated interaction of a regulatory subunit of protein phosphatase 1 with the Snf1 protein kinase in Saccharomyces cerevisiae. Proc Natl Acad Sci U S A 95(11):6245–6250
25. Altschul SF, Madden TL, Schaffer AA, Zhang J, Zhang Z, Miller W, Lipman DJ (1997) Gapped BLAST and PSI-BLAST: a new generation of protein database search programs. Nucleic Acids Res 25(17):3389–3402
26. Fields S, Song O (1989) A novel genetic system to detect protein-protein interactions. Nature (London) 340:245–246
27. Golemis EA, Serebriiskii I, Finley RL Jr, Kolonin MG, Gyuris J, Brent R (2011) Interaction trap/two-hybrid system to identify interacting proteins. Curr Protoc Cell Biol. Chapter 17: Unit 17 13
28. Gimeno-Alcaniz JV, Sanz P (2003) Glucose and type 2A protein phosphatase regulate the interaction between catalytic and regulatory subunits of AMP-activated protein kinase. J Mol Biol 333(1):201–209

Chapter 10

Transient Expression of AMPK Heterotrimer Complexes in Mammalian Cells

Jonathan S. Oakhill, John W. Scott, and Toby A. Dite

Abstract

Regulation of AMP-activated protein kinase (AMPK) signalling is complex and involves contributions from adenine nucleotides, co-/posttranslational modifications, and isoform composition of the AMPK heterotrimer. It is becoming apparent that AMPK activation/inhibition by synthetic drugs involves similar levels of complexity. Major advances in our understanding of these mechanisms have been gained from recombinant expression systems that provide sufficient quantities of highly purified material for structure/function studies. Here, we provide a detailed protocol for transient expression of affinity-tagged AMPK complexes in mammalian cells. We have found this system to be optimal as a source of enzyme possessing regulatory modifications found in vivo.

Key words Recombinant protein, Kinase, Mammalian cell, Transfection, Purification, Biochemistry, Metabolism

1 Introduction

AMP-activated protein kinase (AMPK) is a phylogenetically conserved Ser/Thr kinase that has emerged as an important integrator of signals to control cellular energy balance [1]. At the whole-body level, AMPK also integrates stress responses such as exercise, as well as nutrient and hormonal signals, to control food intake, energy expenditure, and substrate utilization. It is now widely thought that this enzyme is a key component in mechanisms underlying the health benefits of diet and exercise. There is also increasing evidence for a role of AMPK in multiple common diseases including type 2 diabetes, cancer, obesity, and cardiovascular disease. Consequently, a new age of AMPK drug development has emerged that may have profound effects in the treatment of these metabolic diseases in the future [2].

The AMPK complex is an αβγ heterotrimer containing a catalytic α-subunit and regulatory β and γ subunits. Multiple isoforms of each subunit exist in mammals (α1, α2, β1, β2, γ1, γ2, γ3) which

Dietbert Neumann and Benoit Viollet (eds.), *AMPK: Methods and Protocols*, Methods in Molecular Biology, vol. 1732, https://doi.org/10.1007/978-1-4939-7598-3_10,

potentially permit formation of 12 distinct AMPK complexes (α1β1γ1 through α2β2γ3). Much of the pioneering work on AMPK regulation was conducted on enzyme extracted from rat liver (predominantly α1, α2, β1, and γ1 isoforms), purified using extensive multistep protocols. These preparations provided breakthroughs in identifying AMP as a stimulatory signal for AMPK [3] and phosphorylation of the activation loop residue α-Thr-172 as a key mediator of AMPK activity [4]. Development of a bacterial system for expression of milligram quantities of recombinant, heterotrimeric AMPK complexes [5] heralded a new frontier in AMPK research, contributing to the discovery of LKB1 and CaMKK2 as upstream kinases for Thr-172, characterization of regulatory autophosphorylation sites (e.g., β1-Ser108 and α-Ser485), and, of course, providing the opportunity to conduct extensive structural and biophysical studies that now underpin drug development efforts. Expression of AMPK heterotrimers, and in particular specific isoform combinations, has since been described with insect cell- and mammalian cell-based systems [6, 7].

Relevant to the majority of recombinant proteins, selection of the most appropriate expression system is largely determined by final application. The benefit afforded by large-scale expression of AMPK in bacterial hosts is countered to some extent by lack of physiological modifications such as AMPK β-subunit myristoylation, important for full regulation by AMP/ADP, or basal Thr-172 phosphorylation. Conclusions drawn from performing analyses with bacterial-expressed AMPK *in solitude* should therefore be made with caution. Conversely, recombinant AMPK generated in mammalian cells closely resembles the enzyme form found in vivo (low basal Thr-172 and Ser108 phosphorylation, stoichiometric myristoylation) but suffers from inferior yield (Table 1). Additionally, consideration must also be given to the presence of endogenous AMPK isoforms contaminating purified preparations, particularly if the intention is to analyze specific AMPK heterotrimer complexes.

Here, we describe detailed protocols, optimized in our laboratory, to individually produce all 12 AMPK heterotrimers in cultured mammalian cells. The method describes non-liposomal transfection of mammalian cells and harvesting conditions. The use of subunit-specific affinity tags (GST, flag, myc, or HA) enables extraction of specific isoforms for biochemical assay, and postharvest treatments with CaMKK2 or lambda (λ) phosphatase are convenient methods to increase or decrease AMPK phosphorylation and activity, respectively.

Table 1
Comparison of posttranslational modifications present on recombinant AMPK generated by commonly used expression systems. Basal phosphorylation (p) at major sites on α- and β-subunits, and β-subunit myristoylation, are presented as approximate % stoichiometries, derived from intact protein mass spectrometry or immunoblot analyses [8]. Co-expression of AMPK in bacteria with N-myristoyl transferase (NMT) results in fully myristoylated species (−NMT vs. +NMT); expression of β-G2A mutant in mammalian cells abrogates β-subunit myristoylation (WT vs. G2A). n.d., not determined

		Recombinant expression system		
AMPK subunit	**Modification**	**Bacterial**	**Insect Sf21**	**Mammalian**
α1/2	pThr-172	None	~10%	~10%
	pSer485	>70%	n.d.	>70%
β1/2	Myristoylation	None (−NMT) 100% (+NMT)	~50%	100% (WT) None (G2A)
	pSer108	>60%	n.d.	~10%
	pSer182	None	n.d.	>80%

2 Materials

2.1 Expression of Recombinant AMPK

Expression constructs required for the method are described below (*see* **Notes 1** and **2**). All plasmids were prepared by standard miniprep kit and stored (−20 °C) in nuclease-free H_2O at concentrations >200 ng/μl.

1. pDEST27-GST fusion human AMPK α1 or α2. These plasmids are Gateway destination vectors that allow constitutive expression of N-terminally GST-tagged human AMPK subunits α1 (UniProt Q13131) or α2 (P54646). Transcription is under the control of the human cytomegalovirus (CMV) immediate-early promoter/enhancer. pDEST27 plasmids were generated by Gateway recombination technology (Thermo Life Sciences).
2. pcDNA3(-) human AMPK β1 or β2. These plasmids are derived from pcDNA3(-). Transcription is under the control of the CMV promoter. cDNAs for human AMPK subunits β1 (Q9Y478) or β2 (O43741) were inserted into the cloning site using restriction sites XhoI and HindIII. Addition of FLAG or myc affinity tags at the C-terminus, if required, was made possible by incorporating the relevant sequence into the reverse primer used for PCR amplification (*see* **Note 3**).
3. pMT2 AMPK human γ1, γ2, or γ3. These plasmids are derived from expression vector pMT2, in which transcription is directed by the adenovirus major late promoter (Ad-MLP) [9]. cDNAs for human AMPK subunits γ1 (P54619),

γ2 (Q9UGJ0), or γ3 (Q9UGI9) were inserted into the cloning site using restriction sites PstI and EcoRI. Addition of HA affinity tag at the N-terminus was made possible by incorporating the relevant sequence into the forward primer used for PCR amplification.

4. Mammalian cell line (COS7 or HEK293).
5. DMEM + 10% FBS: Dulbecco's Modified Eagle's Medium (DMEM) supplemented with 10% (v/v) fetal bovine serum (FBS).
6. Penicillin/streptomycin.
7. PBS: phosphate buffer saline (pH 7.4).
8. Trypsin/EDTA (pH 7.4).
9. Transfection reagent: FuGENE HD (Promega; *see* **Note 4**).
10. Reduced cell lysis buffer: 50 mM Tris–HCl, pH 7.4, 150 mM NaCl, 50 mM NaF, 1 mM NaPPi, 1 mM EDTA, 1 mM EGTA, 1 mM dithiothreitol (DTT), 1% (v/v) Triton X-100, cOmplete™ mini protease inhibitor cocktail (Sigma-Aldrich; *see* **Note 5**).

2.2 Purification of Recombinant AMPK

1. Glutathione agarose.
2. Glutathione agarose wash buffer: 50 mM Tris–HCl, pH 7.4, 150 mM NaCl, 1 mM DTT, 10% (v/v) glycerol.
3. Glutathione agarose elution buffer: 50 mM Tris–HCl,pH 7.4, 150 mM NaCl, 1 mM DTT, 10% (v/v) glycerol, 20 mM glutathione (*see* **Note 6**).

2.3 Modification of the Protocol for Postharvest Increase or Decrease of AMPK Activity

1. pcDNA3(-) human CaMKK2. cDNA for human CaMKK2 isoform 1 (Q96RR4-1) was inserted into the cloning site using restriction sites XhoI and HindIII. Addition of FLAG affinity tag at the C-terminus was made possible by incorporating the relevant sequence into the reverse primer used for PCR amplification.
2. Nonreducing cell lysis buffer: 50 mM Tris–HCl, pH 7.4, 150 mM NaCl, 50 mM NaF, 1 mM NaPPi, 1 mM EDTA, 1 mM EGTA, 1% (v/v) Triton X-100, cOmplete mini protease inhibitor cocktail (Sigma-Aldrich; *see* **Note 5**).
3. Anti-FLAG M2 affinity agarose gel (Sigma-Aldrich; *see* **Note 7**).
4. FLAG agarose wash buffer: 50 mM Tris–HCl, pH 7.4, 150 mM NaCl, 10% (v/v) glycerol.
5. FLAG agarose elution buffer: 50 mM Tris–HCl, pH 7.4, 150 mM NaCl, 10% (v/v) glycerol, 1 mg/ml FLAG synthetic peptide (*see* **Note 8**).

6. CaMKK2 phosphorylation buffer: 50 mM Tris–HCl, pH 7.4, 150 mM NaCl, 1 mM DTT, 10% (v/v) glycerol, 2 mM $MgCl_2$, 200 μM ATP.
7. λ-phosphatase.
8. λ-phosphatase dephosphorylation buffer: 50 mM Tris–HCl, pH 7.4, 150 mM NaCl, 1 mM DTT, 10% (v/v) glycerol, 2 mM $MnCl_2$.

3 Methods

3.1 Expression of Recombinant AMPK

1. Maintain mammalian cells (COS7 or HEK293) in sterile 10 cm tissue culture dishes in DMEM + 10% FBS, supplemented with penicillin and streptomycin. Incubate at 37 °C and 5% CO_2/humidified air (*see* **Note 9**).
2. 24 h prior to transfection, aspirate media, and wash cells in 8 ml of PBS at 37 °C. Aspirate PBS and detach cells by the addition of 5 ml trypsin/EDTA, followed by incubation at 37 °C. Cell detachment can be aided by gently agitating plates by hand.
3. Seed 10 cm dishes at 30–40% confluency ($1.0–1.3 \times 10^6$ cells per dish), and incubate in DMEM + 10% FBS overnight at 37 °C and 5% CO_2/humidified air.
4. For DNA transfections prepare DNA dilutions. First, prewarm DMEM and DNA expression constructs for each AMPK α, β, and γ subunits, to room temperature. For each 10 cm dish transfection, add 1 μg each of α and γ DNA construct, and 0.5–1.5 μg of β DNA construct (*see* **Note 10**), to 100 μl of DMEM in a sterile 1.5 ml Eppendorf tube, and mix gently by flicking the tube or vortexing. DNA dilutions for multiple plate transfections can be prepared in the same tube. To prepare transfection complexes, add 9 μl of prewarmed transfection reagent per 10 cm dish to DNA dilutions. Mix and incubate for 20 min (*see* **Note 11**).
5. Add transfection reagent/DNA mixture dropwise to each 10 cm dish. Tilt dishes by hand to mix, and return to incubator at 37 °C and 5% CO_2/humidified air.
6. After 48 h, replace medium in transfected plates with fresh, DMEM + 10% FBS at 37 °C, and return to incubator at 37 °C and 5% CO_2/humidified air.
7. After 2 h, remove dishes from incubator and place on ice at a slight angle. We recommend that the following steps proceed directly to avoid unnecessarily stressing cells leading to undesirable AMPK activation.
8. Aspirate media and apply 5 ml of ice cold PBS to the top edge of the dish.

9. Aspirate PBS and add 0.5 ml of ice-cold reduced cell lysis buffer to the top edge of the dish.
10. Using a cell scraper, collect solubilized cell lysate at the bottom edge of the dish, and pipette into a 1.5 ml Eppendorf tube.
11. Vortex briefly, and clarify lysate by centrifugation at 18,000 × *g* for 5 min, 4 °C. Lysate can be flash frozen in liquid nitrogen and stored at −80 °C indefinitely or processed on glutathione agarose as described below.

3.2 Purification of Recombinant AMPK

1. For AMPK immobilization on glutathione agarose (*see* **Note 12**), dispense glutathione agarose (~20 μl of a 50% slurry/0.5 ml cell lysate) into a 1.5 ml Eppendorf tube, and pellet by centrifugation at 3,350 × *g* for 3 min.
2. Wash glutathione agarose three times by resuspension in 1 ml of glutathione agarose wash buffer, followed by centrifugation at 3,350 × *g* for 3 min.
3. After the final centrifugation step, resuspend glutathione agarose in AMPK expression cell lysate. Place on a rotating wheel at 4 °C for 1 h, and pellet glutathione agarose by centrifugation at 3,350 × *g* for 3 min.
4. Wash glutathione agarose three times by resuspension in 1 ml of glutathione agarose wash buffer, followed by centrifugation at 3,350 × *g* for 3 min.
5. For AMPK elution, after the final centrifugation step, resuspend in glutathione agarose elution buffer (10 μl buffer/10 μl agarose), and place on rotating wheel at 4 °C for 5 min. Pellet agarose by centrifugation at 3,350 × *g* for 3 min. Remove 5 μl of the AMPK elution for Western blot analysis (Fig. 1; *see* **Note 13**), and dispense remaining AMPK elution into 50 μl aliquots (*see* **Notes 14** and **15**). Flash freeze aliquots in liquid N_2 for long-term storage at −80 °C.

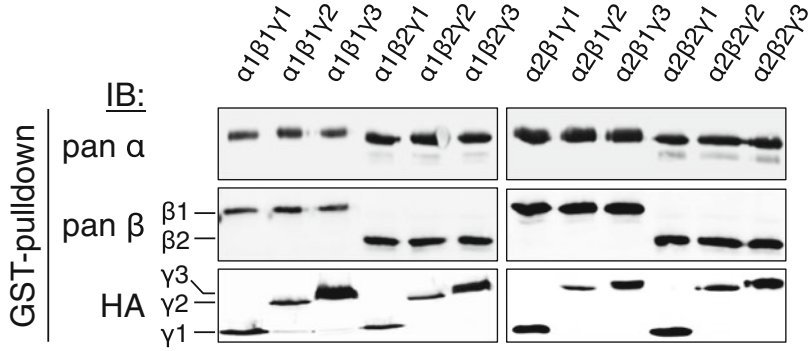

Fig. 1 Immunoblot profiles of 12 recombinant AMPK complexes expressed in COS7 cells. Both β1 (30.4 kDa) and γ3 (54.3 kDa) subunits display reduced electrophoretic mobility on SDS-PAGE, relative to expected mobility based on molecular mass

Table 2
Expected specific activities of recombinant AMPK complexes expressed in COS7 cells. Fold increases in enzyme activity in the presence of 200 μM AMP (+AMP) or CaMKK2 treatment, relative to basal, are indicated

AMPK complex	Basal activity (nmol.min^{-1}.mg^{-1} enzyme)	Fold stimulation	
		+AMP	CaMKK2-treated
α1β1γ1	100–200	2–3×	20–30×
α1β1γ2	100–200	2–3×	20–30×
α1β1γ3	100–200	1.5×	20–30×

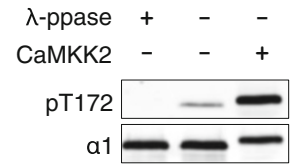

Fig. 2 Postharvest treatments of glutathione-agarose immobilized AMPK α1β1γ1. CaMKK2 or λ-phosphatase treatments either increase, or reduce, α-Thr-172 phosphorylation, respectively

3.3 Modification of the Protocol for Postharvest Increase or Decrease of AMPK Activity

We find that recombinant AMPK extracted from COS7 cells, incubated in high-glucose DMEM, has measurable kinase activity in the low nmol.min^{-1}.mg^{-1} enzyme range (Table 2). For drug screening purposes, it is often useful to obtain AMPK preparations with either higher activity (e.g., amenable to inhibitor screening [10]) or negligible activity (e.g., amenable to screening for AMP synergism [11]). Since AMPK activity is directly related to phosphorylation of Thr-172 in the activation loop, modulation of AMPK activity can be conveniently performed by treatment with CaMKK2 (Thr-172 phosphorylation) or lambda (λ) phosphatase (phospho-Thr-172 dephosphorylation) (Fig. 2). Treatments can be conveniently performed while AMPK is immobilized on glutathione agarose.

1. CaMKK2 can be purchased commercially, but we find expression of recombinant enzyme in mammalian cells a more convenient and economical source in our laboratory. The method is identical to **steps 1–3** in Subheading 3.1, with the exception that 3 μg of pcDNA3-CaMKK2-FLAG DNA is transfected per 10 cm dish and cell lysates are harvested in ice-cold nonreducing cell lysis buffer (*see* **Note 16**).
2. For the purification, dispense anti-FLAG M2 affinity agarose gel (~20 μl of a 50% slurry/0.5 ml cell lysate) into a 1.5 ml Eppendorf tube, and pellet by centrifugation at 3,350 × *g* for 3 min.

3. Wash anti-FLAG M2 affinity agarose gel three times by resuspension in 1 ml of FLAG agarose wash buffer, followed by centrifugation at 3,350 × *g* for 3 min.
4. After the final centrifugation step, resuspend anti-FLAG M2 affinity agarose gel in CaMKK2 expression cell lysate. Place on a rotating wheel at 4 °C for 1 h, and pellet anti-FLAG M2 affinity agarose gel by centrifugation at 3,350 × *g* for 3 min.
5. Wash anti-FLAG M2 affinity agarose gel three times by resuspension in 1 ml of FLAG agarose wash buffer, followed by centrifugation at 3,350 × *g* for 3 min.
6. For elution, after the final centrifugation step, resuspend in FLAG agarose elution buffer (10 μl buffer/10 μl agarose), and place on rotating wheel at 4 °C for 3 h. Pellet agarose by centrifugation at 3,350 × *g* for 3 min, and repeat the 3 h elution step. Combine CaMKK2 elutions and dispense into 20 μl aliquots. Flash freeze aliquots in liquid N_2 for long-term storage at −80 °C.
7. For Thr-172 phosphorylation by CaMKK2, immobilize AMPK on glutathione agarose (*see* **Note 12**), and wash three times in glutathione agarose wash buffer, as described in **step 1** in Subheading 3.2. Uniformly resuspend glutathione agarose in an equal volume of CaMKK2 phosphorylation buffer (room temperature), and add CaMKK2 (20 ng enzyme/10 μl agarose).
8. Place on a rotating wheel at room temperature for 10 min, and pellet glutathione agarose by centrifugation at 3,350 × *g* for 3 min.
9. Wash glutathione agarose three times by resuspension in 1 ml of glutathione agarose wash buffer, followed by centrifugation at 3,350 × *g* for 3 min.
10. For elution, after the final centrifugation step, resuspend in glutathione agarose elution buffer (10 μl buffer/10 μl agarose), and place on rotating wheel at 4 °C for 5 min. Pellet glutathione agarose by centrifugation at 3,350 × *g* for 3 min. Dispense AMPK elution into 50 μl aliquots (*see* **Notes 14** and **15**). Flash freeze aliquots in liquid N_2 for long-term storage at −80 °C.
11. If desired, for Thr-172 dephosphorylation, immobilize AMPK on glutathione agarose, and wash three times in glutathione agarose wash buffer, as described in **steps 1–4** in Subheading 3.2.
12. Uniformly resuspend glutathione agarose in an equal volume of λ-phosphatase dephosphorylation buffer (room temperature), and add λ-phosphatase (200 activity units/10 μl agarose). Place on rotating wheel at room temperature for 30 min.

13. Pellet glutathione agarose by centrifugation at 3,350 × *g* for 3 min. Wash glutathione agarose three times by resuspension in 1 ml of glutathione agarose wash buffer, followed by centrifugation at 3,350 × *g* for 3 min.
14. For elution, after the final centrifugation step, resuspend in glutathione agarose elution buffer (10 μl buffer /10 μl agarose), and place on rotating wheel at 4 °C for 5 min. Pellet glutathione agarose by centrifugation at 3,350 × *g* for 3 min. Dispense AMPK elution into 50 μl aliquots (*see* **Notes 14** and **15**). Flash freeze aliquots in liquid N_2 for long-term storage at −80 °C.

4 Notes

1. We find that maintenance of cDNAs for AMPK subunits on individual expression plasmids provides a highly dynamic platform for rapid generation of mutants, truncations, and isoform combinations of intact heterotrimers. Theoretically, any mammalian cell-compatible expression constructs can be used; however, we find that yields significantly drop if all three plasmids share the same promoter. For this reason we prefer to use a plasmid for γ-subunit expression with a different promoter (Ad-MLP) to that used for α- and β-subunit expression (CMV).
2. COS7 and HEK293 cell lines express endogenous AMPK (e.g., both β1 or β2 [10]) that can associate with recombinant subunits to produce complexes of undetermined isoform composition. In the event that final application is isoform sensitive (e.g., drug screening), or to exclude wild-type subunits if mutant AMPK is desired, it is necessary to preferentially isolate the relevant recombinant subunit under investigation. We have found this is conveniently achieved by placing distinct affinity tags on each subunit (α1/2: GST; β1/2: myc or FLAG; γ1/2/3: HA). We have yet to detect any discernible effect of these (mostly small) tags on AMPK regulation.
3. We have found that overall yield is largely determined by expression levels of the recombinant β-subunit, which forms the stabilizing scaffold for the AMPK heterotrimer. Inclusion of a C-terminal affinity tag can have profound effects on β-subunit expression, for unknown reasons. In particular, we find that protein yield is increased three- to fourfold by expressing the β-subunit as a FLAG fusion. Affinity tags must be incorporated at the β-subunit C-terminus to avoid disrupting the N-terminal myristoylation consensus sequence.
4. We experience higher transfection efficiencies and subsequently greater protein yields using FuGENE HD transfection regent

from Promega; however alternative transfection reagents from other suppliers can be used and their use optimized empirically.

5. We observe negligible protease activity during cell lysis using cOmplete™ mini protease inhibitor cocktail tablets from Sigma-Aldrich. These tablets provide a convenient means to ensure consistency between different lysis buffer preparations. Alternative protease inhibitor cocktails from other suppliers may be used.
6. Glutathione agarose elution buffer can be prepared from glutathione wash buffer by addition of 20 mM glutathione. If this method is used, it is critical to return the pH of the elution buffer to 7.4 with a few drops of 10 M NaOH prior to use. It is not uncommon for inexperienced operators to disregard this step. 20 mM glutathione will acidify the wash buffer to ~pH 3.2. Elution buffer at ~pH 3.2 is an ineffective eluent and prevents subsequent attempts to recover AMPK using elution buffer at correct pH 7.4. The preparation will have to be discarded.
7. We find maximal yields are achieved using anti-FLAG M2 affinity agarose gel from Sigma-Aldrich. This affinity resin contains anti-FLAG M2 monoclonal antibody covalently attached to cross-linked 4% agarose beads, thereby reducing antibody leaching during the prolonged incubation steps.
8. FLAG synthetic peptide (amino acid sequence DYKDDDDK) is commercially available from a number of suppliers but can be expensive in the event of large-scale preparations. We have found custom peptide synthesis from any number of independent services (e.g., GL Biochem (Shanghai)) to be an effective and more economical source.
9. For master cell cultures, maintain confluency between 10% and 90%. Over-confluent cells become resistant to liposomal transfection, resulting in reduced efficiency and lower protein yields. Discard cell cultures at passage 40; transfection efficiency is also diminished using over-passaged cells.
10. As outlined in **Note 3**, AMPK yield is dictated by β-subunit expression. If the β-subunit is untagged, or myc-tagged, we typically add 1.5 μg DNA per 10 cm dish. Conversely, we reduce to 0.5 μg if the β-subunit is being expressed as a FLAG fusion.
11. The 20 min incubation should be strictly observed. Longer incubation times result in drastically reduced protein yields.
12. The method describes purification via the GST-tag on α-subunits but can be adapted accordingly for other affinity tags. For FLAG, myc or HA purification, prepare lysis, wash and elution buffers in the absence of DTT. If required, FLAG-

purified AMPK can be eluted from anti-FLAG M2 affinity agarose gel using FLAG elution buffer instead of glutathione agarose elution buffer. Note that CaMKK2 phosphorylation cannot be performed on anti-FLAG M2 affinity agarose gel because FLAG peptide present in CaMKK2 preparations generated by our method will result in undesirable AMPK elution during the phosphorylation step.

13. Both β1 (30.4 kDa) and γ3 (54.3 kDa) subunits display reduced electrophoretic mobility on SDS-PAGE, relative to expected mobility based on molecular mass.
14. A second elution step can be performed. The second elution typically possesses half the protein concentration of the first with similar volume.
15. Yields can vary significantly between preparations, being influenced mainly by cell viability, transfection efficiency, and the recombinant AMPK complex being expressed. Typically, we achieve yields of 1–2 μg purified AMPK per 10 cm dish.
16. Nonreducing lysis buffer (devoid of DTT or reducing agent equivalents) is necessary to avoid dissociation of the heavy and light chains in the immobilized M2 antibody present on anti-FLAG M2 affinity agarose gel. This consideration is important for maximal yield.

References

1. Oakhill JS, Scott JW, Kemp BE (2012) AMPK functions as an adenylate charge-regulated protein kinase. Trends Endocrinol Metab 23:125–132
2. Jeon S-M (2016) Regulation and function of AMPK in physiology and diseases. Exp Mol Med 48:e245
3. Ferrer A, Caelles C, Massot N et al (1985) Activation of rat liver cytosolic 3-hydroxy-3-methylglutaryl coenzyme a reductase kinase by adenosine 5′-monophosphate. Biochem Biophys Res Comm 132:497–504
4. Hawley SA, Davison M, Woods A et al (1996) Characterization of the AMP-activated protein kinase kinase from rat liver and identification of threonine 172 as the major site at which it phosphorylates AMP-activated protein kinase. J Biol Chem 271:27879–27887
5. Neumann D, Woods A, Carling D et al (2003) Mammalian AMP-activated protein kinase: functional, heterotrimeric complexes by co-expression of subunits in *Escherichia coli*. Protein Expr Purif 30:230–237
6. Iseli TJ, Oakhill JS, Bailey MF et al (2008) AMP-activated protein kinase subunit interactions: beta1:gamma1 association requires beta1 Thr-263 and Tyr-267. J Biol Chem 283:4799–4807
7. Scott JW, van Denderen BJ, Jorgensen SB et al (2008) Thienopyridone drugs are selective activators of AMP-activated protein kinase beta1-containing complexes. Chem Biol 15:1220–1230
8. Oakhill JS, Chen ZP, Scott JW et al (2010) β-subunit myristoylation is the gatekeeper for initiating metabolic stress sensing by AMP-activated protein kinase (AMPK). Proc Natl Acad Sci U S A 107:19237–19241
9. Bonthron DT, Handin RI, Kaufman RJ et al (1986) Structure of pre-pro-von Willebrand factor and its expression in heterologous cells. Nature 324:270–273
10. Scott JW, Galic S, Graham KL et al (2015) Inhibition of AMP-activated protein kinase at the allosteric drug-binding site promotes islet insulin release. Chem Biol 22:705–711
11. Scott JW, Ling N, Issa SM et al (2014) Small molecule drug A-769662 and AMP synergistically activate naïve AMPK independent of upstream kinase signalling. Chem Biol 21:619–627

Chapter 11

Knockdown of Human AMPK Using the CRISPR/Cas9 Genome-Editing System

Adrien Grenier, Pierre Sujobert, Séverine Olivier, Hélène Guermouche, Johanna Mondésir, Olivier Kosmider, Benoit Viollet, and Jérôme Tamburini

Abstract

AMP-activated protein kinase (AMPK) is a critical energy sensor, regulating signaling networks involved in pathology including metabolic diseases and cancer. This increasingly recognized role of AMPK has prompted tremendous research efforts to develop new pharmacological AMPK activators. To precisely study the role of AMPK, and the specificity and activity of AMPK activators in cellular models, genetic AMPK inactivating tools are required. We report here methods for genetic inactivation of AMPK α1/α2 catalytic subunits in human cell lines by the CRISPR/Cas9 technology, a recent breakthrough technique for genome editing.

Key words CRISPR/Cas9, AMPK, AMPKα1, PRKAA1, AMPKα2, PRKAA2, AML, Caco2

1 Introduction

1.1 CRISPR/Cas9 Genome-Editing System

The rapid development of the clustered regularly interspaced short palindromic repeats (CRISPR)/CRISPR-associated protein-9 endonuclease (Cas9) technology provides unprecedented genomic research tools. CRISPR are short DNA sequences found in bacteria. Together with the bacterial Cas9, these sequences are involved in the clearance of foreign DNA from bacteria [1]. Shortly after its discovery, the CRISPR/Cas9 system has been engineered for genome editing including in eukaryotic cells. Indeed, CRISPR/Cas9 offers a specific genomic tool based on the complementation of genomic DNA by a 20-mer oligonucleotide sequence followed by a consensus sequence called PAM for protospacer adjacent motif. This short guide RNA (sgRNA) allows the recruitment of Cas9 to the targeted genomic DNA sequence leading to DNA

Adrien Grenier, Pierre Sujobert, Séverine Olivier contributed equally to this work.

Dietbert Neumann and Benoit Viollet (eds.), *AMPK: Methods and Protocols*, Methods in Molecular Biology, vol. 1732, https://doi.org/10.1007/978-1-4939-7598-3_11,

double-strand breaks (DSB). In case of DSB repair by nonhomologous end joining (NHEJ), small insertions/deletions within coding sequences may be produced leading to a premature stop codon [2, 3]. Alternatively, DSB may be repaired by homologous recombination (HR), which may be exploited for targeted mutagenesis of endogenous genes when using a mutated recombination template [4]. In fact, multiple refinements of the CRISPR/Cas9 technology have been described, and the power of these techniques as well as their potential applications is increasingly growing.

1.2 Why and How Disrupting AMPK Activity?

AMP-activated protein kinase (AMPK) is one of the main cellular energy sensors, activated by the binding of AMP or ADP to its γ-regulatory subunit and by the phosphorylation of its α-catalytic subunit [5]. Once activated, AMPK modifies cell metabolism (inhibition of anabolism and activation of catabolism) to restore cellular energy balance. Tremendous research efforts are therefore ongoing to efficiently activate AMPK in the context of metabolic diseases or cancer [5]. Abrogating AMPK activity may help to define the role of AMPK in a given cellular context. Unfortunately, no specific AMPK inhibitors are currently available and genetic knockdown/knockout approaches are recommended to validate the function of AMPK (*see* Chapter 12). Hence, specific deletion of AMPK genes represents an invaluable tool to assess the specificity of AMPK-targeting small molecules (mostly AMPK activators). While targeting regulatory AMPKβ or γ subunits may be important to disrupt the regulation of AMPK activity and function, AMPKα gene inactivation is sufficient to abrogate AMPK serine/threonine kinase activity [6]. At first glance, we used RNA interference (RNAi) by small hairpin RNA (shRNA) to deplete AMPKα from acute myeloid leukemia (AML) cells as done by other groups in other cellular contexts [7–9]. However, we failed to achieve a complete inhibition of AMPKα, with a residual expression of 10–20% at the protein level [10]. Indeed, Saito and colleagues recently demonstrated the essential pro-survival function of AMPK in AML cells exposed to stress [11], thus explaining the negative selection of cells with efficient AMPKα1 knockdown. Hence, efficient and stable AMPKα knockout in human cell lines represents a challenge. To avoid this limitation, and also to reduce the probability of off-target as observed with shRNA [12], we moved toward a CRISPR/Cas9-based approach to study AMPK function in human cell lines. In this chapter, we describe the use of CRISPR/Cas9 technology to disrupt AMPKα1 expression in acute myeloid leukemia (AML) MOLM-14 and OCI-AML3 cells and concomitant AMPKα1 and AMPKα2 expression in colon carcinoma Caco2 cells that may provide invaluable tools for further studies on AMPK biology and development of specific AMPK activators for the treatment of cancer and metabolic diseases (*see* **Note 1**). We attempted to find common DNA sequences across *PRKAA1* and *PRKAA2* genes (encoding the AMPKα1 and AMPKα2 catalytic subunits,

respectively) for targeting by a single sgRNA, but no such sequence was available within *PRKAA1* or *PRKAA2* coding or non-coding DNA. While multiplexing sgRNA into a single vector is possible [13], we used a sequential procedure to achieve first AMPKα1 and then AMPKα2 knockdown in single-cell clones. We thus developed *PRKAA1*- and *PRKAA2*-targeting CRISPR/Cas9 systems allowing a convenient sequential selection of AMPKα1-depleted single-cell clones based on antibiotic resistance and then isolation of AMPKα2 knockout single-cell clones based on the expression of a fluorescent marker. In particular, we describe procedures to design AMPKα1 and AMPKα2 targeting sgRNAs and cloning into lentiviral vector. We also provide methods for infection, clonal selection, screening, and validation of single-cell CRISPR clones (*see* **Note 2**).

2 Material

2.1 sgRNA Design and Cloning

1. Online bioinformatic sgRNA design tool (e.g., CRISPR design tool) (*see* **Note 3**).
2. plentiCRISPR v2 plasmid (Addgene reference #52961). (*See* **Notes 4** and **5**).
3. pL-CRISPR.EFS.GFP plasmid (Addgene reference #57818).
4. Designed sgRNA oligonucleotides, 100 μM oligonucleotides in H_2O:
   - *PRKAA1 sgRNA#1:* forward 5′-CACCGAGGGCACGCC ATACCCTTG-3′ and reverse 5′-AAACCAAGGGTATGGC GTGCCCT-3′.
   - *PRKAA1 sgRNA#2:* forward 5′-CACCGATCCTGAAA GAGTACCATTC-3′ and reverse 5′-AAACGAATGGTA CTCTTTCAGGAT-3′.
   - *PRKAA2 sgRNA#1:* forward 5′-CACCGAAGATCGGAC ACTACGTGCT-3′ and reverse 5′-AAACAGCACGTAG TGTCCGATCTTC-3′.
   - *PRKAA2 sgRNA#2:* forward 5′-CACCGTCAGCCATC TTCGGCGCGCG-3′ and reverse 5′-AAACCGCGCGCC GAAGATGGCTGAC-3′.
5. 10× kinase buffer: 500 mM Tris–HCl, pH 7.6, 100 mM $MgCl_2$, 50 mM DTT, 10 mM ATP, 1 mM spermidine.
6. T4 PNK: 10 U/μl T4 polynucleotide kinase.
7. Restriction enzyme: 10 U/μl EspI (BsmBI) and 10× FastDigest Green Buffer (Thermo Fisher Scientific).
8. T4 ligase: 1 U/μl T4 ligase.
9. 10× ligation buffer: 500 mM Tris–HCl, pH 7.5, 100 mM $MgCl_2$, 10 mM ATP, 10 mM DTT, 50% (w/v) polyethylene glycol-8000.

10. Stbl3 *Escherichia coli* competent cells.
11. SOC medium: 20 g/L tryptone, 5 g/L yeast extract, 10 mM NaCl, 2.5 mM KCl, 10 mM $MgCl_2$, 10 mM $MgSO_4$, 20 mM glucose. Dissolve to 1 L deionized water, 20 g of tryptone, 5 g of yeast extract, 2 ml of 5 M NaCl, 2.5 ml of 1 M KCl, 10 ml of 1 M $MgCl_2$, and 10 ml of 1 M $MgSO_4$. Autoclave at 121 °C for 15 min, and add 20 ml of filter-sterilized 1 M glucose.
12. LB agar plate: lysogeny broth (LB) agar plate with 100 μg/ml ampicillin.
13. Maxiprep plasmid DNA kit.

2.2 Production of Lentiviral Particles

Before starting work with lentivirus, ensure compliance with your Environmental Health and Safety office and government/organization/university.

1. HEK 293T cells.
2. Phosphate buffer saline (PBS): 137 mM NaCl, 2.7 mM KCl, 10 mM Na_2HPO_4, 1.8 mM KH_2PO_4, pH 7.4.
3. $CaCl_2$ solution: 1 M $CaCl_2$.
4. Lipofectamine® 2000 transfection reagent.
5. PsPAX2 plasmid (encoding Gag and Pol proteins). (Addgene reference #12260).
6. pMD2.G (encoding VSV-G envelope proteins). (Addgene reference #12259).
7. HEPES buffered saline (HBS): 20 mM HEPES, pH 7, 150 mM NaCl.
8. Complete DMEM medium: DMEM, 10% (v/v) foetal bovine serum (FBS), 100 units/ml penicillin and 100 μg/ml streptomycin, 2 mM L-glutamine.
9. Complete MEM alpha medium: MEM alpha medium, 10% (v/v) foetal bovine serum (FBS), 100 units/ml penicillin and 100 μg/ml streptomycin, 2 mM L-glutamine.
10. Opti-MEM culture medium.
11. 0.22 μm filter.
12. G418 (Geneticin®) stock solution: 100 mg/ml G418.

2.3 Infection and Clone Selection

1. Human AML cell lines: MOLM-14 or OCI-AML3 human cell lines.
2. Human Caco2 colon carcinoma cell line.
3. Complete MEM alpha medium: Minimum Essential Medium (MEM) Alpha Medium, 10% (v/v) FBS, 100 units/ml penicillin and 100 μg/ml streptomycin, 2 mM L-glutamine.

4. Complete EMEM culture medium: Eagle's Minimum Essential Medium (EMEM), 20% (v/v) FBS, nonessential amino acids, 100 units/ml penicillin, and 100 μg/ml streptomycin.
5. Trypsin/EDTA solution: 0.25% (w/v) Trypsin, 0.53 mM EDTA.
6. 50 μm cell strainer.
7. Cell sorting buffer: PBS (without Ca^{2+}/Mg^{2+}), 25 mM HEPES, pH 7, 1% (v/v) FBS, 1 mM EDTA.
8. 12 ml FACS tube.
9. Flow cytometer.

2.4 Screening

1. GeneScan™ 500ROX.
2. PCR Primers:
   - *PRKAA1 primers:* forward 5′-FAM-ATCACCAGGATCC TTTGGCA-3′ and reverse 5′-TGCTTTCCTTACACCTT GGTG-3′.
   - *PRKAA2 primers*: forward 5′-FAM-GCTGCACTGTGGG TAGGC-3′ and reverse 5′-GGGCGTCGGCACCTTC-3′.
3. Capillary electrophoresis.
4. GeneMapper® software v3.7.

2.5 Sequencing

1. Sequencing primers:
   - PRKAA1 primers: forward 5′-ATCACCAGG ATCCTTTGGCA-3′ and reverse 5′-TGCTTTCCTTA-CACCTTGGTG-3′.
   - PRKAA2 primers: forward 5′-GCTGCACTGTGGGTAGG C-3′ and reverse 5′-GGGCGTCGGCACCTTC-3′.
2. Cell lysis buffer: 4% Tween 20,100 μg/ml proteinase K in H_2O.
3. DNA polymerase: Phire Hot Start II DNA Polymerase and 5× reaction buffer (Thermo Scientific).
4. Tris-acetate-EDTA (TAE) buffer: 40 mM Tris–HCl, pH 8.3, 20 mM acetic acid, 1 mM EDTA.
5. Agarose gel: 2% (w/v) agarose in TAE.

3 Methods

3.1 sgRNA Design and Cloning

Putative target sites can be identified by simply scanning the region of the particular genomic location that you want to target (but you should check your sgRNA design for potential off-target effects) or by using online bioinformatical tools dedicated to sgRNA design. (*See* **Note 3**).

Human AMPKα catalytic subunit encompasses two isoforms, AMPKα1 and AMPKα2, encoded by the *PRKAA1* and *PRKAA2* genes located at chromosomes 5p13.1 and 1p32.2, respectively. *PRKAA1* is made of 9 exons (Fig. 1**A**) representing 5088 base pairs (bp) and encodes a 559-amino acid (AA) protein of 64 kDa. *PRKAA2* coding sequence is 9280 bp long but with a long 3′ untranslated region and encodes a 552-AA protein of 62 kDa (Fig. 1**B**). To target *PRKAA1* gene, we designed two sgRNAs targeting *PRKAA1* exon 7. To target *PRKAA2* gene, we designed two sgRNAs targeting *PRKAA2* exon 1 (Fig. 1**A** and **B**).

CRISPR Design

1. Identify sgRNA targeting sequences in the genomic region of interest by running the CRISPR design tool (*see* **Notes 6–8**). The output window shows 23 bp genomic sites of the form 5′-N_{20}NGG-3′ within your target region. These sites may reside on the + or − strand (Fig. 2).
2. Remove NGG sequence to leave 20 nt target sequence.
3. Add G to the 5′ end of target sequence if it does not begin with G. (*See* **Note 9**).
4. For cloning into the plentiCRISPR vector using BbsI restriction enzyme, add GATC to the 5′ end of forward oligonucleotide, and add AAAA to the reverse complement oligonucleotide (including any additional G nucleotide). (*See* **Note 10**).
5. Synthetize forward and reverse oligonucleotides corresponding to the selected sgRNAs. (*See* **Notes 11** and **12**).

CRISPR Cloning

6. Mix 1 μl of 100 μM of forward and reverse oligonucleotides with 1 U of T4 PNK in 10 μl of 1× kinase buffer, and incubate for 30 min at 37 °C. (*See* **Note 13**).
7. Incubate at 95 °C for 5 min and gradually cool the solution at room temperature.
8. Digest 5 μg of plentiCRISPRv2 plasmid backbone with 30 U of Esp3I (BsmBI) in a final volume of 60 μl of 1× FastDigest Green Buffer. Incubate for 25 min at 37 °C and then at 65 °C for 15 min. (*See* **Note 14**).
9. Prepare a 10 μl ligation reaction mix by adding 150 ng of plentiCRISPR digestion product, 1 μl of 1 μM annealed sgRNA oligonucleotides, 1 μl of 1 U/μl T4 ligase, 1 μl of 10× T4 ligase buffer. Incubate for 10–30 min at room temperature.

A

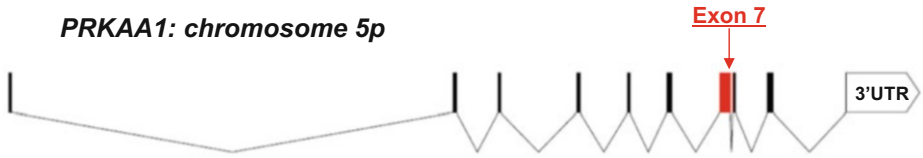

***PRKAA1* exon 7**

TTCAACCATGATTGATGATGAAGCCTTAAAAGAAGTATGTGAAAAGTTTGAGTGCTCAGAAG
AGGAAGTTCTCAGCTGTCTTTACAACAGAA***ATCACCAGGATCCTTTGGCA***GTTGCCTACCA
TCTCATAATAGATAACAGGAGAATAATGAATGAAGCCAAAGATTTCTATTTGGCGACAAGCCC
ACCTGATTCTTTTCTTGATGATCATCACCTGACTCGGCCCCATCCTGAAAGAGTACCATTCT
TGGTTGCTGAAACACCA**AGGGCACGCCATACCCTTG**ATGAATTAAATCCACAGAAATCCAA
A***CACCAAGGTGTAAGGAAAGCA***AAATGGCATTTAGGAATTAGAAGTCAAAGTCGACCAAAT
GATATTATGGCAGAAGTATGTAGAGCAATCAAACAATTGGATTATGAATGGAAG

AMPKα1 sgRNA#1
AMPKα1 sgRNA#2
PRKAA1 foward sequencing primer
PRKAA1 reverse sequencing primer
Underlined: 239 bp predicted amplicon.

B

PRKAA2: chromosome 5p

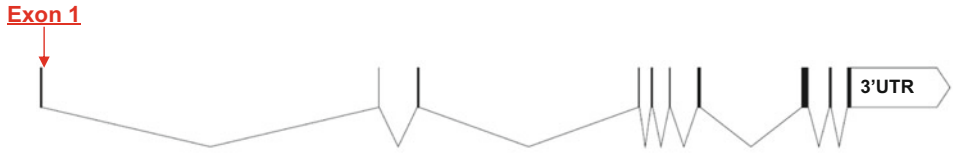

PRKAA2 exon 1

GCGCCCAGCGCCCTCTCCCGGGACCCCGCGCCCGCCCCGCGCCCCTCGCGGCTCGGGG
TCCGCCCCCTCGCCCGCAGGGCCC***GCTGCACTGTGGGTAGGC***GGCGGCGGCGGCGGCT
ACGCGGAGCGGCAGGCGGTGGAGCGAGGCCG**CGCGCGCCGAAGATGGCTGA**GAAGCA
GAAGCACGACGGGCGGGT**GAAGATCGGACACTACGTGCT**GGGCGACACGCT***GGGCGTC***
GGCACCTTCGGCAAAGTGAAGAGTTGAGTACGCGCTCCGGACCGCTGTGCGGGGCTGCC
TGACTTGCGGGAGGCCGAGGGGAGAGGCGGGAGCCCCGGGCCTCCGGCGGGCGCGGG

AMPKα2 sgRNA#1
AMPKα2 sgRNA#2
PRKAA2 foward sequencing primer
PRKAA2 reverse sequencing primer
Underlined: 158 bp predicted amplicon.

Fig. 1 Graphical representation of *PRKAA1* and *PRKAA2* genomic DNA sequences. *PRKAA1* and *PRKAA2* encompass 9 and 10 exons, respectively. Exons are figured as *vertical black rectangles*. *PRKAA1 e*xon 7 is highlighted in *red*. Intronic regions are depicted by connecting roof-shaped lines. 3′ untranslated regions (3′UTR) are indicated. The scale is indicated, 1kd: 10 bases (**A**) AMPKα1 sgRNA#1 (*green*) and sgRNA#2 (*red*), forward (*blue*) and reverse (*pink*) sequencing primers, and predicted amplicon (*underlined*) are represented. (**B**) AMPKα2 sgRNA 1 (*green*) and 2 (*red*), forward (*blue*) and reverse (*pink*) sequencing primers, and predicted amplicon (*underlined*) are represented

A

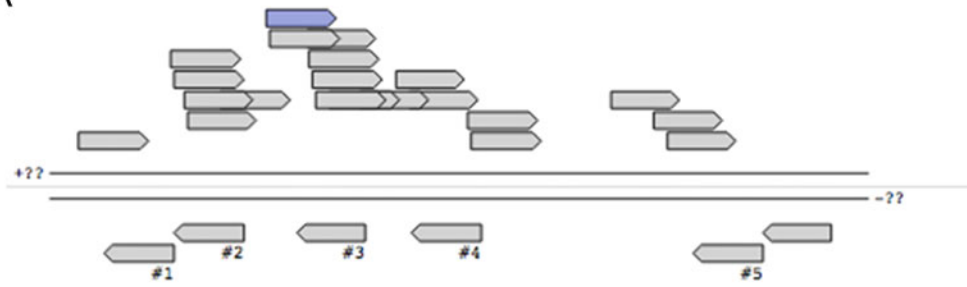

B

all guides

scored by inverse likelihood of offtarget binding

mouse over for details ... show legend

	score	sequence	
Guide #1	90	GAAGATCGGCCACTACATTC	TGG
Guide #2	86	TACATTCTGGGTGACACGCT	GGG
Guide #3	86	CTACATTCTGGGTGACACGC	TGG
Guide #5	84	GCGTGTCACCCAGAATGTAG	TGG
Guide #6	83	CGGCACCTTCGGCAAAGTGA	AGG
Guide #7	82	ATTCGGAGCCTTGATGTGGT	AGG
Guide #8	80	ACATTCTGGGTGACACGCTG	GGG
Guide #9	79	GAAGATTCGGAGCCTTGATG	TGG
Guide #22	48	GGCTGTCGCCATCTTTCTCC	AGG

C

guide #1 quality score: 90

guide sequence: GAAGATCGGCCACTACATTC TGG

on-target locus: unknown

number of offtarget sites: 48 (8 are in genes)

top 20 genome-wide off-target sites — show all exonic

sequence	score	mismatches	UCSC gene	locus
TAAATTCAGCCACTACATTCAAG	1.4	4MMs [1:4:5:8]		chr12:+84595478
CCAGATCGGCCATTACATTCCAG	1.2	3MMs [1:2:13]		chr9:-95924685
CAAAACCTGCCACTACATTCTGG	0.8	4MMs [1:4:6:8]	NM_005570	chr18:-56997420
GAGTAGCCGCCACTACATTCCAG	0.8	4MMs [3:4:6:8]		chr14:-88983876
TAAAATCGGTCACTACATGCAAG	0.5	4MMs [1:4:10:19]		chr6:-150155811
AAAGATTGGACTCTACATTCTGG	0.5	4MMs [1:7:10:12]		chr2:+130783057
GAACAGCCGCCGCTACATTCAGG	0.4	4MMs [4:6:8:12]		chr10:-2957677

Fig. 2 Screenshots from online CRISPR design tool. (**A**) Graphical representation of location for proposed AMPKα1 sgRNA sequence within *PRKAA1* gene. (**B**) Specificity scores for proposed AMPKα1 sgRNA sequence. Each guide has a specificity score from 0 to 100. (**C**) Details about potential off-targets. CRISPR Design application software is available at http:/crispr.mit.edu

10. Transform the ligation product into Stbl3 *Escherichia coli*. (*See* **Note 15**).
11. Incubate ligation product and one aliquot of Stbl3 cells for 10 min on ice.
12. Heat shock at 42 °C for 45 s and return to ice for 2 min.
13. Add 250 μl of room temperature SOC medium, and incubate at 37 °C with shaking for 1 h.
14. Spread the transformation mixture onto a prewarmed LB agar plate containing 100 μg/ml kanamycin. Incubate overnight at 37 °C.
15. Incubate the plates overnight at 37 °C in a microbiological incubator.
16. After incubation, pick 5–10 colonies to identify a correct clone for proper insert identification by Sanger sequencing.
17. After identifying the colonies with the correct sequence, isolate plasmid DNA using a maxiprep kit.

3.2 Lentivirus Production

To produce recombinant lentivirus, HEK293-T packaging cells are transfected with the packaging plasmids pVSVg and psPAX2 encoding lentiviral proteins (Gag, Pol, and Env) and the transfer plentiCRISPR/sgRNA plasmid. We propose here two different methods for lentiviral particles production using HEK293T packaging cells. (*See* **Note 16)**.

Calcium/HBS Transfection

1. Plate 1.5×10^6 HEK293T cells into two T175 flasks in complete DMEM medium containing 1 mg/ml G418 antibiotic (generally 4 days before transfection).
2. The day of transfection, wash cells once with PBS, and add 18 ml of DMEM without FBS or G418. Incubate the cells for 6 h in a humidified 37 °C, 5% CO_2 incubator.
3. Prepare transfection solution by adding 1.5 ml of sterile water, 500 μl of 1 M $CaCl_2$ solution, and a DNA plasmid mix containing 16 μg pMD2.G, 24 μg PsPAX2, and 3 μg of plentiCRISPR/sgRNA plasmids.
4. During a continuous vortex agitation, add dropwise transfection solution into 2 ml of HBS in a 50 ml tube. Incubate the mixture (final volume of 4 ml) for 15 min at room temperature.
5. Add 2 ml of this mix on each T175 flask, and incubate overnight in a humidified 37 °C, 5% CO_2 incubator.

6. Discard culture medium and add 18 ml of complete DMEM culture medium. Incubate in a humidified 37 °C, 5% CO_2 incubator for 24 h.
7. Collect the supernatants using a syringe, and filtrate out the cellular debris using a 0.22 μm filter. The filtered lentivirus supernatant can be either immediately used to transduce a cell line or stored at −80 °C. Avoid freeze-thawing lentivirus supernatant. (*See* **Note 17**).

Lipofectamine Transfection

8. Plate 2×10^6 HEK293T cells into two 10 cm diameter culture dishes with DMEM culture medium containing 1 mg/ml G418 antibiotic, and incubate overnight in a humidified 37 °C, 5% CO_2 incubator.
9. Wash once with PBS, and replace medium with 4.2 ml of Opti-MEM culture medium.
10. Add 12 μl of Lipofectamine 2000 Transfection Reagent to 400 μl of FBS-free OPTIMEM medium. Incubate the mixture at room temperature for 15 min.
11. Add 3 μg of plentiCRISPR/sgRNA, 2 μg of PsPAX2 vector, and 1 μg of pMD2.G plasmids to 400 μl of FBS-free OPTI-MEM medium.
12. Mix diluted plasmid DNA with diluted Lipofectamine mixture. Incubate the mixture at room temperature for 15 min.
13. Add 800 μl of the mixture dropwise to the cells, and incubate in a humidified 37 °C, 5% CO_2 incubator.
14. Replace medium after 3–6 h with fresh DMEM culture medium, and incubate in a humidified 37 °C, 5% CO_2 incubator for 48 h.
15. Collect the supernatants using a syringe, and filtrate out the cellular debris using a 0.22 μm filter. The filtered lentiviral supernatant can be either immediately used to transduce a cell line or stored at −80 °C. Avoid freeze-thawing lentiviral supernatant. (*See* **Note 17**).

3.3 Cell Infection and Clonal Isolation

Determination of MOI

The volume of supernatants used for infection may vary for each cell line and depends on lentiviral titer. Determination of the multiplicity of infection (MOI) for each cell line is recommended and is valid only for a given lentiviral supernatant batch [14]. To ensure that most cells receive only one stably integrated sgRNA, a MOI of 0.3 should be used. (*See* **Note 18**).

MOI theoretically is the number of viral particles per cell; a MOI of 1 means that 1 particle reached a single cell. However, particles may not lead to viral genome integration in all cases, and

transduction is not linear but follows a Poisson distribution considering that each event is independent. MOI can be determined by using the following formula:

$$m = -\ln(1 - P)$$

where m = MOI and P = probability of infection.

1. Plate 12-well plates at a density of 2×10^5/ml AML cells in 2 ml of complete MEM alpha medium.
2. In each well, add 200, 100, 50, 25, or 0 μl of lentiviral supernatant. An additional no antibiotic selection control well without addition of lentivirus is prepared. Incubate for 24 h in a humidified 37 °C, 5% CO_2 incubator.
3. Twenty-four hours after lentiviral transduction, wash the cells twice with PBS to eliminate residual lentiviral particles, and then incubate with complete MEM alpha medium.
4. Twenty-four hours after lentiviral transduction, replace the medium with complete MEM alpha medium containing 1 mg/ml puromycin (or the relevant antibiotic selection). For the no antibiotic selection control well, replace the medium with complete MEM alpha medium without antibiotic.
5. Refresh complete MEM alpha medium with and without antibiotic until the antibiotic selection control well with no virus contains no viable cells.
6. Count the number of cells in each well. For each virus conditions, MOI is estimated. For example, if 37% of transduced cells are recovered after antibiotic selection, MOI = $-\ln(0.37) = 0.994$.

Infection of Cell Lines

7. For AML human cell lines, seed cells at a density of 2×10^5 cells/ml in complete MEM alpha medium.
8. For colon carcinoma Caco2 cells, plate 2×10^5 cells/wells in 24-well plates in 0.5 ml of complete EMEM culture medium.
9. Add lentiviral supernatants at a MOI of 0.3, and incubate for 24 h in a humidified 37 °C, 5% CO_2 incubator.
10. Wash the cells with PBS twice, and then incubate with complete MEM alpha medium for AML cells or complete EMEM culture medium for Caco2 cells.

Antibiotic Selection and Clonal Isolation

11. Two to three days after lentiviral transduction, replace the medium with complete MEM alpha medium containing 1 mg/ml puromycin (or relevant antibiotic selection depending on antibiotic resistance marker expressed on the lentivirus

vector used) for AML cells or complete EMEM culture medium containing 1 mg/ml puromycin (or relevant antibiotic) for Caco2 cells.

12. After antibiotic selection of transduced cells, select clonal cell lines by isolating single cells into 96-well plates through either cell sorting or other isolation procedures. (*See* **Notes 19** and **20**).
13. For single isolation of AML cells, count cells with an automated cell counter, and prepare a cell suspension with 10^6 cells/ml in cell sorting buffer.
14. For single isolation of Caco2 cells, aspirate culture medium, and wash cells with room temperature PBS.
15. Add trypsin/EDTA and incubate for 3 min to detach cells.
16. Resuspend dissociated cells with prewarmed complete EMEM medium, and gently pipet up and down several times to generate a single-cell suspension.
17. Centrifuge the cell suspension for 5 min at 800 × *g* at room temperature.
18. Aspirate the supernatant, and resuspend the cell pellet in appropriate volume of cell sorting buffer to adjust the cell concentration to 10^6 cells/ml.
19. Filter cell suspensions through a 50 μm filter into a FACS tube.
20. Set up the cell sorter and install the required collection device.
21. Collect cells individually into 96-well plates containing 100 μl/well of appropriate culture medium.
22. After isolation of single cells (or single-cell derived clones), culture the cells without selection antibiotic. Allow the bulk cells to expand in a humidified 37 °C, 5% CO_2 incubator. Establishment of new clonal cell lines will vary depending on the doubling time of the cell line used.

Fluorescence-Activated Cell Sorting (FACS) Enrichment and Clonal Isolation

The following steps are performed for clonal isolation without antibiotic selection when using a plentiCRISPR plasmid expressing a fluorescent marker (e.g., pL-CRISPR.EFS.GFP plasmid). This approach can be a useful alternative strategy when working with puromycin (or other antibiotic)-resistant cell lines. Indeed, we used FACS to select cells transduced with "GFP" pL-CRISPR.EFS.GFP/AMPKα2 in puromycin-resistant AMPKα1 knockout Caco2 cells (previously generated by transduction with "puromycin" plenti-CRISPR/AMPKα1) (*see* **Note 21**) (Fig. 3).

23. Two to three days after lentiviral transduction, confirm successful delivery of sgRNA by visualizing fluorescent marker expression using fluorescence microscopy.

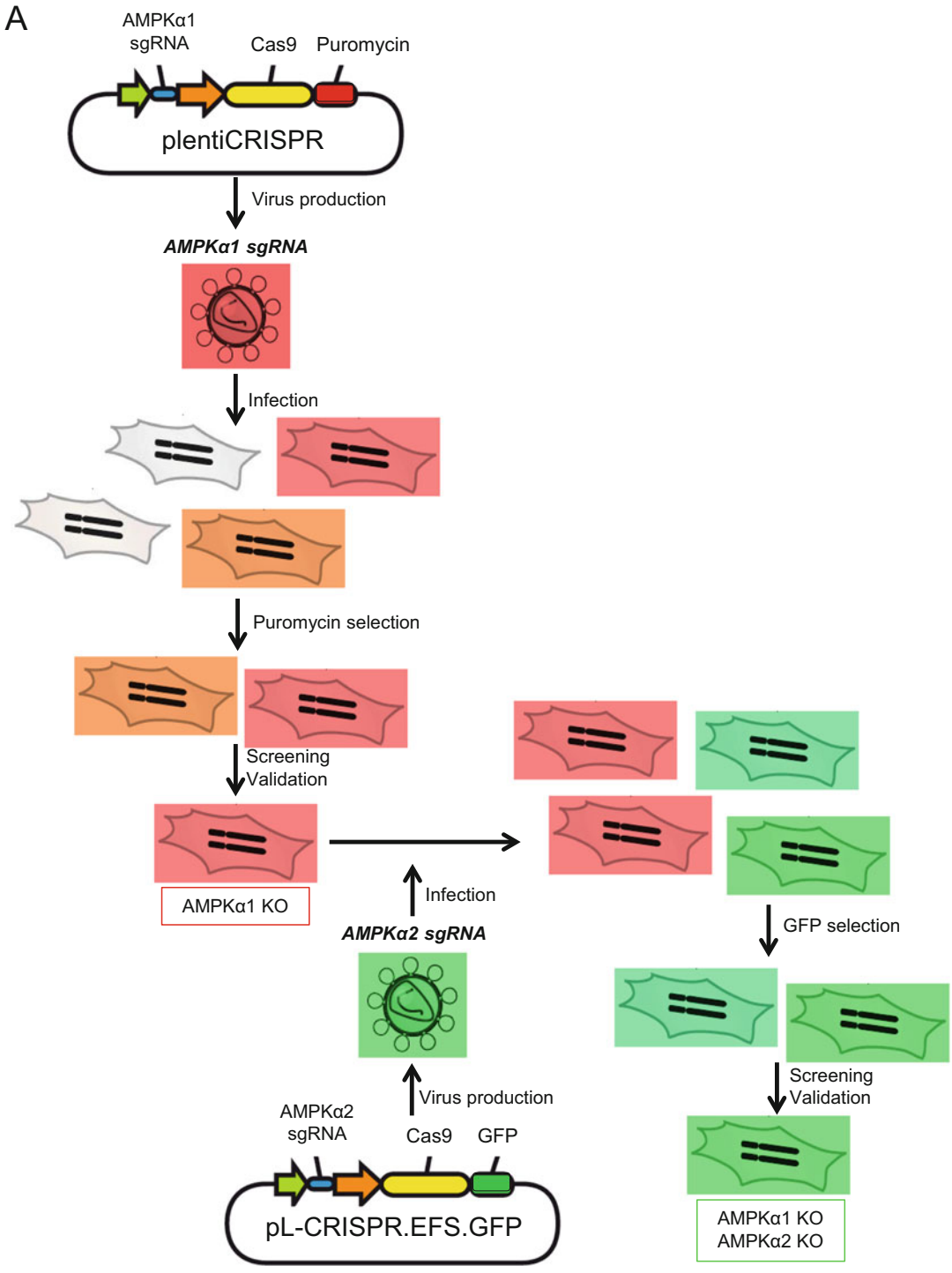

Fig. 3 Experimental workflow for genome engineering of colon carcinoma Caco2 cells. We used a sequential procedure to achieve both AMPKα1 and AMPKα2 knockout in single-cell Caco2 clones. (**A**) PRKAA1-targeting sgRNAs are cloned into the plentiCRISPR plasmid, allowing a selection based on puromycin resistance. PRKAA2-targeting sgRNAs are cloned into the pL-CRISPR.EFS.GFP plasmid allowing a selection based on GFP

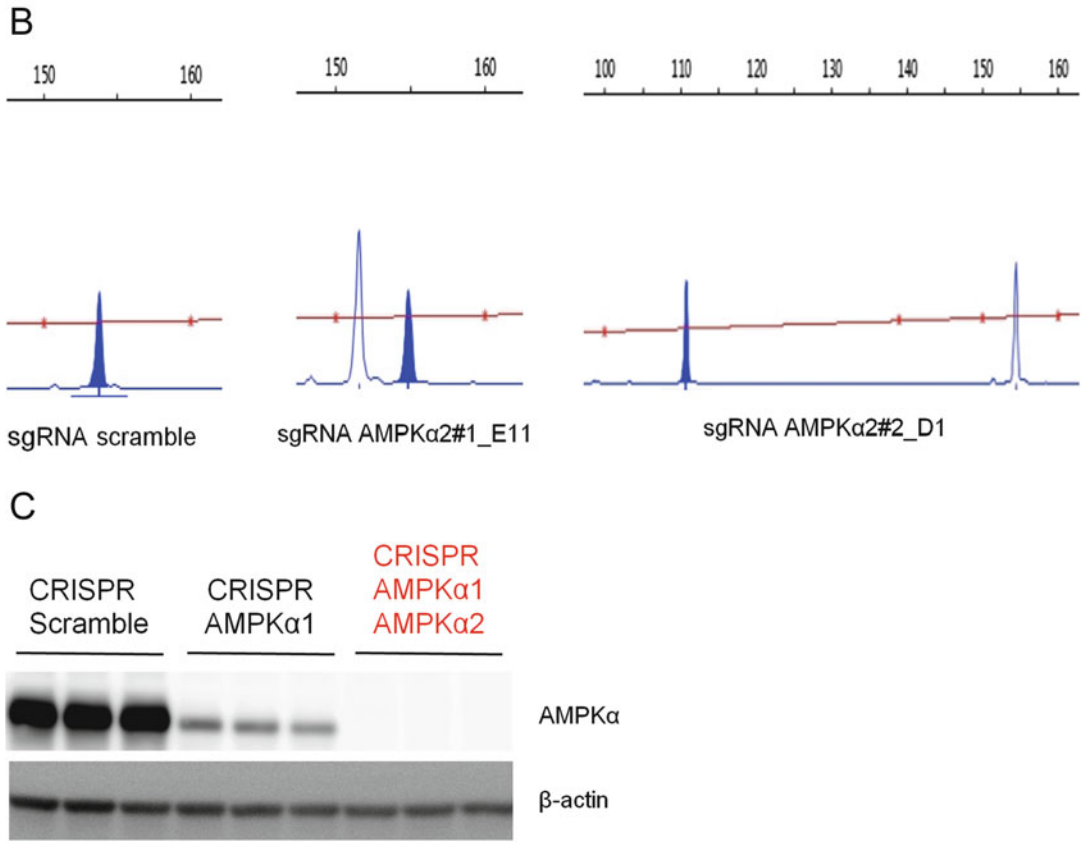

Fig. 3 (continued) detection. Single-cell sgRNA AMPKα1 Caco2 clones were selected based on puromycin resistance (*left part*), and then single-cell sgRNA AMPKα2 Caco2 clones on a AMPKα1 knockout background are isolated based on GFP fluorescence (*right part*). (**B**) Genome editing efficiency of AMPKα2 sgRNA in AMPKα1-knockout Caco2 cells is assessed by capillary electrophoresis fragment analysis. (**C**) Western blot analysis of AMPKα protein expression in single-cell Caco2 clones isolated after sequential transduction with lentivirus expressing "puromycin" CRISPR/AMPKα1 and "GFP" CRISPR/AMPKα2. Western blots were performed using anti-panAMPKα and anti-β-actin antibodies. Each clone was analyzed in triplicate

24. Prepare cells for FACS analysis as described in Subheading 3.3, **steps 13–19** for suspension and adherent cells.
25. Set up the flow cytometer with negative control cells. Adjust the forward scatter (FSC) and side scatter (SSC) to place the population of interest on scale.
26. Run positive control cells, and draw an interval gate to define the populations of interest.
27. Once gates have been determined, sort the top ~10% of fluorescent-positive cells from the experimental samples.

28. Collect cells individually into 96-well plates containing 100 μl/well of culture medium.
29. After sorting, examine the plates under a microscope, and determine the presence of a single cell in most of the wells on the plate. Mark off the wells that are empty or that may have been seeded more than a single cell.
30. When cells exceed 10^5 cells/ml for suspension cells and are 80–90% confluent for adherent cells, prepare replicate plates for screening.
31. Expand the cells for 2–3 weeks. Change medium every 3–5 days as necessary and passage accordingly.

3.4 Screening and Validation

Most mutations induced by sgRNA at target site are small deletions or insertions (±1–20 bp), and knockout cell clones can be simply identified by analyzing successful micro-deletions or micro-insertions by product size analysis. Forward and reverse primers designed to anneal outside of the target locus region are used.

1. Screen a coverage of >20 clones per sgRNA to guarantee that each perturbation will be sufficiently represented in the final screening readout. (*See* **Note 22**).

   Cell Lysis

2. Transfer cells into a 96-well U-bottom plate, and wash once in PBS buffer through centrifugation at 300 × *g* (1200 rpm) for 20 s at 4 °C.
3. Discard culture medium and add 13 μl of cell lysis buffer. (*See* **Notes 23** and **24**).
4. Transfer into PCR tubes, vortex briefly, and heat at 56 °C for 10 min and then at 95 °C for an additional 10 min.

   PCR Amplification

5. Select a 500 bp region around the targeting site, and identify optimal targeting primer sets that amplify 200–300 bp around the targeting site. (*See* **Note 25**).
6. Assemble a 50 μl PCR with 13 μl of cell lysate, 1.5 μl of 10 μM 5′-FAM-labelled forward primer, 1.5 μl of 10 μM nonfluorescent reverse primer, 1 μl of 10 mM dNTP, 10 μl of 5× PCR buffer, and 1 μl of phire taq polymerase.
7. Run sample in thermocycler with the following program: 98 °C for 1 min and for 35 cycles, 98 °C for 7 s, *X* °C for 5 s (*X* depend on the annealing temperature of the primers), 72 °C for 10–15 s/kb, and then 72 °C for 1 min. (*See* **Note 26**).
8. After the reaction is complete, run 1 μl of each amplified target on a 2% (w/v) agarose gel in TAE to verify successful amplification of a single product at the appropriate size.

Fragment Analysis

9. To 1 μl of fluorescent PCR products, add 18.8 μl of water and 0.2 μl of GeneScan™ 500ROX.
10. Perform migration by capillary electrophoresis using a DNA analyzer.
11. Analyze migration profile using GeneMapper® software v3.7 (Applied Biosystems) (Fig. 4C, left panel).

Validation of Genetic Modification by Sanger Sequencing

12. Use nonfluorescent primers to generate amplicons as described above see Sect. 3.4, **steps** 5–7.
13. Sequence the amplicons by using the same primers. Representative chromatograms are provided in Fig. 4C (right panel) for correlation with fragment analysis for the same clone.

Verification of Knockout Cell Clones by Immunoblotting Analysis

After validation of sequence perturbation, Western blot analysis is recommended for verifying protein expression of targeted genes (*see* **Note 24**). Methods for performing Western blot are described in Chapters 24 and 27.

Western blots from CRISPR/AMPKα1-modified MOLM-14- and OCI-AML3-derived clones are shown in Fig. 5**A**–**C**. Western blots from CRISPR/AMPKα1- and CRISPR/AMPKα2-modified Caco2 derived clones are shown in Fig. 3**A** and **B**.

4 Notes

1. Although we provide a comprehensive view of CRISPR/Cas9 use in human AML and colon carcinoma cell lines, the methods described here may be applied to AMPK knockdown in other human cell lines as well as to any gene of interest.
2. Recent breakthrough allows researchers to disrupt the expression of a given gene by multiple means. Among the most popular techniques are RNA interference and CRISPR/Cas9, whose pros and cons are reviewed by other [12]. While both techniques might be used to achieve a partial knockdown of protein expression (e.g., with inactivated dCas9 fused to transcriptional modulators [15]), only CRISPR/Cas9 can achieve a complete and stable inhibition of protein expression. We believe that most of the technical pitfalls in CRISPR/Cas9 assays could be overcome after a careful adaptation of our current canvas to each cell type and sgRNAs, providing an invaluable tool for AMPK pharmacological research and beyond.

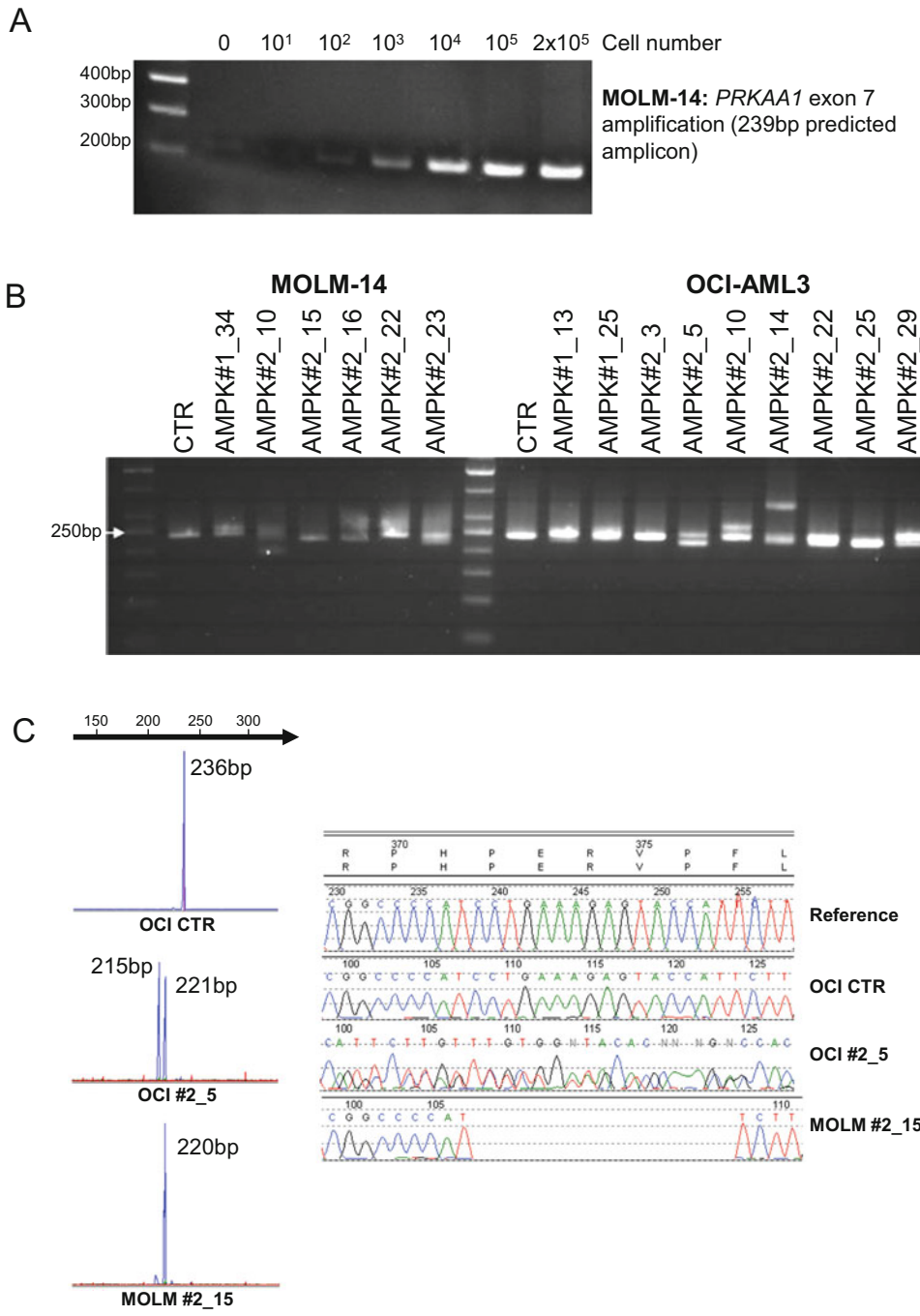

Fig. 4 Fragment and sequencing analysis of single-cell sgRNA AMPKα1 AML clones. (**A**) Limiting dilutions experiments in MOLM-14 cells to assess the sensitivity of H_2O/tween lysis and AMPKα1-targeted locus amplification. (**B**) Agarose gel migration of PCR products (using the sequencing primers described in Fig. 1a) from single-cell MOLM-14 and OCI-AML3 clones isolated after transduction with lentivirus expressing CRISPR/AMPKα1#1 and #2. (**C**) Capillary electrophoresis fragment analysis using FAM-labelled primers in OCI-AML3 CTR, OCI-AML3 AMPKα1#2_5, and MOLM-14 AMPKα1#2_15 clones (*left panel*) and matching Sanger sequencing for OCI-AML3 AMPKα1#2_5 and MOLM-14 AMPKα1#2_15 clones (*right panel*)

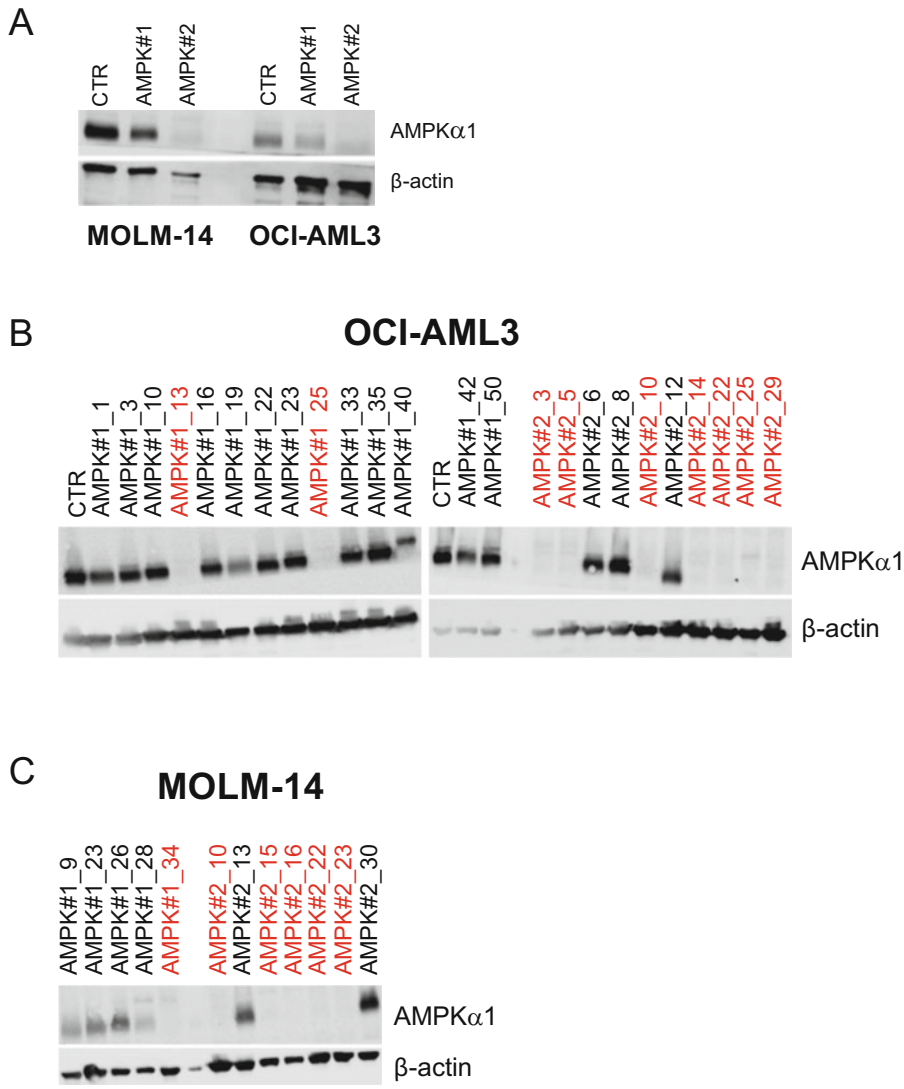

Fig. 5 AMPKα1 protein expression in sgRNA AMPKα1 AML cell lines. (**A**) Western blot analysis of AMPKα1 protein expression in MOLM-14 and OCI-AML3 cell lines bulk populations transduced with lentivirus expressing CRISPR/AMPKα1#1 and #2. (**B**) Western blots analysis of AMPKα1 protein expression in single-cell OCI-AML3 clones after transduction with lentivirus expressing CRISPR/AMPKα1#1 and #2. (**C**) Western blots analysis of AMPKα1 protein expression in single-cell MOLM-14 clones isolated after transduction with lentivirus expressing CRISPR/AMPKα1#1 and #2. Clone numbers highlighted in *red* and in *black* indicate successful AMPKα1 knockout and knockout failure, respectively. Western blots were performed using anti-AMPKα1 and anti-α-actin antibodies

3. Many bioinformatics tools are available online to help in the design of sgRNA (e.g., ZiFit, CRISPR Design Tool). We used the optimized CRISPR Design application software from Dr. Feng Zhang's laboratory (http://crispr.mit.edu). This software provides an accurate analysis of off-target sites. Due to the

growing use of the CRISPR/Cas9 technology, more and more sgRNA sequences will be published to target a given gene/protein. Thus, it will be possible to pick-up already validated sgRNA sequences into published articles. Some companies also offers ready-to-use plasmids containing a validated sgRNA and also services for lentiviral particle production for a given plasmid that may represents a valuable assets, particularly for teams with limited experience with the CRISPR/Cas9 technology.

4. In previous publication, we have used the plentiCRISPRv1 plasmid [10], formerly referenced under the Addgene reference #49545, but this plasmid is currently not available due to the recent development of plentiCRISPRv2 plasmid (Addgene reference #52961). plentiCRISPRv2 is identical to the original plentiCRISPRv1 but produces nearly tenfold higher titer virus.
5. We mostly used the plentiCRISPR v1 plasmid, allowing the expression of sgRNA and Cas9 though a unique vector. While we found this system very convenient for our purposes, facilitating the clonal selection steps by antibiotic selection and allowing further transductions with other lentiviral vectors, such as GFP-expressing vectors (pL-CRISPR.EFS.GFP plasmid, Addgene reference #57818), people may want to use different systems dependent on their cellular model. Among many CRISPR/Cas9 tools currently available, we mention doxycycline-inducible vectors, such as, for example, the pLKO.1-puro U6 sgRNA BfuAI stuffer plasmid (Addgene #50920), using a modified Cas9 inactivated for endonuclease activity (dCas9) and fused to transcription corepressors such as KRAB, allowing a direct and efficient repression of transcription.
6. Appropriate sgRNA sequences are computationally designed based on known sgRNA targeting rules. The selected genomic target sequence should be unique to the genomic target site and be present immediately upstream the PAM sequence that is necessary for Cas9 recognition. Cas9 nuclease cuts 3-nt upstream of the PAM site. Avoid target sequence with homopolymer stretches (e.g., AAAA) and with a GC-rich content. The sequence analysis software analyzes a target sequence of up to 500 nucleotides and searches for PAM sequences either in the positive or negative strand of the corresponding genomic DNA. Every potential sgRNA is then analyzed against a reference genome (e.g., human genome hg19), to search for potential off-target sites in the whole genome. The output assigns a score (from 0 to 100) for each guide, according to an algorithm described on the website, and indicates the potential undesirable targets of this sgRNA. As recommended by Zhang's team, sgRNA with a score above 50 are good candidates, provided the off-targets are outside gene regions.

7. sgRNAs targeting the first exons of the gene are better candidates, to ensure that the premature stop codon will efficiently disrupt protein function. However, when targeting genes encoding multiple isoforms, we recommend targeting exons shared between all isoforms.
8. It is recommended to check the location of the sgRNA on the genomic sequence of the gene of interest, in order to avoid sgRNA that would be complementary to an exon-exon junction and thus would be inefficient at the genomic level.
9. If the 20 bp sequence does not start with a "G," a single "G" nucleotide must be prepended to allow efficient transcription from the RNA polymerase III U6 promoter.
10. Appropriate sites for restriction enzymes should be added for subcloning purpose. If plentiCRISPR plasmid contain a Esp3I (BsmBI) restriction site, add "GATC" to the 5′ end of the forward sequence and "AAAA" to the 5′ end of reverse complementary sequence. The two oligos should anneal to form the following double strands:

    5′-GATCGXXXXXXXXXXXXXXXXXXXG-3′.
    3′-CXXXXXXXXXXXXXXXXXXXXCAAAA-5′.
11. A control sgRNA that does not match any genomic sequence can be also synthesized. We used the following nontargeted guide as a control: 5′-GTAGGCGCGCCGCTCTCTAC-3′ [10].
12. We suggest using two (or more) different sgRNA sequences for each target gene, to be able to conclude that the observed effects are directly due to gene knockout, rather than to off-target activities of the constructs.
13. If phosphorylated oligonucleotides are ordered, the use of T4 PNK is omitted.
14. In order to minimize the risk of self-ligation of the plentiCRISPR plasmid, an additional digestion with 30 U of NsiI in the presence of 3 U of thermosensitive alkaline phosphatase (FastAP, EF0651, Thermo Scientific) is performed.
15. Lentiviral transfer plasmids contain long terminal repeats (LTRs) and must be transformed into recombination-deficient bacteria. We use Stbl3 *E. coli* (Thermo Fisher Scientific, C7373-03) although other RecA$^-$ strains may be used as well.
16. The choice between calcium/HBS and Lipofectamine™2000 to transduce HEK293 cells is mostly based on the cost/efficiency balance. For large lentiviral productions, we generally use calcium/HBS transductions for cost/efficiency reasons. In case of hard-to-transduce cell line, filtrated and concentrated supernatants should be used in priority. Alternatively, lentiviral production can be delegated to commercial companies.

Lentiviral supernatants should be stored at −80 °C, and freezing/thawing cycles should be avoided by aliquoting the supernatants in small fractions.

17. Lentivirus supernatants can be concentrated by ultracentrifugation to increase transduction efficiency that may be helpful for some cell types. Concentration of lentivirus is achieved through centrifugation in a SW32Ti rotor at 82500 × *g* (22,000 rpm) for 1 h 30 min with the following settings: acceleration 3 and deceleration 3. Concentrated supernatants are then stored at −80 °C.
18. Researchers should be aware that lentiviral transduction efficacy is widely different across cell line and that each lentiviral supernatant batch also produces different transduction rates for the same cell line. We recommend the determination of a MOI for each lentiviral supernatant and each cell line used. MOI calculation is based on Poisson's statistics, assuming that cell transduction is a binary process. Indeed, MOI better reflects the true cell transduction rate than quantification of lentiviral particle on cell culture supernatants due to the presence of empty particles. While MOI is ideally evaluated when the vector is directly detected in a given cell, for example, by a fluorescent protein (GFP or other), an approximation of efficiently transduced cells is possible using antibiotic selection such as puromycin, approximating that only transduced cells are alive after adjunction of the selection compound.
19. Among multiple critical steps using this technique described here, people should keep in mind that, dependent on cell type, CRISPR/Cas9-induced knockdown may not be apparent in a bulk cellular population, in contrast to other techniques such as RNA interference. Several parameters may explain this fact, among which are variability in lentiviral transduction efficacy, discrepancy in sgRNA efficacy and also cell ploidy that may affect CRISPR/Cas9 efficacy in the presence of multiple copy of a given gene. Moreover, CRISPR/Cas9 may induce multiple gene modifications at the single-cell level, which may be difficult to genetically characterize when working on a bulk population. For these reasons, we recommend to single-cell clone-transduced cell lines and to choose the optimal clones based on genetic and immunoblotting characterization.
20. Depending on the response of used cell types to FACS, alternative methods can be performed. Cells can be individually sorted by using limiting dilution. We recommend to plate cells at 0.4 cell/well of 96-well plates. Isolation of clonal cell populations can be also performed by platting the cells at low density to isolate individual single-cell-derived clones. Monoclonal colonies can be picked and moved to a flat bottom

96-well plates for expansion. As colony formation could vary among cell types, optimal density of cell population needs to be determined empirically.

21. Beyond genetic and proteomic characterization of AMPK knockdown cells, attention should be given to the evaluation of AMPK activity in these cells. In AML cells, we exploited the fact that only AMPKα1 isoform are expressed, allowing a complete disruption of AMPK activity, as attested, for example, by the absence of induction of ACC phosphorylation upon stimulation by AMPK activators [10]. In other cell types, co-expression of AMPKα2 even at low levels might represent an issue for achieving a complete inhibition of AMPK. In this situation, strategy of sequential targeting of *PRKAA1* and then *PRKAA2* by different CRISPR/Cas9 vectors might represent an option.
22. In our experience, the probability of inducing DNA alterations by CRISPR/Cas9 is variable depending on the vector, sgRNA, and cell line. Therefore, achieving a significant depletion of a target protein on a bulk cellular population by this method is uncommon. In MOLM-14 and OCI-AML3 bulk populations, efficient AMPKα1 knockdown is achieved using AMPK#2 sgRNA, but AMPKα1 protein expression is barely affected by AMPK#1 sgRNA in these cells (Fig. 3A). We may extrapolate the probability of efficient knockdown, as in OCI-AML3 cells, 2/12 (16%) clones were AMPKα1-depleted with AMPK#1 guide and 7/12 (58%) with AMPK#2 guide (Fig. 3B). Similar, we found 1/5 (20%) modified clones with AMPK#1 and 5/7 (71%) with AMPK#2 in the MOLM-14 cell line (Fig. 3C). We thus suggest performing a single-cell selection of cellular clones that will be further genetically characterized.
23. We have developed an easy-to-use assay to amplify a region avoiding DNA extraction and using a limited number of cells. This tool allows searching for genomic DNA modifications in a large number of single-cell-derived clones simultaneously. However, any method for genomic DNA isolation may be utilized.
24. To screen for multiple clones in parallel, we set up an assay based on direct PCR amplification of our target genomic sequence among cells in liquid cultures. By direct cell lysis into the PCR tube, we avoid time-consuming steps of DNA extraction and purification. While we focused on capillary electrophoresis DNA fragment analysis, as we found this technique robust and cost-efficient for our purposes, other techniques may be applied to characterize CRISPR/Cas9-induced genomic modifications including next-generation sequencing [16]. Although time-consuming, it is possible to search for

protein modification across the clones using immunoblotting. Alternatively, we may imagine to directly assess protein expression in single-cell clones using reverse phase protein microarrays (RPPA) that allows to test in parallel up to 100 conditions in a single slide [17]. However in this latter case, we still advise to characterize the selected clones at the genetic level as well.

25. Amplification of fragment smaller than 400 bp is recommended to ensure good resolution of the fluorescence-labelled DNA size analysis. Note that the size of amplicon analysis could vary by ~1 bp.
26. To estimate the appropriate annealing temperature for primer pairs when using the Phire DNA polymerase, we use the Tm calculator application available at https://www.thermofisher.com/us/en/home/brands/thermo-scientific/molecular-biology/molecular-biology-learning-center/molecular-biology-resource-library/thermo-scientific-web-tools/tm-calculator.html.

Acknowledgments

Work from the authors was performed within the Département Hospitalo-Universitaire (DHU) AUToimmune and HORmonal diseaseS (AUTHORS) and was supported by grants from INSERM, CNRS, Université Paris Descartes, and Société Francophone du Diabète (SFD). J.M. was supported by a fellowship from AP-HP. A.G. holds a doctoral fellowship from CARPEM. S.O. received a doctoral fellowship from the Région Ile-de-France (CORDDIM).

References

1. Zhang F, Wen Y, Guo X (2014) CRISPR/Cas9 for genome editing: progress, implications and challenges. Hum Mol Genet 23(R1):R40–R46
2. Ran FA, Hsu PD, Lin CY, Gootenberg JS, Konermann S, Trevino AE, Scott DA, Inoue A, Matoba S, Zhang Y, Zhang F (2013) Double nicking by RNA-guided CRISPR Cas9 for enhanced genome editing specificity. Cell 154(6):1380–1389
3. Ran FA, Hsu PD, Wright J, Agarwala V, Scott DA, Zhang F (2013) Genome engineering using the CRISPR-Cas9 system. Nat Protoc 8 (11):2281–2308
4. Paquet D, Kwart D, Chen A, Sproul A, Jacob S, Teo S, Olsen KM, Gregg A, Noggle S, Tessier-Lavigne M (2016) Efficient introduction of specific homozygous and heterozygous mutations using CRISPR/Cas9. Nature 533(7601):125–129
5. Hardie DG (2013) The LKB1-AMPK pathway-friend or foe in cancer? Cancer Cell 23 (2):131–132
6. Hardie DG, Ross FA, Hawley SA (2012) AMPK: a nutrient and energy sensor that maintains energy homeostasis. Nat Rev Mol Cell Biol 13(4):251–262
7. Chen L, Chen Q, Deng G, Kuang S, Lian J, Wang M, Zhu H (2016) AMPK activation by GSK621 inhibits human melanoma cells in vitro and in vivo. Biochem Biophys Res Commun 480(4):515–521
8. Jiang H, Liu W, Zhan SK, Pan YX, Bian LG, Sun B, Sun QF, Pan SJ (2016) GSK621 targets glioma cells via activating AMP-activated

protein kinase signalings. PLoS One 11(8): e0161017

9. Wu YH, Li Q, Li P, Liu B (2016) GSK621 activates AMPK signaling to inhibit LPS-induced TNFalpha production. Biochem Biophys Res Commun 480(3):289–295
10. Sujobert P, Poulain L, Paubelle E, Zylbersztejn F, Grenier A, Lambert M, Townsend EC, Brusq JM, Nicodeme E, Decrooqc J, Nepstad I, Green AS, Mondesir J, Hospital MA, Jacque N, Christodoulou A, Desouza TA, Hermine O, Foretz M, Viollet B, Lacombe C, Mayeux P, Weinstock DM, Moura IC, Bouscary D, Tamburini J (2015) Co-activation of AMPK and mTORC1 induces cytotoxicity in acute myeloid leukemia. Cell Rep 11(9):1446–1457
11. Saito Y, Chapple RH, Lin A, Kitano A, Nakada D (2015) AMPK protects leukemia-initiating cells in myeloid leukemias from metabolic stress in the bone marrow. Cell Stem Cell 17 (5):585–596
12. Gilbert LA, Horlbeck MA, Adamson B, Villalta JE, Chen Y, Whitehead EH, Guimaraes C, Panning B, Ploegh HL, Bassik MC, Qi LS, Kampmann M, Weissman JS (2014) Genome-scale CRISPR-mediated control of gene repression and activation. Cell 159(3):647–661
13. Sakuma T, Nishikawa A, Kume S, Chayama K, Yamamoto T (2014) Multiplex genome engineering in human cells using all-in-one CRISPR/Cas9 vector system. Sci Rep 4:5400
14. Tiscornia G. SOaVI (2007) Development of lentiviral vectors expressing siRNA. CSH protocols:23–34
15. Konermann S, Brigham MD, Trevino AE, Joung J, Abudayyeh OO, Barcena C, Hsu PD, Habib N, Gootenberg JS, Nishimasu H, Nureki O, Zhang F (2015) Genome-scale transcriptional activation by an engineered CRISPR-Cas9 complex. Nature 517 (7536):583–588
16. Bell CC, Magor GW, Gillinder KR, Perkins AC (2014) A high-throughput screening strategy for detecting CRISPR-Cas9 induced mutations using next-generation sequencing. BMC Genomics 15:1002
17. Kornblau SM, Coombes KR (2011) Use of reverse phase protein microarrays to study protein expression in leukemia: technical and methodological lessons learned. Methods Mol Biol 785:141–155

Chapter 12

Compound C/Dorsomorphin: Its Use and Misuse as an AMPK Inhibitor

Biplab Dasgupta and William Seibel

Abstract

The evolutionary conserved energy sensor AMPK plays crucial roles in many biological processes—both during normal development and pathology. Loss-of-function genetic studies in mice as well as in lower organisms underscore its importance in embryonic development, stress physiology in the adult, and in key metabolic disorders including cardiovascular disease, diabetes, cancer, and metabolic syndrome. In contrast to several other kinases important in human health and medicine where specific/selective inhibitors are available, no AMPK-specific inhibitors are available. The only reagent called dorsomorphin or compound C that is occasionally used as an AMPK inhibitor unfortunately inhibits several other kinases much more potently than AMPK and is therefore highly non-specific. In this chapter, we discuss the pros and cons of using this reagent to study AMPK functions.

Key words AMPK, Compound C, Dorsomorphin, Cancer, Metabolism

1 Introduction

From unicellular organisms to mammals, AMP-activated protein kinase, or AMPK, functions as an evolutionarily conserved energy sensor [1, 2]. Reduced ATP production (e.g., nutrient and oxygen limitation, starvation/caloric restriction) or increased ATP consumption (e.g., exercise, activation of motor proteins, ion channels, and unchecked cellular biosynthesis) increases the cellular AMP-ATP ratio and activates AMPK. Active AMPK inhibits ATP-consuming pathways and augments ATP-producing pathways to restore energy homeostasis by both transcriptional and post-translational regulations. AMPK executes numerous cellular functions and is required for adaptive responses to various physiological and pathological conditions. Studies from AMPK knockout organisms including mice indicate essential as well as redundant functions of the several isoforms of the AMPK heterotrimeric complex [3–11]. Work from knockout mouse models also revealed conflicting results, particularly on AMPK's response to drugs

Dietbert Neumann and Benoit Viollet (eds.), *AMPK: Methods and Protocols*, Methods in Molecular Biology, vol. 1732, https://doi.org/10.1007/978-1-4939-7598-3_12,

including AMPK activators in basal and stress metabolism and in metabolic disease [12–14]. Conflicting reports about its cellular functions, particularly in cancer, are also intriguing, and a growing number of AMPK activators are being developed to treat human diseases such as cancer and diabetes. However, a significant bottleneck in understanding AMPK function both in vitro and particularly in vivo is the absence of a specific AMPK inhibitor.

2 The AMPK Inhibitor Compound C/Dorsomorphin

Compound C ($C_{24}H_{25}N_5O$; 6-[4-(2-piperidin-1-ylethoxy) phenyl]-3-pyridin-4-ylpyrazolo [1, 5-a] pyrimidine) is the primary reagent used as an AMPK inhibitor (Fig. 1). The general cell cycle inhibitor adenine arabinoside or Ara-A, which is highly non-specific to AMPK, has also been used in a few studies. Compound C is widely used in biochemical experiments in vitro and in some in vivo contexts. The history of discovery of this small molecule is probably not known to all Compound C users. Compound C was originally identified as an AMPK inhibitor from a screen of a 10K library by Merck scientists. Their main interest in a selective AMPK inhibitor was as a research tool in the delineation of the mechanism of metformin, and they showed selectivity vs. a few unrelated kinases [15]. While this reagent was being used for over a decade as an AMPK inhibitor, in a high-throughput screen, another small molecule had been identified as the first selective small molecule inhibitor of bone morphogenetic protein (BMP) signaling. It was named dorsomorphin because it caused dorsoventral patterning defects in zebrafish typically seen in BMP-pathway mutant embryos [16–18]; however, dorsomorphin is structurally identical to compound C. Dorsomorphin and its analog LDN-193189 cause stem cell differentiation and thus may have therapeutic implications in the progressive muscle and bone disease called fibrodysplasia ossificans progressiva (FOP). This is an incurable disease where muscle and tendons are slowly replaced by bone due to a mutation in the BMP

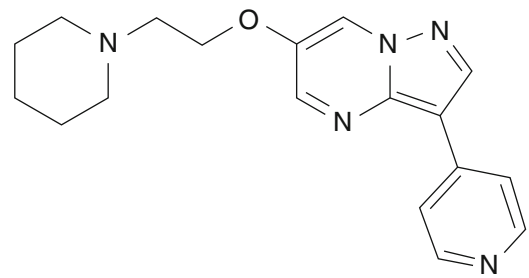

Fig. 1 Chemical structure of compound C/dorsomorphin

type 1 receptor called ALK2 (ACVR1) [19–21]. In addition to inhibiting BMP signaling, dorsomorphin also inhibits the VEGF type 2 receptor (FLK1/KDR) and disrupts angiogenesis during zebrafish development [22]. It is an irony that while the therapeutic potential of dorsomorphin was tempered by its known ability to inhibit AMPK ("off-target" effects), Compound C found its use as an AMPK inhibitor. Very little prudence was used despite its numerous "off-target" effects as detailed below.

3 Doses of Compound C Users Need to Consider

Various concentrations of Compound C as an AMPK inhibitor has been used by laboratories (including ours) for in vitro and in vivo experiments, and often times, doses were chosen to fit anticipated results. In zebrafish embryos, a concentration of 5 μM for 24 h was sufficient to cause dorsoventral patterning defects that were attributed to inhibition of BMP signaling [22]. In vitro, Compound C inhibited BMP signaling in murine pulmonary smooth muscle cells at an IC_{50} of 0.47 μM [17]. At 4 μM, it completely blocked SMAD1/5/8 phosphorylation by BMP, and because SMADs regulate transcription, treatment of human liver cell lines (HepG2/Hep3B) with 10 μM Compound C for 6 h completely blocked BMP-induced transcription of the SMAD-responsive iron regulating hepatic hormone hepcidin [16]. Because hepcidin interacts with the cell surface iron transport protein ferroportin to control plasma iron levels, intravenous administration of Compound C at 10 mg/kg caused 60% increase in serum iron concentrations resulting in hyperferremia in mice in 24 h [16]. Because iron overload causes various systemic pathologies, the use of Compound C in vivo in adult rodents warrants careful consideration of this side effect of Compound C. In another study, 5 μM Compound C inhibited angiogenesis by about 50%, and at 10 μM, it completely disrupted blood vessel formation [22]. However, given that both VEGF and BMP signaling are involved in angiogenesis, the authors could not reach a conclusion based on the results produced by Compound C. Given its effect on the inhibition of angiogenesis, any in vivo study that attempts to connect AMPK with angiogenesis by the use of Compound C alone should be considered inconclusive.

4 Compound C Kinase Profiling Data

While extensive experimental analysis showed that Compound C inhibits BMP and VEGF signaling in zebrafish and mammalian cells at low micromolar concentrations, the reagent found continuous use as an AMPK inhibitor in various in vitro and in vivo studies. This is despite additional reports about the lack of selectivity of this

molecule towards AMPK. For example, in a study involving a panel of 70 human kinases, Compound C was found to inhibit several other kinases including ERK8, MELK1, MNK1, PHK, DYRK, Src, Lck, and HIPK1 at similar concentrations as AMPK. At 1 μM, Compound C inhibited about 73% of AMPK activity. At this concentration, it inhibited 81% of MNK1 activity; 94% of PHKL activity; 43% of Aurora kinase C activity; 95% of MELK1 activity; 91%, 88%, and 76% of DYRK3, DYRK1A, and DYRK2 activities, respectively; 74% of HIPK2; 75% of Src; and 80% of Lck enzymatic activity [23]. It also inhibited kinase activities of the receptor tyrosine kinases FGFR1, Yes and Eph-A2 [23]. These authors suggested that since nearly 40 μM Compound C is required for complete inhibition of AMPK activity in vitro, levels that clearly impact numerous other kinases, the use of this reagent to examine AMPK functions is not recommended. In another kinase profiling study of Compound C against 119 kinases, several kinases including many receptor tyrosine kinases were inhibited by Compound C. The efficiency at which Compound C inhibited AMPK at 10, 1, and 0.1 μM was found to be 90%, 50%, and 25%, respectively. However, at 10 μM, it inhibited the activities of 64 out of the 119 kinases by greater than 50%. At 1 μM, it inhibited the activities of 34 out of 119 kinases more potently than it inhibited AMPK [24]. Some of the kinases that Compound C inhibited similarly or more effectively than AMPK include MARK3, EPHB3, DYRK3, FGFR1, MLK3, Src, EPH-B4, EPH-B2, MINK1, HIPK2, IRAK4, Lck, TES1, PRK2, MELK, NUAK1, CK1, CAMKKβ, ABL, PHK, DYRK1A, CLK2, GCK, ERK8, RIPK2, and VEGFR. At a hundredfold lower concentration (0.1 μM), Compound C inhibited 50% activity of PRK2, YES1, Nuak1, VEGFR, DYRK1, PHK, ABL, ERK8, CLK2, and GCK. Unfortunately, these data are overlooked, and often Compound C is used as a reference inhibitor of AMPK, sometimes at concentrations as high as 40 μM. Further complicating the question of selectivity is the finding by Jester et al. [25], that Compound C also inhibits luciferase, raising concerns about its use in assays that are coupled to luciferase.

5 Use of Compound C in Cancer

Compound C has been widely used in biochemical, cell-based, and in vivo assays as a "selective" AMPK inhibitor. The compound found its greatest use in cancer-related studies given that AMPK functions downstream of a known tumor suppressor gene called LKB1. In nearly all of these reports, the biochemical and cellular effects of compound C have been attributed to its inhibitory action toward AMPK [26–31]. In the study by Yang et al. [31], 10–30 μM Compound C was used in vitro cell proliferation studies to achieve inhibition of proliferation of human colon cancer cell lines.

Compound C was even used to rescue the effects of AMPK activators, although the effects of Compound C alone were not categorically examined in some studies. For example, the compound AICAR and the biguanide metformin activate AMPK through disparate AMPK-dependent and AMPK-independent mechanisms [32]. Strangely, while Compound C was used to rescue the antiproliferative effects of AICAR and metformin [33, 34], we and others have found that each of the three reagents, AICAR, metformin, and Compound C, inhibits cancer cell proliferation in vitro and tumor growth in vivo through AMPK-independent mechanisms [32, 35–37, 38]. In the study by Tang et al. [34], 5 and 10 mM Compound C was used for 72 h to rescue the in vitro antiproliferative effects of the non-specific AMPK activator AICAR in mouse embryonic fibroblasts (MEFs). In contrast to this study, we found that in 72 h, Compound C alone significantly inhibited viability of multiple human glioma cell lines at all concentrations between 1 and 10 μM [35]. Even at 24 h, 10 μM, Compound C caused significant cell cycle arrest at G2M in these glioma cells. All these effects were independent of AMPK. Ironically, we found that AMPK depletion by silencing RNA increased cell death by Compound C indicating not only a promiscuous mode of action of this reagent but also that AMPK protects cells from insults by xenobiotics such as Compound C. We also tested the effect of Compound C in WT and AMPK-null MEFs in the presence and absence of the AMPK activators AICAR and metformin. While metformin (5 mM), AICAR (0.5 mM), and Compound C (5 μM) each reduced viability of both WT- and AMPK-null MEFs following 72 h of treatment, Compound C did not have any protective effects against AICAR or metformin. In fact, Compound C alone killed significantly more MEFs (about 90%) regardless of the presence or absence of AICAR or metformin (our unpublished observations).

AMPK has been shown to play a role in the migration of normal as well as cancer cells. Because we and others have found many AMPK-independent effects of compound C, we also tested the AMPK dependency of this phenotype. Again, Compound C strongly inhibited migration of cancer cells independent of AMPK and at doses (1 and 2.5 μM) where it showed little effect on inhibition of AMPK activity in these cells [35]. In this study, we also reported that Compound C significantly inhibits Akt phosphorylation (at both T308 and S473) and mTOR activity in glioma cells independent of AMPK and induces apoptosis and destructive autophagy, all independent of AMPK. One surprising observation was that while Compound C effectively inhibited Akt phosphorylation in both glioma cells and MEFs, mTOR inhibition was observed specifically in glioma cells but not in MEF = mouse embryo fibroblast (unpublished). The reasons for this discrepancy are unknown to us. Erk1/2 phosphorylation remained unaffected by Compound C (unpublished). We observed that blocking apoptosis was

insufficient to rescue cells from the effect of Compound C. Instead, inhibition of the calpain-/cathepsin-mediated cell death pathway partially rescued the antiproliferative effect of Compound C [35], indicating that one mechanism by which Compound C kills cancer cells independent of AMPK is by activation of the calpain/cathepsin pathway.

6 Conclusion and Perspectives

The function of physiologically active AMPK in cancer is largely unknown. Because AMPK inhibits biosynthetic pathways and increases insulin sensitivity (a beneficial effect for the treatment of type II diabetes), there has been a sustained effort to develop AMPK activators. Unfortunately, Compound C remains the only small molecule that has been widely used to study AMPK signaling and various aspects of cell physiology, including cell proliferation, survival, and migration. The use of Compound C continues despite reports that it inhibits several other kinases with a lower Km than AMPK. Based on clear evidence from our laboratory and others, the use of this reagent as an AMPK inhibitor is not recommended. Even if genetic means such as silencing RNAs are used (which by themselves can have off-target effects), the use of Compound C to corroborate the results from genetic experiments to prove AMPK dependency of a cellular function is unwarranted and could be flawed. We encourage others to include a statement in their manuscripts that due to its proven promiscuity and non-selectivity, Compound C was not used to test AMPK function in their experiments.

References

1. Hardie DG, Hawley SA (2001) AMP-activated protein kinase: the energy charge hypothesis revisited. BioEssays 23(12):1112–1119. https://doi.org/10.1002/bies.10009
2. Hardie DG (2007) AMP-activated/SNF1 protein kinases: conserved guardians of cellular energy. Nat Rev Mol Cell Biol 8 (10):774–785. https://doi.org/10.1038/nrm2249
3. Thelander M, Olsson T, Ronne H (2004) Snf1-related protein kinase 1 is needed for growth in a normal day-night light cycle. EMBO J 23(8):1900–1910. https://doi.org/10.1038/sj.emboj.7600182
4. Spasic MR, Callaerts P, Norga KK (2008) Drosophila alicorn is a neuronal maintenance factor protecting against activity-induced retinal degeneration. J Neurosci 28(25):6419–6429. https://doi.org/10.1523/JNEUROSCI.1646-08.2008
5. Tschape JA, Hammerschmied C, Muhlig-Versen M, Athenstaedt K, Daum G, Kretzschmar D (2002) The neurodegeneration mutant lochrig interferes with cholesterol homeostasis and Appl processing. EMBO J 21 (23):6367–6376
6. Dasgupta B, Ju JS, Sasaki Y, Liu X, Jung SR, Higashida K, Lindquist D, Milbrandt J (2012) The AMPK beta2 subunit is required for energy homeostasis during metabolic stress. Mol Cell Biol 32(14):2837–2848. https://doi.org/10.1128/MCB.05853-11
7. Jorgensen SB, Wojtaszewski JF, Viollet B, Andreelli F, Birk JB, Hellsten Y, Schjerling P, Vaulont S, Neufer PD, Richter EA, Pilegaard H (2005) Effects of alpha-AMPK knockout on exercise-induced gene activation in mouse skeletal muscle. FASEB J 19(9):1146–1148. https://doi.org/10.1096/fj.04-3144fje

8. Viollet B, Andreelli F, Jorgensen SB, Perrin C, Geloen A, Flamez D, Mu J, Lenzner C, Baud O, Bennoun M, Gomas E, Nicolas G, Wojtaszewski JF, Kahn A, Carling D, Schuit FC, Birnbaum MJ, Richter EA, Burcelin R, Vaulont S (2003) The AMP-activated protein kinase alpha2 catalytic subunit controls whole-body insulin sensitivity. J Clin Invest 111 (1):91–98. https://doi.org/10.1172/JCI16567
9. O'Neill HM, Maarbjerg SJ, Crane JD, Jeppesen J, Jorgensen SB, Schertzer JD, Shyroka O, Kiens B, van Denderen BJ, Tarnopolsky MA, Kemp BE, Richter EA, Steinberg GR (2011) AMP-activated protein kinase (AMPK) beta1beta2 muscle null mice reveal an essential role for AMPK in maintaining mitochondrial content and glucose uptake during exercise. Proc Natl Acad Sci U S A 108 (38):16092–16097. https://doi.org/10.1073/pnas.1105062108
10. Viollet B, Athea Y, Mounier R, Guigas B, Zarrinpashneh E, Horman S, Lantier L, Hebrard S, Devin-Leclerc J, Beauloye C, Foretz M, Andreelli F, Ventura-Clapier R, Bertrand L (2009) AMPK: lessons from transgenic and knockout animals. Front Biosci (Landmark Ed) 14:19–44
11. Viollet B, Foretz M (2016) Animal models to study AMPK. EXS 107:441–469. https://doi.org/10.1007/978-3-319-43589-3_18
12. Foretz M, Hebrard S, Leclerc J, Zarrinpashneh E, Soty M, Mithieux G, Sakamoto K, Andreelli F, Viollet B (2010) Metformin inhibits hepatic gluconeogenesis in mice independently of the LKB1/AMPK pathway via a decrease in hepatic energy state. J Clin Invest 120(7):2355–2369. https://doi.org/10.1172/JCI40671
13. Cao J, Meng S, Chang E, Beckwith-Fickas K, Xiong L, Cole RN, Radovick S, Wondisford FE, He L (2014) Low concentrations of metformin suppress glucose production in hepatocytes through AMP-activated protein kinase (AMPK). J Biol Chem 289 (30):20435–20446. https://doi.org/10.1074/jbc.M114.567271
14. Fullerton MD, Galic S, Marcinko K, Sikkema S, Pulinilkunnil T, Chen ZP, O'Neill HM, Ford RJ, Palanivel R, O'Brien M, Hardie DG, Macaulay SL, Schertzer JD, Dyck JR, van Denderen BJ, Kemp BE, Steinberg GR (2013) Single phosphorylation sites in Acc1 and Acc2 regulate lipid homeostasis and the insulin-sensitizing effects of metformin. Nat Med 19 (12):1649–1654. https://doi.org/10.1038/nm.3372
15. Zhou G, Myers R, Li Y, Chen Y, Shen X, Fenyk-Melody J, Wu M, Ventre J, Doebber T, Fujii N, Musi N, Hirshman MF, Goodyear LJ, Moller DE (2001) Role of AMP-activated protein kinase in mechanism of metformin action. J Clin Invest 108(8):1167–1174. https://doi.org/10.1172/JCI13505
16. Yu PB, Hong CC, Sachidanandan C, Babitt JL, Deng DY, Hoyng SA, Lin HY, Bloch KD, Peterson RT (2008) Dorsomorphin inhibits BMP signals required for embryogenesis and iron metabolism. Nat Chem Biol 4(1):33–41. https://doi.org/10.1038/nchembio.2007.54
17. Hao J, Daleo MA, Murphy CK, Yu PB, Ho JN, Hu J, Peterson RT, Hatzopoulos AK, Hong CC (2008) Dorsomorphin, a selective small molecule inhibitor of BMP signaling, promotes cardiomyogenesis in embryonic stem cells. PLoS One 3(8):e2904. https://doi.org/10.1371/journal.pone.0002904
18. Yu PB, Deng DY, Lai CS, Hong CC, Cuny GD, Bouxsein ML, Hong DW, McManus PM, Katagiri T, Sachidanandan C, Kamiya N, Fukuda T, Mishina Y, Peterson RT, Bloch KD (2008) BMP type I receptor inhibition reduces heterotopic [corrected] ossification. Nat Med 14(12):1363–1369. https://doi.org/10.1038/nm.1888
19. Shen Q, Little SC, Xu M, Haupt J, Ast C, Katagiri T, Mundlos S, Seemann P, Kaplan FS, Mullins MC, Shore EM (2009) The fibrodysplasia ossificans progressiva R206H ACVR1 mutation activates BMP-independent chondrogenesis and zebrafish embryo ventralization. J Clin Invest 119(11):3462–3472. https://doi.org/10.1172/JCI37412
20. Kaplan FS, Xu M, Seemann P, Connor JM, Glaser DL, Carroll L, Delai P, Fastnacht-Urban E, Forman SJ, Gillessen-Kaesbach G, Hoover-Fong J, Koster B, Pauli RM, Reardon W, Zaidi SA, Zasloff M, Morhart R, Mundlos S, Groppe J, Shore EM (2009) Classic and atypical fibrodysplasia ossificans progressiva (FOP) phenotypes are caused by mutations in the bone morphogenetic protein (BMP) type I receptor ACVR1. Hum Mutat 30 (3):379–390. https://doi.org/10.1002/humu.20868
21. Shore EM, Xu M, Feldman GJ, Fenstermacher DA, Cho TJ, Choi IH, Connor JM, Delai P, Glaser DL, LeMerrer M, Morhart R, Rogers JG, Smith R, Triffitt JT, Urtizberea JA, Zasloff M, Brown MA, Kaplan FS (2006) A recurrent mutation in the BMP type I receptor ACVR1 causes inherited and sporadic fibrodysplasia ossificans progressiva. Nat Genet 38(5):525–527. https://doi.org/10.1038/ng1783
22. Hao J, Ho JN, Lewis JA, Karim KA, Daniels RN, Gentry PR, Hopkins CR, Lindsley CW, Hong CC (2010) In vivo structure-activity relationship study of dorsomorphin analogues

identifies selective VEGF and BMP inhibitors. ACS Chem Biol 5(2):245–253. https://doi.org/10.1021/cb9002865

23. Bain J, Plater L, Elliott M, Shpiro N, Hastie CJ, McLauchlan H, Klevernic I, Arthur JS, Alessi DR, Cohen P (2007) The selectivity of protein kinase inhibitors: a further update. Biochem J 408(3):297–315. https://doi.org/10.1042/BJ20070797
24. Vogt J, Traynor R, Sapkota GP (2011) The specificities of small molecule inhibitors of the TGFss and BMP pathways. Cell Signal 23 (11):1831–1842. https://doi.org/10.1016/j.cellsig.2011.06.019
25. Jester BW, Cox KJ, Gaj A, Shomin CD, Porter JR, Ghosh I (2010) A coiled-coil enabled split-luciferase three-hybrid system: applied toward profiling inhibitors of protein kinases. J Am Chem Soc 132(33):11727–11735. https://doi.org/10.1021/ja104491h
26. Vucicevic L, Misirkic M, Janjetovic K, Vilimanovich U, Sudar E, Isenovic E, Prica M, Harhaji-Trajkovic L, Kravic-Stevovic-T, Bumbasirevic V, Trajkovic V (2011) Compound C induces protective autophagy in cancer cells through AMPK inhibition-independent blockade of Akt/mTOR pathway. Autophagy 7(1):40–50
27. Hwang JT, Ha J, Park IJ, Lee SK, Baik HW, Kim YM, Park OJ (2007) Apoptotic effect of EGCG in HT-29 colon cancer cells via AMPK signal pathway. Cancer Lett 247(1):115–121. https://doi.org/10.1016/j.canlet.2006.03.030
28. Pan W, Yang H, Cao C, Song X, Wallin B, Kivlin R, Lu S, Hu G, Di W, Wan Y (2008) AMPK mediates curcumin-induced cell death in CaOV3 ovarian cancer cells. Oncol Rep 20 (6):1553–1559
29. Rios M, Foretz M, Viollet B, Prieto A, Fraga M, Costoya JA, Senaris R (2013) AMPK activation by oncogenesis is required to maintain cancer cell proliferation in astrocytic tumors. Cancer Res 73(8):2628–2638. https://doi.org/10.1158/0008-5472.CAN-12-0861
30. Dowling RJ, Zakikhani M, Fantus IG, Pollak M, Sonenberg N (2007) Metformin inhibits mammalian target of rapamycin-dependent translation initiation in breast cancer cells. Cancer Res 67(22):10804–10812. https://doi.org/10.1158/0008-5472.CAN-07-2310
31. Liu X, Chhipa RR, Pooya S, Wortman M, Yachyshin S, Chow LM, Kumar A, Zhou X, Sun Y, Quinn B, McPherson C, Warnick RE, Kendler A, Giri S, Poels J, Norga K, Viollet B, Grabowski GA, Dasgupta B (2014) Discrete mechanisms of mTOR and cell cycle regulation by AMPK agonists independent of AMPK. Proc Natl Acad Sci U S A 111(4):E435–E444. https://doi.org/10.1073/pnas.1311121111
32. Isakovic A, Harhaji L, Stevanovic D, Markovic Z, Sumarac-Dumanovic M, Starcevic V, Micic D, Trajkovic V (2007) Dual antiglioma action of metformin: cell cycle arrest and mitochondria-dependent apoptosis. Cell Mol Life Sci 64(10):1290–1302. https://doi.org/10.1007/s00018-007-7080-4
33. Tang YC, Williams BR, Siegel JJ, Amon A (2011) Identification of aneuploidy-selective antiproliferation compounds. Cell 144(4):499–512. https://doi.org/10.1016/j.cell.2011.01.017
34. Liu X, Chhipa RR, Nakano I, Dasgupta B (2014) The AMPK inhibitor compound C is a potent AMPK-independent antiglioma agent. Mol Cancer Ther 13(3):596–605. https://doi.org/10.1158/1535-7163.MCT-13-0579
35. Dai RY, Zhao XF, Li JJ, Chen R, Luo ZL, Yu LX, Chen SK, Zhang CY, Duan CY, Liu YP, Feng CH, Xia XM, Li H, Fu J, Wang HY (2013) Implication of transcriptional repression in compound C-induced apoptosis in cancer cells. Cell Death Dis 4:e883. https://doi.org/10.1038/cddis.2013.419
36. Jin J, Mullen TD, Hou Q, Bielawski J, Bielawska A, Zhang X, Obeid LM, Hannun YA, Hsu YT (2009) AMPK inhibitor Compound C stimulates ceramide production and promotes Bax redistribution and apoptosis in MCF7 breast carcinoma cells. J Lipid Res 50 (12):2389–2397. https://doi.org/10.1194/jlr.M900119-JLR200
37. Hirose Y, Berger MS, Pieper RO (2001) Abrogation of the Chk1-mediated G(2) checkpoint pathway potentiates temozolomide-induced toxicity in a p53-independent manner in human glioblastoma cells. Cancer Res 61 (15):5843–5849
38. Darzynkiewicz Z, Juan G, Li X, Gorczyca W, Murakami T, Traganos F (1997) Cytometry in cell necrobiology: analysis of apoptosis and accidental cell death (necrosis). Cytometry 27 (1):1–20
39. Yang WL, Perillo W, Liou D, Marambaud P, Wang P (2012) AMPK inhibitor compound C suppresses cell proliferation by induction of apoptosis and autophagy in human colorectal cancer cells. J Surg Oncol 106(6):680–688. https://doi.org/10.1002/jso.23184

Chapter 13

Identifying the Heterotrimeric Complex Stoichiometry of AMPK in Skeletal Muscle by Immunoprecipitation

Jesper B. Birk and Jørgen F. P. Wojtaszewski

Abstract

The 5′-AMP-activated protein kinase is a complicated enzyme consisting of three different subunits, each of which is expressed as two or three isoforms. This gives the possibility of 12 different heterotrimeric complexes, which could have diverse functions within the cell. To map out which of these complexes are present and to what extent in skeletal muscle, we have used the immunoprecipitation technique and analyzed both the precipitates and the remaining supernatants for coprecipitation of complex partners. We have fine-tuned this method to give the best results on lysates from the skeletal muscle, liver, and heart muscle from mouse to man.

Key words AMPK, Homogenization, Protein interaction, Immunoprecipitation, Western blot, In vitro setting, Antibody specificity

1 Introduction

The 5′-AMP-activated protein kinase (AMPK) is a trimeric protein complex consisting of a catalytic α subunit and two regulatory β and γ subunits. Not including splice variants, each of these subunits is expressed as two or three isoforms (α1, α2, β1, β2, γ1, γ2, and γ3) giving the possibility of 12 different heterotrimeric complexes. It is well established that the expression profile of each of these isoforms is more or less tissue specific; α1, γ1, and γ2 being broadly expressed in most tissues throughout the body. The α2 and β2 being more restricted to the skeletal muscle, heart muscle, and liver, while the γ3 subunit isoform is highly restricted to skeletal muscle and especially fast-twitch/white fiber types [1–4]. Although this tissue specificity narrows down the number of possible heterotrimeric complexes in a certain tissue, all seven subunit isoforms have been identified in skeletal muscle leaving the stoichiometry and regulation of AMPK in this tissue highly complex. Adding to this complexity is the heterogeneity of the skeletal muscle tissue containing not only myofibers but also endothelial and adipose

Dietbert Neumann and Benoit Viollet (eds.), *AMPK: Methods and Protocols*, Methods in Molecular Biology, vol. 1732, https://doi.org/10.1007/978-1-4939-7598-3_13,

cells, fibroblasts, and different types of blood cells. Although in minority, these other cell types could contribute with AMPK heterotrimers not present in the myofibers themselves. Little is known about the regulation and substrate specificity of the different heterotrimeric complexes within the muscle cell. There could be differences in upstream and downstream signaling, localization, and metabolite sensitivity. Acknowledging that the analyses were not specific to myofibers alone, but the whole mixed muscle tissue, we set out more than 10 years ago to identify which of the 12 possible heterotrimeric complexes is present in skeletal muscle and what the stoichiometry of these might be [5–7]. To do this, we immunoprecipitated the different subunit isoforms and evaluated these for coprecipitation of complex partners. This method requires strong protein-protein interaction between the complex partners that have to withstand the process of muscle tissue homogenization and the immunoprecipitation procedure itself. The pitfall of this procedure is false negatives that do not show up as complexes because the protein-protein interaction is too weak to last throughout the procedure. Another issue is the specificity of the antibodies used for the precipitation. In theory, these could be more or less specific toward certain complexes and may be blocked out by others if a certain complex partner would hide the epitope. To avoid these problems, we insured that the antibodies used were able to immunoprecipitate all of the specific protein they were targeted against—leaving no fraction out of the equation. This procedure enabled comparison as to how much a specific isoform coprecipitated the others and vice versa. Putting these data together, it was possible to account for the vast majority of the subunit isoforms and the complexes they were part of.

The immunoprecipitation (IP) can be analyzed in two ways. One way is to immunoprecipitate the different subunit isoforms and load an equal amount of the IPs on the same gel and then blot for one of the isoforms. This gives a direct comparison of how much of the subunit isoform blotted for that is coprecipitated with the others. Problems could be uneven antibody-antigen affinity and hence washing away more of some isoforms than others in the various IPs.

Analysis of the Post-IPs is a stronger method to compare coprecipitation. By analyzing the same amount of sample protein on Western blot for the Post-IP and the Pre-IP (~input), it is possible to quantify how much of a specific isoform has been removed by the IP procedure. This analysis is not dependent on the washing steps of the IP, which makes it more consistent than analyzing the IP per se. This way it is possible to control that an antibody is able to immunoprecipitate all of the targeted protein. However, since the samples are being analyzed and verified by Western blot, there are limits to the outer extremes of the spectrum. On one end the analysis is restricted to the lowest detection

limit of Western blotting. If nearly all of a subunit isoform is coprecipitated, then the little remaining protein in the Post-IP might be below the detection limit on the Western blot making it look like all of the protein was coprecipitated. On the other end of the scale, i.e., coprecipitating only a small part of a subunit isoform fraction, it might be hard to determine if the Post-IP band is indeed weaker than the input (Pre-IP) band. In this case, however, the IP itself can help to verify the coprecipitation, because it would show a faint band of the coprecipitated protein.

The Subheading 2 is divided into two subsections: one describing the homogenization of muscle tissue and the other the immunoprecipitation procedure. In theory, the IP procedure could work on any lysates produced by homogenization in different kinds of homogenization buffers. However, a short description is given to the homogenization protocol because we have experienced that other buffers (e.g., RIPA buffer (Sigma R0278) and Rac1 lysis buffer (Cytoskeleton Inc. BK126)) induce problems if the IP is followed by an enzyme activity assay (described in Chapter 14). Due to high salt, but still mild detergent (Nonidet P-40), the homogenization buffer we use is relatively strong and gives a high protein yield in the lysate. This gives a higher extraction yield of AMPK from the muscle tissue and lower chance of losing potentially important fractions in the pellet when the homogenate is centrifuged to get the lysate. The disadvantage could be disruption of certain AMPK complexes, though comparing with milder homogenization buffers this is not our experience. The homogenization buffer is possibly not strong enough to lyse the cell nuclei, and thus our method does not detect AMPK complexes in this compartment, unless mechanically disrupted by the tissue lysing. Adding ionic detergents (e.g., sodium deoxycholate or SDS) would solve this, but at the same time, most likely disrupt the AMPK heterotrimeric complexes making co-IP impossible.

We do not go into details describing the total protein determination procedure, because this is considered as standard and will be done equally on all samples involved in the subsequent IP procedure. The main requirement for the assay for determination of the protein concentration is that it is compatible with the ingredients in the homogenization buffer, which is the case for the bicinchoninic acid (BCA) assay.

The same applies for the SDS-PAGE and Western blot analysis following the IP procedure, which should not change the outcome of the IP procedure. Certainly, it is important that antibodies are appropriately verified for specificity and the blots are tested for signal linearity in relation to the amount of protein loaded on the gel.

2 Materials

Prepare all solutions using ultrapure water (Milli-Q purified demineralized water) and analytical grade reagents. Prepare and store all reagents at room temperature (unless indicated otherwise).

2.1 Muscle Homogenization

1. Homogenization buffer: 50 mM HEPES, pH 7.5, 10% (v/v) glycerol, 20 mM Na-pyrophosphate, 150 mM NaCl, 1% (v/v) Nonidet P-40 (Igepal CA-630), 20 mM beta-glycerophosphate, 10 mM NaF, 2 mM phenylmethylsulfonyl fluoride, 1 mM EDTA, 1 mM EGTA, 10 μg/ml aprotinin, 10 μg/ml leupeptin, 2 mM Na_3VO_4, 3 mM benzamidine. This buffer is stored at 4 °C for up to 1 day.
2. Homogenizer: Retsch TissueLyser II (Qiagen).
3. Rotation apparatus for Eppendorf tubes. Should be placed at 4 °C.
4. Protein determination: Bicinchoninic acid kit.

2.2 Immunoprecipitation

1. IP buffer (*see* **Note 1**): 20 mM Tris-base, pH 7.4, 50 mM NaCl, 1% (v/v) Triton X-100, 50 mM NaF, 5 mM Na-pyrophosphate, 500 μM phenylmethylsulfonyl fluoride, 2 mM dithiothreitol, 4 μg/ml leupeptin, 50 μg/ml soybean trypsin inhibitor, 6 mM benzamidine, 250 mM sucrose. This buffer is stored at 4 °C.
2. Protein A or G agarose (*see* **Note 2**) washed thrice in IP buffer and used as a 50:50 slurry suspension. Stored at 4 °C.
3. IP wash buffer: 120 mM HEPES, pH 7.0, 240 mM NaCl. This buffer is stored at 4 °C.
4. 6× sample buffer (6×SB): 320 mM Tris–HCl, pH 6.8, 550 mM dithiothreitol, 315 mM SDS, 27% (v/v) glycerol, 100–200 μg/ml bromophenol blue sodium salt. This buffer is stored at −20 °C. To get a 2× sample buffer (2×SB), dilute the 6×SB three times in water.
5. Primary antibodies against the various AMPK subunit isoforms (*see* **Note 3**).

3 Methods

3.1 Muscle Homogenization

1. For studies of rodents, it is often possible to dissect well-defined muscles or parts hereof. By visual inspection associated adipose or connective tissue can be removed. Similarly, muscles can be freed of superficial blood contamination by washing in ice-cold phosphate-buffered saline. Human muscle samples obtained by needle biopsies do not offer a fast procedure for such sample cleaning—except a quick rinse in ice-cold buffer.

Thus, to ensure a clean muscle sample, it is recommended that biopsy material is freeze-dried and subsequently dissected free of visible blood, fat, and connective tissue under the microscope.

2. Make up a fresh batch of homogenization buffer and keep it on ice or at 4 °C.
3. Keep the wet weight or freeze-dried tissue on dry ice (−80 °C) in 2 ml Eppendorf tubes until just before the homogenization buffer is added.
4. Open and place the tubes in the TissueLyser plastic racks. These should be stored at −20 °C, so they are cold at all times.
5. Working quickly, add a 5 mm steel ball to each tube (be careful that pieces of tissue will not "jump" out of the tube when the ball hits the bottom).
6. Add homogenization buffer to all samples in a ratio 20 μl to 1 mg of wet weight muscle or 80 μl to 1 mg of freeze-dried muscle (*see* **Note 4**).
7. Close all tubes and place the rack in the TissueLyser.
8. Tissue-lyse two times 1 min at 30 Hz. If there are still large chunks of muscle in some tubes, tissue-lyse again.
9. Place the tubes in another rack, and let them rotate end over end for 1 h at 4 °C.
10. Spin down the pellet at 16,000 × *g* for 20 min and 4 °C.
11. Transfer the supernatant (lysate) to a new set of tubes on ice.
12. Take out a small portion (10–15 μl) for determination of protein concentration, and store the rest at −80 °C.
13. Use a standard protocol for determination of protein concentration with a bicinchoninic acid (BCA) kit. Dilute the samples five times in water for the assay.

3.2 Immunoprecipitation

1. Make up a fresh batch of IP buffer and keep it on ice or at 4 °C.
2. Choose the appropriate Protein A or G agarose (agarose beads) according to the antibody to be used in the immunoprecipitation (IP) (*see* **Note 2**).
3. Wash the agarose beads thrice in IP buffer, and make up a 50:50 slurry suspension (*see* **Note 5**).
4. To get the most correct representation of the input to the IP, make up a **Pre-IP** (*see* **Note 6**). Set up an IP with an irrelevant antibody that does NOT recognize the protein of interest or any of its predicted complex partners. This IP is run in parallel with the "real" IP(s).
5. Add 20 μl of agarose beads (10 μl packed beads) to each IP (use 0.2 or 0.5 ml tubes). Keep these tubes on ice.

6. Add IP buffer according to your calculations. If the total volume of the IP should be 200 µl, then the IP buffer should be 200 µl minus 20 µl of agarose (50:50 slurry), minus 10 µl of antibody, minus *x* µl of lysate (Fig. 1a) (*see* **step 8**).
7. Add 10 µl of antibody (*see* **Note 7**).
8. Add *x* µl of lysate. If you want to IP on 200 µg of lysate and the total protein concentration in that lysate is 5 µg/µl, then add 40 µl of lysate (200 µg divided by 5 µg/µl) (*see* **Note 8**).
9. Let the IPs rotate end over end at 4 °C overnight (*see* **Note 9**).
10. On Day 2, remove the IPs from rotation and spin down the agarose for 1 min at 500 × *g* or quick spin in a small tabletop centrifuge. Place tubes on ice.
11. Prepare a new set of tubes for the Post-IPs.
12. Add 34 µl of 6×SB to each of these tubes (*see* **Note 10**).
13. Transfer 170 µl of the supernatant from the IP to the new tube with 6×SB and mix (Fig. 1b). This is the **Post-IP** (*see* **Note 11**). For the IP with irrelevant antibody, this is the **Pre-IP**.
14. Wash the remaining agarose once in 180 µl of IP buffer and twice in 180 µl of IP wash buffer. Between washes spin the agarose down for 1 min at 500 × *g* and 4 °C or in a small tabletop centrifuge. Use suction to discard the supernatant, but be careful not to take away any agarose. Leave 10–20 µl of wash buffer to be safe.
15. After last wash, aspirate all supernatant, still being careful not to lose any agarose beads.
16. Add 20 µl of 2×SB to the agarose and mix gently without splashing the agarose up the sides of the tube (Fig. 1c). This is the IP (*see* **Note 12**).
17. Heat all samples (IPs and Pre- and Post-IPs) at 96 °C for 5 min. Mix and spin down.
18. The samples are now ready for SDS-PAGE.
19. The protein in the IP is no longer attached to the agarose but is free in the small sample buffer supernatant. Do not load the agarose on the gel but only the supernatant.
20. The resulting protein concentration in the Pre-IP and the Post-IP is the same. The input was 200 µg of lysate protein in 190 µl (half of the 20 µl of agarose (50:50 slurry) was packed beads and is not part of the supernatant, *see* **step 6**). 170 µl of the supernatant was transferred to a new tube and diluted with 34 µl of 6×SB. This gives a concentration of: (200 µg/190 µl * 170 µl)/(170 µl + 34 µl) = 0.88 µg/µl (Fig. 1c) (*see* **Note 13**).

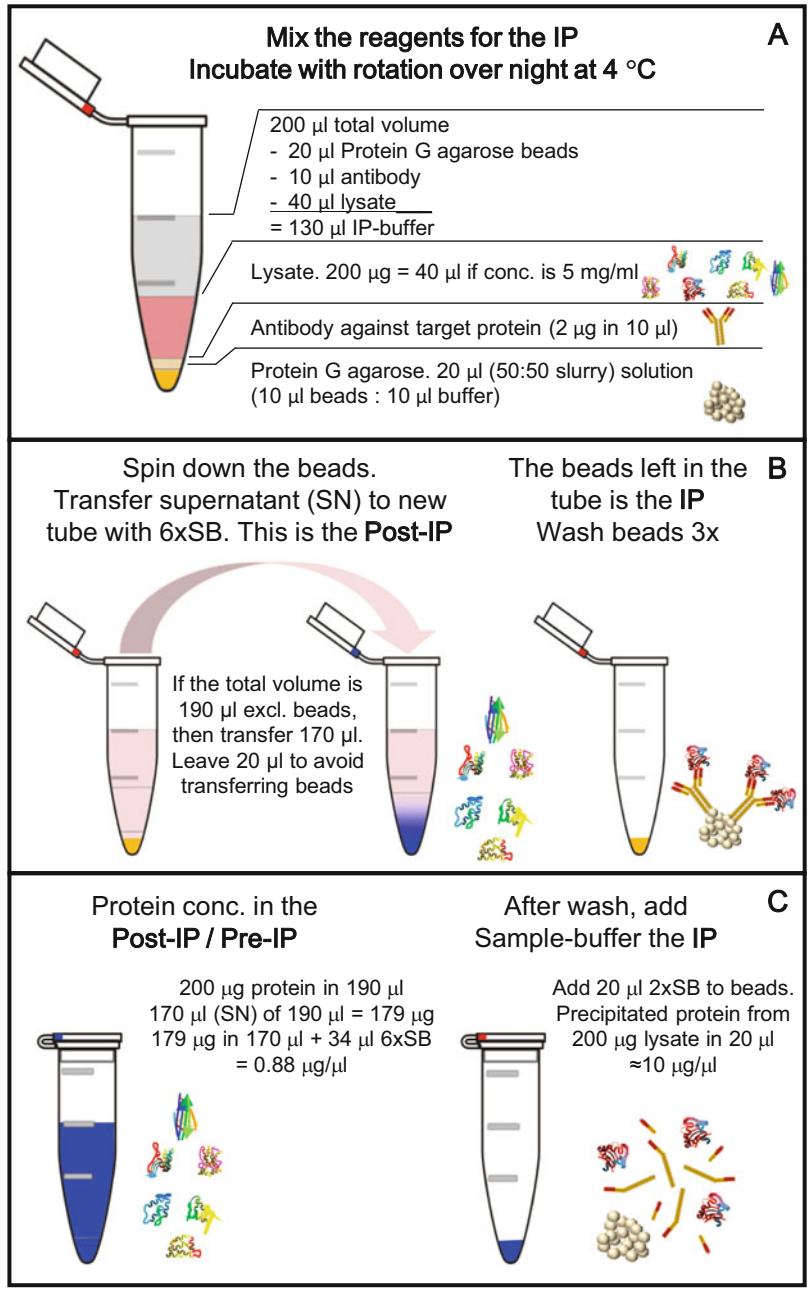

Fig. 1 Schematic representation of the IP procedure. (A) Example of the constituents of an IP sample with indicated volumes of Protein G agarose, antibody, lysate, and IP buffer. (B) Separation of IP and Post-IP, transferring the supernatant from the IP to a new tube with sample buffer. (C) Resulting protein concentration of the Post-IP and the equivalent of the IP for the precipitated protein

21. Compare the signal from the different IPs to see how much of the different subunit isoforms are coprecipitated with the others.

22. Compare the Post-IPs to the Pre-IP to see how much of each specific subunit isoform is missing in the Post-IPs after the various IPs.
23. Do not quantitatively compare signal intensities between the IPs and the Post- or the Pre-IPs (*see* **Note 14**).

4 Notes

1. The IP buffer could be the same as the homogenization buffer or even just phosphate-buffered saline (PBS). Our experience is that analyzing enzyme activity after the IP (*see* Chapter 14) gives higher specific activity with the milder IP buffer compared to the homogenization buffer for reasons unknown. Advantages of the IP buffer compared to PBS is the detergent in the IP buffer which eliminates the surface tension and makes the solution mix better in very small tubes during the end-over-end incubation. Also the addition of extra protease and phosphatase inhibitors during the IP incubation is beneficial.
2. The selection of either Protein A or G agarose is dependent on the species and subgroup of the antibody used in the IP. Most antibodies work best with Protein G, but this should be verified before start. As standard we use Protein G agarose, Fast Flow from Merck (cat. #16-266).
3. It is paramount that the antibodies used for immunoprecipitating each subunit isoform are able to IP all of the particular subunit from the lysate. In case a specific subunit isoform cannot be precipitated (near) quantitatively, there is no way of knowing if the remaining fraction is part of a special heterotrimeric complex or if it is a complex fraction that is posttranslationally modified by signaling that could be important for the distribution and regulation of AMPK. Over the years, we have used many different sources of antibodies as some have run out of stock. All have been tested thoroughly before use and during our search; many have been rejected for precipitating partially or not at all. At the time of writing, we have still not been able to find suitable antibodies for IP of the AMPK γ1 and γ2 isoforms.
4. If homogenizing a large portion of muscle (more than ~12 mg freeze-dried or 50 mg of wet weight muscle), it is not advisable to add more than 800 μl of buffer to the 2 ml tube when tissue-lysing, because too much fluid in the tube will slow down the movements of the steel ball. Add the remaining buffer after tissue-lysing before the samples are set to rotate for 1 h (**step 9**). To speed up the process, add the same amount of buffer to all samples, tissue-lyse, and then fill up the remaining

buffer for each sample. This minimizes the time the muscle is at 4 °C where enzymatic processes slowly start up. Once the tissue is lysed, the proteins and enzymes are extracted and mixed with protease and phosphatase inhibitors, and then the time pressure for having the sample at 4 °C is lowered.

5. The Protein A or G agarose is usually supplied in a suspension containing ethanol and has to be calibrated in the IP buffer. When pipetting the agarose, use wide orifice pipette tips and vortex or stir the suspension just before pipetting.
6. The Pre-IP is the same as the input material to the IP procedure and could be the raw lysate. Mixing the lysate with agarose beads and antibody and incubating it overnight could however make small changes in the appearance of protein bands on a SDS-polyacrylamide gel (also proteins not precipitated). To make the best comparison between Pre- and Post-IP, a control IP with an unspecific/irrelevant antibody should be made, and the Post-IP of this should be used as Pre-IP (input).
7. The amount of antibody to be used in an IP depends on the amount of lysate precipitated on and the affinity of the antibody, which must be tested. Usually 2 μg of antibody is sufficient for IP on 200 μg of lysate. The concentration of antibody varies between batches, and also to avoid pipetting very small volumes, it is recommended to dilute the antibody in IP buffer to a concentration of 0.2 mg/ml and then pipette 10 μl to each IP.
8. The amount of lysate protein put into the IP depends on the purpose of the IP. Searching for co-IP of AMPK heterotrimeric complex partners, the IP and Post-IP must be used for several Western blots detecting all seven subunit isoforms. The amount of protein loaded on gels for these blots depends on the antibodies used for the blots, but are in the range of 5–20 μg, and some isoforms with different molecular weight can even be analyzed on the same gel. Precipitating on 200 μg of lysate protein would give material enough for loading at least five gels.
9. The time and temperature for an IP can vary a lot depending on antibody affinity, considerations for protein complex stability, and workflow. Low temperature (4 °C) lengthens the IP process, but maintains a higher stability for protease and phosphatase inhibitors as well as for protein interactions. Doing consecutive IPs and measuring enzyme activity on each of the IPs would challenge the number of hours in a working day if the time for each IP was set to only a couple of hours. Our experience is that the AMPK heterotrimeric complexes are very stable and can endure at least three consecutive overnight IP incubations at 4 °C.

10. The 6×SB should comprise a sixth of the total volume in a sample made ready for SDS-PAGE. 170 µl Post-IP/5 = 34 µl.
11. Leave a small volume (190–170 = 20 µl) of the supernatant with the IP to minimize the risk of transferring agarose beads to the Post-IP. This small amount of supernatant is washed away afterward. The Post-IP can be used for several Western blots detecting the presence (not coprecipitated) or absence (coprecipitated) of different subunit isoforms and other proteins.
12. If the specific protein was precipitated from 200 µg of lysate protein and all of the specific protein was precipitated successfully, then adding 20 µl of 2×SB to the agarose beads would give a protein concentration corresponding to 10 mg/ml. This is not the real protein concentration, but the amount of the specific precipitated protein would be equivalent to that in 20 µl of lysate with a total protein concentration of 10 mg/ml.
13. The amount of lysate protein to be put into the IP and the volume of the IP are adjustable as one finds suitable. Increasing the amount of protein and/or decreasing the volume gives a higher protein concentration in the Post-IP. The volume should be sufficient to allow for proper fluid mixing in the tube during the IP end-over-end incubation. Smaller tubes (0.2 ml PCR tubes) are suitable for smaller IP volumes.
14. Since the IP only contains a "few" proteins (the precipitated and coprecipitated proteins, plus the antibody and the protein G from the agarose) compared to a lysate, it will often behave differently on SDS-PAGE. Occasionally the specific protein band shifts upward in molecular weight and does not align with the band in the Pre-IP. Furthermore, when loading the same amount of protein based on the input to the immunoprecipitation, the signal intensity of the IP band is different from the corresponding band from the Pre-IP. Often the Western blot signal in the IP is lower with the exception of the γ1 isoform, which is stronger. It is therefore advisable to load twice the amount of protein from the IP compared to the Pre- and Post-IPs to get similar signal intensity on the Western blot. However, due to these and other circumstances mentioned above, *do not quantitatively compare IP signals to the signals of the Pre- and Post-IPs.*

References

1. Stapleton D, Mitchelhill KI, Gao G, Widmer J, Michell BJ, Teh T, House CM, Fernandez CS, Cox T, Witters LA, Kemp BE (1996) Mammalian AMP-activated protein kinase subfamily. J Biol Chem 271:611–614
2. Mahlapuu M, Johansson C, Lindgren K, Hjalm G, Barnes BR, Krook A, Zierath JR, Andersson L, Marklund S (2004) Expression profiling of the gamma-subunit isoforms of AMP-activated protein kinase suggests a major

role for gamma3 in white skeletal muscle. Am J Physiol Endocrinol Metab 286:E194–E200

3. Yu H, Fujii H, Hirshman MF, Pomerleau JM, Goodyear LJ (2004) Cloning and characterization of mouse 5′-AMP-activated protein kinase g3 subunit. Am J Physiol Cell Physiol 286: C283–C292
4. Kristensen DE, Albers PH, Pratz C, Baba O, Birk JB, Wojtaszewski JFP (2015) Human muscle fibre type-specific regulation of AMPK and downstream targets by exercise. J Physiol 593:2053–2069
5. Wojtaszewski JF, Birk JB, Frosig C, Holten M, Pilegaard H, Dela F (2005) 5′AMP activated protein kinase expression in human skeletal muscle: effects of strength training and type 2 diabetes. J Physiol 564:563–573
6. Birk JB, Wojtaszewski JF (2006) Predominant alpha2/beta2/gamma3 AMPK activation during exercise in human skeletal muscle. J Physiol 577:1021–1032
7. Treebak JT, Birk JB, Hansen BF, Olsen GS, Wojtaszewski JF (2009) A-769662 activates AMPK beta1-containing complexes but induces glucose uptake through a PI3-kinase-dependent pathway in mouse skeletal muscle. Am J Physiol Cell Physiol 297:C1041–C1052

Chapter 14

Kinase Activity Determination of Specific AMPK Complexes/ Heterotrimers in the Skeletal Muscle

Jesper B. Birk and Jørgen F. P. Wojtaszewski

Abstract

Measuring the kinase activity of the 5′-AMP-activated protein kinase (AMPK) is an essential part of understanding the regulation of this metabolic master switch. The AMPK heterotrimer can exist in 12 different constellations with potentially diverse activation patterns. It is therefore important to be able to measure heterotrimer-specific activity to discriminate between these patterns. In this chapter we describe how to measure the AMPK activity of specific heterotrimeric complexes by consecutive immunoprecipitations and how the assay can be performed in a medium throughput fashion using 96-well plates.

Key words Immunoprecipitation, AMPK activity, Skeletal muscle, Isoform-specific, Radioactive tracer ^{33}P, AMARA peptide

1 Introduction

A key element of an enzyme is its activity, i.e., for a kinase the ability to phosphorylate its target proteins. The 5′-AMP-activated protein kinase (AMPK) is activated both allosterically and by covalent modifications such as phosphorylation. The allosteric activation by AMP and to a lesser degree ADP increases the kinase activity, but more importantly, it increases the susceptibility for phosphorylation by upstream kinases and reduces the dephosphorylation by phosphatases [1]. The canonical phosphorylation site Thr-172 on the activation loop of the catalytic α subunit is extremely important for the activity of AMPK. Phosphorylation of Thr-172 increases the activity of AMPK with two to three orders of magnitude [2].

The initial measurements of AMPK activity were performed before antibodies were produced against AMPK, and hence no immunoprecipitation allowed AMPK purification from tissue lysates. Using crude tissue extracts and ammonium sulfate precipitation of proteins, the specificity of the kinase activity had to be insured by a substrate peptide constructed to mimic the phosphorylation site on the known AMPK target acetyl-CoA carboxylase

Dietbert Neumann and Benoit Viollet (eds.), *AMPK: Methods and Protocols*, Methods in Molecular Biology, vol. 1732, https://doi.org/10.1007/978-1-4939-7598-3_14,

(ACC). This peptide was modified to omit phosphorylation by cyclic AMP-dependent protein kinase and called the SAMS peptide from the internal sequence of the peptide (HMRSAMSGLHLVKRR) containing the target serine residue phosphorylated by AMPK [3–5].

In an effort to define the recognition motif of mammalian, higher plant, and yeast members of the SNF1 protein kinase subfamily, the synthetic peptide AMARA (AMARAASAAALARRR) was developed and was shown to be a better substrate for AMPK than the SAMS peptide [6]. After this discovery, an increasing number of research groups exchanged SAMS for AMARA peptide in activity measurements of AMPK.

In 1996, the first antibodies against the α subunit isoforms were generated, and AMPK could be purified with immunoprecipitation further increasing the specificity of the activity assay [7]. Furthermore, the activity of AMPK could now be divided into α1 and α2 activities showing diverse regulation in skeletal muscle [8, 9]. In 2005, our research group identified the human heterotrimeric complex composition in the skeletal muscle [10] and, shortly thereafter, started to measure not only the α1 and α2 activities but also the γ3-associated activity [11].

Some considerations should be made when measuring the kinase activity of AMPK. First of all, the assay is depending on immunoprecipitation and the quality of this as described in Chapter 13. This raises demands to the homogenization procedure and the IP procedure itself. During the kinase reaction, the immunoprecipitated AMPK heterotrimeric complex is still bound by the antibody and the Protein G agarose beads. The antibody has approximately the same molecular size as the whole AMPK heterotrimer complex, and depending on the location of the epitope, this could potentially inhibit (or less likely increase) the activity of AMPK. Therefore, comparison of activities between different complexes (precipitated with different antibodies) or between different laboratories using different sources of antibodies should be done with caution.

Secondly, the AMPK activity is measured in vitro under conditions that are different from the in vivo environment inside the cell. The nucleotide status (AMP, ADP, and ATP conc.) in the cell at the time of harvest has tremendous effects on the activity of AMPK both in terms of allosteric and covalent (Thr-172 phosphorylation) activation. The kinase activity assay is run with a saturated concentration of AMP (200 μM), and thus the direct allosteric effect of the intracellular AMP/ATP ratio is lost in the assay. The allosteric activation of AMPK is fortunately relatively small compared to the covalent (Thr-172 phosphorylation), and thus it may not make a substantial difference that the assay is run with a saturated concentration of AMP. In theory, the activity measured should therefore be equivalent to the Thr-172 phosphorylation status of the assayed

heterotrimeric complex. This has previously been shown for the α2β2γ3 complex by correlating the γ3-associated activity to the γ3-associated α-Thr-172 phosphorylation [11]. In line with this, we get strong correlations between our summed activities from measurements of the activity of all heterotrimeric complexes in a set of samples and the result from a phospho-AMPK Thr-172 Western blot. This shows the robustness of the assay but also the importance of dissecting the AMPK activity into different heterotrimeric complexes. The activation of the different complexes differs greatly with various interventions, and these differences are not always observable in a total phospho-AMPK Thr-172 Western blot [11].

The assay described in the following is very similar to that described by Davies SP. et al., in 1989 [3], and with immunoprecipitation by Vavvas D. et al., in 1997 [8]. It can be done either in single Eppendorf tubes or in a medium throughput fashion using 96-well PCR-plates. The principle is the same as is the workflow, but only the medium throughput fashion will be described here. The duration of the assay (4–5 days) is not much shorter with the medium throughput compared to the single-tube assay, but approximately eight times as many samples can be run within the same time frame. The medium throughput assay requires some special equipment, which is not needed for the single-tube assay.

The Subheading 3 is divided into three subsections, the first describing the immunoprecipitation of the various heterotrimeric complexes, the second the kinase reaction itself, and the last the calculations for the specific activity of the samples.

2 Materials

Prepare all solutions using ultrapure water (Milli-Q purified demineralized water) and analytical grade reagents. Prepare and store all reagents at room temperature (unless indicated otherwise).

2.1 Immunoprecipitation (IP)

1. IP-buffer (*see* **Note 1**): 20 mM Tris-base, pH 7.4, 50 mM NaCl, 1% (v/v) Triton X-100, 50 mM NaF, 5 mM Na-pyrophosphate, 500 μM phenylmethylsulfonyl fluoride, 2 mM dithiothreitol (DTT), 4 μg/ml leupeptin, 50 μg/ml soybean trypsin inhibitor, 6 mM benzamidine, 250 mM sucrose. This buffer is stored at 4 °C.
2. Protein A or G agarose (*see* **Note 2**) washed thrice in IP-buffer and used as a 50:50 slurry suspension. Stored at 4 °C.
3. Primary antibodies against desired AMPK subunit isoforms (*see* **Note 3**).
4. 96-Well PCR-plates with V-shaped well bottoms and a volume of 200 μl per well.

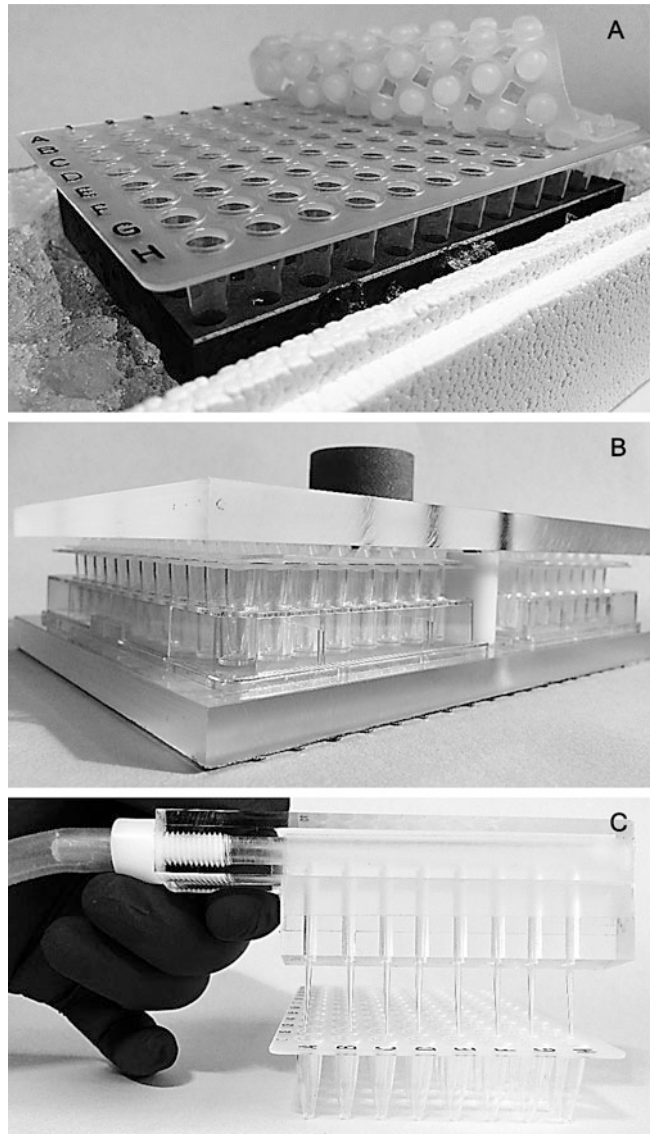

Fig. 1 Pictures showing the special equipment used for the medium throughput AMPK activity assay. (A) The 96-well PCR-plate in the aluminum block on ice with the silicone sealing mat drawn aside. (B) The "sandwich device" with two flat bottom 96-well plates holding two 96-well PCR-plates with silicone sealing mats on top. The "sandwich device" holds the assembly together, so it can rotate end over end without fluid leaking out of the wells of the PCR-plate. (C) Polycarbonate suction device with eight pipette tips for discarding the wash supernatant from the wells of the 96-well PCR-plate. The length of the pipette tips is adjusted so they cannot reach the bottom 10 μl of the wells, safeguarding the agarose beads from accidental disposal

5. Reusable silicone sealing mat for PCR-plate(s) (Fig. 1A).
6. Homemade "sandwich device" to keep the silicone sealing mat firmly in place when the PCR-plate(s) rotates end over end during the IP procedure (Fig. 1B).

7. 96-Well aluminum block for the PCR-plate to keep it cold on ice during the IP procedure and warm on a heating block during the kinase reaction (Fig. 1A).
8. Rotation apparatus able to hold the "sandwich device" with the PCR-plate(s). Should be placed at 4 °C.
9. 96-Well plate swing-out rotor insert for centrifuge.
10. 6×Assay buffer: 240 mM HEPES, pH 7.0, 480 mM NaCl. This buffer is stored at 4 °C.
11. 3×Assay buffer: 120 mM HEPES, pH 7.0, 240 mM NaCl. This buffer is stored at 4 °C.
12. Adjustable eight-channel pipette going up to 200 µl.
13. Homemade eight-channel suction device (Fig. 1C). Used for aspiration of wash buffer. An eight-channel pipette could be used instead.

2.2 Kinase Reaction

1. Kinase reaction buffer (30 µl per sample): 40 mM HEPES, pH 7.0, 80 mM NaCl, 833 µM DTT, 200 µM AMP, 100 µM AMARA peptide (AMARAASAAALARRR), 5 mM $MgCl_2$, 200 µM ATP, 33 µCi/ml ^{33}P γ-labeled ATP (*see* **Note 4**).
2. Heating block for the PCR-plate (30 °C) (*see* **Note 5**).
3. Repeater pipette with options to dispense 10 and 30 µl.
4. Phosphoric acid (1% (v/v) solution).
5. Eight-channel pipette in the range of 20 µl.
6. Whatman™ Grade P81 Ion Exchange Cellulose Chromatography Paper.
7. Acetone.
8. Ultima Gold™ scintillation cocktail.
9. Pico Prias Vials (6 ml).
10. Phosphor imager with storage phosphor screens.
11. Liquid Scintillation Analyzer.

3 Methods

We strongly recommend to homogenize the muscle tissue as described in Chapter 13, as we have seen that muscles homogenized in a standard RIPA buffer (Sigma R0278) or Rac1 lysis buffer (Cytoskeleton Inc. BK126) have no AMPK activity at all (unpublished data).

3.1 Immunoprecipitation (IP) Procedure

1. Prepare a list of your samples, so you will know how much of each buffer and reagent is necessary for the entire assay. The following will be an example of an assay with 100 samples

including blind samples (*see* **step 6**) and three consecutive IPs for measuring the activities of α2β2γ3, α2β2γ1, and α1β2γ1 (in that order).

2. Make up a fresh batch of IP-buffer and keep it on ice or at 4 °C (*see* **Note 6**).
3. Choose the appropriate Protein A or G agarose (agarose beads) according to the antibody to be used in the IP (*see* **Note 7**).
4. Wash the agarose beads thrice in IP-buffer and make up a 50:50 slurry suspension (*see* **Note 2**).
5. Place the PCR-plate in the aluminum block on ice and add 20 μl of agarose beads (50:50 slurry) to each well in the PCR-plate (one well per sample).
6. Prepare to set up a number (e.g., triplicate) of "blind" samples that could be a lysate pool of the samples analyzed. These blind samples must be used as background activity and are subtracted from the other samples in the calculations at the end of the assay. Set up the blind samples as the rest of the samples, but do not add antibody (or choose an irrelevant antibody).
7. Add IP-buffer according to your calculations. The total volume of the IPs should be 200 μl, so the IP-buffer should be 200 μl minus 20 μl of agarose (50:50 slurry), minus 10 μl of antibody, and minus *x* μl of lysate (*see* **step 9**).
8. Add 10 μl of AMPK γ3 antibody to each IP (*see* **Note 8**) and instead 10 μl of IP-buffer to the blind samples.
9. Add *x* μl of lysate (*see* **Note 6**). If assaying the activity of three heterotrimeric complexes with three consecutive IPs, we recommend to IP on at least 250 μg of lysate.
10. Put on the silicone sealing mat and secure it to the PCR-plate in the "sandwich device" (Fig. 1B).
11. Let the IPs rotate end over end at 4 °C overnight (*see* **Note 9**).
12. On Day 2, set up a new PCR-plate like the day before. Add 20 μl of Protein G agarose and 10 μl of AMPK α2 antibody to the IPs and Protein G agarose and 10 μl of IP-buffer to the blind samples.
13. Release the "γ3" PCR-plate from the "sandwich device" after rotation and spin down the agarose for 1 min at 500 × *g* and 4 °C. Place the PCR-plate on ice (in the 96-well aluminum block).
14. Using an eight-channel pipette, transfer 170 μl of the supernatant from each well to the new "α2" PCR-plate (*see* **Note 10**). This is the most difficult part of the assay. Be careful not to transfer any agarose (*see* **Note 11**).

15. When all supernatants are transferred, seal the "α2" PCR-plate and install it to rotate overnight at 4 °C as described for the "γ3" PCR-plate in **steps 10** and **11**.
16. Using the eight-channel pipette, add 180 μl of IP-buffer to the "γ3" PCR-plate and make sure to stir up the agarose beads. If they are not stirred up by the addition of IP-buffer, seal the plate with the silicone mat and shake it gently until they are.
17. Spin down the agarose for 1 min at 500 × *g* and 4 °C.
18. Aspirate the supernatant using the eight-channel suction device (Fig. 1C) or an eight-channel pipette. Be careful not to lose any agarose.
19. Repeat **steps 16–18** once with 6×Assay buffer and twice with 3×Assay buffer.
20. After last wash in 3×Assay buffer, carefully aspirate all supernatant, so that only the 10 μl of packed agarose beads are left in the wells. Leave the PCR-plate on ice and continue with the kinase reaction (below).
21. On Day 3, repeat **steps 12–20** for the "α2" PCR-plate and set up the "α1" PCR-plate for the supernatant from the "α2" PCR-plate (**step 12**).
22. On Day 4, repeat **steps 13–20** for the "α1" PCR-plate. The supernatant from this plate can be discarded (**step 14**).

3.2 Kinase Reaction

1. While the IPs in the PCR-plate are kept on ice in the aluminum block, prepare the kinase reaction buffer. Make up 30 μl for each sample plus a little extra (for 3–4 samples) (*see* **Note 12**).
2. Relocate to a radioisotope-classified laboratory (Class C or higher), and work behind a Plexiglas screen.
3. Add the calculated amount of tracer (^{33}P-ATP) to the kinase reaction buffer.
4. Using a repeater pipette, add 30 μl of kinase reaction buffer to each well in a steady pace.
5. Place the PCR-plate on the heating block (30 °C) for 30 min (*see* **Note 13**).
6. Take out 15 μl from the excess kinase reaction buffer and dilute it in 985 μl of water. This will be used as the specific activity (SA) of the kinase reaction buffer (*see* **Note 14**).
7. During the incubation, prepare a piece of P81 ion exchange filter paper with pencil dots each representing one sample. The distance between the dots (18 mm) should be twice the distance between each tip on an eight-channel pipette both vertically and horizontally, meaning that the area of the filter paper will be four times the area of the PCR-plate (*see* **Note 15**).

8. When the kinase reaction has run for 30 min, remove the PCR-plate from the heating block and stop the reaction by adding 10 μl of 1% phosphoric acid to each well at the same pace as adding the kinase reaction buffer in **step 4**.
9. Place the P81 filter paper on a piece of table paper with wax underside, and start spotting 20 μl of the samples using an eight-channel pipette with only every other tip applied (*see* **Notes 15** and **16**).
10. When all samples are spotted, put the P81 filter paper into a container with 1% phosphoric acid for washing away unbound ^{33}P-ATP. Wash three times for 15 min (*see* **Note 17**).
11. After last wash in phosphoric acid, wash for 2–5 min in acetone to displace water from the filter paper.
12. Let the filter paper air dry in a fume hood.
13. While the P81 filter paper is drying, add 10 μl of the SA to each of three counting vials (size 6 ml) plus 2 ml Ultima Gold scintillation cocktail, cap, and vortex.
14. Count the three vials (triplicate) in a Liquid Scintillation Analyzer with a program designed for ^{33}P (window between 2 and 249 keV, counting time 2 min or stop at 2.0 (2% sigma), and no need for quench curve correction (*see* **Note 18**)). These counts (multiplied by 200) are the specific activity (SA) for the kinase reaction buffer and what was added to all samples (*see* **Note 19**).
15. When the P81 filter paper is dry, spot two times 1 μl and two times 2 μl of the SA on the periphery of the paper where there are no samples spotted.
16. Wrap the P81 filter paper in Vita Wrap and place it in an X-ray exposure cassette with a phosphor-imager screen. Let it expose for 1 or 2 days.
17. After exposure, scan the phosphor-imager screen in a phosphor-imager scanner. Quantify the spots using circular "boxes," and apply background subtraction as local median. The quantification will result in arbitrary "volumes" or intensities that have to be converted into DPM, which will be described in the next section.

3.3 Activity Calculations

1. Only spotting 1 and 2 μl of the SA on the P81 filter paper is a precaution to avoid saturation of the scanner (**step 15** of the Subheading 3.2). Spotting both 1 and 2 μl gives an indication of linearity for the phosphor-imager screen. Multiply the 1 μl spots with 10 and the 2 μl spots with 5 and take the mean. This is the arbitrary "volume" or intensity for 10 μl of the SA on the phosphor-imager screen. As the activity in 10 μl of the SA has been measured by liquid scintillation (**step 14** of the

Subheading 3.2), a relationship between "volume" and DPM is known. Dividing the "volume" with the DPM for the 10 μl of the SA gives "volume"/DPM. Dividing the "volume" of all samples with this factor will convert them into DPM.

2. The background noise of the assay has to be subtracted from the activities of the samples. The blind samples "precipitated" with none or irrelevant antibody will have a small activity that is considered as noise. For this reason, subtract the mean value of the blind samples from all other samples.
3. Because only 20 μl of each sample was spotted onto the P81 filter paper, the DPM has to be corrected to represent the whole sample. The kinase reaction took place in a mixture of 10 μl of agarose beads and 30 μl of kinase reaction buffer. Then 10 μl of 1% phosphoric acid was added to stop the reaction, bringing the total volume up to 50 μl. Spotting 20 μl of the total 50 μl is only 40%, which makes the total activity in the sample 2.5 times higher than measured.
4. The activity of tracer (^{33}P-ATP) represents the total amount of ATP added to the sample of which the amount incorporated into the substrate peptide is measured. The kinase reaction buffer has 200 μM ATP in 30 μl = 6000 pmol ATP (the contribution of ATP from the tracer is negligible (0.33 pmol)). These 6000 pmol ATP are represented by the total radioactive activity in a sample theoretically being 2,220,000 DPM (measured empirically in every assay as the SA).
5. All elements are now ready for the calculation of the AMPK activity in the samples (x):

$$\frac{50\ \mu l * \text{Sample DPM} * 6000\ \text{pmol ATP}}{20\ \mu l * \text{Total DPM} * 30\text{min} * 0.25\ \text{mg}} = x\ \text{pmol/min/mg}$$

50 μl representing the total reaction volume.

20 μl representing the volume spotted onto the P81 filter paper.
Sample DPM representing the amount of ATP incorporated into the substrate peptide.
6000 pmol *ATP* representing the total amount of ATP in the kinase reaction.
Total DPM representing the radioactive activity of the total amount of ATP in the kinase reaction.
30 min representing the duration of the kinase reaction.
0.25 mg representing the total amount of lysate protein from which AMPK was isolated (*see* **Note 10**).

4 Notes

1. The IP-buffer could be the same as the homogenization buffer or even just phosphate-buffered saline (PBS). The importance of this is subject to a large array of optimizations. Our experience is that analyzing enzyme activity after the IP gives higher specific activity with the milder IP-buffer compared to the homogenization buffer described in Chapter 13 for reasons unknown.
2. The Protein A or G agarose is usually supplied in a suspension containing ethanol and has to be calibrated to the IP-buffer. When pipetting the agarose, use wide orifice pipette tips and vortex or stir the suspension just before pipetting.
3. It is paramount that the antibody used for precipitating each subunit isoform is able to IP all of the particular subunit from the lysate. If not all is precipitated, there is no way of knowing if the remaining fraction is part of a special heterotrimeric complex or if it is a complex fraction that is modified by PTM or signaling that could be important for the distribution and regulation of AMPK. Over the years, we have used many different sources of antibodies as some have run out of stock. Do always verify antibodies with IP and Western blot.
4. It is not mandatory to use ^{33}P-labeled ATP; the cheaper ^{32}P-labeled ATP could be used instead. However, the emitted energy from ^{32}P is seven times higher than from ^{33}P. During the process of spotting the samples (*see* **step 9** of the Subheading 3.2), there will be a large area with high activity radiating your hands, and this can be minimized using ^{33}P instead of ^{32}P.
5. There are no special requirements for the heating block. The 96-well aluminum block can be placed on top of the inserted blocks for tubes in the heating block, and if there is metal-metal contact, the heat will transfer easily to the 96-well aluminum block.
6. When setting up the IPs, the lysates are diluted in IP-buffer (*see* **step 7** of the Subheading 3.1). The total volume of the IPs should be 200 μl including 20 μl of Protein G agarose (50:50 slurry), 10 μl of antibody, and the lysate. If the lysate has a protein concentration of 5 mg/ml, then 250 μg is 50 μl. The volume of IP-buffer in that IP will be (200 μl − 20 μl − 10 μl − 50 μl = 120 μl). Calculate how much IP-buffer is needed for all samples in the assay. In addition to this, all IPs must be washed in 180 μl IP-buffer (*see* **step 16** of the Subheading 3.1), and there are three IPs for each sample, one for each heterotrimeric complex, giving 540 μl IP-buffer per sample for washing. If having 100 samples and they on average need 120 μl to fill up the first IP and 540 μl for

washing, then this is a total of (120 µl + 540 µl) * 100 = 66 ml of IP-buffer. Approximately 10 ml of IP-buffer will be used for the initial washing and calibration of the Protein G agarose, and then always make a little extra. Thus, for this assay with 100 samples, make up 90 ml of IP-buffer.

7. The selection of either Protein A or G agarose is dependent on the species and subgroup of the antibody used in the IP. Most antibodies work best with Protein G, but this should be verified before starting. As standard we use Protein G agarose, Fast Flow from Merck (cat. #16-266).
8. The amount of antibody to be used in an IP depends on the amount of lysate put into the IP and the affinity of the antibody, which must be tested. Usually 2 µg of antibody is sufficient for IP on 200 µg lysate. The concentration of antibody varies between batches, and to avoid pipetting very small volumes, it is recommended to dilute the antibody in IP-buffer to a concentration of 0.2 mg/ml and then pipette 10 µl to each IP.

   When doing consecutive IPs on AMPK, it is very important to do the IPs in the right sequence. Working with human muscle samples, only three different heterotrimeric complexes have been identified [10, 11]. The β2 subunit is part of all three complexes, so the IPs cannot be done with a β2-specific antibody. The α2 subunit is part of two of these complexes, so starting with an α2 IP would pull down both these complexes at once. The trick is to IP the γ3 subunit first isolating the α2β2γ3 complex. Then α2 can be precipitated isolating the α2β2γ1 complex. The only complex left in the supernatant then is the α1β2γ1 complex, which can be isolated with an α1 IP.

   Working with mouse muscle makes things a little more complicated, because there are five complexes [12]. All five complexes cannot be isolated with consecutive IPs on the same lysate sample. Two sets of consecutive IPs must be set up as follows to get the individual activity of all five complexes:
   Set1: IP1 γ3 (α2β2γ3), IP2 β1 (α1β1γ1 and α2β1γ1), IP3 α2 (α2β2γ1), and IP4 α1 (α1β2γ1).
   Set 2: IP1 γ3 (α2β2γ3), IP2 β2 (α1β2γ1 and α2β2γ1), IP3 α2 (α2β1γ1), and IP4 α1 (α1β1γ1).

   The proportion of β1 complexes is however quite small and likewise the activity, so it might not be worth the effort to try to isolate the β1 complexes from the β2 complexes, unless specifically interested in the β1 activities. Just doing three consecutive IPs like on human lysates (γ3, α2, α1) would make the assay much simpler, and one might acquire the sufficient level of information.

9. The time and temperature for an IP can vary a lot depending on antibody affinity, considerations for protein complex stability, and workflow. Low temperature (4 °C) lengthens the IP process but maintains a higher stability for protease and phosphatase inhibitors as well as for protein interactions. Doing consecutive IPs and measuring enzyme activity on each of the IPs would challenge the number of hours in a working day if the time for each IP was set to only a couple of hours. Our experience is that the AMPK heterotrimeric complexes are very stable and can endure at least three consecutive overnight IP incubations at 4 °C. We have assayed the α1-, α2-, and γ3-associated activities after 4 h and one, two, and three overnight incubations with similar results.
10. The total volume of each of the first γ3 IPs is 200 μl of which 10 μl is packed agarose beads and 190 μl is supernatant. By only transferring 170 μl to the next IP, protein is lost, but there must be a safety margin to avoid transferring agarose with bound AMPK to the next IP. The second IP (α2) will thus be on (250 μg/190 μl) * 170 μl = 224 μg total protein. The total volume of the α2 IP will be 200 μl (20 μl of Protein G agarose, 10 μl of antibody, and 170 μl of supernatant from the γ3 IP) like the first IP of which 190 μl is supernatant. Transferring 170 μl of supernatant from the second α2 IP to the third α1 IP will give this IP (224 μg/190 μl) * 170 μl = 200 μg total protein. These amounts of total protein precipitated on (input) will be used in the calculations of the specific AMPK activities that are given as pmol ATP incorporated into the AMARA peptide per minute of time for the kinase reaction per mg lysate precipitated on (pmol/min/mg).
11. When transferring the supernatant from one IP to the next, place the first PCR-plate on the table and use plenty of light. Place a mirror on one side of the PCR-plate, so you can see both the first pipette tip of the eight-channel pipette on the side facing you and the eighth tip facing the mirror. This way you will be sure that none of the eight pipette tips reach the agarose at the bottom of the wells. After the transfer of all supernatants, put the PCR-plate back on ice.
12. The stock solutions for preparing the kinase reaction buffer are stored at −20 °C unless otherwise indicated. We use the following stock concentrations: 5 mM DTT, 2 mM AMP, 1.5 mM AMARA peptide, 150 mM $MgCl_2$ (stored at 4 °C), 10 mM ATP, and ^{33}P-ATP (10 μCi/μl) (stored at 4 °C). In order to make up kinase reaction buffer for one sample (30 μl), mix 8.3 μl water, 5 μl DTT, 3 μl AMP, 2 μl AMARA peptide, 1 μl $MgCl_2$, 0.6 μl ATP, 0.1 μl ^{33}P-ATP (on calibration date), and 10 μl 3×Assay buffer (120 mM HEPES and 240 mM NaCl). The amount of water and ^{33}P-ATP depends on the

calibration date for the latter. If the assay is run after the calibration date, then more of the ^{33}P-ATP stock is needed and accordingly less water. If getting a too low activity in the assay (especially in the basal samples), the amount of tracer can be adjusted and easily increased from 1 to 2 μCi per sample.

13. The addition of kinase reaction buffer will stir up the agarose beads. There is no need to shake the PCR-plate during the incubation. Due to the low volume and the V shape of the PCR-plate well bottoms, the agarose beads will sediment and are very hard to stir up during incubation even at 1400 rpm (max) in a thermo-shaker. The reaction will proceed fine without stirring.
14. The reason for diluting the SA is that counting it undiluted will exceed the capacity of the Liquid Scintillation Analyzer.
15. In **step 9** of the Subheading 3.2, 20 μl of the samples are spotted onto the P81 filter paper using an eight-channel pipette. This volume of liquid spotted onto this type of filter paper will spread out in a circular area with a diameter of ~15 mm. If using every tip on the eight-channel pipette, the spots would overlap, so to avoid this, only every other tip is applied to the pipette spotting four samples at a time. Firstly, the samples from the wells in column 1 row A, C, E, and G are spotted; followed by column 1 row B, D, F, and H; and so on. The columns will be the same on the filter paper as in the PCR-plate, but the rows will be arranged differently, which of cause has to be sorted out when quantifying the spots on the phosphor imager (*see* **step 17** of the Subheading 3.2).
16. The agarose beads are included in the 20 μl spotting volume. Put the pipette tip into the well(s) (four at a time), but not all the way to the bottom (pressing the pipette tip through the sedimented agarose could clot the tip), and gently mix up and down three to four times stirring up the agarose. Transfer and spot onto the P81 filter paper. As the total volume in the wells is 50 μl, there is enough for a double determination; however our experience is that the assay variation is not lying in the spotting step.
17. Collect the first wash in a container and store it to let the isotope decay before pouring it into the drain. ^{33}P has a half-life of 25 days and ^{32}P 14 days. This is not necessary for the last two washes as more than 90% of the isotope is in the first wash.
18. There is no need for quench curve correction, because 10 μl of watery ^{33}P solution in 2 ml Ultima Gold gives practically no quenching, so CPM equals DPM. If the assay is run in single Eppendorf tubes and the researcher doesn't have access to a phosphor imager, then it is possible to spot on single pieces of P81 filter paper (~1.5 × 1.5 cm). These can after washing be

analyzed by liquid scintillation by putting them into counting vials with Ultima Gold. In this case the filter paper will "quench" the samples (~20%), and therefore the 10 μl of the SA must also be spotted on a piece of filter paper to quench these accordingly.

19. Adding 1 μCi ^{33}P-ATP to each sample (0.1 μl of a 10 μCi/μl stock) (*see* **Note 12**) equals 2,220,000 DPM (1 μCi = 37,000 Bq = 2,220,000 DPM). The kinase reaction buffer was diluted 67 times in water (15 μl plus 985 μl of water) (*see* **step 6** of the Subheading 3.2), and only 10 μl was added to the counting vial while 30 μl was added to the samples, giving an extra three times dilution making the total dilution 200 times. The counting values obtained measuring the SA should therefore be approximately 11,100 CPM or DPM (2,220,000/200 = 11,100).

References

1. Xiao B, Sanders MJ, Underwood E, Heath R, Mayer FV, Carmena D, Jing C, Walker PA, Eccleston JF, Haire LF, Saiu P, Howell SA, Aasland R, Martin SR, Carling D, Gamblin SJ (2011) Structure of mammalian AMPK and its regulation by ADP. Nature 472:230–233
2. Suter M, Riek U, Tuerk R, Schlattner U, Wallimann T, Neumann D (2006) Dissecting the role of 5′-AMP for allosteric stimulation, activation, and deactivation of AMP-activated protein kinase. J Biol Chem 281:32207–32216
3. Davies SP, Carling D, Hardie DG (1989) Tissue distribution of the AMP-activated protein kinase, and lack of activation by cyclic-AMP-dependent protein kinase, studied using a specific and sensitive peptide assay. Eur J Biochem 186:123–129
4. Winder WW, Hardie DG (1996) Inactivation of Acetyl CoA Carboxylase and activation of AMP-activated protein kinase in muscle during exercise. Am J Physiol 270(Endocrinol Metab 33):E299–E304
5. Hayashi T, Hirshman MF, Kurth EJ, Winder WW, Goodyear LJ (1998) Evidence for 5-′-AMP-activated protein kinase mediation of the effect of muscle contraction on glucose transport. Diabetes 47:1369–1373
6. Dale S, Wilson WA, Edelman AM, Hardie DG (1995) Similar substrate recognition motifs for mammalian AMP-activated protein kinase, higher plant HMG-CoA reductase kinase-A, yeast SNF-1, and mammalian calmodulin-dependent protein kinase I. FEBS Lett 361:191–195
7. Stapleton D, Mitchelhill KI, Gao G, Widmer J, Michell BJ, Teh T, House CM, Fernandez CS, Cox T, Witters LA, Kemp BE (1996) Mammalian AMP-activated protein kinase subfamily. J Biol Chem 271:611–614
8. Vavvas D, Apazidis A, Saha AK, Gamble J, Patel A, Kemp BE, Witters LA, Ruderman NB (1997) Contraction-induced changes in acetyl CoA carboxylase and 5′-AMP-activated protein kinase in skeletal muscle. J Biol Chem 272:13255–13261
9. Hayashi T, Hirshman MF, Fujii N, Habinowski SA, Witters LA, Goodyear LJ (2000) Metabolic stress and altered glucose transport activation of AMP-activated protein kinase as a unifying coupling mechanism. Diabetes 49:1–5
10. Wojtaszewski JF, Birk JB, Frosig C, Holten M, Pilegaard H, Dela F (2005) 5′AMP activated protein kinase expression in human skeletal muscle: effects of strength training and type 2 diabetes. J Physiol 564:563–573
11. Birk JB, Wojtaszewski JF (2006) Predominant alpha2/beta2/gamma3 AMPK activation during exercise in human skeletal muscle. J Physiol 577:1021–1032
12. Treebak JT, Birk JB, Hansen BF, Olsen GS, Wojtaszewski JF (2009) A-769662 activates AMPK beta1-containing complexes but induces glucose uptake through a PI3-kinase-dependent pathway in mouse skeletal muscle. Am J Physiol Cell Physiol 297:C1041–C1052

Chapter 15

Determination of Adenine Nucleotide Concentrations in Cells and Tissues by High-Performance Liquid Chromatography

Noemí García-Tardón and Bruno Guigas

Abstract

The serine/threonine AMP-activated protein kinase (AMPK) is a central player in the regulation of energy homeostasis, and its activity is tightly controlled, among other mechanisms, by subtle changes in cellular adenine nucleotide levels. In this chapter, we describe a step-by-step protocol for rapid, highly sensitive, reproducible, and simultaneous determination of ATP, ADP, and AMP concentrations in cell or tissue samples by reversed-phase high-performance liquid chromatography (HPLC).

Key words HPLC, Adenine nucleotides, Tissue, Cells, Quantification, Adenylate energy charge

1 Introduction

The evolutionary-conserved and ubiquitously expressed serine/threonine AMP-activated protein kinase (AMPK) is a central player in the regulation of energy homeostasis [1]. AMPK is a heterotrimeric protein complex, consisting of a catalytic α subunit and two regulatory β and γ subunits, that functions as an adenylate charge-regulated kinase which constantly senses the cellular energy status by monitoring intracellular AMP, ADP, and ATP levels [2]. In response to metabolic stresses and cellular ATP depletion, a concomitant rise in AMP occurs due to the presence of adenylate kinase, leading to allosteric activation of AMPK by direct binding to the cystathionine β-synthase (CBS) domains on γ subunit. In addition, the interaction between AMP and the CBS domains also promotes phosphorylation of the Thr172 residue within the activation loop of the α-catalytic subunit by upstream AMPK kinases (AMPKK), considerably amplifying AMPK activity. ADP has also been shown to bind instead of ATP to some of the CBS nucleotide-binding sites and to enhance AMPKK-mediated Thr172 phosphorylation [3]. AMP and ADP also sustain AMPK activation through

Dietbert Neumann and Benoit Viollet (eds.), *AMPK: Methods and Protocols*, Methods in Molecular Biology, vol. 1732, https://doi.org/10.1007/978-1-4939-7598-3_15,

inhibition of Thr172 dephosphorylation by still unidentified AMPK-specific protein phosphatase(s) [4]. Once activated, AMPK concomitantly inhibits ATP-consuming anabolic processes and promotes ATP-generating catabolic pathways via direct phosphorylation of multiple downstream effectors, leading to restoration of cellular energy balance [5].

Since subtle changes in cellular energy status would directly affect AMPK activity, accurate determination of adenine nucleotide concentrations is essential in the framework of studies investigating the pleiotropic role of the kinase in cell and tissue functions. Several methods have been reported for measuring cell and/or tissue ATP, ADP, and AMP levels, including luciferase-based bioluminescence assays and ultraviolet (UV)-based high-performance liquid chromatography (HPLC) [6–8]. HPLC has the advantage of high sensitivity and allows the separation and simultaneous quantification of a wide range of nucleotides. Furthermore, taking into account that HPLC systems are among the most common apparatus available in laboratory technical platforms, the cost per sample remains generally lower for large sample size in comparison with single-nucleotide commercial assay kits.

In this chapter, we describe a step-by-step protocol for rapid, highly sensitive, reproducible, and simultaneous determination of ATP, ADP, and AMP concentrations in cell or tissue samples by reversed-phase HPLC. Of note, the accurate determination of adenine nucleotide levels will also depend upon the extraction procedure used. We therefore include a description of such important step that was successfully applied in various cells and tissues [9–13].

2 Materials

Prepare all solutions using ultrapure water (mQ water; sensitivity ≥18 MΩ-cm at 25 °C) and analytical grade reagents. Prepare and store all reagents at room temperature (unless otherwise indicated).

2.1 Equipment

1. Polytron homogenizer.
2. HPLC system (DIONEX UltiMate 3000, Thermo Scientific).
3. SUPELCOSIL™ reversed-phase column (LC-18-DB, Sigma-Aldrich).

2.2 Extraction Buffers

1. Perchloric acid/EDTA solution: 10% (v/v) $HClO_4$, 25 mM EDTA. Add ~70 ml of mQ water to a glass beaker containing a magnet. Add 14.3 ml of 70% perchloric acid. Weigh 930.6 mg of EDTA disodium salt dihydrate and transfer to the glass beaker. Mix gently until complete dissolution. Make up to 100 ml, transfer in a glass bottle, and store at 4 °C.

2. KOH/MOPS solution: 2 N KOH/0.3 M 3-(N-morpholino) propanesulfonic acid (MOPS). Add ~70 ml of mQ water to a glass beaker containing a magnet. Weigh 11.22 g of KOH and 6.28 g of MOPS, and transfer to the glass beaker. Mix gently until complete dissolution. Make up to 100 ml, transfer in a glass bottle, and store at 4 °C.

2.3 HPLC Buffers

1. Pyrophosphoric acid solution: 1 M $H_4P_2O_7$. Pre-warm pyrophosphoric acid bottle at 37 °C in a water bath. Weigh 17.8 g of pyrophosphoric acid in a glass container. Add ~90 ml of mQ water to a glass beaker containing a magnet. Add pyrophosphoric acid step-by-step in water under moderate stirring in a flow hood. Make up to 100 ml and transfer in a glass bottle.
2. Pyrophosphate (saturated) solution. Add sodium pyrophosphate decahydrate in a glass container containing a magnet and ~25 ml mQ water until dissolution is not possible anymore.
3. Pyrophosphate buffer: 25 mM sodium pyrophosphate, pH 5.75. Add ~1.8 L of mQ water to a glass beaker containing a magnet. Weigh 25 g of sodium pyrophosphate decahydrate and transfer to the glass beaker. Mix gently until complete dissolution. Add 50 ml of pyrophosphoric acid solution. Adjust pH to 5.75 with a solution of saturated sodium pyrophosphate decahydrate. Make up to 2 L, filter (0.22 μm; *see* **Note 1**), and transfer in a glass bottle.
4. Acetonitrile: 70% (v/v). Add 700 ml of acetonitrile in a glass cylinder and complete to 1 L with mQ water.
5. Acetonitrile: 5% (v/v). Add 50 ml of acetonitrile in a glass cylinder and complete to 1 L with mQ water.
6. Methanol: 30% (v/v). Add 300 ml of methanol absolute in a glass cylinder and complete to 1 L with mQ water.

2.4 Adenine Nucleotide Standards

1. ATP: 1 mM adenosine 5′-triphosphate (ATP), pH 7.4. Add ~20 ml of mQ water to a glass beaker containing a magnet. Weigh 15.1 mg of ATP disodium salt trihydrate and transfer to the glass beaker container. Mix and adjust pH to 7.4 with Tris–HCl powder. Make up to 25 ml with mQ water. Aliquot (200 μl) in 0.5 ml tubes and store at −80 °C.
2. ADP: 1 mM adenosine 5′-diphosphate (ADP), pH 7.4. Add ~20 ml of mQ water to a glass beaker containing a magnet. Weigh 10.7 mg of ADP sodium salt and transfer to the glass beaker container. Mix and adjust pH to 7.4 with Tris–HCl powder. Make up to 25 ml with mQ water. Aliquot (200 μl) in 0.5 ml tubes and store at −80 °C.
3. AMP: 1 mM adenosine 5′-monophosphate (AMP), pH 7.4. Add ~20 ml of mQ water to a glass beaker containing a magnet.

Weigh 9.1 mg of AMP monohydrate and transfer to the glass beaker container. Mix and adjust pH to 7.4 with Tris–HCl powder. Make up to 25 ml with mQ water. Aliquot (200 µl) in 0.5 ml tubes and store at −80 °C.

The determination of the exact final adenine nucleotide standard concentrations can be performed by UV spectrophotometry using a quartz cuvette and the following formula: [*ATP/ADP/AMP*] in µM = optical density at 259 nm/15.4 ($cm^{-1}.10^3$ M^{-1}).

3 Methods

Carry out all procedures at room temperature unless otherwise specified.

3.1 Extraction of Adenine Nucleotides from Cultured Cells

1. Rinse cell monolayers (e.g., one million hepatocytes plated in a collagen-coated 4-cm-diameter Petri dish) once with ice-cold PBS.
2. Scrape the cells in 250 µl of ice-cold perchloric acid/EDTA with a rubber policeman (*see* **Note 2**).
3. Transfer the cell extracts containing precipitated proteins to 1.5 ml tubes, vortex briefly once, and keep on ice for ~30 min.
4. Spin down precipitated proteins at 8000 × *g* for 2 min at 4 °C.
5. Transfer 200 µl of the supernatant fractions into a new 1.5 ml tube (on ice) and adjust pH to 6.5–7 with ~130 µl of KOH/-MOPS. pH should be checked after brief vortexing using pH-indicator strips. pH > 7 should be avoided.
6. Clarify lysate by centrifugation at 8000 × *g* for 2 min at 4 °C.
7. Transfer 200 µl of the (neutralized) supernatant fractions into a new 1.5 ml tube (on ice) and store at −80 °C until determination of nucleotide concentrations. Neutralization of the samples before storage at −80 °C is recommended in order to minimize adenine nucleotide degradation during freeze-thaw cycle.

3.2 Extraction of Adenine Nucleotides from Frozen Tissues

1. Lyse a piece of frozen tissue (e.g., 50 mg liver; kept at −80 °C) in 500 µl of ice-cold perchloric acid/EDTA using a Polytron homogenizer (three times 10 s).
2. Transfer immediately tissue lysate containing precipitated proteins into a new 1.5 ml tube and keep on ice for ~30 min.
3. Spin down precipitated proteins at 8000 × *g* for 2 min at 4 °C.
4. Neutralize the supernatant fractions as described in Subheading 3.1, **steps 5–7** and store at −80 °C until determination of nucleotide concentrations.

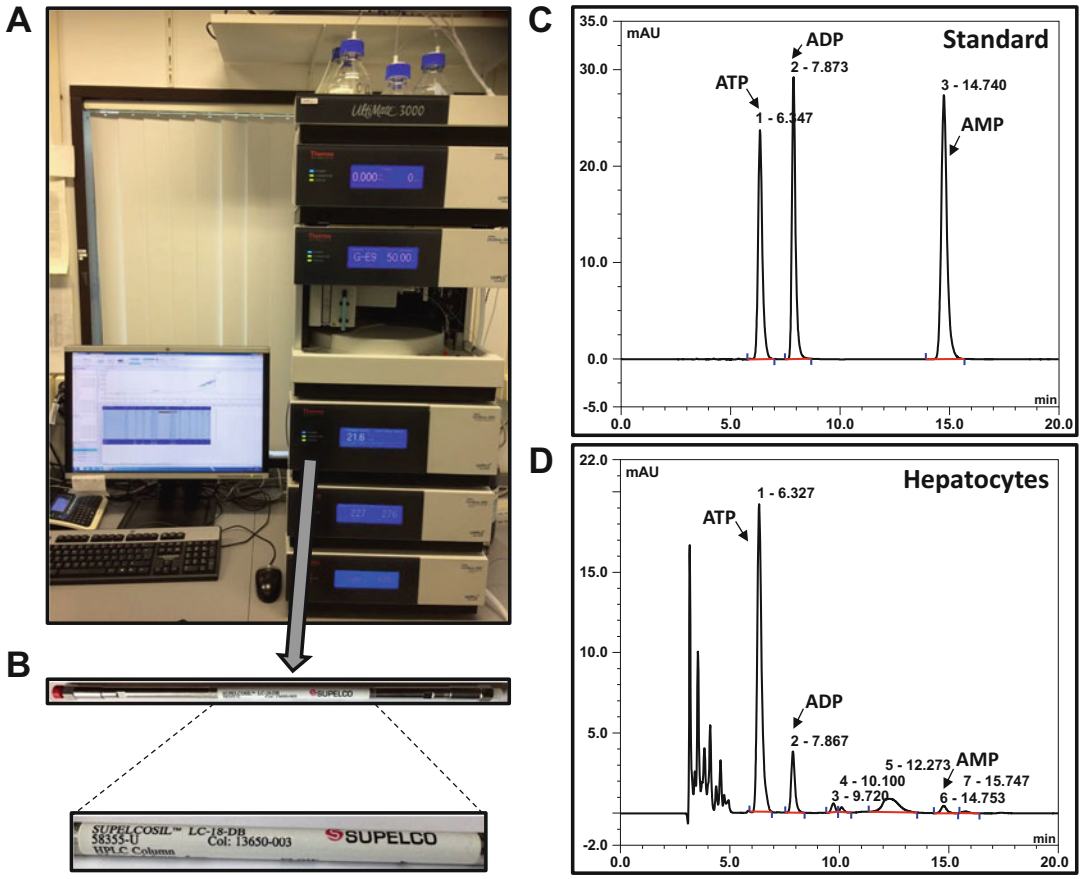

Fig. 1 HPLC system and examples of chromatogram. The HPLC system used (**a**; DIONEX UltiMate 3000, Thermo Scientific) consists of a RS column module with binary pumps, a temperature-controlled RS autosampler with a 50 μl injection valve, a temperature-controlled RS column compartment module containing a SUPELCOSIL™ reversed-phase LC-18 column (**b**), and a RS fluorescent (UV) detector equipped with a 11 μl flow cell. HPLC chromatograms obtained at a wavelength of 254 nm for standard (**c**) or test (**d**) samples are shown as examples

3.3 Preparation of the HPLC System

The HPLC system used (DIONEX UltiMate 3000, Thermo Scientific) consists of a column module with binary pumps, a temperature-controlled autosampler (96-well plate) with a 50 μl injection valve, a temperature-controlled column compartment module, and a fluorescent (UV) detector equipped with a 11 μl flow cell (Fig. 1a). For peak analysis and quantification, the Chromeleon 7 software (version 7.1.2, Thermo Scientific) is used. HPLC chromatograms are obtained at a wavelength of 254 nm (Fig. 1c and d).

1. Sonicate the pyrophosphate buffer during ~10 min (*see* **Note 3**).
2. Fix the SUPELCOSIL™ reversed-phase column (LC-18-DB, 25 cm × 4.6 mm, 5 μm, Sigma-Aldrich 58,355-U SUPELCO; Fig. 1b) to the system in the temperature-controlled column

module (*see* **Note 4**). A security guard cartridge pre-column (SUPELCOSIL™ LC-18-DB Supelguard™ Cartridge, 5 μm, 2 cm × 3 mm, Sigma-Aldrich 59565C30 SUPELCO) is advised (but not mandatory) for protecting the LC-18 column.

3. Set the column compartment temperature at 30 °C.
4. Purge the system.
5. Start the pump with a gradual increase in pyrophosphate buffer flow rate until 0.8 ml/min for ~1 h. The pressure should be continuously monitored and do not exceed the capacity of the system (usually <100 bar, but this could vary depending of the HPLC tubing used).
6. Reduce the flow rate to ~0.1 ml/min and let the system equilibrate overnight.

3.4 Preparation of the Samples

1. Defrost the standard stocks and samples on ice.
2. Vortex briefly and spin down the samples at 8000 × *g* for 2 min at 4 °C.
3. Prepare a standard solution containing ATP, ADP, and AMP at a final concentration of 30 μM by mixing 45 μl of each standard in 1365 μl of pyrophosphate buffer.
4. Transfer 250 μl of the standard solution in triplicate in a 96-well plate. Keep the plate on ice.
5. Prepare each sample on ice in the 96-well plate by mixing 100 μl (for tissue lysate) or 150 μl (for cell lysate) of sample extract with 150 μl or 100 μl of pyrophosphate buffer, respectively.
6. Seal the 96-well plate with an ad hoc plastic film cover.

3.5 HPLC Run

1. Purge the system.
2. Increase gradually the flow rate to 0.8 ml/min and let the system equilibrate for ~30 min.
3. Switch on the UV light.
4. Transfer the 96-well plate in the temperature-controlled autosampler previously set at 4 °C.
5. Program the HPLC software: injection of 20 μl of standard or samples every 20 min.
6. Start the run (*see* **Note 5**).
7. Once the whole run is completed, reduce the pump flow rate. If multiple runs are planned, go back to **step 2** once you are ready to load the next 96-well plate. Stop the pump immediately (set flow rate to 0 ml/min), if you want to store the column (continue with **step 8**). In case of unsatisfactory results, such

as broadening of peaks, consider regenerating the column (go to **step 9**).

8. Column storage: Purge the system. Flush the column in 5% (v/v) acetonitrile at 0.2 ml/min for 30 min. Purge the system. Flush the column in 70% (v/v) acetonitrile at 0.2 ml/min for 30 min. Stop the system, disconnect the column, and close it tight. Store at room temperature.
9. Column regeneration: The column can be regenerated if the sharpness of the nucleotide separation is reduced. Fix the column to the system in the opposite direction of the usual flow and flush with 30% (v/v) methanol at 0.2–0.4 ml/min for ~1 h. Next, wash the column with mQ water by gradually increasing the flow rate until 0.8 ml/min for ~30 min, followed with overnight equilibration with pyrophosphate buffer, as described in Subheading 3.3.

3.6 Calculations

The nucleotides in sample extracts are identified by their retention times in comparison with standards (these later eluted in sharp peaks; *see* Fig. 1c).

1. Calculate nucleotide concentrations (in μmol) using the following formula:

$$[\text{nucleotide}]\,(\mu\text{mol}) = \frac{(\text{Vol.SN} + \text{Vol.KOMO})}{\text{Vol.SN}} \times \frac{(\text{Vol.buffer} + \text{Vol.sample})}{\text{Vol.buffer}} \times \frac{[Std] \times \text{AUC nucleotides}}{\text{AUC Std.}}$$

Vol. SN is the volume of extract supernatant in μl.

Vol. KOMO is the volume of KOH/MOPS used for neutralization in μl.

Vol. buffer is the volume of pyrophosphate buffer in μl.

Vol. sample is the volume of neutralized sample in μl.

[*Std*] is the standard concentration in μM.

AUC nucleotide is the area under the curve in mV * min for the specific nucleotide.

AUC Std is the area under the curve in mV * min for the corresponding nucleotide standard.

The result can be expressed in μmol/million cells, μmol/mg tissue, or μmol/mg protein (if cell count, tissue weight, or protein amount, respectively, were measured in parallel).

2. Calculate the so-called adenylate energy charge, which mainly reflects the energy supply-to-demand relationship, using the following equation:

$$\text{adenylate energy charge} = \frac{([ATP] + 0.5[ADP])}{([ATP] + [ADP] + [AMP])}$$

where [*ATP*], [*ADP*], and [*AMP*] are the respective intracellular/tissue concentrations in μmol.

4 Notes

1. This is advised to remove microparticles that could block the column and lead to increase in system pressure.
2. The hydrolysis of MgATP can take place very rapidly. EDTA is therefore added to the extraction buffer for chelating magnesium in order to avoid ATP degradation by ATPases.
3. This is advised to remove microbubbles that could eventually interfere with the UV spectrophotometer.
4. Pay attention to the direction of the column (*see* the arrow on the side of the column indicating the flow direction).
5. It is important to double-check that the volume of pyrophosphate buffer available is enough for the whole run.

Acknowledgments

Guigas' group is supported by funding from the European Federation for the Study of Diabetes (EFSD/Lilly Research Grant Fellowship), the Société Francophone du Diabète (SFD), and the Dutch Organization for Scientific Research (ZonMW TOP Grant 91214131).

References

1. Hardie DG (2014) AMP-activated protein kinase: maintaining energy homeostasis at the cellular and whole-body levels. Annu Rev Nutr 34:31–55. https://doi.org/10.1146/annurev-nutr-071812-161148
2. Oakhill JS, Scott JW, Kemp BE (2012) AMPK functions as an adenylate charge-regulated protein kinase. Trends Endocrinol Metab 23 (3):125–132. https://doi.org/10.1016/j.tem.2011.12.006
3. Oakhill JS, Steel R, Chen ZP, Scott JW, Ling N, Tam S, Kemp BE (2011) AMPK is a direct adenylate charge-regulated protein kinase. Science 332(6036):1433–1435. https://doi.org/10.1126/science.1200094
4. Gowans GJ, Hawley SA, Ross FA, Hardie DG (2013) AMP is a true physiological regulator of AMP-activated protein kinase by both allosteric activation and enhancing net phosphorylation. Cell Metab 18(4):556–566. https://doi.org/10.1016/j.cmet.2013.08.019
5. Guigas B, Viollet B (2016) Targeting AMPK: from ancient drugs to new small-molecule activators. EXS 107:327–350. https://doi.org/10.1007/978-3-319-43589-3_13
6. Bhatt DP, Chen X, Geiger JD, Rosenberger TA (2012) A sensitive HPLC-based method to quantify adenine nucleotides in primary astrocyte cell cultures. J Chromatogr B Analyt Technol Biomed Life Sci 889–890:110–115. https://doi.org/10.1016/j.jchromb.2012.02.005
7. Manfredi G, Yang L, Gajewski CD, Mattiazzi M (2002) Measurements of ATP in mammalian cells. Methods 26(4):317–326. https://doi.org/10.1016/S1046-2023(02)00037-3
8. Zur Nedden S, Eason R, Doney AS, Frenguelli BG (2009) An ion-pair reversed-phase HPLC method for determination of fresh tissue adenine nucleotides avoiding freeze-thaw degradation of ATP. Anal Biochem 388(1):108–114. https://doi.org/10.1016/j.ab.2009.02.017

9. Guigas B, Bertrand L, Taleux N, Foretz M, Wiernsperger N, Vertommen D, Andreelli F, Viollet B, Hue L (2006) 5-Aminoimidazole-4-carboxamide-1-beta-D-ribofuranoside and metformin inhibit hepatic glucose phosphorylation by an AMP-activated protein kinase-independent effect on glucokinase translocation. Diabetes 55(4):865–874
10. Guigas B, Taleux N, Foretz M, Detaille D, Andreelli F, Viollet B, Hue L (2007) AMP-activated protein kinase-independent inhibition of hepatic mitochondrial oxidative phosphorylation by AICA riboside. Biochem J 404(3):499–507. https://doi.org/10.1042/BJ20070105
11. Kramer DK, Al-Khalili L, Guigas B, Leng Y, Garcia-Roves PM, Krook A (2007) Role of AMP kinase and PPARdelta in the regulation of lipid and glucose metabolism in human skeletal muscle. J Biol Chem 282(27):19313–19320. https://doi.org/10.1074/jbc.M702329200
12. Stephenne X, Foretz M, Taleux N, van der Zon GC, Sokal E, Hue L, Viollet B, Guigas B (2011) Metformin activates AMP-activated protein kinase in primary human hepatocytes by decreasing cellular energy status. Diabetologia 54(12):3101–3110. https://doi.org/10.1007/s00125-011-2311-5
13. Taleux N, De Potter I, Deransart C, Lacraz G, Favier R, Leverve XM, Hue L, Guigas B (2008) Lack of starvation-induced activation of AMP-activated protein kinase in the hypothalamus of the Lou/C rats resistant to obesity. Int J Obes 32(4):639–647. https://doi.org/10.1038/sj.ijo.0803759

Chapter 16

Intact Cell Assays to Monitor AMPK and Determine the Contribution of the AMP-Binding or ADaM Sites to Activation

Simon A. Hawley, Fiona A. Fyffe, Fiona M. Russell, Graeme J. Gowans, and D. Grahame Hardie

Abstract

AMP-activated protein kinase (AMPK) is extremely sensitive to cellular stress, so that nonphysiological activation of the kinase can readily occur during harvesting of cells or tissues. In this chapter we describe methods to harvest cells and tissues, and for kinase assays, that preserve the physiological activation status of AMPK as far as possible. Note that similar care with methods of cell or tissue harvesting is required when AMPK function is monitored by Western blotting, rather than by kinase assays. We also describe methods to determine whether compounds that activate AMPK in intact cells do so indirectly by interfering with cellular ATP synthesis or directly by binding to AMPK and, if the latter, whether this occurs by binding at the AMP-binding sites on the γ subunit or at the ADaM site located between the α and β subunits.

Key words AMP-activated protein kinase, AMPK, Kinase assay, Allosteric activation, Phosphorylation, Dephosphorylation

1 Introduction

AMPK is mainly regulated by ligands that bind either to the adenine nucleotide-binding sites on the γ subunit, with binding to site 3 appearing to be particularly critical [1], or to the ADaM site located between N-lobe of the kinase domain on the α subunit and the carbohydrate-binding module on the β subunit [2]. In Chapter 5 we provided protocols for measuring the effects of regulatory ligands on AMPK in cell-free assays. In this chapter we describe methods to extract AMPK from intact cells to monitor kinase activity and Thr172 phosphorylation and also describe specially constructed cell lines that allow the investigator to determine whether an activating compound is acting either: (1) indirectly, by inhibiting cellular ATP production and increasing cellular AMP/ATP and/or ADP/ATP ratios (e.g., phenformin,

Dietbert Neumann and Benoit Viollet (eds.), *AMPK: Methods and Protocols*, Methods in Molecular Biology, vol. 1732, https://doi.org/10.1007/978-1-4939-7598-3_16,

berberine); (2) directly, by binding at site 3 (e.g., ZMP, derived from intracellular metabolism of the prodrug 5-aminoimidazole-4-carboxamide riboside (AICAR)); or (3) directly, by binding at the ADaM site (e.g., A769662) [3]. Compounds that activate AMPK in intact cells generally fall into one of these categories. AMPK activators that work via mechanism (1) increase the intracellular concentration of AMP or ADP, while those that work via mechanism (2) increase the intracellular concentration of an AMP analogue. In either case, an intact AMP-binding site 3 on the AMPK-γ subunit is required. There are a number of well-characterized mutations within the CBS domains of the γ subunits that disrupt AMP binding, and heterotrimeric complexes containing these mutations are in general less sensitive to changes in AMP levels within the cell [4]. We have used transient transfection of plasmids encoding "RG" mutations affecting the binding of AMP at site 3 in human γ1 (R299G) or human γ2 (R531G) to determine whether AMPK activators require an intact site 3; if they do, this suggests that they mediate their effects via mechanism (1) or (2) [3]. It is sufficient to transiently transfect DNA encoding the γ subunit only; the recombinant γ subunit will compete with the endogenous γ subunit for binding to the available α and β subunits, thus acting as a "quasi knock-in" or dominant negative mutant. Although the transfected γ subunit does not usually completely replace the endogenous γ subunit, this is not a problem if the transfected γ subunit is tagged (e.g., FLAG-tagged) and is immunoprecipitated prior to assay using anti-epitope tag antibody (e.g., anti-FLAG). The endogenous γ subunits will not interfere in such IP-kinase assays, although they may still contribute to phosphorylation of downstream targets, making any studies of the latter difficult to interpret.

Using the Flip-In™ system, we have also made cell lines stably expressing WT or RG mutants, which has the advantages that clones of cells that express the WT and RG mutant at similar levels can be selected, and that the use of expensive transfection reagent is minimized. While we have used these stable cell lines successfully [3, 5], unfortunately the RG mutant cells appear to be rather unstable during serial passage. We find that the expression of the RG mutant declines, and/or expression of the endogenous WT γ subunit is restored. We suspect that the cells are undergoing selection for promoter mutations that either reduce expression of the RG mutant or increase expression of the endogenous WT γ subunit. It is possible that this problem could be overcome by starting with γ1/γ2 knockout cells generated by CRISPR/Cas9, but in the meantime, we describe below the transient transfection approach.

In crystal structures of human α2β1γ1 complexes with ligands (A769662 or 991) bound in the ADaM site, the ligands are bound in a cleft between the carbohydrate-binding module (CBM) on the β1 subunit and the N-lobe of the kinase domain on the α2 subunit

[2]. This binding site appears to be stabilized by an ionic interaction between phosphorylated Ser108 on β1 (which can be modified by autophosphorylation) and the side chain of Lys31 on α2, while the side chain of Lys29 directly interacts with the bound ligand. Consistent with this, mutation of either Ser108 on β1 or of Lys29 and Lys31 on α2, to alanine (β1 S108A, α2 K29A/K31A), abolishes or greatly reduces activation by A769662 or 991. We have shown that AMPK containing the β1-S108A mutation is not activated, or only poorly activated, by the ADaM site ligands salicylate and A769662 but is still activated by quercetin in intact cells [6]. We have also shown that AMPK containing the K40A/K42A mutations in α1 (equivalent to K29A/K31A in α2) is not activated by A769662 in intact cells, although it is still activated by an agent that binds in the catalytic site, SU6656 [7]. Surprisingly, the K40A/K42A mutant, although still allosterically activated by AMP in cell-free assays, is not activated by increased Thr172 phosphorylation in intact cells by agents that increase cellular AMP/ADP (phenformin, berberine, troglitazone, or oligomycin) [7]. Thus, an intact ADaM site is required for the effects of AMP-elevating agents to promote Thr172 phosphorylation, although not for allosteric activation. This may also be true of the S108A mutation in β1, since quercetin, the positive control used in the original study [6], may act in part by an AMP-independent mechanism [3]. Thus, while the RG mutants discriminate between agents acting at the AMP-binding and ADaM sites, the β1-S108A or α1-K40A/K42A mutants appear not to distinguish between them in terms of Thr172 phosphorylation, although doing so in terms of allosteric activation.

The levels of adenine nucleotides in intact cells can be determined either by capillary electrophoresis (CE), high-performance liquid chromatography (HPLC), or liquid chromatography-mass spectrometry (LC-MS). However, due to the low levels of AMP in cells under basal conditions, CE or HPLC may not be sufficiently sensitive to reliably detect and quantify AMP by ultraviolet absorbance alone. The ADP/ATP ratio, which can be used as a surrogate for the AMP/ATP ratio [8], can be readily measured using CE or HPLC, while the large increase in sensitivity of LC-MS also allows AMP to be measured under all conditions. However, since the recoveries of AMP, ADP, and ATP during MS analysis are not the same, it is essential to run appropriate standards to correct for these differences.

As an adjunct to measuring adenine nucleotides, the use of an Extracellular Flux Analyzer to measure oxygen consumption rate (OCR) can help to confirm whether a compound that increases cellular ADP/ATP and/or AMP/ATP ratios is doing so by inhibiting mitochondrial function.

Finally, a crucial point to note when harvesting AMPK for kinase assays, as well as when monitoring the phosphorylation status of AMPK or downstream targets by Western blotting, is

that AMPK is very sensitive to stress and can be readily phosphorylated and activated during harvesting and extraction of cells or tissues. If great care is not taken over the methods used for cell or tissue harvesting, this can lead to many misleading artifacts. The key to success is to achieve rapid cooling of the cells or tissues. This was first realized by Zammit and coworkers when they prepared ER membranes for assays of the downstream target of AMPK, HMG-CoA reductase, which led to the development of a technique known as "cold-clamping" [9]. It was reinforced when our laboratory found that freeze-clamping was necessary to preserve the phosphorylation status of another AMPK target, acetyl-CoA carboxylase, during extraction from rat liver [10]. When sampling human muscle, which is normally achieved using needle biopsies, the biopsies are frozen in liquid nitrogen as soon as they are taken [11]. We describe below (Subheading 2.1) our standard method for harvesting cells that show good adherence to culture plates following growth in two-dimensional culture, which we have developed over many years. We also describe (Subheading 2.2) a method we have developed for harvesting cultured cytotoxic T lymphocytes, which grow in suspension and do not adhere to culture plates. These methods can be adapted to other cell types, according to whether or not the cells are adherent. However, when harvesting AMPK from any tissue or cell type, it is necessary to think carefully about whether the method used could be leading to artificial activation, either *post mortem* when using animal tissues or during harvesting when using cultured cells.

2 Materials

Prepare all solutions with ultrapure water. Reagents are stored at room temperature unless indicated otherwise.

2.1 Methods of Plating and Treating Adherent Cells

1. Laminar flow tissue culture cabinet.
2. Tissue culture incubator.
3. Cells in 6 cm plates.
4. Compounds to activate AMPK, e.g., direct activators such as A.769662 or indirect activators such as phenformin or berberine.
5. Pipette and tips.
6. Culture medium.
7. Fetal bovine serum (FBS).
8. Penicillin-streptomycin solution.

1. Cell scraper.
2. Aspirator.
3. Plastic pastette.

2.2 Methods of Harvesting Adherent Cells for AMPK Assays or Monitoring Thr172 Phosphorylation

4. Liquid nitrogen.
5. Phosphate-buffered saline (PBS): 137 mM NaCl, 2.7 mM KCl, 4.3 mM Na_2HPO_4, 1.47 mM KH_2PO_4, pH 7.4 (*see* **Note 1**).
6. Lysis buffer: 50 mM Tris–HCl, pH 7.2 at room temperature, 50 mM NaF, 5 mM Na pyrophosphate, 1 mM EDTA, 1 mM EGTA, 1% (v/v) Triton X-100, 1.3 mM dithiothreitol, 1.3 mM benzamidine, 100 μM phenylmethane sulphonyl fluoride, 5 μg/ml soybean trypsin inhibitor (*see* **Note 2**).
7. Cells in 6 cm plates at 80–90% confluency.

2.3 Methods of Harvesting Nonadherent Cells (e.g., T Cells) for AMPK Assays or Monitoring Thr172 Phosphorylation

Materials required for this protocol are identical to those listed in Subheading 2.2; additional materials are listed below:

1. Cells in flask at 80–90% confluency.
2. Centrifuge.

2.4 Use of RG Plasmid to Test AMP Dependence of Activators

1. Plasmid DNAs encoding wild-type (WT) and AMP-insensitive forms with RG mutations affecting site 3 on the AMPK-γ subunit (*see* **Note 3**).
2. Cell line expressing LKB1 (*see* **Note 4**), plated in 6 cm plates.
3. Transfection reagent.
4. Direct (e.g., salicylate, A769662, 991, MK8722) or indirect (e.g., berberine, phenformin, troglitazone) activators of AMPK, dissolved in water or DMSO according to solubility.

2.5 Use of S108A and K40A/K42a Cells to Test ADaM Site Dependence

1. Plasmid DNAs encoding wild type AMPK-β1 (WT) and S108A mutant of AMPK-β1 (S108A mutant) (*see* **Note 5**), or AMPK-α1 (WT) or K40A/K42A mutant of AMPK-α1 (AA mutant).

2.6 CE and LC-MS Assays of Adenine Nucleotides

1. Cell scraper.
2. Aspirator.
3. Plastic pastette.
4. Four sets of labeled microcentrifuge tubes.
5. PBS, ice-cold (*see* **Note 1**).
6. Perchloric acid: 5% (w/v) perchloric acid, ice-cold.
7. 1:1 mixture of tri-n-octylamine and 1,1,2-trichlorotrifluoroethane.
8. Chilled centrifuge.
9. Capillary electrophoresis (CE) instrument. We use a Beckman Coulter P/ACE 5500 MDQ with the following buffers:

- Buffer A: 0.8% (v/v) HCl.
- Buffer B: 0.1 M NaOH.
- Buffer C: 50 mM NaH_2PO_4, 25 mM NaCl, adding Na_2HPO_4 to give pH 5.2.
- Buffer D: 0.1 M MES monohydrate/Tris pH 5.2, 0.2% (w/v).

Hydroxyethyl cellulose, 0.2% (w/v), is added to buffers C and D (*see* **Note 6**).

We use a capillary of length 31.2 cm, diameter 75 μm, and aperture size 100 × 800 μm.

10. LC-MS instrument. We use a TSQ Quantiva interfaced with an Ultimate 3000 Liquid Chromatography system, equipped with a porous graphitic carbon column and using the following buffers:
    - Buffer A: 0.3% (v/v) formic acid adjusted to pH 9 with ammonia prior to a 1:10 dilution.
    - Buffer B: 80% (v/v) acetonitrile.

2.7 Analysis of Cellular Oxygen Uptake Using an Extracellular Flux Analyzer

1. Seahorse Extracellular Flux Analyzer (e.g., XF24).
2. Seahorse XF Base Medium.
3. D-Glucose.
4. Sodium pyruvate.
5. L-Glutamine.
6. Seahorse XF Sensor Cartridge.
7. Seahorse XF Cell Culture plate.
8. Seahorse XF Calibrant solution.
9. Phenformin (or similar compound as a positive control).
10. Uncoupler (e.g., 2,4-dinitrophenol).
11. Compound of interest.

3 Methods

3.1 Methods of Plating and Treating Adherent Cells

1. Plate cells in 6 cm dishes in 4 ml of appropriate media supplemented with 10% FBS. Depending on the cell type, media may be changed for one with a more physiological glucose concentration (5 mM) 16 h prior to treatment, when cells are ≈70% confluent (*see* **Note 7**).
2. Activating compounds are made up as described by suppliers. Usually compounds are dissolved in dimethyl sulfoxide (DMSO) and are then added such that the final concentration of DMSO in the culture medium is no greater than 1%. Higher concentrations of DMSO, or incubation periods longer than

1 h in 1% DMSO, may be toxic to the cells and lead to AMPK activation even in vehicle controls. Compounds dissolved in water, culture medium, or other solvents can also be used, as long as the appropriate vehicle control is always included in the experimental design.

3. To preserve activation and phosphorylation status of AMPK and downstream targets, plates must not be removed from the incubator for longer than necessary. To facilitate this, we remove plates from the incubator and treat them in batches of four, at intervals of 3–5 min.
4. Remove four plates from the incubator and place in the laminar flow cabinet. Treat cells with compounds of choice. Swirl plates gently to mix compound in the culture medium, and return to incubator. Repeat at 3–5 min intervals until all cells have been treated.
5. Lyse plates after an appropriate incubation period (for many canonical activators, 1 h is sufficient), as described in Subheading 3.2.

3.2 Methods of Harvesting Adherent Cells for AMPK Assays or Monitoring Thr172 Phosphorylation

1. To preserve activation and phosphorylation status of AMPK and downstream targets, cells must be lysed rapidly on ice. Indeed, "slow lysis" at room temperature is a previously used method for artificially activating AMPK (*see* **Note 8**). For rapid lysis (lysing four dishes at timed intervals), aspirate off the medium and then gently but rapidly wash plates in 2 × 2 ml of ice-cold PBS, aspirating the washing solution each time (*see* **Note 9**).
2. Add 200–300 μl of ice-cold lysis buffer; the exact volume depends on the cell type but is designed to maximize protein concentration in the lysate.
3. Immediately scrape lysing cells off using a cell scraper, and transfer to prelabeled microcentrifuge tubes; vortex briefly and flash freeze in liquid nitrogen.
4. Defrost lysates when required on ice, and clarify by centrifugation at 17,000 × *g* for 10 min at 4 °C.
5. Remove and retain supernatant for subsequent protein quantification assays, Western blotting, and/or AMPK activity assays.
6. Cell lysates are stable at −80 °C for many years. However, avoid repeated freezing/thawing.

3.3 Methods of Harvesting Nonadherent Cells (e.g., T Cells) for AMPK Assays or Monitoring Thr172 Phosphorylation

1. After treatment, transfer cell suspension into a conical or round-bottomed centrifuge tube on ice.
2. Centrifuge at 250 × *g* for 3 min at 4 °C to gently pellet the cells; remove culture medium by aspiration. Do not centrifuge with higher g forces, as this may stress the cells, activating AMPK.

3. Gently wash the pellet in 2 ml of ice-cold PBS and repeat centrifugation.
4. Remove PBS by aspiration and immediately resuspend the cell pellet in ice-cold lysis buffer. Vortex briefly and flash freeze in liquid nitrogen.
5. Now follow **steps 4–6** as for adherent cells (Subheading 3.2).

3.4 Use of RG Mutants to Test AMP Dependence of Activation Mechanism

1. Plate cells in appropriate medium containing 10% FBS.
2. Transfect cells with DNA encoding either FLAG-tagged AMPK-γ WT (γ1 or γ2) or FLAG-tagged RG mutant (γ1 R299G or γ2 R531G) using your preferred transfection reagent, as per manufacturers' instructions.
3. After allowing sufficient time to express the recombinant protein (typically 36–48 h), you may wish to change the medium to 5 mM glucose (*see* **Note 7**) at least 16 h prior to cell treatment and lysis.
4. Treat replicate plates with the compound under test. As controls, also treat plates with activators acting through known mechanisms such as AICAR, phenformin, or berberine (which will activate only WT complexes) or ADaM ligands such as A769662 or 991 or the Ca^{2+} ionophore A23187 (all of which will all activate both WT and RG complexes).
5. Harvest and lyse the cells as in Subheadings 3.2 and 3.3.

3.5 Use of S108A and K40A/K42A Cells to Test Dependence on the ADaM Site

1. Plate cells in appropriate medium containing 10% FBS.
2. Transfect cells with DNAs encoding either WT AMPK-β1 or β1 S108A mutant or encoding WT AMPK-α1 or α1-K40A/K42A mutant, using preferred transfection reagent as per manufacturers' instructions. We recommend a nontoxic transfection reagent, such as FuGENE 6.
3. Follow **steps 3–5** in Protocol 3.4.

3.6 CE and LC-MS Assays of Adenine Nucleotides

Steps 1–7 below relate to sample preparation (identical for both CE, HPLC, and LC-MS), **steps 7** and **8** relate to CE, and **step 9** relates to LC-MS. We have not performed these analyses by HPLC for some time, but previously published a method for this [12].

1. Perform appropriate treatment to disturb cellular energy charge (including controls to establish basal levels of nucleotides) as described in Subheading 3.1.
2. Lyse four dishes at appropriate time intervals, on ice, as follows:
   (a) Aspirate medium and then gently but rapidly wash plates in 2 × 2 ml of ice-cold PBS, aspirating liquid between each wash and after final wash.

(b) For a 6 cm plate, add 150 µl of ice-cold 5% perchloric acid, scrape off cells using a cell scraper, and transfer the liquid into prelabeled 1.5 ml microcentrifuge tubes.

(c) Vortex for 30 s, and store on ice until all plates have been lysed. Cold perchloric acid extracts are stable for 1 or 2 h without significant degradation of adenine nucleotides, although **steps 3** to **6** below should always be performed as soon as possible.

3. Clarify the lysates by centrifugation at 17,000 × *g* for 3 min at 4 °C and transfer the supernatant to a fresh microcentrifuge tube.
4. Add an equal volume of a 1:1 mixture of tri-n-octylamine and 1,1,2-trichlorotrifluoroethane to the tube, vortex for 30 s, and repeat centrifugation.
5. Carefully remove the top (aqueous) phase, transferring it into a fresh tube (*see* **Note 10**), and repeat the extraction by adding an equal volume of a 1:1 mixture of tri-n-octylamine and 1,1,2-trichlorotriflouroethane, vortexing for 30 s, and repeating centrifugation.
6. Carefully remove the top (aqueous) phase, transferring into a fresh tube, and store frozen for subsequent analysis. The extracts should now have a neutral pH with no perchloric acid remaining, and in this form, the nucleotides are stable at −80 °C for many months.
7. Capillary electrophoresis (CE) detects nucleotide peaks by UV absorbance at 254 nm. ADP and ATP levels are measured using peak areas and expressed as ADP/ATP ratios.
8. The capillary is washed as follows: Buffer A 1 min, 20 psi; water 1 min, 20 psi; Buffer B 2 min, 20 psi; and Buffer C 2 min, 20 psi. The nucleotide sample is injected at 1 KV under reverse polarity and chased by an injection of Buffer D for 1 min at 0.5 psi. Nucleotides are separated over Buffer C by reverse polarity at 7 KV for 10 min.
9. The LC-MS column is maintained at a controlled temperature of 30 °C and is equilibrated with 10% Buffer B for 5 min at a constant flow rate of 0.06 ml/min. Samples are loaded onto the column and compounds eluted with a linear gradient of 10%–60% Buffer B over 9 min. Buffer B is then increased to 100% within 1 min and the column washed for 5 min with 100% Buffer B. Eluents are sprayed into the TSQ Quantiva using an Ion Max NG ion source with ion transfer tube temperature set to 350 °C and vaporizer temperature 125 °C. The TSQ Quantiva is run in negative ion mode with a spray voltage of 2600, sheath gas 40, and aux gas 10.

3.7 Analysis of Cellular Oxygen Uptake Using an Extracellular Flux Analyzer

The protocol below assumes the use of a Seahorse XF24 instrument. The use of a different analyzer (e.g., XF96) will require the cell numbers and volumes to be adjusted appropriately, based on the well size.

1. Harvest a healthy culture of cells, wash in pre-warmed growth medium to remove trypsin, and then seed an appropriate number of cells into each well of a Seahorse XF Cell Culture Microplate (*see* **Note 11**). Cells should be dispensed in 100 μl of medium (*see* **Note 12**). We recommend seeding cells in triplicate for each condition. Add an equal volume of medium to control wells that lack cells.
2. Leave cells at room temperature in the tissue culture hood for 1 h (*see* **Note 13**).
3. Place cells in a 37 °C tissue culture incubator until they become adherent.
4. Add 150 μl of growth medium to each well, including controls, and return the cell plate to the incubator overnight.
5. Remove the XF Sensor Cartridge from the utility plate (do not place it facedown as this could damage the sensors). Add 1 ml of Seahorse XF Calibrant solution to each well of the utility plate and then place the sensor cartridge back on the plate, ensuring that the sensors are fully submerged in calibrant solution. Place in a humidified, non-CO_2, 37 °C incubator overnight.
6. Prepare XF Assay Medium. To the XF Base Medium, add appropriate amounts of glucose, sodium pyruvate, and glutamine. Use the same concentrations as normally used in growth medium (*see* **Note 14**). Adjust the pH to 7.4 and filter sterilize. Media can be stored at 4 °C.
7. Aspirate all but 50 μl of the media from the cells with a micropipette, taking care not to disturb the cell monolayer. Wash the cells twice in 1 ml of pre-warmed XF Assay Medium and add an appropriate final volume of Assay Medium (*see* **Note 15**). Check cell adhesion and culture purity by examining with a microscope.
8. Place the cell plate in the 37 °C non-CO_2 incubator for 1 h.
9. Prepare compounds for injection (*see* **Note 16**). Compounds should be prepared at an appropriate concentration in XF Assay Medium and the pH adjusted to 7.4 as required. It is important to include a positive control compound that is expected to alter OCR (*see* **Note 17**) as well as a vehicle control (e.g., DMSO).
10. Load the ports of the sensor cartridge with 75 μl of prepared compounds. To ensure even injections across all wells, each series of port (e.g., all "A" ports, all "B" ports) should have the

same volume of liquid added. All wells, including the control wells and any blanks, must have vehicle or compound loaded in the appropriate ports.

11. Prepare assay protocol (*see* **Note 18**). Load the sensor cartridge plate (containing the compounds of interest) and perform instrument calibration. Replace the utility plate with the cell culture plate when instructed. Run the assay.
12. Once the assay is completed, collect the cells. If required, harvest cells and determine the actual number per well (e.g., by counting with a hemocytometer). This number can be used to normalize the OCR for exact cell number (*see* **Note 19**).
13. Changes in OCR are indicative of a disruption in mitochondrial function and suggest that the compound of interest is likely to activate AMPK via increases in the AMP/ATP or ADP/ATP ratios. If an AMPK activator does not change OCR, it is likely to be acting via a different mechanism. We have previously characterized a number of AMPK activators in this way [3].
14. The extracellular acidification rate (ECAR), measured simultaneously to the OCR, is often used as a measure of the rate of glycolysis and may be useful for assessing the effects of AMPK activators that act by inhibiting glycolysis. However, we have no first-hand experience with that approach.

3.8 Suggested Methods for Analyzing AMPK Activation in Cell Lysates

Once cell lysates have been prepared, some thought should be given to the most appropriate method of determining the degree of AMPK activation. There are two widely used approaches:

1. AMPK immunoprecipitate (IP)-kinase assay (*see* Subheading 3.5 in Chapter 5). This radiometric assay measures AMPK activity due to changes in the covalent modification of Thr172, the key residue on the α subunit phosphorylated by the upstream kinases LKB1 and CaMKK2, and represents a quantitative, sensitive, and reproducible assay for AMPK activation. However, it cannot address effects of allosteric activation, since any allosteric effects due to non-covalent binding of ligands are lost during the preparation of the immunoprecipitate.
2. Western blotting using phosphospecific antibodies that recognize either the phosphorylated, active form of AMPK itself (pT172) or a phosphorylated downstream target such as acetyl-CoA carboxylase (pACC; *see* **Note 20**) or Raptor (p-Raptor, phosphorylated on S792). Similar to the IP-kinase assay, pT172 blots only reflect the degree of AMPK activation that is due to changes in phosphorylation of Thr172 by the upstream kinases and ignore any concomitant allosteric activation. In contrast, pACC and p-Raptor blots should reflect both

covalent modification of Thr172 and allosteric activation and give the most sensitive indication of the degree of AMPK activation within the cell. An example of this is provided by the ADaM site ligand A769662, which usually causes only a modest increase in AMPK activity as measured in IP-kinase assays or pT172 blots yet causes a large allosteric activation that is reflected in a much larger increase in pACC phosphorylation.

4 Notes

1. PBS for washing cells must be ice-cold to preserve the activation and phosphorylation status of AMPK and of downstream targets.
2. Lysis buffer can be made in advance and stored at −20 °C. Lysis buffer must be ice-cold when used, to preserve the activation and phosphorylation status of AMPK and of downstream targets.
3. Such DNAs may encode either the WT or R299G mutant of γ1 or the wild type or R531G mutant of γ2 (human numbering). Although it is also possible to mutate the equivalent arginine in AMPK-γ3 (R454), AMPK complexes containing WT γ3 appear to respond rather differently in that they are not significantly allosterically activated by AMP [13].
4. To detect changes in AMPK activity or phosphorylation of Thr172 in response to energy stress, the cells need to express LKB1 and its accessory subunits, STRAD-α or STRAD-β and MO25-α or MO25-β. Some tumor cell lines, do not express LKB1.
5. The S108A mutation can also be made in AMPK-β2, although β2-containing complexes are usually much less sensitive to ADAM site activators than β1-containing complexes.
6. Addition of hydroxyethyl cellulose decreases electro-osmotic flow; to dissolve it, boil in a microwave with gentle agitation.
7. Some AMPK activators, such as phenformin and berberine, inhibit mitochondrial ATP synthesis and thus activate AMPK by increasing cellular levels of AMP and ADP. However many cell lines, especially when maintained in medium containing 25 mM glucose (as in Dulbecco's Modified Eagle's Medium, DMEM), are highly glycolytic, and mitochondrial inhibitors may fail to elicit much of a response. In such cases, transferring to a more physiological glucose concentration (5 mM) 16 h prior to treatment with mitochondrial inhibitors can lead to greater AMPK activation.

8. "Slow lysis" is performed at room temperature; this causes cell stress, thus activating AMPK. Aspirate medium, add 500 μl of PBS stored at room temperature, scape cells off using a cell scraper, and transfer to labeled microcentrifuge tubes. Centrifuge (17,000 × *g*, 3 min, room temperature), aspirate off the supernatant, and wash the pellet once in 1 ml of PBS. Centrifuge again, remove the supernatant, and resuspend the pellet in 200–300 μl of ice-cold lysis buffer. Samples can then be frozen in liquid nitrogen and clarified as described in Subheading 3.2, **step 4**.
9. The PBS washes are essential to remove all traces of protein derived from serum in the medium.
10. It is important when removing the top (aqueous) phase to take only this layer. This means that a small amount of the aqueous layer, and hence adenine nucleotides, may be lost with each extraction. However, the losses will be the same for AMP, ADP, and ATP, and if the results are always expressed as AMP/ATP or ADP/ATP ratios, any losses during extraction will not matter.
11. To determine the appropriate number of cells to use per well, it is important to perform pilot experiments to find the numbers of cells that give a linear relationship between cell number and measured oxygen consumption rate. This will vary based on the metabolic profiles of the cells used, but for HEK293 cells in an XF24 analyzer, we would typically use 40,000 to 60,000 cells per well, giving around 70% confluence.
12. It is important to seed the cells in a low volume of medium to ensure a consistent monolayer of cells at the bottom of the well.
13. This helps promote even cell distribution across the well.
14. For HEK293 cells, we use 25 mM glucose, 2 mM sodium pyruvate, and 1 mM glutamine.
15. This volume of medium will depend on the number of injections to be performed. For an XF24 analyzer, we inject 75 μl from each port. The recommended capacity of the well is 900 μl, so for four injections, the cells are left in a final volume of 600 μl.
16. The XF24 can perform four injections on the same well, allowing for increasing concentrations of the same drug to be tested in the same experiment. It is also very informative to include injections of known metabolic inhibitors to determine the mode of action of test compounds. For example, we routinely use 2,4-dinitrophenol (DNP) to test whether a particular compound is inhibiting the mitochondrial electron transport chain (ETC). The addition of DNP, which collapses the proton

gradient, causes OCR to reach a maximum, as mitochondria are no longer limited by the supply of ADP. However, prior addition of phenformin, a potent AMPK activator, will reduce OCR and prevent any DNP-induced increases in OCR, confirming that it is an inhibitor of the ETC rather than the F1Fo ATP synthase. As with cell number, it is important to titer the concentration of compounds to achieve the maximum effects. For HEK293 cells, we find that 10 mM phenformin and 100 μM DNP are sufficient to maximally reduce and stimulate OCR, respectively.

17. We routinely use phenformin for this purpose.
18. The assay protocol is determined by a number of parameters, including the number of injections to be performed and the expected OCRs for different cell types. Consult the manufacturer's guidelines to set these. For HEK293 cells, we typically perform the following steps: mix for 2 min and rest for 10 min. To establish a baseline of oxygen consumption rate, we take three measurements as follows: mix for 2 min, rest for 2 min, and measure for 2.5 min. These measurement cycles are then repeated as desired, following each compound injection. To accurately determine the effects of a drug, the OCR should always be allowed to reach a new steady state following injection. The Seahorse allows for the protocol to be changed while the assay is in progress, so adjustments can be made if the OCR is still changing following injection.
19. To determine the effect of a compound on OCR, we found it helpful to express the effects as a percentage change in basal OCR following injection. This normalization removes the need to determine the absolute numbers of cells in each well.
20. The commercially available pACC antibodies appear to recognize both ACC1 phosphorylated on Ser79 and ACC2 phosphorylated on Ser212 (mouse numbering). These two isoforms differ slightly in size (ACC1 265 kDa, ACC2 276 kDa, mouse sequences), and in tissues expressing both (e.g., mouse liver), it should be possible to resolve them.

Acknowledgments

Studies in the Hardie Laboratory were supported by a Senior Investigator Award (097726) from the Wellcome Trust and by a Programme Grant (C37030/A15101) from the Cancer Research UK.

References

1. Li X, Wang L, Zhou XE, Ke J, de Waal PW, Gu X, Tan MH, Wang D, Wu D, Xu HE, Melcher K (2015) Structural basis of AMPK regulation by adenine nucleotides and glycogen. Cell Res 25(1):50–66. https://doi.org/10.1038/cr.2014.150
2. Xiao B, Sanders MJ, Carmena D, Bright NJ, Haire LF, Underwood E, Patel BR, Heath RB, Walker PA, Hallen S, Giordanetto F, Martin SR, Carling D, Gamblin SJ (2013) Structural basis of AMPK regulation by small molecule activators. Nat Commun 4:3017. https://doi.org/10.1038/ncomms4017
3. Hawley SA, Ross FA, Chevtzoff C, Green KA, Evans A, Fogarty S, Towler MC, Brown LJ, Ogunbayo OA, Evans AM, Hardie DG (2010) Use of cells expressing gamma subunit variants to identify diverse mechanisms of AMPK activation. Cell Metab 11(6):554–565. https://doi.org/10.1016/j.cmet.2010.04.001
4. Scott JW, Hawley SA, Green KA, Anis M, Stewart G, Scullion GA, Norman DG, Hardie DG (2004) CBS domains form energy-sensing modules whose binding of adenosine ligands is disrupted by disease mutations. J Clin Invest 113(2):274–284
5. Jensen TE, Ross FA, Kleinert M, Sylow L, Knudsen JR, Gowans GJ, Hardie DG, Richter EA (2015) PT-1 selectively activates AMPK-gamma1 complexes in mouse skeletal muscle, but activates all three gamma subunit complexes in cultured human cells by inhibiting the respiratory chain. Biochem J 467(3):461–472. https://doi.org/10.1042/BJ20141142
6. Hawley SA, Fullerton MD, Ross FA, Schertzer JD, Chevtzoff C, Walker KJ, Peggie MW, Zibrova D, Green KA, Mustard KJ, Kemp BE, Sakamoto K, Steinberg GR, Hardie DG (2012) The ancient drug salicylate directly activates AMP-activated protein kinase. Science 336(6083):918–922. https://doi.org/10.1126/science.1215327
7. Ross FA, Hawley SA, Auciello FR, Gowans GJ, Atrih A, Lamont DJ, Hardie DG (2017) Mechanisms of paradoxical activation of AMP-activated protein kinase by the kinase inhibitors SU6656 and sorafenib. Cell Chem Biol 24(7):813-824. https://doi.org/10.1016/j.chembiol.2017.05.021
8. Gowans GJ, Hawley SA, Ross FA, Hardie DG (2013) AMP is a true physiological regulator of AMP-activated protein kinase by both allosteric activation and enhancing net phosphorylation. Cell Metab 18(4):556–566. https://doi.org/10.1016/j.cmet.2013.08.019
9. Easom RA, Zammit VA (1984) A cold-clamping technique for the rapid sampling of rat liver for studies on enzymes in separate cell fractions. Suitability for the study of enzymes regulated by reversible phosphorylation-dephosphorylation. Biochem J 220:733–738
10. Davies SP, Carling D, Munday MR, Hardie DG (1992) Diurnal rhythm of phosphorylation of rat liver acetyl-CoA carboxylase by the AMP-activated protein kinase, demonstrated using freeze-clamping. Effects of high fat diets. Eur J Biochem 203(3):615–623
11. Wojtaszewski JF, Nielsen P, Hansen BF, Richter EA, Kiens B (2000) Isoform-specific and exercise intensity-dependent activation of 5′-AMP-activated protein kinase in human skeletal muscle. J Physiol 528(Pt 1):221–226
12. Corton JM, Gillespie JG, Hardie DG (1994) Role of the AMP-activated protein kinase in the cellular stress response. Curr Biol 4(4):315–324
13. Ross FA, Jensen TE, Hardie DG (2016) Differential regulation by AMP and ADP of AMPK complexes containing different gamma subunit isoforms. Biochem J 473(2):189–199. https://doi.org/10.1042/BJ20150910

Chapter 17

Cellular Application of Genetically Encoded Sensors and Impeders of AMPK

Takafumi Miyamoto, Elmer Rho, Allen Kim, and Takanari Inoue

Abstract

Unraveling the spatiotemporal dynamics of 5'-AMP-activated protein kinase (AMPK) signaling is necessary to bridge the gap between nutrient signaling and downstream function. Three genetically encoded Förster Resonance Energy Transfer (FRET)-based AMPK biosensors are available yielding insight into how AMPK-derived signal propagates throughout a cell in response to particular inputs. These findings, together with accumulating evidence obtained from biochemical techniques, promise to give a holistic understanding of the AMPK signaling. In this protocol, we describe the procedures and materials required for imaging intracellular AMPK activity in an organelle-specific manner, with a focus on ABKAR, a FRET-based biosensor. In addition, we introduce a novel AMPK inhibitor peptide that allows us to inhibit AMPK activity at specific subcellular compartments.

Key words Organelle-specific, Kinase activity monitoring, Biosensor, Förster resonance energy transfer (FRET), Compartmentalization, Signaling dynamics, Inhibitor peptide

1 Introduction

The mammalian 5'-AMP-activated protein kinase (AMPK) is a heterotrimeric enzyme composed of a catalytic α subunit, scaffold β subunit, and regulatory γ subunits [1]. There are two genes encoding isoforms of both the α and β subunits (α1 and α2, β1 and β2) and three genes encoding isoforms of the γ subunit (γ1, γ2, and γ3) [2]. AMPK senses changes in intracellular energy by responding to the relative levels of ATP compared to either AMP or ADP. For AMPK to be fully activated, AMP and/or ADP binds to the γ subunit of AMPK. This leads to a conformational change of AMPK [3, 4] that exposes amino acid Thr172 within the activation loop of the α subunit, allowing it to be subsequently phosphorylated and activated by the upstream AMPK kinases such as LKB1 [5] and CaMKKβ [6, 7].

Once activated, AMPK phosphorylates downstream substrates to regulate critical cellular functions such as metabolic homeostasis,

Dietbert Neumann and Benoit Viollet (eds.), *AMPK: Methods and Protocols*, Methods in Molecular Biology, vol. 1732, https://doi.org/10.1007/978-1-4939-7598-3_17,

cell growth, proliferation, autophagy, polarity, and transcription. So far, over 50 proteins have been identified as AMPK substrates [8]. Notably, these substrates are present in various subcellular compartments (Table 1), suggesting a role for spatial regulation of AMPK activity.

The signaling dynamics of AMPK have been studied extensively with biochemical assays [1, 2]. However, the experimental methods used to assess the signaling dynamics of AMPK are limited because of the daunting task of visualizing these processes at the subcellular compartment level in living cells in real time. Therefore, the spatio-temporal dynamics of AMPK signaling have remained mostly unknown until the recent advent of imaging techniques based on Förster Resonance Energy Transfer (FRET).

FRET is a physical process by which energy transfers from an excited donor fluorophore to an acceptor fluorophore through non-radiative dipole-dipole coupling [9]. Since the efficiency of the energy transfer depends on the donor-acceptor distance and/or their relative orientation, FRET has been widely used to monitor protein-protein interactions and protein conformational changes. Among many applications, genetically encoded FRET-based biosensors have been exploited to visualize various kinase dynamics in living cells. These kinase activity reporters (KARs) consist of a pair of fluorophores that have sufficient spectral overlap, an optimized substrate motif of the target kinases, and a phosphopeptide-binding forkhead-associated (FHA1) domain. Phosphorylation of the substrate motif increases its affinity toward FHA1 domain, bringing donor and acceptor fluorophores such that FRET. Based on these principles, three FRET-based AMPK biosensors have been developed: AMPKAR, ABKAR, and BimAB-KAR (Fig. 1).

The first generation of the biosensor called AMPKAR is a unimolecular FRET biosensor [10]. The structural layout is similar to many other KARs. It consists of ECFP and circularly permuted variants of Venus cpV E172 as a fluorophore FRET pair, bracketing an FHA1 domain and an AMPK substrate motif. When AMPK is activated, AMPKAR undergoes conformational changes that lead to an increase of the FRET signal. The use of AMPKAR thus allows for visualization of AMPK dynamics in either cytoplasmic or nuclear compartment under different experimental conditions; however, there still exists a need to monitor AMPK activity with subcellular resolution to capture spatially differentiated dynamics. ABKAR, a second-generation AMPK biosensor, lived up to this demand [11–13]. It was achieved by having the donor fluorophore, ECFP, in AMPKAR replaced with Cerulean 3, a brighter version of ECFP, resulting in an approximately two-fold larger dynamic range relative to the original AMPKAR. Additional refinements were

Table 1
A list of AMPK substrates and their main localization

Protein name	Gene name	Main localization
Girdin	CCDC88A	Cell-cell junction
Acetyl-CoA carboxylase 1	ACACA	Cytosol
Insulin receptor substrate 1	IRS1	Cytosol
TBC1 domain family member 4	TBC1D4	Cytosol
Troponin I, cardiac muscle	TNNI3	Cytosol
Tuberous sclerosis complex 2	TSC2	Cytosol
Serine/threonine-protein kinase ULK1	ULK1	Cytosol
Lactate dehydrogenase	LDH	Cytosol
3-Hydroxy-3-methylglutaryl-coenzyme A reductase	HMGCR	ER
Golgi-specific brefeldin A-resistance guanine nucleotide exchange factor 1	GBF1	Golgi apparatus
Sterol regulatory element-binding protein 1	SREBP-1c	Golgi apparatus
Regulatory-associated protein of mTOR	RPTOR	Lysosome
Protein kinase C theta	PRKCQ	Microtubule organizing center
CAP-Gly domain-containing linker protein 1	CLIP-170	Microtubules
Glycogen synthase 1 (muscle isoform)	GYS1	Microtubules, cytosol
Acetyl-CoA carboxylase 2	ACACB	Mitochondria
Mitochondrial fusion factor	MFF	Mitochondria
Histone deacetylase 5	HDAC5	Nuclear speckles
1-Phosphatidylinositol 3-phosphate 5-kinase	PIKFYVE	Nuclear speckles
Glutamine-fructose-6-phosphate aminotransferase [isomerizing] 1	GFPT1	Nucleoli
RNA polymerase I-specific transcription initiation factor RRN3	RRN3	Nucleoli
TBC1 domain family member 1	TBC1D1	Nucleoli
Cell division cycle protein 27 homolog	CDC27	Nucleoplasm
CREB-regulated transcription coactivator 2	CRTC2	Nucleoplasm
Eukaryotic elongation factor 2 kinase	eEF2K	Nucleoplasm
Histone acetyltransferase p300	EP300	Nucleoplasm
Histone H2B	H2B	Nucleoplasm
p53	p53	Nucleoplasm

(continued)

Table 1
(continued)

Protein name	Gene name	Main localization
Peroxisome-proliferator-activated receptor gamma coactivator 1-alpha	PGC1A	Nucleoplasm
Tumor protein p73	TP73	Nucleoplasm
Cyclin-dependent kinase inhibitor 1B	CDKN1B	Nucleus
Forkhead box protein O3	FOXO3a	Nucleus
Mdm4	MDM4	Nucleus
6-Phosphofructo-2-kinase/fructose-2,6-bisphosphatase 2	PFKFB2	Nucleus
Hepatocyte nuclear factor 4	HNF4	Nucleus
Carbohydrate-responsive element-binding protein	MLXIPL	Nucleus
Phosphatase 1 regulatory subunit 12C	PPP1R12C	Nucleus
Serine/threonine-protein kinase PAK 2		
Astrocytic phosphoprotein PEA-15	PEA15	Nucleus, cytosol
Clock component cryptochrome 1	CRY1	Nucleus, nuclear membrane, microtubules
Serine/threonine-protein kinase PAK 2	PAK2	Nucleus, vesicles
Microtubule-associated protein tau	MAPT	Plasma membrane
Phospholipase D1	PLD1	Plasma membrane
Thioredoxin-interacting protein	TXNIP	Plasma membrane
Vasodilator-stimulated phosphoprotein	VASP	Plasma membrane, cell junctions, focal adhesion sites
Brain-specific angiogenesis inhibitor 1-associated protein 2	BAIAP2	Plasma membrane, cytosol
Cingulin	CGN	Tight junctions
Serine/threonine-protein kinase B-raf	BRAF	Vesicle

made by fusing a series of organelle-targeting sequences (OTS) to ABKAR (osABKARs) targeting it to various subcellular localizations. A collection of osABKARs allowed for monitoring the AMPK dynamics at various subcellular compartments such as the plasma membrane, Golgi apparatus, endoplasmic reticulum (ER), mitochondria, and lysosomes as well as previously reported cytosolic and nuclear compartments (Fig. 2).

In addition to these unimolecular AMPK biosensors, bimolecular kinase activity reporter for AMPK (BimABKAR) was also developed [14]. In this system, the donor fluorophore

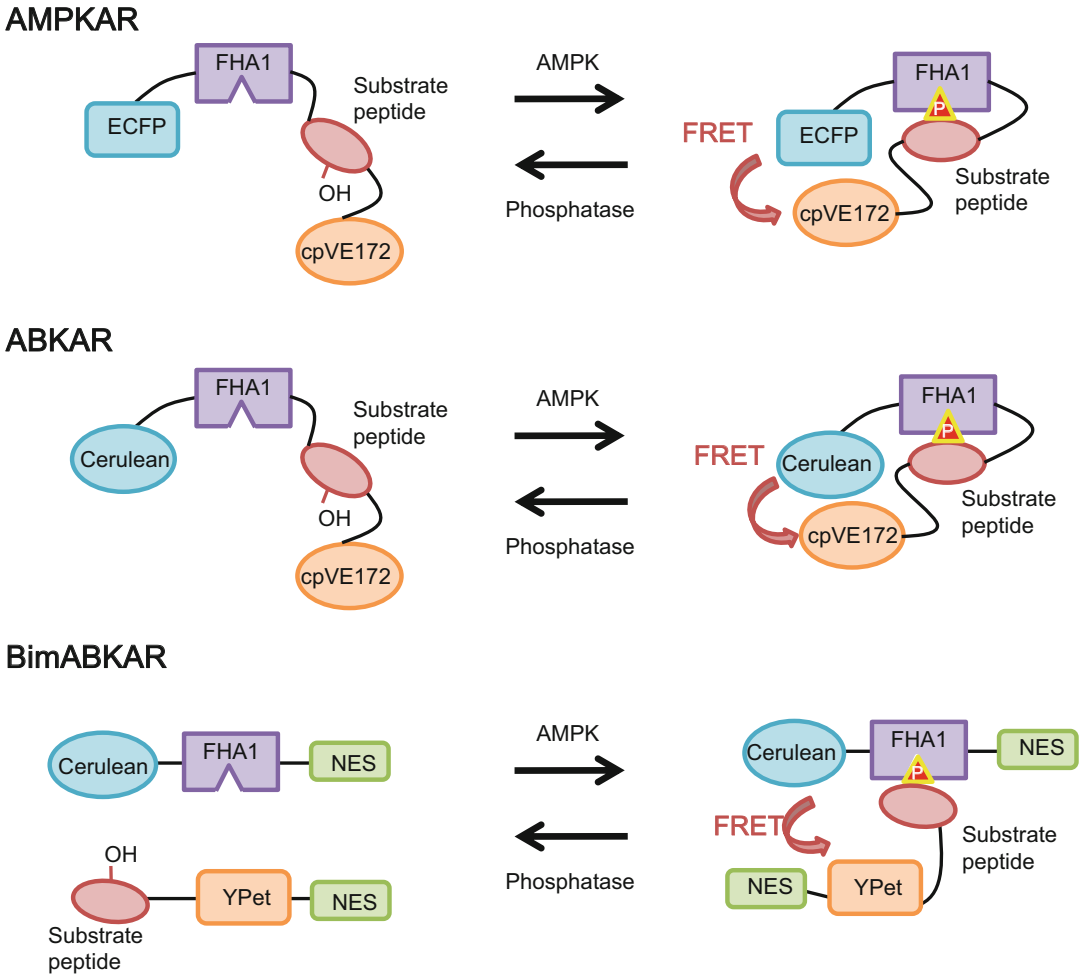

Fig. 1 Schematic diagram of FRET-based AMPK biosensors. *ECFP* enhanced cyan fluorescent protein, *cpVE172* circularly permuted variants of Venus cpV E172, *FHA1* forkhead-associated domain1, *Cerulean* cerulean 3, *YPet* yellow fluorescent protein (YFP) variant, *NES* nuclear export signal. Reproduced from [11] with permission

(Cerulean)-fused FHA1 domain and the acceptor fluorophore (YPet)-fused AMPK substrate motif were expressed as two different proteins. By appending an OTS (e.g., KRAS for plasma membrane) to a YPet-fused AMPK substrate motif, the BimABKARs, like the osABKARs, were also able to reveal activation dynamics of AMPK at specific subcellular compartments. To that end, subcellular compartment-specific BimABKAR succeeded in illuminating the cross talk of AMPK and cAMP-dependent protein kinase signaling at the plasma membrane [14]. Collectively, these reporters have revealed a role for compartmentalized AMPK signaling.

One of the downsides of currently available approaches in manipulating AMPK activity is their spatial non-specificity. For

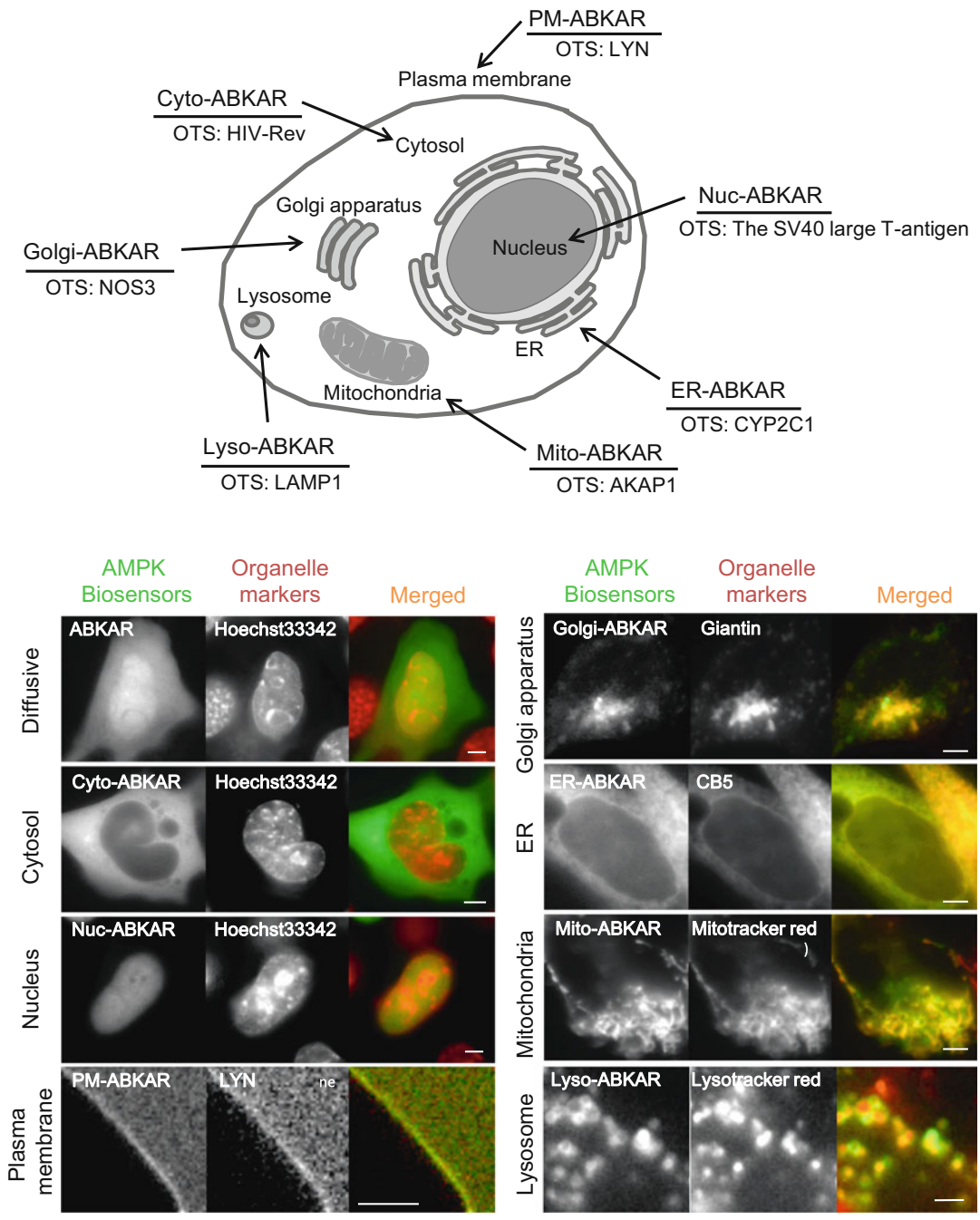

Fig. 2 The localization of organelle-specific ABKARs. Scale bar, 10 μm. Reproduced from [11] with permission

example, 2-deoxyglucose and ionomycin have been used to globally activate AMPK through activation of LKB1 and CaMKKβ, respectively, and Compound C is used for global inhibition of AMPK. Due to the global nature of these perturbations, these

approaches are unsuitable for studying compartmentalized signaling. Development of a tool to precisely target AMPK activity will further enrich our understanding of AMPK signaling. Recently, an AMPK inhibitor peptide (AIP) has been developed which now allows us to inhibit AMPK activity at specific subcellular compartments.

To date, two types of AIPs are available: AIP and the phosphorylation site-mutated version, AIP (TA) (Fig. 5a). Each version is suited for different purposes, and the choice between the two AIPs should be based on the careful discretion of the experimenter. AIP is applicable to experiments where chronic inhibition of AMPK at a subcellular compartment is demanded. In contrast, AIP (TA) is less effective but allows the experimenter to have control of the onset of inhibition at specific compartments with the help of dimerization methods such as chemically induced dimerization (CID) [11, 15].

Although the application of these FRET-based AMPK biosensors has yielded important insights into the AMPK signaling network throughout the cell, our understanding of compartmentalized AMPK signaling is far from complete. In the protocol below, we describe some general principles and optimization schemes to measure the spatiotemporal dynamics of AMPK activity in living cells using ABKAR/osABKARs. Briefly, the experimenter will measure compartmentalized AMPK signaling dynamics via four simple steps: (1) preparation of plasmid DNA encoding ABKAR/osABKARs and AIP, (2) conventional transfection of the plasmid DNA into target cells, (3) imaging the transfected cells using fluorescent microscopy, and (4) data analysis using image analysis software. Details are described below.

2 Materials

2.1 Cell Culture and Transfection

1. CO_2 incubator for cell culture.
2. 6-Well cell culture plate.
3. Opti-MEM reduced serum medium.
4. 0.05% Trypsin-EDTA (*see* **Note 1**).
5. Phosphate-buffered saline (PBS), pH 7.4.
6. Plasmids: 1 mg/ml plasmid DNA encoding ABKAR, osABKARs, and AIP in sterile water. Plasmids encoding osABKARs are available from Addgene.
7. Transfection reagents: In the described experiments, we used FuGENE HD, but other transfection reagents can also be used (*see* **Note 2**).
8. Sterilize round glass cover slips (0.1–0.2 mm thickness and 25 mm diameter).
9. Absolute ethanol.

10. Poly-D-lysine solution (0.1 mg/ml).
11. Milli-Q water.
12. Coverslip holder: serves as a chamber to hold cover slips for cell imaging (for details, *see* [16]).

2.2 Fluorescence Microscopy Imaging and Analysis

1. Physiological stimulant (such as 2-deoxyglucose (2-DG)): 1000× stock solution should be prepared according to manufacturer's instructions (*see* **Note 3**).
2. Imaging medium: phenol red-free DMEM with 25 mM HEPES, pH 7.4 under 5–10% CO_2 environment (*see* **Notes 4–6**).
3. Fluorescence microscopy: In our laboratory, live cell measurements are performed using an epifluorescence microscope. CFP and YFP excitation are carried out by an X-Cite Series 120Q mercury-vapor lamp and processed through appropriate filter cubes. Images are taken using a 63× objective (Plan-Apochromat, NA = 1.4) mounted on an inverted Axiovert 135 TV microscope and are captured by a QIClick charge-coupled device camera. The microscope is operated by the MetaMorph software package. CFP and YFP channels are configured to use the respective excitation and emission filter (427/10 nm excitation and 472/30 nm emission for CFP, 504/12 nm excitation and 542/27 nm emission for YFP), while the FRET channel is configured to use CFP as excitation and YFP as emission.
4. Image analysis software (e.g., MetaMorph imaging software) (*see* **Note 7**).

3 Methods

3.1 osABKAR Design and Preparation

1. Selecting the appropriate OTS is critical for proper osABKAR function. OTSs that were used in previously developed osABKARs are summarized in Fig. 2 (*see* **Note 8**). For targeting to relatively small subcellular compartments (e.g., centrosome, basal body of primary cilia, etc.), it is essential to identify the shortest sequence that effectively targets the sensor to the appropriate compartment. Furthermore, the compartment-specific targeting sequence needs to be as short as possible without degrading the FRET efficiency of ABKAR and is tagged to either the N-terminal or the C-terminal end of ABKAR (*see* **Note 9**). The information on protein localization sequences can be easily obtained online as it is now universally available (e.g., The Human Protein Atlas, http://www.proteinatlas.org/).
2. Prepare the plasmids according to standard subcloning protocols (*see* **Note 10**). Validate all plasmids by sequencing.

3.2 Cell Preparation and Transfection

1. Cultured cells: Maintain cultured cells (e.g., mouse embryonic fibroblasts, HeLa cervical cancer cells, Cos7 African green monkey fibroblasts, etc.), at 37 °C in 5% CO_2 at 90% relative humidity in the appropriate cell culture medium (*see* **Note 11**).
2. Pre-warm cell culture media, Opti-MEM, and trypsin at 37 °C.
3. Prepare the transfection mixture in a 1.5 ml sterile microcentrifuge tube. For FuGENE HD transfection, mix 2 μg of plasmid DNA encoding the desired osABKAR and 6 μl of FuGENE HD in 100 μl Opti-MEM. If multiple constructs are transfected together, the ratio should be optimized by testing the expression of each construct. Transfection reagents are not limited to FuGENE HD, and other transfection reagents (e.g., Lipofectamine) can be used instead. If resorting to a different transfection reagent, the protocol must be modified according to the manufacturer's instruction.
4. Incubate the transfection mixture for 20 min at room temperature (*see* **Note 12**).
5. In the meantime, prepare glass cover slips coated with poly-D-lysine. Store cover slips in individual wells in a 6-well plate (*see* **Note 13**).
6. Trypsinize cells, transfer 210×10^4 number of cells into a 15 ml tube, and spin them down at $362 \times g$ for 3 min (*see* **Note 14**).
7. Resuspend the cells in 10 ml of cell culture medium.
8. Add 500 μl of resuspended cells to 100 μl of the transfection mixture, and mix them well by tapping.
9. Add 80 μl of the cell suspension onto each cover slip.
10. For cell adhesion, leave the cover slips in the incubator for 2 h. Duration of the incubation should be adjusted for individual cell types.
11. Add 2 ml of fresh cell culture medium to each well.
12. Acquire images 36–48 h after transfection (*see* **Note 15**).

3.3 Live Cell Imaging

Monitoring AMPK activity with ABKAR/osABKARs is performed as follows:

1. Replace culture medium with fresh culture medium 2 h before live cell imaging (*see* **Note 16**).
2. Place a cover slip into a metal frame filled with 450 μl of the imaging medium (*see* **Note 17**).
3. Use a fluorescence microscope for image acquisition. Consistent temperature and CO_2 conditions are desirable irrespective of the duration of the imaging session (*see* **Notes 18** and **19**).

4. Under the microscope, select cells for monitoring in the live imaging mode. These cells should contain all the constructs required for the monitoring, which should be confirmed by checking appropriate fluorescence signals. Cells that are unusually dim or bright or that show aberrant organelle morphology should not be selected (*see* **Note 20**).
5. Start the YFP, CFP, and FRET image acquisition in a time-lapse mode. The time frame should be determined depending on the event to be monitored. Usually, observable changes in AMPK activity detected by ABKAR occur within a few minutes after the activation of CaMKKβ-mediated pathway by ionomycin, whereas over 5 min is required for the LKB1-mediated pathway to be activated by perturbing the glycolysis pathways (*see* **Note 21**).
6. Start the imaging without the stimulant to measure the baseline activity of AMPK, and at the desired time point, add the physiological stimulant (*see* **Note 22**).
7. Acquire images until the event of interest is complete. The duration of the imaging session will depend on the expected time range in which you expect to see changes in AMPK activity.

3.4 Data Analysis

The obtained fluorescent images are analyzed as follows:

1. Evaluate AMPK activity by taking regions of interest (ROI) (*see* **Note 23**). Images acquired in a microscope also include contributions from non-FRET fluorescence. The FRET component of the signal can be isolated by calculating the corrected *FRET (FRETc)* (*see* **Note 24**) (Fig. 3).
2. AMPK activity can be calculated from the following equation:

$$\text{AMPK activity} = \frac{\text{FRETc}}{\text{CFP}}$$

3. Once the images are correctly processed, kinase activity will be reflected by the intensity of the pixel in the FRET image. Typically, imaging applications allow various methods of visualizing these intensities. The recommended approach is to visualize the FRET image using a pseudocolor lookup table (LUT). This will create an image where different colors map to different intensity levels (Fig. 4) (*see* **Note 25**).

3.5 Examples of Applications

A genetically encoded AMPK inhibitor peptide (AIP) is a powerful tool to inhibit AMPK activity at specific subcellular compartments (Fig. 5a) (*see* **Note 26**) [11]. The specificity of AIP to AMPK is determined by the amino acid sequence. Thus, the AIP should be rationally designed by utilizing the rich resources that are available

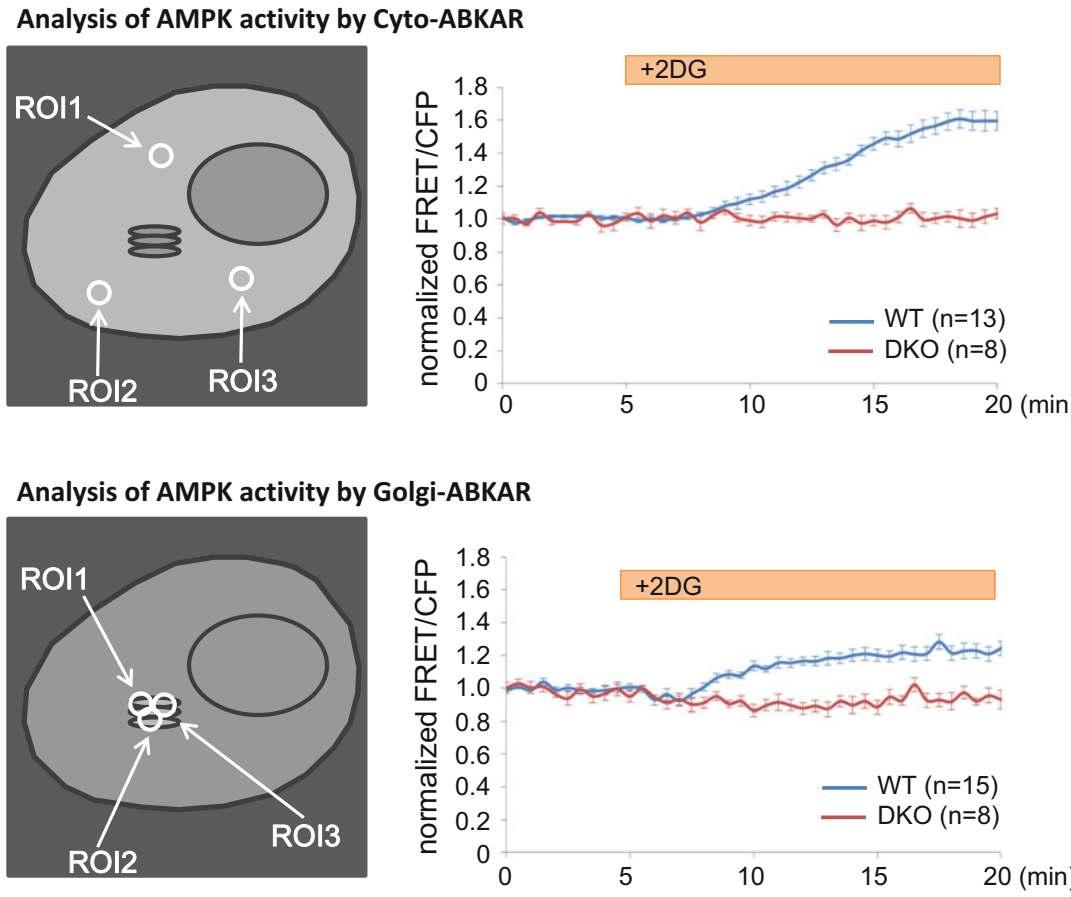

Fig. 3 Examination of AMPK activity by ABKAR. Wild-type MEFs and AMPK α subunit double knockout (DKO) MEFs were treated with 10 mM 2-DG. AMPK activity was measured by indicated AMPK biosensors. Reproduced from [11] with permission

elsewhere [8]. Current versions of the AIP could suppress 10 mM 2-DG-induced AMPK activation in Cos7 cells as measured by ABKAR (Fig. 5b) (*see* **Note 27**) [11]. To develop subcellular compartment-specific AIPs, tag appropriate OTS to the AIP. The inhibitory effect of OTS-fused AIPs can be assessed using the corresponding osABKARs (Fig. 5c). AIPs and organelle-specific AIPs are encoded on plasmids, which can be co-transfected with ABKAR. Hence, the experimental protocol is similar to that described in Subheading 3.

4 Notes

1. Use appropriate concentration of trypsin based on the adhesivity of the cell. Prolonged trypsin treatment will damage cells and may change the phenotype.

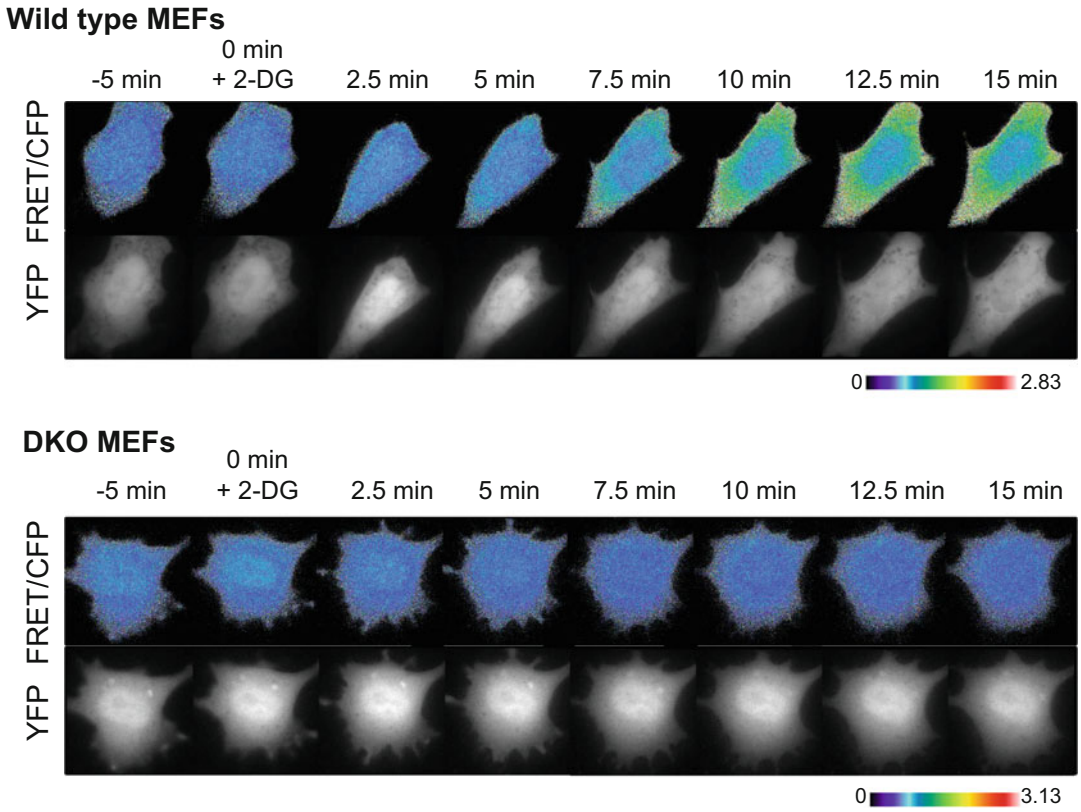

Fig. 4 Representative FRET image in wild-type MEFs and AMPK α subunit double knockout (DKO) MEFs as measured by ABKAR. Cells were treated with 10 mM 2-DG. Reproduced from [11] with permission

2. Our prior experience indicates that the use of FuGENE HD reagent with antibiotics does not cause cytotoxicity nor drop in transfection efficiency for mouse embryonic fibroblasts (MEFs), African green monkey fibroblast cells (Cos7), human cervical cancer cells (HeLa), and human embryonic kidney cells (HEK293).
3. In our protocol, 2-DG was dissolved in distilled Milli-Q water and was used at a final concentration of 10 mM.
4. If the concentration of nutrients, especially glucose, in the cell culture medium is considerably different from the imaging media, it is suggested to check whether the difference affects AMPK activity with a Western blot to detect phosphorylation level of AMPK Thr172 and AMPK substrate ACC Ser79.
5. When imaging in the absence of a stage CO_2 incubator, fluctuations in pH levels become a critical issue in FRET measurements and AMPK activity. Addition of HEPES in medium can mitigate this issue by maintaining the pH at physiological level for at least 30 min.

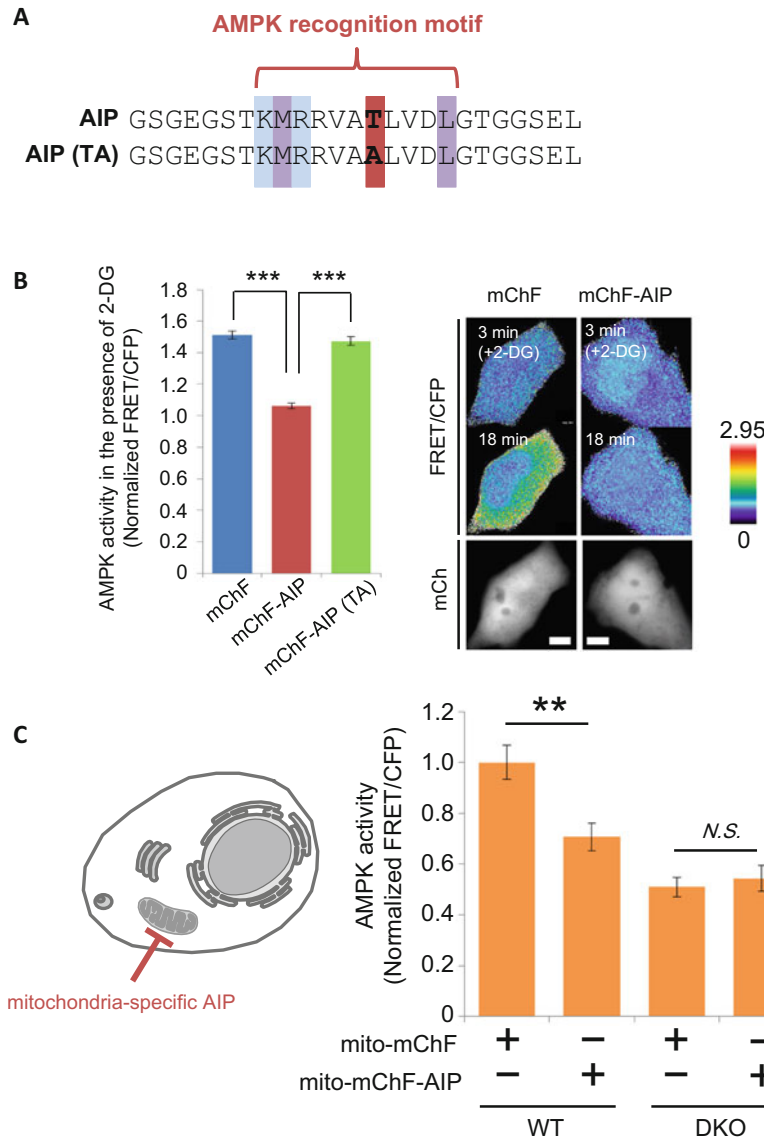

Fig. 5 Development of AIP. (**a**) The alignment of the amino acid sequences of AIP and AIP (TA) is shown. (**b**) The degree of AMPK inhibition of each AIP is shown. Cos7 cells expressing ABKAR and either mChF (control), mChF-AIP, or mChF-AIP (TA) were treated with 10 mM 2-DG for 20 min. (*Left*) The average of normalized FRET/CFP ratio from 15 to 20 min are shown as mean ± SD. (*Right*) Representative pseudocolor images of FRET/CFP ratio in cells expressing either mChF or mChF-AIP are shown. Reproduced from [11] with permission. (**c**) Inhibition of AMPK activity at mitochondria. WT MEFs and AMPK α subunit double knockout (DKO) MEFs were transiently transfected with either mito-mChF or mito-mChF-AIP, and AMPK activity was measured at the mitochondria under nutrient-surplus condition by mito-ABKAR. Quantification was performed on three independent experiments. Data are presented as mean ± SD. Reproduced from [11] with permission

6. Phenol red increases background fluorescence which interferes with the FRET signal; thus it is recommended to use phenol red-free medium for imaging.

7. Alternative image analysis can be used. FRET analysis requires image analysis software capable of performing basic arithmetic operations on images.
8. The information on OTSs for the nucleus, mitochondria, lysosome, peroxisome, ER, plasma membrane, Golgi apparatus, and secretory pathway is available in LocSigDB (http://genome.unmc.edu/LocSigDB/index.html).
9. Some general restriction enzymes are available for appending compartment-targeting sequences at either end of ABKAR. However, in cases where embedded restriction enzyme site (s) exists within the compartment-targeting sequences, infusion cloning may circumvent the problem.
10. OTSs were fused to ABKARs by designing oligonucleotides that were flanked by specific restriction enzyme sites. Cutting them with the respective restrictive enzymes provide sticky ends that can be used to ligate the OTSs to the desired location in the ABKAR containing plasmid.
11. Appropriate culture medium should be used according to ATCC protocol.
12. Prolonged incubation (>1 h) reduces transfection efficiency of FuGENE HD in MEFs. For better reproducibility, incubation time should be fixed.
13. To prepare Poly-D-lysine-coated cover slips, sterilize round glass cover slips with absolute ethanol, air-dry them and apply 100 μl of poly-D-lysine solution to each cover slip. Incubate for 2 min at room temperature and wash twice with 500 μl of sterile Milli-Q water. It is not necessary to coat the entire surface of the glass cover slips. A droplet with diameter of 5 mm is enough for the experiment. Most cell types may require this procedure unless the cell type is highly adherent to the cover slips.
14. AMPK shows disparate activation dynamics at the subcellular compartment level in response to cell confluence status [17]. Therefore, appropriate cell confluency for each experiment should be determined.
15. For better reproducibility, culture time should be fixed.
16. When analyzing metabolic signaling pathways, it is recommended to replace old medium with a fresh one to keep AMPK activity at basal level before imaging, because AMPK activity is highly sensitive to the cellular environment.
17. Imaging medium should be at room temperature unless a different temperature is required.
18. Since AMPK activity fluctuates in response to cellular environmental changes (such as temperature and medium pH),

optimization of imaging conditions is a prerequisite. To optimize imaging conditions, it is advisable to monitor AMPK activity under control condition (e.g., nutrient-rich condition).

19. In addition to optimizing imaging conditions, preparation of AMPK α1 and α2 subunit-deficient cells is important to validate the results obtained from ABKAR. It should be noted that ABKAR is not specific for AMPK; brain-specific kinases 1 and 2 (BRSK1 and BRSK2) are able to phosphorylate and change FRET signals of ABKAR [13]. Appropriate control experiments will help control for any AMPK-independent effects.
20. If the fluorescence measurements of the cell of interest are either saturated or indistinguishable from the background, it is recommended to exclude it from the analysis. To identify abnormal organelle morphology, compare cells with a control in which an appropriate organelle marker is expressed. If the cell of interest does not fall into the pool of control cells which constitutes 95% of the total population of cells when grouped by morphological similarity, the cell of interest should not be considered in the analysis.
21. It has been revealed that 2-DG treatment induces AMPK activation in the cytosol, but not in the nucleus, whereas ionomycin is able to increase AMPK activity in both compartments [10, 11]. It is good to keep in mind that different stimuli could cause different activation pattern of AMPK spatiotemporally.
22. It is advisable to monitor AMPK activity at least 5 min without adding any stimulants to make sure the imaging conditions do not affect AMPK activity as monitored by the osABKARs.
23. It should be kept in mind that AMPK activity in certain organelles is not uniform. Therefore, it is advisable to take at least three ROIs at the compartment of interest per single cell and obtain the average. The size of the ROI should be just enough to cover the compartment so that extraneous signal does not get incorporated into the measurement.
24. To calculate the corrected FRET, it is necessary to go through a number of image processing steps. To obtain the fraction of excitation cross talk "CT_{YFP}," excite cells expressing only YFP with a 504 nm laser, each time collecting the images in the YFP and FRET detection channels. It is best to use a diffusive protein to estimate cross talks to avoid FRET artifacts. Collect ten cells and measure the fluorescence signal of each cell with an image processing software.

$$\Upsilon_i = \frac{\left(\mathrm{FRET}_{\mathrm{ex427nm},i}\right) - \mathrm{background}}{\left(\mathrm{YFP}_{\mathrm{ex504nm},i}\right) - \mathrm{background}}$$

Repeat this calculation for each cell and take the average from the following equation:

$$CT_{YFP} = \sum_{1}^{10} \Upsilon_i / 10.$$

To calculate emission cross talk "CT_{CFP}," excite cells expressing only CFP with a 427 nm laser and collect images in the CFP and FRET detection channels. Again collect ten cells and measure the fluorescence.

$$C_i = \frac{\left(FRET_{ex427nm,i}\right) - \text{background}}{\left(CFP_{ex427nm,i}\right) - \text{background}}$$

Repeat this calculation for each cell and take the average from the following equation:

$$CT_{CFP} = \sum_{1}^{10} C_i / 10.$$

The corrected FRET ($FRET_C$) can be calculated by the following equation:

$$FRET_C = FRET_{raw} - CT_{YFP} * YFP - CT_{CFP} * CFP.$$

For further information, refer to [18].

25. Subcellular compartment-specific AMPK biosensors are powerful tools to detect compartmentalized AMPK signaling. However, one must be aware of the fact that OTS, itself, can influence the sensitivity of the sensor. Accordingly, the dynamic range of the osABKARs varied across subcellular compartments as a result of the modifications (Fig. 6). Therefore, it is vital that one does not directly compare AMPK activity at subcellular compartments with the FRET signals reported by the different osABKARs.
26. The current amino acid sequence of AIP was designed according to the data from a positional scanning peptide library screen (Fig. 5a) [10, 11]. However, it is essential to note that BRSK1 and BRSK2 can phosphorylate AIP as described in **Note 4**, hence, inhibiting BRSK1/2 in a competitive manner. To avoid misinterpreting the results, it is necessary to have an appropriate control experiment (e.g., AMPK-knockout cells).
27. In the case of transfection of MEFs, optimal ratio of plasmids encoding ABKAR and AIP is 1:1. But it is dependent on experimental conditions (cell lines, transfection reagents, etc.).

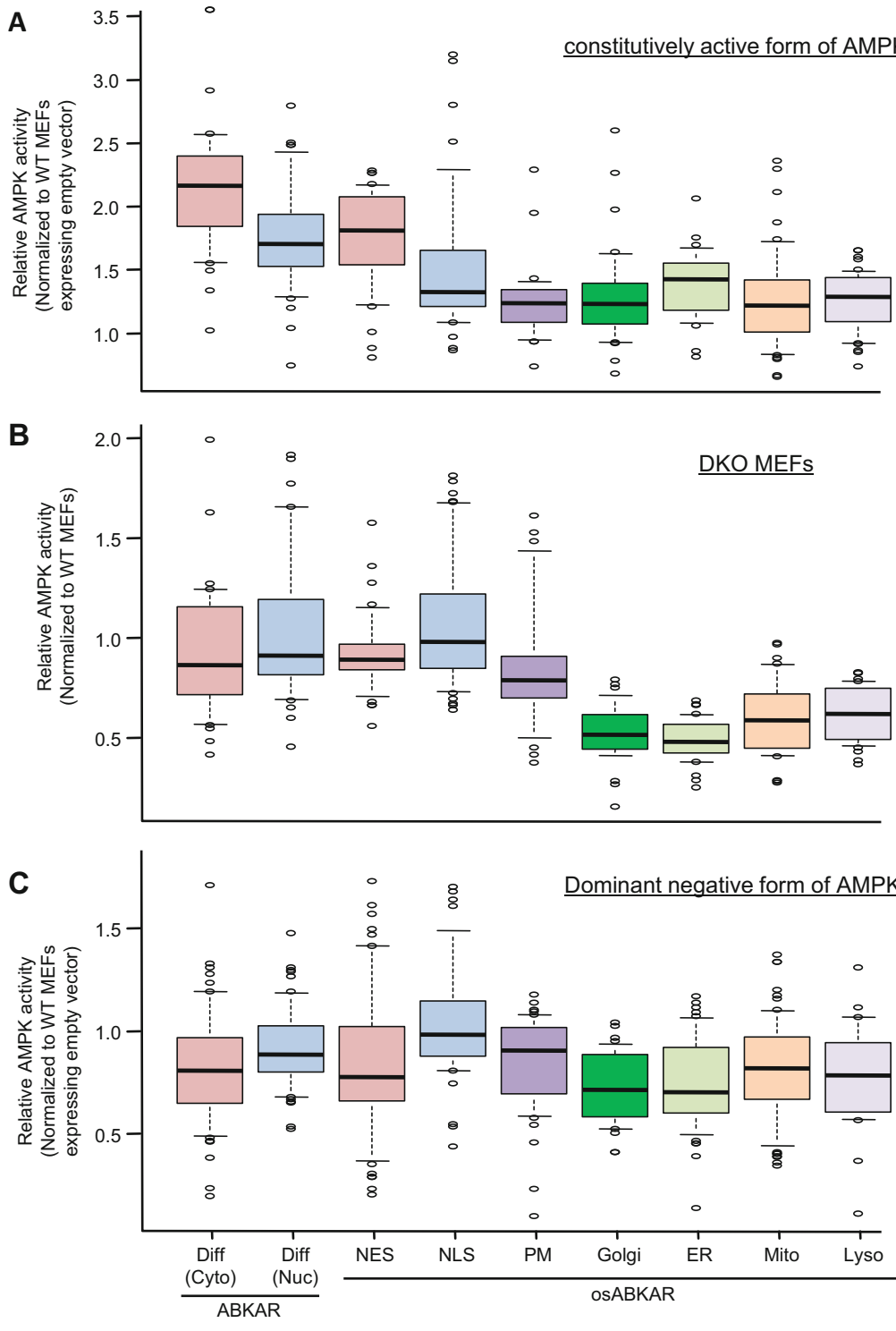

Fig. 6 Dynamic range of ABKAR and osABKARs is shown. The dynamic range of each AMPK biosensor was obtained from wild-type mouse embryonic fibroblasts (MEFs) expressing a constitutively active form of AMPK (**a**), AMPK α subunit double knockout MEFs (**b**), and wild-type MEFs expressing a dominant negative form of AMPK (**c**) under nutrient-rich condition. Reproduced from [11] with permission

Acknowledgments

We are grateful to Robert DeRose and Daniel Frigo for constructive comments. This work was supported in part by the US National Institutes of Health (NIH) grant to T.I. (DK102910).

References

1. Hardie DG, Ross FA, Hawley SA (2012) AMPK: a nutrient and energy sensor that maintains energy homeostasis. Nat Rev Mol Cell Biol 13:251–262
2. Shackelford DB, Shaw RJ (2009) The LKB1-AMPK pathway: metabolism and growth control in tumour suppression. Nat Rev Cancer 9:563–575
3. Xiao B, Sanders MJ, Underwood E et al (2011) Structure of mammalian AMPK and its regulation by ADP. Nature 472:230–233
4. Oakhill JS, Steel R, Chen Z et al (2011) AMPK is a direct adenylate charge-regulated protein kinase. Science 332:1433–1435
5. Woods A, Johnstone SR, Dickerson K et al (2003) LKB1 is the upstream kinase in the AMP-activated protein kinase cascade. Curr Biol 13:2004–2008
6. Hawley SA, Pan DA, Mustard KJ et al (2005) Calmodulin-dependent protein kinase kinase-beta is an alternative upstream kinase for AMP-activated protein kinase. Cell Metab 2:9–19
7. Woods A, Dickerson K, Heath R et al (2005) Ca2+/calmodulin-dependent protein kinase kinase-beta acts upstream of AMP-activated protein kinase in mammalian cells. Cell Metab 2:21–33
8. Schaffer BE, Levin RS, Hertz NT et al (2015) Identification of AMPK phosphorylation sites reveals a network of proteins involved in cell invasion and facilitates large-scale substrate prediction. Cell Metab 22:907–921
9. Medints I, Hildebrandt N (2013) FRET – Förster Resonance Energy Transfer: from theory to applications. Wiley Online Library. http://onlinelibrary.wiley.com/book/10.1002/9783527656028
10. Tsou P, Zheng B, Hsu C-H et al (2011) A fluorescent reporter of AMPK activity and cellular energy stress. Cell Metab 13:476–486
11. Miyamoto T, Rho E, Sample V et al (2015) Compartmentalized AMPK signaling illuminated by genetically encoded molecular sensors and actuators. Cell Rep 11:657–670
12. Miyamoto T, Rho E, Inoue T (2015) Deconvoluting AMPK dynamics. Oncotarget 6:30431–30432
13. Sample V, Ramamurthy S, Gorshkov K et al (2015) Polarized activities of AMPK and BRSK in primary hippocampal neurons. Mol Biol Cell 26:1935–1946
14. Depry C, Mehta S, Li R, Zhang J (2015) Visualization of compartmentalized kinase activity dynamics using adaptable BimKARs. Chem Biol 22:1470–1480
15. DeRose R, Miyamoto T, Inoue T (2013) Manipulating signaling at will: chemically-inducible dimerization (CID) techniques resolve problems in cell biology. Pflugers Arch 465:409–417
16. Komatsu T, Inoue T (2014) A method to rapidly induce organelle-specific molecular activities and membrane tethering. Methods Mol Biol 1174:231–245
17. Kodiha M, Rassi JG, Brown CM, Stochaj U (2007) Localization of AMP kinase is regulated by stress, cell density, and signaling through the MEK-->ERK1/2 pathway. Am J Physiol Cell Physiol 293:C1427–C1436
18. Fivaz M, Bandara S, Inoue T, Meyer T (2008) Robust neuronal symmetry breaking by Ras-triggered local positive feedback. Curr Biol 18:44–50

Chapter 18

Assessing Mitochondrial Bioenergetics by Respirometry in Cells or Isolated Organelles

Guillaume Vial and Bruno Guigas

Abstract

Mitochondrial oxidative phosphorylation is central for generating ATP and maintaining energy homeostasis in most eukaryotic cells. The ex vivo measurement of mitochondrial oxygen consumption rates in intact cells or isolated organelles is a valuable approach to assess mitochondrial bioenergetics in various experimental conditions. In this chapter, we describe several step-by-step protocols for measuring mitochondrial respiration in intact cells, permeabilized cells (in situ mitochondria), and isolated organelles using both Clark-type polarographic oxygen electrode devices and the newly developed oxygen-sensing fluorophore-based Seahorse technology.

Key words Mitochondria, Oxidative phosphorylation, Oxygraph, Oxygen consumption, Respiratory rate, Bioenergetics, Clark electrode, Seahorse, AMPK

1 Introduction

Mitochondria plays a central role in most of the eukaryotic cells by generating ATP and being involved in maintenance of cellular energy homeostasis. Oxidative phosphorylation (OXPHOS) is a set of bioenergetic reactions that take place within the mitochondrial inner membrane and couples the oxidation of substrates to the synthesis of ATP from ADP and inorganic phosphate (P_i) [1]. According to the widely accepted Mitchell's chemiosmotic theory of energy transduction [2], electrons generated by substrate oxidation are transferred by reduced electron carriers, such as NADH and $FADH_2$, to the mitochondrial electron transport chain (ETC). The subsequent electron flow through the ETC, i.e. from the respiratory-chain complex I (NADH) or complex 2 ($FADH_2$) to the respiratory-chain complex IV (cytochrome oxidase), leads to reduction of molecular oxygen, the final electron acceptor, to form water [1]. The electron transfer flavoprotein-ubiquinone oxidoreductase, localized at the matrix side of the mitochondrial inner membrane, can also act as electron acceptor

Dietbert Neumann and Benoit Viollet (eds.), *AMPK: Methods and Protocols*, Methods in Molecular Biology, vol. 1732, https://doi.org/10.1007/978-1-4939-7598-3_18,

from multiple acetyl-CoA dehydrogenases and catalyses the transfer of electrons from flavoproteins to ubiquinone, linking the oxidation of fatty acids to mitochondrial OXPHOS. Altogether, the redox energy generated by electron flow is used to transport protons from mitochondrial matrix to the intermembrane space, generating an electrochemical gradient (or protonmotive force) that is ultimately used for ATP synthesis through ATP synthase or dissipated through passive reentry into the matrix (proton leak) [1].

Specific inhibition of ETC complexes and ATP synthase or uncoupling of OXPHOS using chemical protonophores both lead to cellular ATP depletion and activation of the energy sensor AMP-activated protein kinase (AMPK). AMPK is a heterotrimeric protein complex, consisting of a catalytic α subunit and two regulatory β and γ subunits, that functions as an adenylate charge-regulated kinase which constantly senses the cellular energy status by monitoring intracellular AMP, ADP, and ATP levels [3]. Once activated, AMPK inhibits ATP-consuming anabolic processes and promotes ATP-generating catabolic pathways via direct phosphorylation of multiple downstream effectors, leading to restoration of cellular energy homeostasis [4]. In this context, investigating the impact of AMPK-activating drugs on mitochondrial OXPHOS by measuring oxygen consumption rates in intact cells might provide relevant information in order to elucidate the mechanism underlying AMPK activation in various conditions [5]. Interestingly, the study of mitochondrial bioenergetics has recently faced a renewed interest, notably in the emerging field of immunometabolism, in part due to the development of a user-friendly integrated system for assessing cellular oxygen consumption in a semi-throughout way using oxygen-sensing fluorophores incorporated on a cell plate (Seahorse™). Before this technological breakthrough, the mitochondrial bioenergetics was reliably assessed in isolated organelles from whole tissue or cells using Clark-type polarographic oxygen electrode devices. A Clark electrode is composed of a polarized platinum cathode and a silver anode in contact with a solution of semi-saturated potassium chloride maintained by a thin Teflon membrane permeable to oxygen and is usually connected to a thermostated and stirred chamber containing the mitochondria/cell suspension [6].

In this chapter, using liver and primary hepatocytes as examples of starting materials, we describe several step-by-step protocols for measuring mitochondrial oxygen consumption rates in intact cells, permeabilized cells (in situ mitochondria), and isolated organelles using both Clark-type polarographic oxygen electrode devices and the newly developed Seahorse technology (Fig. 1). Of note, these approaches can easily be translated to other tissues and cell types than liver and hepatocytes.

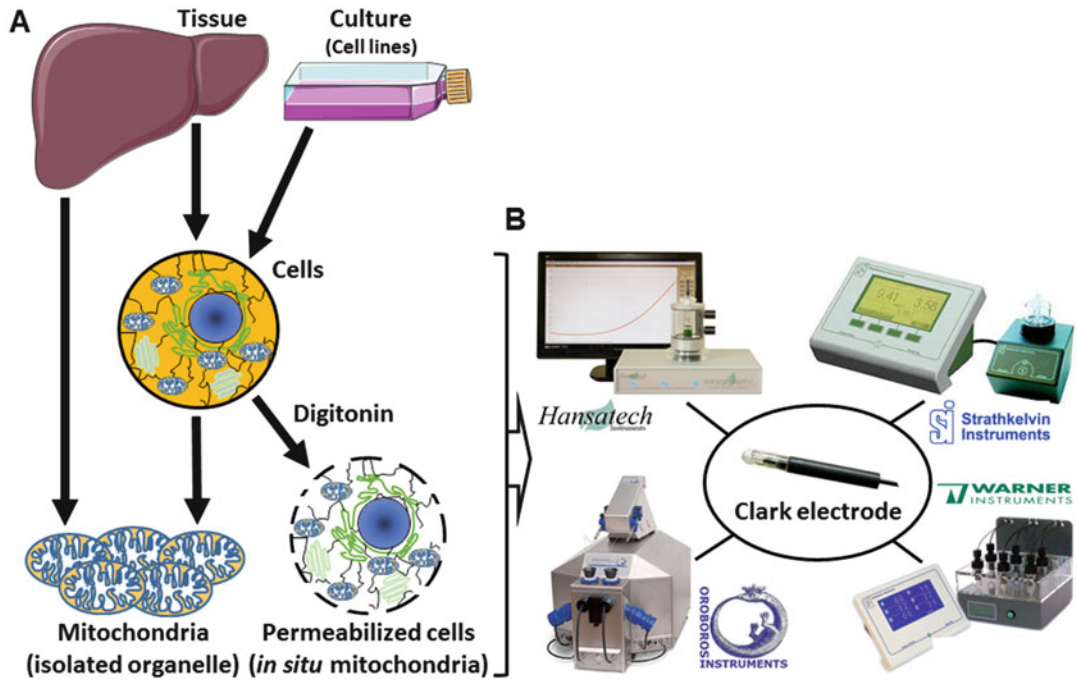

Fig. 1 General approaches for monitoring mitochondrial respiration in cells or isolated organelles using Clark-type oxygen electrode commercial devices. The oxygen consumption rates can be monitored in intact or permeabilized cells (in situ mitochondria) and mitochondria isolated from tissues (e.g., liver) or cultured cell lines (**a**) using various Clark-type oxygen electrode commercial devices (**b**) allowing continuous polarographic measurement of oxygen concentration in sample medium

2 Materials and Reagents

Prepare all solutions using ultrapure water (mQ water; sensitivity ≥18 MΩ-cm at 25 °C) and analytical grade reagents. Prepare and store all reagents at room temperature (unless indicated otherwise).

2.1 Materials and Equipment

1. Primary mouse hepatocytes (*see* **Note 1**).
2. M199 culture medium.
3. Fetal calf serum (FCS).
4. 30-ml Potter-Elvehjem.
5. Temperature-controlled centrifuge.
6. Ethanol absolute.
7. Dimethyl sulfoxide (DMSO).
8. Clark-type electrode device.
9. Hamilton syringes.
10. XF^{e}96 extracellular flux analyzer (Seahorse Bioscience).
11. Seahorse 96-well plate and XF cartridge.

2.2 Culture Medium and Extraction Buffer

1. Culture medium for primary hepatocytes: M199 medium containing 10% (v/v) FCS, 0.1% (w/v) BSA-FFA-free, 1 nM insulin, 100 nM dexamethasone, 100 nM T3, and 100 IU/ml penicillin and streptavidin.
2. Mitochondrial homogenization buffer: 250 mM sucrose, 20 mM Tris–HCl, pH 7.4, 1 mM EGTA. Add ~1.5 L of mQ water to a glass beaker containing a magnet. Weigh 171.2 g of sucrose and transfer to the glass beaker container. Add 4.8 g of Tris-Base powder and 760 mg of ethylene glycol-bis (2-aminoethylether)-N,N,N′,N′-tetraacetic acid (EGTA). Mix and adjust pH to 7.4 with hydrochloric acid. Store at 4 °C overnight and readjust pH to 7.4. Make up to 2 L with mQ water and transfer in glass bottle. Store at 4 °C (weeks) or −20 °C (months).

2.3 Respiration Buffers

1. HEPES solution: 1 M 4-(2-hydroxyethyl)piperazine-1-ethanesulfonic acid, N-(2-hydroxyethyl)piperazine-N-′-(2-ethanesulfonic acid) (HEPES), pH 7.4. Add ~85 ml of mQ water to a glass beaker containing a magnet. Weigh 23.83 g of HEPES. Mix and adjust pH to 7.4 with 10 M sodium hydroxide. Make up to 100 ml with mQ water, filter (0.22 μM), and store at 4 °C.
2. Krebs-HEPES-glucose buffer: 140 mM NaCl, 4.8 mM KCl, 1.2 mM KH_2PO_4, 1.2 mM $MgSO_4$, 1.3 mM $CaCl_2$, 11 mM glucose, 10 mM HEPES, pH 7.4 (*see* **Note 2**). Add ~350 ml of mQ water to a glass beaker containing a magnet. Weigh and add 4.09 g of natrium chloride, 178.9 mg of potassium chloride, 81.7 mg of potassium phosphate monobasic, 72.2 mg of magnesium sulfate, 72.1 mg of calcium chloride, 0.99 g of D-glucose. Add 5 ml of HEPES 1 M, pH 7.4. Mix and adjust pH to 7.4 if necessary. Make up to 500 ml with mQ water and store at 4 °C (weeks) or −20 °C (months).
3. BSA solution: 15% (w/v) bovine serum albumin (BSA). Add ~50 ml of mQ water to a glass beaker containing a magnet. Weigh 15 g of BSA [Fraction V, fatty acids-free] and transfer to the glass beaker container. Mix and make up to 100 ml with mQ water. Aliquot in 15-ml Falcon tubes and store at −20 °C.
4. P_i-Tris: 1 M inorganic phosphate (P_i). Add 100 ml of mQ water to a glass beaker containing a magnet. Add 13.6 ml of phosphoric acid 85%. Mix and adjust pH to 7.2 with Tris-Base powder. Make up to 200 ml with mQ water. Aliquot in 15-ml Falcon tubes and store at −20 °C.
5. KCl buffer: 125 mM KCl, 20 mM Tris, 1 mM EGTA, pH 7.2. Add ~350 ml of mQ water to a glass beaker containing a magnet. Weigh 4.65 g of KCl and transfer to the glass beaker

container. Add 1.2 g of tris(hydroxymethyl)aminomethane and 190 mg of EGTA. Mix and adjust pH to 7.2 with HCl. Make up to 500 ml with mQ water and store at 4 °C (weeks) or −20 °C (months). On the day of use, add 500 µl of bovine serum albumin solution (final concentration of 0.15% BSA) and 25 µl of inorganic phosphate 1 M (final concentration of 5 mM P_i-Tris) for 50 ml of KCl buffer.

6. XF assay medium. Add 0.5 ml of D-glucose 1 M to 49.5 ml of M199 medium.
7. 5% FCS (v/v)/XF assay medium. Add 0.5 ml of D-glucose 1 M and 2.5 ml of heat-inactivated FCS to 47 ml of M199 medium.
8. Ethanol: 70% (v/v). Add 700 ml of ethanol absolute in a glass cylinder and complete to 1 L with mQ water.
9. Ethanol: 30% (v/v). Add 300 ml of ethanol absolute in a glass cylinder and complete to 1 L with mQ water.

2.4 Substrates and Inhibitors

1. Tris-buffer: 50 mM Tris. Add ~50 ml of mQ water to a glass beaker containing a magnet. Weigh 605.7 mg of Tris. Mix and adjust pH to 7.4 with HCl 1 N. Make up to 100 ml with mQ water, aliquot and store at −20 °C.
2. Glutamate/malate: 0.5 M glutamate/0.25 M malate. Dissolve 422.7 mg of L-glutamic acid sodium salt and 222.6 mg of L-malic acid disodium salt in 5 ml of Tris-buffer 50 mM. Aliquot (250 µl) in 0.5-ml tubes and store at −20 °C.
3. Succinate/malate: 0.5 M succinate/0.25 M malate. Dissolve 675 mg of succinate disodium salt hexahydrate and 222.6 mg of L-malic acid disodium salt in 5 ml of Tris-buffer 50 mM. Aliquot (250 µl) in 0.5 ml tubes and store at −20 °C.
4. Malate: 0.25 M malate. Dissolve 222.6 mg of L-malic acid disodium salt in 5 ml of Tris-buffer 50 mM. Aliquot (250 µl) in 0.5 ml tubes and store at −20 °C.
5. Palmitoyl-DL-carnitine: 20 mM palmitoyl-DL-carnitine. Dissolve 43.6 mg of palmitoyl-DL-carnitine chloride in 5 ml of mQ water. Aliquot (250 µl) in 0.5 ml tubes and store at −20 °C.
6. Rotenone: 2 mM rotenone. Dissolve 3.95 mg of rotenone in 5 ml of ethanol absolute. Aliquot (100 µl) in 0.5 ml tubes and store at −20 °C.
7. ADP: 100 mM ADP. Dissolve 213.6 mg of adenosine 5′-diphosphate sodium salt in 5 ml of Tris-buffer 50 mM. Aliquot (200 µl) in 0.5 ml tubes and store at −20 °C.
8. Oligomycin: 1 mg/ml oligomycin. Dissolve 2 mg of oligomycin in 2 ml of DMSO. Aliquot (100 µl) in 0.5 ml tubes and store at −20 °C.

9. CCCP: 100 mM carbonyl cyanide 3-chlorophenylhydrazone (CCCP). Dissolve 20.5 mg of CCCP in 1 ml of DMSO. Aliquot (100 µl) in 0.5 ml tubes and store at −20 °C.
10. DNP: 100 mM 2,4-dinitrophenol (DNP). Dissolve 18.4 mg of DNP in 1 ml of DMSO. Aliquot (100 µl) in 0.5 ml tubes and store at −20 °C.
11. Antimycin: 100 µg/ml antimycin. Dissolve 5 mg of antimycin A in 50 ml of ethanol absolute. Aliquot (250 µl) in 0.5 ml tubes and store at −20 °C.
12. Myxothiazol: 1.6 mM myxothiazol: Dissolve 3.9 mg of myxothiazol in 5 ml of DMSO. Aliquot (100 µl) in 0.5 ml tubes and store at −20 °C.
13. Ascorbate: 0.5 M ascorbate. Dissolve 0.88 g of L-ascorbic acid in 10 ml of Tris-buffer 50 mM. Aliquot (250 µl) in 0.5 ml tubes and store at −20 °C.
14. TMPD/ascorbate: 20 mM N,N,N′,N′-tetramethyl-p-phenylenediamine dihydrochloride (TMPD), 1 mM ascorbate. Add 47.4 mg of TMPD and 20 µl of ascorbate 0.5 M in 10 ml of warm mQ water or medium. Aliquot (250 µl) in 0.5 ml tubes and store at −20 °C.
15. Digitonin solution: 10% digitonin. Dissolve 100 mg of digitonin in 1 ml of DMSO. Aliquot (100 µl) in 0.5 ml tubes and store at −20 °C.
16. Glucose: 1 mM. Dissolve 1.8 g of D-glucose in 10 ml of mQ water. Aliquot (250 µl) in 0.5 ml tubes and store at −20 °C.

3 Methods

3.1 Determination of Mitochondrial Oxygen Consumption Rates in Intact Cells

Experiments are usually carried out at 37 °C.

3.1.1 Clark-Type Oxygen Electrode

1. Calibrate the Clark-type polarographic oxygen electrode device according to the manufacturer's guidelines (*see* **Note 3**).
2. Preincubate freshly isolated primary hepatocytes (~2.10^7 cells; *see* **Notes 4** and **5**) for ~30 min at 37 °C in a shaking water bath in closed vials containing 2 ml of Krebs-HEPES-glucose buffer with or without additional exogenous substrates (*see* **Note 6**).
3. Saturate the cell suspension or not with a gas phase containing O_2/CO_2 (19:1) for ~1 min, depending of the sensitivity of the Clark electrode used.
4. Transfer the cells into the oxygraph chamber.

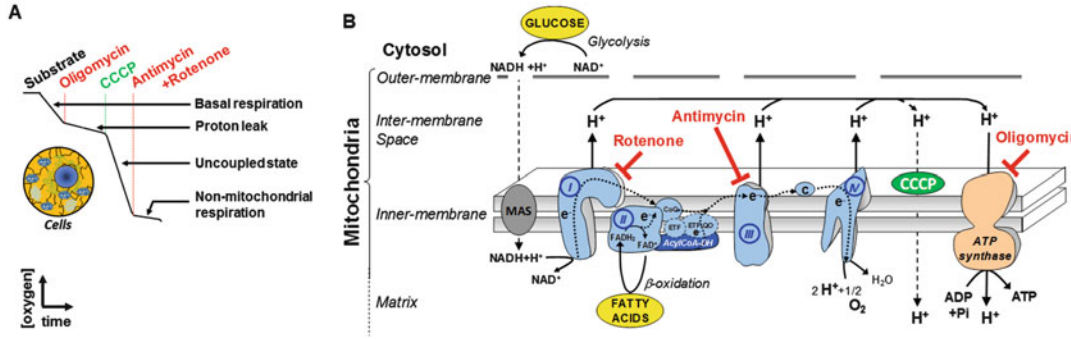

Fig. 2 Methods for studying mitochondrial bioenergetics in intact cells. The oxygen consumption rates (JO_2) of primary or cultured intact cells are determined by measuring the decay of oxygen concentration in time (slope) in various respiratory states (**a**, **b**). The basal JO_2 can be measured in the absence (endogenous) or presence of various exogenous substrates (glucose, fatty acids, etc.). The subsequent step-by-step additions of oligomycin (respiratory-chain ATP synthase inhibitor), CCCP (OXPHOS uncoupler), and antimycin (respiratory-chain complex III inhibitor) plus rotenone (respiratory-chain complex I inhibitor) allow to assess the mitochondrial respiration coupled to ATP synthesis (oligomycin-sensitive JO_2), the proton leak (oligomycin-insensitive JO_2), the maximal respiratory rate in uncoupled state, and the non-mitochondrial respiration (antimycin/rotenone-insensitive JO^2), respectively. Adapted in part from [19]

5. Start the acquisition of the basal oxygen consumption rate (JO_2) until reaching a steady state (usually ~1–2 min, Fig. 2).
6. Add 3 µl of the respiratory-chain ATP synthase inhibitor oligomycin (stock: 1 mg/ml; final concentration: 1.5 µg/ml) with a Hamilton syringe through the cap of the oxygraph chamber and measure JO_2 during 1–2 min until reaching a steady state. The oligomycin-sensitive JO_2 corresponds to the mitochondrial respiration coupled to ATP synthesis and the oligomycin-insensitive JO_2 to the proton leak though the mitochondrial inner membrane.
7. Add 2 µl of the OXPHOS uncoupler CCCP (prepare an intermediate solution of 0.5 mM by mixing 10 µl of the 100 mM stock with 990 µl of DMSO; final concentration: 0.5 µM; *see* **Note 7**) and measure JO_2 during 1–2 min until reaching a steady state in order to assess the maximal mitochondrial respiratory rate in uncoupled state.
8. Add 3 µl of the respiratory-chain complex III inhibitor antimycin (stock: 100 µg/ml; final concentration: 0.15 µg/ml; *see* **Note 8**) and 2.5 µl of the respiratory-chain complex I inhibitor rotenone (stock: 2 mM; final concentration: 2.5 µM). Measure JO_2 during 1–2 min until reaching a steady state in order to assess the non-mitochondrial respiration.
9. Wash carefully the oxygraph chamber after each measure with mQ water (three times), then 70% ethanol (three times) and again mQ water (three times), in order to remove any remaining traces of inhibitors.

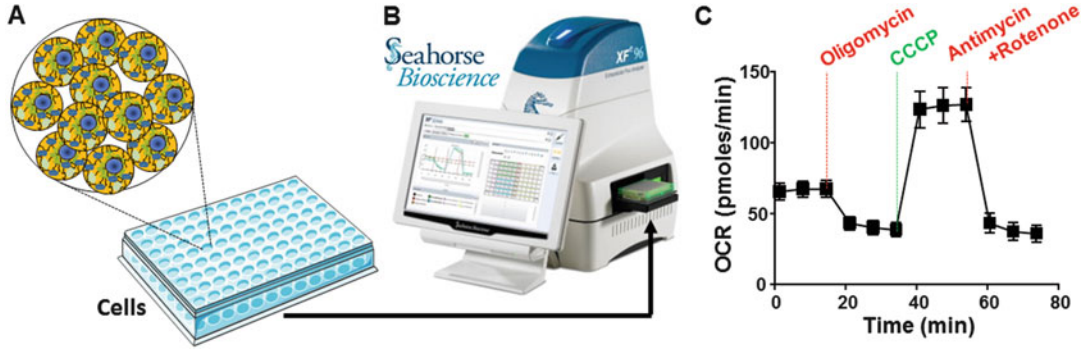

Fig. 3 Determination of mitochondrial respiration in adherent cells using oxygen-sensing fluorophore-based Seahorse™ technology. The oxygen consumption rates can be monitored in adherent cells (~e.g., 6.10^3 primary hepatocytes per well coated with collagen; (**a**) using oxygen-sensing fluorophore-based Seahorse™ technology (**b**) allowing continuous and simultaneous measurement of oxygen concentration in 24 or 96 wells. The computer-controlled administration of up to four respiratory-chain inhibitors/activators (**c**) allows to dissect mitochondrial bioenergetics, as described in Fig. 2

3.1.2 Seahorse

The regulation of mitochondrial oxidative phosphorylation (OXPHOS) can be assessed in intact adherent cells (e.g., primary hepatocytes seeded in collagen-coated 96-well plate) using the newly developed oxygen-sensing fluorophore-based Seahorse technology (Fig. 3). It is worth mentioning that a complete step-by-step procedure for running a Seahorse assay was recently described in details elsewhere for mouse/human dendritic cells [7] and could be used as general guidelines, together with the one provided by the manufacturer (*see* **Note 9**).

1. Add 60 µl of collagen type I (4 mg/ml) in 5 ml of 30% ethanol and pipette 50 µl of this intermediate solution in each well of a Seahorse 96-well plate. Let evaporate at room temperature in a tissue culture hood. Wash twice with PBS. Air-dry the plate and expose to UV light for ~10 min. The plate can be kept for ~1 week at 4 °C in sterile conditions (sealed with parafilm).
2. Hydrate the Seahorse XF cartridge the day before the experiment according to the manufacturer's guidelines.
3. Seed 6×10^4 freshly isolated primary hepatocytes per well in a Seahorse 96-well plate coated with collagen and containing 200 µl of M199 complete medium for at least 4 h.
4. Load the injection ports of the assay cartridge with 20 µl of the following chemicals:
   - Port A (oligomycin): prepare 2.4 ml of intermediate solution by adding 43 µl of oligomycin (stock: 1 mg/ml; final concentration: 1 µg/ml) in 2357 µl of 0% FCS/XF assay medium.

- Port B (CCCP): prepare 2.4 ml of intermediate solution by adding 36 µl of CCCP 1:100 (stock: 100 mM; 1:100 stock: 1 mM; final concentration: 1.5 µM) in 2364 µl of 0% FCS/XF assay medium.
- Port C (antimycin + rotenone): prepare 2.4 ml of intermediate solution by adding 132 µl of antimycin (stock: 100 µg/ml; final concentration: 0.5 µg/ml) and 13.2 µl of rotenone (stock: 2 mM; final concentration: 1 µM) in 2255 µl of 0% FCS/XF assay medium.

5. Replace the M199 complete medium by 180 µl of 5% FCS/XF assay medium.
6. Incubate the cells for 1 h at 37 °C in a dry incubator in order to remove the CO_2 dissolved in the XF assay medium.
7. Set up the assay design (number of measurements, timing of injection, etc.) using the Seahorse XF Wave software.
8. Start the automated calibration of the system.
9. Load the 96-well plate and start the acquisition (*see* **Note 10**).

3.2 Determination of Mitochondrial Oxygen Consumption Rates in Permeabilized Cells

The mitochondrial bioenergetics can be assessed in permeabilized hepatocytes (in situ organelles) using Clark-type polarographic oxygen electrode devices (Fig. 1b). Experiments are usually carried out at 37 °C.

1. Calibrate the Clark-type polarographic oxygen electrode, as described in Subheading 3.1.1.
2. Preincubate freshly isolated primary hepatocytes (2.10^7 cells) for ~30 min at 37 °C in Krebs-HEPES-glucose buffer, as described in Subheading 3.1.1.
3. Spin down the cells in a 2-ml Eppendorf at 1200 × *g* for 2 min and permeabilize membrane by resuspending the cell pellet in 2 ml of KCl medium containing 100 µg/ml digitonin.
4. Transfer the cells into the oxygraph chamber.
5. Add 20 µl of the respiratory-chain complex 1 substrates glutamate/malate (stock: 0.5/0.25 M; final concentrations: 5/2.5 mM), or 20 µl of the respiratory-chain complex 2 substrate succinate/malate (stock: 0.5/0.25 M; final concentrations: 5/2.5 mM), or 5.5 µl of palmitoyl carnitine plus 8 µl of malate (stock palmitoyl carnitine/malate: 20 mM/0.25 M; final palmitoyl carnitine/malate concentrations: 55 µM/1 mM) with a Hamilton syringe through the cap of the oxygraph chamber (*see* **Note 11**).
6. Start the acquisition of the basal (pseudo-state 4) JO_2 until reaching a steady state, usually ~1–2 min (Fig. 4).

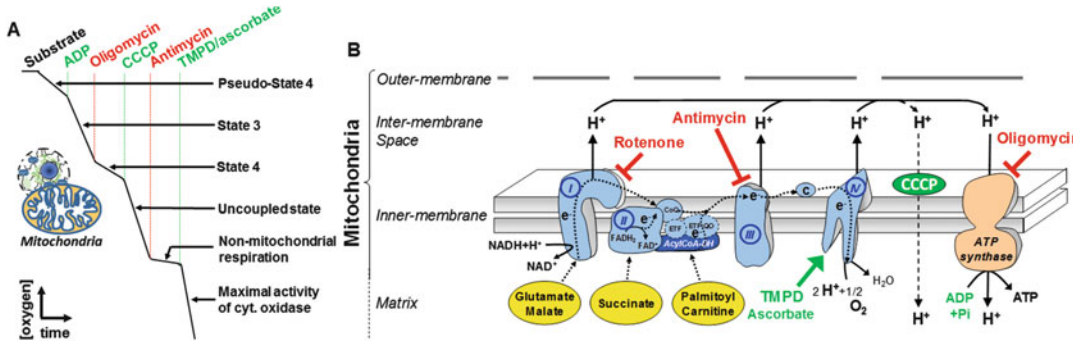

Fig. 4 Methods for studying mitochondrial bioenergetics in permeabilized cells or isolated organelles. The oxygen consumption rates (JO_2) of permeabilized cells (in situ mitochondria) or isolated mitochondria are determined by measuring the decay of oxygen concentration in time (slope) in various respiratory states (**a**, **b**). The basal JO_2 (pseudo-state 4) is measured in the presence of either glutamate/malate (oxidized at respiratory-chain complex I), succinate (oxidized at respiratory-chain complex 2) plus rotenone (to inhibit the reverse electron flow though the respiratory-chain complex I), or palmitoyl carnitine (oxidized by acyl-CoA dehydrogenase). The subsequent step-by-step additions of ADP, oligomycin, CCCP, antimycin, and TMPD/ascorbate (oxidized at respiratory-chain complex IV) allow to assess the respiration coupled to ATP synthesis (state 3), the proton leak (state 4), the maximal respiratory rate in uncoupled state, the non-mitochondrial respiration, and the maximal activity of cytochrome oxidase (respiratory-chain complex IV), respectively. Adapted in part from [19]

7. Add 20 µl of ADP (stock: 100 mM; final concentration: 1 mM) and measure the JO_2 coupled to oxidative phosphorylation (state 3) during 1–2 min until reaching a steady state.
8. Add 1.5 µl of oligomycin (stock: 1 mg/ml; final concentration: 0.75 µg/ml), and measure JO_2 during 1–2 min until reaching a steady state. The oligomycin-insensitive JO_2 corresponds to the proton leak though the mitochondrial inner membrane (state 4).
9. Add 2 µl of the OXPHOS uncoupler CCCP (intermediate stock solution of 0.5 mM; final concentration: 0.5 µM), and measure JO_2 during 1–2 min until reaching a steady state in order to assess the maximal mitochondrial respiratory rate in uncoupled state.
10. Add 3 µl of antimycin (stock: 100 µg/ml; final concentration: 0.15 µg/ml). Measure JO_2 during 1–2 min until reaching a steady state in order to assess the non-mitochondrial respiration.
11. Add 50 µl of the respiratory-chain complex IV substrates TMPD/ascorbate (stock: 20 mM/1 mM; final concentration: 0.5 mM/0.025 mM). Measure JO_2 during 1–2 min until reaching a steady state in order to assess the maximal activity of cytochrome oxidase (respiratory-chain complex IV).

12. Wash carefully the oxygraph chamber after each measure for three times with mQ water, then three times with 70% ethanol and again three times with mQ water, in order to remove any remaining traces of inhibitors.

3.3 Determination of Oxygen Consumption Rates in Isolated Mitochondria

The isolation of liver mitochondria is carried out in a cold room at 4 °C according to the standard differential centrifugation method described by Hogeboom [8] and later optimized by Klingenberg and Slenczka [9].

3.3.1 Isolation of Mitochondria from the Liver

1. Harvest liver after decapitation of animals (*see* **Note 12**).
2. Transfer in a glass beaker containing ~10 ml of ice-cold homogenization buffer, and quickly cut into small pieces with scissors.
3. Rinse twice with the same buffer in order to remove red blood cells.
4. Transfer in a 30-ml Potter-Elvehjem and start homogenization (~15 ups and downs on ice at 500 rpm).
5. Pour the homogenate into a 50-ml plastic tube and spin down at 800 × *g* for 10 min (4 °C).
6. Transfer the supernatant containing mitochondria into another 50-ml tube, and spin down at 8000 × *g* for 10 min (4 °C).
7. Discard the supernatant and resuspend carefully the pellet containing mitochondria with the homogenization buffer (first add ~5 ml and then complete to 50 ml).
8. Spin down again at 8000 × *g* for 10 min (4 °C).
9. Discard the supernatant and carefully resuspend the pellet containing mitochondria in 500 µl of homogenization buffer supplemented with 1% fatty acid-free BSA. The final mitochondria suspension is kept in an Eppendorf tube on ice until use (within a maximal window of ~8 h; *see* **Note 13**).

The determination of mitochondrial protein concentration (usually ~40 mg/ml for rat liver) can be achieved using the bicinchoninic acid assay [10] with BSA as a standard.

3.3.2 Measurement of Oxygen Consumption Rate

1. Calibrate the Clark-type polarographic oxygen electrode, as described in Subheading 3.1.1 (*see* **Note 14**).
2. Add 1 mg/ml of isolated mitochondria from whole liver or cells into the oxygraph chamber containing 2 ml of the KCl medium, as previously reported [11–13].
3. After equilibration for 30 s, the mitochondrial respiratory rate is monitored in the presence of various substrates and inhibitors, as described in Subheading 3.2 (**steps 5–12**) for permeabilized hepatocytes.

4. Wash carefully the oxygraph chamber after each measure for three times with mQ water, then three times with 70% ethanol and again three times with mQ water, in order to remove any remaining traces of inhibitors.

3.4 Calculations

The oxygen consumption rates (JO_2) are calculated by measuring the $\Delta[O_2]/\Delta(t)$, i.e. the slope of the linear regression of oxygen concentration (in nmol O_2) versus time (in min), and expressed toward the number of cells (intact or permeabilized cells) or amount of proteins (isolated mitochondria) placed in the oxygraph chamber. Of note, the antimycin-sensitive JO_2, which corresponds to mitochondrial respiration, is systematically calculated by subtracting the antimycin-insensitive (non-mitochondrial) JO_2 from the JO_2 measured at each state. As an example, $\Delta[O_2]$ at steady state between min 2 and min 4 post addition of CCCP ($\Delta(t)$) = 240 nmol O_2; so $JO_2 = 240/2 = 120$ nmol O_2/min. If the 2-ml chamber contains mitochondria at a concentration of 1 mg protein/ml, the final JO_2 will be: $120/2 = 60$ nmol O_2/min/mg protein.

4 Notes

1. Primary hepatocytes are isolated from rat, mouse, or human liver using the collagenase method, as previously described [14–16].
2. Krebs-Ringer bicarbonate buffer can also be used instead of Krebs-HEPES buffer by lowering NaCl concentration to 120 mM and replacing HEPES with 24 mM $NaHCO_3$.
3. The dissolution of oxygen varies with temperature and the medium composition and should therefore be determined beforehand.
4. ~15 mg of dry hepatocytes corresponds to ~1 million cells [17].
5. Mitochondrial JO_2 can also be measured in cultured cells that are either in suspension or adherent to plates, dishes, or flasks. Once collected by low-speed centrifugation (1200 × *g* for 2 min) or after trypsinization, cells are resuspended at high concentration in a small volume of fresh culture medium without FBS or antibiotics (or eventually in Krebs-HEPES buffer), counted and kept on ice until use. For measurement, 1 ml of cell suspension is transfered into the oxygraph chamber containing 1 ml of culture medium or Krebs-HEPES buffer and, eventually, exogenous substrates. Of note, the culture medium and cell number should be adjusted depending on the cell type and its respiratory rate (e.g., HMEC-1 cells (10^7 cells/ml) in

MCDB-131 medium or KB cells (10^7 cells/ml) in RPMI 1640 medium, as previously reported [16, 17]). After ~30 s of equilibration, the basal JO^2 can start to be recorded until reaching a steady state. Although their respective concentrations need sometimes to be adjusted depending of the cell type, inhibitors and substrates can next be added to the cells in order to assess the mitochondrial respiratory rates in various states, as described in Subheading 3.1 for intact hepatocytes.

6. Glucose can be replaced (or complemented) by various exogenous substrates such as lactate/pyruvate (20/2 mM), glycerol (20 mM), octanoate (4 mM), or BSA-palmitate (2 mM), as previously reported [15, 18].
7. CCCP can be replaced by DNP and used at the final concentration of 150 μM.
8. Antimycin can be replaced by myxothiazol and used at the final concentration of 4 μM.
9. http://www.agilent.com/en-us/solutions/cell-metabolism- (seahorse).
10. The step-by-step addition of oligomycin, CCCP, and antimycin/rotenone every 15–20 min allows to assess the mitochondrial respiration coupled to ATP synthesis (oligomycin-sensitive JO_2), the proton leak (oligomycin-insensitive JO_2), the maximal respiratory rate in uncoupled state (or spare respiratory capacity, SRC), and the non-mitochondrial respiration (antimycin/rotenone-insensitive JO_2), respectively.
11. When using succinate/malate as substrate, add 2.5 μl of rotenone (stock: 2 mM; final concentration: 2.5 μM) in order to prevent reverse flux of electrons through the respiratory-chain complex I.
12. The use of anesthetics should be avoided because they modify mitochondrial functions.
13. Mitochondria can also be prepared from cells according to the same method than the one described in Subheading 3.3. Briefly, cells from culture dishes (~10 millions) are washed once with PBS and then scraped in 2 ml of ice-cold homogenization buffer. After homogenization in an ice-cold 10-ml Potter-Elvehjem (~20 ups and downs on ice at 500 rpm), the suspension is transferred in a syringe and passed through a 25 G needle in order to completely disrupt the cells. The subsequent centrifugation steps and final resuspension are similar to the ones described for mitochondria isolation from whole tissue in Subheading 3.3.
14. Experiments are carried out at 37 °C, but the temperature can also be lowered to 30 °C for prolonged use owing to membrane fragility of isolated mitochondria.

Acknowledgments

Guigas' group is supported by funding from the European Federation for the Study of Diabetes (EFSD/Lilly Research Grant Fellowship), the Société Francophone du Diabète (SFD), and the Dutch Organization for Scientific Research (ZonMW TOP Grant 91214131). To the memory of Dr. Roland Favier and Pr. Xavier Leverve.

References

1. Nicholls DG, Ferguson SJ (2002) Bioenergetics. Academic Press, London
2. Mitchell P (1961) Coupling of phosphorylation to electron and hydrogen transfer by a chemi-osmotic type of mechanism. Nature 191:144–148
3. Oakhill JS, Scott JW, Kemp BE (2012) AMPK functions as an adenylate charge-regulated protein kinase. Trends Endocrinol Metab 23 (3):125–132. https://doi.org/10.1016/j.tem.2011.12.006
4. Hardie DG (2014) AMP-activated protein kinase: maintaining energy homeostasis at the cellular and whole-body levels. Annu Rev Nutr 34:31–55. https://doi.org/10.1146/annurev-nutr-071812-161148
5. Guigas B, Viollet B (2016) Targeting AMPK: from ancient drugs to new small-molecule activators. EXS 107:327–350. https://doi.org/10.1007/978-3-319-43589-3_13
6. Clark LC Jr, Helmsworth JA, Kaplan S, Sherman RT, Taylor Z (1953) Polarographic measurement of oxygen tension in whole blood and tissues during total by-pass of the heart. Surg Forum 4:93–96
7. Pelgrom LR, van der Ham AJ, Everts B (2016) Analysis of TLR-induced metabolic changes in dendritic cells using the seahorse XF(e)96 extracellular flux analyzer. Methods Mol Biol 1390:273–285. https://doi.org/10.1007/978-1-4939-3335-8_17
8. Hogeboom GH, Schneider WC, Pallade GE (1948) Cytochemical studies of mammalian tissues; isolation of intact mitochondria from rat liver; some biochemical properties of mitochondria and submicroscopic particulate material. J Biol Chem 172(2):619–635
9. Klingenberg M, Slenczka W (1959) Pyridine nucleotide in liver mitochondria. An analysis of their redox relationships. Biochem Z 331:486–517
10. Hill HD, Straka JG (1988) Protein determination using bicinchoninic acid in the presence of sulfhydryl reagents. Anal Biochem 170 (1):203–208
11. Batandier C, Guigas B, Detaille D, El-Mir MY, Fontaine E, Rigoulet M, Leverve XM (2006) The ROS production induced by a reverse-electron flux at respiratory-chain complex 1 is hampered by metformin. J Bioenerg Biomembr 38(1):33–42. https://doi.org/10.1007/s10863-006-9003-8
12. Lacraz G, Couturier K, Taleux N, Servais S, Sibille B, Letexier D, Guigas B, Dubouchaud H, Leverve X, Favier R (2008) Liver mitochondrial properties from the obesity-resistant Lou/C rat. Int J Obes 32 (4):629–638. https://doi.org/10.1038/sj.ijo.0803779
13. Vial G, Chauvin MA, Bendridi N, Durand A, Meugnier E, Madec AM, Bernoud-Hubac N, Pais de Barros JP, Fontaine E, Acquaviva C, Hallakou-Bozec S, Bolze S, Vidal H, Rieusset J (2015) Imeglimin normalizes glucose tolerance and insulin sensitivity and improves mitochondrial function in liver of a high-fat, high-sucrose diet mice model. Diabetes 64 (6):2254–2264. https://doi.org/10.2337/db14-1220
14. Guigas B, Bertrand L, Taleux N, Foretz M, Wiernsperger N, Vertommen D, Andreelli F, Viollet B, Hue L (2006) 5-Aminoimidazole-4-carboxamide-1-beta-D-ribofuranoside and metformin inhibit hepatic glucose phosphorylation by an AMP-activated protein kinase-independent effect on glucokinase translocation. Diabetes 55(4):865–874
15. Guigas B, Taleux N, Foretz M, Detaille D, Andreelli F, Viollet B, Hue L (2007) AMP-activated protein kinase-independent inhibition of hepatic mitochondrial oxidative phosphorylation by AICA riboside. Biochem J 404(3):499–507. https://doi.org/10.1042/BJ20070105
16. Stephenne X, Najimi M, Ngoc DK, Smets F, Hue L, Guigas B, Sokal EM (2007) Cryopreservation of human hepatocytes alters the

mitochondrial respiratory chain complex 1. Cell Transplant 16(4):409–419

17. Taleux N, Guigas B, Dubouchaud H, Moreno M, Weitzel JM, Goglia F, Favier R, Leverve XM (2009) High expression of thyroid hormone receptors and mitochondrial glycerol-3-phosphate dehydrogenase in the liver is linked to enhanced fatty acid oxidation in Lou/C, a rat strain resistant to obesity. J Biol Chem 284(7):4308–4316. https://doi.org/10.1074/jbc.M806187200
18. Couturier K, Servais S, Koubi H, Sempore B, Cottet-Emard JM, Guigas B, Lavoie JM, Favier R (2004) Metabolic and hormonal responses to exercise in the anti-obese Lou/C rats. Int J Obes Relat Metab Disord 28(8):972–978. https://doi.org/10.1038/sj.ijo.0802717
19. Vial G, Dubouchaud H, Leverve XM (2010) Liver mitochondria and insulin resistance. Acta Biochim Pol 57(4):389–392

Chapter 19

Study of AMPK-Regulated Metabolic Fluxes in Neurons Using the Seahorse XFe Analyzer

Claudia Marinangeli, Jérome Kluza, Philippe Marchetti, Luc Buée, and Valérie Vingtdeux

Abstract

AMP-activated protein kinase (AMPK) is the intracellular master energy sensor and metabolic regulator. AMPK is involved in cell energy homeostasis through the regulation of glycolytic flux and mitochondrial biogenesis. Interestingly, metabolic dysfunctions and AMPK deregulations are observed in many neurodegenerative diseases, including Alzheimer's. While these deregulations could play a key role in the development of these diseases, the study of metabolic fluxes has remained quite challenging and time-consuming. In this chapter, we describe the Seahorse XFe respirometry assay as a fundamental experimental tool to investigate the role of AMPK in controlling and modulating cell metabolic fluxes in living and intact differentiated primary neurons. The Seahorse XFe respirometry assay allows the real-time monitoring of glycolytic flux and mitochondrial respiration from different kind of cells, tissues, and isolated mitochondria. Here, we specify a protocol optimized for primary neuronal cells using several energy substrates such as glucose, pyruvate, lactate, glutamine, and ketone bodies. Nevertheless, this protocol can easily be adapted to monitor metabolic fluxes from other types of cells, tissues, or isolated mitochondria by taking into account the notes proposed for each key step of this assay.

Key words AMPK, Energy metabolism, Glycolysis, Mitochondrial respiration, Oxidative phosphorylation, Seahorse Analyzer, Glucose, Lactate, Ketone bodies

1 Introduction

As master energy sensor and metabolic regulator, the AMP-activated protein kinase (AMPK) plays a central role in the maintenance of cell energy homeostasis. AMPK is activated when intracellular reduction of ATP/AMP ratio occurs in response to energetic stress conditions. Once activated, AMPK modulates several anabolic and catabolic pathways, such as fatty acid oxidation, glucose metabolism, and mitochondrial biogenesis to reestablish the ATP reservoir [1–3]. For instance, AMPK can increase the intracellular availability and processing of glucose by inducing the translocation of glucose transporters on cell membrane and by

Dietbert Neumann and Benoit Viollet (eds.), *AMPK: Methods and Protocols*, Methods in Molecular Biology, vol. 1732, https://doi.org/10.1007/978-1-4939-7598-3_19,

upregulating the glycolytic flux via 6-phosphofructo-2-kinase phosphorylation [4–7]. Additionally, AMPK is responsible for stimulating mitochondrial biogenesis, via increasing the transcription and the activity of the peroxisome proliferator-activated receptor gamma coactivator 1α (PGC-1 α) [8]. Therefore, AMPK represents a key player in regulating several metabolic pathways to rebalance processes of energy expenses and energy intake. However, the study of metabolic fluxes has remained quite challenging and time-consuming.

A valuable and efficient experimental tool for accessing metabolic fluxes is the Seahorse XFe24 respirometry assay. This technique is based on the use of specific sensors that define a microchamber over the cells in the wells. Once the sensors reach the right position, they monitor in real time the glycolytic flux and mitochondrial respiration, by measuring the extracellular acidification rate (ECAR) and oxygen consumption rate (OCR), respectively. The Seahorse XFe can be run on intact cells, including stable and primary cells [9, 10], tissues (i.e., pancreatic islet, rodent hippocampus slices), as well as isolated mitochondria [11, 12].

In this chapter, we propose a protocol optimized for the analysis of the metabolic fluxes using various energy substrates in primary neuronal cultures. Indeed, neurons consume most of the energy intake of the brain, an organ that per se consumes approximately 20% of the oxygen and 25% of the total glucose spent by the human body. Neuronal functionality is strongly dependent on intracellular metabolic homeostasis and substrates availability. The importance of neuronal dependence on energy homeostasis is underpinned by the observation that several neurodegenerative diseases, such as Alzheimer's disease, are associated to an alteration of glucose metabolism, mitochondrial dysfunctions, and AMPK deregulation [13, 14]. Despite glucose being the obligatory brain energy source, neurons can use alternative energy substrates, such as lactate and ketone bodies [15, 16]. In this context, the Seahorse XFe assay is a powerful experimental approach for studying the role of AMPK in regulating glycolysis and mitochondrial respiration, herein monitoring metabolic fluxes in the presence of distinct energy substrates, ranging from glucose to pyruvate, lactate, ketone bodies, and glutamine.

2 Materials

All solutions should be prepared using ultrapure water (prepared by purifying deionized water to reach the sensitivity of 18 MΩ/cm at 25 °C) and cell culture grade reagents.

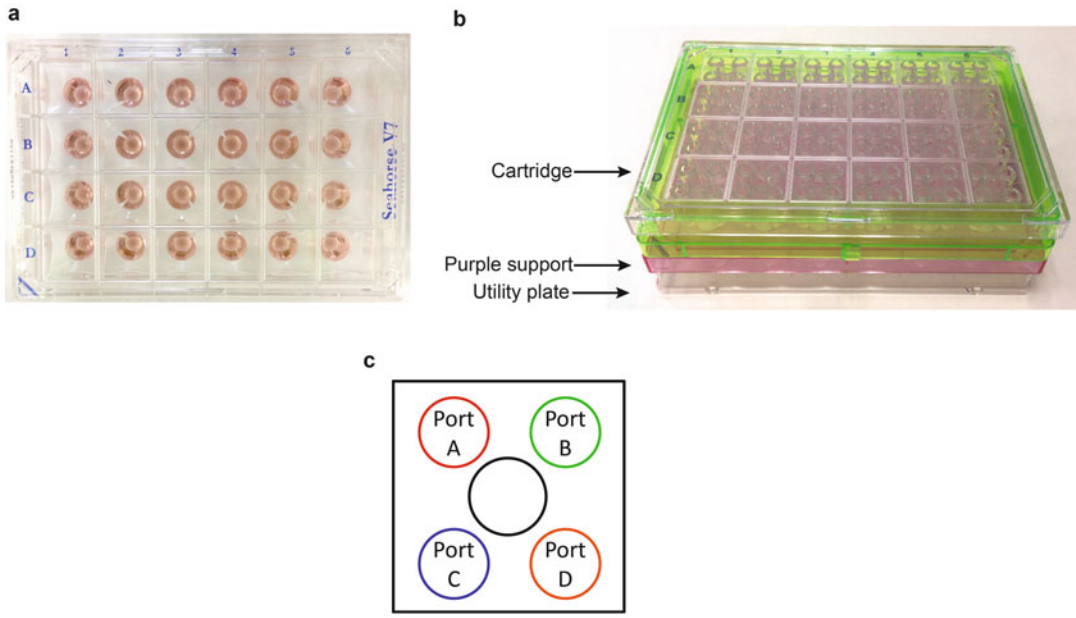

Fig. 1 Picture of Seahorse XFe24 cell plate, cartridge, and port configuration. (**a**) Picture of a Seahorse XFe24 cell culture plate. (**b**) Picture of the Seahorse XFe24 sensor cartridge, indicated by the *upper arrow*, and the utility plate, indicated by the *lower arrow*. The injection ports corresponding to each well are indicated by a *circle*. (**c**) Schematic representation of the injection ports configuration (**a**–**d**)

2.1 Equipment

1. Seahorse XFe24 Analyzer.
2. Seahorse XFe24 cell culture plates and corresponding sensor cartridges (Fig. 1a and b).
3. Incubator without CO_2.

2.2 Buffer and Media

1. XF Calibrant (by Seahorse Bioscience). Store at room temperature.
2. Medium for glycolysis assay (MGA): Dulbecco's Modified Eagle Medium Base (DMEM without glucose, L-glutamine, sodium bicarbonate, sodium pyruvate and phenol red, Sigma cat # D-5030), supplemented with 31.6 mM NaCl, 42,3 μM phenol red, and 20 mM L-glutamine. Bring to 37 °C while stirring. Adjust the pH at 7.35 ± 0.05 using 1 M NaOH when the solution reaches 37 °C (*see* **Note 1**).
3. Medium for mitochondrial respiration assay (MRA): MGA containing 10 mM glucose (*see* **Note 2**). Adjust the pH at 7.35 ± 0.05 using NaOH or HCl when the solution reaches 37 °C.

2.3 Assay Reagents

During the assay it is possible to modulate glycolytic or mitochondrial fluxes via the addition in the cell medium of up to four different reagents via the four injection ports (A, B, C, and D) on

Table 1
Calculation of the dilution factors for the reagents to be loaded in the cartridge injection ports

Injection port sequence	Volume (μl) for each injection	Volume (μl) of medium after the injection	Dilution factor of each reagent to be loaded
A	80	580	7.25×
B	80	660	8.25×
C	80	740	9.25×
D	80	820	10.25×

the sensor cartridge (Fig. 1b and c). For glycolysis assay, glucose, oligomycin, and 2-deoxy-D-glucose (2DG) will be sequentially injected, while for mitochondrial respiration assay, oligomycin, carbonyl cyanide p-trifluoromethoxyphenylhydrazone (FCCP), and rotenone/antimycin A (Rot/AA) will be serially injected.

In order to obtain the desired final concentration for each reagent to be injected, appropriate intermediate solution of each reagent needs to be calculated. This will depend on the volume of the reagent injected and the final volume of the medium once the injection has occurred. In the present protocol, the starting volume of medium in each well is 500 μl, while every injection is of 80 μl.

In this way, following the A to D injection sequence, dilution of each injected reagent will be calculated according to Table 1. The present protocol is based on the use of three of the four injection ports. The remaining port allows the injection of an additional reagent or drug during the Seahorse XFe assay, further increasing the possibilities of metabolic tests and strategies that can be performed.

Reagent Stock Solutions

1. Glucose solution: 20% (w/v) glucose. Prepare a sterile solution by dissolving 20 g of D-glucose in 100 ml of ultrapure water, filter (0.22 μm), and store at 4 °C.
2. Oligomycin: 10 mM oligomycin A in DMSO (*see* **Note 3**).
3. FCCP: 2.5 mM FCCP in DMSO. Keep protected from light (*see* **Note 3**).
4. Rot: 2.5 mM rotenone (Rot) in DMSO (*see* **Note 3**).
5. AA: 2.5 mM antimycin A (AA) in DMSO (*see* **Note 3**).

Reagent Intermediate Solutions for Glycolysis Assay

To run a glycolysis assay, intermediate solutions of glucose, oligomycin and 2DG are calculated and indicated in Table 2.

Prepare the following intermediate solution of each reagent in pre-warmed MGA medium:

Table 2
Calculation of intermediate concentration of reagents to be injected to run a glycolytic assay

Reagent	Injection port	Dilution factor	Final volume (ml)	[Stock]	[Intermediate]	[Final]
Glucose	A	7.25×	3	20%	72.5 mM	10 mM
Oligomycin	B	8.25×	2.1	10 mM	8.25 μM	1 μM
2DG	C	9.25×	2.1	–	1.537 M	150 mM

Table 3
Calculation of intermediate concentration of reagents to be injected to run a mitochondrial assay

Reagent	Port	Dilution factor	[Final]	[Stock]	[Intermediate]	[Final]
Oligomycin	A	7.25×	2.1 ml	10 mM	7.25 μM	1 μM
FCCP	B	8.25×	2.1 ml	2.5 mM	4.125 μM	0.5 μM
Rot/AA	C	9.25×	2.1 ml	2.5 mM	9.25 μM	1 μM

6. Glucose intermediate solution: 72.5 mM glucose. Dilute 20% glucose stock solution accordingly. The final concentration during the assay is 10 mM.
7. Oligomycin intermediate solution for glycolysis: 8.25 μM oligomycin. Dilute 10 mM oligomycin stock solution accordingly. The final concentration during the assay is 1 μM.
8. 2DG intermediate solution: 1.537 M 2DG. The final concentration during the assay is 150 mM. Adjust pH to 7.35 ± 0.05 using NaOH.

Reagent Intermediate Solutions for Mitochondrial Respiration Assay

To run a mitochondrial respiration assay, solutions of oligomycin FCCP and Rot/AA are calculated and indicated in Table 3.

Prepare the following intermediate solution of each reagent in pre-warmed MGA medium:

9. Oligomycin intermediate solution for respiration: 7.25 μM oligomycin. Dilute 10 mM oligomycin stock solution accordingly. The final concentration during the assay is 1 μM.
10. FCCP intermediate solution: 4.125 μM FCCP. Dilute 2.5 mM FCCP stock solution accordingly. The final concentration during the assay is 0.5 μM. The optimal FCCP concentration has been determined from a dose response optimization test (*see* **Note 4** and Fig. 2a and b).
11. Rot/AA: 9.25 μM Rot, 9.24 μM AA. Dilute 2.5 mM Rot/AA stock solutions accordingly. The final concentration during the assay is 1 μM.

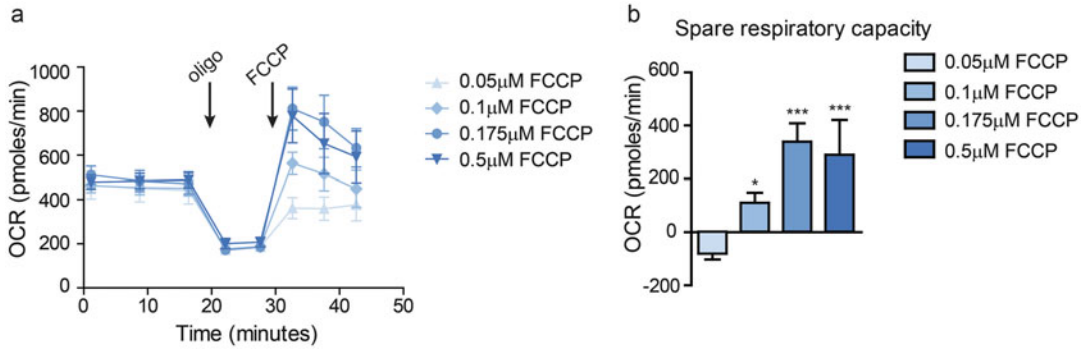

Fig. 2 Optimization of FCCP concentration to induce maximal respiration. Different concentrations of FCCP (0.05, 0.1, 0.175, 0.5 μM) were used to induce maximal respiration in primary neurons. (**a**) OCR (pmoles/min) is monitored at baseline (basal respiration), after the injection of oligomycin and in response to the different concentrations of FCCP. (**b**) Spare respiratory capacity expressed as the difference between maximal OCR upon FCCP injection and basal respiration. Cells were tested between 14 and 17 days in vitro (DIV). Data are mean ± SD of $n = 3$–4. One-way ANOVA, post hoc test Bonferroni $^{**}p < 0.05$, $^{***}p < 0.01$

3 Methods

This present protocol has been optimized for studying metabolic fluxes in primary neuronal cultures, using a Seahorse XFe24. However, this assay can be run on different cell types. In this case all the procedures can be easily adapted and optimized from the present protocol.

Carry out all steps at room temperature (RT) unless otherwise specified.

3.1 Cell Culture

All the procedures for cell plating must be carried under a laminar flux to guarantee sterile conditions. For primary neuronal culture, plate coating is done the day before cell plating (*see* **Note 5**). Here we will not detail the procedures for obtaining primary neuronal culture, as it is beyond the scope of this protocol, but the reader can find further details in Domise et al. [17].

Plate Coating

1. Unpack the box containing the XFe24 multi-well cell plate provided in the kit (Fig. 1a) (*see* **Note 6**).
2. Aliquot in each well 70 μl of 15 μg/ml poly L-ornithine solution.
3. Incubate the plate for 45 min at RT.
4. Substitute the poly L-ornithine with 70 μl of 4 μg/ml poly L-laminin solution.
5. Incubate the plates overnight (ON) at 37 °C.

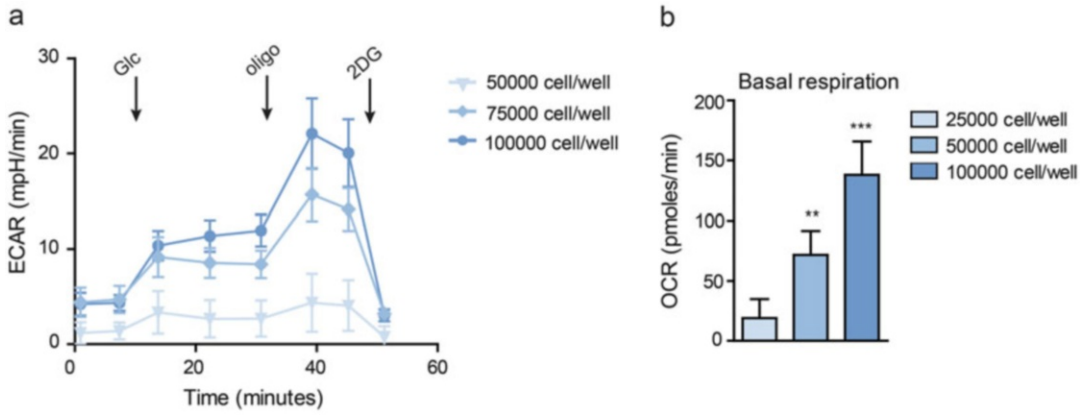

Fig. 3 Test for optimal cell density determination. In this test, primary neurons were plated at a density of 50,000, 75,000, or 100,000 cells per well and tested between 14 and 17 DIV. (**a**) ECAR (expressed in mpH/min) profile, reflecting the glycolytic flux upon sequential injection of 10 mM glucose, 1 μM oligomycin, and 150 mM 2DG, as indicated by *arrows*. (**b**) OCR (expressed in pmoles/min) calculated as mitochondrial respiration at the basal metabolic state of neurons. Data are mean ± SD of $n = 4–6$. One-way ANOVA, post hoc test Bonferroni $^{**}p < 0.05$, $^{***}p < 0.01$

Table 4
Examples of AMPK modulators

Drug	Mode of action	Ref.
AICAR	AIACR is converted by adenosine kinase to AICA ribotide (ZMP). ZMP, an AMP mimetic, allosterically activating AMPK by binding its γ-subunit	[20]
A-769662, 991	A-769662 and 991 reversibly binds at an interface between the β-subunit carbohydrate-binding module (CBM) and the kinase domain of the α-subunit. They preferentially act on AMPK containing β1-subunit	[21, 22]
Compound 2/compound 13	Compound 2 allosterically activates AMPK by binding the γ-subunit. It activates more efficiently AMPK containing α1-subunit	[23]
MT47-100	MT47-100 activates AMPK containing β1-subunit, while it inhibits the AMPK containing β2-subunit	[24]
Compound C	Compound C is an ATP-competitive inhibitor of AMPK	[25]

Primary Neuronal Culture Preparation

6. Dissect and isolate mouse cortical and/or hippocampal neurons using an enzymatic dissociation procedure (*see* **Note 7**).
7. Seed 120,000 cells in 21 wells (*see* **Note 8** and Fig. 3), while add only medium in the remaining three wells (i.e., position A1, C4, D6). The empty wells are required as background signal during the assay.
8. Let cells differentiate for 14–17 days in vitro (DIV) before running the Seahorse XFe test.

Cell Treatment

9. Proceed to AMPK modulation, by using pharmacological approaches (*see* Table 4 for further details). Alternatively it is possible to adopt genetic-based approaches for silencing AMPK expression (e.g., siRNA) or to induce the expression of deregulated forms of AMPK (e.g., constitutive active or dominant negative form of AMPK) [18, 19], using expression vectors or viral vectors (*see* **Note 9**).

3.2 Cartridge Hydration (Day Before the Assay)

1. Open the box containing the sensor cartridge (Fig. 1b).
2. Remove the sensor cartridge with the utility plate from the box.
3. Put away the sensor cartridge with the purple support upside down on the working bench.
4. Fill the 24 wells of the utility plate with 1 ml of XF Calibrant.
5. Reposition the sensor cartridge with the purple support in the utility pate in such a way that the sensors are correctly submerged in the XF Calibrant solution.
6. Place the sensor cartridge with the utility plate in an incubator without CO_2 at 37 °C overnight (*see* **Note 10**).

3.3 Assay Configuration (Day Before the Assay)

The Seahorse Analyzer and the Seahorse Wave software should be turned on the day before the assay to allow the machine to reach 37 °C. The assay configuration will differ for glycolysis and mitochondrial assay as described below. The assay configuration can be set up at any time before the reading and can be used as a template for further assays.

1. Open the Wave software.
2. Design a new template, or open a template previously created, according to the assay.
3. In the group definition tab, define the injection strategies, parameters, assay media, and cell type filling the information following the software wizard.
4. Generate group list according to the assay.
5. In the plate map tab, distribute the groups previously defined on the plate map displayed on the screen, as well as the background well position according to the cell map (*see* above).
6. In the instrument protocol tab, define the injection sequence and the cycles of mix, wait, and measure as detailed in Table 5 for the glycolysis assay and Table 6 for the mitochondrial assay.
7. Save the template.

3.4 Cartridge Loading for Glycolysis Assay

1. Take the cartridge from the incubator. Remove the purple support and place back the cartridge in the utility plate.

Table 5
Instrument protocol for the glycolytic assay on primary neuronal culture

	Basal	Glucose	Oligomycin	2DG
Inj port		A	B	C
Cycles	3	3	2	5
Mix	2:30 min	2:30 min	2:30 min	2:30 min
Wait	2:00 min	2:00 min	2:00 min	2:00 min
Measure	2:30 min	2:30 min	2:30 min	2:30 min

Table 6
Instrument protocol for the mitochondrial respiratory assay on primary neuronal culture

	Basal	Oligomycin	FCCP	Rotenone/antimycin A
Inj port		A	B	C
Cycles	3	3	3	3
Mix	1:30 min	1:20 min	00:20 min	1:20 min
Wait	2:00 min	1:20 min	00:00 min	1:20 min
Measure	3:00 min	2:00 min	2:00 min	2:00 min

2. Distribute each intermediate solution for glycolysis assay prepared as in Subheading 2.3, **items 6–8**, in the sensor cartridge ports as followed:
   - 80 μl of 72.5 mM glucose intermediate solution in the injection port A.
   - 80 μl of 8.25 μM oligomycin intermediate solution for glycolysis in the injection port B.
   - 80 μl of 1.537 M 2DG intermediate solution in the injection port C.

3.5 Cartridge Loading for Mitochondrial Respiration Assay

1. Take the cartridge from the incubator. Remove the purple support and place back the cartridge in the utility plate.
2. Distribute each intermediate solution for mitochondrial respiration assay prepared as in Subheading 2.3, **items 9–11**, in the sensor cartridge ports as followed:
   - 80 μl of 7.25 μM oligomycin intermediate solution in the injection port A.
   - 80 μl of 4.125 μM FCCP intermediate solution in the injection port B.
   - 80 μl of 9.25 μM Rot/AA intermediate solution in the injection port C.

3.6 Equilibration

1. Open the assay template previously configured (*see* Subheading 3.3) on the Seahorse Wave software.
2. Start the running of the assay by clicking on the run assay button on the screen.
3. Place the sensor cartridge with the utility plate on the machine tray taking care of the cartridge orientation (the notch needs to be placed on the bottom left).
4. Confirm the presence of the cartridge to the software by clicking the confirmation button displayed on the screen.
5. Let the calibration and equilibration step to run.

3.7 Cells Washing and Preincubation in Assay Medium

1. Take the cell plate out of the incubator and check the state of the cells under a microscope to verify cell viability, morphology, and confluence.
2. Remove the medium from the each well leaving around 50 μl of medium to avoid cells from drying during the washing steps.
3. Add 650 μl of pre-warmed MGA or MRA at 37 °C to each well (for glycolysis or mitochondrial respiration assay, respectively).
4. Repeat **steps 2** and **3** two more times.
5. Replace entirely the medium with 500 μl of pre-warmed MGA or MRA at 37 °C well by well (for glycolysis or mitochondrial respiration assay, respectively) (*see* **Note 11**).
6. Ensure cell viability and confluence under the microscope (make sure cells did not detach) (*see* **Note 12**).

Incubate the cell plate at 37 °C in an incubator without CO_2 for 40 min. This incubation time is required for the equilibration of the medium with the external environment and the stabilization of cell metabolism after the washing steps (*see* **Notes 13** and **14**).

3.8 Plate Reading

1. Once the calibration is over, remove the cell plate from the incubator and confirm the opening of the tray by clicking on the button displayed on the screen.
2. Substitute the utility plate with the cell plate on the tray. Confirm the presence of the cell plate by clicking on the button displayed on the screen. The assay reading should start automatically.
3. At the end of the reading, confirm the discard of the cartridge and cell plate on the screen. Empty the tray and discard the cartridge in the appropriate waste disposal. Take out the cell plate, check the presence of the cells, remove the media, and store the cell plate at −20 °C if further analyses are needed (*see* **Note 15**).

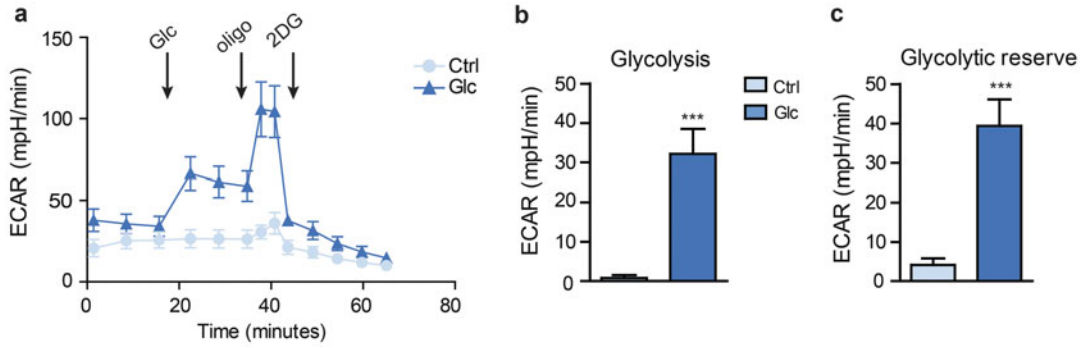

Fig. 4 Glycolytic flux analysis in the presence of glucose as energy substrate. (**a**) Glycolytic flux in primary neuronal culture monitored upon sequential injection of 10 mM glucose (Glc), or medium in the control group (Ctrl), 1 μM oligomycin (oligo), and 150 mM 2DG. (**b**) Glycolysis calculated as the difference in ECAR values before and after glucose injection. (**c**) Glycolytic reserve calculated as the difference between maximal ECAR value after oligomycin, and maximal ECAR value after glucose injection. Cells were tested between 14 and 17 DIV. Data are mean ± SD of $n = 5$. Unpaired *t*-test, $^{**}p < 0.05$, $^{***}p < 0.01$

4. Save the results. The results can be exported in Prism format for further analysis. Alternatively the results can be exported in Excel format and analyzed using dedicated programs, realized and released by Seahorse (report generators).

3.9 Glycolytic Test Analysis

During the glycolytic test, glucose, oligomycin, and 2DG are subsequently injected (Fig. 4a). Due to the absence of glucose in the MGA, the ECAR recorded is dependent on intracellular non-glycolytic processes. Upon the injection of glucose, glycolysis is stimulated, causing an increase of ECAR (Fig. 4b). The following addition of oligomycin maximizes the glycolytic flux (glycolytic capacity), causing a strong increase of ECAR (Fig. 4c). This effect is due to a metabolic compensatory system, in response to the inhibition of mitochondrial respiration induced by oligomycin treatment. Finally, 2DG will inhibit glycolysis, thus causing a decrease of ECAR to the non-glycolytic values (*see* **Note 16**).

3.10 Mitochondrial Respiration Test Analysis

In this assay, oligomycin, FCCP, and Rot/AA are subsequently injected (Fig. 5a). Initially the OCR measured is dependent on mitochondrial respiration at the basal state of the cells (Fig. 5b). The addition of oligomycin, by inhibiting the ATP synthase complex, causes a reduction of OCR. The extent of this effect reflects the oxygen consumption dedicated to the production of ATP (ATP turnover). FCCP maximizes the mitochondrial respiration by disrupting the proton gradient between the intermembrane space and the mitochondrial matrix. The maximal OCR value reached reflects the maximal respiratory capacity (Fig. 5c), and the difference between this pick and the basal respiration is the spare respiratory

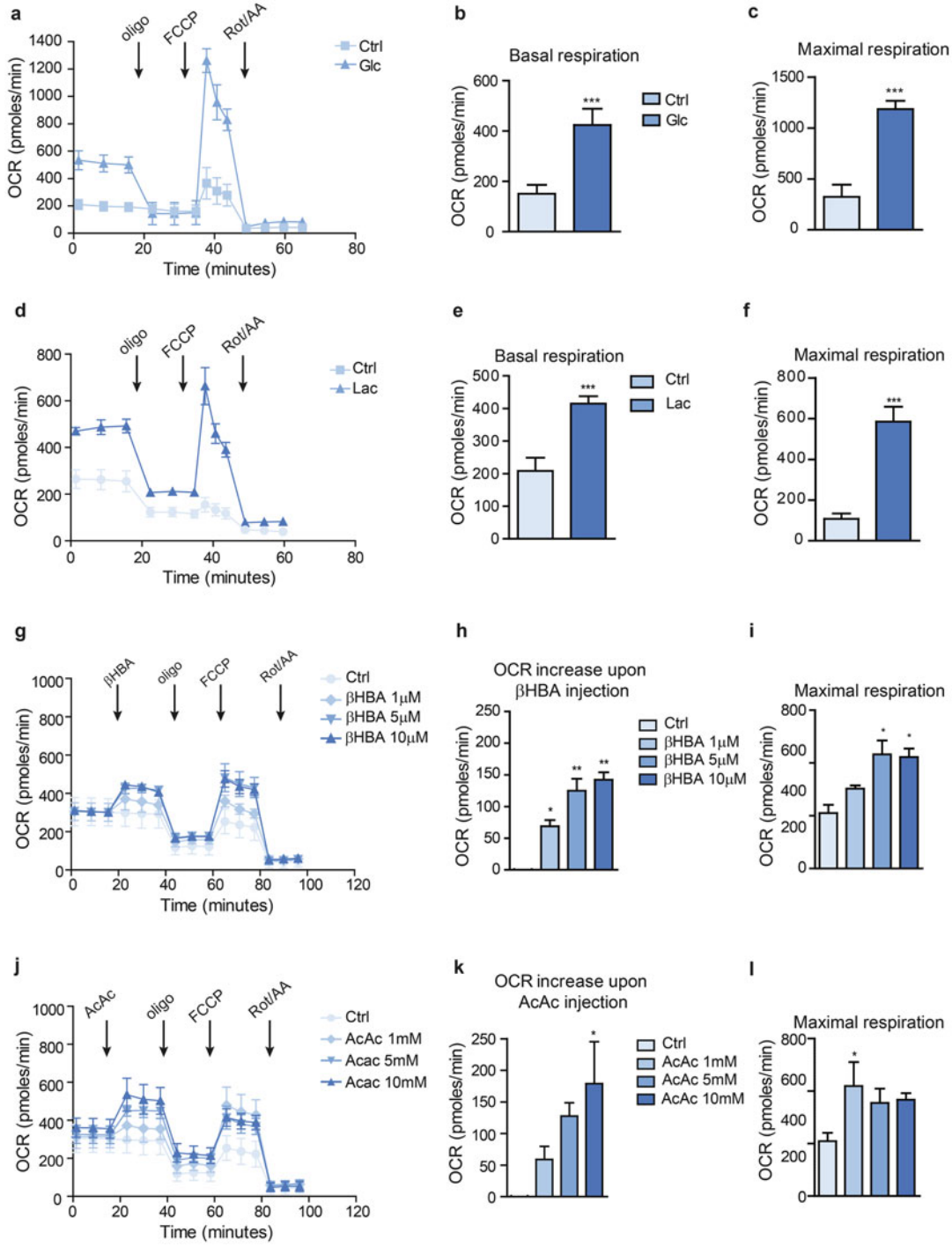

Fig. 5 Mitochondrial respiration analysis in the presence of various energy substrates. Mitochondrial respiration profile of primary neurons in the absence of metabolic substrates (Ctrl) or in the presence of 10 mM glucose (Glc) (**a**), 10 mM L-lactate (Lac) (**d**), or in response to the injection of different concentrations of β-hydroxybutyric acid (1, 5, and 10 μM βHBA) (**g**) or acetoacetate (1, 5, and 10 mM AcAc) (**j**) as metabolic

capacity. Due to their inhibiting action on the complex of the electron transport chain, the addition of Rot/AA totally inhibits the OCR. The residual OCR is determined by non-mitochondrial reactions occurring in the cells (*see* **Note 17**). Besides glucose metabolism, with the Seahorse XFe respirometry assay, it is possible to test alternative substrates, such as lactate and ketone bodies (Fig. 5 and *see* **Note 18**).

4 Notes

1. Do not overheat the medium. The medium should be prepared freshly each time. Medium might be stored at 4 °C for no longer than 48 h.
2. Alternatively, sodium pyruvate, L-lactate, ketone bodies, or fatty acids can be used to assess the mitochondrial capacity to use alternative substrates to glucose.
3. For every reagent resuspended in DMSO, we recommend storage at −20 °C in single use aliquots to avoid freezing/thawing cycles.
4. The optimization test is required to determine the optimal FCCP concentration to inject during mitochondrial test, which can vary according to the cells type and confluence. For this step it is possible to inject FCCP once or twice and to verify if the effect of the first injection can still be increased. In this case, it is of crucial importance to calculate correctly the final concentration of FCCP in the wells upon the second injection.
5. The plate coating described here has been optimized in our laboratory for primary neuronal culture. However, we propose to the reader to use the coating procedure used in his laboratory.
6. The area of a Seahorse XFe24 well is equivalent to a well of a 96 well plate.
7. We invite the reader to proceed with his own protocol to obtain isolated cells, but for further details on the procedure, please refer to Domise et al. [17].

Fig. 5 (continued) substrates and in response to the sequential injection of 1 μM oligomycin, 0.5 μM FCCP, and 1 μM Rot/AA, as indicated by *arrows*. (**b**, **e**) Basal respiration calculated as the difference between OCR before oligomycin injection and OCR after Rot/AA addition. (**h**, **k**) OCR increase upon the injection of βHBA or AcAc. (**c**, **f**, **i**, **l**) Maximal respiration expressed as the difference between OCR after FCCP and Rot/AA injection. Cells were tested between 14 and 17 DIV. Data are mean ± SD of $n = 3$–5. Unpaired *t*-test, $^{**}p < 0.05$, $^{***}p < 0.01$

8. We determined the optimal cell confluence via an optimization test (Fig. 3). As the cell density can vary according to the cell type to be tested, we strongly advise the reader to run an optimization test, to determine the optimal quantity of cells for the experiments to run.
9. The treatment can last from few minutes, accounting for the minimal time required for the drugs to efficiently act on AMPK activity, to several hours, according to the experimental design.
10. The incubation time can vary between 6 and 72 h, the optimal being ON. The purple support is designed to avoid dehydration of the cartridge during the hydration phase, so it is strongly recommended to leave the support during the entire hydration time, and remove it only before loading the cartridge.
11. If needed, addition of pharmacological modulators of AMPK can be added during rinsing and incubation steps.
12. In case cell detachment occurs, we invite the reader to optimize cell adherence, by using an alternative coating procedure.
13. The incubation time can be changed according to the cell type. In some cases, the assay can be run immediately after the washing steps, while in other cases the incubation time can reach 1 h. In both cases, we invite the reader to test different incubation times. The optimal one will be reflected by a stable OCR value during the acquisition of the basal respiration. In any case, due to the limited concentration of nutriments in the medium, absence of serum and CO_2 during the incubation, we strongly discourage to incubate cells for an excessive period.
14. The loading and calibration/equilibration of the cartridge can be performed either before the cell washing and preincubation step or during the cell preincubation time. In this last case, be sure to perform steps in Subheadings 3.5 and 3.6 before the end of the 40 min cells preincubation step.
15. If cells are detached after the assay, we advise the reader to change the coating plate procedure. Alternatively, we advise to reduce the duration of the mix phase during the assay cycles, or even abrogate it. In this case, increase the wait time, so to allow the reagents to diffuse correctly in the medium, once injected. DNA or protein dosage can be realized in order to normalize the assay. Otherwise, dispose of cells and medium appropriately.
16. Figure 4 shows an example of glycolytic test run on primary neuronal culture in presence (Glc), or absence (Ctrl) of glucose as metabolic substrate. The results show that in absence of glucose, glycolysis and glycolytic capacity are strongly abrogated (Fig. 4a and b), confirming that the ECAR monitored is

dependent on glucose metabolism. We invite the reader to perform a similar test to verify the glycolytic profile of the cells to be tested.

17. Figure 5 shows an example of mitochondrial respiration test on primary neuronal culture (Fig. 5a) in presence (Glc), or absence (Ctrl), of glucose as metabolic substrate. The results proposed here show that in absence of glucose, the OCR values of basal respiration and maximal respiratory capacity are abrogated (Fig. 5b and c), confirming that OCR values are dependent on glucose metabolism. We invite the reader to perform a similar test to verify the respiratory profile of the cells to be tested.
18. Using Seahorse XFe technology it is possible to monitor cell metabolism in presence of different energy substrates, including lactate (10 mM Lac) (Fig. 5d–f) and the ketone bodies 3-β hydroxybutyrate (β HBA) and acetoacetate (AcAc) (Fig. 5g–l). Results show that injection of ketone bodies induces a readily increase of OCR, suggesting that ketone bodies are metabolized by neuronal mitochondria.

Acknowledgments

This work was supported by the French Foundation pour la cooperation Scientifique—Plan Alzheimer 2008–2012 (Senior Innovative Grant 2013 to V.V.) and by the Fondation Vaincre Alzheimer, n°FR-16071p (to V.V.) and in part through the Labex DISTALZ (Development of Innovative Strategies for a Transdisciplinary Approach to Alzheimer's Disease). This work received a financial support from INSERM, UNIVERSITE DE LILLE II, a special financial support from the Association pour l'Etude des Anomalies Congénitales Neurodev of Pr. B. Poupard (to J.K. and P.M.) and the support of G. Mulliez.

References

1. Hardie DG (2007) AMP-activated/SNF1 protein kinases: conserved guardians of cellular energy. Nat Rev Mol Cell Biol 8 (10):774–785. https://doi.org/10.1038/nrm2249
2. Hardie DG (2011) AMP-activated protein kinase: an energy sensor that regulates all aspects of cell function. Genes Dev 25 (18):1895–1908. https://doi.org/10.1101/gad.17420111
3. Viollet B, Horman S, Leclerc J, Lantier L, Foretz M, Billaud M, Giri S, Andreelli F (2010) AMPK inhibition in health and disease. Crit Rev Biochem Mol Biol 45(4):276–295. https://doi.org/10.3109/10409238.2010.488215
4. Barnes K, Ingram JC, Porras OH, Barros LF, Hudson ER, Fryer LG, Foufelle F, Carling D, Hardie DG, Baldwin SA (2002) Activation of GLUT1 by metabolic and osmotic stress: potential involvement of AMP-activated protein kinase (AMPK). J Cell Sci 115 (Pt 11):2433–2442
5. Abbud W, Habinowski S, Zhang JZ, Kendrew J, Elkairi FS, Kemp BE, Witters LA, Ismail-Beigi F (2000) Stimulation of

AMP-activated protein kinase (AMPK) is associated with enhancement of Glut1-mediated glucose transport. Arch Biochem Biophys 380 (2):347–352. https://doi.org/10.1006/abbi.2000.1935

6. Weisova P, Concannon CG, Devocelle M, Prehn JH, Ward MW (2009) Regulation of glucose transporter 3 surface expression by the AMP-activated protein kinase mediates tolerance to glutamate excitation in neurons. J Neurosci 29(9):2997–3008. https://doi.org/10.1523/JNEUROSCI.0354-09.2009
7. Marsin AS, Bertrand L, Rider MH, Deprez J, Beauloye C, Vincent MF, Van den Berghe G, Carling D, Hue L (2000) Phosphorylation and activation of heart PFK-2 by AMPK has a role in the stimulation of glycolysis during ischaemia. Curr Biol 10(20):1247–1255
8. Jager S, Handschin C, St-Pierre J, Spiegelman BM (2007) AMP-activated protein kinase (AMPK) action in skeletal muscle via direct phosphorylation of PGC-1alpha. Proc Natl Acad Sci U S A 104(29):12017–12022. https://doi.org/10.1073/pnas.0705070104
9. Corazao-Rozas P, Guerreschi P, Jendoubi M, Andre F, Jonneaux A, Scalbert C, Garcon G, Malet-Martino M, Balayssac S, Rocchi S, Savina A, Formstecher P, Mortier L, Kluza J, Marchetti P (2013) Mitochondrial oxidative stress is the Achille's heel of melanoma cells resistant to Braf-mutant inhibitor. Oncotarget 4(11):1986–1998. https://doi.org/10.18632/oncotarget.1420
10. Corazao-Rozas P, Guerreschi P, Andre F, Gabert PE, Lancel S, Dekiouk S, Fontaine D, Tardivel M, Savina A, Quesnel B, Mortier L, Marchetti P, Kluza J (2016) Mitochondrial oxidative phosphorylation controls cancer cell's life and death decisions upon exposure to MAPK inhibitors. Oncotarget 7 (26):39473–39485. https://doi.org/10.18632/oncotarget.7790
11. Rogers GW, Brand MD, Petrosyan S, Ashok D, Elorza AA, Ferrick DA, Murphy AN (2011) High throughput microplate respiratory measurements using minimal quantities of isolated mitochondria. PLoS One 6(7):e21746. https://doi.org/10.1371/journal.pone.0021746
12. Schuh RA, Clerc P, Hwang H, Mehrabian Z, Bittman K, Chen H, Polster BM (2011) Adaptation of microplate-based respirometry for hippocampal slices and analysis of respiratory capacity. J Neurosci Res 89(12):1979–1988. https://doi.org/10.1002/jnr.22650
13. Marinangeli C, Didier S, Vingtdeux V (2016) AMPK in neurodegenerative diseases: implications and therapeutic perspectives. Curr Drug Targets 17(8):890–907
14. Vingtdeux V, Davies P, Dickson DW, Marambaud P (2011) AMPK is abnormally activated in tangle- and pre-tangle-bearing neurons in Alzheimer's disease and other tauopathies. Acta Neuropathol 121(3):337–349. https://doi.org/10.1007/s00401-010-0759-x
15. van Hall G, Stromstad M, Rasmussen P, Jans O, Zaar M, Gam C, Quistorff B, Secher NH, Nielsen HB (2009) Blood lactate is an important energy source for the human brain. J Cereb Blood Flow Metab 29(6):1121–1129. https://doi.org/10.1038/jcbfm.2009.35
16. Belanger M, Allaman I, Magistretti PJ (2011) Brain energy metabolism: focus on astrocyte-neuron metabolic cooperation. Cell Metab 14 (6):724–738. https://doi.org/10.1016/j.cmet.2011.08.016
17. Domise M, Didier S, Marinangeli C, Zhao H, Chandakkar P, Buee L, Viollet B, Davies P, Marambaud P, Vingtdeux V (2016) AMP-activated protein kinase modulates tau phosphorylation and tau pathology in vivo. Sci Rep 6:26758. https://doi.org/10.1038/srep26758
18. Turban S, Stretton C, Drouin O, Green CJ, Watson ML, Gray A, Ross F, Lantier L, Viollet B, Hardie DG, Marette A, Hundal HS (2012) Defining the contribution of AMP-activated protein kinase (AMPK) and protein kinase C (PKC) in regulation of glucose uptake by metformin in skeletal muscle cells. J Biol Chem 287(24):20088–20099. https://doi.org/10.1074/jbc.M111.330746
19. Woods A, Azzout-Marniche D, Foretz M, Stein SC, Lemarchand P, Ferre P, Foufelle F, Carling D (2000) Characterization of the role of AMP-activated protein kinase in the regulation of glucose-activated gene expression using constitutively active and dominant negative forms of the kinase. Mol Cell Biol 20 (18):6704–6711
20. Corton JM, Gillespie JG, Hawley SA, Hardie DG (1995) 5-Aminoimidazole-4-carboxamide ribonucleoside. A specific method for activating AMP-activated protein kinase in intact cells? Eur J Biochem 229(2):558–565
21. Cool B, Zinker B, Chiou W, Kifle L, Cao N, Perham M, Dickinson R, Adler A, Gagne G, Iyengar R, Zhao G, Marsh K, Kym P, Jung P, Camp HS, Frevert E (2006) Identification and characterization of a small molecule AMPK activator that treats key components of type 2 diabetes and the metabolic syndrome. Cell Metab 3(6):403–416. https://doi.org/10.1016/j.cmet.2006.05.005

22. Xiao B, Sanders MJ, Carmena D, Bright NJ, Haire LF, Underwood E, Patel BR, Heath RB, Walker PA, Hallen S, Giordanetto F, Martin SR, Carling D, Gamblin SJ (2013) Structural basis of AMPK regulation by small molecule activators. Nat Commun 4:3017. https://doi.org/10.1038/ncomms4017
23. Hunter RW, Foretz M, Bultot L, Fullerton MD, Deak M, Ross FA, Hawley SA, Shpiro N, Viollet B, Barron D, Kemp BE, Steinberg GR, Hardie DG, Sakamoto K (2014) Mechanism of action of compound-13: an alpha1-selective small molecule activator of AMPK. Chem Biol 21(7):866–879. https://doi.org/10.1016/j.chembiol.2014.05.014
24. Scott JW, Galic S, Graham KL, Foitzik R, Ling NX, Dite TA, Issa SM, Langendorf CG, Weng QP, Thomas HE, Kay TW, Birnberg NC, Steinberg GR, Kemp BE, Oakhill JS (2015) Inhibition of AMP-activated protein kinase at the allosteric drug-binding site promotes islet insulin release. Chem Biol 22(6):705–711. https://doi.org/10.1016/j.chembiol.2015.05.011
25. Zhou G, Myers R, Li Y, Chen Y, Shen X, Fenyk-Melody J, Wu M, Ventre J, Doebber T, Fujii N, Musi N, Hirshman MF, Goodyear LJ, Moller DE (2001) Role of AMP-activated protein kinase in mechanism of metformin action. J Clin Invest 108(8):1167–1174. https://doi.org/10.1172/JCI13505

Chapter 20

Investigating the Role of AMPK in Inflammation

Sarah J. Mancini and Ian P. Salt

Abstract

In addition to the well-characterized role of AMPK in the regulation of nutrient metabolism, it is increasingly clear that AMPK activation has multiple actions on inflammatory signalling. Here we describe methods to identify effects of AMPK activity on pro-inflammatory signalling, specifically (1) the nuclear localization of the key inflammatory mediators nuclear factor-κB (NFκB) and phosphorylated c-Jun N-terminal kinase (JNK), (2) preparation of conditioned medium to analyze the secretion of cytokines/chemokines, and (3) the pro-inflammatory adhesion of leukocytes to cultured cells.

Key words Inflammation, Nuclear localization, Cytokine, Conditioned medium, Monocyte adhesion

1 Introduction

Inflammatory signalling plays a key role in the development of many chronic pathological disorders, including type 2 diabetes, atherosclerosis, and cancer [1–4]. Intriguingly, AMPK has been reported to have anti-inflammatory actions, dependent and independent of its effects on nutrient metabolism [5–7]. We and others have demonstrated that AMPK activation suppresses multiple distinct pro-inflammatory signalling cascades, including the pro-inflammatory c-Jun N-terminal kinase (JNK), nuclear factor-κB (NFκB), and Janus kinase-signal transducer and activator of transcription (JAK-STAT) pathways [8–13]. Here, we describe methods to investigate the effect of AMPK activation on cultured cells subjected to pro-inflammatory stimuli. In particular, we describe methods to examine translocation of NFκB to and levels of activated JNK in the nucleus, chemokine/cytokine secretion, and adhesion of monocytes to endothelial cells. Translocation of NFκB from the cytosol to the nucleus and nuclear activation of JNK are key stages in pro-inflammatory signalling, as this process ultimately stimulates the transcription of an overlapping set of pro-inflammatory genes encoding cytokines and chemokines, thereby amplifying the inflammatory response [7, 8, 14–16]. Immunofluorescence and confocal

Dietbert Neumann and Benoit Viollet (eds.), *AMPK: Methods and Protocols*, Methods in Molecular Biology, vol. 1732, https://doi.org/10.1007/978-1-4939-7598-3_20,

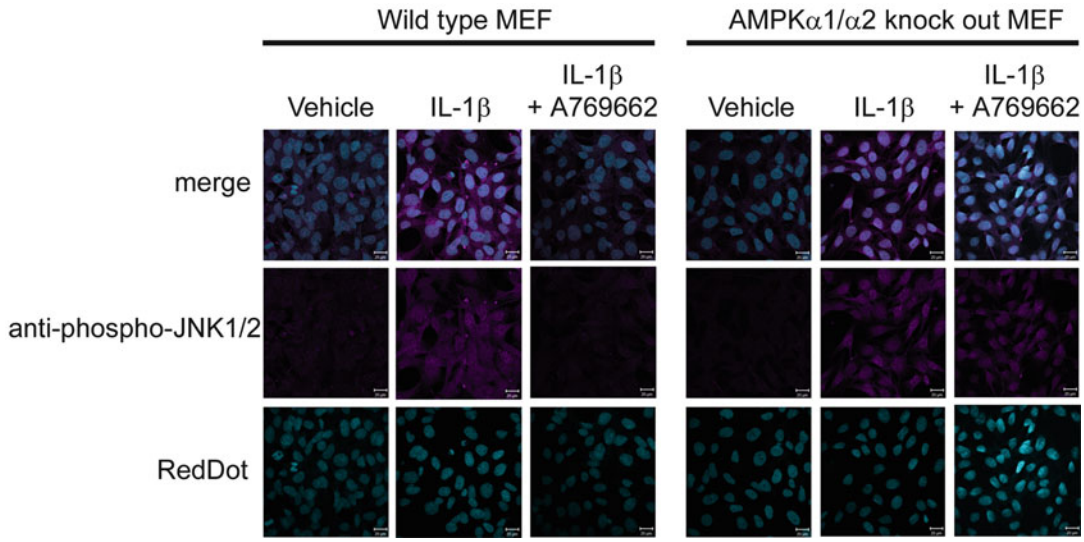

Fig. 1 Immunofluorescence images obtained following anti-phospho-JNK staining. Wild-type and AMPK-α1/α2 knockout mouse embryonic fibroblasts (MEFs) [12, 22] were incubated with IL-1β (10 ng/ml) for 15 min following preincubation for 30 min in the presence or absence of A769662 (100 μM) and stained with anti-phospho-JNK antibodies. RedDot was used to stain the nucleus

microscopy is an effective way to assess the localization of these proteins following exposure to test substances. Cells are fixed and stained with antibodies raised against the protein of interest, and its proximity to the nucleus can be evaluated by co-staining with a nuclear marker or stain (such as RedDot) (Fig. 1). This method also allows the simultaneous visualization of other proteins, which is of use when investigating cells that have been infected or transfected with viruses or DNA-encoding tagged proteins, such as constitutively active or dominant negative mutant AMPK. As a consequence, the infected/transfected cells can be specifically examined by co-staining of cells, of particular value in cells where transfection/infection efficiency is relatively poor, such as 3T3-L1 adipocytes (Fig. 2) [12].

The cytokines and chemokines produced as a result of inflammatory signalling are then secreted from the cell and can function in an autocrine, paracrine, and endocrine manner to exacerbate the pro-inflammatory environment [17, 18]. Here we describe a method to generate and collect culture medium from cells exposed to test substances. Levels of secreted proteins can then be measured quantitatively by an enzyme-linked immunosorbent assay (ELISA).

A consequence of inflammatory chemokine secretion in endothelial cells is the adhesion of monocytes, which is a key step in the infiltration of the vascular wall by leukocytes that occurs early in atherogenesis [19]. Infiltrating monocytes in the blood vessel wall differentiate to macrophages which can become further polarized toward a pro-inflammatory phenotype and avidly take up modified

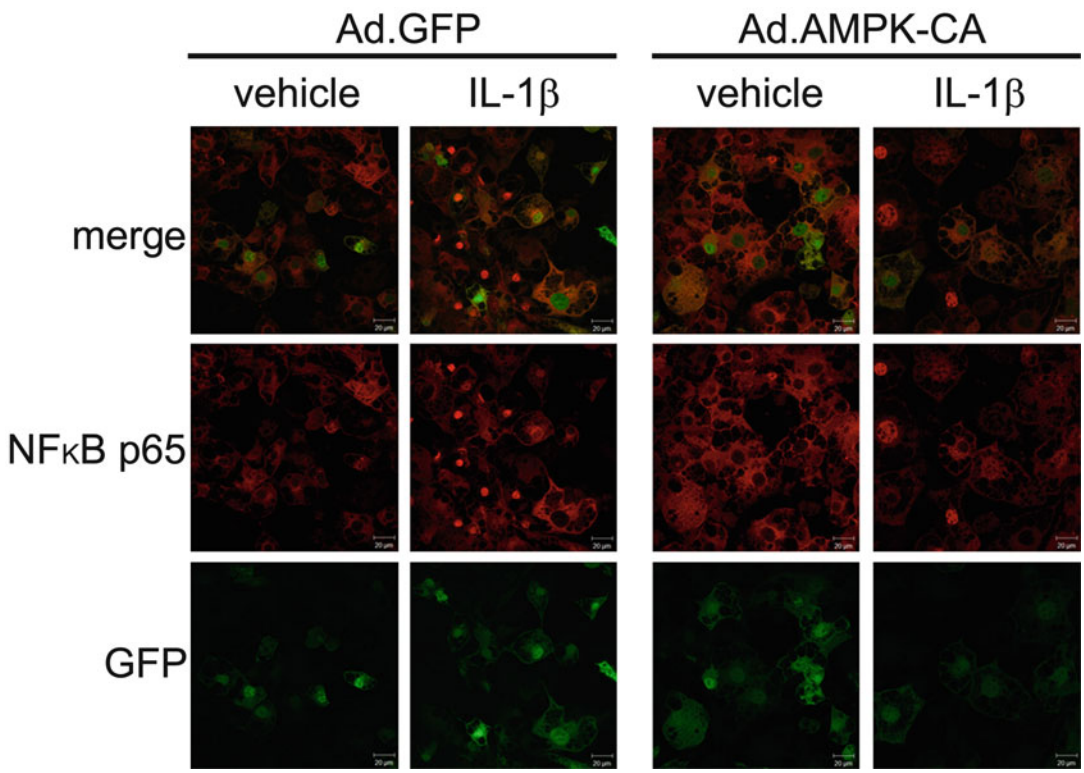

Fig. 2 NFκB nuclear localization in adipocytes overexpressing constitutively active AMPK α1. 3T3-L1 adipocytes which overexpress the coxsackievirus and adenovirus receptor (3T3-L1Δ1CAR) [12, 23] were infected with 100 pfu/cell adenoviruses expressing GFP (Ad-GFP) or constitutively active AMPK-α1 (Ad-AMPK-CA) (which expresses GFP from a separate promotor) [12, 24] for 48 h prior to stimulation with IL-1β (10 ng/ml) for 15 min. NFκB nuclear localization was assessed by confocal microscopy

LDL-cholesterol, leading to the formation of "foam cells" and development of atherosclerotic plaque [20]. The degree of monocyte adhesion in response to test substances can be evaluated in culture by exposing endothelial cells to pro-inflammatory cytokines in the presence or absence of AMPK activators, which are then washed away prior to incubation with a pro-monocytic cell line. Monocytes which are not tightly attached to the endothelial cells are then washed away, before the adherent monocytes are fixed and counted (Fig. 3). These techniques provide multiple methods with which to investigate the role of AMPK in inflammatory pathways in cultured or isolated cells.

2 Materials

AMPK activation can be achieved pharmacologically using direct activators such as A769662 and Compound 991 or the AMP-mimetic AICAR [21]. A769662 and Compound 991 are poorly soluble in aqueous solution, yet are soluble in DMSO,

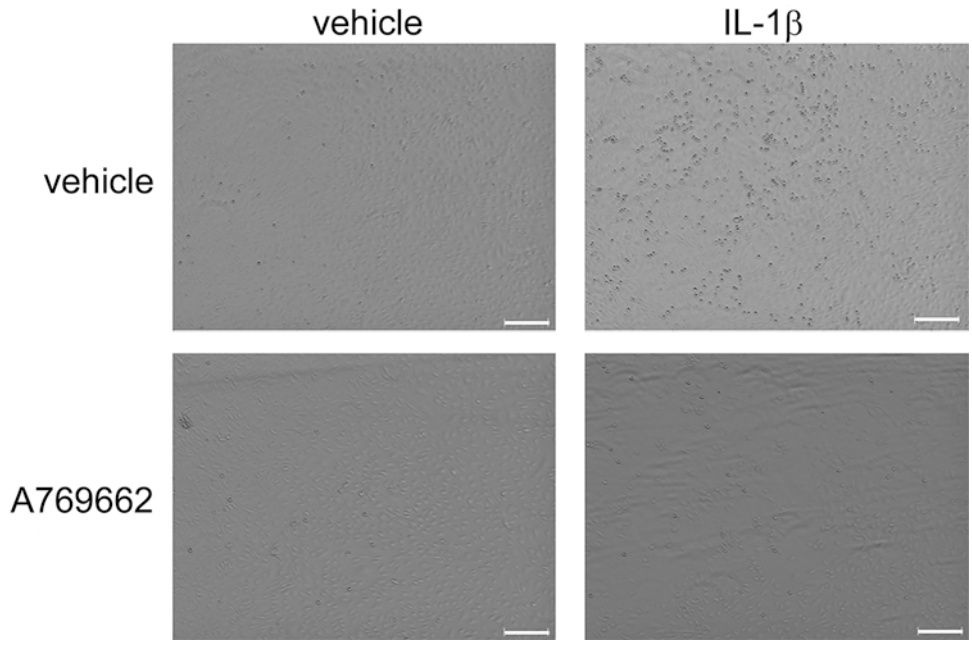

Fig. 3 A769662-mediated inhibition of U937 monocytecell adhesion to HUVECs. HUVECs were incubated with IL-1β (10 ng/ml) for 6 h following preincubation for 30 min in the presence or absence of A769662 (100 μM). Monolayers were washed prior to incubation for 1 h with U937 pro-monocytic cells (2×10^5 cells/ml). Cells were fixed and adherent monocytes visualized by microscopy. Scale bar represents 50 μm

which must be used as a vehicle control in experiments. Activation of AMPK by A769662, Compound 991, and AICAR is cell type-specific and should be optimized for particular cell types prior to use in functional experiments. Cells can be stimulated with species-specific pro-inflammatory cytokines IL-1β or TNF-α (10 ng/ml, incubation time varies depending on application). Care must be taken to follow the supplier's instructions concerning storage of pro-inflammatory cytokines, which are sensitive to freeze-thawing.

2.1 Common Materials to All Techniques

1. Human umbilical vein endothelial cells (HUVECs).
2. MV2 complete endothelial cell medium (Promocell).
3. Medium 199.
4. A769662 stock solution: 50 or 100 mM A769662 in DMSO.
5. IL-1β stock solution: 1 μg/ml human recombinant IL-1β in PBS supplemented with 0.1% (w/v) BSA.

2.2 Preparation of HUVECs for Confocal Immunofluorescence Microscopy

1. Cell culture plasticware (12-well plates).
2. 37 °C incubator (atmospheric CO_2).
3. Krebs ringer HEPES buffer (KRH): 119 mM NaCl, 20 mM HEPES-NaOH, pH 7.4, 5 mM $NaHCO_3$, 5 mM KCl, 1.2 mM $MgSO_4$, 1.2 mM NaH_2PO_4, 2.5 mM $CaCl_2$, and 5 mM

glucose. A 10× solution without $CaCl_2$ or glucose can be prepared and stored at 4 °C. $CaCl_2$ and glucose can be added to a 1× solution on day of use (*see* **Note 1**).

4. Phosphate-buffered saline (PBS).
5. PBS-glycine: PBS, 20 mM glycine.
6. PBS-PFA: PBS, 3% (w/v) paraformaldehyde (*see* **Note 2**).
7. Permeabilization buffer: PBS, 2% (w/v) BSA, 0.1% (v/v) Triton-X-100, 20 mM glycine.
8. IF buffer: PBS, 2% (w/v) BSA, 20 mM glycine, 0.1% (v/v) goat serum.
9. Whatman 3MM paper.
10. Parafilm.
11. Hooked forceps.
12. 21-Gauge needle.
13. 13 mm coverslips and microscope slides.
14. Rabbit anti-NFκB (p65) antibodies.
15. Alexa Fluor® 488-linked goat anti-rabbit antibodies.
16. RedDot far-red nuclear stain (Biotium).
17. Immunomount.
18. Confocal fluorescence microscope.

2.3 Preparation of HUVEC-Conditioned Medium for Cytokine/Chemokine Analysis

1. Cell culture plasticware (6-well plates).
2. Human IL-6 or MCP-1 ELISA kit (R&D Quantikine kits).
3. Spectrophotometer capable of measuring $A_{450/570}$ in 96-well ELISA plates.

2.4 Analysis of U937 Cell Adhesion to HUVECs

1. Cell culture plasticware (24-well plates).
2. U937 cells.
3. RPMI 1640 medium.
4. DMEM.
5. PBS-sucrose-PFA: PBS, 4% (w/v) paraformaldehyde (PFA), 5% (w/v) sucrose, pH 7.2 (*see* **Note 2**).
6. Light microscope with a 5× objective.

3 Methods

3.1 Preparation of HUVECs for Confocal Immunofluorescence Microscopy to Assess Nuclear Localization of NFκB

Here we describe methods to investigate the effect of AMPK activation on the subcellular localization of NFκB p65. The method varies slightly depending on cell type. The method described below has been successfully utilized in HUVECs, while the alternative steps required for fixing and staining mouse embryonic fibroblasts

or 3T3-L1 adipocytes and localizing phosphorylated JNK are found in the Subheading 4.

1. Grow cells to confluence on 13 mm diameter coverslips set inside 12-well plates (two coverslips per condition, plus an extra two coverslips which will become the secondary antibody only control).
2. On the day of the experiment, wash cells with serum-free Medium 199 (0.5 ml/well) (*see* **Notes 3** and **4**).
3. Return plates to 37 °C incubator in appropriate CO_2 atmosphere and starve for 2 h.
4. After 2 h, remove plates from incubator, aspirate serum-free Medium 199, and add 0.5 ml/well KRH buffer. Aspirate and replace with another 0.5 ml/well KRH buffer. Transfer plates to a 37 °C incubator at atmospheric CO_2 and incubate for approximately 30 min (*see* **Note 5**).
5. Add pharmacological AMPK activator (A769662 at final concentration of 100 μM. 1 μl of 50 mM stock/well (*see* **Note 6**)) or equivalent volume of DMSO to control wells (*see* **Note 7**).
6. Return plate(s) to incubator.
7. After 30 min incubation with A769662, remove plate from incubator and add pro-inflammatory cytokine (IL-1β at final concentration of 10 ng/ml—5 μl per well of 1 μg/ml stock) to appropriate wells.
8. Return plate(s) to incubator and incubate for 15 min.
9. At the end of the assay, remove plate(s) from incubator, aspirate, and wash cells with PBS.
10. Fix cells for 25 min at room temperature in PBS-PFA (400 μl/well) (*see* **Note 8**).
11. Aspirate PBS-PFA and quench remaining PFA by washing each well twice with PBS-glycine (0.5 ml/well), followed by two washes with PBS (0.5 ml/well).
12. Lift coverslips into clean 12 well plate(s) containing 0.5 ml/well of PBS using hooked forceps and a needle (*see* **Notes 9** and **10**).
13. Permeabilize cells with 400 μl/well of permeabilization buffer for 10 min (*see* **Note 11**).
14. Aspirate permeabilization buffer and wash with PBS.
15. Block nonspecific binding sites with 400 μl/well of IF buffer (*see* **Note 12**) for 20 min.
16. Cut a section of Whatman 3MM paper, dampen with water, and smooth out on bench (*see* **Note 13**). Lay out strip of parafilm on top, smoothing out.

17. Spot 35 μl of rabbit anti-NFκB (p65) antibodies diluted 1:50 in IF buffer for each coverslip onto parafilm (*see* **Notes 14** and **15**). Do this using a reverse pipetting technique (*see* **Note 16**). Leave the secondary antibody only control coverslips in the plate.
18. Using hooked forceps and needle, remove coverslip from well, dab edge gently on tissue to remove excess liquid, and lay it over the drop of primary antibody (cell-side down) so that the drop is sandwiched between the cells on the coverslip and the parafilm (*see* **Note 17**).
19. Repeat for all coverslips and cover them all with a box/tub (*see* **Note 18**) and incubate for 1 h.
20. Using hooked forceps and needle, move each coverslip back into the 12-well plate so that the cells are facing upward.
21. Wash four times with 400 μl/well of IF buffer.
22. Spot 35 μl of Alexa Fluor® 488-conjugated goat anti-rabbit IgG antibodies and RedDot (both diluted 1:200 (*see* **Note 19**) in IF buffer) per coverslip onto parafilm as described in **step 17**. This should now include the secondary antibody only control coverslips.
23. Transfer coverslips to secondary antibody droplets as described in **steps 18** and **19**.
24. Incubate for 30 min in the dark under a box/tub.
25. Using hooked forceps and needle, move each coverslip back into the 12-well plate so that the cells are facing upward.
26. Repeat wash **step 21**.
27. Add a drop of Immunomount for each coverslip onto a microscope slide (*see* **Note 20**). Using hooked forceps and needle, remove coverslip from plate and dip in PBS. Dab the edge of coverslip and the side lacking cells on a tissue to absorb excess PBS and gently lay each coverslip cell-side down on a drop of Immunomount.
28. Keep coverslips on slides flat, dark and undisturbed overnight, before transferring to a slide box.
29. Visualize with a 63× oil objective and the relevant filter by fluorescence confocal microscopy.
30. Nuclear fluorescence in the resultant images can be quantified using ImageJ software to obtain values corresponding to the density of multiple points within the nucleus. These data can be used to assess the mean density of nuclear fluorescence per cell. A minimum of 50 cells should be analyzed per treatment, and the mean fluorescence taken.

3.2 Preparation of Conditioned Medium from Endothelial Cells for the Analysis of Cytokine and Chemokine Secretion

1. Grow human endothelial cells to confluence in 6-well plates—1-well per condition.
2. On the day of the experiment, wash cells into serum-free Medium 199 (1 ml/well) (*see* **Note 3**).
3. Add pharmacological AMPK activator (A769662 at final concentration of 100 μM. 1 μl of 100 mM stock/well (*see* **Note 6**)) or equivalent volume of DMSO to control wells (*see* **Note 7**).
4. Return plate(s) to 37 °C incubator in atmosphere of CO_2.
5. After 30 min incubation with A769662, remove plate(s) from the incubator and add pro-inflammatory cytokine (IL-1β at final concentration of 10 ng/ml—10 μl per well of 1 μg/ml stock) to appropriate wells.
6. Return plate(s) to incubator and incubate for 6 h.
7. Remove plate(s) from the incubator and immediately transfer culture medium to 1.5 ml centrifuge tubes (*see* **Note 21**).
8. Centrifuge conditioned medium at 3130 × *g* for 20 min at 4 °C to pellet any cell debris. Transfer samples to clean 1.5 ml centrifuge tubes and store at −20 °C.
9. Analyze MCP-1 levels by ELISA. We have obtained good results using the R&D Quantikine kits for MCP-1 or IL-6. We carried out the procedure as follows.
10. Optimize the dilution of conditioned medium required to achieve values within the linear range of the standard curve provided in the kit (*see* **Note 22**).
11. Add 200 μl of standard or sample (diluted as necessary) per well in duplicate and incubate for 2 h at room temperature on a vibrating platform at 200 rpm.
12. Aspirate each well and wash (400 μl/well) three times (*see* **Note 23**).
13. Add 200 μl of MCP-1 conjugate to each well and incubate at room temperature for 1 h on a vibrating platform as described in **step 11**.
14. Repeat the aspiration and wash as in **step 12**.
15. Add 200 μl of "substrate solution" mix to each well. Incubate for 30 min at room temperature (not on shaking platform). Protect plate from light.
16. Add 50 μl of "stop solution" to each well (*see* **Note 24**).
17. Assess the optical density of each well using a microplate reader set to 450 nm (*see* **Note 25**) with wavelength correction set to 540 or 570 nm (if available). If wavelength correction is not available, subtract values obtained at 540/570 nm away from those obtained at 450 nm (*see* **Note 26**).

3.3 Monocyte Adhesion Assay

1. Grow endothelial cells to confluence on 24-well plates—4-wells per condition to give four technical replicates.
2. Grow U937 monocytes in T150 flasks, maintaining a density of 1–2 $\times$ 10^5 cells/ml (*see* **Note 27**).
3. On the day of the experiment, aspirate endothelial cell medium and replace with 0.5 ml/well of fresh medium.
4. Add pharmacological AMPK activator (A769662 at final concentration of 100 μM. 1 μl of 50 mM stock/well (*see* **Note 6**)) or equivalent volume of DMSO to control wells (*see* **Note 7**) and return to a CO_2 incubator at 37 °C.
5. After 30 min incubation with A769662, remove plate from the incubator and add pro-inflammatory cytokine (IL-1β at final concentration of 10 ng/ml—5 μl of 1 μg/ml) to appropriate wells.
6. Return plate(s) to a CO_2 incubator at 37 °C and incubate for 6 h.
7. Wash U937 pro-monocytic cells into serum-free RPMI 1640 medium and resuspend at a concentration of 2 $\times$ 10^5 U937 cells/ml. Do this half an hour before **step 8**.
8. Aspirate medium from endothelial cells and wash monolayers three times with 0.5 ml/well of serum-free RPMI 1640 prior to overlay with 1 $\times$ 10^5 U937 cells/well (0.5 ml per well of 24-well plate) (*see* **Note 28**).
9. Allow cells to adhere for 1 h at 37 °C in a CO_2 incubator, aspirate the medium, and wash monolayers three times with 1 ml/well serum-free DMEM to remove any nonadherent U937 cells (*see* **Note 29**).
10. Fix cells for 25 min at room temperature in PBS-sucrose-PFA (400 μl/well) (*see* **Note 30**).
11. Aspirate PBS-sucrose-PFA and quench remaining PFA by washing each well twice with PBS-glycine (0.5 ml/well), followed by two washes with PBS (0.5 ml/well).
12. Count the number of adhered U937 cells per field of confluent ECs (at least two fields per well) on a light microscope with a 5× objective. Plates can be stored at 4 °C prior to analysis, if preferred.

4 Notes

1. Add dilute NaOH dropwise when adjusting the pH of the working solution, as rapid changes in pH can cause the calcium to precipitate. If this happens, the buffer will become cloudy and should be discarded.

2. Paraformaldehyde is a carcinogen, therefore gloves and a mask should be worn when preparing this solution.
3. Removing serum in this way places cells into a quiescent state, thereby reducing background signalling. In the case of HUVECs and 3T3-L1 adipocytes, cells should not be quiesced for any longer than 7 h, as significant apoptosis occurs after this time.
4. Use serum-free DMEM when quiescing fibroblasts and adipocytes.
5. KRH is a simple buffer that reduces background signalling even further and abrogates the need for an incubation in a CO_2 atmosphere. It is important to let cells adjust to this transition to another buffer prior to adding test substances. This step can be omitted and experiments continued until **step 9** if required, although all incubations in **steps 1–8** would need to occur in a CO_2 incubator.
6. Add the smallest volume of a concentrated stock that is feasible, thereby minimizing the volume of DMSO being added.
7. It is not essential that the test substances such as IL-1β, DMSO, and A769662 are sterile; however, any steps involving washing with Medium 199 or DMEM should be performed in a cell culture hood so as not to contaminate the medium for future use. Using a repeat pipette when adding compounds/cytokines will also improve speed and accuracy.
8. In the case of 3T3-L1 adipocytes, fix for 30 min.
9. Take a 21 G needle, and bend the very tip using a pair of forceps. This, in combination with fine hooked forceps (i.e., one in each hand), allows you to easily maneuver the coverslip in and out of the plate.
10. Fixed cells can be stored at 4 °C in 0.5 ml/well PBS at this point, or the protocol can be continued as described from **step 13**.
11. For 3T3-L1 adipocytes, simultaneously permeabilize and block cells in 400 μl/well of PBS supplemented with 2% (w/v) BSA, 0.1% (w/v) Saponin and 20 mM glycine for 20 min. Adipocytes have cholesterol-rich membranes; therefore saponin is an effective detergent to permeabilize membranes as it selectively removes cholesterol. After this, go to **step 16** and follow the protocol from there.
12. The serum used to block nonspecific interactions should be from the animal the secondary antibody is raised in. If using multiple antibodies for co-staining, ensure that no unintentional cross-reactions can occur between primary and secondary antibodies.

13. The water provides a humid environment for the coverslips when they are being incubated with primary/secondary antibody, thus ensuring they do not dry out.
14. We used rabbit anti-NFκB (p65) (#8242 from Cell Signaling Technologies). If assessing phospho-JNK localization, use mouse anti-phospho-JNK1/2 (#9255 from Cell Signaling Technologies works well) diluted 1:400 in IF buffer.
15. When pipetting antibody ensure that enough space is left between replicates/samples so that they do not end up merging together.
16. Reverse pipetting consists of pushing the pipette plunger down to the second stop, drawing up desired volume, and dispensing liquid by depressing pipette plunger down to the first stop. The purpose of this is to reduce the risk of bubbles which would affect exposure of coverslip to antibody.
17. Incubating coverslips in this way dramatically reduces the volume of antibody required, compared with performing incubations in the well. In the event that there is not even coverage of the coverslip surface, pick the coverslip up and gently wipe away the liquid from the parafilm using tissue. Pipette another droplet of antibody and try again. It is important that you pipette the antibody onto dry parafilm; otherwise it is less likely to sit as a neat drop.
18. Covering in this way helps maintain a humid environment for the coverslips. Cover a box or tub in tinfoil so it can function to protect coverslips from light while incubating in fluorescent secondary antibody.
19. We used Alexa Fluor® 488-linked goat anti-rabbit antibodies. If using mouse anti-phospho-JNK1/2 antibodies as the primary antibody, use Alexa Fluor® conjugated goat anti-mouse IgG as a secondary antibody (Invitrogen, Life Technologies Ltd).
20. Try to minimize the presence of bubbles when spotting mounting agent. Only spot the mounting agent on one or two microscope slides at a time to prevent it drying out before the coverslip is placed over it. Two or three spots of mounting agent and therefore two or three coverslips can be mounted on each slide.
21. The protocol describes collection of simple conditioned media which can be used for ELISA or multiple cytokine analysis, as we have described previously [12]. If that conditioned media are intended to be collected and used to examine the influence of secreted cytokines/chemokines on the behavior of other cells, it is important to ensure that AMPK activators and pro-inflammatory stimuli are washed away such that those

cells are not exposed directly to them. In that case, after washing, the conditioned medium can be collected over an hour and used to examine cell function, as we have previously described for U937 cell migration toward conditioned medium [9].

22. For HUVECs we find a dilution of 1:40 in calibrator diluent RD5L is necessary.
23. Make sure to aspirate the samples entirely using a water/pump-powered aspirator if available. The first two washes can be discarded simply by inverting the plate over a tub or sink and giving a shake. The final wash should be aspirated entirely and the plate blotted against paper towels.
24. This should be added to wells in the same order as the substrate solution was added. The color should change from blue to yellow upon addition of the "stop solution." If the color appears greenish in some wells, use a 200 μl pipette to gently mix. Be sure to change the tip if mixing multiple wells.
25. A wavelength of 485 nm is also adequate if 450 nm is not possible.
26. This is to account for optical imperfections in the plate.
27. U937 cells are grown in suspension, so agitate flask while dispensing cells to ensure they are thoroughly mixed.
28. Washing ensures U937 cells are not exposed to test substances, ensuring observed effects are mediated by ECs and not due to direct actions of pro-inflammatory stimuli or AMPK activators on U937 function.
29. Wash monolayer gently—use a larger pipette for less force, e.g., a 25 ml pipette—and trickle down the side of the well.
30. The presence of sucrose is essential to prevent osmotic lysis of monocytes.

References

1. Nunemaker CS (2016) Considerations for defining cytokine dose, duration, and milieu that are appropriate for modeling chronic low-grade inflammation in type 2 diabetes. J Diabetes Res 2016:2846570
2. Sansbury BE, Spite M (2016) Resolution of acute inflammation and the role of resolvins in immunity, thrombosis, and vascular biology. Circ Res 119:113–120
3. Libby P, Nahrendorf M, Swirski FK (2016) Leukocytes link local and systemic inflammation in ischemic cardiovascular disease: an expanded "cardiovascular continuum". J Am Coll Cardiol 67:1091–1103
4. Musolino C, Allegra A, Pioggia G, Gangemi S (2017) Immature myeloid-derived suppressor cells: a bridge between inflammation and cancer (Review). Oncol Rep 37:671–683
5. Antonioli L, Colucci R, Pellegrini C et al (2016) The AMPK enzyme-complex: from the regulation of cellular energy homeostasis to a possible new molecular target in the management of chronic inflammatory disorders. Expert Opin Ther Targets 20:179–191
6. Steinberg GR, Schertzer JD (2014) AMPK promotes macrophage fatty acid oxidative metabolism to mitigate inflammation: implications for diabetes and cardiovascular disease. Immunol Cell Biol 92:340–345
7. Salt IP, Palmer TM (2012) Exploiting the anti-inflammatory effects of AMP-activated protein

kinase activation. Expert Opin Investig Drugs 21:1155–1167

8. Bess E, Fisslthaler B, Fromel T, Fleming I (2011) Nitric oxide-induced activation of the AMP-activated protein kinase alpha2 subunit attenuates IkappaB kinase activity and inflammatory responses in endothelial cells. PLoS One 6:e20848
9. Rutherford C, Speirs C, Williams JJ et al (2016) Phosphorylation of Janus kinase 1 (JAK1) by AMP-activated protein kinase (AMPK) links energy sensing to anti-inflammatory signaling. Sci Signal 9:ra109
10. Zhang Y, Qiu J, Wang X, Xia M (2011) AMP-activated protein kinase suppresses endothelial cell inflammation through phosphorylation of transcriptional coactivator p300. Arterioscler Thromb Vasc Biol 31:2897–2908
11. Schulz E, Dopheide J, Schuhmacher S et al (2008) Suppression of the JNK pathway by induction of a metabolic stress response prevents vascular injury and dysfunction. Circulation 118:1347–1357
12. Mancini SJ, White AD, Bijland S et al (2017) Activation of AMP-activated protein kinase rapidly suppresses multiple pro-inflammatory pathways in adipocytes including IL-1 receptor-associated kinase-4 phosphorylation. Mol Cell Endocrinol 440:44–56
13. He C, Li H, Viollet B et al (2015) AMPK suppresses vascular inflammation in vivo by inhibiting Signal Transducer and Activator of Transcription-1. Diabetes 64:4285–4297
14. Guma M, Firestein GS (2012) C-Jun N-terminal kinase in inflammation and rheumatic diseases. Open Rheumatol J 6:220–231
15. Pal M, Febbraio MA, Lancaster GI (2016) The roles of c-Jun NH2-terminal kinases (JNKs) in obesity and insulin resistance. J Physiol 594:267–279
16. Zehorai E, Seger R (2014) Beta-like Importins mediate the nuclear translocation of mitogen-activated protein kinases. Mol Cell Biol 34:259–270
17. Griffith JW, Sokol CL, Luster AD (2014) Chemokines and chemokine receptors: positioning cells for host defense and immunity. Annu Rev Immunol 32:659–702
18. Newton K, Dixit VM (2012) Signaling in innate immunity and inflammation. Cold Spring Harb Perspect Biol 4(3). pii: a006049
19. Gerhardt T, Ley K (2015) Monocyte trafficking across the vessel wall. Cardiovasc Res 107:321–330
20. Tabas I, Bornfeldt KE (2016) Macrophage phenotype and function in different stages of atherosclerosis. Circ Res 118:653–667
21. Bultot L, Jensen TE, Lai YC et al (2016) Benzimidazole derivative small-molecule 991 enhances AMPK activity and glucose uptake induced by AICAR or contraction in skeletal muscle. Am J Physiol Endocrinol Metab 311:E706–E719
22. Laderoute KR, Amin K, Calaoagan JM et al (2006) 5′-AMP-activated protein kinase (AMPK) is induced by low oxygen and glucose deprivation conditions found in solid-tumor microenvironments. Mol Cell Biol 26:5336–5347
23. Ross SA, Song X, Burney MW et al (2003) Efficient adenovirus transduction of 3T3-L1 adipocytes stably expressing coxsackie-adenovirus receptor. Biochem Biophys Res Commun 302:354–358
24. Woods A, Azzout-Marniche D, Foretz M et al (2000) Characterization of the role of AMP-activated protein kinase in the regulation of glucose-activated gene expression using constitutively active and dominant negative forms of the kinase. Mol Cell Biol 20:6704–6711

Chapter 21

Studying the Role of AMPK in Cardiac Hypertrophy and Protein Synthesis

Florence Mailleux, Christophe Beauloye, Jean-Luc Balligand, Sandrine Horman, and Luc Bertrand

Abstract

Pathological cardiac hypertrophy, which is a compensatory mechanism established to maintain cardiac function in response to neurohormonal or mechanical stresses, becomes maladaptive with time and frequently leads to heart failure. AMP-activated protein kinase (AMPK) has been extensively described in the literature to act as a break in cardiac hypertrophy development. Its anti-hypertrophic action mostly correlates with the inhibition of several important players of cardiac hypertrophy including protein synthesis and pro-hypertrophic gene expression pathways involving the transcription factor nuclear factor of activated T cells (NFAT) and the mitogen-activated protein kinases ERK1/2. In this chapter, we describe methodologies designed to evaluate cardiomyocyte hypertrophy and its major molecular mechanisms in response to AMPK activation. Two different compounds, AICAr and the biguanide phenformin, were used to promote AMPK activation.

Key words AICAr, AMP-activated protein kinase, Cardiac hypertrophy, eEF2, ERK1/2, NFAT, p70S6K, Phenformin, Protein synthesis

1 Introduction

Cardiac AMP-activated protein kinase (AMPK) has been firstly described to act as a cellular fuel gauge which senses energetic disequilibrium occurring under metabolic stress such as myocardial ischemia [1]. The reduction in substrate and oxygen supply occurring during such circumstances induces the increase in AMP concentration responsible for AMPK activation. Once activated, AMPK protects the ischemic cardiomyocytes by activating energy producing pathways including glycolysis and by inhibiting various anabolic pathways such as protein synthesis [2–5]. However, it is commonly accepted today that AMPK action extends beyond metabolism. Indeed, AMPK can be activated, independently of AMP, by a rise in calcium concentration, and there is an increasing number of AMPK substrates more recently discovered and

Dietbert Neumann and Benoit Viollet (eds.), *AMPK: Methods and Protocols*, Methods in Molecular Biology, vol. 1732, https://doi.org/10.1007/978-1-4939-7598-3_21,

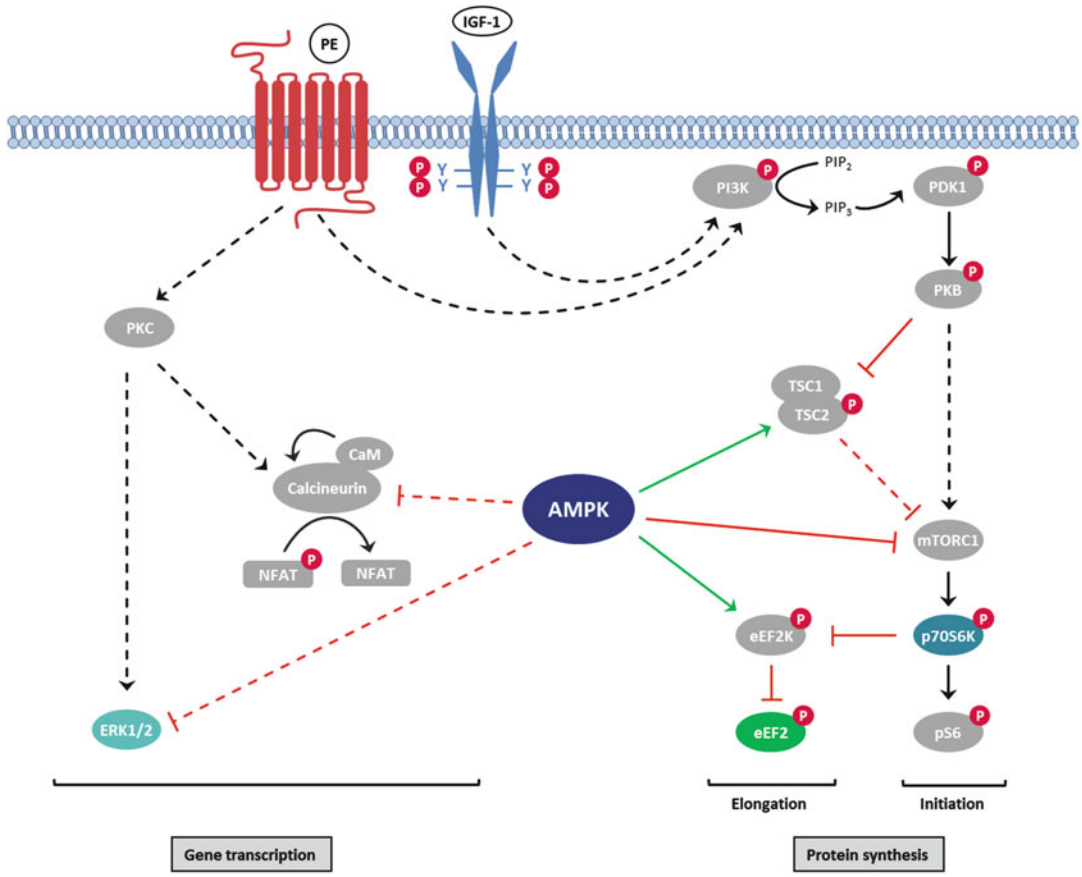

Fig. 1 AMPK activation inhibits different signaling pathways involved in cardiac hypertrophy. This scheme represents the four main pathways involved in hypertrophy development. They comprise the ERK1/2 and NFAT pathways involved in the stimulation of transcription of pro-hypertrophic genes (*left part*) and the p70S6K and eEF2 pathways involved in the stimulation of protein synthesis (*right part*). AMPK inhibits these four pathways (*see* text for more details). *Dashed lines* indicate indirect activation or inhibition. Abbreviations: *CaM* calmodulin, *IGF-1* insulin-like growth factor-1, *PDK1* phosphoinositide-dependent kinase-1, *PE* phenylpehrine, *PI3K* phosphatidylinositol-3-kinase, PIP_2 phosphatidylinositol 4,5-bisphosphate, PIP_3 phosphatidylinositol 3,4,5-triphosphate, *PKB* protein kinase B, *PKC* protein kinase C, *pS6* ribosomal protein S6

unrelated to metabolic issues [2, 3, 6]. Historically, the first connection between AMPK and protein synthesis has been established in hepatocytes [7, 8]. These studies demonstrated an AMPK-mediated reduction of protein translation correlating to the inhibition of two of its important signaling regulators, the p70 ribosomal S6 protein kinase (p70S6K) and the eukaryotic elongation factor-2 (eEF2), involved in the pre-initiation and elongation steps of protein formation, respectively (Fig. 1). The precise molecular mechanism linking AMPK to these elements has been deciphered later and implicates several AMPK substrates. First, AMPK phosphorylates and activates the eEF2 kinase (eEF2K) responsible for eEF2 inactivation [7, 9, 10] (Fig. 1). Second, AMPK inhibits

p70S6K via the inhibition of its upstream kinase, the mammalian target of rapamycin (mTOR) in its hetero-multimeric protein complex called mTOR complex 1 (mTORC1) via a dual mechanism. AMPK phosphorylates and activates the tuberous sclerosis complex 2 (TSC2) [11] (Fig. 1). TSC2 is the GTPase-activating protein of the small G protein Rheb involved in mTORC1 activation. TSC2 activation results in Rheb inactivation and subsequent mTORC1 inactivation. AMPK also phosphorylates the mTOR binding partner raptor inducing mTORC1 inhibition [12] (Fig. 1). Both eEF2 and p70S6K have been proved to be regulated downstream of AMPK in the heart [13, 14].

In line with its inhibitory action on protein synthesis via eEF2 and mTOR/p70S6K, AMPK has been rapidly proposed to be a potent inhibitor of cardiac hypertrophy. In agreement, several studies indicate that AMPK activation blocked cardiomyocyte hypertrophy and, in the same time, inhibited protein synthesis as well as its regulators p70S6K and eEF2 [15, 16]. In addition, AMPK activation also correlated to the inhibition of other important players of cardiac hypertrophy including pro-hypertrophic gene expression pathways involving the transcription factor nuclear factor of activated T cells (NFAT) and the mitogen-activated protein kinases ERK1/2 [15, 17, 18] (Fig. 1).

We describe in this chapter the main experimental procedures employed to investigate protein synthesis, cardiomyocyte hypertrophy development, and their molecular markers (detailed above) in line with AMPK activation in a cellular model, the hypertrophied neonatal rat cardiomyocyte in primary culture [19]. Cardiomyocyte hypertrophy is induced by treatment with the pro-hypertrophic stimulus phenylephrine (PE) [20]. AMPK activation is achieved by using AICAr, which is metabolized into ZMP (an AMP analog), or the biguanide phenformin, which increases intracellular AMP concentration by inhibiting mitochondrial complex 1.

2 Materials

2.1 Isolation and Culture of Neonatal Rat Ventricular Cardiomyocytes for Protein Synthesis and Signaling Analysis

Trypsin digestion of neonatal hearts

1. Hank's balanced salt solution (HBSS) without Ca^{++} and Mg^{++}, with phenol red (Lonza Formulation: KCl (400 mg/L), KH_2PO_4 (60 mg/L), NaCl (8000 mg/L), $NaHCO_3$ (350 mg/L), $NaH_2PO_4{\cdot}7H_2O$ (90 mg/L), glucose (1000 mg/L)). Store at room temperature.
2. Trypsin (stored at 4 °C) (*see* **Note 1**).
3. Two petri dishes.
4. Cleaned scissors with ethanol.
5. Neonatal rats aged from 0- to 3-day-old.

Collagenase type II digestion

6. Full IMDM medium: Iscove's modified Dulbecco's medium (IMDM), 10% (v/v) FBS, 2% (v/v) penicillin/streptomycin. Warm full medium at 37 °C before use.
7. Collagenase type II solution: 0.5 g/L collagenase type II in IMDM medium (*see* **Note 2**).
8. Stirring water bath.
9. 0.2 μm filter.

Cardiomyocyte purification by Percoll gradient

10. 36% (v/v) Percoll (GE Healthcare) in IMDM medium: Mix 11.25 ml of Percoll gradient solution and 1 ml of sterile NaCl (1.5 M). Use 7.8 ml of this mix and add 12.2 ml of warm IMDM medium. Mix slowly and divide the solution into two fractions of 10 ml in 50 ml tube.

Red blood cell lysis

11. Red blood cell (RBC) lysis buffer: 160 mM NH_4Cl, 1 mM EDTA, 10 mM $KHCO_3$ in sterile water. Filter the solution (*see* **Note 3**).
12. 0.2 μm filter.

Dish coating

13. Gelatin: 0.2% gelatin in sterile water (pre-warmed at 37 °C).
14. Cell culture dishes: 3 cm diameter (9.6 cm^2).

Cell counting

15. Burker chamber.
16. Trypan blue.

Cell plating

17. CO_2 incubator: Set to 5% CO_2 and 37 °C.

2.2 Evaluation of Protein Synthesis in Cardiomyocytes During Hypertrophic Treatment

Cardiomyocyte treatments

1. Cultured neonatal cardiomyocytes (750,000 cells per well of 9.6 cm^2).
2. ^{14}C-labeled L-phenylalanine (487 mCi/mmol, PerkinElmer).
3. Phenylephrine (PE) stock solution: 20 mM phenylephrine in H_2O.
4. Phenformin stock solution: 20 mM phenformin in H_2O.
5. AICAr stock solution: 20 mM AICAr in H_2O.
6. Full IMDM medium (*see* Subheading 2.1, **item 6**).
7. IMDM medium without serum: IMDM, 2% (v/v) penicillin/streptomycin (pre-warmed at 37 °C).

Cell harvest

8. 1× phosphate buffer saline (PBS): 138 mM NaCl, 2.7 mM KCl, 1.47 mM KH_2PO_4, 8 mM Na_2HPO_4, pH 7.
9. Cell scraper.
10. Lysis buffer: 50 mM HEPES, pH 7.5, 50 mM KF, 1 mM KPi, 5 mM EDTA, 5 mM EGTA, 5 mM β-mercaptoethanol, 1 mM vanadate, standard protease inhibitor mixture (complete mini, Roche), 1% (v/v) Triton X-100 (*see* **Note 4**).
11. Protein assay kit (Lowry test, e.g., available from BIO-RAD).
12. 96-Well plate (with transparent bottom).

Evaluation of radioactive L-phenylalanine incorporation into proteins

13. Cold trichloroacetic acid (TCA): 100% (w/v) trichloroacetic acid in H_2O.
14. Cold NaOH: 100 mM NaOH.
15. Cold TCA: 5% (v/v) TCA in H_2O.
16. Formic acid: 26.5 M formic acid (store at room temperature).
17. Scintillation liquid (e.g., Ultima Gold, PerkinElmer) (store at room temperature).
18. 20 ml vials for scintillation counter.
19. Scintillation counter.

2.3 Evaluation of p70S6K and eEF2 Signaling Pathway

SDS polyacrylamide gel electrophoresis (SDS PAGE)

1. Sodium dodecyl sulfate (SDS): 5% (w/v) SDS in H_2O.
2. Running gel buffer: 1 M Tris–HCl, pH 8.8.
3. Stacking gel buffer: 0.25 M Tris–HCl, pH 6.8.
4. Acrylamide/bisacrylamide solution: 30% acrylamide/ bisacrylamide (37.5:1 ratio).
5. Ammonium persulfate (APS): 10% (w/v) APS in H_2O (store for long term at −20 °C).
6. *N*,*N*,*N*,*N*′-Tetramethylethylenediamine (TEMED, store at 4 °C).
7. Electrophoresis buffer: 25 mM Tris, 192 mM glycine, 0.1% (w/v), SDS.
8. 4× loading buffer: 200 mM Tris–HCl, pH 6.8, 40% (v/v) glycerol, 8% (w/v) SDS, 0.04% (w/v) bromophenol blue, 25% (v/v) β-mercaptoethanol.
9. Molecular weight markers: PageRuler Prestained Protein Ladder.

Immunoblotting

10. Blotting buffer: 25 mM Tris–HCl, 192 mM glycine.
11. Polyvinylidene fluoride (PVDF) membrane: 0.45 μm pore size.

12. Blotting paper.
13. Tris-buffered saline (TBS): 50 mM Tris–HCl (pH 8), 150 mM NaCl.
14. TBS-T: TBS, 0.1% (v/v) Tween 20.
15. Blocking solution/antibody diluent solution: TBS-T, 5% (w/v) BSA.
16. Stirring plate.
17. ECL substrate solution (e.g., BM chemiluminescence blotting substrate POD, SIGMA). Prepare 30 ml of luminescence substrate solution A with 300 µl of starting solution B.
18. Films: FUJI Super RX 18x24 500 E.
19. Developer buffer: Kodak® X-Ray GBX.
20. Fixator buffer: Kodak® X-Ray GBX.
21. ImageJ software (National Institute of Health, Bethesda).

Antibodies

22. Anti-p70S6K (Cell signaling, 9202): for IB 1:1000 in TBS-T, 5% (w/v) BSA.
23. Anti-p70S6K Thr389 (Cell signaling, 9234): for IB 1:1000 in TBS-T, 5% (w/v) BSA.
24. Anti-eEF2 (Thermo scientific, PA5-17794): for IB 1:1000 in TBS-T, 5% (w/v) BSA.
25. Anti-eEF2 Thr56 (Cell signaling, 2331): for IB 1:2000 in TBS-T, 5% (w/v) BSA.
26. Anti-GAPDH (Cell signaling, 2118): for IB 1:50,000 in TBS-T, 5% (w/v) BSA.
27. Goat anti-rabbit IgG HRP-conjugated (Sigma, A0545): for IB 1:20,000 in TBS-T, 5% (w/v) BSA.

2.4 Evaluation of Cardiomyocyte Hypertrophy by α-Actinin Immunostaining

Cell plating

1. Microscope cover glasses, 12 mm diameter.
2. Gelatin: 0.2% gelatin in sterile water (pre-warmed at 37 °C).
3. Cell culture dishes: 3 cm diameter (9.6 cm^2).
4. Ethanol.
5. 1× PBS.

Cell treatments

6. PE, phenformin and AICAr (as described in Subheading 2.2, **items 3**–**5**).
7. Full IMDM medium (as described in Subheading 2.2, **item 6**).
8. IMDM medium without serum (as described in Subheading 2.2, **item 7**).

9. CO_2 Incubator.

Cell fixation

10. 1× PBS.
11. Paraformaldehyde (PFA): 4% (w/v) PFA, 0.2% (w/v) Triton X-100.

α-Actinin immunostaining

12. Microscope slides.
13. Dako pen for immunohistochemistry.
14. PBS/BSA solutions: PBS, 1% (w/v) BSA and PBS, 0.1% (w/v) BSA.
15. Mouse anti-α-actinin antibody (Sigma, A7811): for immunostaining 1:750 in 1× PBS, 1% (w/v) BSA.
16. Alexa Fluor 594 donkey anti-mouse antibody (Invitrogen, A21203): for immunostaining 1:1000 in 1× PBS, 1% (w/v) BSA.
17. Vectashield mounting medium with 1.5 μg/ml of 4′,6-Diamidine-2′-phenylindole dihydrochloride (DAPI).
18. Structured illumination fluorescent microscope.
19. AxioVision 4.8 (or similar) software.

2.5 Evaluation of NFAT Transcriptional Activity

Cell infection and treatment

1. Cultured neonatal cardiomyocytes (700,000 cells per well).
2. Full IMDM medium (as described in Subheading 2.2, **item 6**).
3. IMDM medium without serum (as described in Subheading 2.2, **item 7**).
4. NFAT/luciferase adenoviral construction: Ad5-NFAT-luciferase reporter (Seven Hills Bioreagents, JMAd-10) [15]. Store at −80 °C (*see* **Note 5**).
5. β-Galactosidase adenoviral construction (used as control). Store at −80 °C.
6. PE, AICAr, and phenformin (as described in Subheading 2.2, **items 3–5**).

Cell lysis

7. Cell culture lysis 5× reagent (CCLR, Promega, E1500). Dilute it in H_2O to make 1× lysis buffer.
8. Cell scraper.
9. 1× PBS.

NFAT-mediated luciferase activity measurement

10. Luciferase assay buffer (Promega, E1500).

11. Luciferase assay substrate (Promega, E1500).
12. Prepare the luciferase assay reagent: Add 10 ml of luciferase assay buffer to the vial containing the lyophilized luciferase assay substrate (*see* **Note 6**).
13. Opaque white 96-well plate.
14. PerkinElmer 2030 program.
15. Plate-reading luminometer (Victor X4, PerkinElmer).

2.6 Evaluation ERK1/2 Signaling Pathway

Except for antibodies, *see* Subheading 2.3 for the materials required.

Antibodies

1. Anti-ERK1/2 (Cell signaling, 9102): for IB 1:1000 in TBS-T, 5% (w/v) BSA.
2. Anti-ERK1/2 Thr202/Tyr204 (Cell signaling, 9101): for IB 1:1000 in TBS-T, 5% (w/v) BSA.
3. Anti-eEF2 (Thermo scientific, PA5–17794): for IB 1:1000 in TBS-T, 5% (w/v) BSA.
4. Goat anti-rabbit IgG HRP-conjugated (Sigma, A0545): for IB 1:20,000 in TBS-T, 5% (w/v) BSA.

3 Methods

3.1 Isolation and Culture of Neonatal Rat Ventricular Cardiomyocytes for Protein Synthesis and Signaling Analysis

Carry out all procedures in sterile conditions under the hood except heart harvesting.

Trypsin digestion of neonatal hearts

1. Sacrifice rat pups (typically 60 pups are used) by cutting the head under aseptic conditions. Remove and place the hearts in a petri dish containing 30 ml of HBSS.
2. Under the hood, transfer all hearts in a second petri dish containing 30 ml of HBSS, and cut them in four pieces with a scalpel.
3. With a 25 ml pipette, transfer the 30 ml of HBSS containing the pieces of heart into 50 ml flask containing 30 mg of trypsin in order to make a trypsin solution of 1 g/L.
4. Digest the hearts at 4 °C in a stirring plate for 3–4 h.

Collagenase type II digestion

5. At the end of trypsin digestion, add 20 ml of warm full IMDM medium, and place the flask in a stirring water bath at 37 °C for 5 min to stop the reaction.
6. Discard the supernatant as much as you can, and leave the cardiomyocyte pieces in the bottom.

7. Add an aliquot of 8–10 ml collagenase type II solution on the cardiomyocytes, and shake the flask in stirring bath at 37 °C for 1 min.
8. Shake the flask vigorously during 10 s. Under the hood, remove the supernatant which is collected into a 15 ml tube. Keep this tube on ice.
9. Add the second aliquot of 8–10 ml collagenase type II solution on the remaining cardiomyocytes in the flask and shake in stirring bath at 37 °C for 15 s.
10. Shake the flask vigorously during 10 s. Under the hood, remove the supernatant which is collected into another 15 ml tube. Keep this tube on ice.
11. Repeat **steps 5** and **6** until hearts are fully digested, increasing number of 15 ml tubes.
12. Adjust the volume of all tubes to the same volume for correct centrifugation.
13. Centrifuge at 183 × *g* for 10 min at 4 °C.
14. Discard the supernatant of each tube (*see* **Note 7**). Resuspend all the pellets in a total of 10 ml of warm full IMDM medium, and pool all resuspended pellets in a 50 ml tube.
15. Homogenize the solution with a 25 ml pipette.

Cardiomyocyte purification by Percoll gradient

16. Slowly, add half of the cardiomyocyte solution on 10 ml of Percoll gradient solution (*see* **Note 8**).
17. Add the other half of cardiomyocyte solution on top of Percoll gradient solution.
18. Centrifuge at 1650 × *g* for 30 min at 15 °C without braking.
19. Remove the pellet containing cardiomyocyte and red blood cells with a 5 ml pipette, and put it in a new 50 ml tube (*see* **Note 9**).

Red blood cell lysis

20. Add 5 ml of RBC lysis buffer on cardiomyocytes and agitate while keeping away from light for 5 min at room temperature in a stirring plate.
21. Add 45 ml of HBSS on the solution containing cardiomyocytes and RBC lysis buffer.
22. Centrifuge for 5 min at 183 × *g* at 4 °C.
23. Discard supernatant and add 50 ml of HBSS, invert the tube, and centrifuge again for 5 min at 183 × *g* at 4 °C.
24. Resuspend the cardiomyocytes in 3.5 ml of warm full IMDM medium.

Dish coating

25. Add 1 ml of 0.2% gelatin solution in each dish and incubate for 15 min (*see* **Note 10**).
26. Remove the solution and leave the dishes opened under the hood until complete drying (*see* **Note 11**).

Cell counting

27. Dilute 10 μl of cardiomyocyte solution in 90 μl of trypan blue (dilution 1/10).
28. Put 10 μl of this mix in the burker chamber.
29. Count living (non-blue) cells (*see* **Note 12**).

Cell plating

30. Dilute cell solution in an adequate volume of warm full IMDM medium knowing that 750,000 cells per dish (9.6 cm^2) are needed for protein synthesis and signaling analysis and wells can contain 2 ml of medium.
31. Let cells to adhere overnight in incubator at 37 °C and 5% CO_2.

3.2 Evaluation of Protein Synthesis in Cardiomyocytes During Hypertrophic Treatment

Cardiomyocyte treatments

1. The day after plating cardiomyocytes, the IMDM medium is changed and replaced by 2 ml of pre-warmed full IMDM medium for 24 h.
2. After 24 h, replace the medium by 2 ml of IMDM medium without serum (pre-warmed at 37 °C) for 2 h before stimulation (*see* **Note 13**).
3. Treat the cells according to the following conditions: controls (no treatment), 20 μM PE (hypertrophic treatment), 1 mM phenformin or 1 mM AICAr (AMPK stimulation), and PE + phenformin or PE + AICAr (simultaneous hypertrophic treatment and AMPK stimulation). At the same time, add 1 μCi/ml C^{14}-labeled L-phenylalanine per well (*see* **Note 14**).
4. Treatments are maintained for 24 h in incubator at 37 °C and 5% CO_2 (*see* **Note 15**).

Cell harvest

5. At the end of the treatment, put dishes on ice.
6. Rinse them twice with cold PBS (*see* **Note 16**).
7. Add 90 μl of lysis buffer and scrap the cells.
8. Transfer lysates into 1.5 ml Eppendorf reaction tubes.
9. Centrifuge lysates for 15 min at 16,100 × *g* at 4 °C and collect supernatants.
10. Protein concentration is measured in supernatants by Lowry method using BIO-RAD protein assay kit in a 96-well plate.

Evaluation of radioactive L-phenylalanine incorporation into proteins

11. Precipitate proteins from supernatants by adding TCA 100% in order to reach a final concentration of 10%. Allow correct precipitation by vortexing.
12. Keep samples on ice for 20 min in order to precipitate proteins.
13. Centrifuge 10 min at 9279 × *g* at 4 °C.
14. Discard supernatants.
15. Add 900 µl of cold NaOH 100 mM in order to dissolve the pellet containing proteins and vortex until the pellet is completely dissolved.
16. Add 100 µl of 100% TCA and vortex.
17. Keep samples on ice for 20 min in order to precipitate proteins.
18. Centrifuge for 10 min at 9279 × *g* at 4 °C.
19. Discard supernatants.
20. Add 500 µl of cold 5% TCA and vortex to detach the pellet (*see* **Note 17**).
21. Centrifuge for 5 min at 9279 × *g* at 4 °C.
22. Discard supernatants, add 1 ml of formic acid (*see* **Notes 18** and **19**), and vortex.
23. Prepare vials for scintillation counter with 5 ml of scintillation liquid (Ultima Gold).
24. Put 800 µl of each protein samples into vials. Shake vials.
25. Count vials in a scintillation counter with appropriate counting program.
26. Radioactivity measured, corresponding to C^{14}-labeled L-phenylalanine incorporated into proteins during all the incubation period, is then normalized to protein concentration (evaluated by protein assay) to allow accurate comparison (*see* Fig. 2a and e).

3.3 Evaluation of p70S6K and eEF2 Signaling Pathway

Such evaluation is performed on cardiomyocytes cultured and treated as described in the previous chapter expect that radioactive L-phenylalanine was not used (*see* **Note 20**).

Cell harvest

For this step, keep dishes on ice and perform cell lysis as quick as possible (*see* **Note 21**).

1. Rinse each dish/well once with cold PBS.
2. Add 90 µl of cold lysis buffer and scraped the cells.
3. Transfer lysates into 1.5 ml Eppendorf reaction tubes.
4. Centrifuge lysates for 15 min at 16,100 × *g* at 4 °C and collect supernatants.

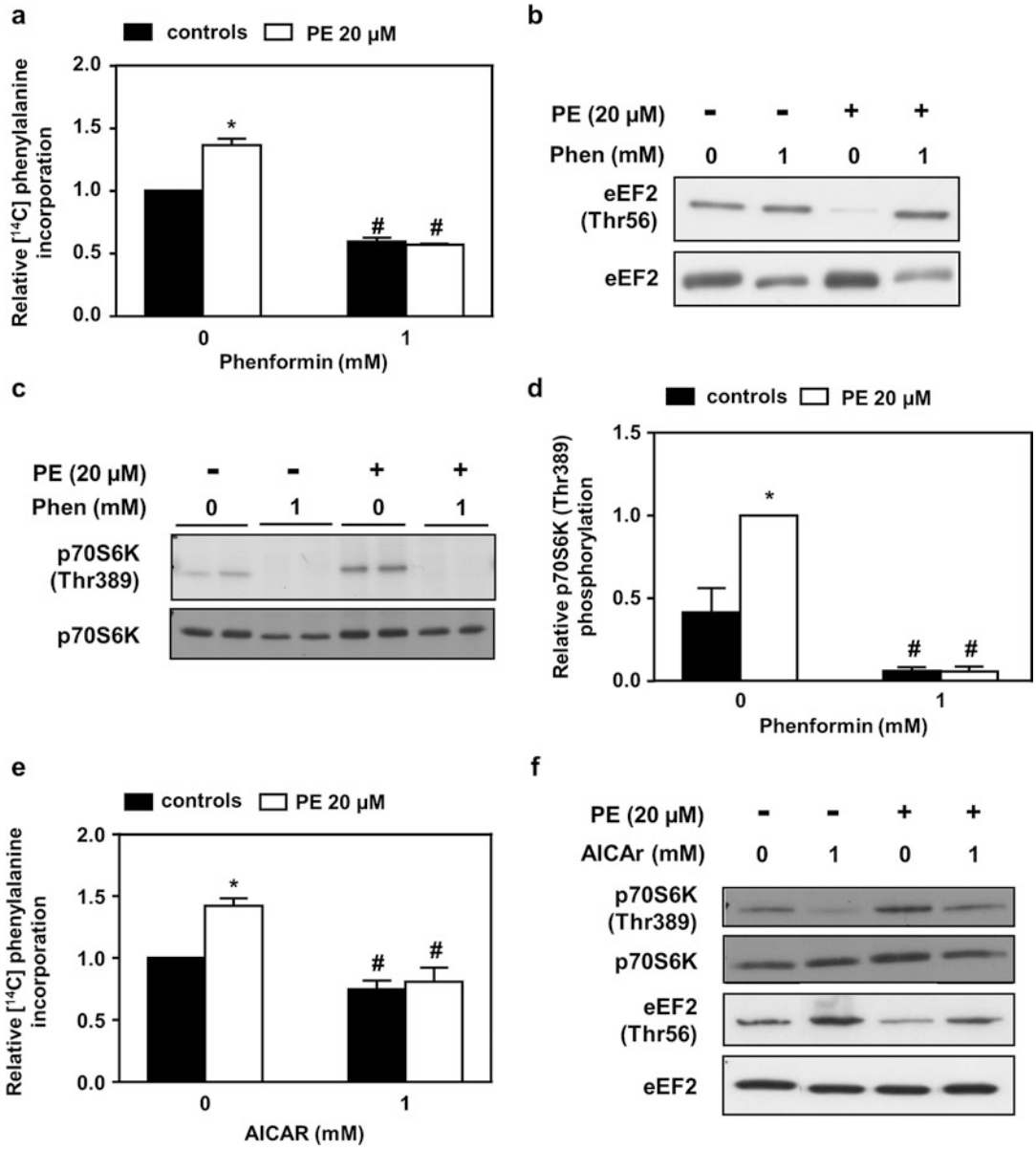

Fig. 2 AMPK activation inhibits phenylephrine-mediated increase in protein synthesis and underlying signaling. (**a**–**d**) Neonatal rat ventricular cardiomyocytes (NRVMs) were treated with (*open bars*) or without (*solid bars*) phenylephrine (PE) in the presence or absence of phenformin (1 mM) for 24 h. (**a**) Amino acid incorporation into proteins measured by [^{14}C]-phenylalanine incorporation. $N = 4$. (**b**) Representative immunoblot of eEF2 (Thr56) phosphorylation state and total eEF2 content. (**c–d**) Representative immunoblot and quantification of p70S6K (Thr389) phosphorylation state and total p70S6K content. $N = 3$. (**e–f**) NRVMs were treated with (*open bars*) or without (*solid bars*) phenylephrine (PE) in the presence or absence of AICAr (1 mM) for 24 h. (**e**) Amino acids incorporation into proteins measured by [^{14}C]-phenylalanine incorporation. $N = 3$. (**f**) Representative immunoblots of p70S6K (Thr389) and eEF2 (Thr56) phosphorylation states and their respective total content. Data are mean ± s.e.m. and were analyzed using two-way ANOVA followed by Bonferroni posttest ($^{*}p < 0.05$ vs. untreated cells, $^{\#}p < 0.05$ vs. PE-treated cells)

5. Protein concentration is measured in supernatants by Lowry method using BIO-RAD protein assay kit in a 96-well plate.
6. 20 μg of total protein is diluted with H_2O to 20 μl total volume, mixed with 5 μl of 4× loading buffer and heated at 100 °C for 3 min. Samples are ready for loading on SDS PAGE (*see* **Note 22**).

SDS polyacrylamide gel electrophoresis

7. For a 10% SDS PAGE, mix 2.65 ml of H_2O, 3.35 ml of acrylamide/bisacrylamide solution, 500 μl of SDS (5%), and 3.75 ml of Tris-HCl (1 M, pH 8.8). Polymerization is started by addition of 75 μl of 10% (w/v) APS and 15 μl of TEMED.
8. For the 3.6% stacking gel, mix 1.75 ml of H_2O, 0.5 ml of acrylamide/bisacrylamide solution, 100 μl of 5% SDS, and 2.5 ml of Tris–HCl (0.25 M, pH 6.8). Polymerization is started by addition of 75 μl of 10% (w/v) APS and 10 μl of TEMED.
9. The samples are loaded and separated electrophoretically at 150 V until the protein reach the running gel and then at 200 V for about 1 h until the bromophenol dye front run off the gel.

Immunoblotting

10. After electrophoresis, separate the gel plates and remove the stacking gel.
11. The PVDF membrane is immerged in ethanol and then in H_2O to make it hydrophilic.
12. The 10% gel can be then blotted according to the wet blotting method.
13. First, two sponges, six Whatman filter papers, and the PVDF membrane are equilibrated in blotting transfer buffer for 30 min.
14. The holder cassette is set inside the container containing blotting transfer buffer with the black side facing down.
15. Then the apparatus is prepared as followed from the cathode: one sponge, three filter papers, the gel, the PVDF membrane, three filter papers, and one sponge.
16. Bubbles are removed by rolling over filter paper using a 15 ml tube. The holder cassette is then closed and placed in the container (*see* **Note 23**).
17. The container is placed into the blotting chamber. Place a cooling unit into the chamber, fill with blotting transfer buffer.
18. The blotting is performed for 1 h at 100 V.

Antibodies

19. After the transfer, incubate the PVDF membrane with blocking solution for 1 h at room temperature on a stirring plate.

20. Incubate the membrane with primary antibody overnight at 4 °C on a rotating device.
21. Then, wash the membrane with TBS-T twice for 5 min, once for 10 min, and twice for 5 min on a stirring plate.
22. Incubate the membrane with the corresponding secondary antibody diluted in TBS-T containing 5% (w/v) BSA for 1 h at room temperature on a stirring plate.
23. After incubation, wash the membrane with TBS-T twice for 5 min, once for 10 min, and twice for 5 min on a stirring plate.
24. ECL solution mixture is prepared for the developing step, and 15 ml is placed on PVDF membrane. Shake membrane with the ECL solution for 1 min.
25. Membrane is then placed between two plastic films and fixed in an autoradiography cassette.
26. In the dark, a film is placed onto the membrane and the cassette was closed. Open the cassette and remove the film after the appropriate time of exposition.
27. Immerse the film in the developer buffer until the chemiluminescence reaction occurs and you can detect a signal. Wash the film with water and place it into the fixator buffer in order to fix the chemiluminescence picture (Fig. 2b, c, and f).
28. Film obtained can be quantified by software such as ImageJ (Fig. 2d) (*see* **Note 24**).

3.4 Evaluation of Cardiomyocyte Hypertrophy by α-Actinin Immunostaining

Cell plating

1. During cardiomyocyte isolation (as presented before), wash coverslips in ethanol and, then, in PBS, under the hood. Place two coverslips per dish.
2. Add 2 ml of 0.2% gelatin solution in each dish for 15 min.
3. Remove the excess and leave the dish open under the hood until complete drying.
4. After cell counting using trypan blue, dilute cells in an adequate volume of full IMDM knowing that 350,000 cells per dish are needed for immunostaining analysis and wells can contain 2 ml of medium.
5. Let cells to adhere overnight in incubator at 37 °C, 5% CO_2.

Cell treatments

6. The day after plating, medium is changed and replaced by 2 ml of fresh full IMDM (pre-warmed at 37 °C).
7. Two days after plating, change and replace IMDM culture medium with 2 ml of IMDM medium without serum (pre-warmed at 37 °C) for 2 h before stimulation.
8. Cells are, then, treated according to the following conditions: controls (no treatment), 20 μM PE (hypertrophic treatment),

1 mM phenformin or 1 mM AICAr (AMPK stimulation), and PE + phenformin or PE + AICAr (simultaneous hypertrophic treatment and AMPK stimulation).

9. Incubate cells for 24 h in incubator at 37 °C, 5% CO_2.

Cell fixation

For this step, keep dishes on ice.

10. Rinse each well once with cold PBS.
11. Add 2 ml of 4% PFA + 0.2% Triton X-100 for fixation during 30 min under the hood.
12. Remove dishes out from ice, remove PFA (*see* **Note 25**), and wash with PBS.

α-Actinin immunostaining

13. Wash coverslips 5 min with PBS + BSA 0.1%. Repeat this step three times.
14. During these washing steps, prepare microscope slides. Draw two circles per slide with dako pen.
15. Put 90 μl of PBS + BSA 1% containing the anti-α-actinin antibody in each drawn circle.
16. After removing the PBS + BSA 0.1% solution from each dish, pick each coverslip and turn it over. Place each coverslip on its corresponding droplet (*see* **Note 26**).
17. Incubate for 1 h at room temperature.
18. Put back each coverslip in the corresponding dish without forgetting to turn it over (*see* **Note 27**).
19. Wash coverslips 5 min with PBS + BSA 0.1%. Repeat this step three times.
20. Remove excess of primary antibody solution. Wash the microscope slides with PBS + BSA 0.1% and, then, with PBS.
21. Remove PBS and put 90 μl of PBS + BSA 1% containing the Alexa Fluor 594 donkey anti-mouse antibody in each drawn circle.
22. After removing the PBS + BSA 0.1% solution from each dish, pick each coverslip in the corresponding dish, and turn it over. Place each coverslip on its corresponding droplet (*see* **Note 26**).
23. Incubate for 1 h at room temperature and away from light.
24. After 1 h, put back each coverslip in the corresponding dish without forgetting to turn it over (*see* **Note 27**).
25. Wash the coverslips three times with PBS and twice with distillated water. Keep away from light.
26. Wash the microscope slides once with PBS then once with distillated water.

27. After removing distillated water on microscope slides, put 7 μl of Vectashield mounting medium with DAPI (*see* **Note 28**) in the middle of the drawn circle.
28. After removing distillated water from each dish, pick the coverslip from the corresponding dish, and turn it over on the mounting medium droplet.
29. After 15 min at room temperature, the coverslip will become immobilized. Microscope slides can be viewed on any structured illumination fluorescent microscope, and cell surface can be quantified on images using AxioVision 4.8 (or similar) software (Fig. 3a–d).

3.5 Evaluation of NFAT Transcriptional Activity

Cell infection

1. Remove full IMDM medium from each well.
2. Rinse cells with PBS.
3. Add 1 ml of IMDM without serum.
4. Infect cardiomyocytes with NFAT luciferase adenovirus at a multiplicity of infection (MOI) of 10 or β-galactosidase adenovirus at similar MOI as control condition (*see* **Note 29**).
5. After 2 h, add 1 ml of full IMDM medium, and incubate cells for 24 h in incubator at 37 °C, 5% CO_2.

Cell treatment

6. After 24 h, remove the medium and add 2 ml of fresh IMDM without serum.
7. After 2 h, treat cells according to the conditions (*see* Subheading 3.4 for details)
8. Incubate cells for 24 h in incubator at 37 °C, 5% CO_2.

Cell lysis

9. Remove the medium and wash the cells once with cold PBS 1×.
10. Remove PBS as much as possible.
11. Add 180 μl of 1× CCLR lysis buffer.
12. Shake culture dishes several times to ensure coverage of all cells with lysis buffer.
13. Scrape attached cells and transfer lysates in 1.5 ml reaction tubes.
14. Vortex tubes for 10–15 s and centrifuge for 90 s at 12,081 × *g* at 4 °C.
15. Transfer supernatants to new tubes.
16. Store samples at −80 °C or proceed to next section.

Luciferase activity measurement

17. Program the luminometer with the appropriate delay time (2 s) and the appropriate measurement time (10 s).

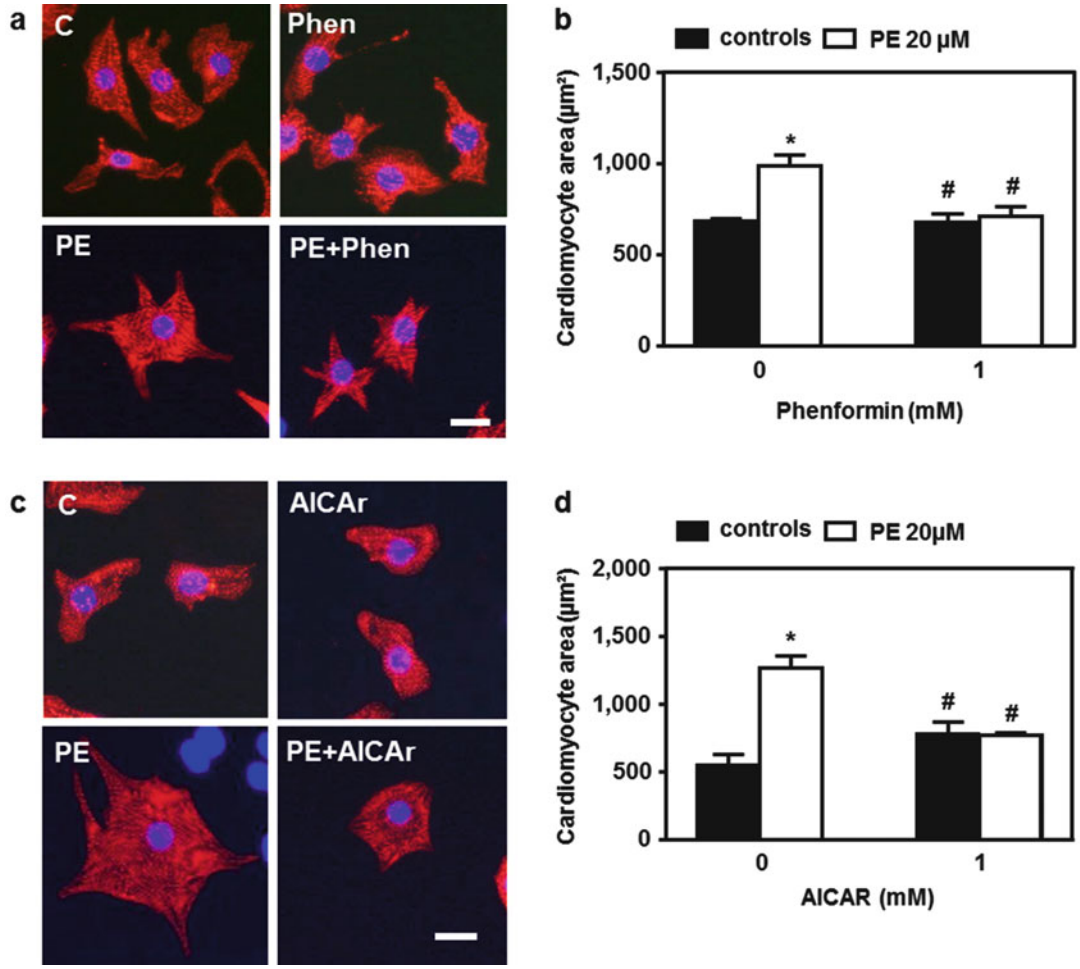

Fig. 3 AMPK activation inhibits phenylephrine-induced cardiomyocyte hypertrophy. (**a**, **b**) NRVMs were treated with (*open bars*) or without (*solid bars*) phenylephrine (PE) in the presence or absence of phenformin (1 mM) for 24 h. (**a**) Representative images of cardiomyocytes after α-actinin immunostaining. (**b**) Quantification of cardiomyocyte area. $N = 3$. (**c**, **d**) NRVMs were treated with (*open bars*) or without (*solid bars*) phenylephrine (PE) in the presence or absence of AICAr (1 mM) for 24 h. (**c**) Representative images of cardiomyocytes after α-actinin immunostaining. (**d**) Quantification of cardiomyocyte area. $N = 3$. Scale bar, 20 µm. Data are mean ± s.e.m. and were analyzed using two-way ANOVA followed by Bonferroni posttest ($^{*}p < 0.05$ vs. untreated cells, $^{\#}p < 0.05$ vs. PE-treated cells)

18. Fill plate wells with 20 µl of each sample in duplicates in 96-well plate (*see* **Note 30**).
19. Wash the luminometer injector with distillated water.
20. Place the plate into the luminometer with injector. The injector adds 100 µl of luciferase assay reagent per well in by one; each well is read 2 s after injection.

21. The luminometer measures the light produced for a period of 10 s. The plate is advanced to the next well for light measurement (Fig. 4a).
22. Wash the luminometer injector with distillated water.

3.6 Evaluation ERK1/2 Signaling Pathway

Such evaluation is performed on cardiomyocytes cultured as described in Subheading 3.3 except that incubation time with PE and AMPK activator phenformin is restricted to 1 h (*see* **Notes 22** and **31**) (Fig. 4b and c).

4 Notes

1. Trypsin (Gibco, ref.: 27250-018) is sensitive to heat and is activated at 37 °C.
2. Collagenase (Gibco, ref.: 17101-015) is activated at 37 °C. Prepare a solution of 80 ml for 60 rat pups. Filter the solution and divide into eight aliquots of 8–10 ml in 15 ml tubes.
3. Protect RBC lysis buffer from the light.
4. Prepare lysis buffer freshly and stored on ice until use.
5. This adenoviral construction contains nine multimerized NFAT binding sites upstream of a minimal TATA-containing promoter fused to luciferase. It allows an efficient evaluation of NFAT transcriptional activity in primary cultures.
6. Equilibrate luciferase assay reagent at room temperature.
7. This step can be done by inverting tubes. Some pellets can be not perfectly stuck on the bottom of the tube; do not hesitate to let a small amount of supernatant to prevent loss of cardiomyocytes.
8. Set the tube in a horizontal position as much as possible, place the pipette perpendicularly to wall tube, and gently add the solution in order to make two separate layers, one under with the Percoll gradient solution and one above with the cardiomyocyte solution.
9. The band in the middle of the tube contains endothelial cells, fibroblasts, and other cell fragments.
10. This step can be performed during the centrifugation of Percoll gradient solution.
11. This step can be performed during red blood cell lysis.
12. Make the mean of three squares in burker chamber. Do not take into account the blue cells which are dead cells. Cell concentration in stock solution (per ml) = number of cells/square multiplied by 10,000 and by 10 (corresponding of the dilution in trypan blue).

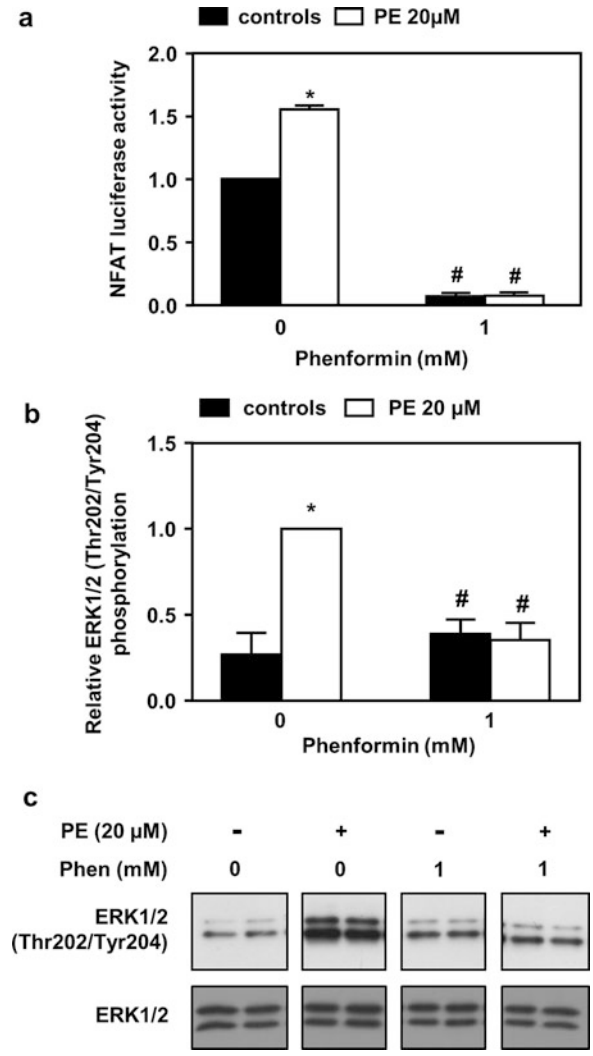

Fig. 4 AMPK activation inhibits phenylephrine-mediated increase in ERK1/2 phosphorylation and NFAT transcriptional activity. (**a**) NRVMs were treated with (*open bars*) or without (*solid bars*) phenylephrine (PE) in the presence or absence of phenformin (1 mM) for 24 h. Evaluation of NFAT transcriptional activity by luciferase activity measurement. $N = 4$. (**b**, **c**) NRVMs were treated with (*open bars*) or without (*solid bars*) phenylephrine (PE) in the presence or absence of phenformin (1 mM) for 1 h. Representative immunoblot and quantification of ERK1/2 (Thr202/Tyr204) phosphorylation state and ERK1/2 total content. $N = 3$. Data are mean ± s.e.m. and were analyzed using two-way ANOVA followed by Bonferroni post test ($^{*}p < 0.05$ vs. untreated cells, $^{\#}p < 0.05$ vs. PE-treated cells)

13. This step is required to allow cardiomyocytes to recover their basal state before to start hypertrophic treatment.
14. 100 nM angiotensin II can be equally used to induce neonatal cardiomyocyte hypertrophy [21].
15. Protein synthesis (radioactive L-phenylalanine incorporation) can be followed during shorter incubation time. Indeed, this

protocol evaluates the final global incorporation of labeled phenylalanine into proteins. It integrates both entry and removal of labeled phenylalanine all along the incubation period. The longer your incubation time, the more your evaluation will take into account putative protein degradation (including autophagy).

16. Use adequate trash for liquid and tips due to the presence of radioactivity.
17. Pellets do not have to be completely dissolved.
18. Formic acid must be added under a hood because of its toxicity.
19. Formic acid allows dissolution of the pellet.
20. Such Western blot analysis can be also performed on cardiomyocytes treated with radiolabeled L-phenylalanine (divided after lysis into two samples, one for protein synthesis analysis and the other for Western blot analysis). However, in this case, all materials should be dedicated for radioactive samples.
21. This will prevent any putative dephosphorylation of the proteins evaluated for its phosphorylation level.
22. It is better to perform two different blots in order to detect phosphorylation and total proteins than to do stripping of a same blot. Indeed, blot stripping is rarely 100% efficient and frequently unequal (principally for the primary antibody) and can falsify data obtained after reprobing with a second antibody detecting the same protein on another epitope (total vs. phosphorylation or vice versa) with the possibility of closed epitope and evident steric hindrance. However, each blot is tripped and reprobed with an antibody directed against a housekeeping protein for which the protein level is known to be unmodified by the different treatments and with a molecular weight sufficiently different form the original target to be easily differentiated (in the present cases, we used GAPDH or eEF2). The data obtained with this loading control will be used to normalize original data.
23. The black side of the holder cassette has to face the black side of the container, and the white side has to face the red one.
24. For a more complete evaluation, you can also follow the phosphorylation state of both p70S6K and eEF2 in a time course experiment all along the 24 h incubation time with hypertrophic agents and AMPK activators.
25. PFA in excess can be removed with a P1000 pipette.
26. Cells have to be on the bottom side facing the antibody solution.
27. Cells have to be on the top side to allow their correct washing.

28. DAPI is a cell permeable fluorescent probe for DNA. It allows nuclear labeling.
29. Once adenoviral construct is used, several biosafety precautions should be taken. All work with adenovirus minimally requires BSL-2 containment. People must wear protective equipment to reduce mucosal or skin exposure. Working surfaces must be disinfected after use. Wastes must be disinfected by bleaching and/or autoclave.
30. The optimal temperature for luciferase activity measurement is room temperature.
31. ERK1/2 phosphorylation is acutely and only temporarily stimulated by pro-hypertrophic stimulation. This stimulation tempts to disappear after longer incubation time such as 24 h.

Acknowledgments

Authors are supported by grants from Fonds National de la Recherche Scientifique et Médicale (FNRS), Belgium, and Action de Recherche Concertée de la Communauté Wallonie-Bruxelles, Belgium, and by unrestricted grants from AstraZeneca. F.M. is supported by the Fund for Scientific Research in Industry and Agriculture, Belgium. S.H. is Research Associate and L.B. is Senior Research Associate of FNRS, Belgium. C.B. is Postdoctorate Clinical Master Specialist of the FNRS, Belgium.

References

1. Kudo N, Barr AJ, Barr RL, Desai S, Lopaschuk GD (1995) High rates of fatty acid oxidation during reperfusion of ischemic hearts are associated with a decrease in malonyl-CoA levels due to an increase in 5′-AMP-activated protein kinase inhibition of acetyl-CoA carboxylase. J Biol Chem 270(29):17513–17520
2. Beauloye C, Bertrand L, Horman S, Hue L (2011) AMPK activation, a preventive therapeutic target in the transition from cardiac injury to heart failure. Cardiovasc Res 90 (2):224–233
3. Horman S, Beauloye C, Vanoverschelde JL, Bertrand L (2012) AMP-activated protein kinase in the control of cardiac metabolism and remodeling. Curr Heart Fail Rep 9 (3):164–173
4. Qi D, Young LH (2015) AMPK: energy sensor and survival mechanism in the ischemic heart. Trends Endocrinol Metab 26(8):422–429. https://doi.org/10.1016/j.tem.2015.05.010
5. Bairwa SC, Parajuli N, Dyck JR (2016) The role of AMPK in cardiomyocyte health and survival. Biochim Biophys Acta 1862 (12):2199–2210. https://doi.org/10.1016/j.bbadis.2016.07.001
6. Daskalopoulos EP, Dufeys C, Bertrand L, Beauloye C, Horman S (2016) AMPK in cardiac fibrosis and repair: actions beyond metabolic regulation. J Mol Cell Cardiol 91:188–200. https://doi.org/10.1016/j.yjmcc.2016.01.001
7. Horman S, Browne G, Krause U, Patel J, Vertommen D, Bertrand L, Lavoinne A, Hue L, Proud C, Rider M (2002) Activation of AMP-activated protein kinase leads to the phosphorylation of elongation factor 2 and an inhibition of protein synthesis. Curr Biol 12 (16):1419–1423
8. Krause U, Bertrand L, Hue L (2002) Control of p70 ribosomal protein S6 kinase and acetyl-CoA carboxylase by AMP-activated protein kinase and protein phosphatases in isolated hepatocytes. Eur J Biochem 269 (15):3751–3759
9. Browne GJ, Finn SG, Proud CG (2004) Stimulation of the AMP-activated protein kinase leads to activation of eukaryotic elongation

factor 2 kinase and to its phosphorylation at a novel site, serine 398. J Biol Chem 279 (13):12220–12231. https://doi.org/10.1074/jbc.M309773200

10. Johanns M, Pyr Dit Ruys S, Houddane A, Vertommen D, Herinckx G, Hue L, Proud CG, Rider MH (2017) Direct and indirect activation of eukaryotic elongation factor 2 kinase by AMP-activated protein kinase. Cell Signal 36:212–221. https://doi.org/10.1016/j.cellsig.2017.05.010
11. Inoki K, Zhu T, Guan KL (2003) TSC2 mediates cellular energy response to control cell growth and survival. Cell 115(5):577–590
12. Gwinn DM, Shackelford DB, Egan DF, Mihaylova MM, Mery A, Vasquez DS, Turk BE, Shaw RJ (2008) AMPK phosphorylation of raptor mediates a metabolic checkpoint. Mol Cell 30 (2):214–226. https://doi.org/10.1016/j.molcel.2008.03.003
13. Horman S, Beauloye C, Vertommen D, Vanoverschelde JL, Hue L, Rider MH (2003) Myocardial ischemia and increased heart work modulate the phosphorylation state of eukaryotic elongation factor-2. J Biol Chem 278 (43):41970–41976. https://doi.org/10.1074/jbc.M302403200
14. Demeulder B, Zarrinpashneh E, Ginion A, Viollet B, Hue L, Rider MH, Vanoverschelde JL, Beauloye C, Horman S, Bertrand L (2013) Differential regulation of eEF2 and p70S6K by AMPKalpha2 in heart. Biochim Biophys Acta 1832(6):780–790. https://doi.org/10.1016/j.bbadis.2013.02.015
15. Chan AY, Dolinsky VW, Soltys CL, Viollet B, Baksh S, Light PE, Dyck JR (2008) Resveratrol inhibits cardiac hypertrophy via AMP-activated protein kinase and Akt. J Biol Chem 283 (35):24194–24201. https://doi.org/10.1074/jbc.M802869200
16. Chan AY, Soltys CL, Young ME, Proud CG, Dyck JR (2004) Activation of AMP-activated protein kinase inhibits protein synthesis associated with hypertrophy in the cardiac myocyte. J Biol Chem 279(31):32771–32779. https://doi.org/10.1074/jbc.M403528200
17. Li HL, Yin R, Chen D, Liu D, Wang D, Yang Q, Dong YG (2007) Long-term activation of adenosine monophosphate-activated protein kinase attenuates pressure-overload-induced cardiac hypertrophy. J Cell Biochem 100(5):1086–1099. https://doi.org/10.1002/jcb.21197
18. Fujita K, Maeda N, Sonoda M, Ohashi K, Hibuse T, Nishizawa H, Nishida M, Hiuge A, Kurata A, Kihara S, Shimomura I, Funahashi T (2008) Adiponectin protects against angiotensin II-induced cardiac fibrosis through activation of PPAR-alpha. Arterioscler Thromb Vasc Biol 28(5):863–870. https://doi.org/10.1161/ATVBAHA.107.156687
19. Louch WE, Sheehan KA, Wolska BM (2011) Methods in cardiomyocyte isolation, culture, and gene transfer. J Mol Cell Cardiol 51 (3):288–298. https://doi.org/10.1016/j.yjmcc.2011.06.012
20. Belge C, Hammond J, Dubois-Deruy E, Manoury B, Hamelet J, Beauloye C, Markl A, Pouleur AC, Bertrand L, Esfahani H, Jnaoui K, Gotz KR, Nikolaev VO, Vanderper A, Herijgers P, Lobysheva I, Iaccarino G, Hilfiker-Kleiner D, Tavernier G, Langin D, Dessy C, Balligand JL (2014) Enhanced expression of beta3-adrenoceptors in cardiac myocytes attenuates neurohormone-induced hypertrophic remodeling through nitric oxide synthase. Circulation 129(4):451–462. https://doi.org/10.1161/CIRCULATIONAHA.113.004940
21. Wang C, Li L, Zhang ZG, Fan D, Zhu Y, Wu LL (2010) Globular adiponectin inhibits angiotensin II-induced nuclear factor kappaB activation through AMP-activated protein kinase in cardiac hypertrophy. J Cell Physiol 222(1):149–155. https://doi.org/10.1002/jcp.21931

Chapter 22

Assessment of AMPK-Stimulated Cellular Long-Chain Fatty Acid and Glucose Uptake

Joost J. F. P. Luiken, Dietbert Neumann, Jan F. C. Glatz, Will A. Coumans, Dipanjan Chanda, and Miranda Nabben

Abstract

Here we describe an assay for simultaneous measurement of cellular uptake rates of long-chain fatty acids (LCFA) and glucose that can be applied to cells in suspension. The uptake assay includes the use of radiolabeled substrates at such concentrations and incubation periods that exact information is provided about unidirectional uptakes rates. Cellular uptake of both substrates is under regulation of AMPK. The underlying mechanism includes the translocation of LCFA and glucose transporters from intracellular membrane compartments to the cell surface, leading to an increase in substrate uptake. In this chapter, we explain the principles of the uptake assay before detailing the exact procedure. We also provide information of the specific LCFA and glucose transporters subject to AMPK-mediated subcellular translocation. Finally, we discuss the application of AMPK inhibitors and activators in combination with cellular substrate uptake assays.

Key words Long-chain fatty acid uptake, Glucose uptake, Initial uptake rate, AMPK inhibitors, AMPK stimuli, CD36 translocation, GLUT4 translocation

1 Introduction

For the majority of mammalian cell types, LCFA and glucose are the most important substrates for cellular energy production. But in order to serve as energy source, both substrates need to be taken up across the plasma membrane. In the remainder of this chapter, we focus on cardiomyocytes, but the general principles of the cellular uptake process are likely to apply to most other mammalian cell types, as has been proven for skeletal muscle cells, adipocytes, hepatocytes, enterocytes, etc. Notably, as observed in cardiomyocytes and skeletal muscle cells, the crossing of the plasma membrane presents the rate-limiting step in the cellular metabolism of both substrates [1–3]. Once inside the cells, both substrates can be readily oxidized according to the metabolic needs of the cells but also stored in times of plenty. Based on its lipophobic properties,

Dietbert Neumann and Benoit Viollet (eds.), *AMPK: Methods and Protocols*, Methods in Molecular Biology, vol. 1732, https://doi.org/10.1007/978-1-4939-7598-3_22,

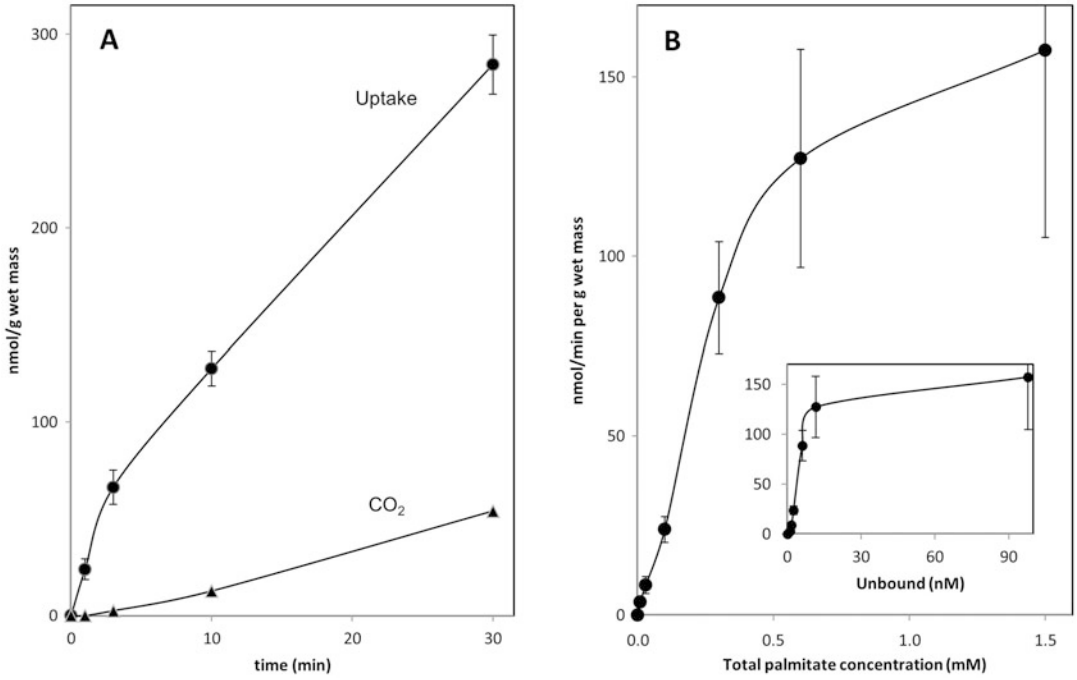

Fig. 1 Kinetics of palmitate uptake and utilization in rat cardiomyocytes. (**a**) Time course of palmitate uptake and utilization. Cardiomyocytes were incubated with palmitate bound to BSA at final concentrations of 90 and 300 μM, respectively (palmitate/BSA molar ratio 0.3), and analyzed at the indicated time points on cellular uptake of palmitate (*filled circle*) and formation of CO_2 (*filled triangle*). (**b**) Palmitate uptake as function of the exogenous palmitate concentration. Cardiomyocytes were incubated with varying concentrations of palmitate bound to BSA (final BSA concentration 300 μM) resulting in palmitate/BSA molar ratios ranging from 0 to 5. Cellular uptake of palmitate was determined at 3 min after substrate addition. In the inset, palmitate uptake is plotted against the unbound palmitate concentration, which is calculated from the palmitate/BSA molar ratio [14]. This figure is modified from Ref. [8]

glucose does not readily cross the plasma membrane, and membrane transporters have long been recognized to mediate the bulk of glucose uptake [4]. These transporters are mainly members of the GLUT family: integral membrane proteins that contain 12 - membrane-spanning helices. In contrast, due to their lipophilic properties, LCFA have been postulated to cross the plasma membrane solely via passive diffusion [5, 6]. Only in the late 1980s of the previous century, transporters emerged as key mediators of bulk LCFA uptake (e.g., *see* [7]). The latter notion followed from several lines of kinetic evidence, including saturation of cellular LCFA uptake (Fig. 1), and sensitivity to competitive substrates and to inhibitors of protein-mediated membrane transport [2]. However, LCFA uptake also displays a non-saturable component, which at physiological LCFA concentrations contributes only modestly to the uptake process, but increases in relative contribution at exceedingly high nonphysiological concentrations [7]. The uptake procedure described below is carried out at low and physiological LCFA concentrations as measured in human plasma [8].

1.1 Considerations of the Uptake Assay

1.1.1 Applicability

This protocol of measurement of cellular substrate uptake is dedicated to primary cells in suspension and is suitable for investigation of the short-term regulation of substrate uptake. Working with primary cells in suspension has the advantage to prevent major cell loss accompanying their maintenance in culture. When one is interested in long-term regulation of substrate uptake, as exerted by transcription factors and subsequent de novo synthesis of substrate transporters, use of primary cells attached to laminin-coated wells is a more appropriate model of study. In that case, we advise to use a modified version of this uptake protocol [9]. On the other hand, cultured cells can be detached from their plates and undergo the uptake protocol as described below.

1.1.2 Radioactive Tracers

The most sensitive method to measure substrate uptake is via radioactive tracers. Uptake is measured as cell-associated radioactivity, which can be determined upon centrifugation and subsequent washing of the cells after a fixed time of incubation with the radioactive substrates. The most commonly used LCFA tracer is [1-^{14}C]palmitate, but also [^{14}C] or [^{3}H] derivatives of oleate are often used, although these have the disadvantage of being considerably more expensive. The radiolabeled LCFA will be taken up into the cells mainly via LCFA transporters. Thereafter, they are intracellularly transported by small cytoplasmic fatty acid-binding proteins (FABP) to the cytoplasmic leaflet of the outer mitochondrial membrane for conversion into CoA esters by fatty acyl-CoA synthetase. This activation is needed for further metabolism, being oxidation within mitochondria, storage as triacylglycerols within lipid droplets and/or conversion into various other lipid species [3]. Depending on cell type and metabolic state, a variable portion of the fatty acyl-CoA will be destined for β-oxidation. Importantly, palmitate uptake needs to be measured during the initial uptake phase, when substrate uptake kinetics proceeds linear with time. Namely, beyond the initial uptake phase, efflux of the ^{14}C-label will gradually increase as a result of equilibration of [1-^{14}C]palmitate with the endogenous non-labeled palmitate pools [8]. Hence, during the initial uptake phase, measurement of uptake provides unbiased information on unidirectional influx of palmitate. Another reason for a rapid measurement of palmitate uptake relates to a progressive loss of ^{14}C-label due to β-oxidation. Specifically using [1-^{14}C]palmitate, the ^{14}C-label at the C1 position will already disappear within the first round of β-oxidation, yielding a radioactive acetyl-CoA and a non-labeled myristoyl-CoA, of which the latter can no longer be traced. The radiolabeled acetyl-CoA subsequently enters the TCA cycle leading to $^{14}CO_2$ production. This CO_2 diffuses away from the cells and the liquid medium into the gas phase. Hence, the portion of $^{14}CO_2$ produced from [1-^{14}C]palmitate escapes the radioactive detection and leads to underestimation of the uptake rates. In metabolically active primary

cardiomyocytes, this initial uptake phase amounts to 3–5 min after addition of the radiolabeled substrates (Fig. 1a) [8]. In most cardiac cell lines, the initial uptake rate is lower compared to primary cardiomyocytes and in the linear phase for up to 30 min [9, 10].

To obtain information about cellular glucose uptake, non-metabolizable glucose analogs such as radiolabeled 2-deoxyglucose (2-deoxy-D-[^{3}H]glucose) are often applied, so that glucose uptake can be assessed independently of metabolism. Glucose and 2-deoxyglucose display similar uptake kinetics in cardiomyocytes (Luiken, unpublished). Whereas glucose is mostly used in uptake studies at physiological millimolar concentrations, it is advisable to use 2-deoxyglucose at submillimolar concentrations in order to minimize undesirable accumulation of 2-deoxyglucose-6-phosphate. The use of non-metabolizable analogs would also be advantageous for LCFA uptake studies. Yet, non-metabolizable LCFA analogs as 2-bromopalmitate [11] display much slower uptake rates due to the bulky bromo group and therefore do not reflect their naturally occurring counterparts. For the same reason, also iodo-fatty acids would display nonphysiologically low uptake rates. These iodo-fatty acids (e.g., 15-(p-iodophenyl)3(R,S)-methylpentadecanoic acid) are, however, suitable for PET imaging of myocardial metabolism [12].

1.1.3 LCFA-Albumin Ratios

Another complication with respect to measuring LCFA uptake is that this substrate is virtually insoluble in aqueous solutions [13]. In the mammalian circulation, LCFA are almost completely bound to albumin. In most cellular systems, high-affinity albumin binding sites have been found, which brings the LCFA-albumin complex in close proximity to the plasma membrane. Subsequently, the LCFA gain access to their membrane transporters. Hence, the cellular uptake of LCFA from the LCFA-albumin complex is an entire protein-mediated process. Conversely, dissolving radiolabeled LCFA in lipophilic solvents, such as DMSO, would lead to the partitioning of LCFA into the outer plasma membrane monolayer rather than being taken up by a physiological process involving membrane-binding proteins. Albumin has 6–8 binding sites for LCFA. When palmitate will be mixed with albumin at ratios exceeding 8:1, palmitate micelles will be formed. Such micelles will readily incorporate into membranes so that nonphysiologically high uptake rates will be recorded. An important point of consideration is that palmitate is taken up as a function of the "free," i.e., non-albumin-bound palmitate concentration and not the total palmitate concentration [8]. At least in media with albumin concentrations >4 μM, the free palmitate concentration is entirely governed by the palmitate-albumin ratio [14]. Therefore in studies on fatty acid uptake regulation, the respective Materials and Methods sections (describing the uptake assay) should detail not only the total LCFA concentration but also the LCFA-albumin ratio. The physiological

LCFA-albumin ratio roughly varies between 0.3 and 3. Of further note, possible changes in LCFA uptake would be most sensitively detected at palmitate-albumin ratios well below the ratio at which the rate is half of V_{max}, thus reflecting an apparent K_m (in analogy to Michaelis-Menten kinetics of enzyme reactions). As an example, in cardiomyocytes, palmitate-albumin ratios should be used below a ratio of 1.45, which amounts to the apparent K_m of palmitate uptake in this cell type (Fig. 1b) [8].

1.1.4 Stop Procedures

Several stop procedures have been applied to terminate the uptake process, for instance, centrifugation of the cells through a layer of silicon oil [5]. This latter stop protocol can be applied to primary hepatocytes but is not suited for every cell type. For studies with cardiomyocytes, we have adopted a stop procedure from Sorrentino et al. [7]. This method brings together three different means contributing to stop radiolabeled substrate uptake: (1) dilution with excess cold substrate, (2) removal of LCFA that are loosely attached to the outer leaflet of the plasma membrane (but have not been taken up) by inclusion of albumin in the stop buffer, and (3) addition of phloretin, a nonselective inhibitor of carrier-mediated membrane transport processes [15].

1.1.5 Limitations

The substrate uptake rates to be calculated from these single-cell suspensions will definitely differ from the in vivo uptake rates, because the cells are incubated in the absence of blood-delivered hormonal and any mechanical stimuli. In primary culture, cardiomyocytes are not stimulated to contract and, at the most, will display some irregular spontaneous contractions. But these occasional contractions do not compare with the metabolic demands of the in vivo contractions. Hence, in vitro uptake rates are expected to be at least a magnitude lower. But nonetheless, single-cell suspensions offer the opportunity to investigate the kinetics and influence of stimulating/inhibiting agents in multiple parallel incubations.

1.2 Regulation of Cellular Substrate Uptake by AMPK

The described protocol of cellular substrate uptake is designed for cells in suspension, which can be maintained in viable shape for periods up to 2 h. Hence only short-term regulation of substrate uptake by AMPK needs to be taken into account. Theoretically these would include posttranslational modification (e.g., phosphorylation) of substrate transporters or, alternatively, translocation of substrate transporters from intracellular stores to the plasma membrane. In particular, there is a wealth of evidence that AMPK modulates substrate uptake through the translocation of substrate transporters [3, 16, 17].

With respect to glucose uptake, mostly GLUT1 and GLUT4 have been investigated in relation to AMPK. Whereas AMPK regulation of GLUT1 has been reported to occur via direct activation at

the plasma membrane in clone-9 cells [18], GLUT1 activity in muscle cells is generally regarded as non-inducible, involved in merely basal glucose uptake [19]. On the other hand, there is ample evidence that GLUT4 translocation is the main mechanism by which AMPK regulates changes in glucose uptake [20]. In case of LCFA uptake, a number of structurally unrelated proteins have been proposed to facilitate LCFA uptake. These proteins include the peripheral membrane protein FABPpm, the channel-forming family of the FATPs, and the scavenger receptor CD36, also referred to as SR-B2, supposedly acting as a flippase [3]. Although FABPpm, FATP1, and FATP4, but not FATP6, appear to translocate to the cell surface upon AMPK activation in skeletal muscle cells [21], this has not been reproduced in cardiomyocytes [22]. It is now well established that regulation of LCFA transport by cardiac AMPK relies entirely on the translocation of CD36 to the cell surface, with a very similar molecular mechanism to that of GLUT4. Of note, the same upstream and downstream signaling components appear to be involved, thereby further reinforcing the similarity of both translocation processes. The upstream and downstream mechanisms involved in AMPK-mediated GLUT4 translocation have been intensively studied (e.g., *see* Ref. [20]). In short, upstream of AMPK, the kinases LKB1 and CaMKK-β have been implicated, dependent on the cell type (LKB1 in the heart and CaMKK-β in skeletal muscle). Downstream of AMPK, AS160 is the most important AMPK target leading to GLUT4 translocation via de-inhibition of specific Rab proteins [23]. Remarkably, AMPK-stimulated CD36 translocation in the heart and muscle shares the same upstream and downstream signaling components as AMPK-stimulated GLUT4 translocation, including LKB1, CaMKK-β, and AS160 [24–26]. Hence the AMPK signaling pathway similarly regulates LCFA uptake and glucose uptake.

2 Materials

2.1 Equipment

1. Shaking water bath (including temperature control and holders for 20-mL vials).
2. Magnetic stirrer.
3. Gas phase system of 95% O_2/5% CO_2.
4. N_2 gas.
5. Liquid scintillation counter (β-counter).
6. Glass β-counter vials.

2.2 Cells

7. Cell suspensions can be obtained as primary cells upon isolation from rodent organs (e.g., heart) or can be derived from cell cultures upon dis-attachment from the culture wells.

2.3 Uptake Assay

1. Ethanol.
2. DMSO.
3. KOH: 1 M KOH.
4. $CaCl_2$: 100 mM $CaCl_2$.
5. Bovine serum albumin (BSA)—Fraction V (fatty acid-free).
6. Palmitic acid.
7. [1-^{14}C]palmitate.
8. 2-Deoxyglucose/2-deoxy-D-[^{3}H]glucose mix: 10 mM 2-deoxyglucose and 2.2 μCi 2-deoxy-D-[^{3}H]glucose.
9. AMPK activators and/or inhibitors.
10. OPTI-FLUOR liquid scintillation cocktail.

Solutions to Be Prepared in Advance

11. 10× MKR: 1.17 M NaCl, 26 mM KCL, 12 mM KH_2PO_4, 12 mM $MgSO_4$, 100 mM $NaHCO_3$, and 100 mM HEPES, pH 7.55. Use a 1 L *glass* cylinder or a *glass* beaker. Weigh the indicated amount of the following chemicals: 68.36 g of NaCl, 1.94 g of KCl, 1.63 g of KH_2PO_4, 2.96 g of $MgSO_4{\cdot}7H_2O$, 8.4 g of $NaHCO_3$, and 23.83 g of HEPES. Add distilled H_2O to a volume of 800 mL. Mix and adjust pH to 7.55 with 1 M NaOH. Make up to 1000 mL with distilled H_2O and store at 4 °C. This stock solution should be diluted in later steps to the indicated dilutions.
12. Stock [1-^{14}C]palmitate label: 1.8 mM palmitate complexed to 0.3 mM (≙2.0% w/v) BSA, 17.4 μM [1-^{14}C]palmitate, and 1 mM $CaCl_2$ in 1× MKR. Prepare pre-warmed BSA solution in a 100 mL *glass* cylinder, by dissolving 1.0 g of BSA in 40 mL of 1,25× MKR. Place in a shaking water bath at 37 °C until further use (100 rpm). Weigh 23.1 mg of palmitic acid in a 100 mL *glass* cylinder, and dissolve in 9.5 mL of pure ethanol**.** Add 50 μCi of [1-^{14}C]palmitate (*see* **Note 1**), and mix thoroughly. Use a 10 mL *glass* cylinder to prepare 10 mL of KOH solution by pipetting 135 μL of 1 M KOH into 10 mL distilled H_2O. Add, drop by drop under constant stirring, the 10 mL of KOH solution to the 10 mL of palmitate-ethanol solution (*see* **Note 2**). Evaporate all ethanol at 45 °C (in water bath) under a constant stream of N_2 gas until the odor of alcohol can no longer be detected and the volume is less than 8 mL. Adjust the volume to 10 mL with distilled H_2O. Add this 10 mL KOH-palmitate solution drop by drop with a *glass* pipette (*see* **Note 3**), under continuous gentle stirring (*see* **Note 2**) to the pre-warmed BSA solution (total volume 50 mL). Add 0.5 mL of 100 mM $CaCl_2$. Transfer into *glass* centrifuge tubes, and spin down for 10 min at 3000 × *g* at room temperature.

Aliquot the supernatant into 2–5 mL portions in *glass* vials and store at −20 °C.

Solutions to Be Prepared Extemporaneously the Day of Experiment

13. Uptake buffer: 1× MKR, 1 mM $CaCl_2$, and 0,45% (w/v) BSA. Take a 100 mL *glass* cylinder. Add 0.23 g of BSA, 49.5 mL of MKR buffer, and 0.5 mL of 100 mM $CaCl_2$. Place uptake buffer in a water bath at 37 °C.
14. Day Label (for up to 20 incubations): 100 μM [1-^{14}C]palmitate, 100 μM deoxy-glucose, and 3.3 μCi 2-deoxy-D-[^{3}H]glucose. Take a 10 mL *glass* vial, and add 9.34 mL of uptake buffer, 0.56 mL of Stock [1-^{14}C]palmitate label, and 100 μL of 10 mM 2-deoxyglucose/2-deoxy-D-[^{3}H]glucose mix. Place the vial in a water bath at 37 °C.
15. Stop solution (for ~20 incubations): 0.2 mM phloretin and 0.1% (w/v) BSA. Prepare phloretin solution by dissolving 21.8 mg of phloretin in 400 μL DMSO. Use a 500 mL **glass** cylinder, and add 400 mL of 1× MKR buffer, 4.0 mL of 100 mM $CaCl_2$, 0.40 g of BSA (Fraction V, essentially fatty acid-free), and the phloretin solution. For each condition, prepare a 15-mL centrifugation tube with 8 mL Stop solution added. Place tubes on ice.
16. Working solutions of desired AMPK stimuli (*see* **Note 4**) and/or inhibitors (*see* **Note 5**).

3 Methods

1. Suspend cells in uptake buffer (50,000–500,000 cells/mL) (depending on metabolic activity of cells; *see* **Notes 6** and 7), and distribute over (20-mL) *glass* vials. Add 2 mL of cell suspension per vial.
2. Preincubate the cell suspension at 37 °C with a gas phase of 95% O_2 /5% CO_2 with inhibitors of AMPK for 20 min in a water bath (shaking at 160 rpm).
3. Subsequently, add activators of AMPK, refill the gas phase, and incubate for another 30 min at 37 °C.
4. Start the uptake assay by adding 0.5 mL of Day Label to the cell suspension, and incubate for 5 min at 37 °C in a water bath with a gas phase of 95% O_2/5% CO_2. Each cellular substrate uptake assay should include a "zero time control" to allow to correct for the background signal (*see* **Note 8**).
5. After 5 min, stop the assay, and transfer 2 mL of cell suspension from each incubation to centrifugation tubes with 8 mL of ice-cold Stop solution.

6. Spin the cells down for ≤2 min at 4 °C (*see* **Note 9**). Remove the supernatant and wash with 10 mL of ice-cold Stop solution. Repeat the centrifugation step.
7. Lyse the pellets in 0.5 mL of distilled H_2O, and transfer the lysates to 20 mL glass β-counter vials containing 5 mL of OPTI-FLUOR liquid scintillation cocktail. Do not forget to include a sample with a fixed volume (e.g., 20 μL) of Day Label for scintillation counting in order to allow for calculation of absolute uptake rates.
8. Vortex the samples, and measure the disintegration counts per minute at the β-counter using a combined $^{3}H/^{14}C$ counting protocol. Uptake values are expressed as nmol/(g wet mass * min), after subtracting the background signal (*see* **Note 8**). A representative data set of a substrate uptake assay using AMPK activators is given in Table 1.

4 Notes

1. It is advised to purchase and use a radiolabeled palmitate product dissolved in ethanol, and not toluene, because toluene is extremely toxic to cells.
2. If precipitate is formed, discard the solution and start again.
3. Work as much as possible with glassware because (radiolabeled) palmitate binds non-specifically to plastic surfaces. In the uptake assay, this can lead to high background counts.
4. For selecting the appropriate AMPK activators to be used in the intended experiments, at least the following five items are relevant: (1) the cellular uptake process of interest, (2) the tissue of interest from which primary cells will be isolated, (3) the type of physiological process one aims to mimic or investigate, (4) the off-target actions of selected compound, and (5) the toxic effects of selected compound depending on the cell type.

   An increasing number of pharmacological AMPK activators have been employed for the study of AMPK activation on cellular LCFA and glucose uptake. We provide here with some tips and consideration about the most commonly used compounds to investigate substrate uptake in muscle cells:

   – *Oligomycin*: It is a very potent stimulator of glucose and LCFA uptake in primary cardiomyocytes and in cardiac cell lines in which the uptake of both substrates increases by ~twofold already within 15–30 min [16]. It is of note that the concentration of oligomycin tolerated by cells differs among cell types. In cardiomyocytes, oligomycin can be used at concentrations of up to 30 μM, but this

Table 1
Data obtained from an example experiment

Condition	dpm ^{14}C	Minus background	Palmitate uptake	Normalized	dpm ^{3}H	Minus background	Deoxyglucose uptake	Normalized
Zero time	76				38			
Control	1590	1514	10.10		372	334	0.81	
Control	1625	1549	10.33	1.00	411	373	0.91	1.00
Control	1669	1593	10.63		414	376	0.91	
Oligomycin	3065	2989	19.94		735	697	1.69	
Oligomycin	3093	3017	20.13	1.94	724	686	1.67	1.97
Oligomycin	3121	3045	20.31		790	752	1.83	
AICAR	2401	2325	15.51		420	382	0.93	
AICAR	2312	2236	14.92	1.47	406	368	0.89	1.03
AICAR	2381	2305	15.38		399	361	0.88	

The described method for substrate uptake measurement was applied. The following values were experimentally determined. Radioactive counts of 20 μL Day Label were 5354 dpm (^{14}C) and 14,705 dpm (^{3}H). The amount of cells per incubation was 7.0 mg wet mass/mL (~70,000 cardiomyocytes/mL). The duration of the uptake assay was 5 min. Values for palmitate uptake and deoxyglucose uptake are calculated as nmol/(g wet mass × min)

concentration is cytotoxic in cell lines, such as HL-1 cells, in which concentrations of up to 1 μM are more advisable. Importantly, besides activation of AMPK [16], oligomycin also stimulates production of reactive oxygen species and subsequent activation of protein kinase-D1, another crucial player in oligomycin-induced GLUT4 translocation and cellular glucose uptake [27].

- *Mitochondrial inhibitors*: Uncoupling agents (such as 2,4-dinitrophenol) and respiratory chain inhibitors (rotenone) stimulate cellular glucose uptake in adipocytes and myocytes [28, 29]. However, these agents cannot be used to study cellular LCFA uptake. Unlike glucose uptake, LCFA uptake across the plasma membrane is dependent on the cellular membrane potential [30], which is destroyed by these agents since their protonophore activity is not restricted to mitochondria [28, 31]. The respiratory chain inhibitor rotenone potently impairs the oxidative metabolism of both substrates. Because uptake and subsequent metabolism are tightly coupled processes, the block in oxidative phosphorylation leads to feedback inhibition of the LCFA uptake process [8]. In contrast, the acceleration of glucose uptake upon rotenone-induced AMPK activation may be accommodated for by a concomitant acceleration in glycolysis so that all incoming glucose is efficiently phosphorylated and feedback inhibition will not occur. In case of specific interest in AMPK-stimulated glucose uptake, DNP and rotenone should preferably be used at low micromolar concentrations.
- *AICAR*: One point of concern with the use of AICAR is the increasing list of AMPK-independent actions of AICAR [32]. Nonetheless, AICAR has been used as activator of LCFA uptake in skeletal muscle [33] and glucose uptake in adipocytes [29] and skeletal muscle [34]. In cardiomyocytes, AICAR, at low millimolar concentrations, stimulates LCFA uptake by ~1.5-fold in an AMPK-dependent fashion [25, 35], but this compound is not effective in stimulation of GLUT4 translocation and cellular glucose uptake (Fig. 2b) [25, 35, 36]. Thus it appears that the stimulation of cellular glucose uptake by AICAR is tissue-specific and should be taken into consideration when studying the effects of AMPK activation on substrate uptake.
- *Metformin and phenformin*: Although these antidiabetic drugs are known to activate AMPK at low millimolar concentrations [37, 38], they failed to increase GLUT4 or CD36 translocation or cellular uptake of LCFA and glucose within 30 min in cardiomyocytes [39] (Luiken, unpublished). However, metformin has been shown to stimulate

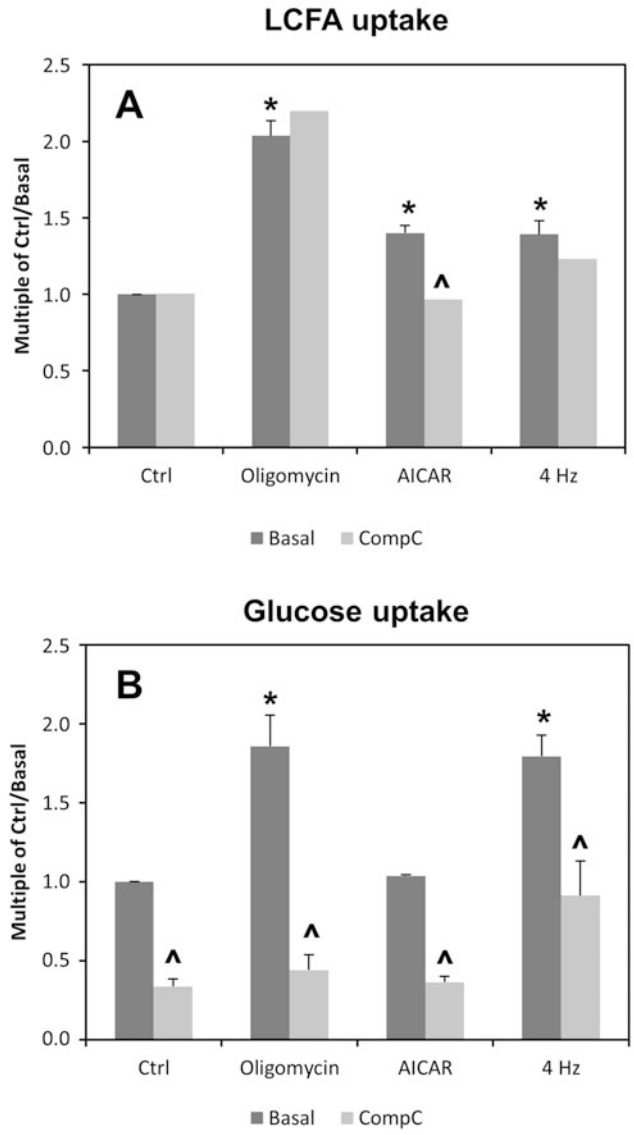

Fig. 2 Effects of Compound C on substrate uptake into rat cardiomyocytes stimulated by various AMPK activators. Cell suspensions were incubated in absence or presence of 50 μM Compound C for 30 min, and subsequently for another 15 min without or with 5 μM oligomycin or 1.5 mM AICAR. Alternatively, electrostimulation was performed for 7 min at 4 Hz. Then, radioactive substrates were added for measurement of (**a**) palmitate uptake or (**b**) deoxyglucose uptake during 5 min. Data are means ± S.E.M ($n = 4$–6). *Significantly different from myocytes without additions (Ctrl) ($p < 0.05$). ^Significantly different from corresponding incubations in the absence of Compound C (Basal) ($p < 0.05$)

GLUT4 translocation in cardiomyocytes upon long-term (18 h) treatment, indicating reliance on synthesis of specific proteins. These proteins might be involved in the negative regulation of GLUT4 endocytosis [39].

- *Small-molecule direct AMPK activators*: A screen by the Abbott Laboratories of >700,000 compounds yielded a non-nucleoside thienopyridone, A-769662, as novel small-molecule AMPK activator [40]. In skeletal muscle strips, it appeared ineffective on stimulation of glucose uptake [41]. In cardiomyocytes at concentrations between 30 and 300 μM, during 30 min, it also failed to stimulate AMPK-Thr172 phosphorylation or LCFA and glucose uptake (Habets and Luiken, unpublished). Compared with β1-containing heterotrimers, β2-containing AMPK isoforms are less efficiently activated by A-769662 [42]. Given that muscle tissues mainly express the AMPK β2 subunit isoform, A-769662 may be a less favorable option for studying the role of AMPK in the heart and skeletal muscle.

  More recently, another small-molecule AMPK activator, 991 (also known as ex229), has been described [41]. Although it shares the same binding site on AMPK as A-769662, it showed a ~tenfold greater potency to activate AMPK [43]. Interestingly, 991 activates both AMPK β1- and β2-containing complexes and efficiently stimulates glucose uptake into skeletal muscle at 100 μM for 60 min [41]. Further studies are required to investigate whether this compound is a suitable tool to study substrate uptake in cardiac cells.

- *Leptin*: This hormone is a physiological AMPK activator and stimulates CD36 translocation in an AMPK-dependent manner at 10 μg/mL for 15–60 min, as well as LCFA uptake in skeletal muscle incubations and cardiomyocytes [44]. With respect to glucose uptake, 20 min leptin was ineffective in stimulating glucose uptake in HL-1 cardiomyocytes [45]. In contrast, 30 min leptin stimulates GLUT4 translocation in C2C12 myotubes, which was dependent on ERK2 [46] and perhaps independent of AMPK. Hence, a pleiotropy of stimulatory actions on intracellular signaling cascades makes leptin less suited as a tool to study AMPK-specific regulation of substrate uptake.

5. Genetic approaches would be the preferable manner to investigate the involvement of AMPK in substrate uptake. An excellent option would be to use primary cells from tissues derived from AMPK knockout mouse models for assessment of cellular substrate uptake. But since at least two isoforms of the catalytic α and regulatory β subunits are expressed in mammals, one needs double-knockout mouse models for these subunits to provide full proof for the involvement of AMPK. But in case that one is only interested in the role of AMPK in a specific tissue, a single-knockout mouse will suffice, when the respective tissue only expresses one isoform. For example, in muscle

tissues, AMPKα2 knockout mice would be suitable, given that the α1 subunit is only marginally expressed in muscles. Furthermore, the muscle-specific kinase-dead AMPKα2 overexpressing mouse [47] provides a very suitable model for the role of AMPK in muscles. A second option would be to silence AMPK in cell lines, e.g., by siRNA approach or CRISPR/Cas9 (*see* Chapter 11). However, when AMPK mouse models or silencing methodologies are not available, one can consider a pharmacological approach and use small-molecule AMPK inhibitors. Below is a list of compounds previously used in substrate uptake studies:

- *5-Iodotubercidin*: 5-Iodotubercidin is not a direct AMPK inhibitor but blocks the formation of AMP from adenosine via inhibition of adenosine kinase [48]. Treatment with 5-iodotubercidin for 10 μM at 15–30 min blocks AICAR-induced LCFA uptake into cardiomyocytes [16] and glucose uptake into clone-9 cells [18] and muscle strips [49], in agreement with its ability to inhibit ZMP formation. In contrast, 5-iodotubercidin does not alter contraction and oligomycin-stimulated LCFA uptake into cardiomyocytes [16], which is readily explained by the fact that AMP formation due to stress or increased energy demands is derived from ATP utilization and not from AMP synthesis. Hence, 5-iodotubercidin is of limited use to study AMPK actions.
- *Adenine 9-β-D-arabinofuranoside (Ara-A)*: This AMP analog decreases AMPK activity in vitro [50]. Ara-A is used in concentrations of 2–3 mM for 15–30 min and entirely inhibits AICAR-induced glucose uptake into muscle strips [49]. It also inhibits stimulation of GLUT4 translocation and glucose uptake in neonatal cardiomyocytes by respiratory chain inhibition using sodium azide (NaN_3). Furthermore, Ara-A inhibits AICAR-stimulated LCFA uptake into primary cardiomyocytes [35] and also leptin-stimulated CD36 translocation and LCFA uptake into skeletal muscle and primary cardiomyocytes [44]. Hence, as AMPK inhibitor, Ara-A has a broader applicability than 5-iodotubercidin in studying AMPK-related actions but has also numerous other inhibitory effects, such as inhibition of adenylyl cyclase [51].
- *Compound C*: As selected from a high-throughput in vitro kinase assay out of >10.000 compounds, Compound C appeared a potent reversible AMPK antagonist via competition with ATP [37]. Compound C is mostly used in concentrations of 10–50 μM and has been shown to inhibit AICAR-induced GLUT4 translocation [52] and AICAR-stimulated glucose uptake [53]. We have used Compound C (50 μM) to study AMPK-mediated LCFA and glucose

uptake into primary cardiomyocytes. AICAR-stimulated LCFA uptake was entirely inhibited, whereas contraction and oligomycin-stimulated LCFA uptake were not significantly altered (Fig. 2a). This inhibition pattern does not match with the presumed direct action of Compound C on AMPK. Furthermore, interpretation of the effects of Compound C on AMPK-stimulated glucose uptake was complicated by a large effect of this inhibitor on basal glucose uptake (Fig. 2b), in agreement with Merlin et al. [53]. Please note that AICAR does not stimulate glucose uptake into rodent cardiomyocytes (Fig. 2b). Finally, the list of off-target actions of Compound C on other kinases, such as ERK8 and MNK1, is growing [54]. As described in Chapter 12, there are serious doubts about the specificity of Compound C and whether it is a useful tool for studying AMPK.

- *STO-609*: STO-609 does not inhibit AMPK directly but rather blocks upstream activation. Specifically, STO-609 is an antagonist of Ca^{2+}/calmodulin-dependent kinase kinase (CaMKK) [55]. Together with liver kinase B1 (LKB1) and transforming growth factor beta-activated kinase 1 (TAK1) [56], CaMKK-β is one of the several kinases able to directly activate AMPK. Hence, STO-609 is of no use to study activation of AMPK by LKB1 and TAK1. Given that most inflammatory stimuli act via TAK1 and given that LKB1 is the major upstream activator of AMPK in several tissues, including the heart [25], STO-609 is often of limited use in AMPK research. We observed that STO-609 (5 μM; 20 min) does not block LCFA and glucose uptake stimulated by oligomycin or AICAR [35].

  But still, STO-609 may be a suitable tool to connect Ca^{2+} signaling to AMPK signaling. In skeletal muscle, the Ca^{2+} signaling activator caffeine stimulates AMPKα2 activation, and also LCFA and glucose uptake. Moreover, LCFA and glucose uptake stimulated by contraction or caffeine is largely blocked by STO-609 indicating an important role of CaMKK-β in AMPK regulation of substrate uptake in contracting muscle [24]. In contrast STO-609 did not inhibit contraction-stimulated LCFA and glucose uptake into primary cardiomyocytes, pinpointing to a less prominent role of Ca^{2+} signaling in contraction-regulated metabolism in the heart [35].

6. The isolation procedure raises cellular stress levels, and primary cells should preferably undergo a recovery period of ~90 min at room temperature after their isolation to allow the metabolic rate to decrease to low "basal" levels. In case of cultured cells, a ~60 min recovery period is recommended after the

dis-attachment from the plates with a low trypsin concentration ($\leq$0.05%) to minimize damage to exposed substrate transporters at the cell surface.

7. Most primary cells can be regarded as metabolically active cells, especially since isolation procedures have been optimized for many years. When these cells are immediately used for substrate uptake assays, their metabolic activity will be highest, likely resulting in relatively high substrate uptake rates. Culturing of primary cells leads to a marked decline in metabolic activity depending on the duration and culturing conditions. Upon their dis-attachment from the culture wells, it is therefore recommended to use higher cell densities in the uptake assay, compared to their freshly used counterparts. Lowest metabolic activity is displayed by the cell lines and likely dependent on the number of passages. Therefore, relatively high cell densities should be used in order to obtain accurately detectable uptake values. Overall, it is recommended to perform a pilot measurement of substrate uptake as function of the cell density.
8. Correction for background signal: At least one incubation per experiment should serve as "zero time control" ($t = 0$). In this case, the cell suspension (1.6 mL) should be transferred to the Stop solution prior to addition of the Day Label (0.4 mL). The remainder of the procedure is similar as described for the other incubations. When performing the calculation of uptake rates, the counts of this "zero time control" should be subtracted from the radioactive counts of each incubation.
9. The centrifugation speed is dependent on the size of the cells (e.g., primary cardiomyocytes are pelleted at 25 $\times g$; several cell lines require centrifugation speeds of ~1000 $\times g$).

References

1. Shulman GI (2000) Cellular mechanisms of insulin resistance. J Clin Invest 106 (2):171–176. https://doi.org/10.1172/JCI10583
2. Luiken JJ, Schaap FG, van Nieuwenhoven FA, van der Vusse GJ, Bonen A, Glatz JF (1999) Cellular fatty acid transport in heart and skeletal muscle as facilitated by proteins. Lipids 34 (Suppl):S169–S175
3. Glatz JF, Luiken JJ, Bonen A (2010) Membrane fatty acid transporters as regulators of lipid metabolism: implications for metabolic disease. Physiol Rev 90(1):367–417. https://doi.org/10.1152/physrev.00003.2009
4. Mueckler M (1994) Facilitative glucose transporters. Eur J Biochem 219(3):713–725
5. Rose H, Hennecke T, Kammermeier H (1990) Sarcolemmal fatty acid transfer in isolated cardiomyocytes governed by albumin/membrane-lipid partition. J Mol Cell Cardiol 22 (8):883–892
6. Hamilton JA, Johnson RA, Corkey B, Kamp F (2001) Fatty acid transport: the diffusion mechanism in model and biological membranes. J Mol Neurosci 16(2–3):99–108.; discussion 151–157. https://doi.org/10.1385/JMN:16:2-3:99
7. Sorrentino D, Stump D, Potter BJ, Robinson RB, White R, Kiang CL, Berk PD (1988) Oleate uptake by cardiac myocytes is carrier mediated and involves a 40-kD plasma membrane fatty acid binding protein similar to that in liver, adipose tissue, and gut. J Clin Invest 82

(3):928–935. https://doi.org/10.1172/JCI113700

8. Luiken JJ, van Nieuwenhoven FA, America G, van der Vusse GJ, Glatz JF (1997) Uptake and metabolism of palmitate by isolated cardiac myocytes from adult rats: involvement of sarcolemmal proteins. J Lipid Res 38(4):745–758
9. Schwenk RW, Dirkx E, Coumans WA, Bonen A, Klip A, Glatz JF, Luiken JJ (2010) Requirement for distinct vesicle-associated membrane proteins in insulin- and AMP-activated protein kinase (AMPK)-induced translocation of GLUT4 and CD36 in cultured cardiomyocytes. Diabetologia 53 (10):2209–2219. https://doi.org/10.1007/s00125-010-1832-7
10. Van Nieuwenhoven FA, Luiken JJ, De Jong YF, Grimaldi PA, Van der Vusse GJ, Glatz JF (1998) Stable transfection of fatty acid translocase (CD36) in a rat heart muscle cell line (H9c2). J Lipid Res 39(10):2039–2047
11. Oakes ND, Kjellstedt A, Forsberg GB, Clementz T, Camejo G, Furler SM, Kraegen EW, Olwegard-Halvarsson M, Jenkins AB, Ljung B (1999) Development and initial evaluation of a novel method for assessing tissue-specific plasma free fatty acid utilization in vivo using (R)-2-bromopalmitate tracer. J Lipid Res 40(6):1155–1169
12. Verberne HJ, Sloof GW, Beets AL, Murphy AM, van Eck-Smit BL, Knapp FF (2003) 125I-BMIPP and 18F-FDG uptake in a transgenic mouse model of stunned myocardium. Eur J Nucl Med Mol Imaging 30(3):431–439
13. Vorum H, Brodersen R, Kragh-Hansen U, Pedersen AO (1992) Solubility of long-chain fatty acids in phosphate buffer at pH 7.4. Biochim Biophys Acta 1126(2):135–142
14. Richieri GV, Ogata RT, Kleinfeld AM (1994) Equilibrium constants for the binding of fatty acids with fatty acid-binding proteins from adipocyte, intestine, heart, and liver measured with the fluorescent probe ADIFAB. J Biol Chem 269(39):23918–23930
15. Andersen BL, Tarpley HT, Regen DM (1978) Characterization of beta-hydroxybutyrate transport in rat erythrocytes and thymocytes. Biochim Biophys Acta 508(3):525–538
16. Luiken JJ, Coort SL, Willems J, Coumans WA, Bonen A, van der Vusse GJ, Glatz JF (2003) Contraction-induced fatty acid translocase/CD36 translocation in rat cardiac myocytes is mediated through AMP-activated protein kinase signaling. Diabetes 52(7):1627–1634
17. Klip A, Schertzer JD, Bilan PJ, Thong F, Antonescu C (2009) Regulation of glucose transporter 4 traffic by energy deprivation from mitochondrial compromise. Acta Physiol (Oxf) 196(1):27–35. https://doi.org/10.1111/j.1748-1716.2009.01974.x
18. Abbud W, Habinowski S, Zhang JZ, Kendrew J, Elkairi FS, Kemp BE, Witters LA, Ismail-Beigi F (2000) Stimulation of AMP-activated protein kinase (AMPK) is associated with enhancement of Glut1-mediated glucose transport. Arch Biochem Biophys 380 (2):347–352. https://doi.org/10.1006/abbi.2000.1935
19. Abel ED (2004) Glucose transport in the heart. Front Biosci 9:201–215
20. Richter EA, Hargreaves M (2013) Exercise, GLUT4, and skeletal muscle glucose uptake. Physiol Rev 93(3):993–1017. https://doi.org/10.1152/physrev.00038.2012
21. Jain SS, Chabowski A, Snook LA, Schwenk RW, Glatz JF, Luiken JJ, Bonen A (2009) Additive effects of insulin and muscle contraction on fatty acid transport and fatty acid transporters, FAT/CD36, FABPpm, FATP1, 4 and 6. FEBS Lett 583(13):2294–2300. https://doi.org/10.1016/j.febslet.2009.06.020
22. Habets DD (2008) Thesis: "Regulation of cardiac long-chain fatty acid and glucose utilization. Studies with cardiomyocytes from genetically manipulated mice" Thesis Chapter 5: AICAR stimulates long-chain fatty acid uptake and oxidation in mouse heart independent of CD36
23. Thong FS, Bilan PJ, Klip A (2007) The Rab GTPase-activating protein AS160 integrates Akt, protein kinase C, and AMP-activated protein kinase signals regulating GLUT4 traffic. Diabetes 56(2):414–423. https://doi.org/10.2337/db06-0900
24. Abbott MJ, Edelman AM, Turcotte LP (2009) CaMKK is an upstream signal of AMP-activated protein kinase in regulation of substrate metabolism in contracting skeletal muscle. Am J Physiol Regul Integr Comp Physiol 297(6):R1724–R1732. https://doi.org/10.1152/ajpregu.00179.2009
25. Habets DD, Coumans WA, El Hasnaoui M, Zarrinpashneh E, Bertrand L, Viollet B, Kiens B, Jensen TE, Richter EA, Bonen A, Glatz JF, Luiken JJ (2009) Crucial role for LKB1 to AMPKalpha2 axis in the regulation of CD36-mediated long-chain fatty acid uptake into cardiomyocytes. Biochim Biophys Acta 1791(3):212–219. https://doi.org/10.1016/j.bbalip.2008.12.009
26. Samovski D, Su X, Xu Y, Abumrad NA, Stahl PD (2012) Insulin and AMPK regulate FA translocase/CD36 plasma membrane recruitment in cardiomyocytes via Rab GAP AS160 and Rab8a Rab GTPase. J Lipid Res 53

(4):709–717. https://doi.org/10.1194/jlr.M023424

27. Luiken JJ, Glatz JF, Neumann D (2015) Cardiac contraction-induced GLUT4 translocation requires dual signaling input. Trends Endocrinol Metab 26(8):404–410. https://doi.org/10.1016/j.tem.2015.06.002
28. Luiken JJ, Coort SL, Koonen DP, van der Horst DJ, Bonen A, Zorzano A, Glatz JF (2004) Regulation of cardiac long-chain fatty acid and glucose uptake by translocation of substrate transporters. Pflugers Arch 448 (1):1–15. https://doi.org/10.1007/s00424-003-1199-4
29. Yamaguchi S, Katahira H, Ozawa S, Nakamichi Y, Tanaka T, Shimoyama T, Takahashi K, Yoshimoto K, Imaizumi MO, Nagamatsu S, Ishida H (2005) Activators of AMP-activated protein kinase enhance GLUT4 translocation and its glucose transport activity in 3T3-L1 adipocytes. Am J Physiol Endocrinol Metab 289(4):E643–E649. https://doi.org/10.1152/ajpendo.00456.2004
30. Weisiger RA, Fitz JG, Scharschmidt BF (1989) Hepatic oleate uptake. Electrochemical driving forces in intact rat liver. J Clin Invest 83 (2):411–420. https://doi.org/10.1172/JCI113899
31. Park KS, Jo I, Pak K, Bae SW, Rhim H, Suh SH, Park J, Zhu H, So I, Kim KW (2002) FCCP depolarizes plasma membrane potential by activating proton and Na+ currents in bovine aortic endothelial cells. Pflugers Arch 443 (3):344–352. https://doi.org/10.1007/s004240100703
32. Liu X, Chhipa RR, Pooya S, Wortman M, Yachyshin S, Chow LM, Kumar A, Zhou X, Sun Y, Quinn B, McPherson C, Warnick RE, Kendler A, Giri S, Poels J, Norga K, Viollet B, Grabowski GA, Dasgupta B (2014) Discrete mechanisms of mTOR and cell cycle regulation by AMPK agonists independent of AMPK. Proc Natl Acad Sci U S A 111(4): E435–E444. https://doi.org/10.1073/pnas.1311121111
33. Bonen A, Han XX, Habets DD, Febbraio M, Glatz JF, Luiken JJ (2007) A null mutation in skeletal muscle FAT/CD36 reveals its essential role in insulin- and AICAR-stimulated fatty acid metabolism. Am J Physiol Endocrinol Metab 292(6):E1740–E1749. https://doi.org/10.1152/ajpendo.00579.2006
34. Russell RR 3rd, Bergeron R, Shulman GI, Young LH (1999) Translocation of myocardial GLUT-4 and increased glucose uptake through activation of AMPK by AICAR. Am J Phys 277 (2 Pt 2):H643–H649
35. Angin Y, Schwenk RW, Nergiz-Unal R, Hoebers N, Heemskerk JW, Kuijpers MJ, Coumans WA, van Zandvoort MA, Bonen A, Neumann D, Glatz JF, Luiken JJ (2014) Calcium signaling recruits substrate transporters GLUT4 and CD36 to the sarcolemma without increasing cardiac substrate uptake. Am J Physiol Endocrinol Metab 307(2): E225–E236. https://doi.org/10.1152/ajpendo.00655.2013
36. Dirkx E, Schwenk RW, Coumans WA, Hoebers N, Angin Y, Viollet B, Bonen A, van Eys GJ, Glatz JF, Luiken JJ (2012) Protein kinase D1 is essential for contraction-induced glucose uptake but is not involved in fatty acid uptake into cardiomyocytes. J Biol Chem 287 (8):5871–5881. https://doi.org/10.1074/jbc.M111.281881
37. Zhou G, Myers R, Li Y, Chen Y, Shen X, Fenyk-Melody J, Wu M, Ventre J, Doebber T, Fujii N, Musi N, Hirshman MF, Goodyear LJ, Moller DE (2001) Role of AMP-activated protein kinase in mechanism of metformin action. J Clin Invest 108(8):1167–1174. https://doi.org/10.1172/JCI13505
38. Musi N, Hirshman MF, Nygren J, Svanfeldt M, Bavenholm P, Rooyackers O, Zhou G, Williamson JM, Ljunqvist O, Efendic S, Moller DE, Thorell A, Goodyear LJ (2002) Metformin increases AMP-activated protein kinase activity in skeletal muscle of subjects with type 2 diabetes. Diabetes 51(7):2074–2081
39. Yang J, Holman GD (2006) Long-term metformin treatment stimulates cardiomyocyte glucose transport through an AMP-activated protein kinase-dependent reduction in GLUT4 endocytosis. Endocrinology 147 (6):2728–2736. https://doi.org/10.1210/en.2005-1433
40. Cool B, Zinker B, Chiou W, Kifle L, Cao N, Perham M, Dickinson R, Adler A, Gagne G, Iyengar R, Zhao G, Marsh K, Kym P, Jung P, Camp HS, Frevert E (2006) Identification and characterization of a small molecule AMPK activator that treats key components of type 2 diabetes and the metabolic syndrome. Cell Metab 3(6):403–416. https://doi.org/10.1016/j.cmet.2006.05.005
41. Lai YC, Kviklyte S, Vertommen D, Lantier L, Foretz M, Viollet B, Hallen S, Rider MH (2014) A small-molecule benzimidazole derivative that potently activates AMPK to increase glucose transport in skeletal muscle: comparison with effects of contraction and other AMPK activators. Biochem J 460 (3):363–375. https://doi.org/10.1042/BJ20131673

42. Rajamohan F, Reyes AR, Frisbie RK, Hoth LR, Sahasrabudhe P, Magyar R, Landro JA, Withka JM, Caspers NL, Calabrese MF, Ward J, Kurumbail RG (2016) Probing the enzyme kinetics, allosteric modulation and activation of alpha1- and alpha2-subunit-containing AMP-activated protein kinase (AMPK) heterotrimeric complexes by pharmacological and physiological activators. Biochem J 473 (5):581–592. https://doi.org/10.1042/BJ20151051
43. Xiao B, Sanders MJ, Carmena D, Bright NJ, Haire LF, Underwood E, Patel BR, Heath RB, Walker PA, Hallen S, Giordanetto F, Martin SR, Carling D, Gamblin SJ (2013) Structural basis of AMPK regulation by small molecule activators. Nat Commun 4:3017. https://doi.org/10.1038/ncomms4017
44. Momken I, Chabowski A, Dirkx E, Nabben M, Jain SS, McFarlan JT, Glatz JF, Luiken JJ, Bonen A (2017) A new leptin-mediated mechanism for stimulating fatty acid oxidation: a pivotal role for sarcolemmal FAT/CD36. Biochem J 474(1):149–162. https://doi.org/10.1042/BCJ20160804
45. Palanivel R, Eguchi M, Shuralyova I, Coe I, Sweeney G (2006) Distinct effects of short- and long-term leptin treatment on glucose and fatty acid uptake and metabolism in HL-1 cardiomyocytes. Metabolism 55 (8):1067–1075. https://doi.org/10.1016/j.metabol.2006.03.020
46. Berti L, Gammeltoft S (1999) Leptin stimulates glucose uptake in C2C12 muscle cells by activation of ERK2. Mol Cell Endocrinol 157 (1–2):121–130
47. Mu J, Brozinick JT Jr, Valladares O, Bucan M, Birnbaum MJ (2001) A role for AMP-activated protein kinase in contraction- and hypoxia-regulated glucose transport in skeletal muscle. Mol Cell 7(5):1085–1094
48. Samari HR, Seglen PO (1998) Inhibition of hepatocytic autophagy by adenosine, aminoimidazole-4-carboxamide riboside, and N6-mercaptopurine riboside. Evidence for involvement of amp-activated protein kinase. J Biol Chem 273(37):23758–23763
49. Musi N, Hayashi T, Fujii N, Hirshman MF, Witters LA, Goodyear LJ (2001) AMP-activated protein kinase activity and glucose uptake in rat skeletal muscle. Am J Physiol Endocrinol Metab 280(5):E677–E684
50. Henin N, Vincent MF, Van den Berghe G (1996) Stimulation of rat liver AMP-activated protein kinase by AMP analogues. Biochim Biophys Acta 1290(2):197–203
51. Iwatsubo K, Bravo C, Uechi M, Baljinnyam E, Nakamura T, Umemura M, Lai L, Gao S, Yan L, Zhao X, Park M, Qiu H, Okumura S, Iwatsubo M, Vatner DE, Vatner SF, Ishikawa Y (2012) Prevention of heart failure in mice by an antiviral agent that inhibits type 5 cardiac adenylyl cyclase. Am J Physiol Heart Circ Physiol 302(12):H2622–H2628. https://doi.org/10.1152/ajpheart.00190.2012
52. Niu W, Bilan PJ, Ishikura S, Schertzer JD, Contreras-Ferrat A, Fu Z, Liu J, Boguslavsky S, Foley KP, Liu Z, Li J, Chu G, Panakkezhum T, Lopaschuk GD, Lavandero S, Yao Z, Klip A (2010) Contraction-related stimuli regulate GLUT4 traffic in C2C12-GLUT4myc skeletal muscle cells. Am J Physiol Endocrinol Metab 298(5):E1058–E1071. https://doi.org/10.1152/ajpendo.00773.2009
53. Merlin J, Evans BA, Csikasz RI, Bengtsson T, Summers RJ, Hutchinson DS (2010) The M3-muscarinic acetylcholine receptor stimulates glucose uptake in L6 skeletal muscle cells by a CaMKK-AMPK-dependent mechanism. Cell Signal 22(7):1104–1113. https://doi.org/10.1016/j.cellsig.2010.03.004
54. Vogt J, Traynor R, Sapkota GP (2011) The specificities of small molecule inhibitors of the TGFss and BMP pathways. Cell Signal 23 (11):1831–1842. https://doi.org/10.1016/j.cellsig.2011.06.019
55. Tokumitsu H, Inuzuka H, Ishikawa Y, Ikeda M, Saji I, Kobayashi R (2002) STO-609, a specific inhibitor of the Ca(2+)/calmodulin-dependent protein kinase kinase. J Biol Chem 277(18):15813–15818. https://doi.org/10.1074/jbc.M201075200
56. Witczak CA, Sharoff CG, Goodyear LJ (2008) AMP-activated protein kinase in skeletal muscle: from structure and localization to its role as a master regulator of cellular metabolism. Cell Mol Life Sci 65(23):3737–3755. https://doi.org/10.1007/s00018-008-8244-6

Chapter 23

Measurement of AMPK-Induced Inhibition of Lipid Synthesis Flux in Cultured Cells

Marc Foretz and Benoit Viollet

Abstract

AMP-activated protein kinase (AMPK) is a master regulator of multiple cellular metabolic pathways, including lipid metabolism. Some of the well-known substrates of AMPK are acetyl-CoA carboxylase (ACC) and 3-hydroxy-3-methylglutaryl-coenzyme A (HMG-CoA) reductase, regulatory enzymes of fatty acid and cholesterol synthesis, respectively. The discovery that both of them are inactivated by AMPK suggested the therapeutic potential of AMPK activation in the treatment of metabolic diseases associated with lipid disorders, such as nonalcoholic fatty liver disease (NAFLD). Here we describe a method to measure lipid synthesis flux in intact cells from the saponifiable (including fatty acids) and non-saponifiable (including sterols) fractions of lipid extracts.

Key words AMP-activated protein kinase, Lipogenesis, Lipid synthesis, Fatty acid synthesis, Sterol synthesis, Indirect AMPK activators, Small-molecule AMPK activators, Metformin, Primary hepatocytes, AMPK knockout

1 Introduction

The regulation of cellular energy metabolism by AMP-activated protein kinase (AMPK) activation is achieved by acute phosphorylation of key enzymes in carbohydrate, lipid, and protein metabolism [1]. In the liver, AMPK activation influences several downstream cellular targets involved in fatty acid and cholesterol synthesis. Acetyl-CoA carboxylase (ACC) and 3-hydroxy-3-methylglutaryl-coenzyme A reductase (HMG-CoA reductase), key enzymes in fatty acid and cholesterol synthesis, respectively, were the first two enzymes shown to be phosphorylated and inhibited by AMPK [2, 3]. AMPK inhibits hepatic fatty acid synthesis through the phosphorylation of ACC1 at Ser79, leading to its inactivation and thus determining cytosolic concentrations of the reaction product malonyl-CoA, a key precursor for the generation of new fatty acids [4]. Given these properties, it is not surprising that AMPK has emerged as an attractive therapeutic target for

Dietbert Neumann and Benoit Viollet (eds.), *AMPK: Methods and Protocols*, Methods in Molecular Biology, vol. 1732, https://doi.org/10.1007/978-1-4939-7598-3_23,

pathological conditions characterized by abnormal hepatic lipid accumulation, such as nonalcoholic fatty liver disease (NAFLD) [5]. Interestingly, recent studies also challenged the therapeutic potential for AMPK activation to limit tumor cell growth and to restrict viral replication by inhibiting the cellular lipid accumulation [6–8]. We and others have demonstrated that single and dual treatment with indirect and direct AMPK activators increases ACC phosphorylation leading to the inhibition of de novo lipogenesis in primary hepatocytes [9–14]. Here, we describe a detailed protocol for testing the potential of various pharmaceutical/nutraceutical compounds on lipid metabolic flux in cultured cells. The quantitative evaluation of lipid synthesis flux is realized by the use of radiolabeled [1-^{14}C]-acetate tracer and monitoring the amount of radioactivity into the lipid fractions. Analysis of the saponifiable and non-saponifiable fractions of lipid extracts enables the quantification of fatty acids and sterols synthesis flux, respectively.

2 Materials

2.1 Cell Culture

1. Mouse primary hepatocytes (*see* **Note 1**).
2. Cell culture plasticware (6-well plates).
3. Hepatocyte culture medium: medium 199, 100 nM dexamethasone, 100 units/mL penicillin, 100 μg/mL streptomycin. Store at 4 °C (*see* **Notes 2** and **3**).
4. [1-^{14}C]-acetic acid, sodium salt, 1 mCi/mL (37 MBq/mL), 45–60 mCi/mmol. Store at 4 °C (*see* **Note 4**).
5. DMSO (dimethyl sulfoxide) (*see* **Note 5**).
6. TOFA (5-tetradecyloxy-2-furoic acid) stock solution: 10 mM TOFA in DMSO. Store at −20 °C (*see* **Note 6**).
7. Metformin stock solution: 500 mM metformin hydrochloride in sterile distilled H_2O. Store at −20 °C (*see* **Note 7**).
8. Compound 991 stock solution: 10 mM in DMSO. Store at −20 °C (*see* **Note 8**).
9. 1× phosphate-buffered saline (PBS): 140 mM NaCl, 2.6 mM KCl; 2 mM Na_2HPO_4, 1.45 mM KH_2PO_4, pH 7.4.
10. Cell scrapers.
11. Humidified 5% CO_2 incubator at 37 °C.

2.2 Lipid Extraction and ^{14}C-Labeled Lipid Counting

1. 13 × 100 mm borosilicate glass tubes.
2. Polytetrafluoroethylene (PTFE)-lined caps.
3. 40% (w/v) KOH in degassed distilled H_2O (*see* **Note 9**).
4. Methanol.

5. Water-saturated petroleum ether (boiling point at 40–60 °C) (*see* **Note 10**).
6. Bromophenol blue stock solution: 0.2% (w/v) bromophenol blue in distilled H_2O.
7. Hydrochloric acid (HCl) fuming 37% (12 N) (*see* **Note 11**).
8. 5 mL polyethylene pipette dropper.
9. Vortex.
10. Oven at 80 °C.
11. Chemical fume hood.
12. 20 mL liquid scintillation vials.
13. Liquid scintillation cocktail.
14. Radiometric beta counter.

3 Methods

3.1 Stimulation of Cells

1. Mouse primary hepatocytes plated at a density of 0.4×10^6 cells/well in 6-well plates are cultured in 1.8 mL of serum-free hepatocyte culture medium at 37 °C in an incubator providing saturated humidity and 5% CO_2 (*see* **Notes 1–3**).
2. Prepare a tenfold concentrated mix of radiolabeled tracer in M199 medium sufficient for the number of wells used. Use 1.2 μL [1-^{14}C]-acetic acid (1.2 μCi) with 198.8 μL M199 medium per well (*see* **Note 12**).
3. Add AMPK activators at various concentrations or equivalent volume of vehicle and 200 μL of 10× tracer mix/well. Wells incubated with 20 μM TOFA could serve as positive control of lipid synthesis inhibition (*see* **Note 6**).
4. Incubate exactly for 3 h at 37 °C in an incubator providing saturated humidity and 5% CO_2.

3.2 Harvesting and Lysing of the Cells

1. Wash the cells three times with 2 mL of ice-cold PBS.
2. Harvest cells by gently scrapping wells in 0.5 mL of PBS.
3. Transfer to glass tubes containing 1 mL of 40% KOH and 2 mL of methanol.
4. Rinse wells with 0.5 mL PBS and combine. Cap the tubes and vortex for 1 min.
5. Heat at 80 °C for 1 h then allow tubes to cool completely at room temperature.

3.3 Lipid Extraction

Extraction of non-saponifiable lipids (*see* **Notes 13** and **14**)

1. Add 3 mL of water-saturated petroleum ether in each tube (*see* **Note 15**).

2. Cap the tubes and vortex for 1 min.
3. Centrifuge at 1000 × *g* for 2 min to separate aqueous and organic phases (*see* **Note 16**).
4. Transfer the upper organic phase with a 5 mL pipette dropper to 20 mL scintillation vials.
5. Repeat extraction with 3 mL of water-saturated petroleum ether and combine the upper phases.
6. Evaporate to dryness the organic extract from scintillation vials under a chemical fume hood (*see* **Note 17**).
7. Add 10 mL of organic scintillation fluid to the dried residues. Vortex thoroughly to dissolve lipids.
8. Count incorporation of ^{14}C into the non-saponifiable fraction (*see* **Note 18**).

Extraction of saponifiable lipids (*see* **Note 19**)

9. Add 50 μL of 2% bromophenol blue to the lower aqueous fraction from previous **step 4**.
10. Perform saponification of lipids by acidifying to the lower aqueous fraction with 700 μL of 37% HCl and vortex for 1 min (*see* **Note 20**).
11. Add 3 mL of water-saturated petroleum ether in each tube (*see* **Note 15**).
12. Cap the tubes and vortex for 1 min.
13. Centrifuge at 1000 × *g* for 2 min to separate aqueous and organic phases (*see* **Note 16**).
14. Transfer the upper organic phase with a 5 mL pipette dropper to new 20 mL scintillation vials.
15. Repeat extraction with 3 mL water-saturated petroleum ether and combine the upper phases.
16. Evaporate to dryness the organic extract from scintillation vials under a chemical fume hood (*see* **Note 17**).
17. Add 10 mL of organic scintillation fluid to the dried residues. Vortex thoroughly to dissolve lipids.
18. Count incorporation of ^{14}C into the saponifiable fraction (*see* **Note 19**).
19. Determine specific activity by counting 50 μL of labeled media (*see* **Note 18**).

4 Notes

1. The method for the measurement of lipid synthesis described here can be adapted to other cell types because lipid synthesis is active in most cultured cells. An important point to respect is the number of cells in each well since there is no internal

control to normalize data. If the cells studied are available in small numbers, the protocol can be adapted to 12- or 24-well plates. However, we found that the 6-well plate format gives better results in terms of reproducibility.

Measurement of [1-^{14}C]-acetate incorporation into lipids is a very sensitive method to assess variations of lipid synthesis induced by AMPK activation or other stimuli. When this measure is coupled with the use of AMPK-deficient cells such as AMPKα1α2 KO hepatocytes [15], it is a powerful functional test to determine the AMPK dependence on lipid synthesis inhibition induced by various drugs or stimuli (Fig. 1).

2. Medium 199 contains 0.6 mM sodium acetate. If an alternative medium is used, supplement or adjust the sodium acetate concentration to 0.6 mM.
3. Dexamethasone is specifically used in primary culture of hepatocytes to limit dedifferentiation [16].
4. We use [1-^{14}C]-acetic acid, sodium salt from Perkin Elmer (NEC084h001MC). The use of radioactive material requires a legal authorization and needs precautions such as designate and label areas for working with radioactive material, use a chemical fume hood to handle radioactive sources, and wear appropriate personal protective equipment. Radioactive waste requires a specific management.
5. In unstimulated cells, the vehicle (DMSO, ethanol, etc.) should be used as a control.
6. TOFA is a competitive inhibitor of acetyl-CoA carboxylase used as a positive control of lipid synthesis inhibition.
7. Metformin is an indirect AMPK activator which stimulates AMPK activity by increasing intracellular AMP/ATP ratio through inhibition of complex I of the mitochondrial respiratory chain [17, 18].
8. Compound 991 is a small molecule that directly activates AMPK through an AMP-independent mechanism by binding at the interface between the carbohydrate-binding domain of the regulatory β subunit and the catalytic α subunit [19].
9. Distilled H_2O is degassed under vacuum to remove CO_2 and to avoid the formation of K_2CO_3.
10. Water-saturated petroleum ether is prepared by mixing one volume of distilled H_2O with one volume of petroleum ether in a glass bottle. After shaking and decanting, water-saturated petroleum ether corresponds to the upper phase.
11. Concentrated HCl can be replaced by concentrated H_2SO_4 (12 N).

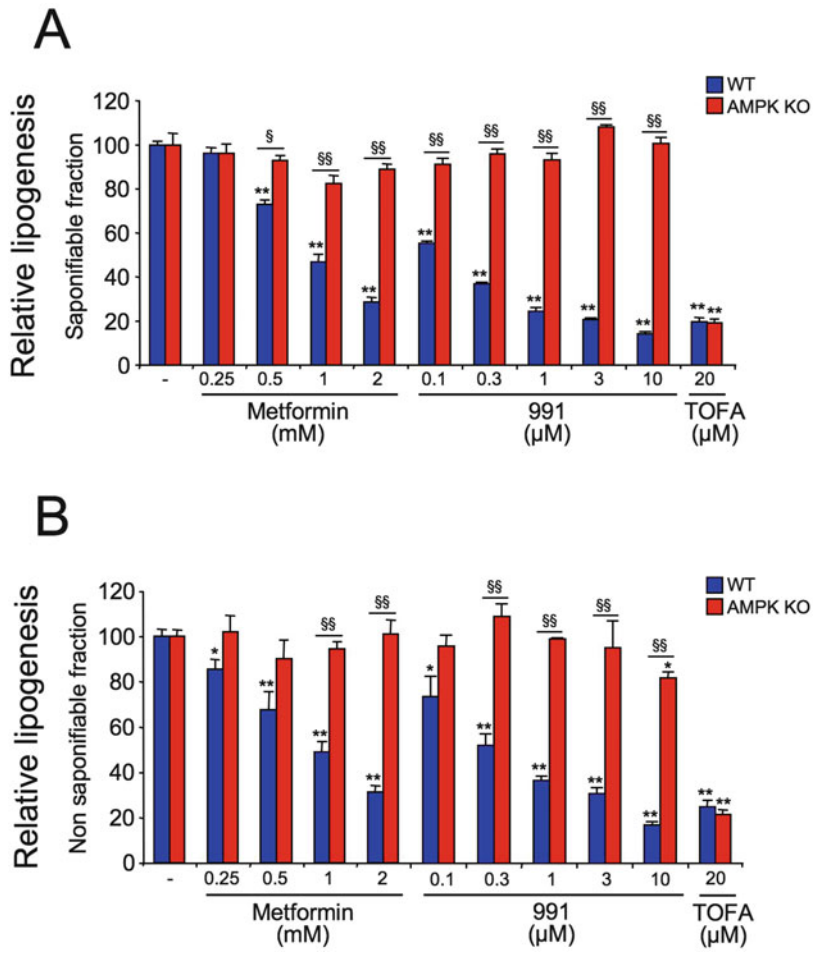

Fig. 1 Effects of metformin and small-molecule 991 on lipid synthesis rates in WT and AMPK-deficient hepatocytes. After plating, WT and AMPKα1α2 knockout primary hepatocytes were cultured for 16 h in serum-free M199 medium containing antibiotics and 100 nM dexamethasone. Hepatocytes were then incubated for 3 h in fresh medium in the absence or in the presence of increasing concentrations of metformin (0.25, 0.5, 1, or 2 mM), an indirect AMPK activator; 991 (0.1, 0.3, 1, 3, or 10 μM), a small-molecule direct activator of AMPK; or TOFA (20 μM), a competitive inhibitor of acetyl-CoA carboxylase, and [1-^{14}C]-acetate tracer was added directly in medium. Rates of fatty acid and sterol synthesis were assessed from incorporation of [1-^{14}C]-acetate into saponifiable (**A**) and non-saponifiable (**B**) lipids, respectively. Results were normalized to protein content and presented as a percentage of [1-^{14}C]-acetate incorporated in WT or AMPK KO hepatocytes incubated in the absence of compounds. Results are representative of three independent experiments. Data are mean ± SEM. $^{*}P < 0.05$, $^{**}P < 0.001$ compared with WT or AMPK KO hepatocytes incubated in the absence of compounds and $^{\S}P < 0.01$, $^{\S\S}P < 0.001$ compared with WT hepatocytes incubated in the same conditions by two-way ANOVA with Bonferroni post hoc test. While TOFA inhibits lipid synthesis both in WT and AMPK-deficient hepatocytes, metformin and 991 inhibit [1-^{14}C]-acetate incorporation in lipids in concentration-dependent manner only in WT hepatocytes. These results demonstrate that the inhibition of hepatic lipid synthesis in response to metformin and 991 is strictly dependent of AMPK

12. [1-^{14}C]-labeled acetate concentration in medium is 0.6 μCi/mL, and cold acetate concentration is 0.6 mM.
13. Non-saponifiable fraction corresponds to neutral lipids, predominantly sterols including cholesterol.
14. Extraction of the non-saponifiable fraction can be skipped (Subheading 3.3, **steps 1–8**), and acidification directly carries out. In this case, extracted lipids after saponification correspond to total lipids (sterols and fatty acids).
15. Petroleum ether is extremely flammable. Precautions should be taken in its handling and storing. Vapors are harmful to the eyes, respiratory system, and skin. Consequently, this solvent should be handling only under a chemical fume hood, and proper personal protective should be worn such as chemical-resistant gloves, laboratory coat, and safety glasses.
16. Centrifugation may be optional because aqueous and organic phases can separate rapidly after a few minutes of decanting.
17. Evaporation of organic extracts in vials takes several hours. Usually, we keep the uncapped vials under a chemical fume hood overnight. Evaporation can be accelerated through the use of an evaporator system which blows down a stream of dry air or nitrogen gas in the vials.
18. Counting is disintegrations per minute (dpm). The blank value obtained from wells without cells but treated as other wells is deducted for each sample. We recommend to perform each condition in triplicate for each experiment. Data are normalized to the protein amount per well. For this, reserve at least a 6-well plate of cells incubated without [1-^{14}C]-labeled acetate to assess the amount of proteins per well. The results can be expressed as a percentage of basal (unstimulated condition) or in absolute values (nanomoles of [1-^{14}C]-acetate incorporated/mg of proteins/h) using the specific activity. Specific activity corresponds to the quantity of radioactivity (in dpm) per nmole of acetate in medium. Specific activity is calculated by dividing the number of total dpm measured per well (in 2 mL) by the number of nmoles of acetate per well (0.6 mM × 2 mL = 1220 nmol; the amount of acetate provided by the tracer is negligible). The value of specific activity thus allows to convert the dpm count values deducted of blank in nmoles of [1-^{14}C]-acetate incorporated in lipids. By dividing these data by the incubation time (3 h) and the amount of proteins per well (mg), the results can be expressed in nmoles of [1-^{14}C]-acetate incorporated in lipids/mg of proteins/h.
19. Saponifiable fraction mainly corresponds to fatty acids.
20. pH indicator (blue bromophenol) should turn yellow to assure complete saponification.

Acknowledgments

Work from the authors was performed within the Département Hospitalo-Universitaire (DHU) AUToimmune and HORmonal diseaseS (AUTHORS) and was supported by grants from INSERM, CNRS, Université Paris Descartes, Agence Nationale de la Recherche (ANR), and Société Francophone du Diabète (SFD).

References

1. Hardie DG (2014) AMP-activated protein kinase: maintaining energy homeostasis at the cellular and whole-body levels. Annu Rev Nutr 34:31–55. https://doi.org/10.1146/annurev-nutr-071812-161148
2. Clarke PR, Hardie DG (1990) Regulation of HMG-CoA reductase: identification of the site phosphorylated by the AMP-activated protein kinase in vitro and in intact rat liver. EMBO J 9 (8):2439–2446
3. Carling D, Clarke PR, Zammit VA, Hardie DG (1989) Purification and characterization of the AMP-activated protein kinase. Copurification of acetyl-CoA carboxylase kinase and 3-hydroxy-3-methylglutaryl-CoA reductase kinase activities. Eur J Biochem 186 (1–2):129–136
4. Foretz M, Viollet B (2011) Regulation of hepatic metabolism by AMPK. J Hepatol 54 (4):827–829. https://doi.org/10.1016/j.jhep.2010.09.014
5. Smith BK, Marcinko K, Desjardins EM, Lally JS, Ford RJ, Steinberg GR (2016) Treatment of nonalcoholic fatty liver disease: role of AMPK. Am J Physiol Endocrinol Metab 311 (4):E730–E740. https://doi.org/10.1152/ajpendo.00225.2016
6. Zadra G, Photopoulos C, Tyekucheva S, Heidari P, Weng QP, Fedele G, Liu H, Scaglia N, Priolo C, Sicinska E, Mahmood U, Signoretti S, Birnberg N, Loda M (2014) A novel direct activator of AMPK inhibits prostate cancer growth by blocking lipogenesis. EMBO Mol Med 6(4):519–538. https://doi.org/10.1002/emmm.201302734
7. O'Brien AJ, Villani LA, Broadfield LA, Houde VP, Galic S, Blandino G, Kemp BE, Tsakiridis T, Muti P, Steinberg GR (2015) Salicylate activates AMPK and synergizes with metformin to reduce the survival of prostate and lung cancer cells ex vivo through inhibition of de novo lipogenesis. Biochem J 469 (2):177–187. https://doi.org/10.1042/BJ20150122
8. Xie W, Wang L, Dai Q, Yu H, He X, Xiong J, Sheng H, Zhang D, Xin R, Qi Y, Hu F, Guo S, Zhang K (2015) Activation of AMPK restricts coxsackievirus B3 replication by inhibiting lipid accumulation. J Mol Cell Cardiol 85:155–167. https://doi.org/10.1016/j.yjmcc.2015.05.021
9. Cool B, Zinker B, Chiou W, Kifle L, Cao N, Perham M, Dickinson R, Adler A, Gagne G, Iyengar R, Zhao G, Marsh K, Kym P, Jung P, Camp HS, Frevert E (2006) Identification and characterization of a small molecule AMPK activator that treats key components of type 2 diabetes and the metabolic syndrome. Cell Metab 3(6):403–416. https://doi.org/10.1016/j.cmet.2006.05.005
10. Hunter RW, Foretz M, Bultot L, Fullerton MD, Deak M, Ross FA, Hawley SA, Shpiro N, Viollet B, Barron D, Kemp BE, Steinberg GR, Hardie DG, Sakamoto K (2014) Mechanism of action of compound-13: an alpha1-selective small molecule activator of AMPK. Chem Biol 21(7):866–879. https://doi.org/10.1016/j.chembiol.2014.05.014
11. Fullerton MD, Galic S, Marcinko K, Sikkema S, Pulinilkunnil T, Chen ZP, O'Neill HM, Ford RJ, Palanivel R, O'Brien M, Hardie DG, Macaulay SL, Schertzer JD, Dyck JR, van Denderen BJ, Kemp BE, Steinberg GR (2013) Single phosphorylation sites in Acc1 and Acc2 regulate lipid homeostasis and the insulin-sensitizing effects of metformin. Nat Med 19 (12):1649–1654. https://doi.org/10.1038/nm.3372
12. Gomez-Galeno JE, Dang Q, Nguyen TH, Boyer SH, Grote MP, Sun Z, Chen M, Craigo WA, van Poelje PD, MacKenna DA, Cable EE, Rolzin PA, Finn PD, Chi B, Linemeyer DL, Hecker SJ, Erion MD (2010) A potent and selective AMPK activator that inhibits de novo lipogenesis. ACS Med Chem Lett 1 (9):478–482. https://doi.org/10.1021/ml100143q

13. Ford RJ, Fullerton MD, Pinkosky SL, Day EA, Scott JW, Oakhill JS, Bujak AL, Smith BK, Crane JD, Blumer RM, Marcinko K, Kemp BE, Gerstein HC, Steinberg GR (2015) Metformin and salicylate synergistically activate liver AMPK, inhibit lipogenesis and improve insulin sensitivity. Biochem J 468 (1):125–132. https://doi.org/10.1042/BJ20150125
14. Ducommun S, Ford RJ, Bultot L, Deak M, Bertrand L, Kemp BE, Steinberg GR, Sakamoto K (2014) Enhanced activation of cellular AMPK by dual-small molecule treatment: AICAR and A769662. Am J Physiol Endocrinol Metab 306(6):E688–E696. https://doi.org/10.1152/ajpendo.00672.2013
15. Foretz M, Hebrard S, Leclerc J, Zarrinpashneh E, Soty M, Mithieux G, Sakamoto K, Andreelli F, Viollet B (2010) Metformin inhibits hepatic gluconeogenesis in mice independently of the LKB1/AMPK pathway via a decrease in hepatic energy state. J Clin Invest 120(7):2355–2369. https://doi.org/10.1172/JCI40671
16. Laishes BA, Williams GM (1976) Conditions affecting primary cell cultures of functional adult rat hepatocytes. II. Dexamethasone enhanced longevity and maintenance of morphology. In Vitro 12(12):821–832
17. Owen MR, Doran E, Halestrap AP (2000) Evidence that metformin exerts its anti-diabetic effects through inhibition of complex 1 of the mitochondrial respiratory chain. Biochem J 348(Pt 3):607–614
18. El-Mir MY, Nogueira V, Fontaine E, Averet N, Rigoulet M, Leverve X (2000) Dimethylbiguanide inhibits cell respiration via an indirect effect targeted on the respiratory chain complex I. J Biol Chem 275(1):223–228
19. Xiao B, Sanders MJ, Carmena D, Bright NJ, Haire LF, Underwood E, Patel BR, Heath RB, Walker PA, Hallen S, Giordanetto F, Martin SR, Carling D, Gamblin SJ (2013) Structural basis of AMPK regulation by small molecule activators. Nat Commun 4:3017. https://doi.org/10.1038/ncomms4017

Chapter 24

Studying the Role of AMPK in Autophagy

Sarah Krieg, Bernhard Lüscher, Jörg Vervoorts, and Marc Dohmen

Abstract

AMPK is an energy-sensing kinase and is required for the induction and progression of the autophagy process. In this chapter, we describe experimental approaches to study the steady state and flux of autophagy in response to AMPK activation. For this purpose, we provide detailed protocols for the measurement of general as well as AMPK-specific autophagy markers by immunoblot and immunofluorescence analysis.

Key words AMP-activated protein kinase, Autophagy, Flux analysis, LC3, Immunofluorescence, Immunoblot, Bafilomycin A1, AICAR, A-769662, Glucose deprivation

1 Introduction

The adenosine monophosphate (AMP)-activated protein kinase (AMPK) is generally considered the master energy sensor because it promotes switching from anabolism to catabolism when activated by an increased ratio of AMP to ATP under energy-deprived conditions. AMPK can be activated selectively by the combination of aminoimidazole-4-carboxamide ribonucleotide (AICAR) and A-769662 or by glucose deprivation [1–4]. AMPK regulates a multitude of metabolic processes by activating or repressing phosphorylation of key enzymes [5, 6]. The most prominent is the phosphorylation of acetyl-CoA carboxylase (ACC) at Ser79 that inhibits fatty acid and isoprenoid synthesis [7, 8]. One of the catabolic processes activated by AMPK is macroautophagy (hereafter autophagy), which is characterized by the engulfing of cytoplasmic components into a double lipid membrane resulting in an isolation membrane and later the autophagosome [9]. Eventually the autophagosome fuses with a lysosome resulting in the autolysosome where the cargo is degraded by the acidic lysosomal hydrolases and recycled to the cytoplasm where it serves as new building blocks and an energy source to maintain homeostasis and prevent apoptosis [5, 9].

Dietbert Neumann and Benoit Viollet (eds.), *AMPK: Methods and Protocols*, Methods in Molecular Biology, vol. 1732, https://doi.org/10.1007/978-1-4939-7598-3_24,

Autophagy relies on a tightly regulated and interconnected cascade of protein complexes encoded by more than 30 *ATG* (*autophagy-related*) genes [10–13]. Focusing on the AMPK-dependent induction of autophagy, AMPK on the one hand inhibits mTORC1 through phosphorylation of its regulatory subunit Raptor at Ser792 [14] and on the other hand through an activating phosphorylation of Unc-51-like autophagy activating kinase 1 (ULK1/ATG1) at several sites including the most prominent Ser555 [15, 16]. The active ULK1 complex initiates the autophagy cascade resulting in the formation of an isolation membrane, which expands to engulf cargo. During the process of expanding this autophagic membrane is marked with the microtubule-associated protein 1 light chain 3 (LC3/ATG8) by conversion of the cytosolic, soluble LC3-I form into the lipidated, autophagosome-incorporated LC3-II. To lipidate LC3, it is first proteolytically cleaved by ATG4 to obtain a processed form (LC3-I) that is covalently modified with phosphatidylethanolamine (PE) by an ubiquitin-like conjugation system resulting in LC3-II [17–19]. The membrane association is documented by the change of the subcellular localization of LC3 from a more diffuse to a dot-like cytoplasmic distribution [20, 21]. The incorporated LC3-II is also involved in the recognition and recruitment of cargo, a process mediated through selective autophagy receptors like p62/SQSTM1 [22]. While p62 is degraded together with the autophagic cargo, LC3 is recycled to the cytoplasm and freed of its lipidation [18, 19, 23, 24].

Based on the knowledge of the autophagic cascade, several techniques have been established to measure general as well as AMPK-dependent induction of autophagy and the autophagic flux employing immunoblotting and immunofluorescence analysis that will be described in detail hereafter [23, 25]. The most common readout for autophagy is the characteristic conversion of LC3-I into lipidated LC3-II. Alternatively, phospho-specific antibodies can visualize the AMPK-dependent phosphorylation of ULK1 and Raptor and thus are a readout specific for AMPK activity. Monitoring autophagy only by measuring steady-state amounts of LC3-II can result in an incorrect interpretation of the autophagy status [26]; therefore the integrity of the autophagic flux has to be assessed, typically by using inhibitors of the flux. Bafilomycin A1 inhibits the fusion of the autophagosome with the lysosome and thus allows estimations of the autophagosomal flux [27]. Moreover, a double-tagged mCherry-EGFP-LC3 construct has been generated that differentiates between autophagosomes and autolysosomes due to the differential sensitivity of mCherry and EGFP to the acidic conditions in lysosomes [28–30]. Furthermore, knockdown and knockout approaches can be used to define the functionality of factors associated with the autophagic process. In particular, the knockdown of AMPKα1/2 can provide evidence for a key role

of AMPK for the induction of autophagy in response to a stimulus of interest.

In the following we describe the protocols that have been used in our lab to measure and evaluate autophagy with the particular emphasis on the role of AMPK in this process. We present cell-based systems to study AMPK-dependent autophagy by biochemical assays using immunoblotting and immunofluorescence as independent approaches.

2 Materials

Store all reagents and solutions at room temperature or according to the manufacturer's instruction unless stated otherwise. Always use double-distilled and autoclaved H_2O.

2.1 Cell Lines

1. U2OS: human bone osteosarcoma cell line (ATCC® HTB-96™).
2. NIH3T3: immortalized murine fibroblasts (ATCC® CRL-1658™).
3. NIH3T3 mCherry-EGFP-LC3: NIH3T3 cells retrovirally transduced with pBABE-puro mCherry-EGFP-LC3 (Addgene #22418) [28–30].

2.2 Cell Culture

1. DMEM high glucose: Dulbecco's Modified Eagle Medium (DMEM), 4.5 g/L glucose, 4 mM L-glutamine, 10% (v/v) heat-inactivated fetal calf serum (FCS), 100 µg/ml penicillin/streptomycin (P/S). Store at 4 °C.
2. Glucose-free DMEM: DMEM without glucose, 4 mM L-glutamine, 10% (v/v) heat-inactivated FCS, 100 µg/ml P/S. Store at 4 °C.
3. Puromycin: 2 mg/ml puromycin in DMSO. Store at −20 °C.
4. Phosphate-buffered saline (PBS) (pH 7.3): 140 mM NaCl, 2.6 mM KCl, 2 mM Na_2HPO_4, 1.45 mM KH_2PO_4.
5. Opti-MEM® medium. Store at 4 °C.
6. AICAR: 150 mM aminoimidazole-4-carboxamide ribonucleotide (AICAR) in H_2O. Store at −20 °C; use within 1 month.
7. A-769662: 50 mM A-769662 in DMSO. Store at −20 °C; use within 1 month.
8. Baf. A1: 200 mM bafilomycin A1 in ethanol. Store at −80 °C.
9. Tissue culture dishes: diameter 6 or 10 cm.
10. Glass coverslips: diameter 18 mm.
11. Cell-counter instrument or Neubauer chamber.
12. CO_2 incubator: Set to 5% CO_2 and 37 °C.

13. Transfection reagent. Store at 4 °C.
14. 5× siRNA buffer (Dharmacon, Cat #B-002000-UB-100). Store at 4 °C. Dilute sterilely 1:5 with RNase-free water to 1× siRNA buffer for usage.
15. siRNA oligo pools: 20 μM stock solution with 1× siRNA buffer. SMARTpool siGENOME (Dharmacon) used: Human PRKAA1 M-005027-02 (siAMPKα1), human PRKAA2 M-005361-02 (siAMPKα2), and nontargeting siRNA pool #2 D-001206-20 (siControl). Dilute sterilely and store at −20 °C.

2.3 SDS Polyacrylamide Gel Electrophoresis

1. Resolving gel buffer: 1.5 M Tris–HCl, pH 8.8, 0.4% (w/v) SDS in H_2O.
2. Stacking gel buffer: 0.5 M Tris–HCl, pH 6.8, 0.4% (w/v) SDS in H_2O.
3. Acrylamide 4 K solution (30%) -Mix 37.5:1.
4. APS: 20% (w/v) ammonium persulfate (APS) in H_2O. Store long term at −20 °C and short term at 4 °C.
5. N,N,N,N′-Tetramethylethylenediamine (TEMED). Store at 4 °C.
6. Isopropanol.
7. PBS. Store at 4 °C.
8. Frackelton buffer: 20 mM HEPES, pH 7.4, 50 mM NaCl, 30 mM $Na_4P_2O_7$, 50 mM NaF, 0.2% (v/v) Triton® X-100, 10% (v/v) glycerol, 5 μM $ZnCl_2$, Protease Inhibitor Cocktail (PIC), 20 mM β-glycerophosphate, 1 mM vanadate (Na_3VO_4), 50 nM okadaic acid. Store at 4 °C (*see* **Note 1**).
9. Lowry protein assay kit.
10. Laemmli buffer: 25 mM Tris–HCl, pH 8.3, 250 mM glycine, 0.1% (w/v) SDS.
11. 4× loading buffer: 320 mM Tris–HCl, pH 6.8, 40% (v/v) glycerol, 20% (w/v) SDS, 0.5% (w/v) bromophenol blue, 200 mM β-mercaptoethanol.
12. Size marker: prestained protein marker (10–250 kDa range).
13. Polyacrylamide protein (mini-)gel system with 1 mm spacer glass plates.

2.4 Immunoblotting

1. Semidry transfer buffer: 25 mM Tris base, 192 mM glycine, 20% (v/v) methanol.
2. Tank blot transfer buffer: 25 mM Tris base, 192 mM glycine, 0.01% (w/v) SDS. Store at 4 °C.
3. Nitrocellulose membrane: 0.2 μm pore size.
4. Grade 3 Qualitative Filter Paper.

5. Semidry blotting apparatus.
6. Tank blotting system. Store cooling element at −20 °C.
7. Tris-buffered saline (TBS): 50 mM Tris–HCl, pH 7.5, 150 mM NaCl.
8. TBS-T: TBS, 0.05% (v/v) Tween-20.
9. IB blocking solution: TBS-T, 5% (w/v) skim milk powder. Store at 4 °C.
10. IB antibody diluent solution: TBS-T, or TBS-T, 5% (w/v) BSA, or TBS-T, 5% (w/v) skim milk powder. Store at 4 °C.
11. Imager for recording of ECL signals.
12. ECL substrate solution.
13. ImageJ software (National Institute of Health, Bethesda).

2.5 Antibodies and Conjugates

Antibodies listed below have been successfully used in this method (*see* **Note 2**).

1. Anti-ACC (Cell Signaling, 3676): for IB 1:1000 in TBS-T, 5% (w/v) BSA (*see* **Note 3**).
2. Anti-ACC pSer79 (Cell Signaling, 11818): for IB 1:1000 in TBS-T, 5% (w/v) BSA (*see* **Note 4**).
3. Anti-actin (C4, MP Biomedicals, 0869100): for IB 1:200,000 in TBS-T.
4. Anti-AMPKα (Cell Signaling, 5831): for IB 1:1000 in TBS-T, 5% (w/v) BSA (*see* **Note 3**).
5. Anti-AMPKα pThr172 (Cell Signaling, 2535): for IB 1:1000 in TBS-T, 5% (w/v) BSA (*see* **Note 4**).
6. Anti-LC3 (Cell Signaling, 2775): for IB 1:1000 in TBS-T, 5% (w/v) BSA.
7. Anti-LC3 (MBL, M152-3B): for IF 1:50 in PBS, 1% (v/v) goat serum.
8. Anti-p62 (Progen, GP62-C): for IB 1:1000 in TBS-T (*see* **Note 5**).
9. Anti-Raptor (Cell Signaling, 2280): for IB 1:1000 in TBS-T, 5% (w/v) BSA (*see* **Note 3**).
10. Anti-Raptor pSer792 (Cell Signaling, 2083): for IB 1:1000 in TBS-T, 5% (w/v) BSA.
11. Anti-ULK1 (Cell Signaling, 8054): for IB 1:1000 in TBS-T, 5% (w/v) BSA (*see* **Notes 3** and **6**).
12. Anti-ULK1 pSer555 (Cell Signaling, 5869): for IB 1:1000 in TBS-T, 5% (w/v) BSA (*see* **Note 6**).

13. Goat anti-guinea pig IgG (H + L) HRP-conjugated (Santa Cruz, sc2438): for IB 1:5000 in TBS-T, 5% (w/v) skim milk powder.
14. Rat anti-mouse IgG (H + L) HRP-conjugated (Jackson ImmunoResearch, 415-035-166): for IB 1:10,000 in TBS-T, 5% (w/v) skim milk powder.
15. Goat anti-rabbit IgG (H + L) HRP-conjugated (Jackson ImmunoResearch, 111-035-144): for IB 1:10,000 in TBS-T, 5% (w/v) skim milk powder.
16. Goat anti-mouse IgG (H + L) Alexa Fluor 488 (Invitrogen/Thermo Fisher Scientific, A-11001): for IF 1:1000 in PBS, 1% (v/v) goat serum.

2.6 Indirect Immunofluorescence and Confocal Laser-Scanning Microscopy

1. Tissue culture dishes: 12-well.
2. Parafilm.
3. Fixation solution: 3.7% (w/v) paraformaldehyde (PFA) in PBS. Store at −20 °C.
4. Permeabilization solution: 40 μg/ml digitonin in PBS. Store at 4 °C (*see* **Notes 7** and **8**).
5. IF blocking solution: 3% (v/v) goat serum in PBS.
6. IF antibody dilution: 1% (v/v) goat serum in PBS.
7. DNA staining solution (Hoechst): 1 mg/ml Hoechst 33258 in H_2O. Store at 4 °C protected from light (*see* **Note 9**).
8. Mounting solution: 10% (w/v) MOWIOL 4-88, 0.1 M Tris–HCl, pH 8.5, 25% (v/v) glycerol. Store long term at −20 °C and short term at 4 °C (*see* **Notes 9** and **10**).
9. Microscope slides 76 × 26 mm with frosted ends.
10. Confocal laser-scanning microscope and instrument software.
11. Precision tissue wipes.
12. Ultrapure water.
13. ImageJ software (National Institute of Health, Bethesda).

3 Methods

If not stated otherwise, carry out all procedures at room temperature and according to the manufacturer's instructions.

3.1 Cultivation of Cell Lines and Stimulation

1. Culture U2OS and NIH3T3 cells in DMEM high glucose at 37 °C in an incubator providing saturated humidity and 5% CO_2. Add 1 μg/ml puromycin to the medium of NIH3T3 cells stably expressing the double-tagged mCherry-EGFP-LC3 construct. Generally, grow the cells in 10 cm dishes and passage every 2–4 days (*see* **Notes 11** and **12**).

2. Seed 1.2×10^6 cells, counted using a cell counter, onto a 10 cm dish containing a glass coverslip to be able to perform immunoblot and indirect immunofluorescence analysis from the same experiment as described in Subheadings 3.5 and 3.6 (*see* **Notes 13–15**). Grow cells under normal growth conditions at 37 °C with 5% CO_2 to reattach overnight (*see* **Note 16**).
3. To induce AMPK-dependent autophagy, stimulate the cells either with 1 mM AICAR and 50 μM A-769662 (A + A) for 16 h (*see* **Note 17**), or after a wash with pre-warmed PBS, replace the full medium with pre-warmed, glucose-free DMEM for 16 h (*see* Fig. 1) (*see* **Notes 18** and **19**). Afterward lyse or fixate the cells for further analysis (*see* Subheadings 3.4 and 3.6)

3.2 Analysis of the Autophagic Flux

A variety of methods can be employed to assess autophagic flux since steady-state analysis alone (*see* Subheading 3.1, **step 3**) can lead to misinterpretations. Two approaches are described in the following:

1. Use Baf. A1, which prevents the fusion of the autophagosome with the lysosome (*see* Figs. 2 and 3). Add Baf. A1 to the cells 4 h prior to lysis at a final concentration of 200 nM (*see* **Notes 17** and **20**).
2. A double-tagged mCherry-EGFP-LC3 fusion protein allows the differentiation between autophagosomes and autolysosomes and an estimation of their ratio (*see* Fig. 3b) (*see* **Note 21**). Seed and stimulate the NIH3T3 cells stably expressing the double-tagged mCherry-EGFP-LC3 construct as described in Subheading 3.1 and in **step 1** of this section (*see* **Note 16**).

3.3 siRNA Transfection

The siRNA-mediated knockdown of AMPKα1/2 or AMPKα1/2 knockout cells can be employed to demonstrate AMPK dependency of the induction of autophagy (*see* Fig. 2). In the following we describe the protocol for using the siRNA-mediated knockdown.

1. Seed 4×10^5 cells onto a 6 cm dish containing a glass coverslip (*see* **Notes 13**, **14**, **15**, and **22**). Grow cells under normal growth conditions at 37 °C with 5% CO_2 for about 2 h until the transfection (*see* **Note 23**).
2. For transfection, incubate 12 μl of the indicated 20 μM siRNA oligo pools with 250 μl of Opti-MEM® and 20 μl of HiPerFect transfection reagent for 10 min at room temperature. Afterward add the mixture to the cells dropwise resulting in a final concentration of 50 nM siRNA oligos in the medium.
3. Thereafter incubate the cells under normal growth conditions at 37 °C with 5% CO_2 for 72 h to allow uptake of the siRNA-containing liposomes (*see* **Note 24**).

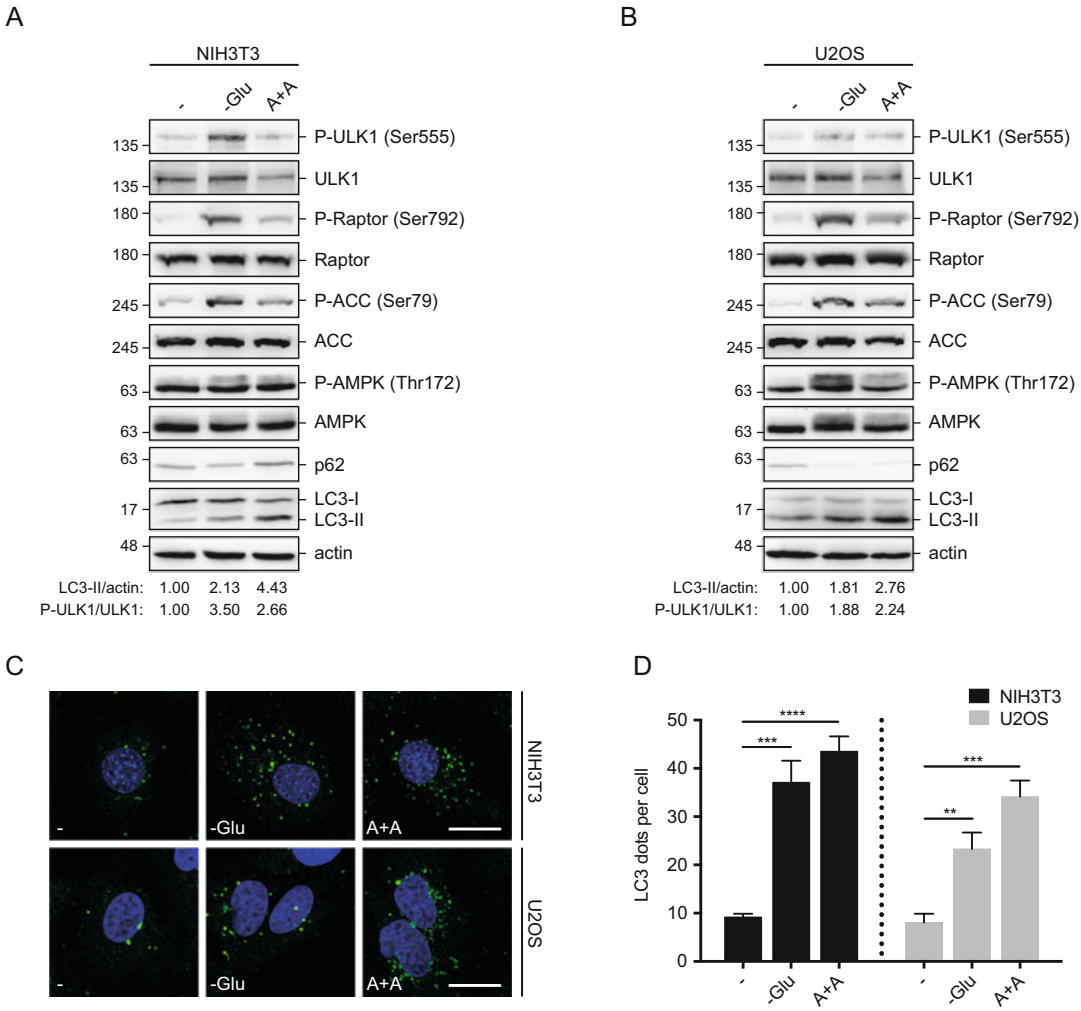

Fig. 1 Evaluation of the induction of AMPK-mediated autophagy by immunoblotting and immunofluorescence. (**a**) NIH3T3 and (**b**) U2OS cells were cultured in glucose-free medium (-Glu) or treated with AICAR and A-769662 (A + A) as indicated and subjected to immunoblot analysis using the indicated pan- and phospho-antibodies. In the two cell lines, both treatments result in an activation of AMPK seen by increased phosphorylation of the AMPK substrates ACC, ULK1, and Raptor and the induction of autophagy displayed by a modest increase in the amount of LC3-II. (**c**) Representative confocal images of NIH3T3 and U2OS cells treated as described in (**a**) and (**b**). Staining of endogenous LC3 was used to monitor autophagy induction measured as an increase in punctate LC3. Scale bar, 20 μm. (**d**) Quantification of the counted LC3 dots per cell of the cells shown in (**c**) for each treatment ($n > 100$). Data are shown as mean values ± SD. The significance was tested by applying a Student's *t*-test (**$p \leq 0.05$, ***$p \leq 0.01$, ****$p \leq 0.001$)

3.4 Harvesting of the Cells

1. After stimulation and/or transfection (*see* Subheadings 3.1–3.3), remove the coverslips from the dishes using a forceps and transfer into a 12-well plate containing PBS (*see* **Note 25**). The continued procedure of immunostaining is described in Subheading 3.6.

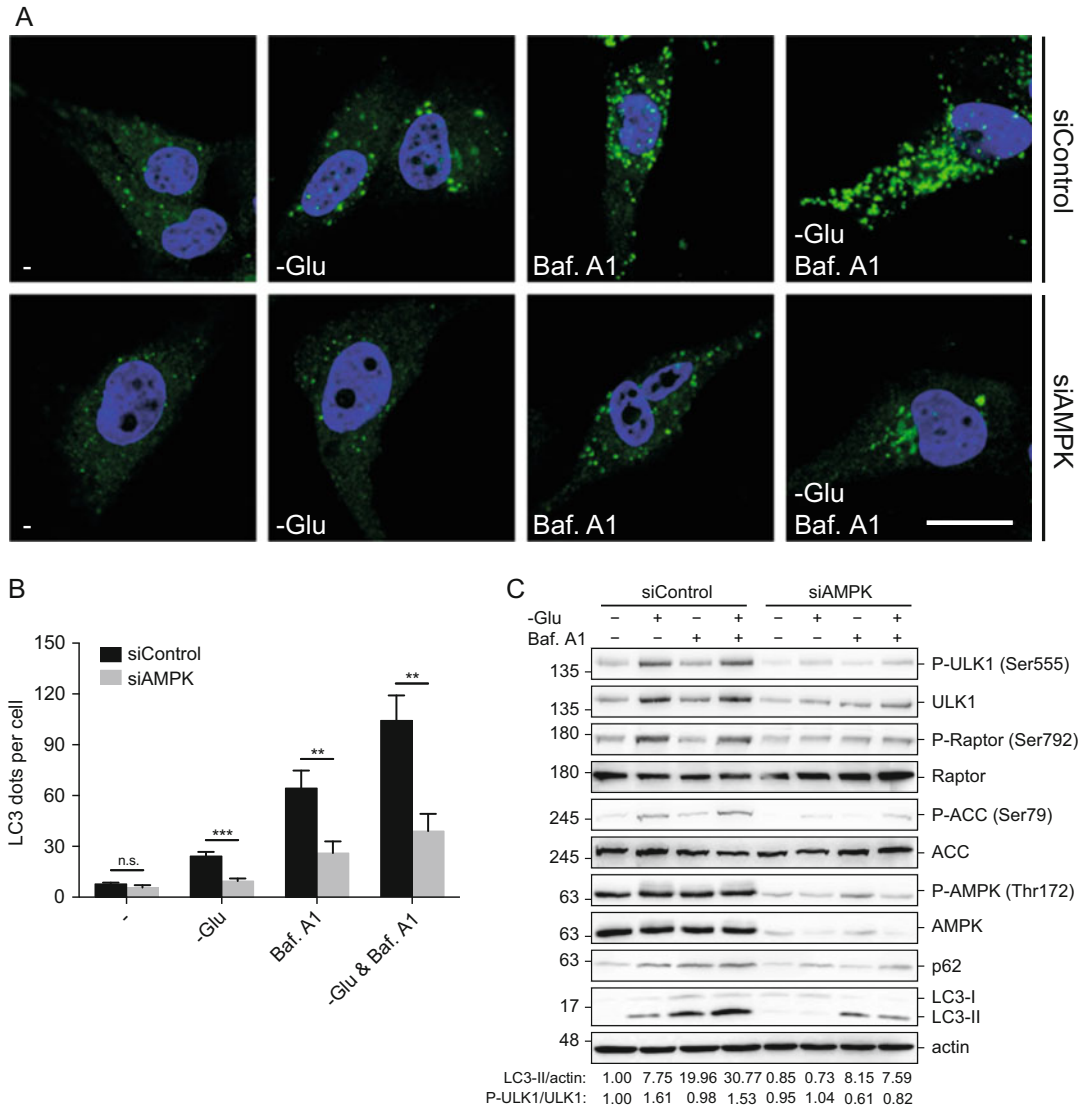

Fig. 2 Assessment of the AMPK dependency of autophagy using siRNA-mediated knockdown. (**a**) Representative confocal images of U2OS cells, which were transfected with the indicated siRNA pools and cultured in glucose-free medium (−Glu). Scale bar, 20 μm. Bafilomycin A1 (Baf. A1) was added to the cells to check for an intact autophagic flux. Endogenous LC3 was used to monitor autophagy through indirect immunofluorescence microscopy. (**b**) The number of endogenous LC3 dots within the cells treated as in (**a**) was counted for each treatment ($n > 100$). The shown results are mean values ± SD. The significance was tested by applying a Student's *t*-test (*n.s.* not significant, $^{**}p \leq 0.05$, $^{***}p \leq 0.01$). The highest number of LC3 dots in the sample treated with glucose deprivation (-Glu) and Baf. A1 in comparison to the single treated samples indicates an intact autophagic flux after glucose deprivation in U2OS cells. (**c**) U2OS cells were transfected and treated as in (**a**). Efficiency of the AMPK knockdown was shown by immunoblot analysis. The AMPK knockdown leads to a reduced substrate phosphorylation and autophagy induction after glucose deprivation. A reduced autophagy flux is observed in the AMPK knockdown cells compared to the cells treated with the control siRNA, because the AMPK knockdown cells accumulate LC3-II in the combined -Glu and Baf. A1 treatment to a lesser degree than the control siRNA-treated cells

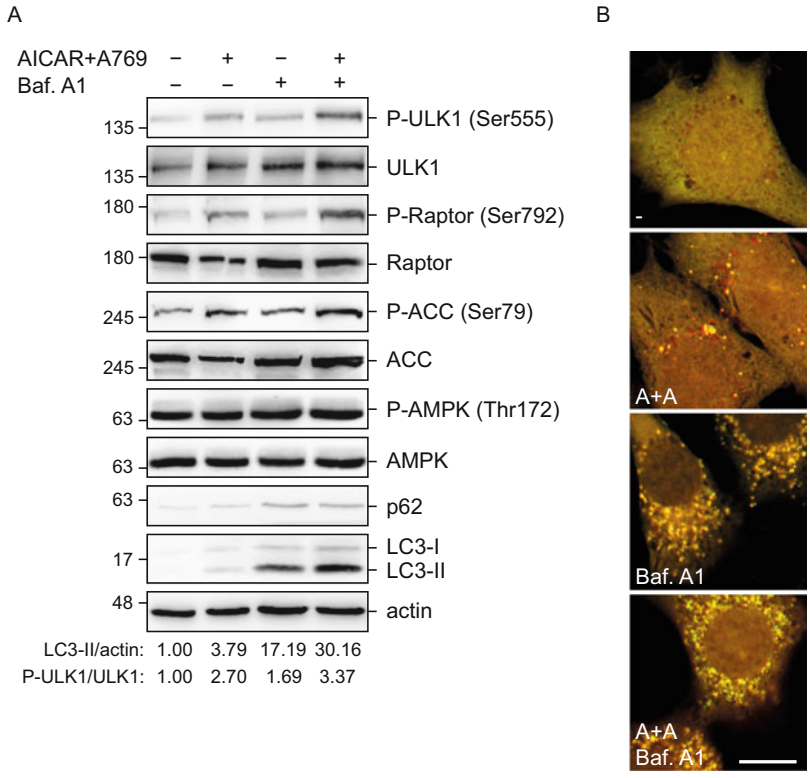

Fig. 3 Measuring the integrity of the autophagy flux with bafilomycin A1 and a double-tagged mCherry-EGFP-LC3 construct. (**a**) NIH3T3 cells stably expressing the mCherry-EGFP-LC3 fusion protein were treated with AICAR and A-769662 (A + A) and bafilomycin A1 (Baf. A1) as indicated. AMPK activity was evaluated by assessing an increase in ACC, ULK1, and Raptor phosphorylation levels by immunoblot analysis. Autophagy induction was monitored by an increase of endogenous LC3-II. The higher amount of LC3-II in the presence of the lysosomal inhibitor Baf. A1 (in comparison to the A + A treatment) indicates an intact autophagic flux after AMPK activation by A + A. (**b**) Representative confocal images of tandem mCherry-EGFP-LC3 expression in NIH3T3 cells showing an overlay of the EGFP and mCherry staining signal. The activation of AMPK by A + A leads to the formation of autophagosomes (*yellow dots*) and acidic autolysosomes (*red dots*). The Baf. A1 treatment blocks the fusion between autophagosomes and lysosomes resulting in an increase of only autophagosomes (*yellow dots*) after inducing autophagy by AMPK activation by AICAR and A-769662. Scale bar, 10 μm

2. Thereafter wash the cells attached to the dish with ice-cold PBS and lyse in 400 μl (10 cm dish) or 150 μl (6 cm dish) of Frackelton buffer (*see* **Note 1**). Perform all subsequent steps on ice or at 4 °C to prevent degradation.
3. After incubation for 10 min, scrape the adherent cells from the dishes and transfer into 1.5 ml reaction tubes.
4. Clear lysates by centrifugation at 16,000 × *g* for 30 min at 4 °C.
5. Measure the protein concentration by Lowry assay according to the manufacturer's instruction in a 96-well plate format (*see* **Note 26**).

6. Dilute 30 μg of total protein with lysis buffer to 15 μl of total volume, mixed with 5 μl of 4× loading buffer, and heat at 95 °C for 5 min. Afterward the samples can be stored at −20 °C until further analysis by SDS-PAGE (*see* Subheading 3.5) (*see* **Note 27**).

3.5 SDS Polyacrylamide Gel Electrophoresis and Immunoblotting

1. For a 7.5% SDS polyacrylamide gel, mix 5 ml of H_2O, 2.5 ml of polyacrylamide solution, and 2.5 ml of resolving gel buffer (*see* **Note 28**). For a 15% SDS polyacrylamide gel, mix 2.5 ml of H_2O, 5 ml of polyacrylamide solution, and 2.5 ml of resolving gel buffer (*see* **Note 29**). Start polymerization by adding 65 μl of APS and 15 μl of TEMED.
2. The 5% stacking gel consists of 3.125 ml of H_2O, 1.25 ml of stacking gel buffer, and 0.625 ml of polyacrylamide solution. To start the polymerization, add 25 μl of APS and 8 μl of TEMED.
3. Load the samples from Subheading 3.4 onto a 7.5% or a 15% SDS gel and separate electrophoretically at 150 V for about 1.5 h until the bromophenol dye front just ran off the gel (*see* **Notes 3** and **27**).
4. Blot the 15% SDS gels with the semidry method. Equilibrate six Whatman filter papers, a nitrocellulose membrane, and the SDS gel for a few minutes with semidry transfer buffer. Afterward stack them on the semidry blotting apparatus in the following order starting from the cathode: three filter papers, SDS gel, nitrocellulose membrane, and three filter papers. Perform the transfer at 1.9 mA per cm^2 of nitrocellulose membrane for 1.25 h and maximal 40 V.
5. Blot the 7.5% SDS gels with the wet blotting method. Equilibrate two sponges, six Whatman filter papers, a nitrocellulose membrane, and the SDS gel in ice-cold tank blot transfer buffer for a few minutes. Afterward stack the holder cassette inside the container with the black side facing down in the following order: a sponge, three filter papers, SDS gel, nitrocellulose membrane, three filter papers, and a sponge. To remove bubbles from the stack, use a glass pipette and roll over it carefully. Close the holder cassette carefully in the container, and place into the blotting chamber with the black side facing black and the white side facing red. Place the cooling unit inside the chamber as well, and fill it up with ice-cold tank blot transfer buffer. Run the tank blot at 100 V for 1 h.
6. After the transfer, incubate the blots with IB blocking solution for at least 1 h at room temperature on a horizontal shaker.
7. Subsequently wash the blocked blots several times in TBS-T (*see* **Note 30**) until the incubation with primary antibody at 4 °C overnight on a rocking device (*see* **Note 2**).

8. Thereafter wash the blots with TBS-T three times for at least 5 min each on a horizontal shaker.
9. Afterward incubate the blot with the according secondary antibody diluted in TBS-T, 5% (w/v) skim milk powder, for 1 h at room temperature on a rocking device.
10. Following the incubation step, wash the blot again with TBS-T three times for at least 10 min each on a horizontal shaker.
11. To develop the blot mix the ECL substrate solutions (Luminol/Enhancer and Stable Peroxide Buffer) in a 1:1 ratio in a reaction tube immediately before usage (*see* **Note 31**).
12. Place the blot on the metal panel of the chemiluminescence imager, cover with the fresh ECL solution mixture, and place inside the imager to take a chemiluminescence picture (*see* **Note 31**).
13. Reuse the blot to detect additional proteins with differing molecular weights. To do so, wash the blot with TBS-T several times to remove the residual ECL solution, and afterward repeat the procedure from **step 7** (*see* **Note 32**).
14. To evaluate and quantify detected protein amounts on the immunoblot, use the ImageJ software for densitometry according to Chapter 30.13 of the ImageJ user guide (*see* **Notes 3** and **33**).

3.6 Immunofluorescence Staining of Adherent Cells and Confocal Microscopy

1. After the cell incubation (*see* Subheading 3.4, **step 1**), transfer coverslips to a 12-well dish with the cells facing up (*see* **Note 34**).
2. Fixate the cells by incubation with 500 µl of fixation solution per well for 20 min. Remove residual PFA by a washing step with 1 ml of PBS.
3. Thereafter treat the fixated cells with 1 ml of permeabilization solution for 15 min to permeabilize their membranes (*see* **Notes 7** and **8**).
4. To reduce unspecific binding of the antibodies, block the coverslips with 1 ml of IF blocking solution for 30 min.
5. Dilute the primary anti-LC3 antibody 1:50 in IF antibody diluent solution, and spot 50 µl per coverslip onto a Parafilm. Place the coverslips on the antibody spots with the cells facing the solution, and incubate in a humid box for 1 h at 37 °C (*see* **Note 35**).
6. Perform the subsequent three washing steps in the 12-well dish again using 1 ml of IF antibody diluent solution.
7. The incubation with the secondary fluorophore-coupled antibody takes place as described for the primary antibody. Use 60 µl of the antibody dilution per coverslip, and keep in the dark for all subsequent steps or at least keep the light exposure to a minimum.

8. Thereupon wash the coverslips two times with PBS and one time with H_2O (*see* **Note 9**).
9. Add 500 μl of Hoechst solution for 5 min for staining of the cellular DNA (*see* **Note 9**).
10. Perform two last washing steps using 1 ml of H_2O (*see* **Note 9**).
11. To mount the coverslips and protect the fluorescence signal from bleaching, spot 12 μl of Mowiol solution onto a glass microscope slide (*see* **Note 10**). Usually up to two coverslips can be placed next to each other on one microscope slide. Place the coverslips onto the Mowiol spots with the cells facing the solution, and incubate for 15 min at room temperature until image acquisition or storage at 4 °C.
12. Acquire all images with the confocal laser-scanning microscope using a 63x water immersion objective. Spot 50 μl of ultrapure water onto the objective before placing the microscope slide on top.
13. Confocal laser-scanning microscopy allows simultaneous acquisition of the Hoechst, Alexa Fluor 488, EGFP, and mCherry fluorescent signal from a single focal plane. Excite Hoechst with an UV laser and detect the emission signal between 425 and 483 nm, while the Alexa Fluor 488 or EGFP fluorophore should be exited with an Argon laser, and the detection takes place between 493 and 550 nm. The excitation of the fluorophore mCherry should be mediated by a helium-neon laser and detected between 562 and 630 nm. Always set the pinhole to 1 airy unit (AU), and choose a resolution of 1024 × 1024 pixels for all pictures (*see* **Notes 36–38**).
14. Perform the editing of the pictures with help of the confocal laser-scanning microscope software (*see* **Note 37**).
15. Quantify the LC3 dots per cell with the ImageJ software. Set the brightness and contrast of the images to isolate the dots and eradicate the background staining. Further analysis requires conversion to an 8-bit binary image. To count the thresholded dots, apply the Analyze Particles algorithm, and set the minimum size and maximal pixel area size >0.1 μm (*see* **Notes 37–39**).

4 Notes

1. Protease and phosphatase inhibitors have to be added freshly to the lysis buffer of every experiment where phosphorylation should be assessed. Suggested phosphatase inhibitor stock solutions: 1 M β-glycerophosphate in H_2O. 100 mM vanadate (Na_3VO_4) in H_2O. 100 μM okadaic acid in DMSO. Store all solutions in aliquots at −20 °C.

2. In our experience, the antibodies listed in Subheading 2.5 worked well, which is why we share the supplier information. However, it does not preclude that antibodies recognizing the same proteins or modifications obtained from other suppliers could also be used in this protocol.
3. If the increase or decrease of a phosphorylation signal should be evaluated in response to a certain treatment, the total level of protein needs to be detected to be able to evaluate the ratio of phosphorylation to total protein. This proceeding excludes the misinterpretation due to possible effects on the total protein level.
4. To evaluate an influence on the AMPK-dependent induction of autophagy, the successful AMPK activation should always be controlled to exclude side effects or misinterpretation. This can be realized by the detection of the AMPK-mediated Ser79 phosphorylation of ACC that is part of an autophagy-independent pathway. The activating phosphorylation of AMPK itself, namely, Thr172, can be utilized for the same purpose but is less reliable, especially with regard to AICAR and A-769662 treatment (*see* Fig. 1a and b) [4].
5. In combination with the degradation of p62, another marker for the induction of autophagy should be evaluated, since the p62 level depends on the experimental setup. During longer periods of starvation or after protein overexpression, p62 is transcriptionally upregulated. This effect abolishes the short-term degradation of p62 seen after autophagy induction (*see* Figs. 2c and 3a) [37, 39].
6. ULK1 phosphorylation level as well as the total protein level change in response to the AMPK-dependent induction of autophagy depending on the temporal and cell type context (*see* Fig. 2c) [40, 41]. Therefore an evaluation of the total protein levels is crucial (*see* **Note 3**).
7. Digitonin solution might form precipitates during storage at 4 °C, which can be resolubilized by warming up to 37 °C and vortexing.
8. To detect LC3 dots by immunofluorescence, it is absolutely required to use digitonin for cell permeabilization since other detergents are too harsh and destroy the autophagosomal membranes.
9. It is crucial to perform the last washing steps with H_2O and to dilute the Hoechst dye in water since PBS would crystalize in combination with Mowiol.
10. The mounting can be facilitated by pre-warming the cold Mowiol solution to room temperature and cutting off the plastic pipette tip to transfer the viscous solution. Not more

than two coverslips should be mounted in parallel since the Mowiol spots would dry out otherwise.

11. Cells need to be tested for mycoplasma, since these pathogens induce autophagy and thus distort the results.
12. For experiments investigating autophagy, the cells should not have a high passage number (<15), because the regulation of autophagy and their sensitivity to stimuli change over time.
13. When evaluating the induction of autophagy, a control transfection with empty vectors should always be included, since transfection already induces autophagy to some extent.
14. If the cell density is too high or the medium is exhausted, the resulting energy deprivation induces autophagy and falsifies the results.
15. It works best to place the coverslip in a dish before adding the medium. Then press the coverslip onto the dish with a plastic pipette tip in order to fixate but not break it.
16. In experiments using the NIH3T3 cells stably expressing the tandem-tagged LC3 construct, the puromycin selection needs to be abolished already one passage prior to seeding for the planned experiment, since puromycin is known to interfere with autophagy [31–33].
17. In the unstimulated cells, the vehicle (DMSO, ethanol, etc.) should be used as a control to exclude effects on the induction of autophagy.
18. If the induction of autophagy is evaluated by the means of the conversion of LC3, the stimulation with AICAR, A-769662, or glucose starvation needs to be applied for longer time periods or overnight. After treatment for 1–2 h, which, e.g., is sufficient for EBSS starvation, only phosphorylation of direct substrates of AMPK can be assessed [2, 34].
19. The stimulation with AICAR, A-769662, or glucose starvation is more specific than, e.g., the broader EBSS starvation and allows the evaluation of AMPK-dependent induction of autophagy in particular [1–4, 35].
20. A longer treatment with bafilomycin A1 leads to a saturation of the LC3-II amount and induces cell death [36, 37].
21. The double-tagged mCherry-EGFP-LC3 fusion protein allows the discrimination between autophagosomes and autolysosomes since EGFP loses its fluorescence in the acidic environment of the autolysosomes resulting in an only red signal while autophagosomes are labeled red and green and thus appear yellow in a merged picture [30, 38].
22. If only an immunoblot from whole cell lysates is performed, a 6 cm dish will usually be sufficient and saves siRNA.

23. The transfection immediately after seeding the cells saves 1 day and increases the transfection efficiency.
24. The time necessary to achieve an efficient knockdown depends on the protein and its half-life. In this case, a knockdown for 72 h is sufficient for the AMPK α-subunits (*see* Fig. 2c). Additionally, an efficient knockdown was also possible using the calcium-phosphate precipitation method, which further enabled co-transfection of desired plasmids.
25. A curved/bent forceps facilitates the handling of the coverslips (e.g., Roth, Dumont #7, 11274-20).
26. Equal amounts of proteins have to be loaded to compare treated with untreated cells with regard to LC3 conversion as well as phosphorylation signals to allow an assessment of the induction of autophagy. This does not substitute the detection of a loading control or total protein levels.
27. To evaluate the conversion of the LC3-I to the autophagosome-associated LC3-II form, the lysates have to be fresh, i.e., not older than 2 or 3 days, since the fragile LC3-II form is prone to degradation.
28. The larger proteins like Raptor (150 kDa), ULK1 (150 kDa), and ACC (280 kDa) are best visualized with the help of a 7.5% SDS gel and a tank blot to facilitate their transfer onto the nitrocellulose membrane.
29. To evaluate the conversion of the LC3-I to the LC3-II form by immunoblotting, a 15% SDS polyacrylamide gel needs to be employed to visualize the difference in size due to proteolytic cleavage and lipidation [18, 19].
30. TBS-T should be used instead of PBS-T when phosphorylation signals should be detected.
31. If the signal is weak, the sensitivity of the ECL solution can be enhanced by using a more sensitive variant of the ECL substrate solution.
32. Stripping the blot to detect the total protein level after detecting the phosphorylation of the same protein or vice versa is not recommended, since stripping might falsify the results due to unequal co-removal of proteins from the membrane.
33. When the induction of autophagy should be assessed, the LC3-II form is the main readout parameter. Therefore a densitometry analysis of LC3-II in relation to a loading control like actin or tubulin can serve as a quantifiable measure for the amount of autophagy in the cells (*see* Fig. 1a and b) [25].
34. In immunofluorescence analysis, the usage of relatively large and strongly adherent cells is recommended in order to have rather large cytoplasmic area that can be recorded in a single plane for the quantification of autophagosomes.

35. To keep the box humid, a wet paper towel was placed in the closed box together with the coverslips on top of the Parafilm.
36. For evaluation of dot-like distribution that is a result of the lipidated LC3-II form associated with the autophagosomes, the pinhole needs to be set to 1 airy unit to visualize only a single focal plane of the cell to eliminate falsification of the results due to fluorescent signals in other focal planes.
37. In order to count and evaluate the number of dots per cell in an unbiased manner in different treatments, it is crucial to always set the same brightness, contrast, and threshold for all pictures of the same experiment to ensure comparability. This needs to be applied strictly when taking the pictures as well as during the later analysis.
38. For statistical analysis of the counted dots per cell, at least 100 cells should be analyzed. For this purpose, the tile scan tool of the confocal microscope can be employed to take rather unbiased pictures of many cells at the same time.
39. It is important not to mistake an increase in the overall fluorescence intensity with the induction of autophagy. The LC3-positive dots mark autophagosomes, while a diffuse cytoplasmic distribution represents the LC3-I form that is not associated with autophagic membranes.

Acknowledgments

This work was supported by a grant ("Alterations of Neuronal Connectivity") from the IZKF Aachen of the Medical School of the RWTH Aachen University to J.V. and by a grant from the START program of the Medical School of the RWTH Aachen University to M.D. This work was also supported by the "Immunohistochemistry and Confocal Microscopy Facility," a core facility of the IZKF Aachen within the Faculty of Medicine at RWTH Aachen University.

References

1. Kim J, Kundu M, Viollet B, Guan KL (2011) AMPK and mTOR regulate autophagy through direct phosphorylation of Ulk1. Nat Cell Biol 13(2):132–141. https://doi.org/10.1038/ncb2152
2. Lee JW, Park S, Takahashi Y, Wang HG (2010) The association of AMPK with ULK1 regulates autophagy. PLoS One 5(11):e15394. https://doi.org/10.1371/journal.pone.0015394
3. Cool B, Zinker B, Chiou W, Kifle L, Cao N, Perham M, Dickinson R, Adler A, Gagne G, Iyengar R, Zhao G, Marsh K, Kym P, Jung P, Camp HS, Frevert E (2006) Identification and characterization of a small molecule AMPK activator that treats key components of type 2 diabetes and the metabolic syndrome. Cell Metab 3(6):403–416. https://doi.org/10.1016/j.cmet.2006.05.005
4. Ducommun S, Ford RJ, Bultot L, Deak M, Bertrand L, Kemp BE, Steinberg GR, Sakamoto K (2014) Enhanced activation of cellular AMPK by dual-small molecule treatment:

AICAR and A769662. Am J Phys Endocrinol Metab 306(6):E688–E696. https://doi.org/10.1152/ajpendo.00672.2013

5. Hardie DG, Ross FA, Hawley SA (2012) AMPK: a nutrient and energy sensor that maintains energy homeostasis. Nat Rev Mol Cell Biol 13(4):251–262. https://doi.org/10.1038/nrm3311
6. Hardie DG (2011) AMP-activated protein kinase: an energy sensor that regulates all aspects of cell function. Genes Dev 25 (18):1895–1908. https://doi.org/10.1101/gad.17420111
7. Dyck JR, Kudo N, Barr AJ, Davies SP, Hardie DG, Lopaschuk GD (1999) Phosphorylation control of cardiac acetyl-CoA carboxylase by cAMP-dependent protein kinase and 5′-AMP activated protein kinase. Eur J Biochem 262 (1):184–190
8. Ha J, Daniel S, Broyles SS, Kim KH (1994) Critical phosphorylation sites for acetyl-CoA carboxylase activity. J Biol Chem 269 (35):22162–22168
9. Tukaj C (2013) The significance of macroautophagy in health and disease. Folia Morphol (Warsz) 72(2):87–93
10. Itakura E, Mizushima N (2010) Characterization of autophagosome formation site by a hierarchical analysis of mammalian Atg proteins. Autophagy 6(6):764–776
11. Thumm M, Egner R, Koch B, Schlumpberger M, Straub M, Veenhuis M, Wolf DH (1994) Isolation of autophagocytosis mutants of Saccharomyces cerevisiae. FEBS Lett 349(2):275–280
12. Tsukada M, Ohsumi Y (1993) Isolation and characterization of autophagy-defective mutants of Saccharomyces cerevisiae. FEBS Lett 333(1–2):169–174
13. Nakatogawa H, Suzuki K, Kamada Y, Ohsumi Y (2009) Dynamics and diversity in autophagy mechanisms: lessons from yeast. Nat Rev Mol Cell Biol 10(7):458–467. https://doi.org/10.1038/nrm2708
14. Gwinn DM, Shackelford DB, Egan DF, Mihaylova MM, Mery A, Vasquez DS, Turk BE, Shaw RJ (2008) AMPK phosphorylation of raptor mediates a metabolic checkpoint. Mol Cell 30 (2):214–226. https://doi.org/10.1016/j.molcel.2008.03.003
15. Egan DF, Shackelford DB, Mihaylova MM, Gelino S, Kohnz RA, Mair W, Vasquez DS, Joshi A, Gwinn DM, Taylor R, Asara JM, Fitzpatrick J, Dillin A, Viollet B, Kundu M, Hansen M, Shaw RJ (2011) Phosphorylation of ULK1 (hATG1) by AMP-activated protein kinase connects energy sensing to mitophagy. Science (New York, NY) 331(6016):456–461. https://doi.org/10.1126/science.1196371
16. Alers S, Loffler AS, Wesselborg S, Stork B (2012) Role of AMPK-mTOR-Ulk1/2 in the regulation of autophagy: cross talk, shortcuts, and feedbacks. Mol Cell Biol 32(1):2–11. https://doi.org/10.1128/mcb.06159-11
17. Dooley HC, Razi M, Polson HE, Girardin SE, Wilson MI, Tooze SA (2014) WIPI2 links LC3 conjugation with PI3P, autophagosome formation, and pathogen clearance by recruiting Atg12-5-16L1. Mol Cell 55(2):238–252. https://doi.org/10.1016/j.molcel.2014.05.021
18. Satoo K, Noda NN, Kumeta H, Fujioka Y, Mizushima N, Ohsumi Y, Inagaki F (2009) The structure of Atg4B-LC3 complex reveals the mechanism of LC3 processing and delipidation during autophagy. EMBO J 28 (9):1341–1350. https://doi.org/10.1038/emboj.2009.80
19. Tanida I, Sou YS, Ezaki J, Minematsu-Ikeguchi N, Ueno T, Kominami E (2004) HsAtg4B/HsApg4B/autophagin-1 cleaves the carboxyl termini of three human Atg8 homologues and delipidates microtubule-associated protein light chain 3- and GABAA receptor-associated protein-phospholipid conjugates. J Biol Chem 279(35):36268–36276. https://doi.org/10.1074/jbc.M401461200
20. Karim MR, Kawanago H, Kadowaki M (2014) A quick signal of starvation induced autophagy: transcription versus post-translational modification of LC3. Anal Biochem 465:28–34. https://doi.org/10.1016/j.ab.2014.07.007
21. Nakatogawa H (2013) Two ubiquitin-like conjugation systems that mediate membrane formation during autophagy. Essays Biochem 55:39–50. https://doi.org/10.1042/bse0550039
22. Svenning S, Johansen T (2013) Selective autophagy. Essays Biochem 55:79–92. https://doi.org/10.1042/bse0550079
23. Mizushima N, Yoshimori T, Levine B (2010) Methods in mammalian autophagy research. Cell 140(3):313–326. https://doi.org/10.1016/j.cell.2010.01.028
24. Kirisako T, Ichimura Y, Okada H, Kabeya Y, Mizushima N, Yoshimori T, Ohsumi M, Takao T, Noda T, Ohsumi Y (2000) The reversible modification regulates the membrane-binding state of Apg8/Aut7 essential for autophagy and the cytoplasm to vacuole targeting pathway. J Cell Biol 151(2):263–276
25. Mizushima N, Yoshimori T (2007) How to interpret LC3 immunoblotting. Autophagy 3 (6):542–545

26. Tanida I, Minematsu-Ikeguchi N, Ueno T, Kominami E (2005) Lysosomal turnover, but not a cellular level, of endogenous LC3 is a marker for autophagy. Autophagy 1(2):84–91
27. Yamamoto A, Tagawa Y, Yoshimori T, Moriyama Y, Masaki R, Tashiro Y (1998) Bafilomycin A1 prevents maturation of autophagic vacuoles by inhibiting fusion between autophagosomes and lysosomes in rat hepatoma cell line, H-4-II-E cells. Cell Struct Funct 23 (1):33–42
28. Vollrath JT, Sechi A, Dreser A, Katona I, Wiemuth D, Vervoorts J, Dohmen M, Chandrasekar A, Prause J, Brauers E, Jesse CM, Weis J, Goswami A (2014) Loss of function of the ALS protein SigR1 leads to ER pathology associated with defective autophagy and lipid raft disturbances. Cell Death Dis 5: e1290. https://doi.org/10.1038/cddis.2014.243
29. N'Diaye EN, Kajihara KK, Hsieh I, Morisaki H, Debnath J, Brown EJ (2009) PLIC proteins or ubiquilins regulate autophagy-dependent cell survival during nutrient starvation. EMBO Rep 10 (2):173–179. https://doi.org/10.1038/embor.2008.238
30. Kimura S, Noda T, Yoshimori T (2014) Dissection of the autophagosome maturation process by a novel reporter protein, tandem fluorescent-tagged LC3. Autophagy 3 (5):452–460. https://doi.org/10.4161/auto.4451
31. Kovacs AL, Seglen PO (1981) Inhibition of hepatocytic protein degradation by methylaminopurines and inhibitors of protein synthesis. Biochim Biophys Acta 676(2):213–220
32. Djehiche B, Segalen J, Chambon Y (1996) Inhibition of autophagy of fetal rabbit gonoducts by puromycin, tunicamycin and chloroquine in organ culture. Tissue Cell 28 (1):115–121
33. Oliva O, Laszlo L, Palfia Z, Rez G (1991) Translational inhibitors cycloheximide, emetine, and puromycin inhibit cellular autophagy in mouse liver parenchymal and pancreatic acinar cells in vivo. Acta Morphol Hung 39 (2):79–85
34. Liang J, Shao SH, Xu ZX, Hennessy B, Ding Z, Larrea M, Kondo S, Dumont DJ, Gutterman JU, Walker CL, Slingerland JM, Mills GB (2007) The energy sensing LKB1-AMPK pathway regulates p27(kip1) phosphorylation mediating the decision to enter autophagy or apoptosis. Nat Cell Biol 9(2):218–224. https://doi.org/10.1038/ncb1537
35. Shang L, Chen S, Du F, Li S, Zhao L, Wang X (2011) Nutrient starvation elicits an acute autophagic response mediated by Ulk1 dephosphorylation and its subsequent dissociation from AMPK. Proc Natl Acad Sci U S A 108(12):4788–4793. https://doi.org/10.1073/pnas.1100844108
36. Yan Y, Jiang K, Liu P, Zhang X, Dong X, Gao J, Liu Q, Barr MP, Zhang Q, Hou X, Meng S, Gong P (2016) Bafilomycin A1 induces caspase-independent cell death in hepatocellular carcinoma cells via targeting of autophagy and MAPK pathways. Sci Rep 6:37052. https://doi.org/10.1038/srep37052
37. Klionsky DJ, Abdelmohsen K, Abe A, Abedin MJ, Abeliovich H, Acevedo Arozena A, Adachi H, Adams CM, Adams PD, Adeli K, Adhihetty PJ, Adler SG, Agam G, Agarwal R, Aghi MK, Agnello M, Agostinis P, Aguilar PV, Aguirre-Ghiso J, Airoldi EM, Ait-Si-Ali S, Akematsu T, Akporiaye ET, Al-Rubeai M, Albaiceta GM et al (2016) Guidelines for the use and interpretation of assays for monitoring autophagy (3rd edition). Autophagy 12 (1):1–222. https://doi.org/10.1080/15548627.2015.1100356
38. Kimura S, Noda T, Yoshimori T (2007) Dissection of the autophagosome maturation process by a novel reporter protein, tandem fluorescent-tagged LC3. Autophagy 3 (5):452–460
39. Sahani MH, Itakura E, Mizushima N (2014) Expression of the autophagy substrate SQSTM1/p62 is restored during prolonged starvation depending on transcriptional upregulation and autophagy-derived amino acids. Autophagy 10(3):431–441. https://doi.org/10.4161/auto.27344
40. Nazio F, Carinci M, Valacca C, Bielli P, Strappazzon F, Antonioli M, Ciccosanti F, Rodolfo C, Campello S, Fimia GM, Sette C, Bonaldo P, Cecconi F (2016) Fine-tuning of ULK1 mRNA and protein levels is required for autophagy oscillation. J Cell Biol. https://doi.org/10.1083/jcb.201605089
41. Allavena G, Boyd C, Oo KS, Maellaro E, Zhivotovsky B, Kaminskyy VO (2016) Suppressed translation and ULK1 degradation as potential mechanisms of autophagy limitation under prolonged starvation. Autophagy 12 (11):2085–2097. https://doi.org/10.1080/15548627.2016.1226733

Chapter 25

Determining AMPK Activation via the Lysosomal v-ATPase-Ragulator-AXIN/LKB1 Axis

Chen-Song Zhang, Mengqi Li, Yue Zong, and Sheng-Cai Lin

Abstract

Recent studies have revealed how AMPK is activated inside the cell and animal tissues: in response to low glucose, AXIN tethers LKB1, by virtue of their constitutive association, to AMPK located on the surface of late endosome/lysosome. Importantly, the lysosomal v-ATPase (vacuolar ATPase)-Ragulator complex, when primed by glucose starvation or concanamycin A, facilitates AXIN/LKB1 to interact with AMPK. Here, we describe the experimental procedures of the assays for detecting the translocation of AXIN/LKB1 or the assembly of the AXIN-based AMPK-activating complexes on the late endosome/lysosome. The methods in this chapter will be useful for determining whether various metabolic stresses or pharmacological stimuli activate AMPK via the v-ATPase-Ragulator-AXIN/LKB1 axis, which also concomitantly inactivates mTORC1. Detailed protocols for determining the levels of adenylates are also described.

Key words AMPK, LKB1, AXIN, Ragulator, v-ATPase, Lysosome, Detergent-resistant membrane, Light organelles

1 Introduction

AMPK is a heterotrimer, comprised of a catalytic α subunit and regulatory β and γ subunits [1, 2]. The adenylates AMP, ADP, and ATP can all bind to the γ subunit and allosterically modulate AMPK activity [3–7]. AMP binding leads to AMPK activation through promoting the upstream kinase LKB1 to phosphorylate threonine 172 of the α subunit of AMPK (Thr-172) and subsequently serine 79 of ACC (Ser-79), which is a "gold standard" for evaluating the activity of AMPK [8–11]. Binding of ADP as well as AMP protects p-Thr-172 from being dephosphorylated, whereas ATP binding inhibits AMPK activation [7, 11–14]. However, it is now clear that activation of AMPK in vivo entails much more complex steps and involves many more factors. It has been recently shown that AMPK activation in response to glucose starvation or after treatment of metformin occurs on the surface of late endosome/lysosome (hereafter only lysosome is referred to) [15, 16]. This process

Dietbert Neumann and Benoit Viollet (eds.), *AMPK: Methods and Protocols*, Methods in Molecular Biology, vol. 1732, https://doi.org/10.1007/978-1-4939-7598-3_25,

requires concerted action of AXIN, the lysosomal v-ATPase, and the Ragulator complex (a pentamer consisting of LAMTORs 1-5) [15, 17]. The scaffold protein AXIN tethers LKB1 by virtue of its ability to directly interact with the upstream kinase, to AMPK located on the surface of lysosome. The lysosomal v-ATPase-Ragulator complex plays an important part in the docking of AXIN/LKB1, allowing for the formation of the stable complex of v-ATPase-Ragulator-AXIN/LKB1-AMPK on the surface of lysosome [18] and the ultimate activation of AMPK by LKB1. Moreover, subcellular fractionation identified that the AMPK-activating complex resides on the lysosomal detergent-resistant membrane (DRM) which is known as lipid raft [15, 19].

To obtain genetic evidence whether a given AMPK activation is through the lysosomal pathway, *AXIN*$^{-/-}$ and *LAMTOR1*$^{-/-}$ mouse embryonic fibroblasts (MEFs) or mouse individuals are starved of glucose or food or treated with other metabolic stresses and pharmacological stimuli. The various cells or animal tissues can be analyzed for AMPK activity by assessing p-Thr-172-AMPKα and p-Ser-79-ACC. As mentioned above, the lysosome is where AMPK phosphorylation occurs after AXIN in complex with LKB1 interacts with v-ATPase-Ragulator. Therefore, isolation of lysosomes of different purity is a direct and efficient way to monitor the "turning on" and "turning off" of the lysosomal pathway (Fig. 1). In addition, it has been well established that Ragulator complex is localized on the DRM region (lipid raft) of lysosome [19–21]. In this protocol, we describe how to isolate intact lysosomes and their DRMs by using the method originally developed by Sigma-Aldrich LLC and Kawabuchi et al. [22]. Through these methods, the dynamic association of the AXIN/LKB1 with the lysosomal DRM, as well as the phosphorylation status of AMPK, in animal tissues or cells can be conveniently determined by immunoblotting after immunoprecipitation (IP) [15]. We also describe the procedures for immunofluorescent staining to visualize the complex formation in intact cells.

Although the above-described method for isolating lysosome and DRM has allowed us to analyze specific protein components on the membrane before and after glucose starvation, they are "less active" and are not suitable for reconstituting the binding of AXIN/LKB1 to the lysosome in vitro. To obtain active membrane structures, Steinberg et al. [23] and Zoncu et al. [24] brilliantly developed a method to isolate crude cytosolic membranes, named as light organelles, in a relatively mild condition. The light organelles have been applied to investigate mechanisms for regulation of mTORC1, which is also activated through v-ATPase and Ragulator [20, 24]. We have demonstrated that the light organelles isolated from glucose-starved cells and cells cultured in complete medium preserve activities for a series of in vitro reconstitution assays for AMPK regulation through the lysosomal pathway [15].

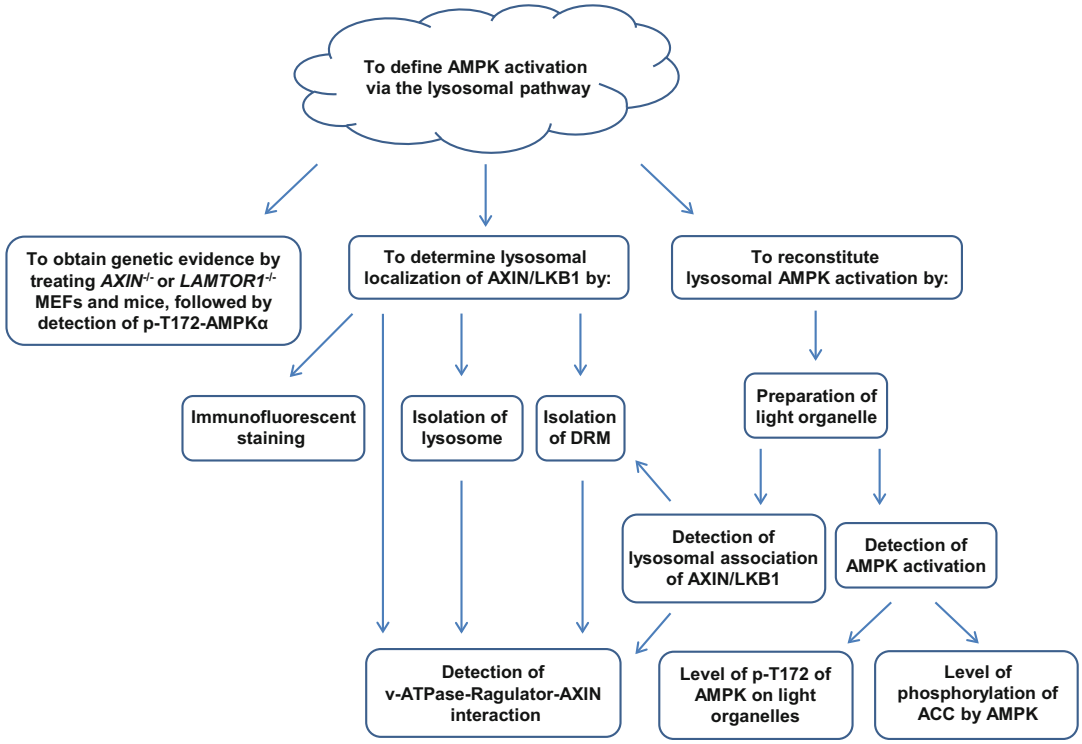

Fig. 1 Diagram of workflow for studying the lysosomal AMPK activation. To study the lysosomal AMPK activation under a desired metabolic stress or pharmacological stimulus, p-Thr-172-AMPKα and p-Ser-79-ACC are analyzed in *AXIN*$^{-/-}$ and *LAMTOR1*$^{-/-}$ mouse embryonic fibroblasts (MEFs) or mouse individuals. The dynamic association of the AXIN/LKB1 with the lysosomal DRM can be determined in purified lysosomes/DRMs, as well as in intact cells. The complex formation of v-ATPase-Ragulator-AXIN/LKB1-AMPK can be determined by co-immunoprecipitation. In addition, the light organelle-based assay system provides a way to determine whether a particular protein or drug of interest activates AMPK directly through triggering the lysosomal pathway in vitro

The adenine nucleotides AMP, ADP, and ATP exert various effects on AMPK activity [11, 12]. Moreover, the cellular energy levels are better reflected by AMP:ATP and ADP:ATP ratios [1, 25–27]. Since the levels of AMP are of extreme low ranges, and ADP, as well as ATP, is rather unstable, it is challenging to precisely measure the levels of AMP, ADP, and ATP. Here, we describe a sensitive method for determining the cellular levels of AMP, ADP, and ATP by using the capillary electrophoresis-mass spectrometry (CE-MS)-based assays [28, 29].

All of the methods described here are summarized in Fig. 1. Of note, for simplicity, we only mention glucose starvation as a representative stress in some parts of the chapter.

2 Materials

2.1 Analysis of AMPK Activation in Cells or Mice

1. Glucose-free DMEM: glucose-free Dulbecco's Modified Eagle's Medium (DMEM), 10% (v/v) fetal bovine serum (FBS) (*see* **Note 1**).
2. Complete DMEM medium: DMEM medium (containing 25 mM glucose), 10% (v/v) FBS.
3. Phosphate-buffered saline (PBS): 137 mM NaCl, 2.68 mM KCl, 10 mM Na_2HPO_4, 1.76 mM KH_2PO_4, pH 7.4. Store at room temperature (RT).
4. *AXIN*$^{-/-}$, *LAMTOR1*$^{-/-}$ MEFs, and the control wild-type MEFs (*see* **Notes 2** and **3**).
5. Male mice (C57BL/6 J) at 4–6 weeks old. The mice are housed individually (*see* **Note 4**) for at least 24 h prior to the experiment, with free access to water and standard diet (65% carbohydrate, 11% fat, 24% protein). The light-dark cycle for mice is from 8 a.m. to 8 p.m.
6. Lysis buffer: 20 mM Tris–HCl, pH 7.5, 150 mM NaCl, 1 mM EDTA, 1 mM EGTA, 1% (v/v) Triton X-100, 2.5 mM sodium pyrophosphate, 1 mM β-glycerophosphate, with protease inhibitor cocktail. Store at 4 °C (*see* **Note 5**).
7. 2× SDS sample buffer: 125 mM Tris–HCl, pH 6.8, 4% (w/v) SDS, 20% (v/v) glycerol, 100 mM DTT, 0.02% (w/v) bromophenol blue. Store at RT.
8. 8% SDS-PAGE gel.
9. Vertical "wet" transfer apparatus (*see* **Note 6**).
10. Blocking solution: TBS (1× Tris-buffered saline): 50 mM Tris–HCl, PH 7.5, 150 mM NaCl, 0.01% Tween-20, 5% (w/v) nonfat dry milk or bovine serum albumin (BSA).
11. Antibodies: anti-phospho-AMPKα-Thr-172, anti-AMPKα, anti-phospho-ACC-Ser79, and anti-ACC (*see* **Note 7**).
12. Sonicator equipped with a 5/64″ (2 mm) stepped microtip.
13. Electrical disperser (*see* **Note 8**).
14. Tabletop centrifuge.

2.2 Analysis of Lysosomal Localization of AXIN

1. Lysosome Isolation Kit (Sigma, cat. LYSISO1) (*see* **Note 9**), containing 5× Extraction Buffer, 20× OptiPrep Dilution Buffer, OptiPrep Density Gradient Medium, 2.5 M $CaCl_2$ solution, and 2.3 M sucrose solution. Store at 4 °C.
2. 7-mL Dounce Glass Tissue Grinder with small clearance pestle. The grinder should be precooled to 4 °C prior to use.
3. Ultracentrifuge equipped with SW60 Ti rotor. The rotor should be precooled to 4 °C prior to use.

4. 11 × 60 mm centrifuge tubes.
5. Buffer A: 50 mM Tris–HCl, pH 7.4, 150 mM NaCl, 1 mM EDTA, 5 mM β-mercaptoethanol, 0.25% (v/v) Triton X-100, with protease inhibitor cocktail. Stored at 4 °C.
6. Sucrose solutions: 5%, 35%, and 80% (w/v) sucrose in Buffer A (*see* **Note 10**). Store at 4 °C.
7. Ultracentrifuge equipped with SW41 Ti rotor. The rotor should be precooled to 4 °C prior to use.
8. 14 × 89 mm centrifuge tubes.
9. Microscope: confocal microscope equipped with argon gas laser and HeNe gas laser.
10. Formaldehyde solutions: 4% and 8% (w/v) formaldehyde in PBS.
11. Antibodies for IP: rabbit anti-LAMTOR1 and goat anti-AXIN (*see* **Note 11**).
12. Antibodies for immunofluorescent staining: goat anti-AXIN, rat anti-LAMP2 primary antibodies (*see* **Note 12**), and Alexa-Fluor 488-conjugated anti-goat, Alexa-Fluor 594-conjugated anti-rat secondary antibodies.
13. Mountant (*see* **Note 13**).
14. ODG buffer: 50 mM Tris–HCl, pH 8.0, 50 mM NaCl, 1 mM EDTA, 1 mM EGTA, 2% (w/v) octyl β-D-glucopyranoside (ODG), 5 mM β-mercaptoethanol, with protease inhibitor cocktail (*see* **Note 14**). Store at 4 °C.
15. Protein A/G beads: mix rProtein A Sepharose Fast Flow with an equal volume of Protein G Sepharose 4 Fast Flow. Store at 4 °C.
16. PBS-T: PBS, 0.1% (v/v) Triton X-100.
17. DRM buffer: 2% (w/v) ODG, 1% (v/v) Nonidet P-40 (NP-40) in Buffer A.

2.3 In Vitro Reconstitution of Lysosomal AMPK Activation

1. Fractionation buffer: 50 mM KCl, 90 mM potassium gluconate, 1 mM EGTA, 5 mM $MgCl_2$, 50 mM sucrose, 20 mM HEPES, pH 7.4, supplemented with 2.5 mM ATP, amino acids, and protease inhibitor cocktail. Store at 4 °C.
2. 22 G needles and 1-mL syringes.
3. AMP: 100 mM AMP in H_2O. Store at −20 °C.
4. ATP: 500 mM ATP in H_2O. Store at −20 °C.
5. Protein phosphatase 2Ac ($PP2A_c$): 1 μg/μL $PP2A_c$, 50 mM Tris–HCl, pH 7.0, 14 mM β-mercaptoethanol, 1 mM benzamidine, 0.1 mM PMSF, 1 mM EDTA, and 50% (v/v) glycerol. Store at −20 °C.

6. Okadaic acid: 10 μg/mL okadaic acid in DMSO. Store at −20 °C.
7. Recombinant His-AXIN (full length), expressed in *E. coli*.
8. Recombinant GST-ACC1 (aa 34–100), expressed in *E. coli*.
9. Thermomixer equipped with 1.5-mL reaction vessels.

2.4 Measurement of AMP, ADP, and ATP

The reagents listed below should be of HPLC or higher grade. Methanol and chloroform should be precooled to 4 °C prior to use.

1. Mannitol solution: 5% (w/v) mannitol in H_2O.
2. Methanol.
3. Chloroform.
4. Ammonium acetate: 50 mM ammonium acetate, pH 8.5, in H_2O.
5. Electrolyte containing phosphate buffer (*see* **Note 15**), stored at 4 °C.
6. Sheath liquid: methanol/water (50% v/v) containing 0.1 μM 2,2-difluoroethoxy phosphazene, stored at 4 °C.
7. Internal standard 1 (IS1): 50 μM L-methionine sulfone, 50 μM D-camphor-10-sulfonic acid in ultrapure water. Store at 4 °C.
8. Internal standard 2 (IS2): 50 μM 3-aminopyrrolidine dihydrochloride, 50 μM N,N-diethyl-2-phenylacetamide, 50 μM trimesic acid, 50 μM 2-naphthol-3,6-disulfonic acid disodium salt in methanol. Store at 4 °C.
9. Ultrafree-MC-PLHCC centrifugal filters.
10. Freeze Dry System: Refrigerated CentriVap Vacuum Concentrators.
11. Capillary electrophoresis equipped with a pump and a splitter (1:100).
12. Mass spectrometry.
13. Fused-silica capillary (i.d. 50 μm × 80 cm).
14. Injection vial.
15. Aluminum clamp (*see* **Note 16**). The clamp should be prefrozen in liquid nitrogen prior to use.

3 Methods

3.1 Analysis of AMPK Activation in Low Glucose (See Notes 17 and 18)

All media should be preheated at a 37 °C water bath prior to use.

Glucose Starvation and Determination of p-AMPKα-Thr-172 in MEFs

1. MEFs are cultured to 70–80% confluence (*see* **Note 19**) in 6-well dishes containing 2 mL of complete DMEM medium per well in a 5% CO_2 incubator.

2. Rinse cells twice with 2 mL of PBS (RT).
3. Add 2 mL of complete DMEM medium or glucose-free DMEM supplemented with desired concentrations of glucose into the control cells or cells to be starved. Incubate cells for desired periods of time at 37 °C in the CO_2 incubator.
4. Aspirate medium, and quickly add 250 μL of ice-cold lysis buffer into each well, and then place the dishes on ice (*see* **Notes 20** and **21**).
5. Scrape and collect the lysed cells, and then sonicate for 3–5 s at 30% maximum power on ice (*see* **Note 22**). The lysates are then centrifuged at 20,000 × *g* for 10 min at 4 °C.
6. Transfer 250 μL of each supernatant into a new tube containing 250 μL of 2× SDS sample buffer, mix well, and then boil the mixture for 10 min.
7. Load 10 μL of each sample into the wells of an 8% SDS-PAGE gel, along with molecular weight marker. Run the gel for 1–2 h at 100 V.
8. Activate PVDF with methanol for 1 min and transfer the protein from the gel to the PVDF membrane by a vertical "wet" transfer apparatus at 100 V for 1 h.
9. Block the membrane for 1 h at room temperature using blocking solution containing 5% (w/v) nonfat dry milk (for blocking AMPKα and ACC) or 5% (w/v) bovine serum albumin (for blocking p-AMPKα and p-ACC).
10. Incubate the membrane with primary antibody in blocking solution overnight at 4 °C, and then incubate the membrane with the HRP-conjugated secondary antibody in blocking solution at RT for 1 h.
11. Acquire images using techniques for chemiluminescence.

Starvation of Mice and Determination of p-AMPKα-Thr-172 in the Mouse Liver

12. Withdraw the diet at 5 p.m.
13. Sacrifice mice at 9 a.m. the next day by cervical dislocation (*see* **Note 23**). Liver tissues are excised and instantly frozen in liquid nitrogen (*see* **Note 24**).
14. To begin homogenization, thaw the frozen liver tissues on ice and add 10 μL of ice-cold lysis buffer per mg of liver tissue (*see* **Note 25**).
15. Homogenize the tissues using an electrical disperser, and sonicate the lysates on ice for 5 s at 30% maximum power on ice.
16. Centrifuge the lysates at 20,000 × *g* for 10 min at 4 °C, recover supernatant in a new tube and add an equal amount of 2× SDS sample buffer, and then analyze p-AMPK and p-ACC as described in previous **steps 6–11**.

3.2 Analysis of the Lysosomal Localization of AXIN/LKB1

Preparation of Lysosomes

In this section, the method preparation of lysosome is described. The method was originally developed by Sigma-Aldrich LLC, with some modifications. All procedures, unless otherwise indicated, should be carried out at 4 °C or on ice.

1. Collect MEFs from 60 10-cm dishes (60–80% confluence) by directly scraping, at RT (*see* **Note 26**).
2. Centrifuge the cells at 500 × *g* at 37 °C (*see* **Note 26**) for 5 min.
3. Resuspend the cells in 7 mL of 1× Extraction Buffer (diluted with ultrapure water) containing protease inhibitor cocktail at RT (*see* **Note 26**).
4. Move the suspended cells to ice bucket and immediately break the cells in a 7-mL Dounce homogenizer for 120 strokes.
5. Centrifuge the sample at 1000 × *g* for 10 min, yielding post-nuclear supernatants (PNS).
6. Transfer the PNS equally to six new tubes. Centrifuge the PNS at 20,000 × *g* for 20 min.
7. Suspend the pellet in each tube in 1× Extraction Buffer to 400 μL final volume (*see* **Note 27**) by gentle pipetting. The resuspension is the crude lysosomal fraction (CLF).
8. Add 253 μL of OptiPrep and 137 μL of 1× OptiPrep Dilution Buffer (diluted with ultrapure water) to each CLF in the tube. Mix the CLF well by gentle pipetting. The mixture is defined as the Diluted OptiPrep Fraction (DOF).
9. Prepare 10 mL of each OptiPrep density gradient medium solutions (Table 1).
10. Prepare six 11 × 60-mm centrifuge tubes, each sequentially loaded with 0.4 mL of 27% and 0.5 mL of 22.5% OptiPrep solution, and overlay with 0.8 mL of DOF, and then with 1 mL of 16%, 0.9 mL of 12% and 0.3 mL of 8% OptiPrep solution.
11. Install each 11 × 60-mm centrifuge tube onto precooled SW60 Ti rotor, and then separate the mixture by ultracentrifugation at 150,000 × *g* for 4 h.
12. The fraction at the top of 12% OptiPrep solution (approximately 200 μL per tube *see* **Note 28**) is collected as the lysosome fraction.
13. Add $CaCl_2$ to the lysosome fraction to an 8 mM final concentration, and centrifuge the fraction at 5000 × *g* for 15 min. Move the supernatant to a new tube.
14. Mix the supernatant with two volumes of PBS. Centrifuge the mixture at 20,000 × *g* for 20 min.

Table 1
Preparation of OptiPrep density gradient medium solutions

OptiPrep (final concentration, %)	OptiPrep (mL)	20× dilution buffer (mL)	2.3 M sucrose (mL)
27	4.5	0.245	0.6
22.5	3.75	0.282	0.62
16	2.67	0.334	0.65
12	2	0.364	0.71
8	1.33	0.395	0.77

Add ultrapure water to 10 mL final volume. Store at 4 °C

15. Aspirate the supernatant, and the sediment is the lysosome fraction.
16. The purified lysosome can be used for IB by mixing with ten volumes of 2× SDS sample buffer or IP analysis of the lysosomal AMPK-activating complex.

Preparation of DRM

In this section, the method for isolating DRM is described. Of note, DRM can be isolated from light organelles after in vitro reconstitution assays (Fig. 1). All procedures, unless indicated otherwise, should be carried out at 4 °C or on ice.

17. MEFs collected from five 10-cm dishes (60–80% confluence), or 0.3 g of freshly excised liver tissue (handled as described in **steps 12–14** of Subheading 3.1) is homogenized in 2 mL of Buffer A.
18. Incubate the homogenates on rotator at 40 rpm for 1 h in cold room.
19. The homogenates are mixed well with 2 mL of 80% sucrose solution by gentle pipetting (*see* **Note 29**).
20. Load the mixture to the bottom of a 14 × 89-mm centrifuge tube and overlay sequentially with 5 mL of 35% and 1 mL of 5% sucrose solutions.
21. Install each tube onto precooled SW41 rotor, and then separate the mixture by ultracentrifugation at 100,000 × *g* for 16 h.
22. The gradient is collected into ten fractions, 1 mL each. Fractions 2 and 3 contain DRM, and fractions 7–10 (the bottom fractions) are cytosolic fractions (non-DRM).
23. Dissolve DRM proteins with an equal volume of DRM buffer, and then add the same volume of 2× SDS sample buffer for immunoblotting (described in **steps 7–11** of Subheading 3.1; *see* **Note 30**), or for IP with AXIN or LAMTOR1 antibody.

Immunofluorescent Analysis of Lysosomal Localization of AXIN

For monitoring dynamic translocation of AXIN onto the surface of lysosome in intact cells, immunofluorescent staining is performed, with LAMP2 as a lysosomal marker.

24. Cells are placed on glass coverslips in 6-well dishes and cultured to 60–80% confluence.
25. Aspirate the medium and fix the cells with 1 mL of 4% (v/v) formaldehyde at RT for 20 min (*see* **Note 31**).
26. Rinse the cells twice with 1 mL of PBS (RT), and permeabilize cells with 1 mL of PBS-T for 5 min at 4 °C.
27. Rinse the permeabilized cells twice with 1 mL of PBS, and incubate the cells with primary antibodies against AXIN and LAMP2 overnight at 4 °C.
28. Rinse the cells for three times with 1 mL of PBS, and then incubate the cells with Alexa-Fluor 488-conjugated anti-goat secondary antibody and Alexa-Fluor 594-conjugated anti-rat secondary antibody for 8 h at RT in the dark.
29. Wash the cells for four times with 1 mL of PBS, and then mount the coverslip on a slide by 20 μL of mountant.
30. Visualize the cells under a confocal microscopy. The samples are excited with argon gas laser using a 488-nm laser line for Alexa-Fluor 488 dye (green channel) and with HeNe gas laser using a 594-nm laser line for Alexa-Fluor 594 dye (red channel). Confocal microscopic pictures are taken with a 63× oil objective using the confocal microscope (*see* **Note 32**). The colocalization percentages are analyzed by using ZEN 2010 software (Zeiss).

Determining the Complex Formation Between v-ATPase-Ragulator and AXIN/LKB1-AMPK by Co-immunoprecipitation Analysis

Cell lysis and co-immunoprecipitation analysis are carried out as described in Rui et al. [30] with some modifications. In particular, to ensure that the membrane-associated proteins such as Ragulator are adequately extracted in the lysis buffer, a series of detergents were screened and titrated. We have found ODG as the most adequate detergent to be included in the lysis buffer [15].

31. MEFs are cultured to 70–80% confluence in 15-cm dishes. To immunoprecipitate AXIN or LAMTOR1, 4–10 dishes (15 cm) of MEFs are collected.
32. Aspirate the medium and quickly lyse the cells with 750 μL/dish of ice-cold ODG buffer (*see* **Note 33**). To immunoprecipitate AXIN or LAMTOR1, lyse lysosomes prepared from ten 10-cm dishes or DRMs from five 10-cm dishes with 750 μL/dish of ice-cold ODG buffer.

33. Sonicate the lysates (*see* **Note 34**), and centrifuge at 20,000 × *g* at 4 °C for 15 min.
34. Incubate the centrifuged supernatants with antibody against AXIN or LAMTOR1 overnight on a rotator at 40 rpm at 4 °C.
35. Overnight protein aggregates are precleared by centrifugation at 20,000 × *g* at 4 °C for 10 min, and protein A/G beads are added into the supernatant into the 7.5 mL of supernatant and mixed on a rotator at 40 rpm for 3 h at 4 °C. Some 75 and 30 μL of net volumes of beads are needed to immunoprecipitate AXIN and LAMTOR1, respectively.
36. Wash the beads with 100 volumes of ODG buffer for three times at 4 °C. Aspirate the ODG buffer, mix the beads with an equal volume of 2× SDS sample buffer, and boil the mixture for immunoblotting (described in **steps 7–11** of Subheading 3.1).

3.3 In Vitro Reconstitution of Lysosomal AMPK Activation

In this section, the methods for the purification of light organelles, and the versatile applications of these membrane structures in monitoring the binding of AXIN/LKB1 to lysosome and activation of AMPK, are described.

Purification of Light Organelles

1. Treat MEFs with desired stimuli.
2. Scrape and spin down cells at 200 × *g* at RT, and then resuspend the cells in 500 μL per 10-cm dish of fractionation buffer at RT.
3. Mechanically break the cells by passing each cell resuspension through a 22 G needle attached to a 1-mL syringe for six times (*see* **Note 35**), and then spin down the homogenates at 2000 × *g* for 10 min, yielding PNS.
4. The PNS is then spun at 20,000 × *g* for 15 min at 4 °C. The pellets are light organelles, and the supernatants are membrane-cleared cytosolic fractions.

In Vitro Reconstitution Assay for Lysosomal Association of AXIN/LKB1

To recapitulate starvation-induced translocation of AXIN onto the surface of lysosome, we incubated light organelles purified from glucose-starved or unstarved cells with AXIN in the membrane-cleared cytosols or purified bacterially expressed AXIN [30]. We found that after glucose starvation or v-ATPase inhibition, the v-ATPase-Ragulator complex becomes more accessible to AXIN-LKB1 [15]. Similarly, the effects of other metabolic stresses or pharmacological stimuli on the lysosomal v-ATPase-Ragulator complex can be easily determined in vitro through applying this method.

5. Each reconstitution reaction requires light organelles from two 15-cm dishes of MEFs.
6. Resuspend the light organelles with 500 μL of cytosolic fractions (containing AXIN) purified from four 15-cm dishes of MEFs or 500 μL of fractionation buffer containing 1 μg of bacterially expressed His-AXIN at 4 °C.
7. Incubate the cytosolic fractions or His-AXIN with light organelles at 37 °C in a thermomixer at 600 rpm for 25 min. The mixture can be used to determine:
   - Localization of AXIN in DRM: treat the mixture with 1.5 mL of ice-cold Buffer A and leave the tubes on a rotator at 40 rpm for 1 h at 4 °C, and then prepare and analyze proteins remaining with DRM fractions by following **steps 21–23** of Subheading 3.2.
   - Immunoprecipitation: lyse the mixture with 500 μL of ODG buffer at 4 °C, and then analyze the interaction between LAMTOR1 and AXIN as described in **steps 33–36** of Subheading 3.2.

Light Organelle-Based AMPK Phosphorylation Assay

The light organelles from the cell in which the lysosomal pathway is "turned on" allows for phosphorylation of AMPK by LKB1 tethered onto the lysosomal surface by AXIN.

8. For each reaction, light organelles (one 10-cm dish of cells) are resuspended in 100 μL of ice-cold fractionation buffer containing 0.5 μg of $PP2A_c$.
9. Incubate the mixtures in a thermomixer at 600 rpm for 30 min (*see* **Note 36**) at 32 °C to dephosphorylate AMPK.
10. Terminate the reaction by adding okadaic acid (10 ng/mL final concentration) into the mixture.
11. Add additive of interest, e.g., various concentrations of AMP (e.g., 0–200 μM final concentrations), to the mixture containing ATP (e.g., 200 μM final concentration), and incubate the mixture at 30 °C for 20 min. The reaction is terminated by addition of 2× SDS sample buffer for immunoblotting (described in **steps 7–11** of Subheading 3.1). Of note, ATP is included to better reflect cellular situations of the ratio of AMP over ATP [11].

Light Organelle-Based ACC Phosphorylation Assay

As described above, ACC phosphorylation (Ser-79 for ACC1 and Ser-212 for ACC2) is primarily catalyzed by AMPK [11]. Light organelles purified from various treated cells are applicable for determining AMPK activities toward ACC in vitro.

12. Light organelles of two 15-cm dishes of MEFs for each reaction are resuspended with 50 μL of fractionation buffer containing 1 μg of recombinant GST-ACC1 as substrate at 4 °C.
13. Add ATP (200 μM final concentration) and/or appropriate concentrations of desired drugs, e.g., AMP, and incubate the mixtures on a thermomixer at 800 rpm for 30 min at 30 °C. The reactions are terminated by addition of 2× SDS and are analyzed by immunoblotting (described in **steps 7–11** of Subheading 3.1).

3.4 Measurement of AMP, ADP, and ATP

In this section, we describe a CE-MS method, developed by Zhao JY et al. and Zhao Y et al. [28, 29], to measure the levels of the cellular adenylate nucleotides. This method is sensitive and effectively protects ATP and ADP from degradation if cautions are properly taken.

Extraction of AMP, ADP, and ATP from Cultured Cells

1. MEFs are cultured to 70–80% confluence in 10-cm dishes.
2. Aspirate culture medium quickly and rinse cells with 20 mL of mannitol solution (*see* **Note 37**).
3. Soak the whole dish in liquid nitrogen, immediately (*see* **Note 38**).
4. Add 1 mL of methanol containing IS1 (1:200) into the dish.
5. Scrape off the cells and transfer the cell-methanol mixture in to a 5-mL reaction tube. Vortex the mixture for 20 s.
6. Add 1 mL of chloroform and 400 μL of ultrapure water into the mixture, sequentially, and vortex for 20 s after each addition.
7. Centrifuge the mixture at 15,000 × *g* for 15 min at 4 °C. Collect 450 μL of aqueous phase.
8. The aqueous phase is then ultrafiltrated through an Ultrafree-MC-PLHCC centrifugal filter at 10,000 × *g* for 3 h at 4 °C (*see* **Note 39**).
9. Freeze-dry the ultrafiltrated product.
10. Dissolve the dried sample in 100 μL of ultrapure water containing IS2 (1:200).
11. Load 20 μL of sample into the injection vial for the CE-MS analysis.

Extraction of AMP, ADP, and ATP from Mouse Liver

12. Mice are starved overnight as described in **step 12** of Subheading 3.1.
13. Anesthetize mouse (*see* **Note 40**).

14. Open the abdomen to expose the organs in the peritoneal cavity and tightly clamp the edge of liver with the prefreezed clamp for 20 s.
15. Homogenate some 50 mg of frozen liver using an electrical disperser in 1 mL of methanol containing IS1 (1:200; *see* **Note 41**).
16. Extract ATP, ADP, and AMP as described in **steps 4–11** of Subheading 3.4.

Measure the Levels of AMP, ADP, and ATP Using CE-MS

17. Maintain the fused-silica capillary at 20 °C prior to use (*see* **Note 42**).
18. Couple CE unit with TOF-MS unit by passing the sheath liquid through the coaxial sheath at 10 μL/min for 30 min.
19. Run CE-TOF-MS at anion mode and analyze the levels of adenylates. In detail, the fused-silica capillary is first filled with ammonium acetate solution and then preconditioned with the electrolyte containing phosphate buffer. At the beginning of each run, the capillary is washed by electrolyte containing phosphate buffer. Sample is injected by Agilent 1100 series pump at a pressure of 50 mbar for 25 s and is driven by a constant voltage at 30 kV (for 40 min). The fragmentor voltage of MS unit at three directions is set at 125, 50, and 650 V, respectively. The voltage for ionization is set at 3500 V, with a drying gas flow at 7 L/min at 300 °C. The separation is assisted by a nebulizer at 15 mbar pressure. The isotope of the deprotonated acetic acid (m/z 60.0172) and 2,2-difluoromethoxy phosphazene plus deprotonated acetic acid (m/z 680.03554) are used as the reference masses. The scanning range is 50–1000 m/z, and the scan rate is 1.5 spectra/s.

4 Notes

1. Dialysis of FBS is not necessary, since the glucose brought by 10% (v/v) FBS is not sufficient to affect the activation of AMPK under glucose starvation.
2. *LAMTOR1*$^{-/-}$ or *AXIN*$^{-/-}$ MEFs are generated by infecting SV40 T-immortalized *LAMTOR1*$^{F/F}$ or *AXIN*$^{F/F}$ MEFs with adenovirus expressing Cre recombinase for 12 h. To avoid the elevated basal levels of p-Thr-172-AMPKα in the infected cells, we strongly recommend that cells be incubated in fresh DMEM for another 8–10 h before further treatments.
3. According to our experience, the genomes of *LAMTOR1*$^{-/-}$ MEFs are unstable. We therefore recommend generating knockout MEFs fresh for each experiment.

4. We strongly recommend that the mouse be housed individually particularly during sacrifice.
5. The lysis buffer can be prepared in large batches, as 10× stock solutions and frozen in aliquots.
6. It is convenient to use Mini Trans-Blot® Cell from Bio-Rad Laboratories.
7. For immunoblotting, the antibodies against phospho-AMPK-α-Thr-172 (cat. #2535), anti-AMPKα (cat. #2532), anti-phospho-ACC-Ser79 (cat. #3661), and anti-ACC (cat. #3662) can be purchased from Cell Signaling Technology. All of these antibodies are 1:1000 diluted for immunoblotting.
8. The T 10 basic ULTRA-TURRAX® from IKA equipped with an S10N-5G Dispersing element (cat. 0003304000) is suggested.
9. The method for the preparation of lysosome was originally developed by Sigma-Aldrich LLC, and the materials used here were purchased from Sigma.
10. To prepare the sucrose solution, dissolve sucrose at 37 °C in Buffer A. Vigorous shaking or vortexing should be avoided, since it would make bubbles.
11. For IP, the antibody against LAMTOR1 was raised with purified bacterially expressed GST-tagged fragment of amino acids 1–64 of human LAMTOR1. The antibody against AXIN can be purchased from Santa Cruz Biotechnology (cat. sc-8567, diluted 1:100).
12. For immunofluorescent staining, the antibody against AXIN can be purchased from Santa Cruz Biotechnology (cat. sc-8567, diluted 1:60), and the antibody against LAMP2 from Abcam (ab13524, diluted 1:120).
13. It is convenient to use ProLong Diamond Antifade Mountant (Molecular Probes, P36970). 90% (v/v) glycerol can also be used as mountant.
14. Keep the concentration of NaCl below 100 mM; otherwise, the efficacy of ODG will be dampened.
15. It is convenient to use the electrolyte containing phosphate buffer from Human Metabolome Technologies (cat. H3302-1022).
16. The size of clamp should be slightly larger than that of a hepatic lobe. Make sure that the lobe can be tightly clamped by the clamp.
17. Only glucose starvation is mentioned as a representative of AMPK-activating stresses in this section. For starvation of other nutrients, just choose appropriate media accordingly. For treatment of drugs, the drug of interest can be added to

the complete DMEM medium directly or administered into animals at chosen doses.

18. It should be noted that AMPK could be artificially activated during collection of cells or dissection of animal tissues. Therefore, cautions must be taken to avoid elevation of basal AMPK activities.
19. According to our experience, never let the cells reach 100% confluence; the basal activity of AMPK will increase otherwise. In addition, contamination of mycoplasma would also inflict an increase of basal AMPK activity.
20. Rinsing cells with PBS (especially at RT) is not recommended; it will raise the basal level of activated AMPK, otherwise.
21. Cells should be kept at ambient temperature before lysis. Cold shock will directly activate AMPK.
22. Pay special attention to temperature rising during the sonication. Hence, sonication should be intermittent.
23. Decapitation must be avoided to prevent draining of blood, because AMPK will otherwise be phosphorylated by CaMKKβ in response to ischemia [31, 32].
24. Liver tissue can also be harvested after anesthesia is applied to mouse.
25. As an alternative choice, homogenize the frozen tissue in ice-cold buffer directly.
26. The cells should be kept at ambient temperature until they are broken by Dounce homogenizer to avoid AMPK activation by cold shock.
27. We find that it is a critical step for lysosome isolation. Make sure that the pellet is sufficiently suspended and volume of the suspension should be precisely adjusted to 400 μL.
28. Avoid collecting too much lysosome fraction (e.g., more than 300 μL); it would otherwise reduce the purification efficiency of **step 12**.
29. Avoid bubbles when mixing the sample—it is critical for the isolation of DRM.
30. If the concentration of protein is too low to be detected, precipitate the protein by adding trichloroacetic acid to the DRM fraction (10% (v/v) final concentration). Wash the precipitant with ice-cold acetone for two times and dissolve the precipitant with ODG buffer. The sample is then sonicated, centrifuged, and mixed with SDS sample buffer for immunoblotting (described in **steps 7–11** of Subheading 3.1).
31. Dilute the formaldehyde prior to use, and do not rinse the cells with PBS before fixation. As an alternative choice, add 2 mL of

8% (v/v) formaldehyde directly into the well containing a similar volume of DMEM medium.

32. The parameters, including PMT voltage, offset, pinhole, and gain, should be kept unchanged between each picture taken to ensure the accuracy of colocalization percentage calculation.
33. Note that lysosomes or DRM fractions can also be used for co-immunoprecipitation analysis (start from **step 2**) (Fig. 1).
34. Make sure that the lysates are sufficiently sonicated; otherwise protein aggregates will form during the immunoprecipitation.
35. The specific rounds of passing the lysates through the syringe vary between different cell types. Six times of passing through is sufficient for breaking MEFs.
36. Determine the efficiency of dephosphorylation at the end of the reaction.
37. The cells should be rapidly rinsed. It is strongly recommended to thoroughly rinse the cells: tilt the culture dish and apply the mannitol solution (25 mL in total, per plate) to the upper side of the dish by using a 25-mL serological pipette, and aspirate the waste liquid at the bottom of the dish.
38. We find that it is better to label the dish on its bottom rather than lid to prevent the lid from unscrewed in liquid nitrogen.
39. The filter should be prevented from drying at all time.
40. Avoid cervical dislocation. It has been reported to cause degradation of ATP and ADP [33]. We anesthetize mice with 100 mg/kg sodium pentobarbital. Use of chloral hydrate is also suitable for this assay.
41. Try to homogenate the tissue as quickly as possible to prevent the degradation of ATP and ADP.
42. At the same time, cool the sample tray to 4 °C.

Acknowledgments

We thank the members of the Hai-Long Piao laboratory from Dalian Institute of Chemical Physics, Chinese Academy of Sciences for the technical instruction on the CE-MS analysis of nucleotides. This work was supported by grants from the National Key Research and Development Project of China (2016YFA0502001) and National Natural Science Foundation of China (#31430094, #31690101, #31571214, and #31601152).

References

1. Hardie DG, Ross FA, Hawley SA (2012) AMPK: a nutrient and energy sensor that maintains energy homeostasis. Nat Rev Mol Cell Biol 13(4):251–262. https://doi.org/10.1038/nrm3311
2. Hardie DG (2014) AMP-activated protein kinase: maintaining energy homeostasis at the cellular and whole-body levels. Annu Rev Nutr 34:31–55. https://doi.org/10.1146/annurev-nutr-071812-161148
3. Scott JW, Hawley SA, Green KA, Anis M, Stewart G, Scullion GA, Norman DG, Hardie DG (2004) CBS domains form energy-sensing modules whose binding of adenosine ligands is disrupted by disease mutations. J Clin Invest 113(2):274–284. https://doi.org/10.1172/JCI19874
4. Kemp BE (2004) Bateman domains and adenosine derivatives form a binding contract. J Clin Invest 113(2):182–184. https://doi.org/10.1172/JCI20846
5. Xiao B, Heath R, Saiu P, Leiper FC, Leone P, Jing C, Walker PA, Haire L, Eccleston JF, Davis CT, Martin SR, Carling D, Gamblin SJ (2007) Structural basis for AMP binding to mammalian AMP-activated protein kinase. Nature 449(7161):496–500. https://doi.org/10.1038/nature06161
6. Chen L, Jiao ZH, Zheng LS, Zhang YY, Xie ST, Wang ZX, Wu JW (2009) Structural insight into the autoinhibition mechanism of AMP-activated protein kinase. Nature 459(7250):1146–1149. https://doi.org/10.1038/nature08075
7. Xiao B, Sanders MJ, Underwood E, Heath R, Mayer FV, Carmena D, Jing C, Walker PA, Eccleston JF, Haire LF, Saiu P, Howell SA, Aasland R, Martin SR, Carling D, Gamblin SJ (2011) Structure of mammalian AMPK and its regulation by ADP. Nature 472(7342):230–233. https://doi.org/10.1038/nature09932
8. Shackelford DB, Shaw RJ (2009) The LKB1-AMPK pathway: metabolism and growth control in tumour suppression. Nat Rev Cancer 9(8):563–575. https://doi.org/10.1038/nrc2676
9. Hawley SA, Davison M, Woods A, Davies SP, Beri RK, Carling D, Hardie DG (1996) Characterization of the AMP-activated protein kinase kinase from rat liver and identification of threonine 172 as the major site at which it phosphorylates AMP-activated protein kinase. J Biol Chem 271(44):27879–27887
10. Oakhill JS, Chen ZP, Scott JW, Steel R, Castelli LA, Ling N, Macaulay SL, Kemp BE (2010) beta-Subunit myristoylation is the gatekeeper for initiating metabolic stress sensing by AMP-activated protein kinase (AMPK). Proc Natl Acad Sci U S A 107(45):19237–19241. https://doi.org/10.1073/pnas.1009705107
11. Gowans GJ, Hawley SA, Ross FA, Hardie DG (2013) AMP is a true physiological regulator of AMP-activated protein kinase by both allosteric activation and enhancing net phosphorylation. Cell Metab 18(4):556–566. https://doi.org/10.1016/j.cmet.2013.08.019
12. Hardie DG, Carling D, Gamblin SJ (2011) AMP-activated protein kinase: also regulated by ADP? Trends Biochem Sci 36(9):470–477. https://doi.org/10.1016/j.tibs.2011.06.004
13. Davies SP, Helps NR, Cohen PT, Hardie DG (1995) 5′-AMP inhibits dephosphorylation, as well as promoting phosphorylation, of the AMP-activated protein kinase. Studies using bacterially expressed human protein phosphatase-2C alpha and native bovine protein phosphatase-2AC. FEBS Lett 377(3):421–425. https://doi.org/10.1016/0014-5793(95)01368-7
14. Oakhill JS, Steel R, Chen ZP, Scott JW, Ling N, Tam S, Kemp BE (2011) AMPK is a direct adenylate charge-regulated protein kinase. Science 332(6036):1433–1435. https://doi.org/10.1126/science.1200094
15. Zhang CS, Jiang B, Li M, Zhu M, Peng Y, Zhang YL, Wu YQ, Li TY, Liang Y, Lu Z, Lian G, Liu Q, Guo H, Yin Z, Ye Z, Han J, Wu JW, Yin H, Lin SY, Lin SC (2014) The lysosomal v-ATPase-Ragulator complex is a common activator for AMPK and mTORC1, acting as a switch between catabolism and anabolism. Cell Metab 20(3):526–540. https://doi.org/10.1016/j.cmet.2014.06.014
16. Zhang CS, Li MQ, Ma T, Zong Y, Cui JW, Feng JW, Wu YQ, Lin SY, Lin SC (2016) Metformin activates AMPK through the lysosomal pathway. Cell Metab 24(4):521–522. https://doi.org/10.1016/j.cmet.2016.09.003
17. Zhang YL, Guo H, Zhang CS, Lin SY, Yin Z, Peng Y, Luo H, Shi Y, Lian G, Zhang C, Li M, Ye Z, Ye J, Han J, Li P, Wu JW, Lin SC (2013) AMP as a low-energy charge signal autonomously initiates assembly of AXIN-AMPK-LKB1 complex for AMPK activation. Cell Metab 18(4):546–555. https://doi.org/10.1016/j.cmet.2013.09.005

18. Chapel A, Kieffer-Jaquinod S, Sagne C, Verdon Q, Ivaldi C, Mellal M, Thirion J, Jadot M, Bruley C, Garin J, Gasnier B, Journet A (2013) An extended proteome map of the lysosomal membrane reveals novel potential transporters. Mol Cell Proteomics 12 (6):1572–1588. https://doi.org/10.1074/mcp.M112.021980
19. Nada S, Hondo A, Kasai A, Koike M, Saito K, Uchiyama Y, Okada M (2009) The novel lipid raft adaptor p18 controls endosome dynamics by anchoring the MEK-ERK pathway to late endosomes. EMBO J 28(5):477–489. https://doi.org/10.1038/emboj.2008.308
20. Sancak Y, Bar-Peled L, Zoncu R, Markhard AL, Nada S, Sabatini DM (2010) Ragulator-Rag complex targets mTORC1 to the lysosomal surface and is necessary for its activation by amino acids. Cell 141(2):290–303. https://doi.org/10.1016/j.cell.2010.02.024
21. Bar-Peled L, Schweitzer LD, Zoncu R, Sabatini DM (2012) Ragulator is a GEF for the rag GTPases that signal amino acid levels to mTORC1. Cell 150(6):1196–1208. https://doi.org/10.1016/j.cell.2012.07.032
22. Kawabuchi M, Satomi Y, Takao T, Shimonishi Y, Nada S, Nagai K, Tarakhovsky A, Okada M (2000) Transmembrane phosphoprotein Cbp regulates the activities of Src-family tyrosine kinases. Nature 404 (6781):999–1003. https://doi.org/10.1038/35010121
23. Steinberg BE, Huynh KK, Brodovitch A, Jabs S, Stauber T, Jentsch TJ, Grinstein S (2010) A cation counterflux supports lysosomal acidification. J Cell Biol 189 (7):1171–1186. https://doi.org/10.1083/jcb.200911083
24. Zoncu R, Bar-Peled L, Efeyan A, Wang S, Sancak Y, Sabatini DM (2011) mTORC1 senses lysosomal amino acids through an inside-out mechanism that requires the vacuolar H(+)-ATPase. Science 334 (6056):678–683. https://doi.org/10.1126/science.1207056
25. Kahn BB, Alquier T, Carling D, Hardie DG (2005) AMP-activated protein kinase: ancient energy gauge provides clues to modern understanding of metabolism. Cell Metab 1 (1):15–25. https://doi.org/10.1016/j.cmet.2004.12.003
26. Steinberg GR, Kemp BE (2009) AMPK in health and disease. Physiol Rev 89 (3):1025–1078. https://doi.org/10.1152/physrev.00011.2008
27. Carling D, Mayer FV, Sanders MJ, Gamblin SJ (2011) AMP-activated protein kinase: nature's energy sensor. Nat Chem Biol 7(8):512–518. https://doi.org/10.1038/nchembio.610
28. Zhao J, Hu C, Zeng J, Zhao Y, Zhang J, Chang Y, Li L, Zhao C, Lu X, Xu G (2014) Study of polar metabolites in tobacco from different geographical origins by using capillary electrophoresis–mass spectrometry. Metabolomics 10(5):805–815. https://doi.org/10.1007/s11306-014-0631-4
29. Zhao Y, Zhao J, Zhao C, Zhou H, Li Y, Zhang J, Li L, Hu C, Li W, Peng X, Lu X, Lin F, Xu G (2015) A metabolomics study delineating geographical location-associated primary metabolic changes in the leaves of growing tobacco plants by GC-MS and CE-MS. Sci Rep 5:16346. https://doi.org/10.1038/srep16346
30. Rui Y, Xu Z, Lin S, Li Q, Rui H, Luo W, Zhou HM, Cheung PY, Wu Z, Ye Z, Li P, Han J, Lin SC (2004) Axin stimulates p53 functions by activation of HIPK2 kinase through multimeric complex formation. EMBO J 23 (23):4583–4594. https://doi.org/10.1038/sj.emboj.7600475
31. Rousset CI, Leiper FC, Kichev A, Gressens P, Carling D, Hagberg H, Thornton C (2015) A dual role for AMP-activated protein kinase (AMPK) during neonatal hypoxic-ischaemic brain injury in mice. J Neurochem 133 (2):242–252. https://doi.org/10.1111/jnc.13034
32. McCullough LD, Tarabishy S, Liu L, Benashski S, Xu Y, Ribar T, Means A, Li J (2013) Inhibition of calcium/calmodulin-dependent protein kinase kinase beta and calcium/calmodulin-dependent protein kinase IV is detrimental in cerebral ischemia. Stroke 44(9):2559–2566. https://doi.org/10.1161/STROKEAHA.113.001030
33. Faupel RP, Seitz HJ, Tarnowski W, Thiemann V, Weiss C (1972) The problem of tissue sampling from experimental animals with respect to freezing technique, anoxia, stress and narcosis. A new method for sampling rat liver tissue and the physiological values of glycolytic intermediates and related compounds. Arch Biochem Biophys 148(2):509–522

Chapter 26

Manipulation and Measurement of AMPK Activity in Pancreatic Islets

Aida Martinez-Sanchez, Marie-Sophie Nguyen-Tu, Isabelle Leclerc, and Guy A. Rutter

Abstract

The role of the energy sensor AMPK-activated protein kinase (AMPK) in the insulin-secreting β-cell remains unclear and a subject of intense research. With this chapter, we aim to provide a detailed description of the methods that our group routinely applies to the study of AMPK function in mouse and human pancreatic islets. Thus, we provide detailed protocols to isolate and/or culture mouse and human islets, to modulate and measure AMPK activity in isolated islets, and to evaluate its impact on islet function.

Key words Mouse and human islets, Islet isolation, AMPK activity, Insulin secretion, Pharmacological AMPK activators

1 Introduction

Pancreatic β-cells are responsible for insulin release in response to elevated glucose concentration in the blood and are therefore essential for normal glucose homeostasis. Diabetes affects 8.5% of the global population [1], and type 2 diabetes (T2D), fueled by the global obesity epidemic, is one of the major modern health concerns. Central to the development of diabetes is the failure of β-cells, unable to secrete enough insulin to lower blood sugar levels. A high prevailing blood sugar will itself further accelerate β-cell failure in a vicious circle.

AMP-activated protein kinase (AMPK) is an energy sensor involved in the control of glucose homeostasis and a suggested target for some of the most commonly used antidiabetic drugs, such as metformin, rosiglitazone, and the SGLT2 inhibitor canagliflozin [2, 3]. Despite the glucose-lowering effects of AMPK activation in the liver and muscle, the impact in other tissues is still debated. In the β-cell, AMPK activity is promoted by glucose deprivation [4], but its role in processes central to β-cell function,

Dietbert Neumann and Benoit Viollet (eds.), *AMPK: Methods and Protocols*, Methods in Molecular Biology, vol. 1732, https://doi.org/10.1007/978-1-4939-7598-3_26,

such as glucose-stimulated insulin secretion, growth, or apoptosis, remains controversial [5, 6]. Moreover, recent studies suggest that chronic alteration of β-cell AMPK function might aggravate the disease [5–8]. Several variables, including the type of cells studied (β-cell lines versus isolated β-cells and/or islets), the context (in vitro or in vivo), conditions of cell culture (glucose concentration, length of the experiments), or the use of different approaches to AMPK activity modulation (e.g., pharmacological versus genetic), have surely contributed to the mixed, even controversial, results obtained by different research groups throughout the years.

AMPK consists of three subunits: α (catalytic), β (regulatory), and γ (regulatory), each of them with 2 (α, β) or 3 (γ) isoforms. In islets, AMPKα1 accounts for most of the catalytic activity [5]. The kinase activity of the catalytic subunit is increased by phosphorylation of a threonine residue (in rat, Thr-172) by upstream kinases such as LKB1 [9]. Binding of AMP allosterically activates AMPK, promotes its phosphorylation by LKB1, and prevents its dephosphorylation by phosphatases (reviewed in [10]). Giving the central role of AMP in increasing AMPK activity, it is not surprising that adenosine analogues are often used by researchers and clinicians as AMPK activators. One of the most widely used AMPK activators is 5-aminoimidazole-4-carboxamide riboside (AICAR), which is intracellularly converted into the AMP analogue ZMP [11, 12]. Nevertheless, being a potent analogue of AMP, ZMP also affects the activity of multiple other enzymes important for cell metabolism and has been recently demonstrated to act through multiple AMPK-independent pathways [13–15]. Thus, our current protocols for the study of AMPK function in human islets favor the use of more potent and selective AMPK activators, such as compound 13 (C-13, [16]) or compound 991 (C-991, [17]). On the other hand, compound C has also been widely used as a rather unspecific inhibitor of AMPK (*see* Chapter 12) [18].

Recently, we have generated mice with highly β-cell-restricted deletion of both catalytic (α1 and α2) AMPK subunits [7]. These animals represent a valuable model for study of AMPK function in the β-cell in vivo and also provide a convenient source of islets for in vitro studies which are null for AMPK. Islets from AMPKdKO animals (AMPKα1flox/flox, AMPKα2flox/flox, Ins1Cre/−) and littermate controls (AMPKα1flox/flox, AMPKα2flox/flox) were isolated as described in Subheading 3.1 and used for RNA sequencing [7, 19] and insulin secretion (Fig. 1 [7]) as detailed in Subheadings 3.4 and 3.5, respectively.

Here we aim to provide a detailed description of the protocols that our group has applied to the study of AMPK function in mouse and human pancreatic islets over the last 15 years.

The main methods described in this chapter are briefly listed below.

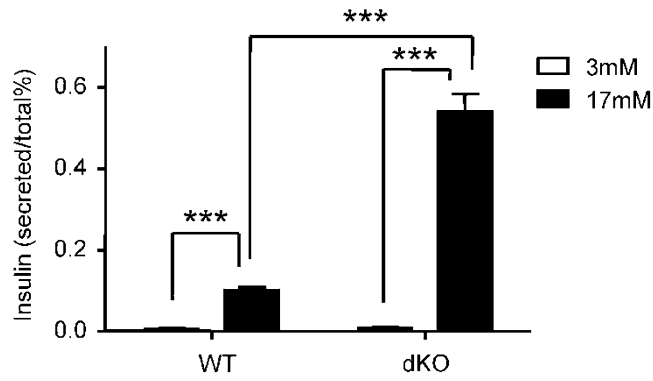

Fig. 1 Glucose-stimulated insulin secretion is increased in AMPK α1 and α2 double knockout (dKO) islets, compared to wild type (WT). After generating mutant mice lacking AMPK α1 and α2 specifically in pancreatic beta cells, 8–10 size-matched islets were isolated and stimulated with low concentration of glucose (3 mM) and high concentration of glucose (17 mM) during 30 min in static incubation. Data normalized to total insulin. $^{*}p < 0.05$, $^{**}p < 0.01$, $^{***}p < 0.001$. Reproduced from Kone et al. 2014 with permission from FASEB [7]

1.1 Isolation and Maintenance of Pancreatic Islets

We provide a brief description of the method based in collagenase injection into the pancreatic duct, which includes all the minor modifications currently applied by our group to result in a high yield and quality of isolated islets. We also detail the conditions at which we maintain both mouse and human islets in culture.

1.2 Approaches to AMPK Modulation in Islets

We describe the main methods we use to modulate islet AMPK activity in vitro that are pharmacological activators and virus expressing a dominant-negative or a constitutively active form of AMPK.

1.3 Measurement of AMPK Activity in Isolated Islets

In this section, we detail the procedures of SAMS peptide assay and Western blot for phosphorylated AMPK and its targets ACC and Raptor, as methods to determine AMPK activity in islets.

1.4 Preparation of Islet RNA for RNA-seq (or qPCR)

We provide a detailed description of RNA isolation using TRIzol, which provides high purity/quality RNA for downstream applications such as RNA sequencing or RT-qPCR.

1.5 Assessing the Impact of AMPK on Glucose-Stimulated Insulin Secretion in Isolated Islets

Healthy β-cells in the pancreatic islet respond to high glucose concentrations by secreting insulin. Therefore, we have chosen to describe in detail an assay to evaluate insulin secretion in response to glucose as a direct method to evaluate islet function.

2 Materials

2.1 Isolation and Maintenance of Pancreatic Islets

1. Dissection tools: Surgical scissors (blunt/blunt and sharp/blunt), Adson forceps (12 cm), and pean hemostatic clamp artery forceps (straight or curved).
2. 70% (v/v) ethanol.
3. 5 and 50 ml syringes.
4. Nontreated 10 cm plates.
5. 30 G needles.
6. 15 and 50 ml conic tubes.
7. 100 μm nylon mesh cell strainer.
8. Plastic Pasteur pipettes.
9. Water bath.
10. Benchtop centrifuge (for 15 and 50 ml tubes).
11. Zoom stereomicroscope, 10× objective.
12. Temperature and CO_2-regulated cell incubator.
13. Histopaque 1119 and 1083.
14. Collagenase solution: 1 mg/ml collagenase (Ref 17,456, SERVA) prepared in RPMI. Sterilize by filtration with a 0.22 μm pore size filter.
15. Mouse islet medium: RPMI (containing 11 mM glucose), 10% (v/v) fetal bovine serum (FBS), 1% (v/v) penicillin/streptomycin.

2.2 Reagents for Modulation of AMPK Activity

1. Isolated islets.
2. Nontreated 6-well plates.
3. 1.5 ml tubes.
4. Mouse islet medium (*see* Subheading 2.1, **item 10**).
5. Dimethyl sulfoxide (DMSO), molecular grade.
6. AMPK pharmacological activators.
7. Benchtop microcentrifuge (1.5 ml tubes).

2.3 Measurement of AMPK Activity in Isolated Islets

SAMS Peptide Assay

1. Isolated islets.
2. Ice-cold PBS with the appropriate glucose concentration.
3. Ice-cold lysis buffer: 50 mM Tris–HCl (pH 7.4 at 4 °C), 250 mM sucrose, 50 mM NaF, 1 mM Na pyrophosphate, 1 mM EDTA, 1 mM EGTA, 1 mM DTT, 0.1 mM benzamidine, 0.1 mM PMSF, 5 μg/ml soybean trypsin inhibitor, and 1% (v/v) Triton X-100.

4. Nontreated 24-well plates.
5. Bicinchoninic acid protein assay reagent from Pierce.
6. Synthetic SAMS peptide (HMRSAMSGLHLVKRR).
7. [γ-^{32}P]ATP 3000 Ci/mmol, 10 mCi/ml.
8. Assay buffer (5×): 20 mM HEPES (pH 7), 400 mM NaCl, 5 mM DTT, 25 mM $AcMg^{2+}$, 1 mM SAMS peptide, 1 mM AMP.
9. Hot ATP (5×), for 200 ml: 10 ml of ATP 3000 Ci/mmol, 10 ml mCi/ml; 40 ml of 10 mM ATP (cold, in 25 mM Tris, pH 8.0), H_2O up to 200 ml.
10. Whatman P81 paper (2 cm^2 square pieces, labeled)
11. Orthophosphoric acid.
12. Acetone.
13. Scintillation liquid or water.
14. Scintillation vials.
15. Scintillation counter.

Western Blot of AMPK Targets

16. Isolated islets.
17. Benchtop microcentrifuge (1.5 ml tubes).
18. Phosphate-buffered saline (PBS): 137 mM NaCl, 2.7 mM KCl, 10 mM Na_2HPO_4, 1.8 mM KH_2PO_4, pH 7.4.
19. RIPA buffer: 150 mM NaCl, 10 mM Tris, pH 7.2, 5 mM EDTA, 0.1% (w/v) SDS, 1% (w/v) sodium deoxycholate, 1% (v/v) Triton X-100, protease and phosphatase inhibitors cocktails.
20. 6× SDS sample buffer: 375 mM Tris–HCl, pH 6.8, 12% (w/v) SDS, 60% (v/v) glycerol, 0.6 M DTT, 0.06% (w/v) bromophenol blue.
21. Mini-Protean electrophoresis system (BioRad).
22. 8% polyacrylamide gels.
23. PVDF membrane.
24. Transfer buffer: 25 mM Tris-base, 192 mM glycine, and 10% (v/v) methanol.
25. Blocking solution: PBS, 0.1% (v/v) Tween 20, 5% (w/v) semi-skimmed milk.
26. Washing buffer: PBS, 0.1% (v/v) Tween 20.
27. Antibodies: anti-ACC (3662, cell signaling), phospho-ACC (Ser79) (3661, cell signaling), Raptor (2280, cell signaling), phospho-raptor (Ser792) (2083, cell signaling), AMPKα (2532, cell signaling), phospho-AMPKα (Thr172) (2535, cell signaling), goat anti-rabbit IgG-HRP (AB6721, Abcam).

28. ECL Prime Western.
29. Re-blot plus strong antibody stripping solution (Millipore).

2.4 Preparation of Islet RNA for RNA-seq

1. Isolated islets.
2. 1.5 ml tubes.
3. Benchtop microcentrifuge (1.5 ml tubes).
4. TRIzol (Invitrogen).
5. Chloroform, molecular grade.
6. Isopropanol, molecular grade.
7. Ethanol, molecular grade.
8. Glycogen, molecular grade.
9. Sodium acetate.
10. Ultrapure, RNAse-free H_2O.
11. DNase I, amplification grade (18068-015, ThermoFisher Scientific).

2.5 Impact of AMPK on Glucose-Stimulated Insulin Secretion in Isolated Islets

1. Isolated islets (30 per condition).
2. KRBH stock solutions (can be kept for 1–2 months at 4 °C):
   - Mixed HEPES-bicarbonate (4×): HEPES 40 mM, 8 mM $NaHCO_3$, 40 mM NaCl.
   - Mixed salts (5×): 650 mM NaCl, 18 mM KCl, 2.5 mM NaH_2PO_4, 2.5 mM $MgSO_4$, 7.5 mM $CaCl_2$.
3. Krebs-Ringer Bicarbonate HEPES (KRBH) (1×): This buffer is made fresh from the stock solutions above in water and equilibrated with 95% O_2 and 5% CO_2 for 10 min. pH is adjusted at 7.4 preceding supplementation with 0.1% (w/v) BSA.
4. KRBH-glucose: Prepare the solution of a range of glucose concentration (typically low glucose is 3 mM (KRBH-3 mM Glu) and high glucose is 17 mM or 11 mM (KRBH-17 mM Glu/KRBH-11 mM Glu), for mouse and human islets, respectively) and KCl (KRBH-30 mM KCl) in KRBH. KRBH-glucose solutions are kept at 37 °C.
5. 95% O_2/5% CO_2 gas cylinders.
6. Nontreated 10 cm and 12-well plates.
7. Temperature and CO^2-regulated cell incubator.
8. Water bath.
9. Zoom stereomicroscope, 10× objective.
10. Benchtop microcentrifuge (1.5 ml tubes).
11. Lysis buffer: Acidic ethanol (75 ethanol: 23.5 H_2O: 1.5 1 M HCl), 0.1% (v/v) Triton X-100.

12. Probe sonicator (Ultrasonic homogenizer).
13. Insulin Ultra-sensitive kit (62IN2PEH, Cisbio).
14. 384 wells, low volume plates (white).

3 Methods

3.1 Isolation and Maintenance of Pancreatic Islets

Isolation of Mouse Pancreatic Islets

To isolate mouse pancreatic islets, we use the method based in collagenase injection into the pancreatic duct. This method has been thoroughly detailed before by Carter and colleagues [20] and ourselves [21]. Here we provide a brief description of the protocol with some minor modifications that our lab currently applies, which results in maximum yields of 250–300 islets per mouse.

1. Prepare 3 (for C57/BL6 mice) to 5 (for CD1 mice) ml of collagenase solution per mice.
2. Cull the animal by cervical dislocation following locally regulated guidelines.
3. Wet fur with 70% (v/v) ethanol and open the abdomen to expose the organs in the peritoneal cavity.
4. With the help of sharp scissors, cut the lower ribs and the xiphoid cartilage. This will provide an adequate angle for needle insertion and will therefore facilitate the subsequent injection of collagenase inside the duct.
5. Position the animal under a Zoom stereomicroscope (10× objective), on top of a 15 ml tube transversally located underneath the liver area (also to provide a good angle for needle insertion in the duct), tail pointing away from the researcher. Flip the intestine toward the left-hand side.
6. Clamp the duct entry into the small intestine (*see* **Note** 1). Leave the clamp toward the left-hand side of the mouse. Holding and directing the clamp with one hand while injecting with the other one will aid the positioning of the needle inside the duct.
7. Pull the liver down, which should expose the Y-like junction between the ducts originating from the liver and gallbladder. Using a 30G (for C57/BL6 mice) or 27G (for CD1 mice) needle attached to a 5 ml syringe, cannulate and steadily inject through the duct 3 (for C57/BL6 mice) to 5 (for CD1 mice) ml of collagenase solution (*see* **Notes 2–4**).
8. Excise the inflated pancreas and place it inside a 50 ml tube on ice until all the samples have been taken (*see* **Note 5**).

9. Incubate the pancreas in a water bath at 37 °C for exactly 10 min (*see* **Note 6**).
10. Add 15 ml of RPMI and shake vigorously for ~20 s. The pancreas should be then fully dissociated with very few clumps. Spin down at 200 × g for 1 min.
11. Discard supernatant and wash with 15 ml of RPMI. Spin down at 200 × *g* for 1 min. Repeat this step an additional two times.
12. Resuspend the pellet in 4 ml of Histopaque 1119, mixing by hand. Transfer the resulting homogenous milky solution into a 15 ml tube.
13. Drop by drop, add 4 ml of Histopaque 1083 to create a density gradient.
14. On top, add 4 ml of RPMI, also drop by drop.
15. Spin at 1200 × *g* in a centrifuge set with maximum acceleration and minimum deceleration for 20 min, at room temperature (RT).
16. Once spun, the islets are found in a ring between the RPMI and Histopaque 1083 layers. Remove the islets using a plastic Pasteur pipette and place into a 10 cm nontreated plate with 8 ml of mouse islet medium. At this point we recommend the use of a 100 μm nylon mesh cell strainer to separate the islets by size.
17. To eliminate all the remaining Histopaque (*see* **Note 7**), hand-pick the islets into a new plate containing mouse islet medium.

Maintenance of Pancreatic Islets

18. The islets are maintained in a 5% CO_2 incubator at 37 °C in mouse islet medium at least overnight before performing any downstream experiments (*see* **Notes 8–10**).

3.2 Approaches to AMPK Modulation in Islets

Besides genetically and by manipulation of glucose concentration in the medium islet, AMPK activity can be modulated pharmacologically or through viral transduction (*see* **Note 11**).

Pharmacological Modulation of AMPK Activity

Pharmacological AMPK activators can be used to assess the effect of "short-term" (i.e., 1.5–2 h), which normally correspond to the duration of an in vitro GSIS experiment (*see* Subheading 3.3) or "long-term" (24–48 h) AMPK activation in islet function, as detailed below:

1. Prepare 6-well plates (for suspension culture, to avoid the attachment of the islets to the surface) with 2.5–3 ml of mouse islet medium containing 20 μM C-13, 50 μM C-991, or both (concentrations chosen to give close to maximal effects on AMPK activity, unpublished data and [22]). A control well is prepared containing an equivalent amount of diluent (DMSO).

2. Handpick islets (*see* **Note 9**) into a 1.5 ml tube, spun for 2 min at 200 × *g*, and resuspend in a small volume (50–100 μl per condition) of mouse islet medium. Equal volumes of the resuspended islets are subsequently added into each well.
3. Incubation is carried out for 48 h.
4. Following incubation, lyse islets in TRIzol for RNA extraction (*see* Subheading 3.4) or in RIPA buffer for protein analysis (*see* Subheading 3.3). As hinted above, our studies on the effect of acute (short-term) modulation of AMPK activity are normally aimed to assess its impact on insulin secretion. Therefore, we used the protocol described in Subheading 3.3 with minor modifications as indicated in **Note 12**.

Modulation of AMPK Using Virus Expression Dominant-Negative (DN) and Constitutively Active (CA) AMPK Proteins

The group of David Carling designed a constitutively active AMPK and a dominant-negative inhibitor of endogenous AMPK [23] which were used by our group [12] to generate adenovirus for islet infection (*see* **Note 11**). These viruses have been successfully used to modify AMPK activity in islets applying the following guidelines:

5. Handpick 30–100 islets <100 μm (*see* **Note 9**) per sample (depending on downstream application) and place in 6-well plates containing 2.5–3 ml of mouse islet medium.
6. Use a multiplicity of infection of 50–100 MOI for 16–48 h. An islet of 100 μm diameter will typically contain ~1000 cells.

We have previously demonstrated that changes in AMPK activity, using both mouse and human islets, can be detected 36 h [12] or 48 h [24] after infection, respectively.

See **Notes 13 and 14** for additional tips/recommendations.

3.3 Measurement of AMPK Activity in Isolated Islets

It should be stressed that the demonstration of changes in AMPK activity requires close attention to several aspects of the islet isolation and incubation protocols that are detailed in **Note 9**.

SAMS Peptide Assay

AMPK activity is measured using the so-called SAMS peptide assay, where a synthetic peptide (HMRSAMSGLHLVKRR) is phosphorylated by AMPK in the presence of radioactive γATP [25]. AMPK activity can be assayed from whole cell lysates (Fig. 2a, reproduced from Leclerc et al. 2004 with permission from *APS*) or after immunoprecipitation using a specific anti-AMPK subunit antibody [26]. To measure AMPK activity from whole islet lysates:

1. Approximately 100–150 islets are required for each sample (duplicates recommended).

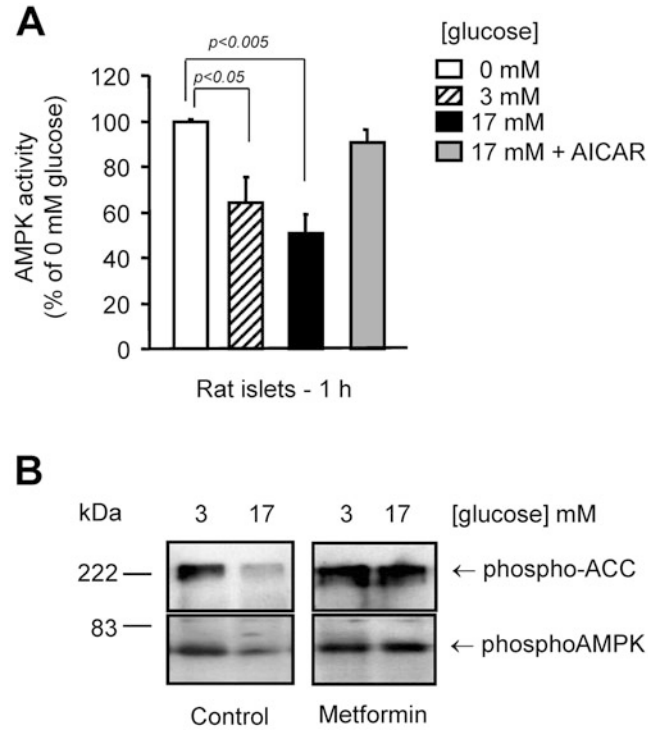

Fig. 2 Measurement of AMPK activity in isolated islets. (**a**) AMPK activity is modulated by overnight incubation at different glucose concentrations and/or with AICAR in human islets, as determined by SAMS peptide assay. Reproduced from Leclerc et al. 2004 with permission from *APS* [24]. (**b**) In MIN6 cells, AMPK activity is regulated by glucose and increased by treatment with metformin during 16 h. Increased AMPK and acetyl-CoA carboxylase (ACC) phosphorylation were measured by immunoblotting in MIN6 cells after treatment with metformin (1 mM). Reproduced from Leclerc et al. 2004 with permission from *APS* [24]

2. Prepare PBS at required glucose concentration (i.e., 3, 11, 17 mM).
3. Add 1 ml of PBS in each well of a nontreated 24-well plate.
4. Wash islets six times by taking across wells with care.
5. Place islets in 1.5 ml microfuge tube, centrifuge at 350 × *g* for 1 min, and remove PBS.
6. Add 25 μl of lysis buffer.
7. Aspirate several times to dissociate the islets with a p200 pipette and incubate on ice for 30 min.
8. Determine protein concentration using BCA protein kit (Pierce).
9. To assay, place in 1.5 ml tube: 10 μg of protein extract (*see* **Note 15**), 10 μl of 5× assay buffer, and 10 μl of 5× ATP (hot/cold). Adjust with H_2O to a total volume of 50 μl.

10. Incubate at 37 °C and spot 10 μl (or 5 μl if using 25 μl) of reaction mix on labeled p81 papers at 10, 20, and 30 min (a different paper for each spot).
11. Wash papers three times in 1% (v/v) orthophosphoric acid (500 ml per wash).
12. Pour off acid and rinse with acetone.
13. Air-dry samples or use a hair dryer until dry.
14. Prepare scintillation vials containing 10 ml H_2O or scintillation liquid.
15. Place paper in appropriate vial and count on ^{32}P channel for 1 min.
16. Express results as picomoles of ^{32}P incorporated per microgram of protein per minute (pmol/μg/min) or as a percentage of control conditions. The counts should increase in a linear way over the 30 min period. Also, include a no kinase sample (just lysis buffer) that should be flat over 30 min and subtract the counts as background.

Western Blot of (Phosphorylated) AMPK Targets

AMPK is known to phosphorylate serine residues in well-defined AMPK recognition motifs [27], and it therefore has multitude of downstream targets (reviewed in [28, 29]). Two of the best characterized AMPK targets are acetyl-CoA carboxylase (ACC), a metabolic enzyme implicated in fatty acid and cholesterol synthesis [30], and Raptor (regulatory associated protein of mTOR complex I), whose inhibition is required for energy stress-induced cell cycle arrest [31]. Thus, (inhibitory-) phosphorylation status of ACC (Fig. 2b, reproduced from Leclerc et al. 2004 with permission from *APS*) and Raptor has been widely used by us and others to assess AMPK activity in islets and β-cells [12, 24, 32]. To determine AMPK activity through the levels of phosphorylated ACC (pACC) and Raptor (pRaptor) in islets, Western immunoblot (WB) can be used as follows:

17. Handpick 10–100 islets (*see* **Note 9**) into 1.5 ml tubes, keeping the picked islets on ice. Spin for 2 min at 200 rcf at 4 °C. Wash once with ice-cold PBS (add 1 ml of PBS, manually resuspend the islets and spin for 2 min at 200 rcf at 4 °C). Remove the supernatant completely.
18. Lyse the islets in 50 μl of RIPA buffer (containing protease and phosphatase inhibitors) per sample. Pipette up and down to facilitate the lysis of the islets and incubate on ice for 20 min. The lysates can now be frozen for posterior analysis.
19. Spin the lysate for 15 min at 4 °C, to pellet DNA and cell debris (*see* **Note 16**). Add 10 μl of 6× SDS sample buffer to the supernatant.

20. Boil the samples for 5 min at 95 °C and place them on ice ready to be loaded onto an 8% polyacrylamide gel. We generally use a Mini-Protean electrophoresis system (BioRad), with a 10-well comb and a 1.5 mm glass plate, which allows the loading of the full sample (~60 μl) per well. Run and transfer onto PVDF membrane as detailed elsewhere [33]. We generally perform the transfer for 75 min at 100 mV in transfer buffer.
21. Following 30 min of blocking with PBS-Tween-5% semi-skimmed milk, cut the membrane longitudinally in three pieces to separately blot overnight with antibodies against pAMPKα (Thr172, 1:1000, 62 kDa), pRaptor (Ser792, 1:1000, 150 kDa), and pACC (Ser79, 1:500, ~280 kDa), in PBS-Tween-5% semi-skimmed milk.
22. The following day, wash the membranes three times with PBS-Tween for 5 min at RT and incubate with HRP-anti-rabbit IgG during 1 h. Following three further 5 min washes with PBS-Tween, develop with the ECL system following manufacturer's instructions (*see* **Note 17**).
23. Strip the antibodies from the membrane by incubating for 10 min with re-blot solution.
24. Repeat previous steps using antibodies for analysis against AMPKα (1:1000), Raptor (1:1000), and ACC (1:1000).

3.4 Preparation of Islet RNA for RNA-seq (or qPCR)

We recommend the use of TRIzol reagent (Invitrogen) for RNA isolation from purified islets.

1. Handpick 20–100 islets (*see* **Note 9**) into 1.5 ml tubes. Spin for 2 min at 200 rcf at RT to remove any leftovers of medium.
2. Resuspend the islets in 250 μl of TRIzol by pipetting up and down or briefly vortexing. Incubate for 10–20 min at RT. Samples can be frozen at this point.
3. Follow manufacturer's instructions for RNA extraction. Importantly, perform the optional step indicated in the manual of adding 30 μg glycogen (or equivalent reagent, such as glycoblue) preceding the RNA precipitation. This step will increase the RNA yield, which is otherwise low from such a small number of islets.
4. When working with a small number of islets, it is common to obtain low RNA concentration of poor purity, as estimated by the ratio of absorbance A260/A280 by a NanoDrop Spectrophotometer. We have found that a simple way to improve sample purity is to reprecipitate the RNA (performed after DNase treatment if this step is required) as follows.
5. Top up the volume with H_2O to 100 μl.
6. Add 0.1 volumes of 3 mM sodium acetate (pH 5.2). Vortex.

7. Add 2.2 volumes of ethanol. Vortex.
8. Incubate the tubes at RT for 10 min or for a longer (20 min–days) period of time on ice or at −20 °C (*see* **Note 18**).
9. Spin the tube at 12,000 × *g* for 15 min at 4 °C.
10. Wash the pellet with 850 μl of 70% (v/v) ethanol, spinning at 12,000 rcf for 5 min at 4 °C.
11. Remove ethanol, dry, and resuspend in ultrapure RNase-free H_2O.
12. Optional DNase treatment (*see* **Note 19**).

3.5 Assessing the Impact of AMPK on Glucose-Stimulated Insulin Secretion in Isolated Islets

The effects of AMPK on insulin secretion and pancreatic β-cell function could be studied by static conditions or by perfusing islets to measure the kinetics of insulin release in response to stimulating factors including glucose, amino acids, or chemical compounds (Fig. 1, Reproduced from Kone et al. 2014 with permission from *FASEB*). Here we describe the static glucose-stimulated insulin secretion (GSIS). Typically, glucose is used in various ranges of concentration and potassium chloride (KCl). The media used is a Krebs-Ringer buffer, with a basal low glucose concentration, and then the islets are stimulated with a higher glucose concentration.

1. Each condition is performed in triplicates (*see* **Note 20**).
2. Wash the isolated islets by picking the islets (*see* **Note 9**) into a new 10 cm petri dish containing 8 ml of KRBH solution (without glucose).
3. Preincubate the islets in unstimulated condition with a "low" glucose KRBH-3 mM Glu solution for 1 h at 37 °C, CO_2 5%, and O_2 95% (*see* **Note 21**).
4. After 1 h, stimulate the islets with different concentrations of glucose in KRBH (KRBH-3 mM Glu, KRBH-17 mM Glu) and KCl (KRBH-30 mM KCl). The KCl is used as a control, because it acts as non-specific membrane depolarizer.
5. Under the microscope, pick 10 size-matched islets for each condition into each well a 12-well plate (*see* **Note 22**).
6. Add 500 μl of KRBH + glucose or KCl into specific wells containing islets.
7. Incubate in a water bath for 30 min with gentle shaking (70 rpm/min).
8. Transfer the content of each well (islets and KRBH solution) into 1.5 ml standard microfuge tubes and place it on ice (*see* **Note 23**).
9. Centrifuge at 350 × *g* for 3 min at 4 °C.
10. Collect supernatant containing the secreted insulin into new tubes.

11. Add to islet pellet 1 ml of lysis buffer.
12. Sonicate the islets in lysis buffer for 10 s at 10 W, then place on ice.
13. Proceed to insulin level measurement or store at −20 °C or lower.
14. Insulin levels analysis by HTRF Cisbio Insulin Ultra-Sensitive Kit. The principle is based on homogeneous time-resolved fluorescence (HTRF) technology in which the insulin is detected in a sandwich assay format using two different monoclonal antibodies (one donor and one acceptor) [34]. Dilute sample with assay buffer (KRHB without glucose), no dilution for low glucose condition of secreted samples, 1:3 for high glucose and KCl conditions of secreted insulin samples, and 1:200 for samples containing total islets in order to fit in the standard range of HTRF kit (0.03–8 ng/ml).

4 Notes

1. Clamp as far inside the intestine as desired, but avoid obstructing the duct outside the intestine which would result in the blockage of the collagenase flow into the pancreatic area.
2. Inserting the needle in the junction will aid needle penetration into the duct and will allow for space to reintroduce the needle if failure. Introduce ~0.5 cm of the needle inside the duct and keep constant pressure. If the needle has been adequately located inside the duct, resistance should be encountered when injecting. If a very localized site of inflation is observed, chances are that the needle has been inserted outside the duct, probably between the duct and the fat that often surround the duct. Patiently removing that fat with the aid of the needle before attempting the insertion inside the duct might help the less experienced researcher to succeed.
3. The degree of inflation will largely correlate with the yield of isolated islets. It is important for the collagenase to reach the whole pancreatic surface.
4. In bigger animals, such as CD1 mice, it might be useful to clamp the duct entry to the liver, to minimize the amount of collagenase leaking inside this organ. This is not necessary if the needle used is thick enough to prevent the reflow of collagenase in the liver direction.
5. It is safe to leave the pancreas on ice for 2–3 h if necessary.
6. The length of the incubation might vary with the collagenase used and should be optimize for each type of collagenase/batch.

7. The islets can be first placed in a fresh tube and washed by adding islet media into the tube, spinning during 2 min at 1000 rpm, and afterward resuspended in fresh mouse islet media and placed in a 10 cm nontreated plate to skip **steps 15** and **16**. Nevertheless, we have found that, due to Histopaque being carried with the islets, the islets sometimes don't pellet adequately at the bottom of the 15 ml tube, in which case some of the islets are lost.
8. This is to allow recovery from the collagenase digestion. Also, note that the mouse islet medium contains 11 mM glucose, which corresponds to the concentration found in plasma in fed mice.
9. Isolation, manipulation, and maintenance of islets in vitro might lead to undesired AMPK activation. First, any contamination of fresh rodent islet preparations with exocrine tissue will markedly increase the measured AMPK activity. This is consistent with the higher levels of the enzyme in the exocrine tissue [24]. Secondly, very large islets have a hypoxic central core [35] and doubtless high AMPK activity. Maintenance of islets in culture for $\geq$3 days before the assay was found to overcome this problem, probably by allowing time for contaminating exocrine tissue and the hypoxic central cores of large islets, to necrose [36]. Another way of avoiding the problem is to either handpick the islets or filter the islets preparation on a 100 μM cell strainer and only use the small ones for the assay. This is particularly important if overexpressing adenoviruses as they will not infect the core of large islets [37]. Nevertheless, this might not be possible when a high amount of islet material is required for downstream applications (such as measurement of activity with SAMS peptide assay). And thirdly, washing the islets in PBS before protein isolation can activate AMPK, this can be prevented by adding glucose in the PBS at the same concentration as in the culture conditions or by strictly using ice-cold PBS and keeping the samples on ice at all times.
10. Human pancreatic islets are generally provided to our lab from several research groups around the world. Human islets are maintained in medium containing a low glucose concentration (5.5 mM glucose), which mimics blood glucose concentration after a meal. Human islet medium: RPMI without glucose (add glucose up to 5.5 mM), 10% (v/v) FBS, 1% (v/v) penicillin/streptomycin, and 2.5 mg/L amphotericin B.
11. The potent and selective AMPK activators compound 13 and compound 991 were described previously [16, 17]. AMPK-DN and AMPK-CA virus [12] are available from our lab.
12. The number of islets to be used will greatly vary depending on the sensitivity of the downstream application. We have used as

little as ten islets (<100 μm) per lane when immunoblot was performed using a WES system (http://www.proteinsimple.com/wes.html) (unpublished data) as in [38]. Nevertheless, detection of pRaptor with the antibody used for standard WB, as described above, failed to provide a detectable signal by WES.

13. AMPK activity is regulated by glucose, over the physiological range of concentrations, in primary rodent and human islets of Langerhans [24]. AMPK is strongly activated by glucose concentrations of 5.5 and 3 mM in mouse and human islets, respectively (unpublished data and [24]). It is important to adjust the glucose concentration at which the islets are maintained when performing experiments aimed to modulate AMPK activity. This is due to the strong effect that glucose has on the activity of this enzyme. We have found that AMPK (as well as its targets ACC and Raptor) is strongly phosphorylated at concentrations <3 mM or <5 mM in human and mouse islets, respectively, while almost completely dephosphorylated at concentrations >11 mM or >17 mM in human and mouse islets, respectively. Thus, we recommend to perform experiments with AMPK-DN at low glucose concentrations and, conversely, at high glucose concentrations with AMPK-CA.
14. Even though no major differences were observed in β-cell mass or the number of islets of AMPKdKO mice in vivo (unpublished data and [7]), the yield of isolated islets was consistently and substantially lower than that of the control (or of wild-type animals of the same background-C57BL/6). We still don't know the cause of this difference, but we hypothesize that it arises during the islet purification steps, possibly due to a higher fragility of the islets. Whereas we are working toward adapting the protocol to improve the islet yield from these animals, this is currently of ~30–80 islets per mice.
15. If less than 10 μg of total protein extracts are available, the assay can be performed with as little as 2.5 μg of protein, but reducing the amount of the other reagents by half and in a total volume of 25 μl.
16. If a very low number of islets are used, the pellet will be barely visible. In that case, just add the loading dye to the whole sample. If a high number of islets are used, the pellet might be gelatine-like (high content of DNA), and the samples will need to be handled with care to obtain a clean supernatant. In that case, a longer centrifugation time may help or, alternatively, it might be easier to pipette out the gelatinous pellet and keep the rest of the sample (supernatant) in the original tube.

17. The amount of protein loaded per lane is low (we estimate ~1–2 μg of total protein/100 < 100 μm islets), and therefore signals tend to be weak, especially for pACC. Therefore, exposure times tend to be long (5–20 min).
18. Other researchers have described that long incubation times (4–24 h) at −20 °C increase the yield of precipitated RNA. Nevertheless, in our hands, the differences are minimal, if any, and we therefore adjust this step just for convenience.
19. For DNase treatment, we recommend the use of DNase I, amplification grade from Invitrogen (18068-015), following manufacturer's instructions. This step is absolutely required if the RNA is going to be used for RNA-seq but can be skipped if the samples are used for other applications, such as qPCR, if adequate primers (spanning exon junctions) are used.
20. The experience is run in triplicate. We recommend performing a minimum of three independent experiments with mouse islets. With human islets, a much higher number of experiments might be required, due to the variability in the response to glucose that is normally observed between donors/batches.
21. These experiments can be performed in combination with pharmacological AMPK activators, such as 991 or C13. In that case, the compounds are added to the KRBH buffer for the duration of the experiment, including the preincubation.
22. More than ten islets per condition can be used. This is especially advisable if these are small (<100 μm).
23. It is critical to make sure that all the islets used for each condition have been collected, with the use of a microscope.

References

1. Organization WH (2016) Global report on diabetes. Geneva
2. Hawley SA, Ford RJ, Smith BK, Gowans GJ, Mancini SJ, Pitt RD, Day EA, Salt IP, Steinberg GR, Hardie DG (2016) The Na+/GLUCOSE cotransporter inhibitor canagliflozin activates AMPK by inhibiting mitochondrial function and increasing cellular AMP levels. Diabetes 65(9):2784–2794. https://doi.org/10.2337/db16-0058
3. Coughlan KA, Valentine RJ, Ruderman NB, Saha AK (2014) AMPK activation: a therapeutic target for type 2 diabetes? Diabetes Metab Syndr Obes 7:241–253. https://doi.org/10.2147/DMSO.S43731
4. Salt IP, Johnson G, Ashcroft SJ, Hardie DG (1998) AMP-activated protein kinase is activated by low glucose in cell lines derived from pancreatic beta cells, and may regulate insulin release. Biochem J 335(Pt 3):533–539
5. Sun G, Tarasov AI, McGinty J, McDonald A, da Silva Xavier G, Gorman T, Marley A, French PM, Parker H, Gribble F, Reimann F, Prendiville O, Carzaniga R, Viollet B, Leclerc I, Rutter GA (2010) Ablation of AMP-activated protein kinase alpha1 and alpha2 from mouse pancreatic beta cells and RIP2.Cre neurons suppresses insulin release in vivo. Diabetologia 53(5):924–936. https://doi.org/10.1007/s00125-010-1692-1
6. Fu A, Eberhard CE, Screaton RA (2013) Role of AMPK in pancreatic beta cell function. Mol Cell Endocrinol 366(2):127–134. https://doi.org/10.1016/j.mce.2012.06.020
7. Kone M, Pullen TJ, Sun G, Ibberson M, Martinez-Sanchez A, Sayers S, Nguyen-Tu MS, Kantor C, Swisa A, Dor Y, Gorman T,

Ferrer J, Thorens B, Reimann F, Gribble F, McGinty JA, Chen L, French PM, Birzele F, Hildebrandt T, Uphues I, Rutter GA (2014) LKB1 and AMPK differentially regulate pancreatic beta-cell identity. FASEB J 28 (11):4972–4985. https://doi.org/10.1096/fj.14-257667

8. Yavari A, Stocker CJ, Ghaffari S, Wargent ET, Steeples V, Czibik G, Pinter K, Bellahcene M, Woods A, Martinez de Morentin PB, Cansell C, Lam BY, Chuster A, Petkevicius K, Nguyen-Tu MS, Martinez-Sanchez A, Pullen TJ, Oliver PL, Stockenhuber A, Nguyen C, Lazdam M, O'Dowd JF, Harikumar P, Toth M, Beall C, Kyriakou T, Parnis J, Sarma D, Katritsis G, Wortmann DD, Harper AR, Brown LA, Willows R, Gandra S, Poncio V, de Oliveira Figueiredo MJ, Qi NR, Peirson SN, McCrimmon RJ, Gereben B, Tretter L, Fekete C, Redwood C, Yeo GS, Heisler LK, Rutter GA, Smith MA, Withers DJ, Carling D, Sternick EB, Arch JR, Cawthorne MA, Watkins H, Ashrafian H (2016) Chronic activation of gamma2 AMPK induces obesity and reduces beta cell function. Cell Metab 23(5):821–836. https://doi.org/10.1016/j.cmet.2016.04.003
9. Hong SP, Leiper FC, Woods A, Carling D, Carlson M (2003) Activation of yeast Snf1 and mammalian AMP-activated protein kinase by upstream kinases. Proc Natl Acad Sci U S A 100(15):8839–8843. https://doi.org/10.1073/pnas.1533136100
10. Hardie DG, Schaffer BE, Brunet A (2016) AMPK: an energy-sensing pathway with multiple inputs and outputs. Trends Cell Biol 26 (3):190–201. https://doi.org/10.1016/j.tcb.2015.10.013
11. Corton JM, Gillespie JG, Hawley SA, Hardie DG (1995) 5-aminoimidazole-4-carboxamide ribonucleoside. A specific method for activating AMP-activated protein kinase in intact cells? Eur J Biochem 229(2):558–565
12. da Silva Xavier G, Leclerc I, Varadi A, Tsuboi T, Moule SK, Rutter GA (2003) Role for AMP-activated protein kinase in glucose-stimulated insulin secretion and preproinsulin gene expression. Biochem J 371 (Pt 3):761–774. https://doi.org/10.1042/BJ20021812
13. Hasenour CM, Ridley DE, Hughey CC, James FD, Donahue EP, Shearer J, Viollet B, Foretz M, Wasserman DH (2014) 5-Aminoimidazole-4-carboxamide-1-β-D-ribofuranoside (AICAR) effect on glucose production, but not energy metabolism, is independent of hepatic AMPK in vivo. J Biol Chem 289 (9):5950–5959. https://doi.org/10.1074/jbc.M113.528232
14. Rao E, Zhang Y, Li Q, Hao J, Egilmez NK, Suttles J, Li B (2016) AMPK-dependent and independent effects of AICAR and compound C on T-cell responses. Oncotarget 7 (23):33783–33795. https://doi.org/10.18632/oncotarget.9277
15. Liu X, Chhipa RR, Pooya S, Wortman M, Yachyshin S, Chow LM, Kumar A, Zhou X, Sun Y, Quinn B, McPherson C, Warnick RE, Kendler A, Giri S, Poels J, Norga K, Viollet B, Grabowski GA, Dasgupta B (2014) Discrete mechanisms of mTOR and cell cycle regulation by AMPK agonists independent of AMPK. Proc Natl Acad Sci U S A 111(4): E435–E444. https://doi.org/10.1073/pnas.1311121111
16. Gómez-Galeno JE, Dang Q, Nguyen TH, Boyer SH, Grote MP, Sun Z, Chen M, Craigo WA, van Poelje PD, MacKenna DA, Cable EE, Rolzin PA, Finn PD, Chi B, Linemeyer DL, Hecker SJ, Erion MD (2010) A potent and selective AMPK activator that inhibits de novo lipogenesis. ACS Med Chem Lett 1 (9):478–482. https://doi.org/10.1021/ml100143q
17. Xiao B, Sanders MJ, Carmena D, Bright NJ, Haire LF, Underwood E, Patel BR, Heath RB, Walker PA, Hallen S, Giordanetto F, Martin SR, Carling D, Gamblin SJ (2013) Structural basis of AMPK regulation by small molecule activators. Nat Commun 4:3017. https://doi.org/10.1038/ncomms4017
18. Bain J, Plater L, Elliott M, Shpiro N, Hastie CJ, McLauchlan H, Klevernic I, Arthur JS, Alessi DR, Cohen P (2007) The selectivity of protein kinase inhibitors: a further update. Biochem J 408(3):297–315. https://doi.org/10.1042/BJ20070797
19. Martinez-Sanchez A, Nguyen-Tu MS, Rutter GA (2015) DICER inactivation identifies pancreatic beta-cell "disallowed" genes targeted by microRNAs. Mol Endocrinol 29 (7):1067–1079. https://doi.org/10.1210/me.2015-1059
20. Carter JD, Dula SB, Corbin KL, Wu R, Nunemaker CS (2009) A practical guide to rodent islet isolation and assessment. Biol Proced Online 11:3–31. https://doi.org/10.1007/s12575-009-9021-0
21. Ravier MA, Rutter GA (2010) Isolation and culture of mouse pancreatic islets for ex vivo imaging studies with trappable or recombinant fluorescent probes. Methods Mol Biol 633:171–184. https://doi.org/10.1007/978-1-59745-019-5_12

22. Hunter Roger W, Foretz M, Bultot L, Fullerton Morgan D, Deak M, Ross Fiona A, Hawley Simon A, Shpiro N, Viollet B, Barron D, Kemp Bruce E, Steinberg Gregory R, Hardie DG, Sakamoto K (2014) Mechanism of action of compound-13: an α1-selective small molecule activator of AMPK. Chem Biol 21 (7):866–879. https://doi.org/10.1016/j.chembiol.2014.05.014
23. Woods A, Azzout-Marniche D, Foretz M, Stein SC, Lemarchand P, Ferré P, Foufelle F, Carling D (2000) Characterization of the role of AMP-activated protein kinase in the regulation of glucose-activated gene expression using constitutively active and dominant negative forms of the kinase. Mol Cell Biol 20 (18):6704–6711
24. Leclerc I, Woltersdorf WW, da Silva Xavier G, Rowe RL, Cross SE, Korbutt GS, Rajotte RV, Smith R, Rutter GA (2004) Metformin, but not leptin, regulates AMP-activated protein kinase in pancreatic islets: impact on glucose-stimulated insulin secretion. Am J Physiol Endocrinol Metab 286(6):E1023–E1031. https://doi.org/10.1152/ajpendo.00532.2003
25. Davies SP, Carling D, Hardie DG (1989) Tissue distribution of the AMP-activated protein kinase, and lack of activation by cyclic-AMP-dependent protein kinase, studied using a specific and sensitive peptide assay. Eur J Biochem 186(1–2):123–128
26. da Silva Xavier G, Leclerc I, Salt IP, Doiron B, Hardie DG, Kahn A, Rutter GA (2000) Role of AMP-activated protein kinase in the regulation by glucose of islet beta cell gene expression. Proc Natl Acad Sci U S A 97(8):4023–4028
27. Scott JW, Norman DG, Hawley SA, Kontogiannis L, Hardie DG (2002) Protein kinase substrate recognition studied using the recombinant catalytic domain of AMP-activated protein kinase and a model substrate. J Mol Biol 317(2):309–323. https://doi.org/10.1006/jmbi.2001.5316
28. Hardie DG, Ross FA, Hawley SA (2012) AMP-activated protein kinase: a target for drugs both ancient and modern. Chem Biol 19(10):1222–1236. https://doi.org/10.1016/j.chembiol.2012.08.019
29. Mihaylova MM, Shaw RJ (2011) The AMPK signalling pathway coordinates cell growth, autophagy and metabolism. Nat Cell Biol 13 (9):1016–1023. https://doi.org/10.1038/ncb2329
30. Carling D, Zammit VA, Hardie DG (1987) A common bicyclic protein kinase cascade inactivates the regulatory enzymes of fatty acid and cholesterol biosynthesis. FEBS Lett 223 (2):217–222
31. Gwinn DM, Shackelford DB, Egan DF, Mihaylova MM, Mery A, Vasquez DS, Turk BE, Shaw RJ (2008) AMPK phosphorylation of raptor mediates a metabolic checkpoint. Mol Cell 30 (2):214–226. https://doi.org/10.1016/j.molcel.2008.03.003
32. Meares GP, Hughes KJ, Naatz A, Papa FR, Urano F, Hansen PA, Benveniste EN, Corbett JA (2011) IRE1-dependent activation of AMPK in response to nitric oxide. Mol Cell Biol 31(21):4286–4297. https://doi.org/10.1128/MCB.05668-11
33. Mahmood T, Yang PC (2012) Western blot: technique, theory, and trouble shooting. N Am J Med Sci 4(9):429–434. https://doi.org/10.4103/1947-2714.100998
34. Degorce F, Card A, Soh S, Trinquet E, Knapik GP, Xie B (2009) HTRF: a technology tailored for drug discovery - a review of theoretical aspects and recent applications. Curr Chem Genomics 3:22–32. https://doi.org/10.2174/1875397300903010022
35. Vasir B, Aiello LP, Yoon KH, Quickel RR, Bonner-Weir S, Weir GC (1998) Hypoxia induces vascular endothelial growth factor gene and protein expression in cultured rat islet cells. Diabetes 47(12):1894–1903
36. Kemp BE, Mitchelhill KI, Stapleton D, Michell BJ, Chen ZP, Witters LA (1999) Dealing with energy demand: the AMP-activated protein kinase. Trends Biochem Sci 24(1):22–25
37. Diraison F, Parton L, Ferré P, Foufelle F, Briscoe CP, Leclerc I, Rutter GA (2004) Overexpression of sterol-regulatory-element-binding protein-1c (SREBP1c) in rat pancreatic islets induces lipogenesis and decreases glucose-stimulated insulin release: modulation by 5-aminoimidazole-4-carboxamide ribonucleoside (AICAR). Biochem J 378 (Pt 3):769–778. https://doi.org/10.1042/BJ20031277
38. Chennell G, Willows RJ, Warren SC, Carling D, French PM, Dunsby C, Sardini A (2016) Imaging of metabolic status in 3D cultures with an improved AMPK FRET biosensor for FLIM. Sensors (Basel) 16(8). https://doi.org/10.3390/s16081312

Chapter 27

Analyzing AMPK Function in the Hypothalamus

Patricia Seoane-Collazo and Miguel López

Abstract

Hypothalamic AMPK plays a key role in the control of energy homeostasis by regulating energy intake and energy expenditure, particularly modulating brown adipose tissue (BAT) thermogenesis. The function of AMPK can be assayed by analyzing its phosphorylated protein levels in tissues, since AMPK is activated when it is phosphorylated at Thr-172. Here, we describe a method to obtain hypothalamic (nuclei-specific) protein extracts and the suitable conditions to assay AMPK phosphorylation by Western blotting.

Key words AMPK, Hypothalamus, Protein extraction, Immunoblot

1 Introduction

AMP-activated protein kinase (AMPK) acts as a cellular gauge that under certain conditions, such as low energy status, is activated, which leads to increased energy production and reduce energy expenditure [1–5].

AMPK is a highly conserved serine/threonine kinase, formed by a heterotrimer complex comprising a catalytic α (α1, α2) subunit, with a serine/threonine protein kinase domain, and two regulatory subunits, β (β1, β2) and γ (γ1, γ2, γ3), encoded by different genes [3, 5, 6]. AMPK is activated by phosphorylation on Thr-172 of the α subunit, a process that can be allosterically induced by AMP (but not ADP) [7] and catalyzed by several upstream kinases, such as liver kinase B1 (LKB1) [8–10], the pseudokinase, STRAD, the scaffold protein, mouse protein-25 (MO25) [11–13], and calmodulin-dependent kinase kinases (CaMKKs), especially CaMKK2 [14–16]. AMP and ADP enable phosphorylation at Thr-172 by LKB1 and CaMKK2 [7, 8, 17–19], but also inhibit dephosphorylation by protein phosphatases, such as protein phosphatase 2C alpha (PP2Cα) [20–22]. A more exhaustive description of AMPK structure and regulation is beyond the scope of the present chapter but has been excellently reviewed by others recently [3, 4, 23–28].

Dietbert Neumann and Benoit Viollet (eds.), *AMPK: Methods and Protocols*, Methods in Molecular Biology, vol. 1732, https://doi.org/10.1007/978-1-4939-7598-3_27,

In the hypothalamus, AMPK integrates peripheral hormonal signals to modulate both sides of the energy balance equation, namely, feeding and energy expenditure [5]. For example, in the case of ghrelin, an orexigenic stomach-derived hormone, activation of AMPK modulates mitochondrial fatty acid oxidation, ceramide synthesis in the endoplasmic reticulum, and intracellular levels of reactive oxygen species. This ultimately regulates the expression orexigenic neuropeptides in the arcuate nucleus of the hypothalamus (ARC), leading to increased appetite [5, 29–35]. On the other hand, inhibition of AMPK in the ventromedial nucleus of the hypothalamus (VMH) induces energy expenditure by boosting sympathetic tone, leading to increased expression of uncoupling protein 1 (UCP1) in brown adipose tissue (BAT) [5]. This mechanism mediates the effects of thyroid hormones (THs) [36–39], estradiol [40], leptin [41], glucagon-like peptide-1 (GLP-1) [42], bone morphogenetic protein 8B (BMP8B) [43, 44], and nicotine [45] on BAT thermogenesis, as well as the browning of white adipose tissue (WAT) induced by THs [38] and BMP8B [44]. The relevance of this interaction is noteworthy, because some agents with known actions on metabolic homeostasis, such as metformin [46, 47], liraglutide [42], and olanzapine [48–51], and also natural molecules, such as resveratrol [52, 53] and flavonoids [54–57], exert their actions by modulating hypothalamic AMPK. This evidence highlights the possibility that hypothalamic AMPK might be a potential target for the treatment of obesity [5, 58, 59].

In physiology, functional analyses are generally related to biochemical changes in proteins. One of the most commonly used techniques to analyze these changes is Western blotting, in which proteins are separated through electrophoresis, transferred to a solid support, and then analyzed using antibodies for specific protein detection. Thus, for assaying AMPK function (activation or inactivation) in the hypothalamus, it is possible to use phospho-specific antibodies that recognize the phosphorylation of AMPKα at Thr-172.

2 Materials

2.1 Administration of Substances

1. Polyethylene tube for intracerebroventricular cannulae (BD Intradermic®).
2. Non-sterile polyethylene tubing (Becton Dickinson and Company, PE-20 for rats and PE-50 for mice).
3. Anesthesia. Xylazine hydrochloride and ketamine.
4. Surgical blade stainless steel n°21.

5. Surgical drill. Tungsten carbide drill (KOMPH141010 for stereotaxic surgery and KOMPH141014 for intracerebroventricular (ICV) surgery, Komet Dental).
6. Cyanoacrylate adhesive.
7. Gavage needle for rat (Fine Science Tools, Item No. 18061-10.)
8. Hamilton syringe for ICV (Hamilton, model #7001N 22 gauge).
9. Hamilton syringe for rat stereotaxic administration (Hamilton, model #7001N 25 gauge).
10. Hamilton syringe for mouse stereotaxic administration (Hamilton, model #7001KH 32 gauge).
11. Osmotic minipumps (Alzet, models 2001, 1007D, 1004D).
12. Stereotaxic frame.
13. Silk suture (rat/mouse) 2-0/4-0.

2.2 Dissection and Protein Extraction

1. PBS (phosphate buffer saline): 138 mM NaCl, 2.7 mM KCl, 1.5 mM KH_2PO_4, 8 mM $Na_2HPO_4{\cdot}7H_2O$, pH 7.4.
2. Precision scissors.
3. Surgical blade stainless steel n°15.
4. Razor blades.
5. 1 mm coronal acrylic brain matrix for rat or mouse.
6. Lysis buffer with protease inhibitor ($BLYS^{pi}$): 50 mM Tris–HCl, pH 7.5, 10 mM EGTA, 10 mM EDTA, 1% (v/v) M Triton X-100, 1 mM sodium orthovanadate, 50 mM sodium fluoride, 10 mM sodium pyrophosphate, 0.25 M sucrose, protease inhibitor cocktail. Store at 4 °C. Weight 6.057 g Tris–HCl, 0.38 g EGTA, 0.37 g EDTA, 0.184 g sodium orthovanadate, 2.099 g sodium fluoride, 2.23 g sodium pyrophosphate, 85.5 g sucrose. Add 10 mL of Triton X-100. Make up to 1 L with distilled water. Mix and adjust pH 7.5 with HCl (*see* **Note 1**). Use one tablet of protease inhibitor in 50 mL of lysis buffer (*see* **Note 2**).
7. Stainless steel grinding beads and bead mill homogenizer.
8. 1 mg/mL bovine serum albumin (BSA) in distilled water.
9. Bradford solution (protein assay dye reagent concentrate). Dilute in distilled water 1:4. Prepare enough for 250 μL for each sample and standard in duplicate. Keep protected from light. Incubate 10 min at 37 °C before use.
10. 96-well plate: clear plates for colorimetric assay.
11. Microplater reader. Thermo Fisher multiskan go.

12. Loading buffer 5×: 250 mM Tris–HCl, pH 6.8, 10% (w/v) sodium dodecyl sulfate (SDS), 50% (v/v) glycerol, 0.0005% (w/v) bromophenol blue, and 5% (v/v) β-mercaptoethanol. Prepare 1 M Tris–HCl, pH 6.8, by dissolving 121.14 g of Tris–HCl in 1 L of distilled water, and adjust the pH with HCl. Mix 12.5 mL of Tris–HCl 1 M pH 6.8, 5 g SDS, 25 mL glycerol, 2.5 mL β-mercaptoethanol, 25×10^{-3} g bromophenol blue. Make up with mQ water to 50 mL. Store at −20 °C (*see* **Note 3**).

2.3 Sodium Dodecyl Sulfate-Polyacrylamide Gel Electrophoresis

1. Buffer A, pH 8.8: 750 mM Tris–HCl, pH 8.8, 0.2% (w/v) SDS. Weight 90.1 g Tris–HCl, 2 g SDS. Make up to 1 L with distilled water. Adjust the pH with HCl.
2. Buffer B, pH 6.8: 250 mM Tris–HCl, pH 6.8, 0.2% (w/v) SDS. Weight 30.2 g Tris–HCl, 2 g SDS. Make up to 1 L with distilled water. Adjust the pH with HCl.
3. APS: 10% (w/v) ammonium persulfate (APS). Dissolve 5 g APS in 50 mL distilled water. Prepare ready-to-use aliquots. Store at 4 °C.
4. 60% (v/v) 2-propanol: Mix 60 mL of 2-propanol in 40 mL of distilled water.
5. Mini-PROTEAN vertical electrophoresis system and 1.5 mm glass plates.
6. Running buffer 5×: 20 mM glycine, 200 mM Tris–HCl, 1% (w/v) SDS. Weigh 72 g glycine, 15 g Tris–HCl, and 5 g SDS. Make up to 1 L with distilled water. Prepare running buffer 1× by adding 100 mL of running buffer 5× in 400 mL of distilled water.
7. Protein ladder.

2.4 Semi-dry Transfer

1. Transfer buffer 1×: 40 mM glycine, 40 mM Tris–HCl, 0.36% (w/v) SDS, 20% (v/v) methanol. Dissolve in distilled water. Store at 4 °C.
2. Extra-thick blot paper (filter paper). Cut two pieces of filter paper per gel with the necessary size to cover the gel. Submerge them in transfer buffer 1× before use.
3. Polyvinylidene difluoride (PVDF) membrane. Cut one piece of PVDF per gel larger enough to match the gel size.
4. Plastic container (to activate the membranes).
5. Trans-Blot SD semi-dry transfer cell.
6. Tris-buffered saline (TBS) 10×: 200 mM Tris–HCl, pH 7.6, 1.3 mM NaCl. Weight 24.2 g Tris–HCl, 80 g NaCl. Dissolve in distilled water. Adjust pH. Make up to 1 L.

7. TBST: 1% (v/v) Tween-20 in TBS. Mix 100 mL TBS 10× and 1 mL Tween-20. Make up to 1 L with distilled water.
8. Blocking solution (BSA-TBST): 3% (v/v) BSA in TBST. Mix 3 g BSA in 100 mL of TBST. Store at 4 °C.

2.5 Antigens and Conjugates

1. Primary antibody. Use a primary antibody that recognizes the phosphorylation of AMPKα at Thr-172. Dilute the antibody in BSA-TBST. As controls, antibodies against non-phosphorylated AMPKα1 and AMPKα2 are used. β-actin is used as loading control.
2. Secondary antibody. Use an HRP conjugated secondary antibody. Dilute the antibody in BSA-TBST.
3. Peroxidase substrate for enhanced chemiluminescence (ECL).

3 Methods

3.1 Induction of Changes in Hypothalamic AMPK Phosphorylation

3.1.1 Feeding/Fasting Experiments

Hypothalamic AMPK can be regulated by energetic status. In the context of food deprivation (after 24-h fasting), increased ghrelin levels stimulate the phosphorylation of hypothalamic AMPKα and its downstream target ACCα, thus inducing feeding through the modulation of hypothalamic fatty acid metabolism [5, 29–35]. After an overnight fasting, refeeding reduces AMPK phosphorylation in all hypothalamic nuclei [60].

3.1.2 Administration of Hormones, Peptides, and Chemicals

Routes of Administration

1. *ICV cannulae*. This procedure is used in experiments that require administration of substances in the brain ventricles, such as the third ventricle (3V) and the lateral ventricle [30, 32, 36, 42–45, 61]. The cannula consists in a polyethylene tube of (rat/mice) 1.09/0.965 mm of external diameter and 0.38/0.58 mm of internal diameter. The length (rat/mouse) is 3.5/2.5 cm. In one of the extremes, cut a bevel of 0.5 mm, and from this point, at 4/2.5 mm, insert a stopper that limits how far the tube goes into the brain. Seal the other side until drug administration. The ICV cannula is stereotaxically inserted using the following coordinates: 1.5/1.2 mm lateral to sagittal suture and 0.9/0.6 mm posterior to the bregma. Under ketamine/xylazine anesthesia, open the scalp (transversal cut) with a surgical blade and identify the bregma. Using a surgical drill, pierce the skull and insert the cannula until the stop, and glue it to the skull with cyanoacrylate adhesive. Allow the animals to recover 3–4 days before the injection of substances (*see* **Note 4**).
2. *Stereotaxic microinjection*. This procedure is performed when it is necessary to inject substances in a specific nucleus of the hypothalamus. Place the animal in a stereotaxic frame under ketamine/xylazine anesthesia. Open the scalp (transversal cut)

with a surgical blade and identify the bregma. Target the specific nucleus bilaterally using a 25 gauge needle connected to a Hamilton 1 μL syringe using specific coordinates. In rat, for the VMH, perform two injections in each cerebral hemisphere (2.4–3.2 mm posterior to bregma, 0.6 mm lateral to midline, 10.1 mm deep); for the ARC, perform one injection in each hemisphere (2.8 mm posterior to bregma, 0.3 mm lateral to midline, 10.2 mm deep); and for the LHA, 2.9 mm posterior to bregma, 2 mm lateral to midline, and 8.1 mm deep. In mice, perform one injection in each cerebral hemisphere: for the VMH, 1.7 mm posterior to bregma, 0.5 mm lateral to midline, and 5.5 mm deep; for the ARC, 1.5 mm posterior to bregma, 0.2 mm lateral to midline, and 6 mm deep; and for the LHA, 1.3 mm posterior to bregma, 1.1 mm lateral to midline, and 5.2 mm deep. Using a surgical drill, pierce the skull in each point. The substances should be delivered at a rate of 200 nL/min during 5 min for rats and 10 min for mice. The entire injector system needs to be left in place for an additional 5 min after the injections are completed. Close the cut with silk suture.

3. *Stereotaxic implantation of nucleus-specific cannulae.* For chronic administration of substances in specific nuclei of the rat hypothalamus, insert bilaterally a 28 gauge stainless steel cannula with different length and gap between the injectors for each hemisphere, according to the coordinates for each specific nuclei: for VMH, 2.8 mm posterior to bregma, 0.6 mm lateral to midline, and 10.1 mm ventral; for ARC, 2.8 mm posterior to bregma, 0.3 mm lateral to midline, and 10.2 mm ventral; and for LHA, 2.9 mm posterior to bregma, 2 mm lateral to midline, and 8.1 mm ventral [44]. Using a surgical drill, pierce the skull in each point. Insert the cannula and glue it to the skull with cyanoacrylate adhesive. Connect a catheter tube from each infusion cannula to an osmotic minipump flow moderator, which should be inserted in a subcutaneous pocket on the dorsal surface created using blunt dissection. Close the cut with silk suture.
4. *Oral gavage administration.* Restrain the animal grasping skin over the shoulders to immobilize the head, and thus the forelegs are extended. Check the length of the gavage needle by measuring the tip of the nose to the last rib. Hold the animal in a vertical position and introduce the gavage needle following the roof of the mouth, moving the needle toward the esophagus. The animal will naturally gag and have a swallow reflex. After the needle pass to the correct length, the compound may be injected [62].

Activators of Hypothalamic AMPK

1. *Ghrelin*. ICV administration of ghrelin to fed satiated rats induced a time-dependent increase in AMPK and ACCα phosphorylation levels, peaking acutely at 1 and 2 h and returning to normal levels by 6 h posttreatment [30, 32, 63]. Rats received an ICV administration of 5 μg of ghrelin in 5 μL of saline or vehicle [30, 32, 63].
2. *5-Aminoimidazole-4-carboxamide-1-d-ribofuranoside (AICAR)*. In rats, ICV administration of the AMPK activator AICAR increases AMPK phosphorylation in the hypothalamus or restore a previously inhibited state. In mice, a single dose of AICAR induces hypothalamic AMPK activation within 6 h. For acute pharmacological AMPK activation with AICAR in rats, inject a single dose of 5 μg dissolved in DMSO, and changes in pAMPK levels can be induced with treatment after 30 min to 2–4 h [40, 62]. For acute ICV treatment in mice, inject 3 μg of AICAR dissolved in saline and sacrificed after 6 h [64].

Inhibitors of Hypothalamic AMPK

1. *Thyroid hormones*. Either hyperthyroidism (excess of circulating levels of thyroid hormones) or central administration of triiodothyronine (T3) decreases the activity of AMPK in the hypothalamus [36–39]. In this sense, stereotaxic administration of T3 into the VMH caused a rapid decreased of pAMPK in this nucleus [36, 39, 65]. The induction of hyperthyroidism is achieved by chronic subcutaneous (SC) administration of L-thyroxine (T4; 100 μg/day, dissolved in 200 μL of saline) or saline for a period of 3 weeks (21 days) [36, 38, 39]. For acute T3 ICV treatment (1 h), inject a single dose of 4 ng dissolved in 5 μL of DMSO [36]. For chronic ICV treatment, in rats and mice, administrate a single ICV daily injection of T3 (for rats 4 ng/day for 5 days, dissolved in 5 μL of saline; for mice 8 ng/day, during 5 days, dissolved in 1 μL of saline) at 8 p.m. just before turning the lights off [36]. In the case of targeting specific nuclei in the rat, acutely inject 8 ng of T3 in 1 μL of 1:50 saline/DMSO or vehicle as control during 3–12 h [36–39]. For chronic treatment delivered via a permanent stainless steel cannula connected to an osmotic minipump flow moderator, rats receive a 4 ng/day of T3 (in saline containing 1 mM NaOH) or vehicle as control.
2. *Estradiol*. 17β-Estradiol (E2), as the major endogenous estrogen, induces a decrease in the phosphorylation of hypothalamic AMPK in female rats when given either ICV or injected stereotaxically in the VMH [40, 66]; nevertheless, when injected directly into the ARC, no clear effect is detected. For the ICV treatment, female rats are administered with a dose of 10 mM 17β-estradiol in 5 μL of volume (dissolved in DMSO/saline 1:1), every 12 h, just before the start of the photoperiod, during 7 days [40, 66]. For the nucleus-specific injections,

the rats receive 1 μL of 1 nM 17β-estradiol in each bilateral injection (total 2 μL in the ARC/4 μL in the VMH). Rats are sacrificed after 3–12 h [40].

3. *Liraglutide*. The clinically used glucagon-like peptide 1 (GLP1) agonist liraglutide stimulates BAT thermogenesis and adipocyte browning independent from nutrient intake and by the inhibition of hypothalamic AMPK [42]. Liraglutide is given at a dose of 3 μg in mouse and 10 μg in rat either ICV or in the VMH [42]
4. *Olanzapine*. Animals treated sub-chronically by oral gavage with olanzapine present decreased hypothalamic AMPK phosphorylation. To deliver the drug (3 mg/kg) into the stomach, use a gavage needle attached to a syringe twice daily (total daily dose, 6 mg/kg) at 9 a.m. and 3 p.m. for 6 days and sacrifice on day 7 after an overnight fasting. Dissolve the drug in 0.1 M HCl and adjust to pH 5.5 using 0.1 M NaOH. Prepare a stock solution of 1.5 mg/mL and administer the appropriate volume to the rats via gavage (actual volume is modified for variation in body weight so that for each rat, each of the two daily doses is 3 mg/kg) [62].
5. *Compound C*. Also known as dorsomorphin, it is a nonspecific AMPK inhibitor (*see* Chapter 12) [67]. When treated ICV, compound C decreases AMPK phosphorylation in the hypothalamus. The dose for ICV treatment (2 h) in rats is 10 μg in 5 μL of DMSO [30].

3.1.3 Administration of Adenovirus

AMPK phosphorylation can be modulated by genetic inhibition or overexpression in specific nuclei. This can be achieved through stereotaxic microinjection of adenoviral expression vectors expressing dominant-negative (DN) or constitutively active (CA) isoforms of AMPKα [30, 36, 40, 42–45]. To induce the overexpression of AMPK, inject following specific coordinates 1 μL of a solution of adenoviral vectors that overexpress the isoform AMPKα1 constitutively active protein (AMPKα1-CA) with a concentration of 1×10^{12} pfu/mL diluted 1:50 in PBS. To induce inhibition of AMPK, inject following specific coordinates 1 μL of a mix of adenoviral particles overexpressing 1:1 of AMPKα1-DN and AMPKα2-DN with a concentration each of 1.2×10^{12} pfu/mL. For control group, inject 1 μL of adenoviral particles expressing green fluorescent protein (GFP) during 5–7 days (*see* **Note 5**). Infection efficiency is demonstrated by GFP expression by the adenoviral construct specifically in the targeted nucleus (use GFP immunohistochemistry or direct GFP immunofluorescence for detection) and by the corroboration of pACCα levels by Western blot (*see* **Note 6**).

3.2 Dissection of the Hypothalamus and Protein Extraction

Carry out all procedures in ice otherwise specified.

The whole hypothalamus can be dissected in fresh tissue with a precision scissors. For nucleus-specific dissection, the brain needs to be frozen.

1. Immediately after sacrifice, position the brain with the hypothalamus upward and the cerebral hemispheres downward in foil, over dry ice. Allow the tissue to completely freeze before closing the foil to stock at −80 °C.
2. Before dissection, let the brain half-thaw in ice and put it in the brain matrix with the hypothalamus upward. Rinse it with few drops of PBS and position a razor blade at the start of median eminence (ME; for the dissection of hypothalamic nuclei). Position the other razor blade at 2 mm of the first one. Cut the brain and position the slice in a plastic plate. With a surgical blade n°15, dissect the area of the specific nuclei with the help of a Brain Atlas [68] (*see* Fig. 1). Immediately introduce the tissue in a 2 mL plastic tube with a stainless steel grinding bead, add the appropriate $BLYS^{pi}$ quantity (*see* **Note 7**), and disrupt it in the bead mill homogenizer for 2 min at 30 Hz (1800 oscillations/min) (*see* **Note 8**). Keep the homogenate always in ice. Collect it to a new plastic tube and centrifuge for 30 min at 13,200 rpm (16100 × *g*) at 4 °C (*see* **Note 9**). Collect the supernatant and transfer to a clean plastic tube.
3. Determine protein concentration with the traditional Bradford assay reagent. Prepare BSA standard curve as follows: Prepare a 1 mg/mL BSA standard by diluting 1 mg BSA in 1 mL of distilled water. Using 1 mg/mL standard, prepare standard

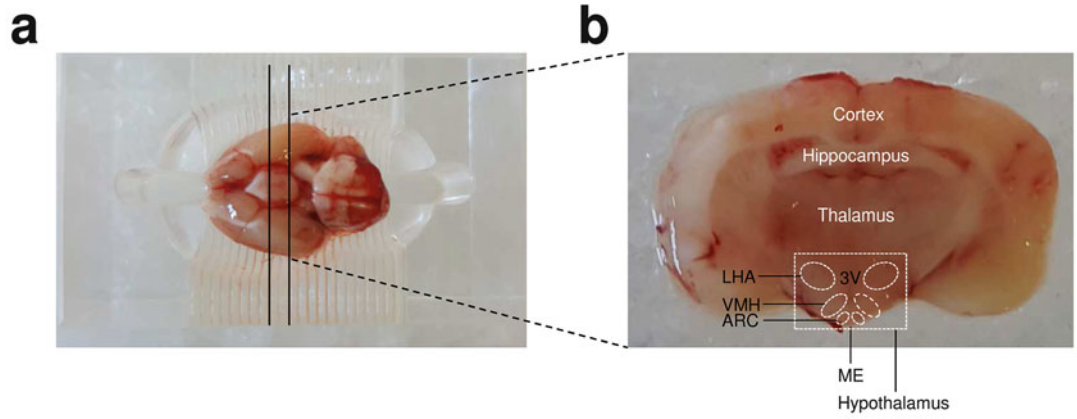

Fig. 1 Specific dissection of hypothalamic nuclei. (**a**) Position of rat brain in the acrylic brain matrix. Black lines are signaling the position of razor blades for delimitation of hypothalamic region containing ARC, VMH, and LHA. (**b**) Coronal section of rat brain showing the localization of the nuclei. *3V* third ventricle, *ARC* arcuate nucleus of the hypothalamus, *LHA* lateral hypothalamic area, *ME* median eminence, *VMH* ventromedial nucleus of the hypothalamus

curve dilution as described: 0.7 mg/mL = 350 μL of 1 mg/mL standard in 150 μL of distilled water; 0.5 mg/mL = 250 μL of 1 mg/mL standard in 250 μL of distilled water; 0.25 mg/mL = 250 μL of 0.5 mg/mL standard in 250 μL of distilled water, 0.125 mg/mL = 250 μL of 0.25 mg/mL standard in 250 μL of distilled water, 0.0625 mg/mL = 250 μL of 0.125 mg/mL standard in 250 μL of distilled water; 0.03125 mg/mL = 250 μL of 0.0625 mg/mL standard in 250 μL of distilled water. Make a dilution to quantify the protein. Take 10 μL of the supernatant and add 250 μL of distilled water. Vortex. Add 10 μL of the standard curve (in ascendant concentration) and the diluted sample in duplicates in a 96-well plate. Add 250 μL of Bradford solution into each standard and sample wells. Eliminate the bubbles. Incubate protected from light 5 min at 37 °C. Measure output (OD 590 nm) on a microplate reader.

3.3 6.5% Sodium Dodecyl Sulfate-Polyacrylamide Gel Electrophoresis

1. Mix 2.45 mL of H_2O, 5.06 mL of buffer A, and 2.18 mL acrylamide. Add 56.25 μL of APS 10% and 28.125 μL of TEMED. Vortex it and cast gel within a 7.2 cm × 10 cm × 1.5 mm gel cassette. Fill to 0.5–1 cm below bottom of the comb teeth and fill up with 60% 2-propanol. Allow polymerization and remove 60% 2-propanol. Rinse the gel with distilled water to wash residual 2-propanol and let it dry.
2. Prepare the stacking gel by mixing 1.77 mL of distilled water, 2.5 mL of buffer B, and 0.65 mL of acrylamide. Add 25 μL of APS 10% and 12.5 μL of TEMED. Vortex it. Insert a 15-well comb immediately without introducing air bubbles.
3. Prepare aliquots. Calculate the amount of protein of the samples extrapolating the ABS with the standard curve, and prepare aliquots for WB mixing sample, loading buffer 1× and $BLYS^{pi}$. For the hypothalamus, calculate volume of protein homogenate to reach 20 μg of protein (10 μg if analyzing a hypothalamic-specific nuclei), loading buffer 3.2 μL (loading buffer is prepared at 5× but is use at 1×; thus, the volume of loading buffer is calculated by dividing the final volume by 5), complete the volume up to 16 μL with $BLYS^{pi}$, and vortex (*see* **Note 10**).
4. Heat the aliquots at 95 °C for 5 min. Centrifuge the heated samples at 13,200 rpm for 9 s to bring down the condensate. Perform the electrophoresis in ice or in a cold chamber at 4 °C. Fill the mini-PROTEAN electrophoresis cell with 1 L of cold running buffer. Pull comb straight up to remove. Load 5 μL of protein ladder (pre-thaw; do no heat). Add 16 μL of protein aliquots in the following wells. Run the electrophoresis at a constant voltage of 140 V and 108 mA, and let the migration front reach the 0.5 cm to edge of the gel (*see* **Note 11**).

3.4 Semi-dry Transfer

1. Prepare the filter paper (extra-thick blot paper) and submerge it into transfer buffer 1×. Activate the PVDF membranes by submerging them first in methanol, secondly in distilled water, and thirdly in transfer buffer 1× (5 min in each).
2. Put the filter paper in the Trans-Blot semi-dry transfer and then the PVDF membranes, the gels, and on top of it another filter paper. Remove the air bubbles in each step (*see* **Note 12**).
3. Perform the transfer in constant amperage of 0.25 A and 25 V approximately during 1 h and 40 min.
4. Block the membranes with BSA 3%-TBST 1×, in agitation at RT (*see* **Note 13**).

3.5 Immuno-detection

1. Remove the blocking and incubate the membranes during 3 h (or overnight) in agitation in the cold chamber (4 °C) with primary antibody (*see* **Note 14**).
2. Remove the primary antibody.
3. Perform three washes in agitation in TBST (5 min each).
4. Incubate the membranes during 1 h with secondary antibody in agitation at RT.
5. Remove the secondary antibody.
6. Perform three washes in agitation in TBST (5 min each).
7. Prepare the ECL with a dilution of 1:1. Incubate the membrane with ECL during 4 min protected from light. Remove the excess ECL and put the membrane in a cassette between acetate papers. Remove the air bubbles.
8. Develop in a dark chamber.

3.6 Analysis

1. Scan the autoradiographic images with a resolution of 800 dpi, and save in TIFF format (*see* Fig. 2).
2. Quantify digital images with *ImageJ Software* (National Institutes of Health, USA), which detects the number of pixels in all the samples of the same autoradiographic plate. Draw a rectangle, with the same dimensions in each case, enclosing the signal, and over the adjacent background. Determine the optical density of the signal and subsequently correct it by the optical density of its background value. Express the data in relation to a housekeeping protein (normally, β-actin for hypothalamic samples) or the non-phosphorylated AMPKα (*see* **Note 15**).

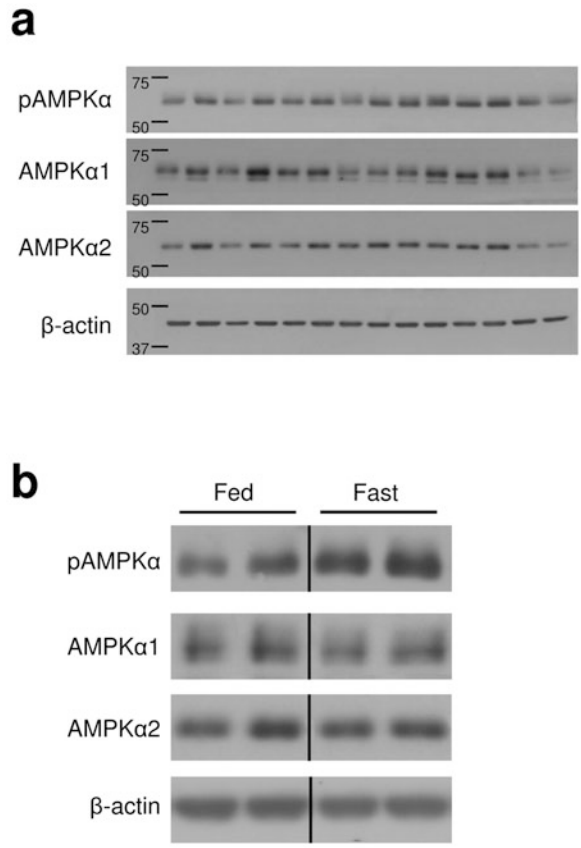

Fig. 2 Western blot autoradiographic images. (**a**) Autoradiographic images of pAMPKα, AMPKα1, AMPKα2, and β-actin from hypothalamic samples of rats separated by 6.5% SDS-PAGE electrophoresis. (**b**) Representative autoradiographic images of pAMPKα, AMPKα1, AMPKα2, and β-actin from hypothalamic samples of fed and fasted rats separated by 6.5% SDS-PAGE electrophoresis. Vertical lines show spliced bands coming in all the cases from the same gels [61]

4 Notes

1. After adjusting the pH, the solution turns to pale green color.
2. If stored at 4 ° C, use the reagent within 15 days. You can make aliquots and store them at −20 ° C for longer preservation.
3. Store in ready to use aliquots. Preheat (95 ° C) before use to solubilize the reagent.
4. It is important to habituate the animals to handling before ICV injections; thus, for acute procedures, the stress induced during the injection is minimized.
5. Due to the biological features of adenoviruses, the infection and overexpression are immediate, but the effect is transitory,

lasting approximately 7 days. It is mandatory to daily check the food intake and body weight.

6. The specificity of dissection can be tested by detection of contamination from adjacent nuclei by measurement of specific markers of each nucleus, such as steroidogenic factor-1 (SF1) as a marker of the VMH, proopiomelanocortin (POMC) for the ARC, or orexin for the LHA. Analysis should be carried by RT-PCR [40]
7. For the whole hypothalamus (rat/mouse), use 400/200 μL $BLYS^{pi}$, while for a nucleus-specific dissection, use 200/100 μL $BLYS^{pi}$.
8. Increase time if necessary. It is very important to complete the disaggregation of the tissue in order to achieve a high protein concentration. With low volumes of $BLYS^{pi}$, some foam may form. Centrifuge the tubes for 10 s at maximum speed in a benchtop centrifuge. You should be able to see the clear homogenate with no bubbles. We recommend using safe-lock tubes.
9. It is recommended putting all tubes in the same orientation into the centrifuge. This way it is possible to know the position of the pellet in the tube even if it is not possible to see it.
10. If the protein concentration is too low, it is possible to increase the final volume of the loading, i.e., without altering the amount of protein loaded to the gel.
11. During the electrophoresis, the migration front can fade. This may be due to a change in the pH of buffers or to abrupt temperature changes.
12. Do not let the filter paper or the membranes become dry. Wet with more transfer buffer 1× when necessary.
13. Avoid using milk-based blocking since it may contain phosphatases.
14. To detect changes in the phosphorylation of AMPKα at Thr-172, we use a Cell Signaling Technology antibody (rabbit monoclonal anti-phospho-AMPKα (Thr-172), Cat#2535S) diluted 1:2000 for total hypothalamic (20 μg of protein per sample) detection or 1:1000 (10 μg of protein per sample) for nucleus-specific detection. pAMPK is normalized with β-actin protein levels, although AMPKα1 and AMPKα2 (or total-AMPK) levels should always be displayed. To detect the levels of AMPKα1 and AMPKα2, we use Merck Millipore antibodies (rabbit polyclonal anti-AMPKα1 and anti-AMPKα2, Refs 07-350 and 07-363, respectively) diluted 1:1000. To detect the total levels of AMPKα, we use a Cell Signaling Technology antibody (rabbit polyclonal anti-AMPKα, Cat#2532) diluted 1:1000.

15. Two ways to represent protein data are used in literature, namely, correction by non-phosphorylated protein levels and by a proper loading control (i.e., β-actin). The latter might be problematical if total protein levels are not displayed. Nevertheless, it is important to keep in mind that independent of the origin in the phosphorylation status (increased/decreased upstream kinase/phosphatase activity or increased/decreased non-phosphorylated levels), the activity of the enzyme (increased/decreased) is what matters.

References

1. Kahn BB, Alquier T, Carling D, Hardie DG (2005) AMP-activated protein kinase: ancient energy gauge provides clues to modern understanding of metabolism. Cell Metab 1:15–25
2. Lage R, Diéguez C, Vidal-Puig A, López M (2008) AMPK: a metabolic gauge regulating whole-body energy homeostasis. Trends Mol Med 14:539–549
3. Carling D, Mayer FV, Sanders MJ, Gamblin SJ (2011) AMP-activated protein kinase: nature's energy sensor. Nat Chem Biol 7:512–518
4. Hardie DG, Schaffer BE, Brunet A (2016) AMPK: an energy-sensing pathway with multiple inputs and outputs. Trends Cell Biol 26:190–201
5. López M, Nogueiras R, Tena-Sempere M, Dieguez C (2016) Hypothalamic AMPK: a canonical regulator of whole-body energy balance. Nat Rev Endocrinol 12:421–432
6. Hardie DG, Ross FA, Hawley SA (2012) AMPK: a nutrient and energy sensor that maintains energy homeostasis. Nat Rev Mol Cell Biol 13:251–262
7. Gowans GJ, Hawley SA, Ross FA, Hardie DG (2013) AMP is a true physiological regulator of AMP-activated protein kinase by both allosteric activation and enhancing net phosphorylation. Cell Metab 18:556–566
8. Woods A, Johnstone SR, Dickerson K et al (2003) LKB1 is the upstream kinase in the AMP-activated protein kinase cascade. Curr Biol 13:2004–2008
9. Hardie DG (2013) The LKB1-AMPK pathway-friend or foe in cancer? Cancer Cell 23:131–132
10. Hardie DG, Alessi DR (2013) LKB1 and AMPK and the cancer-metabolism link - ten years after. BMC Biol 11:36
11. Hawley SA, Boudeau J, Reid JL et al (2003) Complexes between the LKB1 tumor suppressor, STRAD alpha/beta and MO25 alpha/beta are upstream kinases in the AMP-activated protein kinase cascade. J Biol 2:28
12. Shaw RJ, Kosmatka M, Bardeesy N et al (2004) The tumor suppressor LKB1 kinase directly activates AMP-activated kinase and regulates apoptosis in response to energy stress. Proc Natl Acad Sci U S A 101:3329–3335
13. Alessi DR, Sakamoto K, Bayascas JR (2006) LKB1-dependent signaling pathways. Annu Rev Biochem 75:137–163
14. Hawley SA, Pan DA, Mustard KJ et al (2005) Calmodulin-dependent protein kinase kinase-beta is an alternative upstream kinase for AMP-activated protein kinase. Cell Metab 2:9–19
15. Hurley RL, Anderson KA, Franzone JM, Kemp BE, Means AR, Witters LA (2005) The Ca2+/calmodulin-dependent protein kinase kinases are AMP-activated protein kinase kinases. J Biol Chem 280:29060–29066
16. Woods A, Dickerson K, Heath R et al (2005) Ca(2+)/calmodulin-dependent protein kinase kinase-beta acts upstream of AMP-activated protein kinase in mammalian cells. Cell Metab 2:21–33
17. Woods A, Vertommen D, Neumann D et al (2003) Identification of phosphorylation sites in AMP-activated protein kinase (AMPK) for upstream AMPK kinases and study of their roles by site-directed mutagenesis. J Biol Chem 278:28434–28442
18. Oakhill JS, Steel R, Chen ZP et al (2011) AMPK is a direct adenylate charge-regulated protein kinase. Science 332:1433–1435
19. Gowans GJ, Hardie DG (2014) AMPK: a cellular energy sensor primarily regulated by AMP. Biochem Soc Trans 42:71–75
20. Davies SP, Helps NR, Cohen PT, Hardie DG (1995) 5′-AMP inhibits dephosphorylation, as well as promoting phosphorylation, of the AMP-activated protein kinase. Studies using bacterially expressed human protein phosphatase-2C alpha and native bovine protein phosphatase-2AC. FEBS Lett 377:421–425

21. Steinberg GR, Michell BJ, van Denderen BJ et al (2006) Tumor necrosis factor alpha-induced skeletal muscle insulin resistance involves suppression of AMP-kinase signaling. Cell Metab 4:465–474
22. Xiao B, Sanders MJ, Underwood E et al (2011) Structure of mammalian AMPK and its regulation by ADP. Nature 472:230–233
23. Carling D, Thornton C, Woods A, Sanders MJ (2012) AMP-activated protein kinase: new regulation, new roles? Biochem J 445:11–27
24. Hardie DG (2014) AMPK–sensing energy while talking to other signaling pathways. Cell Metab 20:939–952
25. Hardie DG (2014) AMP-activated protein kinase: maintaining energy homeostasis at the cellular and whole-body levels. Annu Rev Nutr 34:31–55
26. Hardie DG, Ashford ML (2014) AMPK: regulating energy balance at the cellular and whole body levels. Physiology (Bethesda) 29:99–107
27. Hardie DG (2014) A new protein kinase cascade. Nat Rev Mol Cell Biol 15:223
28. Ross FA, Jensen TE, Hardie DG (2016) Differential regulation by AMP and ADP of AMPK complexes containing different gamma subunit isoforms. Biochem J 473:189–199
29. Minokoshi Y, Alquier T, Furukawa N et al (2004) AMP-kinase regulates food intake by responding to hormonal and nutrient signals in the hypothalamus. Nature 428:569–574
30. López M, Lage R, Saha AK et al (2008) Hypothalamic fatty acid metabolism mediates the orexigenic action of ghrelin. Cell Metab 7:389–399
31. Andrews ZB, Liu ZW, Walllingford N et al (2008) UCP2 mediates ghrelin's action on NPY/AgRP neurons by lowering free radicals. Nature 454:846–851
32. Lage R, Vázquez MJ, Varela L et al (2010) Ghrelin effects on neuropeptides in the rat hypothalamus depend on fatty acid metabolism actions on BSX but not on gender. FASEB J 24:2670–2679
33. Al MO, López M, Tschop M, Dieguez C, Nogueiras R (2017) Current understanding of the hypothalamic ghrelin pathways inducing appetite and adiposity. Trends Neurosci 40:167–180
34. Cui H, López M, Rahmouni K (2017) The cellular and molecular bases of leptin and ghrelin resistance in obesity. Nat Rev Endocrinol 13:338–351
35. Ramírez S, Martíns L, Jacas J et al (2013) Hypothalamic ceramide levels regulated by CPT1C mediate the orexigenic effect of ghrelin. Diabetes 62:2329–2337
36. López M, Varela L, Vázquez MJ et al (2010) Hypothalamic AMPK and fatty acid metabolism mediate thyroid regulation of energy balance. Nat Med 16:1001–1008
37. Alvarez-Crespo M, Csikasz RI, Martinez-Sanchez N et al (2016) Essential role of UCP1 modulating the central effects of thyroid hormones on energy balance. Mol Metab 5:271–282
38. Martinez-Sanchez N, Moreno-Navarrete JM, Contreras C et al (2017) Thyroid hormones induce browning of white fat. J Endocrinol 232:351–362
39. Martínez-Sánchez N, Seoane-Collazo P, Contreras C et al (2017) Hypothalamic AMPK-ER stress-JNK1 axis mediates the central actions of thyroid hormones on energy balance. Cell Metab 26:212–219
40. Martínez de Morentin PB, Gónzalez-García I, Martins L et al (2014) Estradiol regulates brown adipose tissue thermogenesis via hypothalamic AMPK. Cell Metab 20:41–53
41. Tanida M, Yamamoto N, Shibamoto T, Rahmouni K (2013) Involvement of hypothalamic AMP-activated protein kinase in leptin-induced sympathetic nerve activation. PLoS One 8:e56660
42. Beiroa D, Imbernon M, Gallego R et al (2014) GLP-1 agonism stimulates brown adipose tissue thermogenesis and browning through hypothalamic AMPK. Diabetes 63:3346–3358
43. Whittle AJ, Carobbio S, Martíns L et al (2012) Bmp8b increases brown adipose tissue thermogenesis through both central and peripheral actions. Cell 149:871–885
44. Martins L, Seoane-Collazo P, Contreras C et al (2016) A functional link between AMPK and orexin mediates the effect of BMP8B on energy balance. Cell Rep 16:2231–2242
45. Martínez de Morentin PB, Whittle AJ, Ferno J et al (2012) Nicotine induces negative energy balance through hypothalamic AMP-activated protein kinase. Diabetes 61:807–817
46. Foretz M, Guigas B, Bertrand L, Pollak M, Viollet B (2014) Metformin: from mechanisms of action to therapies. Cell Metab 20:953–966
47. Foretz M, Viollet B (2015) Therapy: metformin takes a new route to clinical efficacy. Nat Rev Endocrinol 11:390–392
48. Ikegami M, Ikeda H, Ishikawa Y et al (2013) Olanzapine induces glucose intolerance through the activation of AMPK in the mouse hypothalamus. Eur J Pharmacol 718:376–382
49. Ikegami M, Ikeda H, Ohashi T et al (2013) Olanzapine increases hepatic glucose production through the activation of hypothalamic adenosine 5′-monophosphate-activated

protein kinase. Diabetes Obes Metab 15:1128–1135

50. Skrede S, Martins L, Berge RK, Steen VM, Lopez M, Ferno J (2014) Olanzapine depot formulation in rat: a step forward in modelling antipsychotic-induced metabolic adverse effects. Int J Neuropsychopharmacol 17:91–104
51. He M, Zhang Q, Deng C, Wang H, Lian J, Huang XF (2014) Hypothalamic histamine H1 receptor-AMPK signaling time-dependently mediates olanzapine-induced hyperphagia and weight gain in female rats. Psychoneuroendocrinology 42:153–164
52. Breen DM, Sanli T, Giacca A, Tsiani E (2008) Stimulation of muscle cell glucose uptake by resveratrol through sirtuins and AMPK. Biochem Biophys Res Commun 374:117–122
53. Vingtdeux V, Giliberto L, Zhao H et al (2010) AMP-activated protein kinase signaling activation by resveratrol modulates amyloid-beta peptide metabolism. J Biol Chem 285:9100–9113
54. Ahn J, Lee H, Kim S, Park J, Ha T (2008) The anti-obesity effect of quercetin is mediated by the AMPK and MAPK signaling pathways. Biochem Biophys Res Commun 373:545–549
55. Lu J, Wu DM, Zheng YL et al (2010) Quercetin activates AMP-activated protein kinase by reducing PP2C expression protecting old mouse brain against high cholesterol-induced neurotoxicity. J Pathol 222:199–212
56. Martínez de Morentin PB, González CR, López M (2010) AMP-activated protein kinase: 'a cup of tea' against cholesterol-induced neurotoxicity. J Pathol 222:329–334
57. Eid HM, Nachar A, Thong F, Sweeney G, Haddad PS (2015) The molecular basis of the antidiabetic action of quercetin in cultured skeletal muscle cells and hepatocytes. Pharmacogn Mag 11:74–81
58. López M, Tena-Sempere M (2017) Estradiol effects on hypothalamic AMPK and BAT thermogenesis: a gateway for obesity treatment? Pharmacol Ther 178:109. https://doi.org/10.1016/j.pharmthera.2017.03.014
59. López M (2017) EJE PRIZE 2017: hypothalamic AMPK: a golden target against obesity? Eur J Endocrinol 176:R235–R246
60. Minokoshi Y, Kim YB, Peroni OD et al (2002) Leptin stimulates fatty-acid oxidation by activating AMP-activated protein kinase. Nature 415:339–343
61. Vázquez MJ, González CR, Varela L et al (2008) Central resistin regulates hypothalamic and peripheral lipid metabolism in a nutritional-dependent fashion. Endocrinology 149:4534–4543
62. Ferno J, Varela L, Skrede S et al (2011) Olanzapine-induced hyperphagia and weight gain associate with orexigenic hypothalamic neuropeptide signaling without concomitant AMPK phosphorylation. PLoS One 6:e20571
63. Sangiao-Alvarellos S, Varela L, Vázquez MJ et al (2010) Influence of ghrelin and GH deficiency on AMPK and hypothalamic lipid metabolism. J Neuroendocrinol 22:543–556
64. Velasquez DA, Martinez G, Romero A et al (2011) The central Sirtuin 1/p53 pathway is essential for the orexigenic action of ghrelin. Diabetes 60:1177–1185
65. Varela L, Martínez-Sánchez N, Gallego R et al (2012) Hypothalamic mTOR pathway mediates thyroid hormone-induced hyperphagia in hyperthyroidism. J Pathol 227:209–222
66. Martinez de Morentin PB, Lage R, Gonzalez-Garcia I et al (2015) Pregnancy induces resistance to the anorectic effect of hypothalamic malonyl-CoA and the thermogenic effect of hypothalamic AMPK inhibition in female rats. Endocrinology 156:947–960
67. Bain J, Plater L, Elliott M et al (2007) The selectivity of protein kinase inhibitors: a further update. Biochem J 408:297–315
68. Paxinos G, Watson C (eds) (1986) The rat brain in stereotaxic coordinates. Academic Press, Sydney

Chapter 28

Using Ex Vivo Kidney Slices to Study AMPK Effects on Kidney Proteins

Renee Rao, Kazuhiro Omi, Roshan Rajani, Hui Li, and Nuria M. Pastor-Soler

Abstract

The ex vivo kidney slice technique has been used extensively in the fields of kidney physiology and cell biology. Our group and others have used this method to study epithelial traffic of transport proteins in situ in kidney tissue. In this methodology chapter, we summarize our adaptation of this classic protocol for the study of the effect of AMPK in the modulation of transport protein regulation, especially in kidney epithelial cells. Briefly, slices were obtained by sectioning freshly harvested rodent (rat or mouse) kidneys using a Stadie-Riggs tissue slicer. The harvested kidney and the kidney slices are kept in a physiological buffer equilibrated with 5% CO_2 at body temperature (37 °C) in the presence of different AMPK activating agents vs. vehicle control followed by rapid freezing or fixation of the slices to prevent non-specific AMPK activation. Thus, homogenates of these frozen slices can be used to study AMPK activation status in the tissue as well as the downstream effects of AMPK on kidney proteins via biochemical techniques, such as immunoblotting and immunoprecipitation. Alternatively, the fixed slices can be used to evaluate AMPK-mediated subcellular traffic changes of epithelial transport proteins via immunolabeling followed by confocal microscopy. The resulting micrographs can then be used for systematic quantification of AMPK-induced changes in subcellular localization of transport proteins.

Key words Hanks buffer, Ringer buffer, Kidney lysate, Homogenization

1 Introduction

The kidney is one of the most metabolically active tissues in the body. For example, via gluconeogenesis, the kidney generates more glucose per gram of tissue than any other organ [1]. The kidney is less than 1% of the total body mass, yet it receives 20% of the cardiac output and utilizes approximately 7% of the oxygen consumed by the body. Proper kidney function requires that a large portion of the energy available for cellular function be used toward epithelial membrane transport [2]. Therefore, the subject of the regulation of membrane transport processes in the kidney has had a special focus

Dietbert Neumann and Benoit Viollet (eds.), *AMPK: Methods and Protocols*, Methods in Molecular Biology, vol. 1732, https://doi.org/10.1007/978-1-4939-7598-3_28,

trying to uncover links between metabolism and transport, especially in kidney epithelial cells.

One of the important results in this search is that of the discovery that the metabolic sensing kinase AMP-activated protein kinase (AMPK) is a key regulator of membrane transport in kidney epithelial cells [3, 4]. The cellular heterogeneity of the nephron and the structural intricacy of kidney tissue have traditionally presented many technical difficulties to uncovering kidney regulatory mechanisms. Researchers have used segment-specific immortalized cell culture models for studies of membrane transport regulation. However, these cell culture models only reliably replicate proximal tubule and collecting duct principal cell epithelia [5]. There are other cell culture models that replicate intercalated cells and inner medullary collecting duct epithelial cells [6–10]. On the other hand, reliable models of the distal convoluted tubule, thick ascending limb, and thin limb are either not available or still being established. Therefore, research that involves evaluation of tubular function by micropuncture and isolated perfused tubules are still being used to confirm cell culture findings.

In our laboratory, we have been using the kidney slice system to evaluate the links between transport and metabolism, especially in kidney intercalated cells. Using this method with rat kidney tissue, we have studied how AMPK regulates the vacuolar H^+-ATPase (V-ATPase) in proximal tubule, the potassium channel KCNQ1 in collecting duct, the creatine transporter in proximal tubule, and aquaporin-2 in collecting duct principal cells [11–13]. This method is useful in evaluating acute changes in transporter subcellular localization by immunolabeling, as well as in determining protein abundance and measuring the levels of posttranslational modifications (e.g., levels of phosphorylated protein) by performing immunoblots of treated slice lysates. We are currently trying to establish the use of kidney slices in using mouse tissue, and although preliminary results show that the tissue is equally responsive to rat tissue, the size of the mouse kidney significantly limits the number of conditions that can be used to treat kidney slices in one experiment. On the other hand, the availability of more mouse models that are genetically engineered to knock out or to overexpress certain proteins offers advantages to study regulatory cascades in situ in kidney tissue without having to use pharmacologic inhibitors or activators that may have non-specific effects.

AMPK is a Ser/Thr kinase ubiquitously expressed in the body and throughout the kidney, which senses cellular metabolic stress. Under hypoxic or energy stress conditions, this kinase is exquisitely sensitive to cellular increases in the [AMP]/[ATP] ratio leading to AMPK activation [3, 14]. When AMPK is activated, threonine-172 in the alpha subunit (catalytic subunit) becomes phosphorylated (phospho-Thr172) [15]. This phosphorylation event can occur via upstream kinases or autophosphorylation. As AMPK becomes

quickly activated if samples are not properly handled, many researchers harvest the kidney following specific protocols to prevent non-specific AMPK activation. For example, the recommended harvesting protocol for the kidney to prevent non-specific AMPK activation involves freezing the kidney in situ while the animal is under anesthesia [16].

The purpose of this chapter/protocol is to document the kidney slice technique and the tissue preparation for immunolabeling and biochemistry preparations. However, we do not describe the specifics of the latter techniques beyond the tissue lysis and fixation steps.

2 Materials

1. 300 g male Sprague-Dawley rats matched in age (*see* **Note 1** for rat selection). All protocols should be approved by the appropriate institutional regulatory committee at the appropriate institution.
2. 25 g mice (*see* **Note 2** for mouse selection).
3. Millipore purified water or equivalent to prepare all buffers.
4. Anesthetic agent: pentobarbital sodium i.p. (*see* **Note 3**).
5. Alternative anesthetic agent: isoflurane to be used with vaporizer machine (*see* **Note 4**).
6. Solution stock A: 2.4 M NaCl. Weigh 70.13 g sodium chloride, then transfer to 1 L graduated cylinder, and add pure water to final volume of 500 mL. Mix until dissolved at RT and store at 4 °C until needed.
7. Solution stock B: 0.5 M $NaHCO_3$. Weigh 21.003 g of $NaHCO_3$, then transfer to 1 L graduated cylinder, and add pure water to final volume of 500 mL. Mix until dissolved at RT and store at 4 °C until needed.
8. Solution stock C: 66.6 mM KH_2PO_4, 16 mM K_2HPO_4. Weigh 4.532 g potassium phosphate monobasic (KH_2PO_4) and 1.393 g potassium phosphate dibasic (K_2HPO_4), then transfer both to 1 L graduated cylinder or glass beaker, and add pure water to final volume of 500 mL. Mix at RT until dissolved and store at 4 °C until needed.
9. Solution stock D: 24 mM $CaCl_2$, 24 mM $MgCl_2$. Weigh 1.332 g calcium chloride anhydrous ($CaCl_2$) and 2.440 g magnesium chloride hexahydrate ($MgCl_2$), then transfer to 1 L graduated cylinder or glass beaker, and add water to final volume of 500 mL. Mix at RT until dissolved and store at 4 °C until needed.
10. D-Glucose.

11. Ringer solution: 120 mM NaCl, 25 mM $NaHCO_3$, 3.3 mM KH_2PO_4, 0.8 mM K_2HPO_4, 1.2 mM $MgCl_2$, 1.2 mM $CaCl_2$, 10 mM D-glucose, pH 7.4, equilibrated with 5% CO_2 (*see* **Note 5**).
12. Alternatively, normal Hank's Balanced Salt Solution can be used: 110 mM NaCl, 5 mM KCl, 1.2 mM $MgSO_4$, 1.8 mM $CaCl_2$, 4 mM NaAcetate, 3 mM $Na_3Citrate$, 6 mM D-glucose, 6 mM L-alanine, 1 mM NaH_2PO_4, 3 mM Na_2HPO_4, 25 mM $NaHCO_3$, pH 7.4 equilibrated with 5% CO_2 (*see* **Note 6**).
13. Mouse vs. rat surgery tools such as hemostats, forceps, scissors.
14. 8G needle (21G for smaller animals such as mice).
15. Paper laboratory tissues/wipes (dry) and/or cotton applicators.
16. Clean disposable razor blades or scalpels.
17. Clean disposable plastic petri dishes.
18. Stir bars and stir plate.
19. Transfer pipets.
20. Sterile water in squeeze bottle and two waste buckets.
21. P1000 pipettor and tips.
22. Perfusion setup with a pump, preferably peristaltic (alternatively via gravity; *see* **Note 7**).
23. CO_2 impermeant tubing (*see* **Note 8**).
24. Manifolds.
25. Vacuum setup (with safety trap to capture liquids from the perfusion procedure).
26. Laboratory tape or labeling adhesive tape.
27. Several timers with multiple channels.
28. Flowchart summarizing experimental conditions, additives, times for addition of reagents, etc.
29. Water-resistant markers.
30. Parafilm or plastic wrap.
31. Stadie-Riggs tissue slicer.
32. Stadie-Riggs tissue slicer blade handle.
33. Stadie-Riggs tissue slicer disposable blades (for slices of approximately 0.5 mm in thickness). Use a new clean disposable blade for each separate experiment (Thomas Scientific).
34. Hemostat for handling of the blade as it is placed and removed from the handle.
35. Blunt forceps for handling the slices from the tissue slicer.
36. Plastic disposable transfer pipettes to dispense Ringer buffer intermittently during slicing.

37. For mice preparations, use lighter pressure or the kidney tissue, and/or a thinner cover (based on the original cover depicted in Fig. 2d) can be built to modify the Stadie-Riggs tissue slicer.
38. AMPK activator: 5-Amino-1-β-$_D$-ribofuranosyl-imidazole-4-carboxamide (AICAR). Use at a final concentration of 1–2 mM.
39. AMPK activator: 200 μM A769662 (*see* **Note 9**).
40. Glass scintillation vials for incubation of the slices. Label one vial per incubation condition. The vial must have a perforated cap through which to feed a "capillary" tubing through the cap.
41. At least two beakers with CO_2-equilibrated Ringer buffer to hold slices until they are placed in the treatment vials.
42. Set up a system of manifolds for gas delivery to the Ringer buffer solution (stock and for each of the slice incubation conditions). Use CO_2 impermeant tubing.
43. Water bath with holders for the scintillation vials. Set the bath at 37 °C.
44. Gas tank with appropriate regulator (5% CO_2/balance air).
45. 1× phosphate-buffered saline (PBS) without calcium and magnesium: 138 mM NaCl, 2.7 mM KCl, 1.5 mM KH_2PO_4, 8 mM $Na_2HPO_4{\cdot}7H_2O$, pH 7.4. Check pH prior to use. Prepare on the day of the experiment and keep at RT.
46. Fixative for slices: 4% (w/v) paraformaldehyde in 1× PBS without calcium and magnesium (*see* **Note 10**).
47. Liquid nitrogen container with liquid nitrogen ready at the start of the experiment.
48. Prepare at least one microcentrifuge tube per slice incubation condition for rapid freezing (with one venting hole in the cover). Storage of frozen slices at −80 °C.
49. Quenching buffer: 0.2 M NH_4Cl in PBS. Add 2.1 g dry ammonium chloride (NH_4Cl) to 500 mL glass beaker. Add 1× PBS to 200 mL and use a stir bar to dissolve the ammonium chloride at RT. Quench buffer can be stored at RT.
50. Cryoprotectant solution: 30% (w/v) sucrose, 0.02% (w/v) sodium azide in PBS. Prepare several days before the experiment and keep at 4 °C. Prepare 1 L of 1× PBS with 0.02% sodium azide. Weigh 300 grams of sucrose and combine with ~800 mL of 1× PBS with 0.02% sodium azide. Use a stir bar to slowly dissolve the sucrose in solution at room temperature. After the sucrose is completely dissolved, bring the solution to a total volume of 1 L by adding more 1× PBS with 0.02% sodium azide.
51. OCT from Tissue-Tek (cryo-embedding material).

52. Cryostat (to slice to 4 μm; −30 °C).
53. +/+ poly-L-lysine coated glass slides.
54. Diamond pen for labeling of the glass slides with the tissue slice treatment condition information.
55. Lysis solution: 10 mM Tris–HCl, pH 7.4, 160 mM NaCl, 0.05% (v/v) IGEPAL CA-630, 1% (v/v) Triton X-100, 2.5 mM EDTA, 1 mM EGTA, 0.5 mg/mL AEBSF, protease inhibitor cocktail (*see* **Note 11**).
56. Ice bucket.
57. Microcentrifuge tubes.
58. Kit for protein concentration measurement.

3 Methods

3.1 Kidney Harvesting for Kidney Slice Preparation (Rats and Mice) Without Kidney Perfusion

1. This is a two-person procedure from Subheadings 3.1–3.3. To keep the slices in solution as much as possible, two people need to be present, one to section the other to ensure that slices are submerged in the buffer. Once the slices are distributed in the vials under different conditions, then one person can manage the actions required by the protocol (*see* **Note 12**).
2. For each condition and time point, there should be an experimental vial and a control vial with no reagent: Prepare a glass scintillation vials for incubation of the slices. Label one vial per incubation condition. The vial must have a perforated cap through which to feed a segment of "CO_2 impermeant" capillary tubing through the cap.
3. In a separate labeled vials (one per condition), place 5–7 mL of fixative per vial. Keep these vials at RT and near the water bath.
4. Prior to kidney perfusion and harvest (or harvest alone), prepare all the vials with the CO_2-equilibrated Ringer buffer at 37 °C, place the reagents needed for the incubation, and continue to bubble the gas through the buffer for all the vials needed. For example, this is a good time in the protocol to add the desired AMPK activator (AICAR or A769662) to the vials (*see* **Note 13**).
5. Anesthetize the adult male Sprague-Dawley rats with sodium pentobarbital or with isofluorane.
6. Harvest the kidneys as in Fig. 1.
7. Verify each rat is well anesthetized by pinching the tail near the body. The rat should not react to pain and should have a slow respiratory rate (Fig. 1a).
8. Lift the abdominal skin with a set of grasping forceps and pull the skin away from the muscle layer (Fig. 1b).

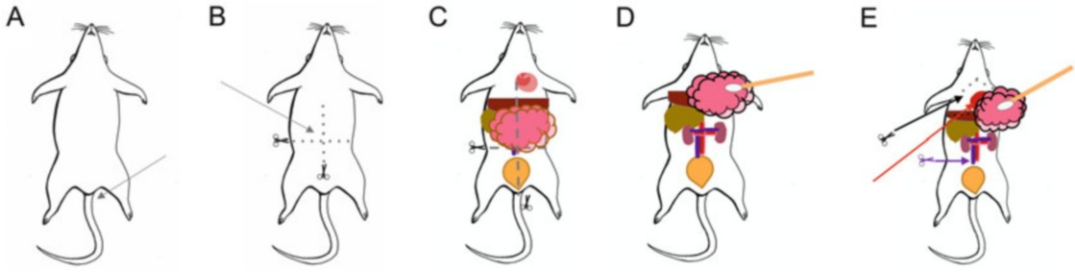

Fig. 1 Diagram of the tissue-harvesting surgery. The depicted procedure relates to Subheading 3.1 (without kidney perfusion) (**a**–**d**) and Subheading 3.2 (with kidney perfusion) (**a**–**e**). (**a**) Verify each rat is well anesthetized by pinching the tail (arrow: position tail pinch). The rat should not react to pain and should have a slow respiratory rate. (**b**) Expose the abdominal muscle layer by placing two additional incisions on the skin perpendicular to the first cut toward each flank taking care to avoid major blood vessels. Using the same grasping forceps, lift the muscle layer away from major intra-abdominal organs underneath (gray arrow). (**c**) Place a small incision in the middle of the abdominal muscle layer, and by carefully visualizing that the scissors are not perforating any internal organs, cut the muscle along the linea alba toward the xiphoid and the pelvis. Avoid touching the diaphragm and the bladder. Place two additional incisions in the abdominal muscle layer perpendicular to the initial xiphoid to pelvis incision toward the flanks. (**d**) Using a paper tissue or cotton applicator (depicted), displace the intestines to visualize the right kidney. At this point, both kidneys can be harvested and sectioned (if no perfusion is required, e.g., go to Subheading 3.3 for instructions to prepare kidney slices). (**e**) Carefully using a paper tissue or cotton applicator, dissect away the skin and fascia from the inferior vena cava. Quickly visualize the diaphragm (black dotted line). Ensure that the perfusion pump is functioning and the perfusion tubing is pumping slowly (one drop every 2–3 s) and that the suction tubing is functional and the vacuum suction is on. With scissors, place an incision in the rightmost aspect of the diaphragm and quickly dissect it frontally toward the left flank with care not to puncture the heart (black arrow and scissors, cut along the gray dashed line). You may need to place two flank incisions to open the rib cage upward. Place the needle in the left ventricle (red arrow). Ask an assistant to increase the pump speed to 4 mL/min. Once the kidneys and the inferior vena cava appear expanded, place a small puncture (purple arrow and scissors) on the inferior vena cava and perfuse the kidney until it becomes pale, using the suction to keep the field clean. When kidneys appear pale, harvest immediately

9. Using scissors, make an incision in this ventral skin from the direction caput to cauda along the central abdominal line (xiphoid to pelvic area) (Fig. 1b).
10. Expose the abdominal muscle layer by placing two additional incisions on the skin perpendicular to the first cut toward each flank taking care to avoid major blood vessels (Fig. 1b).
11. Using the same grasping forceps, pull the muscle away from major intra-abdominal organs (Fig. 1c).
12. Place a small incision in the middle of the abdominal muscle layer, and by carefully visualizing that the scissors are not perforating any internal organs, cut the muscle along the linea alba toward the xiphoid and the pelvis. Avoid touching the diaphragm and the bladder (Fig. 1c).

13. Place two additional incisions in the abdominal muscle layer perpendicular to the initial xiphoid to pelvis incision toward the flanks (Fig. 1c).
14. Using a tissue paper or cotton applicator, displace the intestines to visualize the right kidney (Fig. 1d).
15. At this point, both kidneys can be harvested and sectioned (if no perfusion is required, go to Subheading 3.3) (Fig. 1d).

3.2 Kidney Harvesting for Kidney Slice Preparation (Rats and Mice) with Kidney Perfusion

1. This is also a two-person procedure.
2. If you chose to perform kidney perfusion (Fig. 1a–d) *prior to the harvest* carefully using a paper tissue or cotton applicator, dissect away the skin and fascia from the inferior vena cava (Fig. 1e; *see* **Note 14**).
3. Quickly visualize the diaphragm.
4. Ensure that the perfusion pump is functioning and the perfusion tubing is free of air and the buffer container is at 37 °C and equilibrated with the CO_2/air mix prior to stating the experiment.
5. Ensure that at the start of the perfusion, the buffer is pumping slowly (one drop every 2–3 s) and that the suction tubing is functional and the vacuum suction is on.
6. With scissors, place an incision in the rightmost aspect of the diaphragm and quickly dissect it frontally toward the left flank with care not to puncture the heart. You may need to place two flank incisions to open the rib cage upward.
7. Place the needle in the left ventricle (if obtaining slices from mice, use a smaller needle; *see* Subheading 2).
8. Ask an assistant to increase the pump speed to 4–5 mL/min.
9. Once the kidney and the inferior vena cava appear expanded, place a small puncture on the inferior vena cava and perfuse the kidney until it becomes pale, using the suction to keep the field clean for continued observation.
10. After the kidneys are well perfused, immediately harvest both kidneys and place them in a petri dish.

3.3 Kidney Slice Preparation

1. Ensure that the Stadie-Riggs microtome and blade are ready (Fig. 2).
2. Quickly with a scalpel or blade, cut the kidney into ~5 mm sections transversally and radially (each thick section should have some papilla).
3. Place these thicker kidney sections in a beaker with Ringer buffer at 37 °C equilibrated with the CO_2.

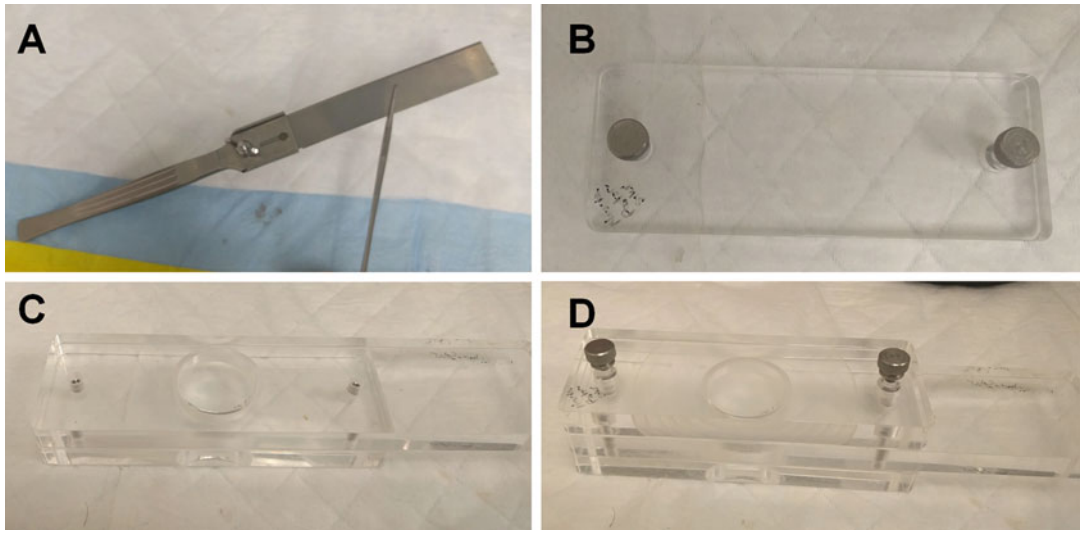

Fig. 2 Stadie-Riggs tissue slicer (microtome) parts and assembly. (**a**) Place a blade (new for each experiment) on the handle using a needle holder or hemostat. The blades are extremely sharp and should not be handled directly with hands (**b**–**d**). To assemble the slicer, the three parts must fit Stadie-Riggs slicer. Cap the slicer. Tighten knobs until kidney section is held firmly in place leaving enough space for the blade to fit. Usually the long piece of the microtome is held with the left hand and the blade with the right hand (*see* Fig. 3)

4. Place one of these thick sections on the Stadie-Riggs slicer (Fig. 3a–h) and quickly obtain a thin kidney tissue slice (~0.5 mm in thickness).
5. Retrieve the thin kidney slice quickly to place it in a second beaker with CO_2-equilibrated Ringer at 37 °C.
6. Continue to obtain slices and place them in the beaker with the other slices.
7. The entire procedure of sectioning both kidneys from the same animal should be performed in less than 5 min.
8. At the end of the sectioning, incubate all the thin kidney slices for 15 min in equilibrated Ringer solution before beginning treatment.
9. Place the slices into the vials for the treatments (Fig. 3h).
10. For AICAR and A769662 treatment, we suggest a minimum of 75-min incubation prior to fixation or rapid freezing.
11. At the end of the incubation time, rapidly place the slices in either fixative or in a microcentrifuge tube that must be rapidly submerged in liquid nitrogen.

3.4 Kidney Slice Sectioning for Immunolabeling or Histology

1. After the above treatments, always keep the slices for each treatment in a separate appropriately labeled container, and place the slices in fixative (4% paraformaldehyde in PBS).

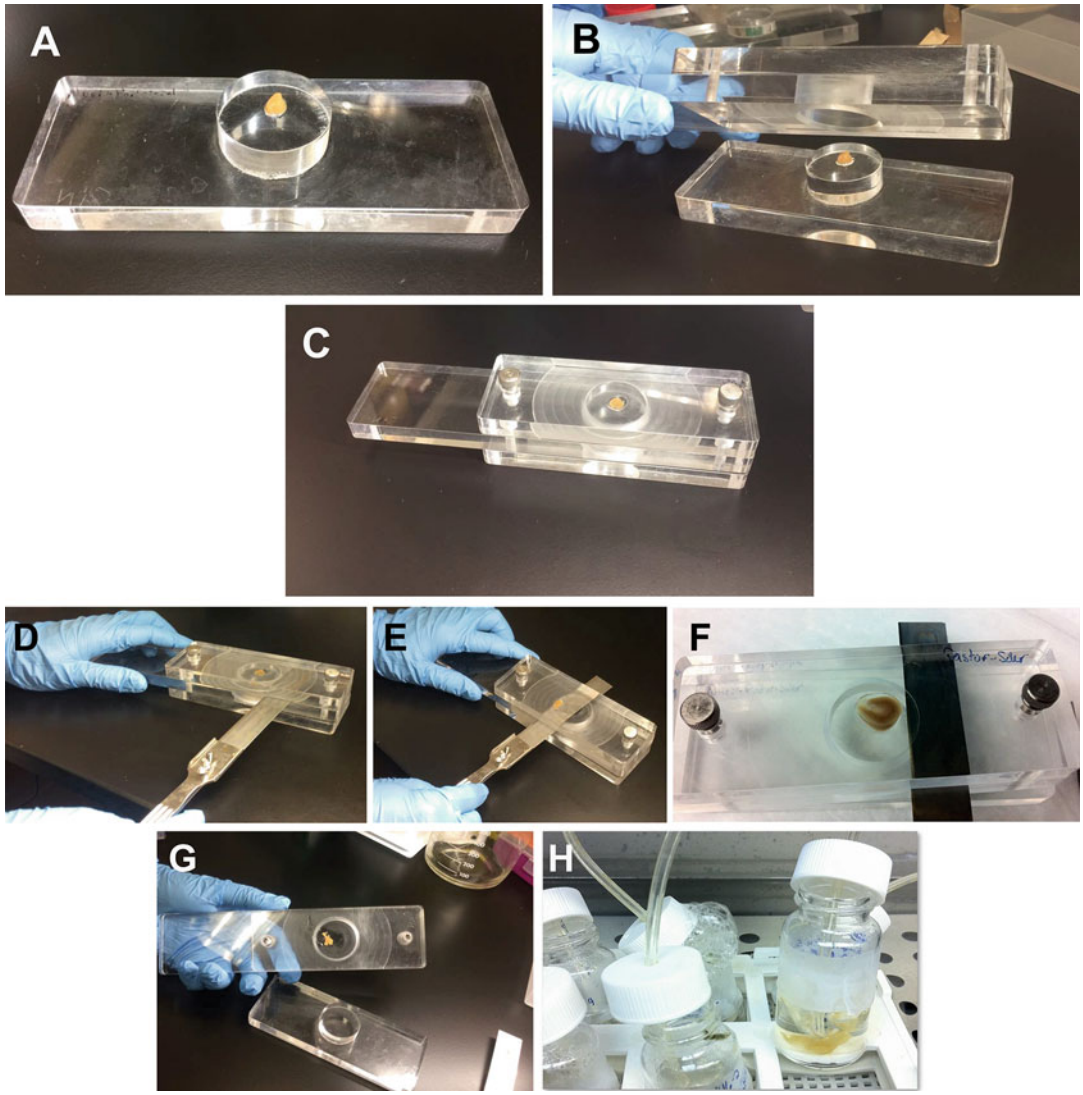

Fig. 3 Kidney slice preparation of the harvested kidney. (**a**) Place the 5 mm section of kidney on the Stadie-Riggs slicer. (**b**) Cap the slicer. (**c**) Tighten knobs until kidney section is held firmly in place. (**d**) Insert the blade into the Stadie-Riggs slicer. (**e**, **f**) Cut horizontally through the kidney slice, slicing into 0.5 mm section, in a right-to-left motion. (**g**) Remove the top of the Stadie-Riggs slicer. (**h**) Add slice of kidney to equilibrated Ringer solution to incubate before treatment

2. Keep the kidney slices in the containers either overnight at 4 °C or at room temperature for 4 h.
3. To proceed with the kidney slice tissue processing at the end of the fixation time period, remove fixative from the vial (dispose of fixative in the hood according to standard operating procedures in the laboratory) (*see* **Note 15**).
4. Place tissue in 1× PBS for 15 min at RT and repeat twice.

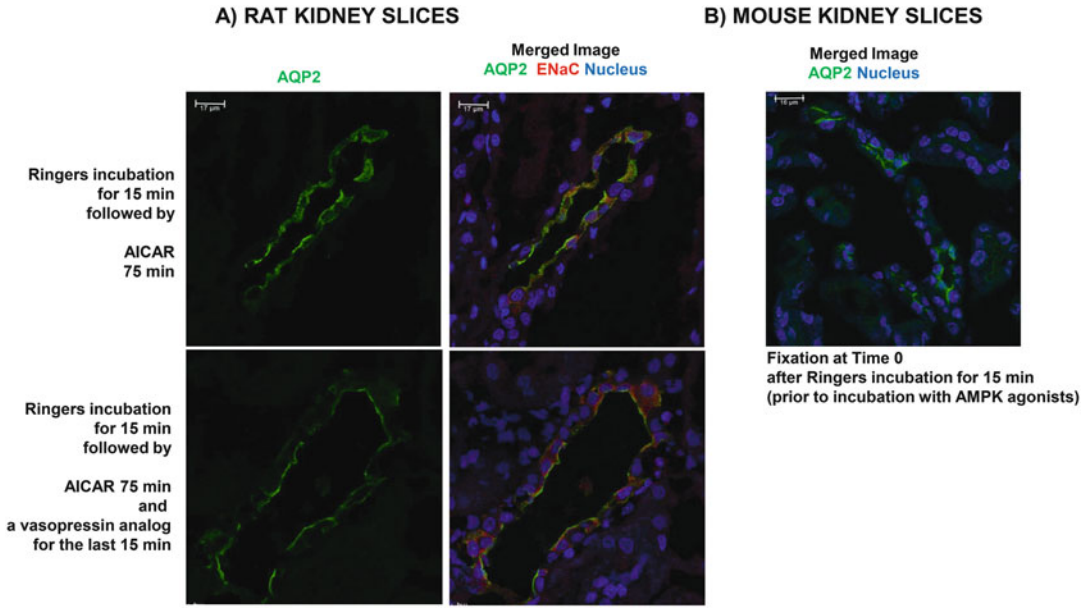

Fig. 4 Confocal images of tissue slices. Kidney slices from rats (**a**) and mouse (**b**) kidney immunolabeled for transport proteins aquaporin-2 (AQP2) and epithelial sodium channel (ENaC). The slices were treated with an AMPK activator (AICAR) in the absence or presence of a vasopressin (**a**) or untreated (**b**). After fixation and cryopreservation, slices were immunolabeled with antibodies against the different transport proteins and imaged using a confocal microscope

5. Placing the kidney slices once for 15 min in quenching buffer (quench step).
6. Rinse tissue again three times, each time for 15 min in 1× PBS at RT (*see* **Notes 16** and **17**).
7. The kidney slices can now be stored at 4 °C in PBS azide and can now be processed for paraffin sections and histology.
8. For immunolabeling, proceed by placing tissue in 30% sucrose overnight at 4 °C or at RT for a few hours until it floats.
9. Place the slice onto a plastic cryomold and flatten it to the bottom of the mold. Freeze in the cryostat chamber at −30 °C. Mount onto the cryostat chuck and section (usually 4 μm thickness) (*see* **Note 18**). For immunolabeling, *see* ref. 11–13 (Fig. 4).

3.5 Kidney Slice Frozen Tissue Lysis Preparation

1. Obtain frozen tissue from −80 °C freezer and transport on ice (*see* **Note 19**).
2. Incubate on ice in cold room for ~30 min until thawed and/or soft enough to homogenize.
3. Put necessary tools in cold room to chill (there must be sufficient tubes for all samples).

4. Prepare tissue lysis buffer (5 mL is sufficient for two whole mouse kidneys).
5. Weigh empty sample tube, and then determine tissue weight.
6. Calculate the required amount of lysis buffer for each tissue sample; ideally there should be 0.5 g tissue per mL buffer.
7. Put tools on ice.
8. Mince tissue in cold petri dish with razor blade until slurry is produced.
9. Transfer slurry to mortar/pestle. Add predetermined tissue lysis buffer volume and grind tissue carefully. Twist and pull slowly until there are no visible tissue chunks remaining (clean mortar/pestle with water between samples).
10. Transfer tissue to clean microfuge tube with a transfer pipet.
11. Centrifuge at maximum speed (13,000 rpm or 16,000 × *g*) for 30 min at 4 ° C (*see* **Note 20**).
12. Transfer supernatant to a clean microfuge tube and discard pellet. Keep supernatant on ice.
13. Prepare a 1:10 dilution of lysate (10 μL in 90 μL tissue lysis buffer) and measure protein concentration of dilution. Calculate actual lysate concentration.
14. Aliquot samples and store at −80 ° C with protein concentration written on tube.

4 Notes

1. When selecting rats, it is important to match the included rats by weight and age if the different animal experiments are going to be compared. Our studies have been carried out using male Sprague-Dawley rats of ~250–300 g who are 8–12 weeks of age. The key in selecting the animal model and animal characteristics is that in order to compare results from a series of replicate experiments, the animals used for one experiment should be of the same sex and approximate age.
2. Two littermate mice of the same sex may need to be used for a preparation if the number of conditions is more than four to five.
3. Difficult to obtain in the US due to regulatory hurdles.
4. Pentobarbital sodium is difficult to procure, isoflurane may be substituted the only caveat is that the time under isofluorane anesthesia must be kept constant for all the animals used for the same study, as anesthetic gases may induce "preconditioning" which makes the tissue resistant to ischemic insult, and is equivalent to AMPK pre-activation [17]. Such preconditioning

would be an important confounder in evaluating the effects of AMPK activation on cellular function, as it would act as an AMPK activator even in the control incubation conditions.

5. This solution is prepared from the four stock solutions (A–D): Add 25 mL of each stock solution (A–D) to a 1 L glass beaker, adding water to final volume of ~400 mL and then adding 0.9 g of D-glucose to the final solution. Bring the solution to 37 °C by placing it on a water bath. Then equilibrate the solution by bubbling through it 5% CO_2 (balance air) while keeping it at 37 °C for ~15 min. Then check the pH of this solution. It should be close to 7.4 without major adjustments.
6. This Hank's Balanced Salt Solution must be prepared using a volumetric flask adding water first and carefully adding the different reagents from stock solutions and adding the calcium containing stock solution last to prevent calcium phosphate precipitation [12, 18].
7. Either a peristaltic or a syringe pump will work. Speed of perfusion pump is ~4.0 mL/min. One end of the tubing should be connected to a needle to be inserted into the left ventricle and the other end of the tubing to be submerged into a container of warm (37 °C) CO_2-equilibrated Ringer buffer. Alternatively, the perfusion pressure could be equilibrated with the animal's blood pressure to prevent changes in the kidney due to perfusion pressures that are either too low or too high.
8. There should be as many tubing pieces for the gas mix as there are condition vials, plus an additional four tubing pieces to allow equilibration of slice holding containers.
9. We have not used metformin in this system as it requires hours to days to induce AMPK activation.
10. Prepare the fixative in PBS fresh every time on the day of the slice preparation. Do not reuse the fixative, and do not save for another slice preparation at a later date. Please discard according to laboratory safety department policies.
11. Lysis solution detailed preparation: 100 µL of 1 M Tris–HCl, pH 7.4; 1.6 mL of 1 M NaCl solution; 5 µL of IGEPAL CA-630 (Sigma-Aldrich #1-3021); 100 µL of Triton X-100 (Sigma-Aldrich #T8787); 20 µL of 0.5 M EDTA; 50 µL of 0.2 M EGTA; one complete protease inhibitor tablet—Roche complete mini, EDTA-free (Sigma-Aldrich #11836170001); one PhosStop tablet (Roche); 50 µL of 100 mg/mL AEBSF (Pefabloc, Sigma-Aldrich #76307); add pure water up to 10 mL; use a stir bar to dissolve ingredients at RT.
12. Until the method is established in the laboratory, the presence of two people throughout the procedure decreases the chances of mishaps.

13. Do not microwave "sugar" containing solutions as the microwave process may "caramelize" the solution.
14. This procedure is optional, as some of the transporter proteins may change their subcellular localization upon kidney perfusion via the left ventricle. However, this procedure helps keep tubules open after sectioning and washes the vasculature of the kidney to remove hormones that may affect intracellular protein traffic.
15. The first and second washes will have high concentrations of paraformaldehyde and should be properly discarded as chemical waste. All other rinses can be disposed of as normal liquid waste.
16. The tissue should be processed at room temperature, but samples should not be allowed to sit out longer than necessary. Perform all steps for the times indicated. Do not allow rinse steps to exceed 20 min unless the tissue is unusually thick.
17. For a particularly helpful setup, place a small funnel over the spout of an empty bottle (i.e., an empty media bottle). Line the funnel with a clean tissue paper. Pour solutions into the tissue paper, using a Pasteur pipet, to direct flow and prevent the tissue from falling. If any tissue does fall out, it will catch in the tissue paper and can be retrieved with forceps.
18. Cryostat use tips: These are not necessarily part of the protocol but are good introductory advice while handling the kidney slices. Be careful with the blade; it is very sharp. It is recommended to change the blade before each sectioning. Be especially careful not to damage the glass of the anti-roll plate with the metal part of the brushes. Use brushes without metal, which often chinks the glass plate. Be sure to judge the distance of the anti-roll plate to the blade; it has to be just right to prevent rolling without jamming the tissue. When leaving the cryostat unattended, place a thin layer of OCT to protect the tissue block; lock handle to prevent tissue damage; when finished sectioning, place the tissue back in cryomold, wrapped in aluminum foil, labeled, and placed at −20 °C for later use.
19. There are many different methodologies/protocols to generate a kidney homogenate. Our protocol of immediately freezing the kidney tissue and then processing at a later time is done solely for the purpose of ensuring that AMPK activity matches the level of AMPK activation that would be expected from the condition. If needed, side-by-side comparisons of homogenization and immunoblot protocols should be performed. It is an important point that all tissues being examined for AMPK downstream effects must be frozen right after the incubation in the Ringer buffer. If tissue is left on ice for lysis at a later time,

the control and treated tissue will likely show the same degree of AMPK activation.

20. Depending on whether the protein of interest is intracellular or in the plasma membrane, different centrifugation techniques can be used [19].

Acknowledgments

This work was in part supported by the Wright Foundation, the Dean's Pilot Project Program, and the Department of Medicine at the Keck School of Medicine of USC. We thank Dr. Kennneth R. Hallows, Dr. Alicia McDonough, and Dona Ralph for technical advice and helpful suggestions.

References

1. Gerich JE, Meyer C, Woerle HJ, Stumvoll M (2001) Renal gluconeogenesis: its importance in human glucose homeostasis. Diabetes Care 24(2):382–391
2. Mandel LJ (1986) Primary active sodium transport, oxygen consumption, and ATP: coupling and regulation. Kidney Int 29 (1):3–9. https://doi.org/10.1038/ki.1986.2
3. Hallows KR (2005) Emerging role of AMP-activated protein kinase in coupling membrane transport to cellular metabolism. Curr Opin Nephrol Hypertens 14 (5):464–471. https://doi.org/10.1097/01.mnh.0000174145.14798.64
4. Hardie DG, Scott JW, Pan DA, Hudson ER (2003) Management of cellular energy by the AMP-activated protein kinase system. FEBS Lett 546(1):113–120. https://doi.org/10.1016/s0014-5793(03)00560-x
5. Bens M, Vandewalle A (2008) Cell models for studying renal physiology. Pflugers Arch - Eur J Physiol 457(1):1–15. https://doi.org/10.1007/s00424-008-0507-4
6. Gekle M, Wünsch S, Oberleithner H, Silbernagl S (1994) Characterization of two MDCK-cell subtypes as a model system to study principal cell and intercalated cell properties. Pflugers Arch 428(2):157–162
7. Guntupalli J, Onuigbo M, Wall S, Alpern RJ, TD DB Jr (1997) Adaptation to low-K+ media increases H(+)-K(+)-ATPase but not H(+)-ATPase-mediated pHi recovery in OMCD1 cells. Am J Phys 273(2 Pt 1):C558–C571
8. Edwards JC, van Adelsberg J, Rater M, Herzlinger D, Lebowitz J, al-Awqati Q (1992) Conditional immortalization of bicarbonate-secreting intercalated cells from rabbit. Am J Phys 263(2 Pt 1):C521–C529
9. Sun X, Yang LV, Tiegs BC, Arend LJ, McGraw DW, Penn RB, Petrovic S (2010) Deletion of the pH sensor GPR4 decreases renal acid excretion. J Am Soc Nephrol 21(10):1745–1755. https://doi.org/10.1681/asn.2009050477
10. Schwartz JH, Li G, Yang Q, Suri V, Ross JJ, Alexander EA (2007) Role of SNAREs and H -ATPase in the targeting of proton pump-coated vesicles to collecting duct cell apical membrane. Kidney Int 72(11):1310–1315. https://doi.org/10.1038/sj.ki.5002500
11. Gong F, Alzamora R, Smolak C, Li H, Naveed S, Neumann D, Hallows KR, Pastor-Soler NM (2010) Vacuolar H+-ATPase apical accumulation in kidney intercalated cells is regulated by PKA and AMP-activated protein kinase. Am J Physiol Renal Physiol 298(5): F1162–F1169. https://doi.org/10.1152/ajprenal.00645.2009
12. Alzamora R, Gong F, Rondanino C, Lee JK, Smolak C, Pastor-Soler NM, Hallows KR (2010) AMP-activated protein kinase inhibits KCNQ1 channels through regulation of the ubiquitin ligase Nedd4-2 in renal epithelial cells. Am J Physiol Renal Physiol 299(6): F1308–F1319. https://doi.org/10.1152/ajprenal.00423.2010
13. Al-Bataineh MM, Li H, Ohmi K, Gong F, Marciszyn AL, Naveed S, Zhu X, Neumann D, Wu Q, Cheng L, Fenton RA, Pastor-Soler NM, Hallows KR (2016) Activation of the metabolic sensor AMP-activated protein kinase inhibits aquaporin-2 function in kidney principal cells. Am J Physiol Renal Physiol 311(5):

F890–F900. https://doi.org/10.1152/ajprenal.00308.2016

14. Pastor-Soler NM, Hallows KR (2012) AMP-activated protein kinase regulation of kidney tubular transport. Curr Opin Nephrol Hypertens 21(5):523–533. https://doi.org/10.1097/MNH.0b013e3283562390
15. Stein SC, Woods A, Jones NA, Davison MD, Carling D (2000) The regulation of AMP-activated protein kinase by phosphorylation. Biochem J 345(3):437. https://doi.org/10.1042/0264-6021:3450437
16. Mount PF (2005) Acute renal ischemia rapidly activates the energy sensor AMPK but does not increase phosphorylation of eNOS-Ser1177. Am J Physiol Renal Physiol 289(5): F1103–F1115. https://doi.org/10.1152/ajprenal.00458.2004
17. Lotz C, Fisslthaler B, Redel A, Smul TM, Stumpner J, Pociej J, Roewer N, Fleming I, Kehl F, Lange M (2011) Activation of adenosine-monophosphate–activated protein kinase abolishes desflurane-induced preconditioning against myocardial infarction in vivo. J Cardiothorac Vasc Anesth 25(1):66–71. https://doi.org/10.1053/j.jvca.2010.02.007
18. Breton S, Brown D (1998) Cold-induced microtubule disruption and relocalization of membrane proteins in kidney epithelial cells. J Am Soc Nephrol 9(2):155–166
19. Sachs AN, Pisitkun T, Hoffert JD, Yu M-J, Knepper MA (2008) LC-MS/MS analysis of differential centrifugation fractions from native inner medullary collecting duct of rat. Am J Physiol Renal Physiol 295(6):F1799–F1806. https://doi.org/10.1152/ajprenal.90510.2008

Chapter 29

A Flow Cytometry-Based Protocol to Measure Lymphocyte Viability Upon Metabolic Stress

Sébastien Denanglaire, Tiphène Pirnay, Oberdan Leo, and Fabienne Andris

Abstract

Distinct lymphocyte subpopulations display discrete metabolic profiles and are differently affected by metabolic resource variations, making the analysis of lymphocyte survival in a complex tissue in response to metabolic stress highly challenging. Here we describe a flow cytometry-based method allowing simultaneous cell identification and viable cell counting in mixed lymphocyte populations without extensive cell subset purification procedures. The example provided herein illustrates the role of AMPK in T lymphocyte survival in response to the mitochondrial poison oligomycin.

Key words Flow cytometry, Polystyrene beads, Lymphocytes, Cell counting, Antibodies, Metabolic stress

1 Introduction

AMP-activated protein kinase (AMPK) is a critical energy sensor adapting cellular metabolism in response to environmental variations, thus playing a crucial role in maintaining cellular energy metabolism homeostasis [1, 2]. AMPK is switched on by cellular stresses that either increase ATP consumption (i.e., muscle contraction) or by stresses that interfere with ATP production (i.e., hypoxia, glucose deprivation, or mitochondrial poisons) [3, 4].

Differentiation of immune cells in effector or long-term memory cells is tightly associated with changes in energy metabolic activity that allow the cells to balance requirements for energy or molecular biosynthesis [5–8]. Moreover, during immune responses, activated lymphocytes encounter distinct metabolic environments with altered availability of nutrients and must adapt to survive [9]. This is particularly relevant in antitumor immunity

Sébastien Denanglaire and Tiphène Pirnay are Co-first authors

Dietbert Neumann and Benoit Viollet (eds.), *AMPK: Methods and Protocols*, Methods in Molecular Biology, vol. 1732, https://doi.org/10.1007/978-1-4939-7598-3_29,

where infiltrating tumor-specific lymphocytes may face severe hypoxia and/or reduced glucose availability [10–13].

Studies on lymphocytes deficient for AMPK have revealed that this enzyme plays an important role in promoting lymphocyte resistance to an energy crisis [14]. In particular, AMPK-deficient lymphocytes are unable to maintain adequate ATP levels and cell viability during metabolic mitochondrial stresses induced by ATP synthase inhibition [14].

Recent evidence indicates that T lymphocyte subsets display distinct metabolic profiles with effector T helper (Th) cells expressing strong glycolytic metabolic profile, whereas regulatory T cells (Tregs) display increased mitochondrial fatty acid oxidation-based metabolism [15, 16]. Thus local metabolic stresses may differently affect distinct lymphocyte subsets.

1.1 Lymphocyte Identification by Flow Cytometry

Lymphocyte cell types differ by the expression of selective surface molecules (e.g., CD for cluster of differentiation) [17]. Panels of fluorescent anti-CD-specific antibodies represent a powerful tool for the identification of lymphocyte subpopulations by flow cytometry and offer interesting potential for measuring selective viable cell subset recovery in mixed populations exposed to metabolic stress.

1.2 Lymphocytes Counting

Manual counting of recovered cell (i.e., trypan blue exclusion) combined with cell subset distribution information (given by flow cytometry) is often used to estimate cell recovery of a particular lymphocyte population without extensive cell subset purification procedures (numbers of viable cells from "subset A" = total number of viable cells x percentage of cells in "subset A"). However, manual counting is time consuming and difficult to apply to a large-scale analysis, in particular in the setting of kinetic studies, and most standard cytometers are not equipped with an absolute cell counting mode.

1.3 Protocol Outline

Here we describe a method allowing simultaneous lymphocyte subset identification and relative cell counting by flow cytometry. Subheading 3.1 (illustrated in Fig. 1) is devoted to the validation of the technique in the local setup. The method relies on adding a fixed amount of easily recognizable (due to distinct size and light opacity) polystyrene beads to cell suspensions resulting from a serial twofold dilution of splenocytes. Plotting the relative cell numbers corresponding to the same number of beads and theoretical cell dilution curve reveals a very good correlation over a wide range of cell numbers (Fig. 1b). In Subheading 3.2, we will describe the step-by-step procedure allowing the analysis of T helper lymphocyte ($CD4^+$), cytotoxic T lymphocyte ($CD8^+$), and B lymphocyte ($CD45R^+$) viability in unfractionated spleen cells from wild-type and T cell conditional AMPKα1-KO mice treated with the F0/F1 ATP synthase inhibitor oligomycin. In Subheading 3.3, we will

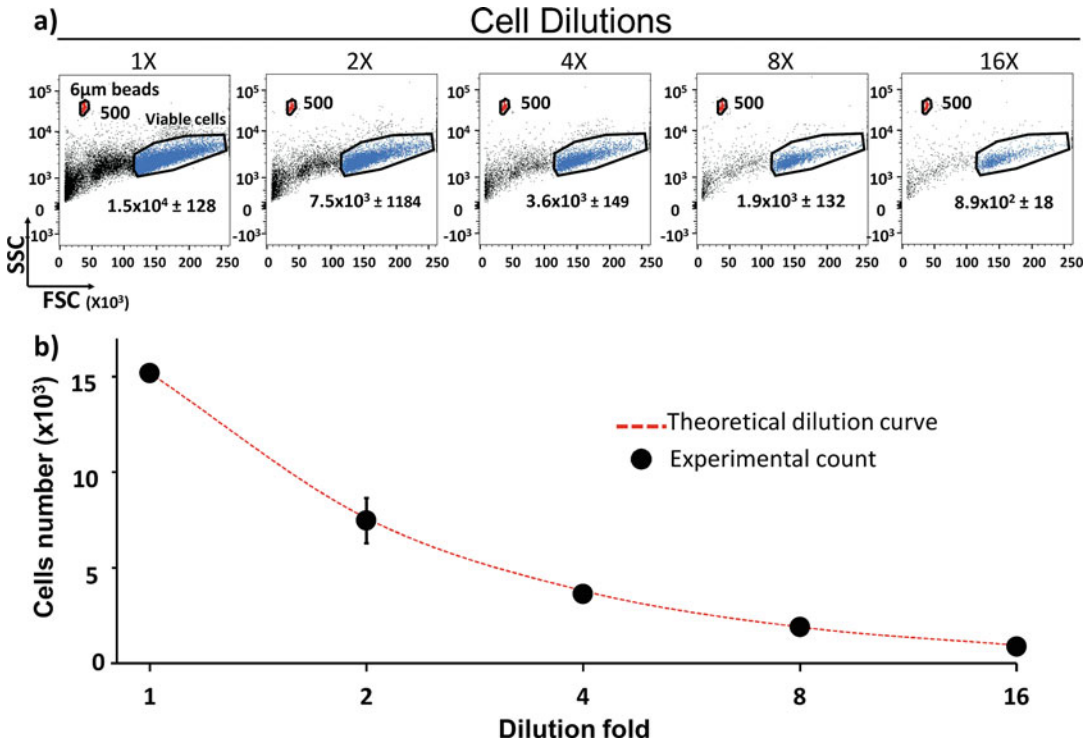

Fig. 1 Correlation of flow cytometry bead-based cell counting and theoretical cell dilution curve. Serial twofold dilutions of splenocytes were mixed with equal number of 6 µm beads. (**a**) Cytometer profiles showing 6 µm beads and viable cells. Acquisition was stopped at 500 events in the bead gate. Number of acquired lymphocytes is indicated in each cell gate (mean duplicates ± SD). (**b**) Experimental cell counts from (**a**) were plotted on theoretical curve of twofold dilutions

further explain the cytometry analysis procedure and viable cell calculation for T lymphocytes identified by flow cytometry (Fig. 2). Finally, with this technique, we illustrate the selective sensitivity of AMPK-deficient $CD4^+$ and $CD8^+$ T lymphocytes to a mitochondrial metabolic stress (Fig. 3).

Importantly, this technique is also applicable to the assay of any cell type viability in response to panels of drugs.

2 Materials

2.1 Solutions, Buffers, and Media

1. Red blood cell lysis solution: 17 mM Tris–HCl, pH 7.65, 144 mM NH_4Cl. Mix 9 volumes of 0.16 M NH_4Cl and 1 volume of 0.17 M Tris–HCl, pH 7.65.
2. Cell culture medium: RPMI 1640 supplemented with 5% (v/v) fetal bovine serum, 2 mM L-glutamine, 1 mM Na-pyruvate, 100 µM nonessential amino acids, and 50 U/mL penicillin/streptomycin.

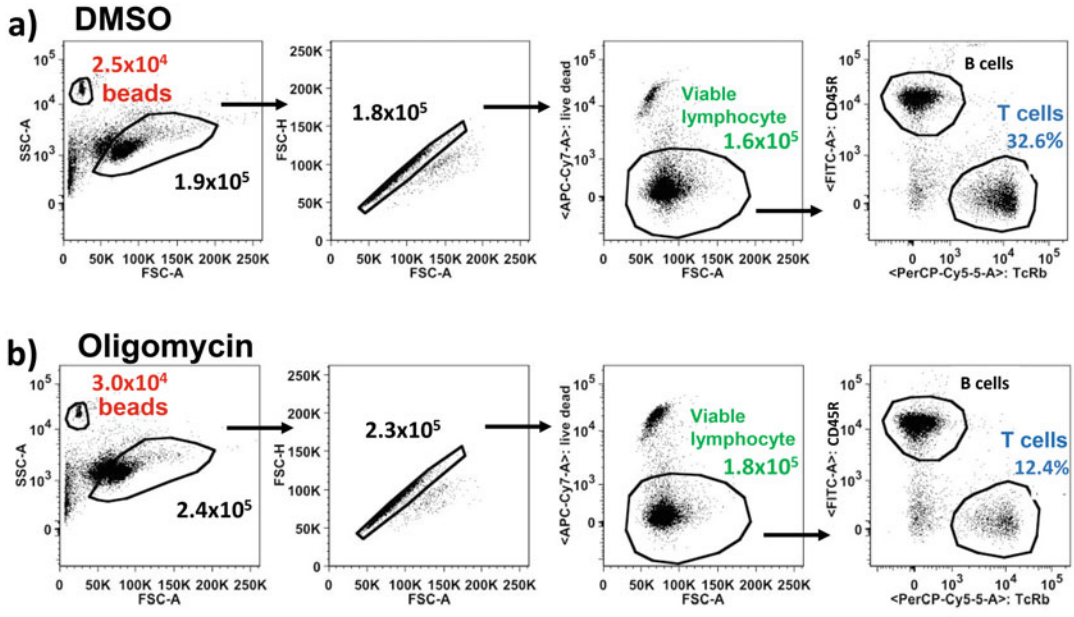

c) -> Relative numbers of T cells for 1000 beads :

$$\frac{1000 \times \text{number of viable lymphocytes} \times \%\,\text{LT}}{\text{number of beads}}$$

DMSO: $\frac{1000 \times 159796 \times 0.326}{24885} = 2093.37$ (A)

Oligo: $\frac{1000 \times 183662 \times 0.124}{30340} = 750.63$ (B)

-> % of T cell recovery (oligomycin VS DMSO treatment)

$$\frac{100 \times B}{A} = \frac{100 \times 750.63}{2093.37} = \mathbf{35.86\ \%}$$

Fig. 2 Combination of bead-based cell counting and flow cytometry analysis allows calculation of T cell recovery upon metabolic stress. Splenocytes from AMPK$\alpha 1^{flox/flox}$-CD4-CRE^{+} mice were incubated for 6 h with (**a**) DMSO or (**b**) 10 nM oligomycin. Splenocytes from left panels were gated for single cells only (exclusion of doublets), then gated for viability (exclusion of dead cells), and further gated for B cells or T cells, as indicated in right panels. Percentages or numbers of cells in each gate are indicated. (**c**) Calculation of relative viable T cell recovery from examples in (**a**, **b**)

3. Phosphate-buffered saline (PBS): 145 mM NaCl, 2.7 mM KCl, 1.5 mM KH_2PO_4, 8 mM Na_2HPO_4, pH 7.
4. Flow medium: PBS, 0.1% (w/v) BSA, 0.1% (w/v) NaN_3.

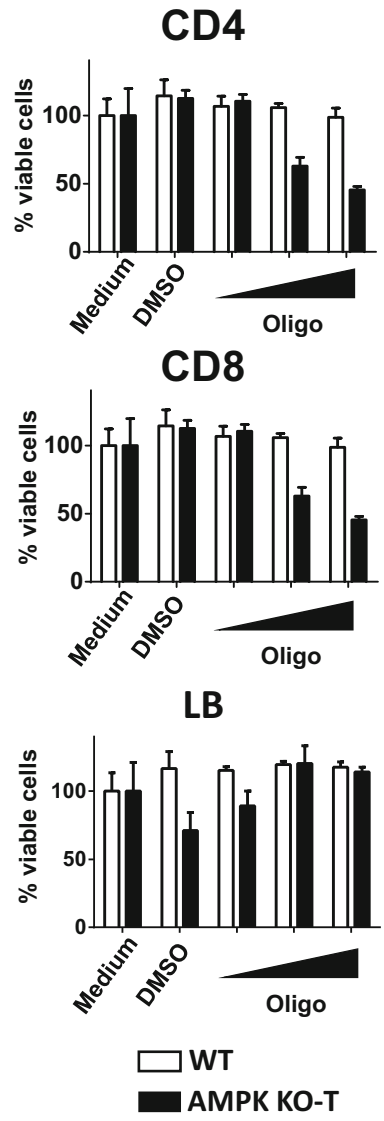

Fig. 3 AMPK-deficient T lymphocytes are more susceptible to metabolic mitochondrial stress. Splenocytes (10^6 cells in 500 μL of culture medium) were incubated for 6 h with graded doses of oligomycin (1.1, 3.3, and 10 nM), with the DMSO solvent or with medium. The relative numbers of viable $CD4^+$, $CD8^+$, and B cells in each experimental sample were estimated as described in Fig. 2. Results are expressed as % of viable cells found in the control (medium alone) group

2.2 Reagents and Materials

1. Dimethyl sulfoxide (DMSO).
2. Oligomycin stock solution: 100 μM oligomycin in DMSO. Prepare a 10 mM oligomycin solution by dissolving 5 mg of oligomycin in 633 μL of DMSO. Make several aliquots to avoid freeze-thaw cycles. Further dilute the 10 mM oligomycin

solution in culture medium by adding 10 μL of 10 mM stock oligomycin into 990 μL of culture medium (this 100-fold dilution leads to the 100 μM oligomycin stock solution). Dilute the DMSO solvent in parallel (10 μL + 990 μL of culture medium) in a separate tube. Diluted stocks can be kept at 4 °C and used for up to 1 month.

3. 6 μm-polystyrene beads (*see* **Note 1**).
4. Fluorescent-coupled monoclonal antibodies: anti-mouse TcR-β-PerCP-Cy5.5; anti-CD4-PECy7; anti-CD8-PE; anti-CD45R-FITC.
5. Anti-mouse CD16/32: 1/200 (*see* **Note 2**).
6. Near-IR viability dye.
7. Petri dishes.
8. 15 mL tubes.
9. 5 mL cytometer-adapted tubes.
10. 70 μm nylon mesh cell strainer.
11. Flow cytometer.
12. FlowJo (or any other) cell analysis software.

2.3 Mice

1. T lymphocyte-conditional AMPKα1-KO mice ($AMPK\alpha1^{flox/flox}$-CD4-CRE^{+}) (*see* **Notes 3** and **4**).
2. Control mice: $AMPK\alpha1^{+/+}$-CD4-CRE^{+} or $AMPK\alpha1^{flox/flox}$-CD4-CRE^{-}. Wild-type C57BL/6 mice can also be used.

3 Methods

3.1 Validation of the Bead-Based Cell Counting Method (Fig. 1)

1. Collect the spleen of a mouse, and mechanically disrupt it with the wide side of a syringe piston, in a 5 mL culture Petri dish containing 1 mL of red blood cell lysis solution.
2. After 1 min, stop the lysing reaction by adding 10 mL of cell culture medium.
3. Filter the cell suspension using a 70 μm nylon mesh cell strainer on top of a 15 mL tube, and centrifuge at 400 × *g* for 5–10 min at 4 °C.
4. Discard supernatant and suspend the pellet in 10 mL of culture medium.
5. Prepare five cytometer tubes containing twofold serial dilutions of cells:
   (a) The first tube will receive 500 μL of the cell suspension.
   (b) The four other tubes will receive 250 μL of culture medium.

(c) Transfer 250 µL of cells from tube 1 to tube 2, mix well, and transfer again 250 µL of twofold diluted cell suspension from tube 2 to tube 3.

(d) Repeat the 250 µL transfer from tube 3 to tube 4 and from tube 4 to tube 5.

(e) Discard 250 µL of diluted cells from tube 5.

6. Carefully vortex the 6 µm polystyrene bead stock solution, and prepare a 1/250 solution (4 µL of 6 µm beads/mL) in flow medium (*see* **Note 5**).
7. Mix well the solution and add 250 µL of pre-diluted 6 µm bead stock solution per tube.
8. Gently mix the tubes and directly analyze by flow cytometry.
9. Adjust forward-scattered light (FSC) and side-scattered light (SSC) to allow simultaneous bead and cell detection: set the SSC axis into log scale. Beads are very small and you can miss them in a linear scale (*see* **Note 6**).
10. Verify correlation between relative bead-based cell count and theoretical cell dilution curve (see theoretical example in Fig. 1).

3.2 Oligomycin Treatment and Lymphocyte Subpopulation Staining

1. Prepare oligomycin working solutions from oligomycin stock solution (*see* **Note 7**):

(a) 20 nM oligomycin: add 2 µL of 100 µM oligomycin solution to 10 mL of cell culture medium. Mix well.

(b) 6.6 nM oligomycin: collect 1 mL from the 20 nM oligomycin solution and add 2 mL of cell culture medium. Mix well.

(c) 2.2 nM oligomycin: collect 1 mL from the 6.6 nM oligomycin solution and add 2 mL of cell culture medium. Mix well.

(d) DMSO control solution: proceed as for the 20 nM oligomycin solution by adding 2 µL of the intermediary solution in 10 mL of cell culture medium. Mix well (*see* **Note 8**).

2. Distribute 250 µL of each oligomycin working solution in cytometer-adapted tubes. Prepare additional tubes containing 250 µL of cell culture medium only. Prepare at least two tubes for each experimental condition.
3. Collect spleen cells from control and AMPKα1$^{flox/flox}$-CD4-CRE^{+} mice as in Subheading 3.1 (**steps 1–3**), and estimate total spleen cell numbers by trypan blue exclusion.
4. Adjust spleen cell concentrations to 4×10^6/mL, mix well, and distribute 250 µL in tubes containing cell culture medium with DMSO or oligomycin working solutions. Mix gently.
5. Incubate 5–6 h in a CO_2 incubator at 37 °C.

6. Centrifuge the tubes at 400 × *g* for 5–10 min at 4 °C.
7. Prepare a "master mix" cell staining solution for lymphocyte subpopulation cell staining. Dilute near-IR viability dye and fluorescent-coupled anti-mouse TcRβ, CD4, CD8, and CD45R monoclonal antibodies, in 50 μL of PBS per tube to stain (*see* **Note 9**). Total volume solution to be prepared = [number of tubes to stain + 1] × 50 μL (*see* **Note 10**).
8. Discard the cell supernatant (*see* **Note 11**) and gently resuspend the cells in 50 μL of master mix cell staining solution.
9. Incubate at 4 °C for 25 min.
10. Add 2 mL of cold PBS and centrifuge the tubes at 400 × *g* for 5–10 min at 4 °C.
11. Carefully homogenize the 6 μm polystyrene bead solution, and prepare a 1/250 solution (4 μL of 6 μm beads/mL) in flow medium (*see* **Note 5**).

    Total volume solution to be prepared = [number of tubes to stain + 1] × 500 μL.
12. Discard the cell supernatant (*see* **Note 11**), and gently resuspend the cells in 500 μL of 6 μm polystyrene bead-containing flow medium (*see* **Notes 12** and **13**).
13. Adjust forward-scattered light (FSC) and side-scattered light (SSC) to allow simultaneous bead and cell detection: regulate SSC axis into log scale (*see* **Note 6**). Gently vortex the tubes before analyzing by the cytometer.

3.3 Flow Cytometry Analysis and Lymphocyte Subset Viability Determination

A representative example and calculation procedure are shown in Fig. 2.

1. From the FSC/SSC dot plot diagram, draw the bead and lymphocyte gates.
2. Select "lymphocyte gate" and open a FSC-A/FSC-H dot plot diagram, and then draw a single-cell gate (*see* **Note 14**).
3. Select "single-cell gate" and open the FSC/viability marker dot plot diagram. Draw a new gate = single live lymphocytes.
4. From this new gate, open the fluorescent marker-associated diagrams (i.e., in Fig. 2a, b: TcRβ versus CD45R). Draw gates corresponding to T lymphocytes ($TcR\beta^+$) and B lymphocytes ($CD45R^+$).
5. From the different gate/plot previously described in **steps 1–4**, record the numbers of beads, numbers of viable lymphocytes, and percentage of T cell subset. The data collected in the Fig. 2 will allow calculation of the relative recovery (i.e., for 1000 beads) of T lymphocyte subset, in each experimental condition, according to the formula:

$$\text{Recovered cells per 1000 beads} = \frac{1000 \times (\text{nb of events in viable lymphocyte gate}) \times \%\text{T cell subset}}{\text{Number of events in bead gate}}$$

The percentage of recovery between treated (oligomycin) and control (medium or DMSO) groups will be further calculated as [number of cells recovered in oligomycin/number of cells recovered in control] × 100 (*see* Fig. 2c for detailed example).

6. Percentage of cell recovery can be plotted in graphs to allow visual representation of lymphocyte viability upon metabolic stress (*see* Fig. 3 for the representative experiment depicted herein: comparison of graded oligomycin dose effects on B cells and helper and cytotoxic T cells from wild-type and conditional T cell-deficient AMPKα1 mice).

4 Notes

1. It is convenient to use 6 μm beads from Polysciences (#07312), but any 5–10 μm laser-detectable beads would also be suitable.
2. Anti-CD16/32 monoclonal antibody will block binding of immunoglobulin to Fc receptors expressed on B cells, monocytes/macrophages, NK cells, granulocytes, mast cells, and dendritic cells.
3. AMPKα1flox/flox-CD4-CRE$^+$ mice were generated by breeding AMPKα1 (Prkaa1)flox/flox mice (kindly provided by Dr. Benoit Viollet, Paris, France) with CD4-CRE mice (Jackson Laboratory strain 017336, provided by Dr. Geert Van Loo, University of Gent, Belgium), both on a C57BL/6 genetic background. The AMPKα1 subunit is the only AMPK catalytic isoform present in hematopoietic cell lineages, and disruption of the AMPKα1 gene does not lead to a compensatory expression of the α2 subunit in the immune system [14].
4. T lymphocytes develop in the thymus where they transiently express both CD4 and CD8 co-receptors (double positive thymocytes) before giving rise to either CD4$^+$ T helper or CD8$^+$ cytotoxic T cells. Therefore AMPKα1$^{flox/flox}$-CD4-CRE$^+$ mice are deficient in AMPK expression in both CD4$^+$ and CD8$^+$ T cell subsets.
5. The bead suspension that we ordered is supplied in the form of a dropper bottle. The stock solution corresponds to a concentration of approximately 200,000 beads/μL. Thoroughly shake the vial and take a few drops in a 1.5 mL tube to allow easier pipetting. This aliquot solution can be stored at 4 °C up to 3 months. Check for drying. Once again, thoroughly shake

the 1.5 mL tube by pipetting up and down before taking a few microliters.

6. Be careful of the instrument threshold settings. Beads are indeed very small and you can miss them if your threshold is set too high.
7. The final volumes of each solution should be adapted depending on the number of experimental condition to be tested. Perform each experimental condition at least in duplicate.
8. Do not exceed a final concentration of 0.1% (v/v) DMSO in any of the samples, to limit interference by this solvent on the biological response analyzed.
9. Dilution of fluorescent-labeled antibodies and viability dye in this particular example:

   Near-IR viability dye, 1/1000 (Life Technologies, L10119); anti-mouse CD16/32, 1/200 (BioXCell, CUS-HB-197); anti- TcRβ-PerCP-Cy5.5, 1/100 (BD, 560657); anti-CD4-PECy7, 1/250 (BD, 552775); anti-CD8-PE, 1/250 (BD, 553033); anti-CD45R-FITC, 1/100 (BD, 553087).
10. Additional tubes with control (untreated) cells stained by single antibody only are required to allow proper instrument calibration (for details, see http://flowjo.typepad.com/the_daily_dongle/2017/03/demystifying-compensation-in-flowjo.html or http://www.drmr.com/compensation/indexDetail.html).
11. This step is very crucial: it is important to discard supernatant with a minimal loss of cells and to proceed in exactly the same way for all the tubes for adequate comparison.
12. Homogenate the bead solution immediately before distribution as beads will rapidly sediment to the bottom of the tube. It is important to distribute the same amount of beads in each experimental tube to ensure reliability and reproducibility of the results.
13. If the identification of lymphocyte subsets requires extensive centrifugation steps and treatments that may lead to loss of viable cells during the procedure (i.e., cell fixation/permeabilization for intracellular transcription factor staining), it is recommended to separate the cell counting procedure and the estimation of cell subset relative frequencies. After metabolic stress treatment, cells may therefore be divided in two tubes:
    (a) In tube 1, cells are mixed with viability dye and 6 μm polystyrene beads (for total viable cell counting).
    (b) Tube 2 is used for classical flow cytometry analysis (estimation of subset cell frequencies).

14. The plot FSC-H vs. FSC-A is used to discriminate doublets from single cells. In this plot, all events falling outside the diagonal are considered as a doublet. Doublet cells representing less than 5% of total cells can be ignored. If doublet cells represent more than 5% of total cells, the formula to calculate the number of cells in the population should be adapted as follow:

$$\text{Recovered cells per 1000 beads} = \frac{1000 \times (2 \times \text{nb of events in doublet cell gate} + \text{nb of events in single cell gate}) \times \%\text{studied cell subset}}{\text{Number of events in bead gate}}$$

Acknowledgments

The laboratory is supported by the European Regional Development Fund (ERDF), the Walloon Region (Wallonia-Biomed portfolio, 411132-957270), a Research Concerted Action of the Communauté Française de Belgique, a grant from the Fonds Jean Brachet, and a research credit from the National Fund for Scientific Research, FNRS, Belgium, and by the Belgian Program in Interuniversity Poles of Attraction initiated by the Belgian State, Prime Minister's office, Science Policy Programming. F.A. is a Research Associate at the FNRS. T.P. was supported by a FNRS/Télévie fellowship.

References

1. Suter M, Riek U, Tuerk R, Schlattner U, Wallimann T, Neumann D (2006) Dissecting the role of 5′-AMP for allosteric stimulation, activation, and deactivation of AMP-activated protein kinase. J Biol Chem 281:32207–32216
2. Viollet B, Horman S, Leclerc J, Lantier L, Foretz M, Billaud M et al (2010) AMPK inhibition in health and disease. Crit Rev Biochem Mol Biol 45:276–295
3. Hardie DG (2004) Minireview: the AMP-activated protein kinase cascade: the key sensor of cellular energy status. Endocrinology 144:5179–5183
4. Marsin A-S, Bouzin C, Bertrand L, Hue L (2002) The stimulation of glycolysis by hypoxia in activated monocytes is mediated by AMP-activated protein kinase and inducible 6-phosphofructo-2-kinase. J Biol Chem 277:30778–30783
5. Frauwirth KA, Riley JL, Harris MH, Parry RV, Rathmell JC, Plas DR et al (2002) The CD28 signaling pathway regulates glucose metabolism. Immunity 16:769–777
6. van der Windt GJW, Everts B, Chang C-H, Curtis JD, Freitas TC, Amiel E et al (2012) Mitochondrial respiratory capacity is a critical regulator of CD8+ T cell memory development. Immunity 36:68–78
7. Pearce EL, Poffenberger MC, Chang C-H, Jones RG (2013) Fueling immunity: insights into metabolism and lymphocyte function. Science 342:1242454
8. Andris F, Leo O (2015) AMPK in lymphocyte metabolism and function. Int Rev Immunol 34:67–81
9. Loftus RM, Finlay DK (2016) Immunometabolism: cellular metabolism turns immune regulator. J Biol Chem 291:1–10
10. Vuillefroy de Silly R, Dietrich P-Y, Walker PR (2016) Hypoxia and antitumor CD8(+) T cells: an incompatible alliance? Oncoimmunology 5:e1232236
11. Hirayama A, Kami K, Sugimoto M, Sugawara M, Toki N, Onozuka H et al (2009) Quantitative metabolome profiling of colon and stomach cancer microenvironment

by capillary electrophoresis time-of-flight mass spectrometry. Cancer Res 69:4918–4925

12. Ho P-C, Bihuniak JD, Macintyre AN, Staron M, Liu X, Amezquita R et al (2015) Phosphoenolpyruvate is a metabolic checkpoint of anti-tumor T cell responses. Cell 162:1217–1228
13. Chang C-H, Qiu J, O'Sullivan D, Buck MD, Noguchi T, Curtis JD et al (2015) Metabolic competition in the tumor microenvironment is a driver of cancer progression. Cell 162:1229–1241
14. Mayer A, Denanglaire S, Viollet B, Leo O, Andris F (2008) AMP-activated protein kinase regulates lymphocyte responses to metabolic stress but is largely dispensable for immune cell development and function. Eur J Immunol 38:948–956
15. Michalek RD, Gerriets VA, Jacobs SR, Macintyre AN, MacIver NJ, Mason EF et al (2011) Cutting edge: distinct glycolytic and lipid oxidative metabolic programs are essential for effector and regulatory CD4+ T cell subsets. J Immunol 186:3299–3303
16. Macintyre AN, Gerriets VA, Nichols AG, Michalek RD, Rudolph MC, Deoliveira D et al (2014) The glucose transporter Glut1 is selectively essential for CD4 T cell activation and effector function. Cell Metab 20:61–72
17. Zola H, Swart B, Banham A, Barry S, Beare A, Bensussan A et al (2007) CD molecules 2006 – human cell differentiation molecules. J Immunol Methods 319:1–5

Chapter 30

Methods to Evaluate AMPK Regulation of Macrophage Cholesterol Homeostasis

Nicholas D. LeBlond and Morgan D. Fullerton

Abstract

Macrophages are a driving force in the development and progression of atherosclerosis, a chronic condition that can lead to cardiovascular disease. In this chapter we describe methods that monitor macrophage cholesterol homeostasis such as cholesterol synthesis, uptake, and efflux, all with the use of AMPK activators and potential genetic models that could help shed light on the role of this metabolic regulator in atherosclerosis and other chronic diseases.

Key words Cholesterol homeostasis, Macrophages, Atherosclerosis, AMP-activated protein kinase, Reverse cholesterol transport

1 Introduction

Atherosclerosis is a chronic inflammatory disease preceding numerous acute coronary artery complications, the combination of which accounts for ~25% of deaths worldwide [1]. Macrophages are a key player in the progression and potential therapeutic targeting of atherosclerosis [2, 3]. Atherosclerotic plaque, in addition to other cell types, is recognized for the accumulation of cholesterol-rich, lipid-laden macrophages (termed "foam cells"). In response to environmental cues, plaque macrophages upregulate scavenger receptors that bind and internalize cholesterol-rich low-density lipoproteins (LDL) that have been modified (usually oxidized or aggregated). The LDL receptor-mediated uptake of lipoproteins is under intricate feedback mechanisms that tightly control the amount of cellular cholesterol taken into the cell. However, modification of LDL particles results in the unregulated uptake and retention of cholesterol within cytoplasmic lipid droplets [4], which can lead to plaque instability and rupture. Moreover, cellular lipid burden contributes to a vicious cycle of impaired lipid efflux, defective macrophage efferocytosis and egress, and can further promote the infiltration and activation of numerous adaptive and

Dietbert Neumann and Benoit Viollet (eds.), *AMPK: Methods and Protocols*, Methods in Molecular Biology, vol. 1732, https://doi.org/10.1007/978-1-4939-7598-3_30,

innate immune cells, hence furthering a pro-inflammatory plaque microenvironment [5, 6].

Macrophages are dynamic innate immune cells that have the tremendous ability to store, mobilize, and efflux cholesterol. There are numerous pathways that contribute to the process of exporting esterified cholesterol (stored as cholesteryl esters; CE); however, the ATP-binding cassette transporters, ABCA1 and ABCG1, are the main transport proteins that facilitate the efflux of free cholesterol to lipid-poor apolipoprotein A-1 (apoA-I) and high-density lipoprotein (HDL), respectively [7–9]. Macrophage cholesterol efflux, in the context of atherosclerosis, represents the first step in reverse cholesterol transport (RCT), the physiological process where cholesterol is removed from peripheral tissue for eventual recycling or elimination. This process is anti-atherogenic and has garnered intense therapeutic interest [10–13]. This chapter focuses on methods that are critical for monitoring macrophage cholesterol synthesis, uptake, and efflux and that have shed light on the importance of AMP-activated protein kinase (AMPK) in the past.

Playing a fundamental role in regulating energy metabolism, AMPK lies at the nexus of macrophage lipid homeostasis and inflammation. In macrophages (and most other myeloid-derived cells) AMPK is expressed exclusively as a α1β1γ1 heterotrimer [14]. Although the immunometabolic aspects of AMPK have been recently reviewed [15–17], some of the first evidence linking AMPK to a protective role in atherosclerosis used a macrophage cell line with the indirect and non-specific activator 5-aminoimidazole-4-carboxamide ribonucleotide (AICAR) [18]. The first in vivo evidence linking macrophage AMPK to a protection against atherogenesis used a myeloid AMPKα1 knockout crossed to the atherosusceptible LDL receptor knockout mouse, which demonstrated that myeloid AMPK regulates macrophage migration, adhesion, and ultimately content within atherosclerotic plaque, functions above and beyond some of the classically described roles [19]. However, the protective role for myeloid AMPK in atherosclerosis was recently challenged when myeloid AMPK α1 knockout mice were crossed to the apolipoprotein E (apoE)-deficient atherogenic background. In this model, AMPKα1 was shown to promote monocyte to macrophage differentiation, and the deletion of AMPK was linked to a defect in autophagy that diminished the number of plaque macrophages [20]. Although there are technical variations between the various in vivo publications, the role for macrophage AMPK in atherosclerosis remains unclear [19–22].

Atherosclerosis represents a complex chronic disease whose initiation and progression requires and affects numerous different cell types, and AMPK has been the focus of many non-macrophage investigations [15]. However, we recently reported that AMPK can regulate numerous aspects of macrophage cholesterol homeostasis in primary mouse macrophage, and moreover, activation of AMPK

had the protective effect of inhibiting foam cell formation through the induction of cholesterol efflux [23], suggesting a protective role for AMPK during atherogenesis. The methodological details of these experiments and notes pertaining to future AMPK-related work are explained below.

2 Materials

2.1 Isolation and Culture of Bone Marrow-Derived Macrophage (BMDM)

L929-Conditioned Medium

1. Class II biological safety cabinet (BSCII).
2. Bead bath (alternatively, hot water bath) set at 37 °C.
3. Humidified 5% CO_2 incubator at 37 °C.
4. 175 cm^2tissue culture flasks (T175).
5. Dulbecco's modified Eagle's medium (DMEM): DMEM containing 4.5 g/L glucose and 1 mM sodium pyruvate.
6. L929 medium: DMEM, 10% (v/v) heat-inactivated fetal bovine serum (FBS), 100 units/mL penicillin, and 100 μg/mL streptomycin.
7. Sterile 1× phosphate-buffered saline (PBS): 137 mM NaCl, 2.7 mM KCl, 10 mM Na_2HPO_4, 1.8 mM KH_2PO_4, pH 7.4.
8. 1× trypsin, 0.05% EDTA in PBS.
9. L929 murine fibroblast cell line (American Tissue Culture Collection).
10. 50 mL sterile conical tubes.
11. 0.22 μm sterile bottle-top filter.
12. Tabletop centrifuge capable of 4 °C refrigeration for 50 mL tubes.
13. Sterile 2 L bottle.

Bone Marrow-Derived Macrophage (BMDM) Isolation

14. Surgical scissors, forceps, and scalpel.
15. 70% (v/v) ethanol diluted in water.
16. Ketamine/xylazine cocktail: 150 mg/mL ketamine, 20 mg/mL xylazine.
17. 1 mL syringe.
18. 23-Gauge needle.
19. Sterile 0.5 and 1.5 mL microcentrifuge tube.
20. 18-Gauge needle.
21. 100 mm tissue culture plates.
22. 40 μm cell strainers fitted for 50 mL conical tube.

23. BMDM medium: DMEM containing 4.5 g/L glucose and 1 mM sodium pyruvate, 10% (v/v) heat-inactivated FBS, 100 units/mL penicillin, and 100 μg/mL streptomycin.
24. L929-conditioned medium.
25. Hemocytometer.
26. Trypan blue.
27. Benchtop microcentrifuge.
28. 2 cm cell scraper.

2.2 Cholesterol Synthesis (^{3}H-Acetate Incorporation)

1. Cells of interest: BMDM.
2. Class II biological safety cabinet (BSCII).
3. Bead bath (hot water bath) set at 37 °C.
4. Humidified 5% CO_2 incubator at 37 °C.
5. 12-Well tissue culture plates.
6. BMDM medium.
7. A-769662: 50 mM A-769662 in dimethyl sulfoxide (DMSO) (or AMPK activator of choice, *see* Table 1).
8. Sodium acetate (500 mM).
9. ^{3}H-Sodium acetate (75–150 mCi/mmol) (Perkin Elmer).
10. DMSO.
11. Sterile 1× PBS.
12. Sterile 1.5 mL microfuge tube.
13. 1 cm cell scraper.
14. Methanol/chloroform (2:1) (v/v).
15. Chloroform.
16. Double-distilled H_2O (ddH_2O).
17. Thin-layer chromatography (TLC) plates (silica gel 60).
18. Solvent system: heptane/isopropyl ether/acetic acid (60:40:3) (v/v/v).
19. Cholesterol standard.
20. Hamilton syringe.
21. Nitrogen gas.
22. Iodine crystals.
23. Flat-edged razor blade.
24. Weigh paper.
25. Scintillation cocktail.
26. 7 mL scintillation vials (or equivalent).
27. Scintillation counter (e.g., Tri-Carb 2910 TR, Perkin Elmer).
28. Bicinchoninic acid assay (BCA) protein determination kit (or equivalent assay).

2.3 Acetylated Low-Density Lipoprotein (acLDL) Uptake

1. Cells of interest: BMDM.
2. Class II biological safety cabinet (BSCII).
3. Bead bath (hot water bath) set at 37 °C.
4. 37 °C and 5% CO_2 cell incubator.
5. 24-Well tissue culture plates.
6. BMDM medium.
7. 1× PBS.
8. A-769662:100 μM A-769662 in DMSO (or AMPK activator of choice, *see* Table 1).
9. DMSO.
10. Recombinant human low-density lipoprotein (LDL) (Alfa Aesar).
11. Recombinant human acLDL (Alfa Aesar).
12. 1,1′-Dioctadecyl-3,3,3′,3′-tetramethylindocarbocyanine (Dil)-acLDL (Alfa Aesar).
13. Isopropyl alcohol.
14. Parafilm.

Table 1
Commonly used compounds for activating macrophage AMPK

Compound name	Mechanism of action	Working concentration	Reference
Metformin	↑AMP/ATP	0.2–2 mM	[24]
Berberine	↑AMP/ATP	5 μM	[25]
Resveratrol	↑AMP/ATP	0.1–10 μM	[26]
Troglitazone	↑AMP/ATP	10 μM	[27]
Phenformin	↑AMP/ATP	100 μM	[28]
Curcumin	↑AMP/ATP	0.5–10 μM	[29]
Thienopyridone (A-769662)	Allosteric activation/ inhibition of dephosphorylation	100 μM	[14, 23]
Salicylate	Allosteric activation	3 mM	[23]
5-Aminoimidazole-4-carboxamide ribonucleotide (AICAR)	AMP mimetic	0.1–2.5 mM	[18]
Benzimidazole (Compound 911)	Allosteric activation	Presumed to be 0.1–5 μM	Yet to be tested in macrophages
Compound 13	Allosteric activation	Presumed to be 10–100 μM	Yet to be tested in macrophages

15. Aluminum foil.
16. 1.5 mL microfuge tube.
17. Fluorometric plate reader (e.g., Biotek Synergy H1 plate reader).
18. Microplate for fluorescence based assays (96-well).
19. Scientific rocker.

2.4 Cholesterol Efflux

1. Cells of interest: BMDM.
2. Class II biological safety cabinet (BSCII).
3. Bead bath (hot water bath) set at 37 °C.
4. Humidified 5% CO_2 incubator at 37 °C.
5. 24-Well tissue culture plates.
6. 1× PBS.
7. Recombinant human acLDL (Alfa Aesar).
8. ^{3}H-Cholesterol (49 Ci/mmol) (Perkin Elmer).
9. Bovine serum albumin (BSA), fatty acid-free, low endotoxin (Sigma).
10. A-769662:50 mM A-769662 in DMSO (or AMPK activator of choice, *see* Table 1).
11. DMSO.
12. Recombinant human high-density lipoprotein (HDL) (Alfa Aesar).
13. Recombinant human apolipoprotein A-I (apoA-I) (Alfa Aesar).
14. Lipoprotein-deficient fetal bovine serum (LPDS) (Alfa Aesar).
15. BMDM medium.
16. Lipid loading medium: DMEM containing 4.5 g/L glucose and 1 mM sodium pyruvate, 5% (v/v) heat-inactivated LPDS, 50 μg/mL acLDL.
17. Equilibration medium: DMEM containing 4.5 g/L glucose and 1 mM sodium pyruvate, 5% (v/v) heat-inactivated LPDS, 0.2% BSA fatty acid free, low endotoxin (w/v).
18. HDL efflux medium: Equilibration medium supplemented with 50 μg/mL HDL.
19. ApoA-I efflux medium: Equilibration medium supplemented with 5 μg/mL ApoA-I.
20. Basal efflux medium: DMEM containing 4.5 g/L glucose and 1 mM sodium pyruvate, 5% (v/v) heat-inactivated LPDS, 0.2% BSA fatty acid free, low endotoxin (w/v).
21. NaOH: 0.1 M NaOH.
22. Scintillation cocktail.

23. 7 mL Scintillation vials (or equivalent).
24. Scintillation counter (e.g., Tri-Carb 2910 TR, Perkin Elmer).
25. Tabletop centrifuge capable of 4 °C refrigeration.

2.5 In Vivo Reverse Cholesterol Transport

1. Class II biological safety cabinet (BSCII).
2. Bead bath (hot water bath) set at 37 °C.
3. Humidified 5% CO_2 incubator at 37 °C.
4. 100 mm cell culture dishes.
5. 1× PBS.
6. Recombinant human acLDL (Alfa Aesar).
7. ^{3}H-Cholesterol (49 Ci/mmol) (Perkin Elmer).
8. A-769662: 50 mM A-769662 in DMSO (or AMPK activator of choice).
9. DMSO.
10. LPDS.
11. 2 cm cell scraper.
12. Trypan blue.
13. Hemocytometer.
14. 1 mL syringe.
15. 23-Gauge needle.
16. L929 medium.
17. BMDM medium.
18. 50 mL sterile conical tube.
19. 1.5 mL sterile microfuge tube.
20. Container with liquid nitrogen.
21. Scintillation cocktail.
22. 7 mL scintillation vials (or equivalent).
23. Scintillation counter (e.g., Tri-Carb 2910 TR, Perkin Elmer).

3 Methods

3.1 Isolation and Culture of BMDM

L929-Conditioned Medium

1. Seed L929 cells at a density of 3.0×10^3 in 50 mL of L929 medium in a T175 flask.
2. Incubate cells in a humidified 5% CO_2 incubator at 37 °C.
3. Once cells reach 80–100% confluency, let the flask incubate for 10 days (*see* **Note 1**).
4. Remove the media (volume will be slightly less than 50 mL) on day 10 and place in a sterile 50 mL conical tube.

5. Spin down the media at 1500 × *g* for 10 min to remove any detached cells.
6. Pool the medium collected from all flasks and filter-sterilize media using a 0.22 μm, bottle-top filter.
7. Aliquot and store L929-conditioned media at −80 °C.

BMDM Isolation

8. Anesthetize and euthanize mouse by overdose of ketamine (150 mg/kg) and xylazine (10 mg/kg) or equivalent locally approved protocol.
9. Spray the mouse with 70% ethanol.
10. Expose the musculature on each leg by removing the skin manually or with scissors (*see* **Note 2**).
11. Remove each exposed leg by gently cutting around the head of the femur to detach ligaments and musculature, while being careful not to cut or crack the femur (*see* **Note 3**).
12. Surgically remove all muscles from each leg (*see* **Note 4**), and then sever tendons between the tibia and femur (discard fibula).
13. When the bones are devoid of muscle, cut the ends off each of the bones, and then place the femur and tibia from one leg into a sterile 0.5 mL tube (which has had a hole punctured by a sterile 18-gauge needle at the very bottom).
14. Place the 0.5 mL microfuge tube containing bones in a sterile 1.5 mL tube, and add 100 μL of BMDM medium to the 0.5 mL tube.
15. Centrifuge the tubes on a benchtop microcentrifuge at 3000 × *g* for 5 min.
16. Dispose of 0.5 mL tube containing bones (*see* **Note 5**).
17. Add 900 μL of BMDM medium to the 1.5 mL microfuge tube containing the pelleted bone marrow and gently resuspend (*see* **Note 6**).
18. Pipette the resuspended bone marrow through a 40 μm cell strainer fixed on a sterile 50 mL conical tube.
19. Pass an additional 25 mL of BMDM medium through the 40 μm cell strainer.
20. Transfer the bone marrow media into a T175 flask containing 60 mL of BMDM medium (making the final volume 85 mL).
21. Incubate cells in a humidified 5% CO_2 incubator at 37 °C for 4 h so that differentiated cells adhere.
22. Add 15 mL of L929-conditioned medium to the T175 flask and mix thoroughly (*see* **Note 7**).

23. Plate bone marrow cells in 100 mm tissue culture plates (10 mL per plate) (*see* **Note 8**).
24. Incubate the cells in a humidified 5% CO_2 incubator at 37 °C for 7–8 days (*see* **Note 9**).
25. Following 7–8-day incubation, remove the media, wash once with 1× PBS, and then gently scrape cells in 2–3 mL BMDM medium.
26. Dilute cell suspension 1:1 in trypan blue and count the number of live cells using a hemocytometer.
27. Plate cells as necessary for future experiments.

3.2 ^{3}H-Acetate Incorporation into Cholesterol (Cholesterol Synthesis)

1. After BMDM have differentiated, seed cells at 5×10^5 in 12-well plates.
2. The following day, remove medium and wash the cells with 1× PBS (*see* **Note 10**).
3. Add 1 mL/well of BMDM medium containing 0.5 mM sodium acetate and 1 μCi/mL ^{3}H-sodium acetate.
4. Add 2 μL of a 50 mM A-769662 stock for a final concentration of 100 μM. Vehicle-treated wells should receive 2 μL of DMSO (other AMPK activators can be substituted as required; *see* Table 1 for partial list of AMPK agonist drugs previously used in macrophages) (*see* **Note 11**).
5. Incubate cells in a humidified 5% CO_2 incubator at 37 °C for the desired time (usually 4–16 h) (*see* **Note 12**).
6. Remove radioactive medium and wash twice with 1× PBS.
7. Scrape cells in 250 μL of PBS and remove 200 μL to a new 1.5 mL centrifuge tube (keep the remaining volume for protein determination).
8. Add 750 μL of methanol/chloroform (2:1) and vortex vigorously for 10 s.
9. Let sit on ice for ~10 min.
10. Add 250 μL of chloroform and vortex.
11. Add 250 μL of ddH_2O, vortex briefly, and spin at 3000 × *g* for 5 min.
12. Remove lower lipid phase and evaporate to dryness under a stream of nitrogen gas (*see* **Note 13**).
13. Resuspend samples in 20 μL of chloroform and spot onto a TLC plate with a Hamilton syringe, including a nonradioactive cholesterol standard (preferably in each lane).
14. Develop the TLC plate in a previously equilibrated TLC tank with heptane/isopropyl ether/acetic acid (60:40:3), until the solvent front is approximately 2 cm from the top of the plate.

15. Visualize the TLC plate by transferring plate to a new TLC tank containing iodine pellets (or by preferred visualization technique).
16. Mark the location of the cholesterol standard, and using a straight razor blade, scrape the silica onto a piece of weigh paper before transferring to a 7 mL scintillation vial.
17. Add 4–5 mL of scintillation fluid and count using a liquid scintillation counter (LSC).
18. Perform a bicinchoninic acid assay (BCA) with a protein determination kit (or equivalent protein quantification assay) of original cell suspension in1× PBS.
19. For BCA assay: prepare BSA (bovine serum albumin) protein serial dilutions ranging from 0 to 2 mg protein/mL for known protein standards.
20. Pipette 25 μL of each protein standard into a 96-well plate to generate a standard protein concentration curve (known protein value absorption vs. known concentration).
21. Pipette 25 μL of 1× PBS into the 96-well plate as a blank.
22. Pipette 25 μL of each experimental sample into the 96-well plate.
23. For each reaction, add 196 μL of reagent A to 4 μL of reagent B (20:1 ratio); scale this master mix to accommodate all standard, blank, and sample wells (in duplicate if preferable).
24. Add 200 μL of 20:1 working reagent (A + B) to each well.
25. Incubate at 37 °C for 30 min.
26. Read each samples absorbance at 562 nm on a microplate reader.
27. Generate a line of best fit for the absorbance value versus known protein concentrations for all the protein standards:

$$y = x + b$$

y = absorbance.
m = slope of line.
x = protein concentration.
$b = y -$ intercept where the line crosses the y axis.

28. Generate equation solving for "x":

$$x = (y - b)/m$$

29. Subtract the averaged absorbance value for the duplicates of 1× PBS samples from each experimental sample replicate.

30. Enter the average absorbance value from each experimental duplicate into the rearranged equation (as the *y*-value), and then proceed to solve equation to produce the known protein concentration.
31. Normalize disintegrations per minute (DPM) to milligram of protein for each sample (*see* **Note 14**).

3.3 acLDL Uptake

1. After BMDM have differentiated, seed cells at a density of 2.5×10^5 cells per 24-well.
2. The following day, remove medium and wash cells with 1× PBS.
3. Add 0.5 mL of BMDM medium containing 10 μg/mL Dil-acLDL, and incubate in a humidified 5% CO_2 incubator at 37 °C for 1–2 h.
4. Remove the medium and wash twice with 1× PBS.
5. Add 250 μL of isopropyl alcohol to each well, seal plates with parafilm, and cover with aluminum foil.
6. Incubate plate at room temperature for 10 min and then at 4 °C overnight with gentle rocking.
7. Collect isopropyl alcohol from each well in a 1.5 mL microfuge tube (*see* **Note 15**).
8. Load 70 μL on a fluorescence compatible 96-well plate.
9. Add a serial dilution of Dil-acLDL as standards to calibrate fluorescence, as well as non-Dil-acLDL loaded samples and isopropyl alcohol controls.
10. Read the plate using a fluorometric plate reader with an excitation of 545 nm and emission wavelength of 580 nm (or comparable fluorescent plate reader) (*see* **Note 16**).

3.4 Cholesterol Efflux

1. After BMDM have differentiated, seed cells at 2.5×10^5 cells/well in 24-well plates.
2. Incubate lipid-loading DMEM with 1 μCi/mL ^{3}H-cholesterol at 37 °C overnight to conjugate.
3. The following day, remove the media from the cells and wash with 1× PBS.
4. Add 0.5 mL of the lipid-loading medium supplemented with 1 μCi/mL ^{3}H-cholesterol to each well (*see* **Note 17**).
5. Incubate cells in a humidified 5% CO_2 incubator at 37 °C for 30 h to induce acLDL uptake and accumulation.
6. Remove the medium and wash the cells twice with 1× PBS to remove all exogenous lipid and radioactivity.
7. To allow time for the cholesterol pools to equilibrate, add 0.5 mL of equilibration medium.

8. Add 1 μL of 50 mM A-769662 stock for a final concentration of 100 μM or desired AMPK activator.
9. Incubate in a humidified 5% CO_2 incubator at 37 °C for 2–18 h (*see* **Note 18**).
10. Remove the medium and wash the cells twice with 1× PBS.
11. Initiate the efflux of cholesterol by adding 0.5 mL of HDL efflux medium, ApoA-I efflux medium, or strict BMDM efflux media as a control. Importantly, AMPK activators are either replenished or introduced at this step (*see* **Note 19**).
12. Incubate cells in a humidified 5% CO_2 incubator at 37 °C for 4–24 h (*see* **Note 20**).
13. Remove the medium from each condition into a 1.5 mL microfuge tube.
14. Spin down efflux media at 4000 × *g* for 15 min, and then transfer supernatant into a new 1.5 mL microfuge tube.
15. Pipette an aliquot of each efflux medium sample into a 7 mL scintillation vial containing 4 mL of liquid scintillation fluid.
16. Wash the plates twice with 1× PBS.
17. Lyse cells by adding 0.5 mL of 0.1 M NaOH to each well and place on rocker at 4 °C overnight.
18. Remove an aliquot of each cell suspension sample into a 7 mL scintillation vial containing 4 mL of liquid scintillation fluid.
19. Count all scintillation samples using LSC (*see* **Note 21**).
20. Calculate the percent cholesterol efflux of each sample by:

$$\text{Cholesterol Efflux} = \frac{\text{Radioactivity in medium}}{\text{Radioactivity in medium} + \text{Radioactivity in cells}} \times 100\%.$$

21. Calculate the percent-specific efflux to HDL by:

    % Specific Cholesterol HDL Efflux = HDL Efflux % − Basal Efflux %
22. Calculate the percent-specific efflux to ApoA-I by:

    % Specific Cholesterol ApoA-I Efflux = ApoA-I Efflux % − Basal Efflux %

3.5 In Vivo Reverse Cholesterol Transport

1. Plate differentiated BMDM at 5×10^6 cells in 100 mm plates.
2. Conjugate lipid-loading medium with 5 μCi/mL of ^{3}H-cholesterol overnight at 37 °C.
3. Lipid-load the cells by adding 10 mL of lipid-loading medium supplemented with 5 μCi ^{3}H-cholesterol to plated BMDMs.

4. Incubate cells in a humidified 5% CO_2 incubator at 37 °C for 30 h.
5. Cells can be treated simultaneously with AMPK activators (*see* **Note 22**).
6. Remove medium and wash twice with 1× PBS.
7. Add 2–3 mL of BMDM medium to each plate.
8. Gently scrape cells and place in 50 mL conical tube.
9. Dilute each genotype or treatment cell suspension 1:1 in trypan blue, and count the number of live cells using a hemocytometer.
10. Inject 8×10^6 cells into the intraperitoneal cavity (*see* **Note 23**) of a wild-type mouse (*see* **Note 24**).
11. Place at least one aliquot of cells (8×10^6 cells) from each experimental group into a 7 mL scintillation vial containing 4 mL of scintillation cocktail to determine the initial radioactivity of the injected cells.
12. Singly house mice after the injection, preferably in a cage with wire bottom or without bedding (for collection of feces).
13. Sample radioactivity in the serum by taking blood at 12 and 24 h post injection from the tail vein, and centrifuge at 4000 × *g* for 5 min. Add 10 μL of aliquot of serum to scintillation vial for LSC.
14. At 48 h post injection, sacrifice mice according to institutional recommendations (either CO_2 or a lethal anesthetic overdose to keep vasculature intact). Perform a cardiac puncture by opening the plural cavity to collect terminal (48 h) blood sample for serum.
15. Perfuse the entire circulation with 10 mL of 1× PBS via the left ventricle by making a cut in the right atrium.
16. Remove the liver and place into a 15 mL tube.
17. Digest in 10 mL of 0.1 M NaOH at 60 °C for 3 h.
18. Centrifuge debris at 14,000 × *g* for 10 min and count an aliquot of the supernatant via LSC.
19. Collect all fecal pellets produced by the mouse over the course of the 48 h experiment into a 50 mL tube.
20. Digest the feces in excess volume of 0.1 M NaOH at 60 °C for 3 h, followed by a 14,000 × *g* spin for 10 min.
21. Remove an aliquot of the supernatant to a scintillation vial and determine radioactivity via LSC.
22. Serum results are expressed as a percent of the initial radioactivity per mL of serum, whereas liver and feces results are expressed as a percent of the initial radioactivity.

4 Notes

1. Large volumes of L929-conditioned medium can be obtained by simply scaling up the number of T175 flasks. Typical batches of L929-conditioned medium can use upwards of 50 flasks, each containing 50 mL of media. In this case, it is important to decant and filter-sterilize all media into a large (sterile) bottle to ensure a homogenous preparation.
2. Cell recovery from the femur and tibia is typically sufficient; however, the humerus can also be isolated for collection of a larger quantity of the bone marrow.
3. If removal of the femur from the pelvis proves difficult, it is possible to cut the entire pelvis (a potential approach for those who have little experience with tissue dissections).
4. Kim wipes are very useful at this step, as the wipes act as sandpaper to remove the musculature off the bone.
5. After this spin, the bone marrow may still be visible with the bones. If this is the case, the 0.5 mL tube containing the bones can be placed into a fresh 1.5 mL tube (**steps 7** and **8** can be repeated).
6. Be careful not to suck up the cellular pellet within the pipette tip since this may sheer cells.
7. A final concentration of 20% L929 medium may be used if 15% is not providing sufficient macrophage differentiation in 7–8 days.
8. It is also possible to plate cells in 150 mm dishes with 20 mL media.
9. The described experiments take advantage of AMPK activators (Table 1), which are added post macrophage differentiation. Simultaneous bone marrow differentiation and AMPK activation would likely affect this process. Moreover, it is important to consider that when using AMPK-deficient mouse models, differentiation of hematopoietic progenitors can be impaired.
10. This protocol describes the use of media containing 10% FBS. Past works in other cell types and in other genetic models have serum-starved cells prior to conducting the ^{3}H-acetate incorporation experiment; however, although there are growth factors in FBS that affect AMPK, we have seen that serum starvation feeds back to induce AMPK activation. This complicates the use of additional AMPK activators. Therefore, these experiments are conducted in the presence of FBS.
11. Macrophages require higher concentrations of A-769662 as compared to hepatocytes, hence the use of 100 μM A-769662.

12. Longer time points could potentially skew interpretation given the metabolism of lipids into which ^{3}H-acetate has been incorporated. This may not reflect only synthesis.
13. At this point, the chloroform (lipid-containing) phase can be evaporated to dryness under a stream of nitrogen gas for TLC separation or saponified with KOH to extract ^{3}H-containing fatty acid and sterols, as described in other chapters of this issue.
14. To calculate the nmol incorporation of ^{3}H-acetate into cholesterol, use the molar amount of sodium acetate and the radioactivity in the initial media to determine specific activity.
15. If cell debris is present in tubes, this can be pelleted by centrifuging at 12,000 $\times$ *g* for 5 min and the supernatant transferred into a fresh 1.5 mL tube.
16. It is important to note that the uptake of Dil-acLDL can be assessed under any permutation of lipid-loaded and AMPK activation treatments. The protocol detailed above assesses Dil-acLDL uptake in basal BMDM. Past work has demonstrated that there is no difference between wild-type and AMPK β1-deficient macrophages in the presence or absence of A-769662 treatment.
17. Each respective plate should be done in triplicate independent of how many technical replicates within treatment groups. One plate is to be used to assess HDL-mediated efflux, one for ApoA-I-mediated efflux, and basal efflux (used to calculate the percent-specific efflux).
18. During the equilibration treatments, AMPK activators may be added to "prime" the system prior to the efflux phase of the experiment. Shorter equilibration times may be used ranging from 2 to 18 h.
19. It is important to consider that AMPK activator treatment and AMPK deficiency can and do alter total cellular cholesterol pools. For example, if A-769662 is added to macrophages during the initial lipid-loading phase, there is a significant reduction in total cholesterol content, which confounds the assessment of ^{3}H-cholesterol. For this reason, it is critical to also measure total cellular cholesterol pools when introducing new AMPK genetic models or pharmacological activators/inhibitors. To this point, timing of AMPK activator treatment can also be tailored to suit investigations into transcriptional vs. acute posttranslational effects by modulating overall treatment time.
20. Kinetics of cholesterol efflux in response to various AMPK activators can be observed by including numerous time points.
21. Scintillation vials can be left to equilibrate overnight and should be counted after at least 24 h.

22. In vivo reverse cholesterol transport assay can employ the use of wild-type or AMPK-deficient cells. In addition, AMPK activators can be used to "prime" cells prior to injection into the mice. In this case, it will be critical not only to assess initial radioactivity but also to determine cholesterol content in these cells.
23. Cells can also be delivered via subcutaneous injection.
24. This experiment can test the inherent capacity of cells from normal and AMPK-deficient mice, as well as normal and AMPK-activator-treated cells. However, there is also the potential to use identically treated wild-type cells injected into both wild-type and AMPK-deficient mice as recipients. This would test whether AMPK could regulate endogenous cholesterol acceptors (such as HDL and apoA-I).

References

1. Benjamin EJ, Blaha MJ, Chiuve SE, Cushman M, Das SR, Deo R, de Ferranti SD, Floyd J, Fornage M, Gillespie C, Isasi CR, Jimenez MC, Jordan LC, Judd SE, Lackland D, Lichtman JH, Lisabeth L, Liu S, Longenecker CT, Mackey RH, Matsushita K, Mozaffarian D, Mussolino ME, Nasir K, Neumar RW, Palaniappan L, Pandey DK, Thiagarajan RR, Reeves MJ, Ritchey M, Rodriguez CJ, Roth GA, Rosamond WD, Sasson C, Towfighi A, Tsao CW, Turner MB, Virani SS, Voeks JH, Willey JZ, Wilkins JT, Wu JH, Alger HM, Wong SS, Muntner P, American Heart Association Statistics C, Stroke Statistics S (2017) Heart disease and stroke statistics-2017 update: a report from the American Heart Association. Circulation 135(10): e146–e603. https://doi.org/10.1161/CIR.0000000000000485
2. Ross R (1999) Atherosclerosis is an inflammatory disease. Am Heart J 138(5 Pt 2): S419–S420
3. Moore KJ, Sheedy FJ, Fisher EA (2013) Macrophages in atherosclerosis: a dynamic balance. Nat Rev Immunol 13(10):709–721. https://doi.org/10.1038/nri3520
4. Tabas I (2002) Cholesterol in health and disease. J Clin Invest 110(5):583–590. https://doi.org/10.1172/JCI16381
5. Tabas I (2010) Macrophage death and defective inflammation resolution in atherosclerosis. Nat Rev Immunol 10(1):36–46. https://doi.org/10.1038/nri2675. nri2675 [pii]
6. Maxfield FR, Tabas I (2005) Role of cholesterol and lipid organization in disease. Nature 438(7068):612–621. https://doi.org/10.1038/nature04399
7. Aiello RJ, Brees D, Bourassa PA, Royer L, Lindsey S, Coskran T, Haghpassand M, Francone OL (2002) Increased atherosclerosis in hyperlipidemic mice with inactivation of ABCA1 in macrophages. Arterioscler Thromb Vasc Biol 22(4):630–637
8. Wang X, Collins HL, Ranalletta M, Fuki IV, Billheimer JT, Rothblat GH, Tall AR, Rader DJ (2007) Macrophage ABCA1 and ABCG1, but not SR-BI, promote macrophage reverse cholesterol transport in vivo. J Clin Invest 117 (8):2216–2224. https://doi.org/10.1172/JCI32057
9. Westerterp M, Murphy AJ, Wang M, Pagler TA, Vengrenyuk Y, Kappus MS, Gorman DJ, Nagareddy PR, Zhu X, Abramowicz S, Parks JS, Welch C, Fisher EA, Wang N, Yvan-Charvet L, Tall AR (2013) Deficiency of ATP-binding cassette transporters A1 and G1 in macrophages increases inflammation and accelerates atherosclerosis in mice. Circ Res 112(11):1456–1465. https://doi.org/10.1161/CIRCRESAHA.113.301086
10. Khera AV, Cuchel M, de la Llera-Moya M, Rodrigues A, Burke MF, Jafri K, French BC, Phillips JA, Mucksavage ML, Wilensky RL, Mohler ER, Rothblat GH, Rader DJ (2011) Cholesterol efflux capacity, high-density lipoprotein function, and atherosclerosis. N Engl J Med 364(2):127–135. https://doi.org/10.1056/NEJMoa1001689
11. Khera AV, Rader DJ (2013) Cholesterol efflux capacity: full steam ahead or a bump in the road? Arterioscler Thromb Vasc Biol 33 (7):1449–1451. https://doi.org/10.1161/ATVBAHA.113.301519

12. Larach DB, deGoma EM, Rader DJ (2012) Targeting high density lipoproteins in the prevention of cardiovascular disease? Curr Cardiol Rep 14(6):684–691. https://doi.org/10.1007/s11886-012-0317-3
13. Rader DJ, Tall AR (2012) The not-so-simple HDL story: is it time to revise the HDL cholesterol hypothesis? Nat Med 18 (9):1344–1346. https://doi.org/10.1038/nm.2937. nm.2937 [pii]
14. Galic S, Fullerton MD, Schertzer JD, Sikkema S, Marcinko K, Walkley CR, Izon D, Honeyman J, Chen ZP, van Denderen BJ, Kemp BE, Steinberg GR (2011) Hematopoietic AMPK beta1 reduces mouse adipose tissue macrophage inflammation and insulin resistance in obesity. J Clin Invest 121 (12):4903–4915. https://doi.org/10.1172/JCI58577
15. Fullerton MD, Steinberg GR, Schertzer JD (2013) Immunometabolism of AMPK in insulin resistance and atherosclerosis. Mol Cell Endocrinol 366(2):224–234. https://doi.org/10.1016/j.mce.2012.02.004
16. O'Neill LA, Hardie DG (2013) Metabolism of inflammation limited by AMPK and pseudo-starvation. Nature 493(7432):346–355. https://doi.org/10.1038/nature11862
17. Day EA, Ford RJ, Steinberg GR (2017) AMPK as a therapeutic target for treating metabolic diseases. Trends Endocrinol Metab. https://doi.org/10.1016/j.tem.2017.05.004
18. Li D, Wang D, Wang Y, Ling W, Feng X, Xia M (2010) Adenosine monophosphate activated protein kinase induces cholesterol efflux from macrophage-derived foam cells and alleviates atherosclerosis in apolipoprotein E-deficient mice. J Biol Chem 285(43):33499–33509. https://doi.org/10.1074/jbc.M110.159772. M110.159772 [pii]
19. Cao Q, Cui X, Wu R, Zha L, Wang X, Parks JS, Yu L, Shi H, Xue B (2016) Myeloid deletion of alpha1AMPK exacerbates atherosclerosis in low density lipoprotein receptor knockout (LDLRKO) mice. Diabetes. https://doi.org/10.2337/db15-0917
20. Zhang M, Zhu H, Ding Y, Liu Z, Cai Z, Zou MH (2017) AMP-activated protein kinase alpha1 promotes atherogenesis by increasing monocyte-to-macrophage differentiation. J Biol Chem. https://doi.org/10.1074/jbc.M117.779447
21. Pinkosky SL, Newton RS, Day EA, Ford RJ, Lhotak S, Austin RC, Birch CM, Smith BK, Filippov S, Groot PH, Steinberg GR, Lalwani ND (2016) Liver-specific ATP-citrate lyase inhibition by bempedoic acid decreases LDL-C and attenuates atherosclerosis. Nat Commun 7:13457. https://doi.org/10.1038/ncomms13457
22. Wang J, Ma A, Zhao M, Zhu H (2017) AMPK activation reduces the number of atheromata macrophages in ApoE deficient mice. Atherosclerosis 258:97–107. https://doi.org/10.1016/j.atherosclerosis.2017.01.036
23. Fullerton MD, Ford RJ, McGregor CP, LeBlond ND, Snider SA, Stypa SA, Day EA, Lhotak S, Schertzer JD, Austin RC, Kemp BE, Steinberg GR (2015) Salicylate improves macrophage cholesterol homeostasis via activation of Ampk. J Lipid Res 56(5):1025–1033. https://doi.org/10.1194/jlr.M058875
24. Kim J, Kwak HJ, Cha JY, Jeong YS, Rhee SD, Kim KR, Cheon HG (2014) Metformin suppresses lipopolysaccharide (LPS)-induced inflammatory response in murine macrophages via activating transcription factor-3 (ATF-3) induction. J Biol Chem 289 (33):23246–23255. https://doi.org/10.1074/jbc.M114.577908
25. Jeong HW, Hsu KC, Lee JW, Ham M, Huh JY, Shin HJ, Kim WS, Kim JB (2009) Berberine suppresses proinflammatory responses through AMPK activation in macrophages. Am J Phys Endocrinol Metab 296(4):E955–E964. https://doi.org/10.1152/ajpendo.90599.2008
26. Buttari B, Profumo E, Segoni L, D'Arcangelo D, Rossi S, Facchiano F, Saso L, Businaro R, Iuliano L, Rigano R (2014) Resveratrol counteracts inflammation in human M1 and M2 macrophages upon challenge with 7-oxo-cholesterol: potential therapeutic implications in atherosclerosis. Oxidative Med Cell Longev 2014:257543. https://doi.org/10.1155/2014/257543
27. Tsai JS, Chuang LM, Chen CS, Liang CJ, Chen YL, Chen CY (2014) Troglitazone and Delta2Troglitazone enhance adiponectin expression in monocytes/macrophages through the AMP-activated protein kinase pathway. Mediat Inflamm 2014:726068. https://doi.org/10.1155/2014/726068
28. Namgaladze D, Snodgrass RG, Angioni C, Grossmann N, Dehne N, Geisslinger G, Brune B (2015) AMP-activated protein kinase suppresses arachidonate 15-lipoxygenase expression in interleukin 4-polarized human macrophages. J Biol Chem 290 (40):24484–24494. https://doi.org/10.1074/jbc.M115.678243
29. Lin XL, Liu MH, HJ H, Feng HR, Fan XJ, Zou WW, Pan YQ, Hu XM, Wang Z (2015) Curcumin enhanced cholesterol efflux by upregulating ABCA1 expression through AMPK-SIRT1-LXRalpha signaling in THP-1 macrophage-derived foam cells. DNA Cell Biol 34 (9):561–572. https://doi.org/10.1089/dna.2015.2866

Chapter 31

Modulation of Vascular Function by AMPK: Assessment of NO Bioavailability and Surrogates of Oxidative Stress

Swenja Kröller-Schön, Andreas Daiber, and Eberhard Schulz

Abstract

The endothelium plays a pivotal role in the development of vascular disease. Decreased bioavailability of nitric oxide, a condition known as "endothelial dysfunction," is considered an early step in this process before atherosclerotic changes of the vessel wall occur. Endothelium-derived nitric oxide (•NO) may be rapidly scavenged by superoxide anions; therefore, the equilibrium between •NO production on one hand and its inactivation by oxidative stress on the other hand is of particular interest. Metabolic enzyme systems such as AMP-activated protein kinase (AMPK) may affect the cellular production of •NO or reactive oxygen species (ROS), while AMPK activity itself can also be modulated by ROS. Therefore, the analysis of •NO as well as ROS levels is essential to understand how metabolism regulating enzymes like AMPK may modulate vascular disease.

Key words Reactive oxygen species, Nitric oxide, Endothelial function, Electron paramagnetic resonance spectroscopy, Amplex red, Dihydroethidium staining, Peroxynitrite, Tyrosine nitration

1 Introduction

In a healthy vessel, nitric oxide (•NO) produced by the endothelial nitric oxide synthase (eNOS) causes vasodilation, while it prevents the infiltration of inflammatory cells and thrombus formation. In order to assess endothelial function, the easiest way is to analyze vasodilation in response to endothelial-dependent stimulators such as acetylcholine (e.g., by isometric tension studies of isolated vascular rings). However, these functional studies require a high level of handling experience especially in small vessels (e.g., mouse aorta) in order to prevent injury during the preparation process. Another option is the specific analysis of •NO bioavailability by electron paramagnetic resonance (EPR) spectroscopy using Fe(II)$(DETC)_2$ as spin trap [1]. EPR spectroscopy is used to study compounds with unpaired electrons such as free radicals or paramagnetic metal species. Since most radicals like •NO have a short half-life, their reaction with another compound (as Fe(II)$(DETC)_2$

Dietbert Neumann and Benoit Viollet (eds.), *AMPK: Methods and Protocols*, Methods in Molecular Biology, vol. 1732, https://doi.org/10.1007/978-1-4939-7598-3_31,

in the case of •NO) is used for spin trapping as this more stable adduct formation allows measurement of •NO at a specific point in time.

Oxidative stress is the most important pathological modulator of endothelial function as •NO may react with superoxide anions under formation of peroxynitrite ($ONOO^-$) [2]. Peroxynitrite and its derived free radicals in turn are highly reactive compounds that may cause protein modifications such as nitration of tyrosine residues [3, 4]. Therefore, tyrosine nitration can be used as a surrogate for $ONOO^-$ levels in the vessel and as an estimate whether oxidative stress plays a functional role with respect to •NO scavenging. Here we describe a method that utilizes the dot blot technique for a quantitative analysis of this interaction. As soon as endothelial dysfunction is present and increased 3-nitrotyrosine levels are observed, the level of oxidative stress in the vasculature should be assessed for a thorough understanding of vascular pathology. Since ROS assays usually have limitations with respect to their sensitivity (e.g., EPR-based assays) or specificity (e.g., chemiluminescence compounds such as lucigenin), it is important to combine at least two different methods.

In this chapter, we will therefore describe two assays (dihydroethidium cryo-staining and Amplex red assay) that can be used for this purpose. Dihydroethidium is a compound that reacts with $\bullet O_2^-$ to form 2-hydroxyethidium, which intercalates with endogenous DNA and causes red fluorescence [5]. By fluorescence microscopy, the local $\bullet O_2^-$ production can be visualized and analyzed within the different vascular layers (endothelium, media, adventitia) [6]. Of note, without the additional use of superoxide dismutase and successful suppression of the fluorescence signal, a part of dihydroethidium cryo-staining can originate from "unspecific" oxidation and formation of ethidium. Therefore, it is more accurate to define the dihydroethidium cryo-staining signal as overall vascular ROS formation. The strengths of the assay are a good sensitivity and spatial resolution of vascular ROS production, while the semiquantitative analysis is a weakness.

The Amplex red assay utilizes a horseradish peroxidase catalyzed oxidation of the non-fluorescent substrate by H_2O_2 to form resorufin that can be detected by fluorescence plate reader or HPLC assays as described in detail below [7]. This assay has a good sensitivity and specificity for H_2O_2 but is not useful if ROS other than H_2O_2 play a role in vascular pathology (e.g., the signal is even diminished when high superoxide formation rates are obtained as in activated granulocytes).

2 Materials

Prepare all solutions using ultrapure water (prepared by purifying deionized water, to attain a sensitivity of 18 MΩ/cm at 25 °C) and

analytical grade reagents. Prepare and store all reagents at room temperature (unless indicated otherwise). Diligently follow all waste disposal regulations when disposing waste materials.

2.1 Vascular Nitric Oxide Analysis by EPR Spectroscopy with Fe (II)(DETC)$_2$ as Spin Trap

1. Argon gas.
2. Phosphate buffered saline (PBS): 145 mM NaCl, 2.7 mM KCl, 1.5 mM KH_2PO_4, 8 mM Na_2HPO_4, pH 7. Aerate PBS in a conical tube for 30 min with argon gas.
3. $FeSO_4$ solution: 1.49 M $FeSO_4$. Weigh 3.4 mg of Fe(II)SO_4 and put it in a 50 mL conical tube. Add 15 mL of the PBS solution to the $FeSO_4$ and mix thoroughly. The $FeSO_4$ has to be dissolved completely. Aerate the solution for another 30 min with argon gas.
4. DETC solution: 1.62 M DETC. Weigh 5.4 mg of DETC (diethyldithiocarbamic acid) and put it in a 50 mL conical tube. Add 15 mL of PBS to the DETC and mix thoroughly. The DETC has to be resolved completely. Aerate the solution for another 30 min with argon gas.
5. Krebs-Hepes buffer (KH): 99.01 mM NaCl, 4.69 mM KCl, 2.5 mM $CaCl_2$, 1.2 mM $MgSO_4$, 25 mM $NaHCO_3$, 1.03 mM K_2HPO_4, 20 mM sodium-Hepes, 11.1 mM D-glucose, adjust pH to 7.35 (*see* **Note 1**).
6. Ca ionophore: 10 mM Ca ionophore. Ca ionophore stock solution solved in dimethyl sulfoxide (DMSO) should be thawed and stored at room temperature till usage.
7. 1 mL syringes: remove the small end of 1 mL syringes and the small end of the plunger inside of the syringe. Label every syringe according to the treatment group.
8. EPR machine (e.g., Magnettech, Berlin).
9. Plastic ware: 1 m syringes (removed caps).

2.2 Amplex Red Assay for the Detection of Hydrogen Peroxide

1. Master mix: 20 μM myxothiazol, 100 μM Amplex red, 0.2 μM horseradish peroxidase (HRP). For preparation to 250 μL of PBS (w/o Ca/Mg), add 1.25 μL of myxothiazol (4 mM in DMSO), 0.5 μL of Amplex red solution (100 μM), and 0.5 μL of HRP (100 μM). Prepare master mix in a conical tube (volumes are meant per sample!).
2. H_2O_2 standard solution: 10 μM H_2O_2 (30% H_2O_2 = 10 M) in 150 μL master mix.
3. Buffer sample: 250 μL of PBS in a HPLC vial.
4. Organic solvent: 90% acetonitrile/10% water (v/v).
5. Mobile phase: 50 mM citrate buffer, pH 2.2.
6. HPLC setup: we are using a system that consists of a control unit, two pumps, a mixer, detectors, a column oven, a degasser,

an autosampler (AS-2057 plus) from Jasco (Groß-Umstadt, Germany), and a C_{18} Nucleosil 100-3 (125/4) column from Macherey and Nagel (Düren, Germany).

2.3 Dihydroethidium (DHE) Staining for the Detection of Superoxide Anions in Vascular Cryosections

1. Krebs-Hepes buffer (KH).
2. Aprotinin: 1 mg/mL H_2O (stock solution).
3. Pepstatin: 2 mg/mL EtOH (stock solution).
4. Leupeptin 5 mg/mL H_2O (stock solution).
5. Krebs-Hepes inhibitory buffer (KH-I): KH, 10 μg/mL aprotinin, 8 μg/mL pepstatin, 5 μg/mL leupeptin. Take 100 μL of aprotinin, 40 μL of pepstatin, and 10 μL of leupeptin, and fill up to 10 mL with KH buffer (*see* **Note 2**).
6. Dihydroethidium (DHE): 1 μM DHE in PBS. Since DHE is UV sensitive, it is essential to use dark 1.5 mL tube cups. For preparation we suggest to start with a stock solution of 5 mM DHE in DMSO. To get a final concentration of 1 μM DHE in PBS, different dilution steps are necessary, e.g.:
   - Dilute 20 μL stock solution (5 mM) with 80 μL of DMSO to get a 1 mM solution (1:5).
   - Dilute 20 μL of the 1 mM solution with 80 μL of DMSO and 100 μL of PBS to get a 100 μM solution (1:10).
   - Dilute 20 μL of the 100 μM solution with 180 μL of PBS to get a 10 μM solution (1:10).
   - To get the final concentration of 1 μM, dilute 100 μL of the 10 μM solution with 900 μL of PBS. The 1 μM solution is the working solution which is used on the aortic cryosections (*see* **Note 3**).

2.4 Assessment of Protein Nitration via Dot Blot Technique

1. SDS solution: 10% sodium dodecyl sulfate (SDS) in PBS.
2. Wash buffer (PBS-T): PBS, 0.1% (v/v) Tween-20.
3. Blocking buffer: (PBS +5% milk): PBS, 5% milk powder.
4. Antibody: anti-nitrotyrosine antibody (e.g., millipore 05-233). Antibody solution should be freshly prepared at 1 μg/ml in PBS + 5% milk (*see* **Note 4**).
5. Contents to determine protein concentrations for standard Bradford assay or Lowry assay.
6. S-Monovettes for plasma preparation.
7. Homogenization buffer (Hg buffer): 20 mM Tris-HCl, 250 mM sucrose, 3 mM EGTA, 20 mM EDTA.
8. Homogenization solution (Hg solution): 0.5 mM PMSF, 2.5 mM sodium fluoride, 0.5 mM sodium vanadate, 1% (v/v) Triton-X in Hg buffer (see above). Add appropriate amount of phosphatase inhibitory cocktail and protease inhibitory cocktail.

3 Methods

Carry out all procedures at room temperature unless otherwise specified.

3.1 Vascular Nitric Oxide Analysis by EPR Spectroscopy with Fe (II)$(DETC)_2$ as Spin Trap

For good results you should perform every step very clean and quickly. Be prepared with everything you will need for the following steps.

3.1.1 Sample Preparation

1. Remove all connective tissue as well as vascular fat tissue from aortic sections. Dissect the aorta into pieces of 5 mm.
2. Put 1 mL of KH in each well of a 12-well plate, and add two aortic sections of 5 mm into every well (two pieces per well).
3. Add 2 μL of the Ca ionophore to the solution and indirectly to the aortic sections (*see* **Note 5**).
4. Add the prepared 15 mL of $FeSO_4$ solution quickly to the 15 mL of DETC solution, and mix it carefully. Avoid too much bubbling (*see* **Note 6**).
5. Give 1 mL of the $FeSO_4$/DETC solution to each well.
6. Incubate the samples for 1 h at 37 °C.
7. After incubation of the samples, the aortic rings are embedded in KH *inside of the capless syringes*: put 200 μL of KH into the syringe; withdraw it with air to 700 μL. Avoid air bubble inside of the solution. Freeze it upside down in liquid nitrogen.
8. Clean the syringe with a wipe from condensed water.
9. Add 100 μL of KH without air bubbles, and put two pieces of the aortic sections to this solution using forceps, and freeze the syringe again upside down in liquid nitrogen. This makes sure that the solutions are fixed in the syringe.
10. Clean the syringe with a wipe from condensed water.
11. Add again 160 μL of KH to the syringe.
12. Freeze the syringe again upside down in liquid nitrogen.

3.1.2 Measurement

1. Apply the following parameters: B_0-field: 3274 G, sweep = 110 G, sweep time = 60 s, modulation = 7000 mG, power = 10 mW.
2. Cool down the EPR tube with liquid nitrogen.
3. Remove sample carefully out of the capless syringe by pushing the plunger without breakage, and transfer it to the EPR tube.
4. Fill up the EPR tube with liquid nitrogen, and cover everything with cotton batting.

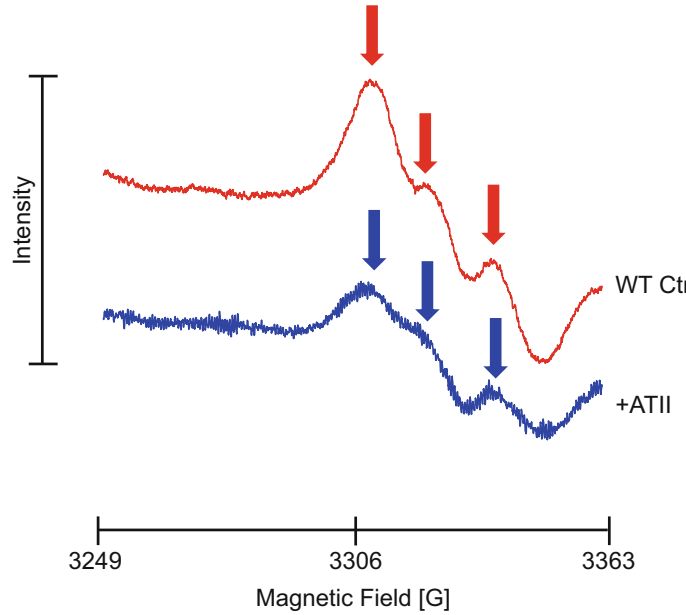

Fig. 1 NO quantification by EPR using Fe(II)$(DETC)_2$. Representative EPR spectra of aortic sections; angiotensin II in vivo treatment was used to establish endothelial dysfunction with diminished NO bioavailability. EPR-based NO analysis from untreated mouse aorta shows the characteristic triplet signal (highlighted by the red arrows), which is significantly weaker after in vivo angiotensin II treatment (highlighted by the blue arrows). Figure modified from [8], Copyright © 2014, Mary Ann Liebert, Inc.

5. Transfer the tube to the EPR machine and start the measurement. Figure 1 shows representative EPR tracings from murine aortic rings treated with and without angiotensin II, a potent stimulator of ROS production that results in diminished vascular •NO levels.

3.2 Amplex Red Assay for the Detection of Hydrogen Peroxide

This is an HPLC method. You should prepare all solutions using ultrapure water and analytical grade reagents.

1. Remove all connective tissue as well as vascular fat from aortic sections. Cut the aorta into pieces of 3 mm in length. One sample consists of two pieces (*see* **Note 7**).
2. Transfer two pieces of the aortic sections to one 1.5 mL tube; add 150 µL of master mix. Make sure that the sections are completely covered with solution.
3. Incubate the samples for 20 min on a shaker at 37 °C, 500 rpm.

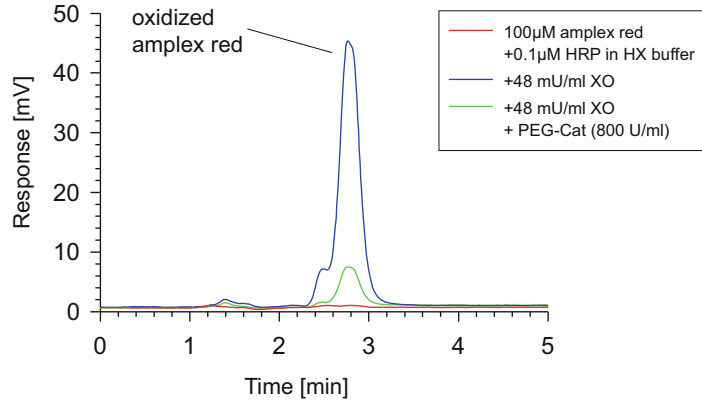

Fig. 2 Amplex red/HRP assay: HPLC tracings. Characteristic HPLC tracings obtained from the Amplex red/HRP assay. The red line shows the negative control (only hypoxanthine added); the blue line shows the oxidized Amplex red signal (ROS generated in vitro by addition of xanthine oxidase) at the retention time of 2.8 min. Addition of PEG catalase in order to remove H_2O_2 from the system diminished the signal (green line)

4. After 20 min remove the samples from the heater at the same time, and transfer the solution to the HPLC vials. Make sure that the aortic sections remain in the 1.5 mL tube.
5. Measure the standard, the buffer sample, and your unknown samples in the HPLC machine using the following settings: a high-pressure gradient is employed with the organic solvent **B** (90 vv% acetonitrile/10 vv% water) and aqueous solvent **A** (50 mM citrate buffer pH 2.2) as mobile phases with the following percentages of the organic solvent **B**: 0 min, 41%; 7 min, 45%; 8–9 min, 100%; 10–12 min, 41% (linear gradient increases within the indicated time windows). The remaining percentages of the mobile phase are the aqueous buffer **B**. The flow should be 1 mL/min, compounds are detected by their absorption at 300 nm, and resorufin is also detected by fluorescence (Ex. 570 nm/Em. 590 nm). Inject 50 μL of the sample to the HPLC system. Typical retention time of resorufin is 2.8 min, and its formation is sensitive to the presence of catalase (Fig. 2).

3.3 Dihydroethidium (DHE) Staining for the Detection of Superoxide Anions in Vascular Cryosections

DHE is a UV-sensitive compound. For the next method, it is necessary to use dark reaction cups, and every step using the compound or the solutions should be done in a darkened room.

3.3.1 Sample Preparation

1. Remove all connective tissue as well as vascular fat tissue from aortic sections. Dissect the aorta into pieces of 3 mm.
2. Prepare one 1.5 mL tube by adding 500 μL of KH-I for each sample.
3. Add one aortic section per tube and incubate for 10 min at 37 °C.
4. Prepare aluminum foil cups for embedding the aortic section. Be sure that the size of the so formed cups is small enough to fit into the storage cups.
5. Fill up the aluminum foil cups with Tissue-Tek O.C.T. compound.
6. After incubation the aortic sections are embedded in a matrix for cryostat sectioning. Therefore remove the aortic section out of the incubation cups, remove the remaining buffer out of the rings, and put them upright into the prepared Tissue-Tek filled cups.
7. Freeze the cups carefully over liquid nitrogen (*see* **Note 8**).
8. If the Tissue-Tek O.C.T. is totally frozen, remove the aluminum foil and store the sample at −80 °C.
9. For microscopical analysis and DHE staining, the prepared aortic samples are cut in 8 μm sections using a cryotome and transferred to microscope slides.
10. Warm the microscope slide with your finger to fix the aortic section.

3.3.2 DHE Staining

The DHE dye is light sensitive. Working in a dark or at least shaded room is preferred.

1. Thaw the microscope slides and put 1 mL of the 1 μM DHE working solution on the slide and incubate for 30 min at 37 °C.
2. After 30-min incubation, remove the surplus solution and cover the samples with a coverslip.
3. Take the pictures using a fluorescence microscope. Figure 3 shows representative DHE staining obtained from murine aortic sections. When compared to the control group, global AMPKα1 deficiency significantly increased red fluorescence as an indicator of increased oxidative stress.

3.4 Assessment of Protein Nitration via Dot Blot Technique

1. Prepare EDTA plasma samples using S-Monovettes according to the manufacturer's protocol, and determine the protein concentration of each sample (*see* **Note 9**).

3.4.1 Preparation of Plasma Samples

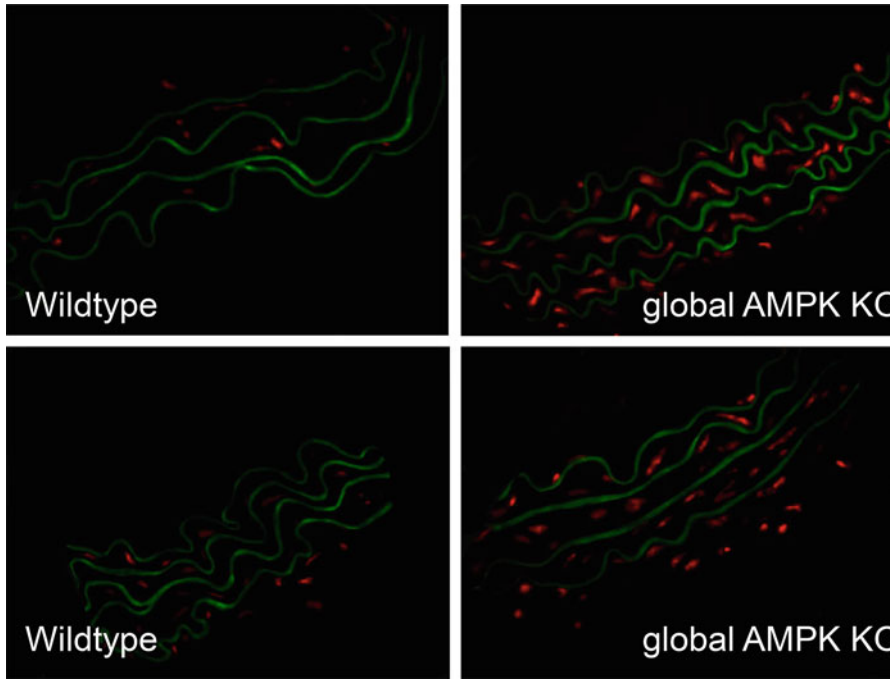

Fig. 3 Visualization of vascular superoxide production by DHE staining. Dihydroethdium-stained aortic cryosections from wildtype mice are shown on the left side. Aortas from α1AMPK knockout mice displayed increased oxidative stress in all layers of the vascular wall as indicated by the intense red fluorescence signal

3.4.2 Preparation of Tissue Samples

1. Homogenate frozen tissue samples on liquid nitrogen using a mortar and pestle. Tissue should be completely pulverized.
2. Transfer the samples to a 1.5 mL tube and dilute with Hg solution. Volume of Hg solution should correlate with the amount of powder.
3. Resuspend the tissue powder thoroughly.
4. Centrifuge at 10,000 × *g* for 10 min at 4 °C.
5. Transfer the supernatant to a new 1.5 mL tube and discard the cell debris.
6. Proteins are solved in the supernatant.

3.4.3 Assay

1. Determine the protein content of each plasma sample according to standard Bradford or Lowry assay.
2. Adjust the protein concentration of each sample to 0.5 μg/μL with PBS (prepare enough sample volume to have 50 μg protein per dot, application of 100 μL per dot).
3. Add the appropriate volume of 10% SDS to get a final concentration of 0.01% SDS per sample.
4. Samples can be stored at −20 °C or used immediately.

3.4.4 Dot Blot

1. Prepare the filter paper and the nitrocellulose membrane for dot botting by equalizing both in PBS for 5 min.
2. Samples should be stored on ice till finale usage.
3. Vortex samples thoroughly before usage.
4. Apply 200 μL of PBS to each dot to purge the system. Make sure that the solutions are gone before moving to the next step (*see* **Note 10**).
5. Apply 100 μL of the samples slowly in the center of the grid. Avoid air bubbles which are preventing the normal flow-through (*see* **Note 11**).
6. Apply 200 μL of PBS to each dot again to purge the system. Make sure that the solutions are gone before moving to the next step.
7. Let the lift pump work for another 10 min.
8. Remove the filter paper and let the nitrocellulose membrane dry for 60 min at 60 °C.
9. Block the membrane with PBS + 5% milk for 1 h at room temperature.
10. Incubate the antibody in PBS + 5% milk overnight at 4 °C. Antibody concentration 1 μg/mL.
11. Wash the membrane five times for 5 min at room temperature with PBS-T.
12. Incubate the secondary antibody according to the manufacturer's protocols in PBS + 5% milk for 2 h at room temperature.
13. Wash the membrane five times for 5 min at room temperature with PBS-T.
14. Detect the membrane with chemiluminescent detection reagents of choice.

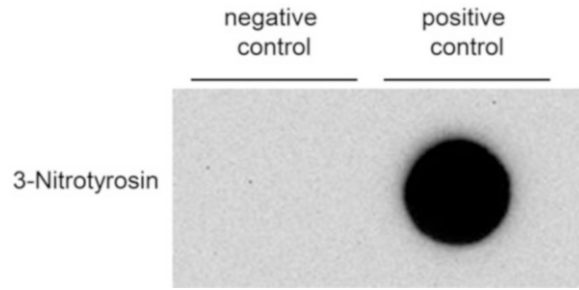

Fig. 4 Tyrosine nitration as a measure of peroxynitrite formation (dot blot). Dot blot signals of bovine serum albumin samples without pretreatment (negative control) and with peroxynitrite (100 mM) preincubation as a positive control

15. Expose to film or analyze with a chemiluminescent detection system.
16. For quantification purposes, a densitometric analysis of each dot is preferred. Figure 4 shows a dot blot of control (negative control) and nitrosylated EDTA plasma samples (positive control).

4 Notes

1. Krebs-Hepes buffer can be prepared 1 day before usage, but adjustment of pH should be done right before usage.
2. Krebs-Hepes inhibitory buffer should be prepared freshly every day.
3. Since dihydroethidium is a fluorescent dye dissolved in pure DMSO, the dilutions have to be prepared freshly before use.
4. Antibodies can be reused. After first usage, add sodium azide (6% solution) at a final concentration of 0.03% and store it at 4 °C.
5. Endothelium-denuded aortic sections can be used as a negative control.
6. Repeater pipette (e.g. Eppendorf®) is useful to allow a quick addition of the $Fe(II)(DETC)_2$ for several samples.
7. If the aortic segments are shorter than 3 mm in length, a total of three pieces per sample may be used. Since radicals are highly reactive species and proteins are still biologically active, preparation steps and sample handling should be done quickly.
8. If the freezing process is too fast, the matrix for cryosectioning (e.g., Tissue-Tek O.C.T.) will break and the sample is lost.
9. Centrifuge S-Monovettes for 10 min/1600 × *g* at room temperature.
10. Make sure that the sample volumes are flown through before moving to the next step.
11. Do not puncture the membrane while applying the sample to the grid.

References

1. Kleschyov AL, Mollnau H, Oelze M, Meinertz T, Huang Y, Harrison DG, Munzel T (2000) Spin trapping of vascular nitric oxide using colloid Fe(II)- diethyldithiocarbamate. Biochem Biophys Res Commun 275:672–677
2. Kissner R, Nauser T, Bugnon P, Lye PG, Koppenol WH (1997) Formation and properties of peroxynitrite as studied by laser flash photolysis, high-pressure stopped-flow technique, and pulse radiolysis. Chem Res Toxicol 10:1285–1292
3. Beckman JS, Koppenol WH (1996) Nitric oxide, superoxide, and peroxynitrite: the good, the bad, and ugly. Am J Physiol 271: C1424–C1437

4. Zou M, Martin C, Ullrich V (1997) Tyrosine nitration as a mechanism of selective inactivation of prostacyclin synthase by peroxynitrite. Biol Chem 378:707–713
5. Rothe G, Valet G (1990) Flow cytometric analysis of respiratory burst activity in phagocytes with hydroethidine and 2′,7′-dichlorofluorescin. J Leukoc Biol 47:440–448
6. Miller FJ Jr, Gutterman DD, Rios CD, Heistad DD, Davidson BL (1998) Superoxide production in vascular smooth muscle contributes to oxidative stress and impaired relaxation in atherosclerosis. Circ Res 82:1298–1305
7. Zhou M, Diwu Z, Panchuk-Voloshina N, Haugland RP (1997) A stable nonfluorescent derivative of resorufin for the fluorometric determination of trace hydrogen peroxide: applications in detecting the activity of phagocyte NADPH oxidase and other oxidases. Anal Biochem 253:162–168
8. Kroller-Schon S, Steven S, Kossmann S, Scholz A, Daub S, Oelze M, Xia N, Hausding M, Mikhed Y, Zinssius E, Mader M, Stamm P, Treiber N, Scharffetter-Kochanek K, Li H, Schulz E, Wenzel P, Munzel T, Daiber A (2014) Molecular mechanisms of the crosstalk between mitochondria and NADPH oxidase through reactive oxygen species-studies in white blood cells and in animal models. Antioxid Redox Signal 20:247–266

Chapter 32

Measurement of Reactive Oxygen Species (ROS) and Mitochondrial ROS in AMPK Knockout Mice Blood Vessels

Qilong Wang and Ming-Hui Zou

Abstract

Reactive oxygen species (ROS) are a group of unstable and highly reactive molecules or free radicals typically generated as by-products of cellular processes involving molecular oxygen. In vascular cells, the excessive ROS generation results in the initiation and progression of cardiovascular diseases (CVD). Therefore, a dynamic, robust, and accurate ROS detection method in the blood vessels is essential for pathophysiological research studies of the cardiovascular system.

In this chapter, we describe a fluorescence dye-based detection method for assaying superoxide and mitochondrial superoxide in mouse aorta using dihydroethidium (DHE) and MitoSOX. The protocol includes preparation of frozen aortic tissue sections, monitoring DHE oxidation-derived fluorescence by fluorescence microscopy, and high-performance liquid chromatograph-based analysis of MitoSOX and its oxidation products. For studying the role of AMP-activated protein kinase (AMPK) in the redox regulation, we employed AMPKα2 knockout mice and observed increased superoxide and mitochondrial superoxide levels in the aorta of AMPK knockout mice relative to the wild-type group. This novel ROS detection method will be valuable for investigating the roles of cellular and/or mitochondrial ROS in the pathogenesis of CVDs.

Key words ROS, Mitochondria, HPLC, AMP-activated protein kinase, Cardiovascular disease

1 Introduction

Reactive oxygen species (ROS) are high reactive oxygen-containing molecules and include superoxide ($O_2^{\bullet -}$), hydrogen peroxide (H_2O_2), hydroxyl radical (OH•), as well as hydroxyl ion (OH^-). Under physiological conditions, low ROS concentrations regulate essential cellular functions and signaling transduction pathways to maintain vascular homeostasis. However, when endothelial cells are exposed to pathological stimuli, such as hyperglycemia or hyperlipidemia, excessive ROS are continuously generated as the natural by-product of aerobic metabolic reactions in mitochondria. Aberrant ROS production causes oxidative modification on proteins and/or nucleic acids (such as DNA). Heightened oxidative stress is widely considered as common pathways for the initiation and

Dietbert Neumann and Benoit Viollet (eds.), *AMPK: Methods and Protocols*, Methods in Molecular Biology, vol. 1732, https://doi.org/10.1007/978-1-4939-7598-3_32,

progression of CVD, including atherosclerosis, hypertension, and heart failure [1]. Therefore, alterations to physiologic ROS levels represent a common and potent mediator of pathogenic risk factors associated with cardiovascular dysfunction. Accurate and dynamic quantification of cellular ROS levels is therefore essential for providing clarity with respect to mechanistic links to CVDs.

1.1 $O_2^{\bullet-}$ Detection in Mammalian Cells Using Dihydroethidium

During the past decade, several fluorescent dyes have been widely used to quantify cellular $O_2^{\bullet-}$ and H_2O_2, for example, by dihydroethidium (DHE) or dichlorodihydrofluorescein diacetate (DCFH-DA) [2]. DHE can freely permeate cell membrane and be oxidized by cellular $O_2^{\bullet-}$ to produce two red fluorescent products, namely, ethidium (E^+), which is typically formed by a non-specific redox reaction, and 2-hydroxyethidium (2-OH-E^+), a specific adduct of cellular $O_2^{\bullet-}$ (Fig. 1). The fluorescent spectrum of 2-OH-E^+ (Ex 500–530 nm/Em 590–620 nm) and E^+ (Ex 520 nm/Em 610 nm) is very similar. Thus, specific detection of 2-OH-E^+ is a challenge due to overlapping fluorescence of 2-OH-E^+ and E^+ spectrum. Scientists routinely employed a modified high-performance liquid chromatography (HPLC) method to separate two fluorescent products and directly quantify 2-OH-E^+ in cells in vitro. However, the HPLC method has big limitation to distinguish the type of cells that contributes to ROS production in tissue responses to pathological stimuli, e.g., tumor, atherosclerosis lesion, in vivo. Recently, many investigators use fluorescent microscopy to measure DHE-derived fluorescence in the artery from diabetes [3], hypertension [4], and atherosclerosis [5]. In Subheadings 3.1 and 3.2, we describe a specific method for detection of $O_2^{\bullet-}$ level in mice aorta using cryosectioning technique and fluorescence microscopy.

1.2 Mitochondrial $O_2^{\bullet-}$ Detection in Mammalian Cells Using MitoSOX

Mitochondrion is an important source of ROS produced by abnormalities of electron transport chain in cardiovascular cells, e.g., endothelial cells (ECs) and vascular smooth muscle cells (VSMCs). Excessive production of mitochondrial $O_2^{\bullet-}$ initiates endothelial dysfunction and atherosclerosis [6, 7]. MitoSOX Red indicator is a modified DHE analog derived by the addition of a triphenylphosphonium group, which specifically targets to mitochondria. MitoSOX is oxidized to form two fluorescent products, mito-ethidium (mito-E^+) and 2-hydroxy-mito-ethidium (2-OH-mito-E^+). 2-OH-mito-E^+ is the sole reaction product of MitoSOX with mitochondrial $O_2^{\bullet-}$. Investigators perform double staining using MitoSOX Red and MitoTracker Green and measure mitochondrial $O_2^{\bullet-}$ using confocal fluorescent microscopy in live cells [8, 9]. However, it possesses serious disadvantages in tissue due to tissue autofluorescence interference. Recently, the MitoSOX fluorescence/HPLC combination is the most accepted measure of qualitative mitochondrial $O_2^{\bullet-}$ production in biological systems [10–12]. In Subheading 3.3, we show new optimized

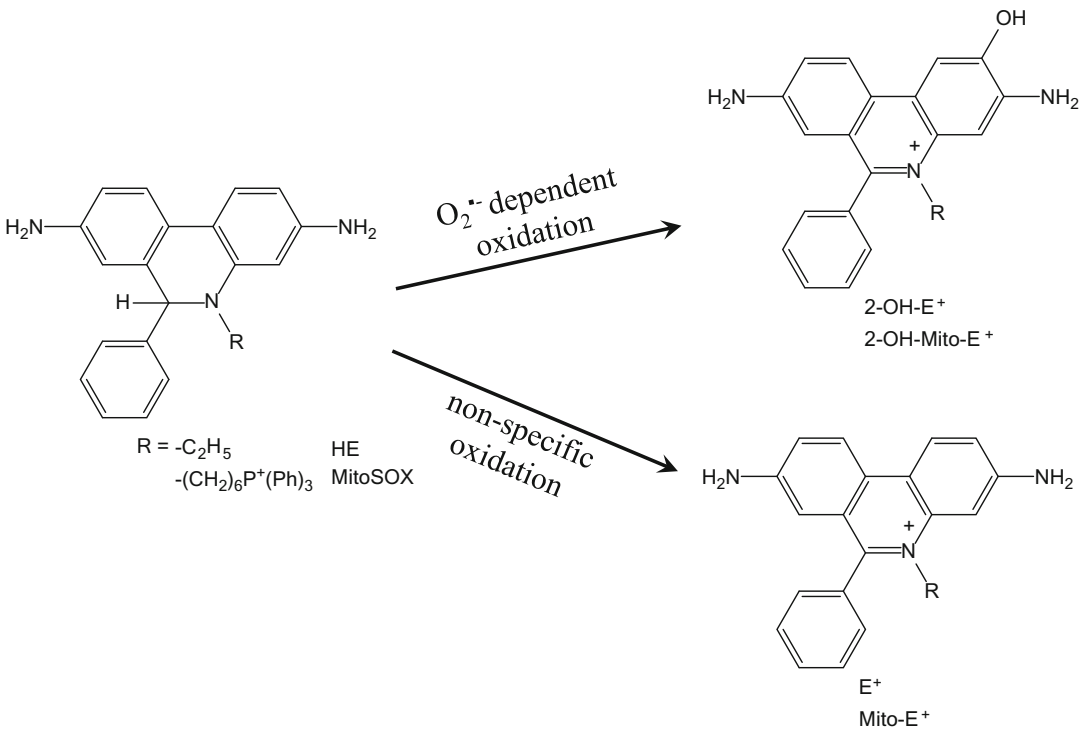

Fig. 1 Superoxide anions ($O_2\bullet^-$)-specific and non-specific oxidation of DHE and MitoSOX

HPLC-fluorescence protocol that allows specific measurement of mitochondrial $O_2\bullet^-$ using MitoSOX. 2-OH-mito-E^+ is identified and quantified by HPLC.

1.3 Role of AMP-Activated Protein Kinase on Cellular Redox Homeostasis

AMP-activated protein kinase (AMPK) is a serine/threonine kinase that is composed of catalytic α subunit and regulatory β and γ subunits. AMPK functions as a regulator of cellular energy metabolism and redox homeostasis. Accumulating evidences suggest cardiovascular protective effects of AMPK via the regulation of the redox system [13]. In diabetes mellitus, the activation of AMPK results in decreased mitochondrial ROS production in ECs via the upregulation of mitochondrial antioxidative enzyme expression [14], acceleration of mitochondrial turnover [15], and maintenance of normal mitochondrial morphology [7]. In addition, AMPK activation reduces hyperglycemia-induced NADPH oxidase expression and NADPH oxidase-derived $O_2\bullet^-$ production in ECs. Conversely, AMPKα2 deficiency causes generation of excess $O_2\bullet^-$ from NADPH oxidase and the mitochondria, resulting in acceleration of atherosclerotic lesion formation [16]. Therefore, we employed the use of AMPKα2 knockout (AMPKα2 KO) mice as a positive model to measure cellular ROS and mitochondrial ROS.

In this chapter, we describe a novel fluorescence dye-based $O_2^{\bullet -}$ and mitochondrial $O_2^{\bullet -}$ measurement method in blood vessels using a combination of HPLC and fluorescence microscopy. Employing blood vessels of AMPKα2 KO mice, we demonstrate that this method successfully and accurately measures cellular and mitochondrial $O_2^{\bullet -}$ levels. In summary, this method provides a valuable tool for investigations related to the roles of cellular or mitochondrial ROS in the pathogenesis of CVD.

2 Materials

2.1 Measurement of $O_2^{\bullet -}$ in Mouse Aorta

1. A 2–3-month-old male C57BL/6J wild-type (WT) mice and AMPKα2 KO mice are housed in humidity- and temperature-controlled (20–22 °C) environments using a 12-h light and 12-h dark cycle. Mice are fed with autoclaved water and regular rodent chow diet.
2. 70% ethanol: Ethanol diluted in deionized H_2O 70% (v/v).
3. Phosphate-buffered saline (PBS): 137 mM NaCl, 2.7 mM KCl, 10 mM Na_2HPO_4, 1.8 mM KH_2PO_4 in deionized H_2O; adjust the pH to 7.4 with HCl, autoclave, and store at room temperature.
4. Optimal cutting temperature (OCT) compound.
5. DHE staining solution: 5 μM DHE dissolved in Milli-Q pure H_2O.
6. Carbon dioxide (CO_2) tank.
7. Dry ice.
8. Surgical tools: Polycarbonate surgery board, dissecting scissors (one straight, one curved), spring scissors, Graefe forceps (curved), Dumont forceps (two angled), sterile syringe (1 and 10 mL), needle (25 G × 5/8, 26 G × 1/2).
9. Sterile gauze pad.
10. 100 mm × 20 mm tissue culture dish.
11. Surgical microscopy.
12. Cryostat.
13. −80 °C ultra-deep freezer.
14. Fluorescence microscopy with green and red fluorescence filter.
15. ImageJ software.

2.2 Measurement of Mitochondrial $O_2^{\bullet -}$ in Mouse Aorta

1. Krebs buffer: 118.3 mM NaCl, 4.7 mM KCl, 1.2 mM $MgSO_4$, 1.2 mM KH_2PO_4, 2.5 mM $CaCl_2$, 25 mM $NaHCO_3$, 0.026 mM EDTA, 11 mM glucose in deionized H_2O.

2. MitoSOX staining solution: 2 μM MitoSOX dissolved in Krebs buffer (*see* **Note 1**).
3. 50% methanol: Methanol diluted in Milli-Q pure H_2O 50% (v/v).
4. Bicinchoninic acid assay (BCA) protein assay reagent.
5. $HClO_4$ protein precipitation solution: 0.2 M $HClO_4$ diluted in methanol.
6. MitoTEMPO: 5 μM MitoTEMPO dissolved in Krebs buffer.
7. HPLC mobile phase A: 0.1% trifluoroacetic acid (TFA) in 1 L pure water.
8. HPLC mobile phase B: 0.1% TFA in 1 L acetonitrile. Keep the mobile phase at 4 °C until use.
9. HPLC-certified non-sterile syringe filter, pore size 0.22 μm.
10. NovaPak C18 (3.9 × 150 mm, 5 μm particle size) column.
11. Refrigerated centrifuge.
12. HPLC: High-pressure pump, autosampler, fluorescence detector.

3 Method

3.1 Isolation of Mouse Thoracic Aorta (~2 h)

1. Asphyxiate WT mouse or AMPKα2 KO mouse with CO_2 for 5 min (*see* **Note 2**).
2. Sanitize the chest region of the mouse by spraying with 70% ethanol.
3. Place and tape the mouse on a surgical board in the supine position.
4. Remove the superficial skin to expose the superior portion of the peritoneum and inferior portion of the thoracic cavity.
5. Open abdominal cavity and thoracic cavity to expose the heart and lungs without cutting any blood vessels to avoid bleeding.
6. Insert 25 G needle attached to the 10 mL syringe into the apex of the heart. Perfuse with 5 mL of sterile ice-cold PBS over 2–3 min. Cut the right atrium with scissor once perfusion has begun. Remove all fluid in the chest cavity gently with sterile gauze.
7. Remove the organs, including the liver, lung, and stomach, to allow a clear view of the aorta. Grasp the heart gently using forceps and carefully separate the thoracic aorta from dorsal spine using curved dissecting scissors. Place thoracic aorta in tissue culture dish with ice-cold PBS buffer.

8. Remove the heart and fat tissue around the aortic region without cutting aortic wall under dissecting microscope (*see* **Note 3**).
9. Cut the aorta into two pieces, one below the arch for measurement of mitochondrial $O_2^{\bullet -}$, the other at the proximity of the diaphragm for measurement $O_2^{\bullet -}$.

3.2 Measurement of $O_2^{\bullet -}$ in Mouse Aorta

1. Cut the cleaned aortic rings into approximate 5 mm long segments using surgical scissors.
2. Embed aorta vertically into OCT Compound. Immediately place the sample on crushed dry ice to freeze.
3. Cut frozen section 8 μm thick using a cryostat at −20 °C. Thaw mount the sections onto gelatin-coated histological slides. Slides containing cryostat sections are stored at −80 °C (*see* **Note 4**).

3.2.1 Preparing Frozen Sections of Mouse Aorta (~3 h)

3.2.2 DHE Staining (~1 h)

1. Prepare 50 mL fresh 5 μM DHE staining solution in slide box prior to use. Dissolve 1 mg DHE in 317 μl of dimethyl sulfoxide (DMSO) for 10 mM stock solution. Dilute 25 μL of DHE stock solution in 50 mL Milli-Q pure H_2O for 5 μM staining solution (*see* **Note 5**) .
2. Rinse slides in pure H_2O for 30 s to wash out OCT compound.
3. Immediately place slides in DHE staining solution. Incubate for 5–20 min at room temperature and avoid exposure to light (*see* **Note 6**).
4. Transfer slides to beaker with deionized H_2O for washing for 1 min. Repeat the washing twice and keep slides in deionized H_2O. Take fluorescence imaging immediately (*see* **Note 7**).

3.2.3 Fluorescence Imaging and Analysis Fluorescence Intensity (~1 h)

1. Visualize slides using fluorescence microscope with red excitation filter and green excitation filter. DHE-derived 2-OH-E^+ can be visualized with red excitation filter, and autofluorescence of elastin in the internal elastic lamina can be visualized with green excitation filter. 2-OH-E^+ in endothelium layer and VSMC can be clearly observed (*see* **Note 8**) .
2. Use 10× magnifications to focus on the sample. Adjust the objective to 40×. Set up exposure time to get optimized imaging and minimal background.
3. Acquire fluorescence images of aortic sections using equal identical laser power, exposure time, sensitivity, and resolution. Choose at least three different fields for each sample (Fig. 2).
4. Open the red fluorescence imaging with ImageJ software. Measure fluorescence intensity of the 2-OH-E^+ signals, and export the value as the relative signal intensity (*see* **Note 9**).

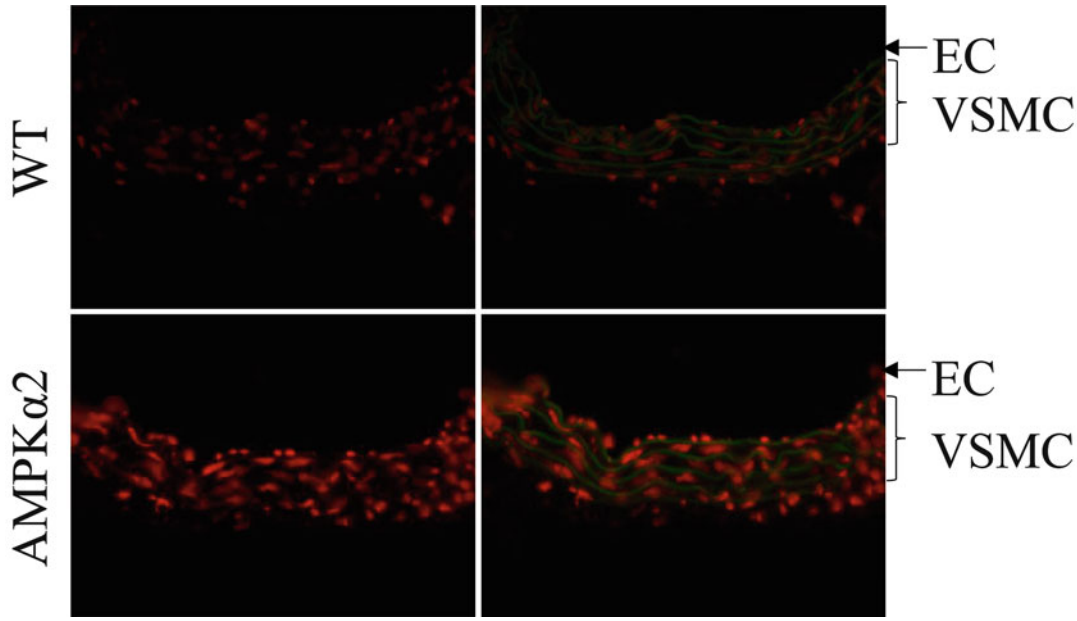

Fig. 2 Detection of $O_2^{\bullet -}$ in frozen aortic section from WT and AMPKα2 KO mice using DHE. Fluorescent micrographs of frozen sections of aorta from WT mice and AMPKα2 KO mice are obtained after staining with DHE (5 μM) for 20 min. AMPKα2 deficiency increased $O_2^{\bullet -}$ production in both aortic endothelial cells (EC) and vascular smooth muscle cell (VSMC)

3.3 Measurement of Mitochondrial $O_2^{\bullet -}$ in Mouse Aorta

3.3.1 Preparing Aortic Samples for HPLC Analysis (~3 h)

1. Prepare fresh 2 μM MitoSOX staining solution prior to use. Dissolve 50 μg MitoSOX in 33 μL of DMSO for 2 mM stock solution. Dilute 5 μL MitoSOX stock solution in 5 mL of Krebs buffer (*see* **Note 10**).
2. Place fresh WT mice and AMPKα2 KO mice aorta in 5 mL of Krebs buffer or buffer containing 5 μM MitoTEMPO (*see* **Note 11**).
3. Incubate at 37 °C for 30 min.
4. Place aorta to 5 mL of 2 μM MitoSOX Red staining solution in tissue culture dish. Perfuse the artery lumen with staining solution using 26 G needle attached to the 1 mL syringe. Wrap the dish with aluminum foil to avoid light exposure. Incubate at 37 °C for 20 min (*see* **Note 12**).
5. Place aorta into 5 mL ice-cold Krebs buffer for washing, and repeat the washing three times (1 min each).
6. Transfer aorta to new Eppendorf tube with 100 μL of ice-cold 50% methanol. Homogenize aorta rings with tissue grinder (*see* **Note 13**).
7. Transfer 2 μL of tissue lysis into an empty Eppendorf tube for measurement of protein concentration by BCA.

8. Transfer 90 μL of cell lysate to new Eppendorf tube containing 90 μL of 0.2 M $HClO_4$, vortex, and keep on ice for 1 h to allow protein precipitation.
9. Centrifuge tissue suspension at 4 °C, 12,000 × *g* for 15 min.
10. The tissue supernatant is passed through a 0.22 μm syringe filter.
11. Transfer the methanol filtrate into HPLC vial with 300 μL conical insert. Seal the vial. Place it in the HPLC refrigerated autosampler at 4 °C.

3.3.2 HPLC Operating Conditions (~4 h)

1. Prepare 1 L mobile phase A (0.1% TFA in H_2O) and 1 L mobile phase B (0.1% TFA in acetonitrile).
2. Filter the mobile phase through a 0.22 μm nylon membrane filter under vacuum to remove undissolved solids.
3. Ultrasound mobile phase A and B for degasification for 30 min.
4. HPLC separations are performed by NovaPak C18 column and monitored with a fluorescence detector (Ex/Em = 510/580 nm). Gradient HPLC method is used for the analysis of oxidized MitoSOX products. The initial mobile phase composition is maintained at 100% mobile phase A, changed linearly to 100% mobile phase B (0–20 min), then followed by a return to the initial conditions within 5 min (20–25 min) and kept 5 min for the chromatograph column equilibrium. Flow rate is maintained at 1.0 mL/min and injection volume of 10 μL (*see* **Note 14**).

3.3.3 Analysis HPLC Results (~1 h)

1. Comparing the HPLC trace of AMPKα2 KO mice aorta in Fig. 3b, c, the HPLC peak with a retention time of 13.8 min is reduced after MitoTEMPO treatment. Thus, this peak is identified as 2-OH-mito-E^+ (*see* **Note 15**).
2. Measure the area of the 2-OH-mito-E^+ peak using the software provided with the HPLC system (*see* **Note 16**).
3. Normalize the 2-OH-mito-E^+ peak areas with the protein concentration of aorta tissue lysates.
4. Statistical analysis of 2-OH-mito-E^+ level in WT mice aorta and AMPKα2 KO mice aorta is performed with one-way ANOVA. $P < 0.05$ is considered statistically significant (*see* **Note 17**).

4 Notes

1. MitoSOX™ Red mitochondrial superoxide indicator is novel fluorogenic dye specifically targeted to mitochondria that is available from ThermoFisher Scientific.

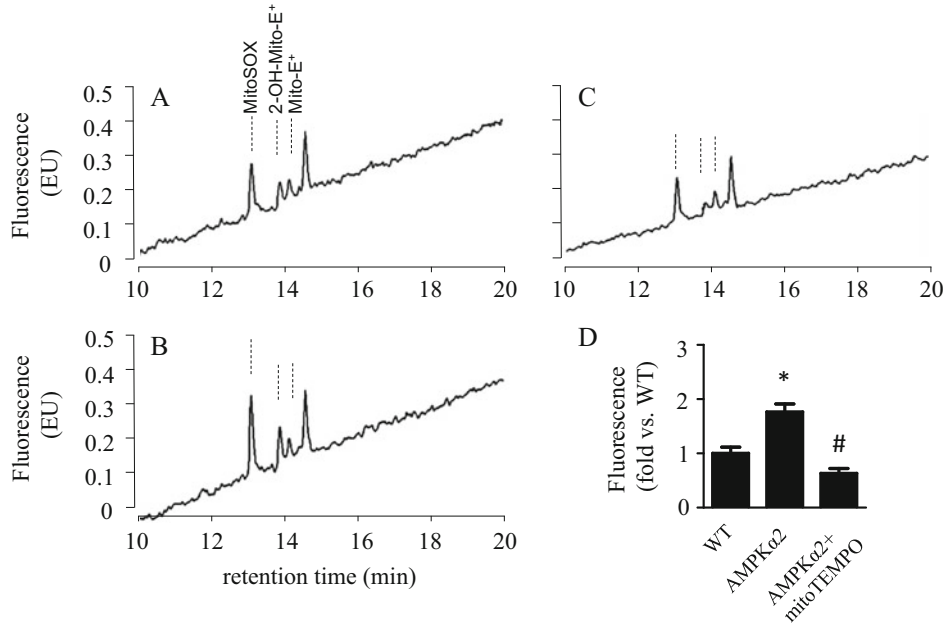

Fig. 3 Detection of mitochondrial $O_2^{\bullet -}$ in WT and AMPKα2 KO mice aorta using HPLC. Fresh WT mice aorta (**a**), AMPKα2 KO mice aorta pretreatment without (**b**) or with (**c**) MitoTEMPO (5 μM), are incubated with MitoSOX (2 μM) for 20 min. Typical HPLC chromatograms of aorta extracts are present (**a**–**c**). Quantification of 2-OH-mito-E^+ peak area in mice aorta (**d**). $n = 3$. *$p < 0.05$ vs. WT, # $p < 0.05$ vs. no MitoTEMPO treatment

2. CO_2 asphyxiation is a safe and humane method of euthanasia for mouse. It causes less oxidative stress, no observable histological changes in tissue. All animal procedures are in accordance with the NIH Guide for the Care and Use of Laboratory Animals.
3. Caution should be applied in the removal of adhering perivascular tissue using surgical forceps. Do not clamp the vessel, which could result in damaged endothelial layer.
4. Cryosectioning and DHE staining could be performed on other mouse arteries, including extrapulmonary artery, carotid artery, mesentery artery, or abdominal aorta.
5. Both H_2O and PBS could be used to dilute DHE staining solution. We observed low-background and high-contrast fluorescence imaging using Milli-Q pure H_2O-diluted DHE solution.
6. Time-course imaging studies, e.g., 5, 10, 15, 20 min, need to be performed to optimize incubation time for DHE staining.
7. The DHE-derived fluorescence intensity is stable over the first 30 min. Thus, all fluorescence images should be taken within 30 min.

8. E^+ intercalates with DNA becoming highly fluorescent in nucleus. 2-OH-E^+ is majorly localized in cytosol. Therefore, 2-OH-E^+ and E^+ could be distinguished according to their localization.
9. Sacrificing mice, preparing frozen aortic section, and DHE staining should be performed on the same day. If not, do not store frozen sections at −80 °C more than 3 days.
10. Krebs buffer is more suitable than cell culture medium for dissolving MitoSOX. Because cell culture medium may include less amount of superoxide radical scavengers which remove superoxide, resulting in underestimation mitochondrial $O_2\bullet^-$.
11. MitoTEMPO is a specific mitochondrial $O_2\bullet^-$ scavenger. AMPKα2 KO mice aorta was treated with MitoTEMPO as a negative control.
12. MitoSOX staining must be performed in fresh aorta, but not frozen sections. In fresh tissue, MitoSOX translocates into the mitochondria and reacts with mitochondrial superoxide. But in frozen aortic section, MitoSOX reacts with both cytoplasmic $O_2\bullet^-$ and mitochondrial $O_2\bullet^-$ to form oxidative products.
13. During preparing HPLC samples, aortic sample should always be kept on ice under reduced light in avoiding to fluorescence quenching.
14. If 2-mito-OH-E^+ peak is becoming wide and difficult to separate with mito-E^+, check column pressure. If column pressure increases significantly, please stop running samples and start to rinse column using 50 mL water, methanol, and acetonitrile, respectively.
15. To identify MitoSOX, mito-E^+, and 2-OH-mito-E^+ in HPLC, we compare HPLC trace from aorta treatment with or without MitoTEMPO and identify reduced peak as 2-OH-mito-E^+. In addition, Jacek Zielonka et al. synthesize 2-OH-mito-E^+ and mito-E^+ by reacting MitoSOX with nitrosodisulfonate or chloranil and then use them as standard to quantify mitochondrial $O_2\bullet^-$ in cells and tissue [10, 12].
16. If fluorescence signaling of 2-mito-OH-E^+ is undetectable, collect at least 2–3 mice aortas and homogenize together as a group for HPLC assay.
17. Besides $O_2\bullet^-$ and mitochondrial $O_2\bullet^-$, some stable by-products modified under conditions of oxidative stress are measured as biomarkers of oxidative stress, e.g., nitrotyrosine-, 4-hydroxy-nonenal-, or S-glutathionylation-modified protein, oxidized low-density lipoprotein, and oxidized phospholipids [17]. Additionally, ROS-producing enzymes (e.g., NADPH oxidase and myeloperoxidase) and antioxidative enzymes (e.g., MnSOD, glutathione peroxidase) are measured in tissues

to evaluate oxidative stress using immunohistochemistry and Western blot [1, 18].

References

1. Song P, Zou MH (2014) Redox regulation of endothelial cell fate. Cell Mol Life Sci 71 (17):3219–3239
2. Dikalov S, Griendling KK, Harrison DG (2007) Measurement of reactive oxygen species in cardiovascular studies. Hypertension 49 (4):717–727
3. Oak JH, Cai H (2007) Attenuation of angiotensin II signaling recouples eNOS and inhibits nonendothelial NOX activity in diabetic mice. Diabetes 56(1):118–126
4. Zhao Q, Zhang J, Wang H (2015) PGC-1alpha overexpression suppresses blood pressure elevation in DOCA-salt hypertensive mice. Biosci Rep 35(3):e00217
5. Miller JD, Chu Y, Brooks RM, Richenbacher WE, Pena-Silva R, Heistad DD (2008) Dysregulation of antioxidant mechanisms contributes to increased oxidative stress in calcific aortic valvular stenosis in humans. J Am Coll Cardiol 52(10):843–850
6. Mercer JR, Yu E, Figg N, Cheng KK, Prime TA, Griffin JL, Masoodi M, Vidal-Puig A, Murphy MP, Bennett MR (2012) The mitochondria-targeted antioxidant MitoQ decreases features of the metabolic syndrome in ATM+/-/ApoE-/- mice. Free Radic Biol Med 52(5):841–849
7. Wang Q, Zhang M, Torres G, Wu S, Ouyang C, Xie Z, Zou MH (2017) Metformin suppresses diabetes-accelerated atherosclerosis via the inhibition of Drp1-mediated mitochondrial fission. Diabetes 66(1):193–205
8. Quijano C, Castro L, Peluffo G, Valez V, Radi R (2007) Enhanced mitochondrial superoxide in hyperglycemic endothelial cells: direct measurements and formation of hydrogen peroxide and peroxynitrite. Am J Physiol Heart Circ Physiol 293(6):H3404–H3414
9. Madesh M, Zong WX, Hawkins BJ, Ramasamy S, Venkatachalam T, Mukhopadhyay P, Doonan PJ, Irrinki KM, Rajesh M, Pacher P, Thompson CB (2009) Execution of superoxide-induced cell death by the proapoptotic Bcl-2-related proteins Bid and Bak. Mol Cell Biol 29(11):3099–3112
10. Dikalova AE, Bikineyeva AT, Budzyn K, Nazarewicz RR, McCann L, Lewis W, Harrison DG, Dikalov SI (2010) Therapeutic targeting of mitochondrial superoxide in hypertension. Circ Res 107(1):106–116
11. Itani HA, Dikalova AE, McMaster WG, Nazarewicz RR, Bikineyeva AT, Harrison DG, Dikalov SI (2016) Mitochondrial cyclophilin D in vascular oxidative stress and hypertension. Hypertension 67(6):1218–1227
12. Zielonka J, Srinivasan S, Hardy M, Ouari O, Lopez M, Vasquez-Vivar J, Avadhani NG, Kalyanaraman B (2008) Cytochrome c-mediated oxidation of hydroethidine and mito-hydroethidine in mitochondria: identification of homo- and heterodimers. Free Radic Biol Med 44(5):835–846
13. Song P, Zou MH (2012) Regulation of NAD(P)H oxidases by AMPK in cardiovascular systems. Free Radic Biol Med 52(9):1607–1619
14. Cai Y, Martens GA, Hinke SA, Heimberg H, Pipeleers D, Van de Casteele M (2007) Increased oxygen radical formation and mitochondrial dysfunction mediate beta cell apoptosis under conditions of AMP-activated protein kinase stimulation. Free Radic Biol Med 42(1):64–78
15. Zhu H, Foretz M, Xie Z, Zhang M, Zhu Z, Xing J, Leclerc J, Gaudry M, Viollet B, Zou MH (2014) PRKAA1/AMPKalpha1 is required for autophagy-dependent mitochondrial clearance during erythrocyte maturation. Autophagy 10(9):1522–1534
16. Wang S, Zhang M, Liang B, Xu J, Xie Z, Liu C, Viollet B, Yan D, Zou MH (2010) AMPKalpha2 deletion causes aberrant expression and activation of NAD(P)H oxidase and consequent endothelial dysfunction in vivo: role of 26S proteasomes. Circ Res 106(6):1117–1128
17. Dikalov SI, Harrison DG (2014) Methods for detection of mitochondrial and cellular reactive oxygen species. Antioxid Redox Signal 20 (2):372–382
18. Panth N, Paudel KR, Parajuli K (2016) Reactive oxygen species: a key hallmark of cardiovascular disease. Adv Med 2016:9152732

Chapter 33

Studying the Role of AMPK in Angiogenesis

Katrin Spengler, Silke Große, Nderim Kryeziu, Anne Knierim, and Regine Heller

Abstract

The role of AMPK in angiogenesis can be studied using in vitro and in vivo assays. The endothelial spheroid assay is a robust three-dimensional in vitro test, which allows investigation of tubular morphogenesis by integrating cell-cell as well as cell-matrix interactions. The Matrigel plug assay validates the process of angiogenesis in vivo and allows studies in genetically modified mice. Here, we give a detailed description of both assays and their application in AMPK research.

Key words Angiogenesis, Spheroid assay, Sprouting, Tube formation, Matrigel plug assay

1 Introduction

AMPK has been demonstrated to play a role in angiogenesis in vitro and in vivo [1]. Our own study has shown that vascular endothelial growth factor (VEGF) activates AMPK via Ca^{2+}/calmodulin-dependent protein kinase kinase 2 and that AMPKα1 depletion reduces VEGF-induced angiogenesis in cultured endothelial cells and in mice [2]. The mechanisms underlying angiogenic effects of AMPK are still obscure and may involve endothelial NO synthase (eNOS) activation [3] and eNOS-independent pathways [2]. Recent data from our group suggested that the suppression of the hexosamine biosynthetic pathway by AMPK promotes VEGF-induced angiogenesis [4]. However, additional processes may contribute to angiogenic effects of AMPK, and more detailed knowledge about the role of AMPK in angiogenesis is required.

In general, angiogenesis is monitored in in vitro and in vivo settings with each having advantages and disadvantages. While in vitro assays allow the evaluation of distinct processes and components of angiogenesis, in vivo assays reflect the complexity of angiogenesis and verify the biological relevance of specific observations [5]. In vitro angiogenesis assays include the evaluation of endothelial functions required for angiogenesis, i.e., proliferation,

Dietbert Neumann and Benoit Viollet (eds.), *AMPK: Methods and Protocols*, Methods in Molecular Biology, vol. 1732, https://doi.org/10.1007/978-1-4939-7598-3_33,

migration, and differentiation into tubular structures. Differentiation is best measured in three-dimensional assays, which integrate cell-cell and cell-matrix interactions and allow lumen formation in the developing sprouts. In these assays, endothelial cells are placed within an extracellular matrix such as collagen, fibrin, or Matrigel, which may contain pro- or antiangiogenic compounds [5]. Cells are added as single-cell suspension, spheroids (cell aggregates stabilized by addition of a scaffold molecule such as methylcellulose), or endothelial cell-coated beads, and tube formation is monitored over time by counting the length and/or number of the formed sprouts. However, given the heterogeneity of endothelial cells, the alteration of their phenotype in culture, and the lack of interaction with mural cells, it is essential that results from in vitro assays are validated in vivo. In vivo angiogenesis assays utilize an intact organism to model vessel formation. The most common in vivo assays include chorioallantoic membrane assay, fluorescent zebrafish assay, and tests, which assess mammalian angiogenesis, i.e., matrix invasion assays, dorsal air sac or chamber assays, and tumor mouse models [5]. All of these assays can be employed for studying the effect of compounds on angiogenesis, but molecular mechanisms of sprouting are preferentially investigated in the mammalian models. Among them, in vivo matrix invasion assays facilitate angiogenesis in natural extracellular biomaterials, e.g., Matrigel. They allow not only the analysis of a given molecule that is incorporated into the matrix but can also reveal the impact of host molecules on angiogenesis when performed in genetically modified mice.

1.1 Endothelial Cell Spheroid Assay

The use of endothelial spheroids to study angiogenesis was first described by Korff et al., who discovered that in contrast to an endothelial monolayer, the surface layer of endothelial spheroids is able to differentiate in response to VEGF [6] and that VEGF-treated spheroids form lumenized capillary-like tubes when embedded in collagen or fibrin [7]. Tubulogenesis is controlled by $\alpha 2\beta 1$ integrins in collagen and by $\alpha_v\beta 2$ and $\alpha 5\beta 1$ in fibrin matrices [8, 9]. Spheroid assays can be performed with endothelial cells from different sources. Among them, human umbilical vein endothelial cells (HUVEC) are widely used due to their availability, the relatively easy preparation, and the high purity of cultures. The HUVEC-based spheroid assay has been characterized as a versatile tool to study the impact of pro- and antiangiogenic determinants on angiogenesis under standardized conditions (i.e., low passage numbers or immortalized cells) [10]. HUVEC gene expression can be modified efficiently using siRNA techniques [2, 4], which is another requirement for a qualified in vitro angiogenesis assay [11]. In line with this, we performed assays with HUVEC spheroids, in which both AMPKα isoforms were individually or jointly downregulated to investigate the role of AMPK in angiogenesis [2, 4].

1.2 Matrigel Plug Assay

The Matrigel plug assay is a widely used in vivo assay, which allows the evaluation of angiogenesis within a few days. Matrigel is a soluble basement membrane extract of the Engelbreth-Holm-Swarm mouse sarcoma, which includes the components laminin, collagen IV, heparan sulfate proteoglycan, and entactin. It is liquid at 4 °C, reconstitutes into a gel when injected subcutaneously into mice, and finally forms a solid plug, into which endothelial cells can immigrate and form vessels. The angiogenic process can be modulated by adding growth factors or pro- and antiangiogenic drugs to the Matrigel [12–14]. The angiogenic response is quantified after harvesting and sectioning the plugs by assessing CD31-positive structures in immunofluorescent stainings. Alternatively, cells can be released from the plugs by mild protease treatment and analyzed by flow cytometry [15]. Matrigel has the advantage that angiogenesis is initiated in a natural environment. However, since it contains endogenous growth factors and cytokines itself (even if the growth factor-reduced Matrigel is used), interference with test compounds and spontaneous sprouting can occur. We employed the Matrigel plug assay to investigate angiogenesis in AMPKα1 knockout mice [2].

2 Materials

2.1 Endothelial Cell Spheroid Assay

2.1.1 siRNA-Mediated Downregulation of AMPKα in HUVEC

1. HUVEC: Primary HUVEC isolated from anonymously acquired umbilical cords according to the Declaration of Helsinki 'Ethical Principles for Medical Research Involving Human Subjects' (1964) (*see* **Note 1**).
2. Endothelial cell growth medium: Medium 199, 17.5% (v/v) fetal calf serum (FCS), 2.5% (v/v) human serum, 7.5 μg/mL endothelial mitogen, 7.5 U/mL heparin, 680 μM glutamine, 100 U/mL penicillin, 100 μg/mL streptomycin, 100 μM ascorbic acid (*see* **Note 2**).
3. Hank's balanced salt solution (HBSS).
4. M199/HSA: Medium 199 with 0.25% (w/v) human serum albumin.
5. siRNA duplex oligonucleotides based on human cDNA encoding AMPKα1 or AMPKα2 (*see* **Note 3**).
6. Transfection kit: SAINT-sRNA transfection reagent (*see* **Note 4**).
7. HEPES-buffered saline (HBS): 20 mM HEPES, 150 mM NaCl, pH 7.4.
8. Cell culture incubator (5% CO_2, 37 °C, 100% humidity).

2.1.2 Generation of Spheroids

1. Methylcellulose stock solution: 1.2% (w/v) methylcellulose. Weigh 6 g of methylcellulose, transfer to a 500 mL glass bottle,

and add a magnetic stirrer and autoclave (*see* **Note 5**). Add 250 mL of prewarmed medium 199 (37 °C) to autoclaved methylcellulose, transfer the bottle to a sterile 60 °C water bath, and incubate for 20 min interrupted by four to five times stirring at room temperature (*see* **Note 6**). Add 250 mL of medium 199, and stir for 1 h at room temperature and then overnight at 4 °C. Transfer the solution into 50 mL tubes, and centrifuge for 2 h at 4000 × *g* at room temperature. Transfer the upper 45 mL into new tubes using a pipette, and store at 4 °C (*see* **Notes 7** and **8**).

2. Trypsin/EDTA: 0.05% (w/v) trypsin, 0.02% (w/v) EDTA.
3. Phosphate-buffered saline (PBS): 145 mM NaCl, 2.7 mM KCl, 1.5 mM KH_2PO_4, 8 mM $Na_2HPO_4 \cdot 2H_2O$, pH 7.4, autoclaved.
4. Stop medium: Medium 199, 10% (v/v) FCS.
5. Endothelial cell growth medium (*see* Subheading 2.1.1., **item 2**).
6. 96-well plates (round bottom, for suspension culture).
7. Sterile 50 mL Falcon tubes.
8. Pipettors, multistepper pipette.
9. Cell culture incubator (*see* Subheading 2.1.1., **item 8**).

2.1.3 Embedding and Stimulation of Spheroids

1. HEPES buffer: 10 mM HEPES-Na, pH 7.4, 145 mM NaCl, 5 mM KCl, 1 mM $MgSO_4$, 10 mM glucose. Sterilize by filtration (*see* **Note 9**).
2. Aprotinin: 10,000 U/mL aprotinin. Dissolve 10,000 U in 1 mL of sterile ddH_2O, and store aliquots at −20 °C (*see* **Note 10**).
3. Fibrinogen: 3.5 mg/mL fibrinogen. Weigh approximately 3.5 mg fibrinogen under sterile conditions into a U-shaped tube (*see* **Notes 11** and **12**). Add 1 mL of sterile prewarmed HEPES buffer (37 °C) to the rim of the tube, and let it carefully run down; do not mix (*see* **Note 13**). Transfer the tube into a 37 °C water bath, and let the fibrinogen dissolve for 4 h without agitation. Subsequently, mix the solution carefully, and determine protein content (*see* **Note 14**). Dilute fibrinogen to a concentration of 1.8 mg/mL with sterile HEPES buffer. Add 20 µL of the antifibrinolytic agent aprotinin per 1 mL.
4. HEPES/Ca buffer: HEPES buffer plus 1.5 mM $CaCl_2$, sterilize by filtration.
5. Thrombin: Dissolve 100 U in 1 mL of sterile ddH_2O, and store aliquots at −20 °C (*see* **Note 15**).
6. Spheroid growth medium: Medium 199, 2% (v/v) FCS, 680 µM glutamine, 100 U/mL penicillin, 100 µg/mL streptomycin (*see* **Note 16**).

7. Reagents for protein determination (according to Lowry or Bradford).
8. Multichannel pipettor for 100–200 µL, sterile reservoir.
9. Sterile tubes.
10. 24-well plates.
11. Cell culture incubator (*see* Subheading 2.1.1, **item 8**), incubator without CO_2 (37 °C) or heating plate (37 °C).

2.1.4 Fixation and Analysis of Spheroids

1. Phosphate buffer: 200 mM sodium phosphate, pH 7.4. Prepare stock solutions of 200 mM $Na_2HPO_4 \cdot 2H_2O$ (35.6 g in 1000 mL ddH_2O, buffer A) and of 200 mM $NaH_2PO_4 \cdot H_2O$ (27.6 g in 1000 mL ddH_2O, buffer B), and mix 770 mL of buffer A and 230 mL of buffer B. Check the pH of the solution at room temperature. If necessary, adjust the pH to 7.4.
2. PFA stock solution: 4% (w/v) paraformaldehyde (PFA). Weigh 40 g of paraformaldehyde powder into a glass beaker, and put it on a magnetic stirrer in a ventilated hood. Add 400 mL ddH_2O, and heat to 60 °C while stirring (check temperature!). Add 1 N NaOH dropwise to clear the solution. Heat again to 60 °C. Adjust the volume to 500 mL ddH_2O, and let the solution cool down to room temperature. Filter the PFA solution into 500 mL of phosphate buffer (pH 7.4) in a 1 L round bottom flask. Freeze aliquots. After thawing the solution can be stored at 2–8 °C for up to 1 month.
3. Inverse microscope with software for taking photos.
4. Software for analyzing sprout length and number.
5. Sodium azide: 200 mg/mL sodium azide. Dissolve 200 mg sodium azide in 1 mL ddH_2O, and store at 4 °C.
6. Parafilm.

2.2 Matrigel Plug Assay

2.2.1 Generation of Matrigel Plugs in Mice

1. Mice: Wild-type and AMPKα1 knockout mice as previously reported [16, 17].
2. Matrigel, growth factor-reduced, phenol red-free (*see* **Note 17**).
3. PBS: 145 mM NaCl, 2.7 mM KCl, 1.5 mM KH_2PO_4, 8 mM $Na_2HPO_4 \cdot 2H_2O$, pH 7.4, autoclaved.
4. Recombinant VEGF 165 protein: Prepare a stock solution of 10 µg/mL in PBS containing 0.1% (w/v) albumin.
5. Heparin: 12.5 mg/mL stock solution in sterile ddH_2O.
6. 70% (v/v) ethanol (disinfectant).
7. Anesthetics: 0.1 mg/mL medetomidine, 0.01 mg/mL fentanyl, 1 mg/mL midazolam.

8. Antidotes to anesthetics: 5 mg/mL atipamezole, 2.4 mg/mL naloxone, 1 mg/mL flumazenil.
9. 1 mL syringes, 20- and 27-gauge needles.
10. 2 mL Eppendorf tubes, 15 mL Falcon tubes, pipette tips.
11. Scissors, scalpel.
12. Zinc fixative (*see* **Note 18**).

2.2.2 Embedding of Matrigel Plugs in Paraffin and Sectioning

1. Tissue cassettes.
2. Spin tissue processor (Histokinette).
3. Ethanol (99%, 96%, 70% (v/v)).
4. Xylene.
5. Ethanol:xylene: 2:1 and 1:2.
6. Paraffin.
7. Modular tissue embedding center.
8. Microtome.
9. Paintbrush, 20- and 27-gauge needles.
10. Water bath at room temperature and 37 °C.
11. Polylysine-coated microscope slides.

2.2.3 Staining of Matrigel Plugs (CD31 Immunofluorescence)

In addition to **items 3** and **4** in Subheading 2.2.2. above, the following material is required:

1. Ethanol (50% (v/v)).
2. Citrate buffer: 0.01 M $Na_3C_6H_5O_7 \cdot 2H_2O$, pH 6.0.
3. Microwave.
4. PBST: PBS including 0.01% (v/v) Triton X-100.
5. Immunostaining system.
6. Blocking solution: PBST, 10% (v/v) serum (*see* **Note 19**), 0.25% (w/v) bovine serum albumin-c (BSA-c) (*see* **Note 20**).
7. Anti-CD31 antibody applicable on paraffin sections (*see* **Note 21**).
8. Secondary antibody coupled to a fluorescent dye (*see* **Note 22**).
9. Fluoromount-G aqueous mounting medium.
10. Coverslips (0.17 mm thickness).
11. Laser scanning microscope or epifluorescent microscope with software including stitching function.
12. ImageJ (NIH) or comparable analyzing software.

3 Methods

3.1 Endothelial Cell Spheroid Assay

3.1.1 siRNA-Mediated Downregulation of AMPKα in HUVEC

1. Seed HUVEC of the first passage 1 day prior to transfection; cells should be 50–80% confluent on the day of transfection.
2. Dilute non-targeting or AMPKα-isoform-specific siRNA in HBS. Vortex SAINT-sRNA for 30 s and dilute it in HBS (1:5). Prepare siRNA/SAINT-sRNA complexes by gently pipetting diluted siRNA into diluted SAINT-sRNA and add 4 volumes M199/HSA to obtain the final transfection solution. Gently invert the tube, do not vortex. Usually, 2.5 mL transfection solution consisting of 1.25 μg/250 μL siRNA solution, 250 μL diluted SAINT-sRNA and 2 mL M199/HSA is added to a 60-mm cell culture dish.
3. Wash cells twice with HBSS.
4. Remove HBSS and add the prepared transfection medium to the cells.
5. Incubate cells for 4 h at 37 °C at 5% CO_2, and then add 2 volumes of endothelial cell growth medium without removing the transfection medium (for instance, 5 mL growth medium is added to 2.5 mL transfection solution on a 60-mm culture dish).
6. Incubate for 48–72 h.
7. Check siRNA-mediated downregulation of target genes in Western blotting experiments parallel to spheroid assays.

3.1.2 Generation of Spheroids

1. Wash siRNA-treated confluent HUVEC monolayers twice with PBS.
2. Add trypsin/EDTA (for instance, 0.5 mL per 60-mm cell culture dish) for maximal 3 min to detach cells.
3. Transfer the cell suspension into a Falcon tube containing stop medium (2 mL/10^6 cells).
4. Rinse the cell culture dish with stop medium (2 mL/60-mm dish), and pool the rinsing solution with the initial cell suspension (*see* **Note 23**).
5. Centrifuge the pooled cell suspension for 6 min at 500 × *g* at room temperature without brake.
6. Aspirate the supernatant, and resuspend the cell pellet in 5 mL of endothelial cell growth medium (*see* **Note 24**).
7. Take an aliquot of the suspension, and count the cells (for instance, using a Neubauer chamber).
8. Calculate the number of spheroids and the cell number required for the respective experiment. Perform each treatment condition in duplicates. One spheroid should contain 3000 cells; approximately 30–40 spheroids per sample have to be planned (*see* **Note 25**).

9. Prepare a cell suspension of 37,500 cells/mL, and add 1.2% methylcellulose at a ratio of 5:1 to receive a cell concentration of 30,000 cells/mL. Mix carefully by inverting the tube.
10. Add 100 μL of this cell suspension per well of a round bottom 96-well plate using a multistepper pipette. Each well provides one spheroid (*see* **Note 26**).
11. Incubate the plates for 24 h at 37 °C and 5% CO_2 to obtain spheroids.

3.1.3 Embedding and Stimulation of Spheroids

1. Prepare fibrinogen solution 4 h before starting embedding of spheroids.
2. Harvest spheroids from the 96-well plates using a multichannel pipettor, and collect them in a pipetting reservoir (*see* **Notes 27** and **28**). Use a separate reservoir per treatment condition.
3. Transfer the spheroids into a 50 mL tube, and centrifuge for 4 min at 200 × *g* at room temperature without brake (*see* **Note 29**).
4. Aspirate supernatant carefully to avoid damage of spheroids. Add 10 mL of HEPES/Ca buffer to the spheroids, mix carefully by gently inverting the tube, and centrifuge again for 4 min at 200 × *g* at room temperature without brake.
5. Calculate the amount of required thrombin (10 μL of 20 U/mL thrombin is needed for each well with embedded spheroids). Dilute thrombin stock solution (100 U/mL) 1:5 with HEPES/Ca buffer to obtain the final concentration of 20 U/mL (*see* **Note 30**).
6. Aspirate the supernatant of spheroids carefully. Add 2 mL of the diluted fibrinogen solution (1.8 mg/mL) including aprotinin to approximately 200 spheroids, and mix carefully (*see* **Note 28**).
7. Add 10 μL of 20 U/mL thrombin per well of a non-coated 24-well cell culture plate (*see* **Note 31**).
8. Immediately add 300 μL of the spheroid/fibrinogen suspension to each thrombin-containing well of the 24-well plate, and gently pipette it up and down twice (*see* **Note 32**).
9. Incubate the plate at 37 °C without CO_2 supply for 20 min for polymerization of fibrin (*see* **Notes 33** and **34**).
10. When the fibrin gel is formed, add 350 μL of spheroid growth medium, and incubate for 30 min at 37 °C and 5% CO_2. Within this time, change the medium carefully after 10 and 20 min without touching the gel (*see* **Note 35**).
11. Aspirate the medium carefully and add 300 μL of spheroid growth medium.

12. Add compounds of interest (growth factors, drugs), and mix carefully by gently moving the plate (*see* **Note 36**).
13. Incubate the plate with spheroids at 37 °C, 5% CO_2 for 24 or 48 h (*see* **Note 37** and **38**).

3.1.4 Fixation and Analysis of Spheroid Sprouting

1. Fix the spheroids 24 or 48 h after stimulation. Carefully aspirate the medium without touching the gel, add 500 µL cold 4% PFA to each well, and incubate for 10 min on ice. Aspirate PFA, wash the gel twice with 500 µL of PBS, and add 500 µL of PBS. At this stage spheroids can be stored (*see* **Note 39**).
2. Take 50× magnification pictures of the fixed spheroids in bright-field microscopy using an inverse microscope (*see* **Notes 40–42**). Save TIFF-files and corresponding meta-files.
3. For analysis, load the TIFF-files into a software, which is able to process meta-files and to acquire the correct scale information of the picture.
4. Determine the number and length of sprouts per spheroid. For this, zoom into the pictures, and trace the sprouts from their origin to the end using the "polyline" tool of the software (*see* Fig. 1). Export data on the number and length of polylines (i.e., sprouts) into a spreadsheet program (*see* **Note 43**). Calculate mean values of sprout number and length per condition.
5. Calculate mean values from several independent experiments, and perform statistical analysis (representative images shown in Figs. 2 and 3).

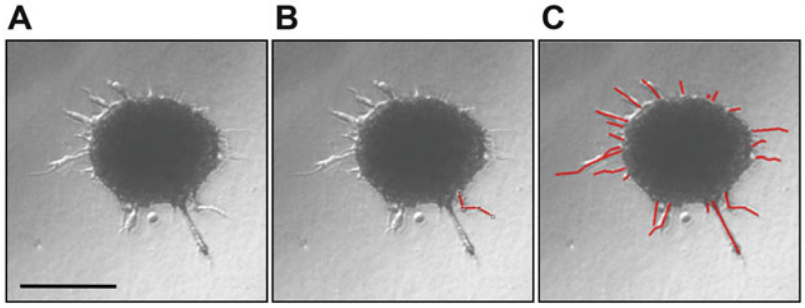

Type	Length (µm)
Polyline	45.35
Polyline	62.88
Polyline	19.90
Polyline	23.75
...	...
Count	21
Mean	47.35

Fig. 1 Analysis of sprouting from HUVEC spheroids. (**a**) TIFF-files of spheroid images (50× magnification) are loaded into an appropriate software for quantification. (**b**, **c**) Spheroid sprouts are traced with the tool *polyline* from their origin to the end including kinks. (**d**) Data are exported into a spreadsheet program. The number of polylines and their length in µm correspond to the number and length of the sprouts. Five to ten spheroids per experimental condition are quantified and averaged. Mean values and standard deviations need to be calculated from several independent experiments. Scale bar 200 µm

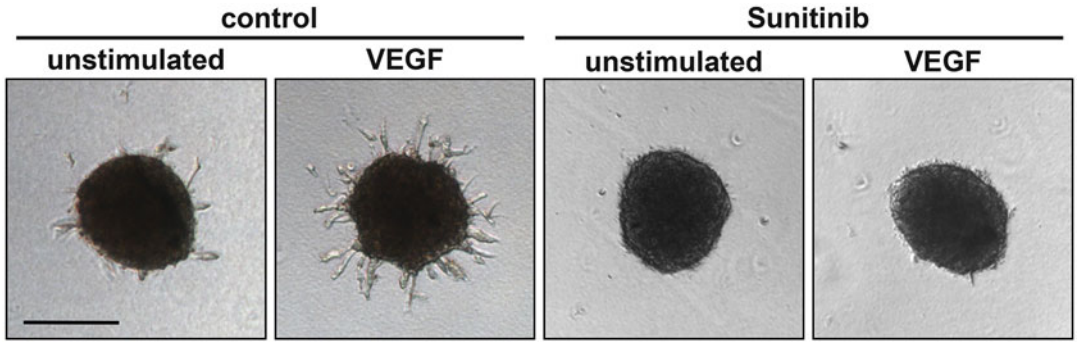

Fig. 2 VEGF induces sprouting in HUVEC spheroids. Embedded HUVEC spheroids were treated with 50 nM sunitinib, a VEGF receptor 2 inhibitor, or vehicle. After 30 min, 10 ng/mL VEGF was added. Spheroids were fixed after 48 h, and images were taken at 50× magnification. VEGF induced strong sprouting, which was completely inhibited by sunitinib. Scale bar 200 μm

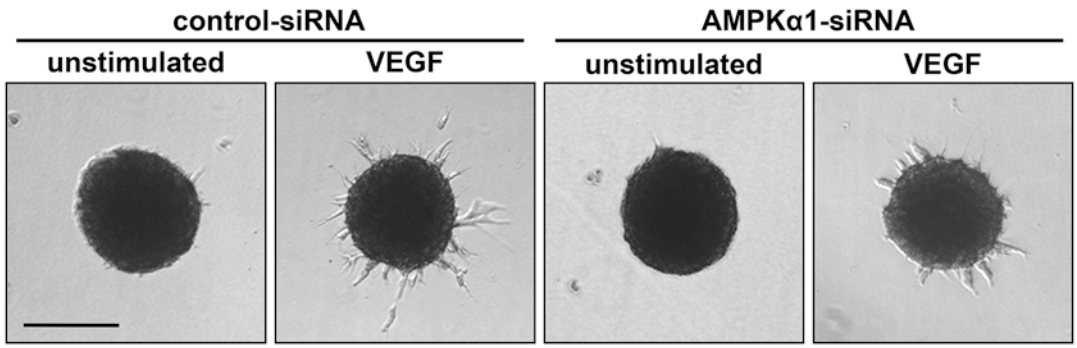

Fig. 3 AMPKα1 is involved in VEGF-induced sprouting. HUVEC were seeded on 60-mm cell culture dishes and transfected with 0.5 μg/mL control-siRNA or 0.5 μg/mL AMPKα1-siRNA, respectively, using the SAINT-sRNA transfection reagent. After 72 h, spheroids were generated from control and AMPKα1-depleted cells, embedded in fibrin gels and stimulated with 10 ng/mL VEGF for 48 h. After fixation of spheroids images were taken. VEGF-induced sprouting was inhibited in AMPKα1-depleted cells by approximately 45% as described previously [2]. Note that in the paper published by Stahmann et al. [2], the sprouting effect induced by VEGF was lower. This is likely related to differences in growth conditions, especially in the applied serum, and to an optimized protocol as described here. Scale bar 200 μm

3.2 Matrigel Plug Assay

3.2.1 Mouse Model

1. Perform experiments with sex-matched 3-month-old wild-type and AMPKα1 knockout mice. Carry out all animal procedures in accordance with the guidelines of the local and national committees for animal experiments.
2. Use a mouse identification system (i.e., ear punch or tag, tattoo).

3.2.2 Generation of Matrigel Plugs in Mice

1. Calculate the amount of Matrigel needed for your experiment. For adult mice 2× 500 μL per mouse are required to generate control and experimentally treated plugs, respectively (*see* **Note 44**). Thaw the Matrigel overnight in an ice bath.

2. Cool all required solutions and materials to 4 °C (PBS, pro- and antiangiogenic compounds, 15 mL tubes, 2 mL tubes, pipette tips, 1 mL syringes, 20- and 27-gauge needles) (*see* **Note 45**). All solutions and materials have to be sterile. Work under a laminar flow hood.
3. After thawing, mix the Matrigel carefully by slowly pipetting it up and down ten times with precooled tips (*see* **Note 46**). Prepare 1.5 mL aliquots in 2 mL tubes.
4. Add the required agents (growth factors, inhibitors) or vehicles to the Matrigel solution; vortex and spin briefly in a precooled 4 °C centrifuge (*see* **Note 47**). All solutions have to be kept at 4 °C before being added to Matrigel. VEGF is applied at a final concentration of 400 ng/mL together with 400 μg/mL of heparin (*see* **Note 48**).
5. Fill 500 μL of Matrigel with or without added compounds into a 1 mL syringe using a 20-gauge needle. Keep the syringe with Matrigel flat on ice until use (*see* **Note 49**).
6. Determine the body weight of each mouse, and inject a mixture of anesthetics intraperitoneally (final concentrations: 0.5 mg/kg medetomidine, 0.05 mg/kg fentanyl, 5 mg/kg midazolam).
7. Disinfect the flanks of the mice with 70% ethanol using a Q-tip.
8. Remove the Matrigel-containing syringe from the ice, and keep it at room temperature 5 min before injection (*see* **Note 50**).
9. For injection, a 27-gauge needle is placed to the syringe. Remove remaining bubbles before injection. Inject 450–500 μL of Matrigel subcutaneously into the flank of the mice, and leave the needle at this site for 30 s to avoid backflow. Press a Q-tip on the injection site for 1–2 min until polymerization starts. Each mouse needs to receive two implants, i.e., the control Matrigel and the experimentally treated Matrigel in the right or left flank, respectively. Make sure that the two plugs are sufficiently distant from each other.
10. Inject the antidote mixture intraperitoneally (final concentrations: 2.5 mg/kg atipamezole, 1.2 mg/kg naloxone, and 0.5 mg/kg flumazenil).
11. Leave the mouse for 7 days in the animal facility under normal housing conditions.
12. Sacrifice the mouse by cervical dislocation.
13. Take off the plug from each flank by carefully excising it from the surrounding tissue. Take pictures from plugs for documentation (*see* **Note 51**).
14. Transfer the plug into 5 mL of zinc fixative (*see* **Note 52**).
15. Incubate the plugs in zinc fixative for 24 h at room temperature.

3.2.3 Embedding of Matrigel Plugs in Paraffin

1. Transfer the fixed plugs into labelled tissue cassettes. Labelling has to be performed with a lead pencil (*see* **Note 53**). Collect the cassettes in a basket (belonging to the tissue processing equipment), and put it into a container filled with tap water. Close the basket with the metal lid, and place the container under gently running tap water for 2 h.
2. Take out the basket from the container, let the water drip off, and wipe off the remaining water with a dry tissue (*see* **Note 54**).
3. Insert the basket into a tissue processing equipment, and perform dehydration of samples according to the following protocol: 2× 1 h in 70% ethanol, 1 h in 96% ethanol, 2× 2 h in 96% ethanol, 2× 2 h in 99% ethanol, 1 h in ethanol:xylene 2:1, 1 h in ethanol:xylene 1:2, 1 h in xylene, 2 h in melted paraffin, and another 3 h in a second vessel with melted paraffin.
4. Transfer the tissue cassettes to an embedding station. Place the Matrigel plugs with the help of a warm forceps into a metal casting mold with the flat side to the bottom. Fill the mold with melted paraffin and let the plug sink for 5 s (*see* **Note 55**). Put the labelled part of the tissue cassette on top of it, add more paraffin, and transfer the whole mold to the cold plate to solidify the paraffin. After 30 min, remove the paraffin block from the mold, and store it at room temperature.
5. Obtain sections of the Matrigel plugs for staining using a microtome. Cut the paraffin block down till the plug is visible (*see* **Note 56**). Discard 500 μm and start sectioning with four 5 μm sections (level 1). Repeat this step for up to 12 more levels with 100 μm distance in between. Transfer sections into a water bath at room temperature using a small paintbrush, and keep them there until mounting (*see* **Note 57**).
6. For mounting, transfer sections into a 37 °C water bath using a glass slide (*see* **Note 58**). Let them float on a labelled polylysine-coated glass slide, and fix them with the help of a needle. Mount two sections on one slide. Dry sections at room temperature for 24 h. They can be stored at room temperature or at 2–8 °C in slide storage boxes for several years.

3.2.4 Analysis of Angiogenesis in Matrigel Plugs by CD31 Staining

1. Rehydrate the Matrigel plug sections by incubating them 3× 10 min in xylene, followed by subsequent 5 min incubations in 99%, 96%, 70%, and 50% ethanol and ddH_2O.
2. For antigen retrieval, transfer the slides into citrate buffer (prewarmed for 5 min in a microwave, 630 W), and boil them for 12 min in a microwave set to 630 W. Afterwards, leave the slides in the buffer until they cool down to room temperature.

3. Wash the slides 8 min in PBS and incubate them for 8 min in PBST. Transfer the slides into an immunostaining system, and add PBST to prevent drying.
4. Add blocking solution and incubate for 30 min at room temperature (*see* **Note 59**).
5. Wash 2 × 5 min with PBST.
6. Add the primary anti-CD31 antibody diluted in blocking solution, and incubate for 2 h at room temperature or longer times at 4 °C.
7. Wash 3 × 5 min with PBST.
8. Add the fluorescent-labelled secondary antibody diluted in blocking solution, and incubate for 60 min at room temperature in the dark.
9. Wash 3 × 5 min with PBST and 2 × 5 min with PBS.
10. Embed the slides with fluoromount-G and mount a glass coverslip over the Matrigel section (*see* **Note 60**).
11. Let the slides dry overnight at room temperature and store them in slide storage boxes in the dark at 4 °C (*see* **Note 61**).
12. Scan the sections at 50× magnification at a laser scanning microscope or 200× magnification with an epifluorescent microscope, and allow stitching of single images (*see* **Note 62**).
13. For analyzing open the stitched pictures in ImageJ or a comparable analyzing software.
14. Manually define the plug area and set an automatic threshold ("Otsu") (*see* Fig. 4).
15. Analyze CD31-positive pixels in the total plug area.

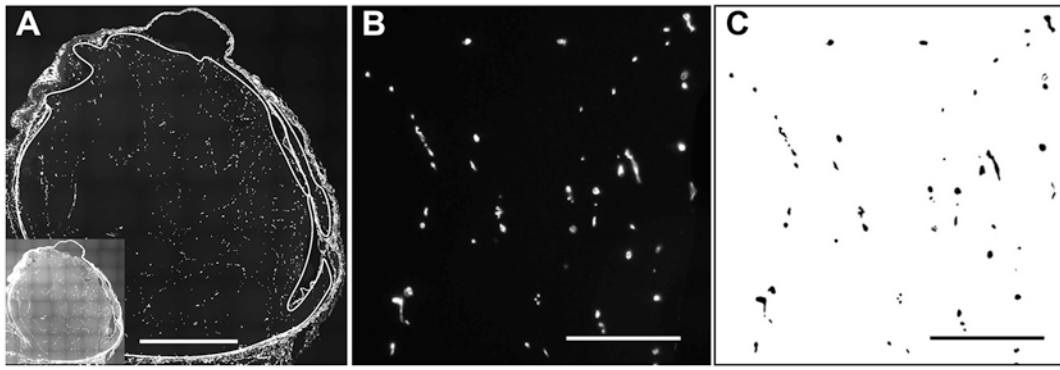

Fig. 4 Analysis of Matrigel plug sections with ImageJ. (**a**) The plug section is scanned at a 200× magnification with an epifluorescent microscope, stitched automatically (see the adjusted brighter insert), and loaded into ImageJ. The plug area is defined manually, an automatic threshold is set using the "Otsu" method, and the CD31-positive area is normalized to the whole plug area. (**b**, **c**) An enlarged section of the whole plug is shown to illustrate the vessels before (**b**) and after (**c**) thresholding. Scale bars 1000 μm (**a**) or 100 μm (**b**, **c**)

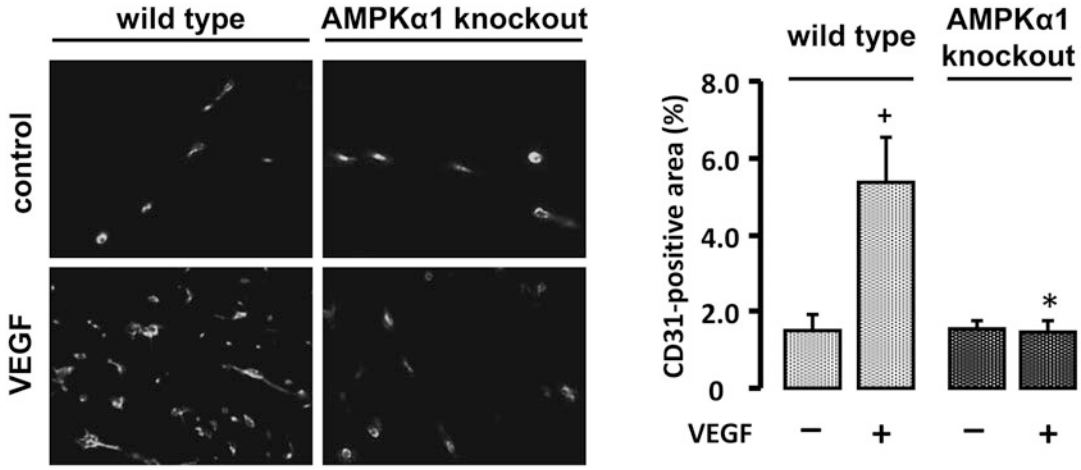

Fig. 5 VEGF-induced tube formation is inhibited in AMPKα1 knockout mice§. 500 μL of Matrigel including 200 ng of VEGF and 200 μg of heparin or 500 μL Matrigel without VEGF was injected subcutaneously into the right or left flank, respectively, of wild-type or AMPKα1 knockout mice. Plugs were removed after 7 days, fixed in zinc fixative, and embedded in paraffin. Tissue sections were stained with an anti-CD31 antibody and evaluated by fluorescence microscopy. Representative images (400×) and an analysis of the vascularized area are shown. Mean ± SEM; $n = 4$ for control plugs, $n = 13$ or 14 for VEGF-containing plugs in wild-type or AMPKα1 knockout mice, respectively. $^{+}p < 0.05$ versus non-VEGF-treated controls; $^{*}p < 0.05$ versus the respective values in wild-type mice. §This research was originally published in The Journal of Biological Chemistry: Stahmann N, Woods A, Spengler K, Heslegrave A, Bauer R, Krause S, Viollet B, Carling D, Heller R. Activation of AMP-activated protein kinase by vascular endothelial growth factor mediates endothelial angiogenesis independently of nitric-oxide synthase. *J Biol Chem* 2010; 285: 10638-52. © the American Society for Biochemistry and Molecular Biology

16. To obtain a representative evaluation for each plug, monitor two sections from at least four levels, respectively, and calculate the final average from all values.
17. Representative images from Matrigel plugs in wild-type and AMPKα1 knockout mice as published by Stahmann et al. [2] are shown in Fig. 5.

4 Notes

1. HUVEC are prepared from umbilical cords by filling the vein with 0.01% collagenase and incubating it for 3 min at 37 °C. Dissociated cells are collected and seeded in endothelial growth medium on culture flasks coated with 0.2% gelatine. After reaching confluency, cells are detached with Trypsin/EDTA and split at a 1:3 ratio. Cells of the first passage are used to generate spheroids.
2. We have good experiences with endothelial mitogen from BTI Inc. or endothelial growth supplement from Sigma-Aldrich.

3. We obtain approximately 90% downregulation using AMPKα1- and AMPKα2-specific siGENOME SMARTpool siRNA from Dharmacon (GE Healthcare).
4. The transfection reagent SAINT-sRNA (formerly SAINT-RED, Synvolux Products and Therapeutics) uses the principle of lipofection and shows good results in HUVEC.
5. Autoclaving is required for sterility and does not affect the structure of methylcellulose.
6. Initial dissolving at 60 °C is critical; methylcellulose will not dissolve at lower temperatures and will precipitate at higher temperatures. Use a water bath rather than a heating plate. Warm up the methylcellulose solution at 60 °C in a water bath for 20 min, and take it out four to five times for 1 min of stirring on a magnetic stirrer. The final overnight stirring at 4 °C will lead to complete dissolution.
7. Use only the upper 45 mL from 50 mL. The sediment may contain residual cellulose fibers.
8. Prepare fresh methylcellulose stock solution regularly; it should be stored not longer than 6 months.
9. HEPES buffer cannot be autoclaved since it contains glucose.
10. Aliquots can be stored at −20 °C for up to 1 year. Avoid repeated thawing/freezing.
11. Prepare approximately 200 μL of the fibrin stock solution per sample. Some of the fibrinogen is lost during dissolving, and an extra volume may be needed for additional wells (*see* **Note 32**).
12. U-shaped tubes provide a larger contact area between fibrinogen powder and HEPES buffer.
13. By adding HEPES buffer to the rim of the tube, you can wash away the fibrinogen powder on the wall. Pipetting the buffer directly onto fibrinogen leads to clumping.
14. Protein determination can be done according to Lowry or Bradford. Perform measurement at least in triplicates.
15. Aliquots can be stored at −20 °C for up to 1 year. Avoid repeated thawing/freezing. Keep thrombin aliquots on ice during use.
16. Low serum concentration in spheroid growth medium is required to reduce spontaneous sprouting.
17. We use Matrigel from BD Biosciences (BD 356231), which has a protein concentration between 9 and 12 mg/mL. Since the composition of Matrigel batches may vary significantly, it is essential to test the batch in a small pilot study before performing a bigger experiment.

18. We use zinc fixative from BD Biosciences (BD 550523). Alternatively, it can be prepared by adding 0.5 g/L calcium acetate, 5.0 g/L zinc acetate, and 5.0 g/L zinc chloride to 0.1 M Tris buffer, pH 7.4.
19. Use serum from the same species as the secondary antibody source.
20. BSA-c is a 10% (w/v) solution of acetylated BSA, which prevents charge-based background by blocking polycationic sites of specimen.
21. We obtain good results with the polyclonal anti-CD31 antibody from Acris (AP06560PU-N).
22. We use an Alexa-Fluor 488-labelled goat anti-rabbit secondary antibody.
23. Prepare pooled cell suspension for each experimental condition (i.e., siRNA treatment).
24. Suspend cells in 1 mL of growth medium before adding the remaining 4 mL.
25. Embed approximately 20–30 spheroids per well of a 24-well cell culture plate. Calculate for 30–40 spheroids since losses occur during washing procedures. Higher numbers of spheroids per well may limit space for individual sprouting and lead to fusion of adjacent sprouts. Run positive (treatment with basic fibroblast growth factor (bFGF)) and negative controls (no treatment).
26. To prepare 96 spheroids in a 96-well plate, mix 8 mL of cell suspension with a concentration of 37,500 cells/mL and 2 mL methylcellulose.
27. Check spheroids under the microscope before harvesting. Instability may be related to poorly dissolved methylcellulose.
28. Use pipette tips with a sufficiently wide diameter at the end to avoid damaging spheroids due to shear stress.
29. Do not pool spheroids from more than three 96-well plates to restrict shear stress during future pipetting.
30. Dilution of thrombin is preferentially done during the last centrifugation of spheroids.
31. Add thrombin as a drop in the middle of each well. Thrombin will convert the subsequently added fibrinogen into a solid fibrin gel.
32. Mix gently to obtain homogeneous fibrin formation. Avoid the formation of air bubbles. Control each well under the microscope for the number of spheroids and equal distribution. If required, prepare additional wells from the residual spheroid suspension.

33. Use an incubator without CO_2 supply or a heating plate at 37 °C to allow pH maintenance via HEPES buffer.
34. Control fibrin formation in parallel in a reaction tube. Disturbed fibrin formation may be due to (1) decay of fibrinogen, (2) insufficient activity of thrombin (repeated thawing/freezing, storage at room temperature), and (3) insufficient mixing of thrombin with the fibrinogen/spheroid suspension.
35. This step is required to equilibrate spheroids with medium and to remove residual thrombin.
36. The concentration of added compounds has to be calculated for a total volume of 600 μL per well (300 μL of fibrin gel + 300 μL of spheroid medium).
37. The standard incubation time is 48 h. If sprouting is enhanced (*see* **Note 38**) or spheroids are unstable, evaluation after 24 h is advisable.
38. Spheroids may exhibit high basal sprouting due to robust pipetting, insufficient removal of thrombin, transfection, and/or age of cells. In the latter case, incubation of spheroids in low serum conditions before embedding may be of use. VEGF-induced sprouting may be low when VEGF is inappropriately stored or repeatedly thawed/frozen.
39. For storage, add the lid of the plate and seal the plate with parafilm. Plates with spheroids can be stored for approximately 2 weeks at 4 °C. In case longer storage is required, add 0.2 mg/mL sodium azide. Note that prolonged storage will affect the quality of the spheroids.
40. For quality improvement of the pictures, remove the lid of the plate.
41. Take pictures from 5 to 10 representative spheroids per well.
42. Do not evaluate spheroids at the edge of the well because sprout formation may be spatially impaired. Use phase contrast in case spheroids appear too bright.
43. If the meta-file is read correctly, the program should give the length of the polylines in μm range (in average between 10 and 100 μm per sprout).
44. Some Matrigel gets lost during pipetting due to its high viscosity; thaw about 30% more than the volume required for injections. Non-used Matrigel can be frozen again but avoid multiple thawing/freezing cycles.
45. Pipette tips are cooled by putting them into sterile tubes in an ice bath.
46. The Matrigel flask can be slightly rotated but avoid inverting it upside-down.

47. Inclusion of positive (for instance, bFGF) and negative controls (no treatment, inhibitors only) in an experimental series is essential.
48. Heparin supports efficient binding of VEGF 165 to the VEGF receptors.
49. Be careful to fill the syringe slowly and to avoid bubbles. Matrigel is highly viscid.
50. Keeping Matrigel at room temperature 5 min before injection leads to a faster polymerization in vivo and helps to prevent leakage.
51. The plugs can cause an inflammatory response, which may interfere with the effect of the added compounds on angiogenesis. Occasionally, the Matrigel plugs can be absorbed.
52. We obtain best whole plug CD31 stainings when plugs are processed with zinc fixative compared to 4% PFA.
53. Ball pen or marker labels will disappear when the cassette is treated with solvents at a later stage.
54. Remaining water will dilute the ethanol, in which the basket will be transferred afterwards.
55. Use a warm forceps if the plug has moved and needs to be repositioned. If the plug is placed on the bottom of the mold, it will be located on top of the paraffin block, which is of advantage for cutting sections.
56. The Matrigel plug can be macroscopically distinguished from the normal tissue.
57. At room temperature the section will not stick to the slide.
58. Fragmentation of the sections may be due to too high temperature of the water bath.
59. We use a volume of 150 μL of blocking solution or diluted antibody per slide and 1 mL of PBS per washing step when using the Shandon Sequenza® immunostaining center together with the Shandon coverplate technology.
60. Pressing carefully but firmly on the coverslip during embedding gives a flatter surface which helps with focusing on the microscope.
61. Slides with paraffin-embedded sections can be stored at 2–8 °C for several years in slide storage boxes. Long-term storage may reduce the staining intensity for certain antigens.
62. The stitching settings should be optimized before starting imaging.

References

1. Fisslthaler B, Fleming I (2009) Activation and signaling by the AMP-activated protein kinase in endothelial cells. Circ Res 105(2):114–127. https://doi.org/10.1161/CIRCRESAHA.109.201590
2. Stahmann N, Woods A, Spengler K, Heslegrave A, Bauer R, Krause S, Viollet B, Carling D, Heller R (2010) Activation of AMP-activated protein kinase by vascular endothelial growth factor mediates endothelial angiogenesis independently of nitric-oxide synthase. J Biol Chem 285 (14):10638–10652. https://doi.org/10.1074/jbc.M110.108688
3. Youn JY, Wang T, Cai H (2009) An ezrin/calpain/PI3K/AMPK/eNOSs1179 signaling cascade mediating VEGF-dependent endothelial nitric oxide production. Circ Res 104 (1):50–59. https://doi.org/10.1161/CIRCRESAHA.108.178467
4. Zibrova D, Vandermoere F, Goransson O, Peggie M, Marino KV, Knierim A, Spengler K, Weigert C, Viollet B, Morrice NA, Sakamoto K, Heller R (2017) GFAT1 phosphorylation by AMPK promotes VEGF-induced angiogenesis. Biochem J 474 (6):983–1001. https://doi.org/10.1042/BCJ20160980
5. Irvin MW, Zijlstra A, Wikswo JP, Pozzi A (2014) Techniques and assays for the study of angiogenesis. Exp Biol Med 239 (11):1476–1488. https://doi.org/10.1177/1535370214529386
6. Korff T, Augustin HG (1998) Integration of endothelial cells in multicellular spheroids prevents apoptosis and induces differentiation. J Cell Biol 143(5):1341–1352
7. Korff T, Augustin HG (1999) Tensional forces in fibrillar extracellular matrices control directional capillary sprouting. J Cell Sci 112 (Pt 19):3249–3258
8. Bayless KJ, Davis GE (2003) Sphingosine-1-phosphate markedly induces matrix metalloproteinase and integrin-dependent human endothelial cell invasion and lumen formation in three-dimensional collagen and fibrin matrices. Biochem Biophys Res Commun 312 (4):903–913
9. Carnevale E, Fogel E, Aplin AC, Gelati M, Howson KM, Zhu WH, Nicosia RF (2007) Regulation of postangiogenic neovessel survival by beta1 and beta3 integrins in collagen and fibrin matrices. J Vasc Res 44(1):40–50. https://doi.org/10.1159/000097976
10. Heiss M, Hellstrom M, Kalen M, May T, Weber H, Hecker M, Augustin HG, Korff T (2015) Endothelial cell spheroids as a versatile tool to study angiogenesis in vitro. FASEB J 29 (7):3076–3084. https://doi.org/10.1096/fj.14-267633
11. Nakatsu MN, Hughes CC (2008) An optimized three-dimensional in vitro model for the analysis of angiogenesis. Methods Enzymol 443:65–82. https://doi.org/10.1016/S0076-6879(08)02004-1
12. Passaniti A, Taylor RM, Pili R, Guo Y, Long PV, Haney JA, Pauly RR, Grant DS, Martin GR (1992) A simple, quantitative method for assessing angiogenesis and antiangiogenic agents using reconstituted basement membrane, heparin, and fibroblast growth factor. Lab Investig 67(4):519–528
13. Malinda KM (2001) In vivo matrigel migration and angiogenesis assays. Methods Mol Med 46:47–52. https://doi.org/10.1385/1-59259-143-4:047
14. Staton CA, Reed MW, Brown NJ (2009) A critical analysis of current in vitro and in vivo angiogenesis assays. Int J Exp Pathol 90 (3):195–221. https://doi.org/10.1111/j.1365-2613.2008.00633.x
15. Adini A, Fainaru O, Udagawa T, Connor KM, Folkman J, D'Amato RJ (2009) Matrigel cytometry: a novel method for quantifying angiogenesis in vivo. J Immunol Methods 342 (1-2):78–81. https://doi.org/10.1016/j.jim.2008.11.016
16. Viollet B, Andreelli F, Jorgensen SB, Perrin C, Geloen A, Flamez D, Mu J, Lenzner C, Baud O, Bennoun M, Gomas E, Nicolas G, Wojtaszewski JF, Kahn A, Carling D, Schuit FC, Birnbaum MJ, Richter EA, Burcelin R, Vaulont S (2003) The AMP-activated protein kinase alpha2 catalytic subunit controls whole-body insulin sensitivity. J Clin Invest 111 (1):91–98. https://doi.org/10.1172/JCI16567
17. Jorgensen SB, Viollet B, Andreelli F, Frosig C, Birk JB, Schjerling P, Vaulont S, Richter EA, Wojtaszewski JF (2004) Knockout of the alpha2 but not alpha1 5′-AMP-activated protein kinase isoform abolishes 5-aminoimidazole-4-carboxamide-1-beta-4-ribofuranoside-but not contraction-induced glucose uptake in skeletal muscle. J Biol Chem 279 (2):1070–1079. https://doi.org/10.1074/jbc.M306205200

Chapter 34

Analysis of Muscle Stem Cell Fate Through Modulation of AMPK Activity

Marine Theret, Linda Gsaier, Sabrina Ben Larbi, Michèle Weiss-Gayet, and Rémi Mounier

Abstract

In this chapter, we describe the methods to isolate and culture muscle stem cells (MuSCs) from murine skeletal muscle in order to decipher the intrinsic effect of AMP-activated kinase activity on MuSC fate. Culture of MuSCs is a powerful model to recapitulate every step of stem cell behavior observed in vivo: activation, proliferation, differentiation, fusion and also self-renewal. We provide the detailed procedures to isolate pure MuSCs by a flow cytometry-based method using the selection of a combination of specific markers and to characterize MuSC fate (quiescence, activation, and differentiation) in response to AMPK activity modulation by assessing of the expression of stem cell (*e.g.*, Pax7) and myogenic marker (*e.g.*, MyoD).

Key words Metabolism, Stem cell behavior, Myogenesis, Muscle, Quiescence, Differentiation, Pax7, Flow cytometry

1 Introduction

Skeletal muscle stem cells (MuSCs) are widely recognized for their contributions to muscle regeneration [1]. At resting state, MuSCs (also named satellite cells) express the intracellular marker paired-box domain transcription factors Pax7 and remain quiescent under the basal lamina attached to the myofiber. During skeletal muscle regeneration, these cells are able to recapitulate the myogenic program to repair damaged myofibers [2]. Upon activation and expression of proliferation and activation markers such as Ki67 and myogenic differentiation 1 (MyoD), these cells are capable of both differentiating (leading to the downregulation of Pax7 and upregulation of MyoD and then myogenin expression) to repair muscle tissue after injury and self-renewing to replenish the stem cell pool by upregulating Pax7 and downregulating Ki67 and MyoD expression [3]. In order to maintain the pool of MuSCs for future needs, controlling the return into quiescence is crucial [2]. We recently

Dietbert Neumann and Benoit Viollet (eds.), *AMPK: Methods and Protocols*, Methods in Molecular Biology, vol. 1732, https://doi.org/10.1007/978-1-4939-7598-3_34,

identified AMP-activated protein kinase (AMPK), the master metabolic regulator of the cell, as an important player in MuSC self-renewal [4]. Thus, manipulating metabolic pathways might aid to regulate stem cell fate between self-renewal and differentiation.

This chapter provides full information on how to harvest muscles, sort MuSCs, and then study their fate in vitro. Here, we describe methods for muscle stem cell extraction and culture in order to investigate the importance of AMPK in metabolic pathway acting on MuSC fate in a cell-autonomous manner. A selection of a combination of specific cell surface receptor markers is used to isolate pure MuSCs *via* fluorescence-activated cell sorting (FACS). MuSC pool is defined through positive selection of cells expressing both α7-integrin and CD34, combined with negative selection of CD45 (marker of hematopoietic lineage), CD31 (endothelial cells), and Sca-1 (mesenchymal and hematopoietic stem cells) [5]. Then, to study MuSC behavior upon modulation of AMPK activity, the cell population is entirely assessed by a combination of Pax7 (muscle stem cell marker), Ki67 (proliferation marker) and MyoD (activation marker and commitment into the myogenic lineage marker) staining by immunochemistry. MuSC population can be deciphered in four groups of cells found: $Pax7^{+}Ki67/MyoD^{-}$ cells are quiescent, $Pax7^{+}Ki67/MyoD^{+}$ cells are activated, $Pax7^{-}Ki67/MyoD^{+}$ are committed cells that are mostly into the myogenic lineage and finally $Pax7^{-}Ki67/MyoD^{-}$ cells.

2 Materials

All culture media and sterile reagents are from Gibco-Life Technologies and plastics from BD Biosciences, unless otherwise indicated.

2.1 Mouse Dissection and MuSC Extraction

1. Material for mouse dissection (thin forceps, razor blade or thin scissors, thin sharp scissors).
2. Shaking water bath setup at 37 °C.
3. Vortex.
4. Ethanol diluted in water 70% (v/v).
5. Petri dishes 60 mm.
6. 30 ml polystyrene containers.
7. 0.22 μm Millex Syringe filter (Millipore, #SLGP033RS) and 20 ml syringe (TERUMO, #SS+20ES1)
8. 70 μm cell strainers.
9. 30 μm CellTrics® strainers.
10. 15 and 50 ml Falcon tubes.
11. Polypropylene round bottom FACS tubes.

12. Polystyrene round bottom FACS tubes.
13. 1× PBS: 138 mM NaCl, 2.7 mM KCl, 1.5 mM KH_2PO_4, 8 mM $Na_2HPO_4{\cdot}7H_2O$, pH 7.4.
14. Digestion buffer: DMEM/F-12, 10 mg/ml Collagenase B (Roche, #11 088 831 001), 2.4 U/ml Dispase (Roche, #04 942 078 001). Sterilize by filtration.
15. Heat-inactivated fetal bovine serum (FBS).
16. FACS buffer: 1× PBS, 2% (v/v) FBS.
17. Ammonium-chloride-potassium (ACK) buffer: 8 mg/l Nh_4Cl, 1 mg/l $KHCO_3$, 3.7 mg/l EDTA.$Na_2{\cdot}2H_2O$ (Lonza, #10-548E) .
18. Antibody mix: FACS buffer, 5 μg/ml anti α7integrin-647 (AB lab, #AB0000538), 2.5 μg/ml anti CD34-FITC (ebioscience, #11-0341-82), 0.2 μg/ml anti CD45-PE (ebioscience, #12-0451-82), 0.2 μg/ml anti CD31-PE (ebioscience, #12-0311-82), 0.2 μg/ml anti Sca1-PE (ebioscience, #12-5981-82).
19. 4′,6-diamidino-2-phénylindole (DAPI): 1 mg/ml stock solution.
20. Cell sorting machine (*e.g.*, Aria I).

2.2 Murine MuSC Culture

1. 0.22 μm sterile bottle-top filter.
2. 1× PBS: 138 mM NaCl, 2.7 mM KCl, 1.5 mM KH_2PO_4, 8 mM $Na_2HPO_4{\cdot}7H_2O$, pH 7.4.
3. Trypsin EDTA 0.25%: 0.25% (w/v) trypsin, 0.02% (w/v) EDTA.
4. Coating solution: 10% (v/v) Matrigel in DMEM/F-12. Keep the solution in ice until use (*see* **Note 1**).
5. MuSC medium: DMEM/F-12, 20% (v/v) FBS, 100 U/ml penicillin/streptomycin. Filter sterilizes using 0.22 μm filter unit.
6. MuSC growth medium: MuSC medium, 2% (v/v) Ultroser™ G serum substitute (*see* **Note 2**).

2.3 AMPK Activation/ Inhibition During MuSC Differentiation

1. MuSC differentiation medium: DMEM/F-12, 2% (v/v) horse serum, 100 U/ml penicillin/streptomycin.
2. 5-aminoimidazole-4-carboxamide-1-β-D-ribofuranoside (AICAR): 75 mM stock solution in DMSO.
3. 991 compound: 10 mM stock solution in DMSO.
4. 2 Deoxy-D-glucose (2-DG) .
5. STO-609: 10 mM stock solution in DMSO.

2.4 Immunolabeling of MuSCs

1. 1× PBS: 138 mM NaCl, 2.7 mM KCl, 1.5 mM KH_2PO_4, 8 mM $Na_2HPO_4{\cdot}7H_2O$, pH 7.4.
2. Paraformaldehyde (PFA): 1× PBS, 4% (w/v) PFA.
3. Mounting medium.
4. Permeabilization buffer: 1× PBS, 0.5% (v/v) Triton X-100.
5. Saturation buffer: 1× PBS, 2% (w/v) bovine serum albumin (BSA).
6. First antibody mix: 1× PBS, 1% (w/v) BSA, 1/100 anti-Pax7 antibody (Hybridoma bank, concentrate), 1/50 anti-MyoD antibody (Santa Cruz, #sc760) and 1/100 anti-Ki67 antibody (Abcam, #ab15580) (*see* **Note 3**) or 60 μg/ml anti-Desmin antibody (Abcam #ab32362) or 1/50 anti-active form of caspase 3 (Abcam, #ab32042).
7. Second antibody mix: 1× PBS, 1/200 anti-Mouse IgG Biotin-conjugated (Vector, #B1-2000), 1/200 anti-Rabbit IgG Cy3-conjugated (Jackson, #711-165-152).
8. Streptavidin mix: 1× PBS, 0.1% (v/v) DTAF-conjugated Streptavidin (Jackson, #016-010-084) .
9. Nuclei staining solution: 1× PBS, 2 nM (v/v) Hoechst (*see* **Note 4**).

3 Methods

3.1 MuSCs Extraction

From one adult healthy mice (3–6-month old) using the two hind limbs, 50,000–120,000 MuSCs can be sorted.

1. Keep on ice a 30 ml container and petri dishes. Fill the petri dishes with 5 ml of ice-cold 1× PBS (*see* **Note 5**).
2. Prepare digestion buffer and preheat at 37 °C.
3. Euthanize mice according to your local regulation. Harvest muscles of both hind limbs (including *tibialis anterior*, *gastrocnemius*, *quadriceps*, *ischio*, and *gluteus*), and put them in the petri dish previously filled with 1× PBS. Then discard fat, tendons, fascia, vessels, and nerves (*see* **Note 6**).
4. Pour muscle (without taking the PBS) in the cold 30 ml container, and crush in very small pieces to obtain a pulp.
5. Add 8 ml of the digestion buffer on the muscle slop and incubate for up to three rounds of 10 min in a shaking water bath at 37 °C (*see* **Note 7**).
6. Vortex the mixture between each round.
7. From here, all the next steps have to be made on ice and in sterile conditions.
8. Stop the digestion by adding 2 ml of FBS. Mix by pipetting up and down.

9. Add 20 ml of DMEM/F-12. Mix by pipetting up and down.
10. Filtrate the mixture on a 70 μm cell strainer (*see* **Note 8**).
11. Wash the 30 ml container with 10 ml of DMEM/F-12, and pass it through the same cell strainer.
12. Centrifuge at 350 × *g* for 10 min at 4 °C.
13. Eliminate supernatant and lyse red cells with 1 ml of ACK Buffer. Vortex until the solution become pink/red (3–5 s) .
14. Stop lysis by adding 10 ml of FACS buffer.
15. Centrifuge at 350 × *g* for 7 min at 4 °C.
16. Resuspend the pellet into 2 ml of FACS buffer.
17. Distribute in polystyrene round bottom FACS tubes in order to perform non-labeled, single labeling, CD34-FITC fluorescence minus one (FMO) and cell sorting tubes (*see* **Note 9**).
18. Add 2 ml of FACS buffer in each tube.
19. Centrifuge at 350 × *g* for 5 min at 4 °C.
20. Remove the supernatant, leave around 100 μl and homogenize the pellet.
21. Add 1 ml of the antibody mix (*see* **Note 10**).
22. Incubate the tubes protected from light for 20–40 min at 4 °C.
23. Stop labeling by adding 2 ml of FACS buffer.
24. Centrifuge at 350 × *g* for 5 min at 4 °C.
25. Resuspend the pellet with 0.5 ml of FACS buffer and filtrate using a 30 μm CellTrics strainer.
26. Wash the tube with 0.5 ml of FACS buffer and filter as above. Keep the tubes on ice and protected from light until cell sorting.
27. Just before sorting, add DAPI at final concentration of 1 μg/ml (*see* **Note 11**).
28. To sort MuSC, please follow our gating strategy. Gate cells based on their size and granularity, and then select single cell by eliminating high FSC-H and SSC-H cells. To follow, gate on negative cells for DAPI and CD45/CD31/Sca1. Finally, MuSCs are the double-positive population for CD34 and α7integrin (*see* Fig. 1).
29. Recover cells in polypropylene round bottom FACS tubes containing 0.5 ml of FBS, and note the number of cells you recovered for the cell culture part.
30. *Quantum satis* the FACS tube with MuSC growth medium to 4 ml.
31. Centrifuge at 350 × *g* for 10 min at 4 °C.
32. Discard carefully the supernatant.
33. Resuspend the pellet in 1 ml of MuSC growth medium.

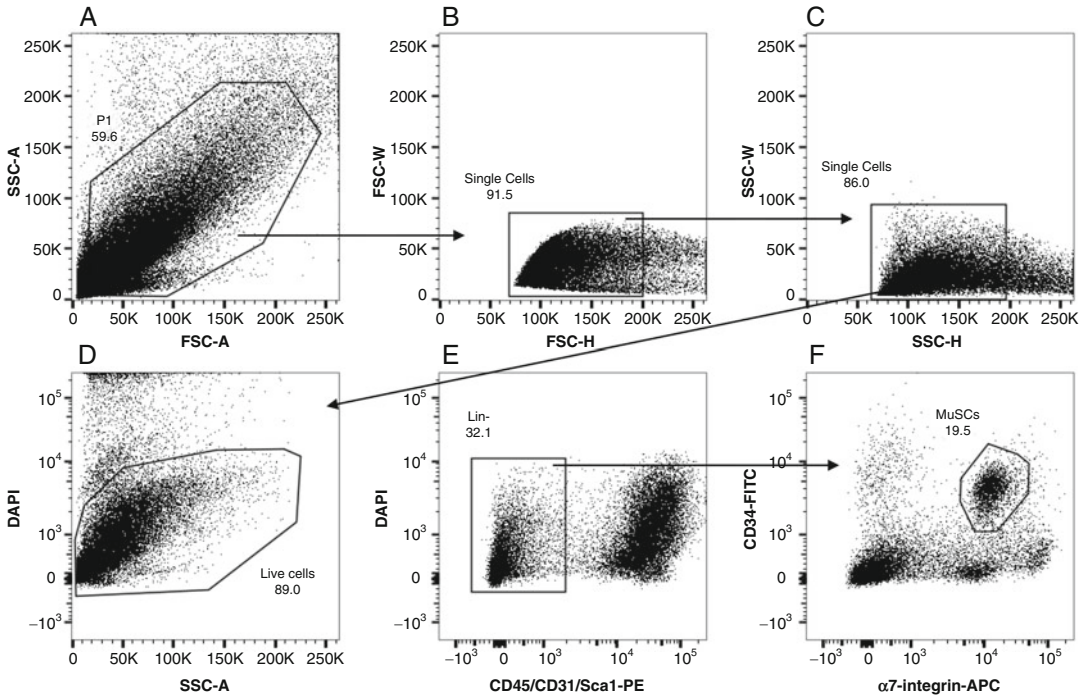

Fig. 1 Muscle stem cell extraction by cell sorting. Gating strategy to sort muscle stem cells (MuSCs) from hind limbs. MuSCs are sorted on DAPI^{neg}, CD45/CD31/Sca1^{neg} and CD34/α7int^{pos} cells. (**a**) Cells are selected on their SSC/FSC localization and then (**b**, **c**) double selected on low FSC-H and SSC-H to avoid cell doublets. (**d**) Cells are then negatively selected for DAPI and (**e**) CD31/CD45/Sca1. (**f**) Finally, the MuSC population is the double positive for CD34 and α7integrin. This last gate is the population that has to be sorted

3.2 Measure of MuSC Proliferation

1. Coat 48-well plate by adding 80 µl of coating solution in each well and incubate for 30 min at 37 °C. Wash twice with 1× PBS to avoid Matrigel lump (*see* **Note 1**).
2. Plate 50 MuSCs (numbers from the sorting) *per* well in the coated 48-well plate in MuSC growth medium containing AMPK activators or not (*see* Table 1). Appropriate control treatment should be done (*e.g.*, DMSO).
3. From day 2 to day 7, under the microscope and with a cell counter, calculate the number of cells in each clone and in each well to assess MuSC proliferation and the impact of AMPK activation or inhibition on it.

3.3 MuSC Amplification

This method is continuing from Subheading 3.1.

1. Coat 12-well plate by adding 500 µl of coating solution in each well and incubate for 30 min at 37 °C. Wash twice with 1× PBS to avoid Matrigel lump (*see* **Note 1**).
2. Plate cells in the coated 12-well plate at 3000 cells/cm² in MuSC growth medium.

Table 1
List of AMPK activators or inhibitor and their range of concentration to be used in vitro

Molecules	Concentration range (min–max)
5-aminoimidazole-4-carboxamide-1-β-D-ribofuranoside (AICAR)	0.1–1 mM
Compound 991	0.1–10 μM
2 deoxy-D-glucose (2-DG)	50–500 nM
STO-609	1–10 μM

3. Change the media every day during 4 days (rinse once with DMEM/F-12 and then add fresh MuSC growth medium) and then every 2 days until the cells entirely recover the well (from 4 to 7 days).
4. Harvest the cells by washing the well once with 1× PBS. Then, incubate the plate with 100 μl of 0.25% trypsin EDTA at 37 °C for 1 min. Check cell detachment under a microscope. Stop cell detachment by adding 200 μl of FBS. Harvest and spin cells at room temperature (RT) at 350 × *g* for 7 min. Resuspend the pellet in 1 ml of MuSC growth medium.
5. Count the cells using a hemocytometer, a cell counted and viability dye (*e.g.*, trypan blue).
6. Plate cells in 48-well plate coated with Matrigel (*see* **Note 1**) at 30,000 cells/cm² in MuSC growth medium (*see* **Notes 12** and **13**).
7. Six hours after plating, perform Pax7/Ki67/MyoD labeling to check MuSC activation (*see* Subheading 3.5).

3.4 Activation/Inhibition of AMPK in MuSCs

1. Six hours after plating, switch the media for MuSC differentiation medium, containing AMPK activators or not (*see* Table 1). Appropriate control should be done (*e.g.*, DMSO or water).
2. Forty-eight hours after switching the media, check that your cells form myotubes and perform Pax7Ki67MyoD labeling (*see* Subheading 3.5 and Fig. 2). For all molecules and concentrations, you should check that apoptosis is not highly induced. To proceed, perform an immunolabeling against the active form of caspase 3 (*see* Subheading 3.5).

3.5 Immunolabeling of MuSCs

To determine the percentage of $Pax7^{+}Ki67/MyoD^{-}$ (quiescent cells), $Pax7^{+}Ki67/MyoD^{+}$ (activated cells), $Pax7^{-}Ki67/MyoD^{+}$ (differentiating cells) and $Pax7^{-}Ki67/MyoD^{-}$ cells (differentiated

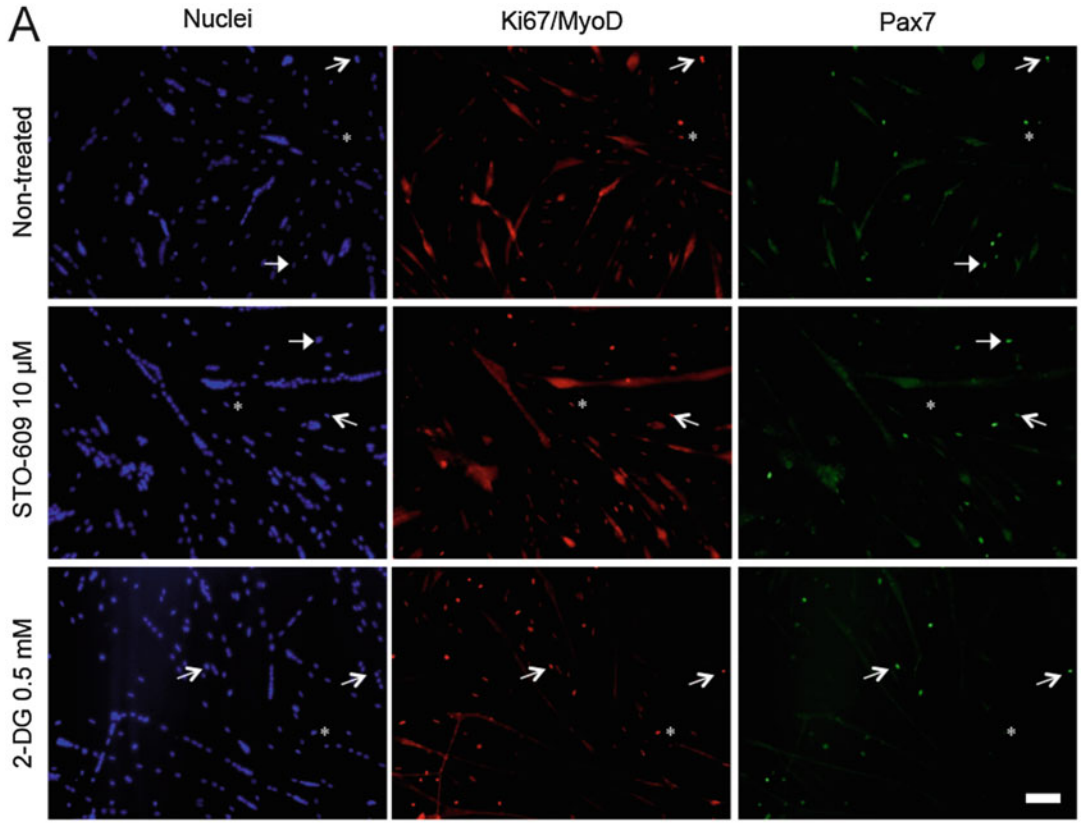

B

Populations (%)	Pax7⁺Ki67/MyoD⁻	Pax7⁺Ki67/MyoD⁺	Pax7⁻Ki67/MyoD⁺	Pax7⁻Ki67/MyoD⁻
Non-Treated	1.8	4.5	62.8	30.9
STO-609 10 µM	1.9	1.9	58.7	37.5
2-DG 0.5 mM	0.0	7.0	47.0	46.0

Fig. 2 Pax7Ki67MyoD labeling and analysis. MuSCs were extracted from total hind limbs as described. (**a**) Pax7Ki67MyoD labeling was performed after 48 h of culture in differentiation conditions: Non-treated (top panel), supplemented with STO-609 (10 µm, middle panel) or 2-deoxy-D-glucose (2-DG, 0.5 mM, bottom panel). Nuclei (Hoescht-Blue), Ki67/MyoD (red), and Pax7 (green) labeling. Full white arrows show $Pax7^{+}Ki67/MyoD^{-}$ quiescent cell; empty white arrows show activated $Pax7^{+}Ki67/MyoD^{+}$cell; Star shows $Pax7^{-}Ki67/MyoD^{+}$ cell. Scale bar = 100 µm. (**b**) Example of quantification of $Pax7^{+}Ki67/MyoD^{-}$ (quiescent), $Pax7^{+}Ki67/MyoD^{+}$ (activated), $Pax7^{-}Ki67/MyoD^{+}$ (committed), $Pax7^{-}Ki67/MyoD^{-}$ (differentiated) cells

cells), labeling for Pax7 (muscle stem marker), Ki67 (proliferation marker) and MyoD (activation marker and commitment into the myogenic lineage marker) is performed (*see* **Note 14**). You can also perform desmin labeling to determine fusion of myogenic cells (*see* **Note 15**) or active caspase 3 labeling to test apoptosis induced by AMPK activators.

1. Wash the 48-wells plate once with 1× PBS (*see* **Note 16**).
2. Add 100 µl of 4% PFA *per* well and incubate for 10 min at RT.
3. Wash wells with 1× PBS for 5 min. Repeat three times.
4. Add 100 µl of permeabilization buffer *per* well and incubate for 10 min at RT.
5. Wash wells with 1× PBS for 5 min. Repeat three times.
6. Add 100 µl of saturation buffer *per* well and incubate at least 1 h at RT.
7. Wash wells with 1× PBS for 5 min. Repeat three times.
8. Add 80 µl of the first antibody mix *per* well, and incubate overnight at 4 °C in humid chamber.
9. Wash wells with 1× PBS for 5 min. Repeat three times.
10. Add 80 µl of the second antibody mix *per* well, and incubate for 1 h at 37 °C in humid chamber.
11. Wash wells with 1× PBS for 5 min. Repeat three times.
12. Add 100 µl of the streptavidin mix *per* well and incubate for 45 min at 37 °C in humid chamber (except for act-casp3 labeling alone).
13. Wash wells with 1× PBS for 5 min. Repeat three times.
14. Add 100 µl of the nuclei staining solution; incubate 10–20 s at RT.
15. Wash wells with 1× PBS for 5 min. Repeat three times.
16. Add 100 µl of mounting medium in each well.
17. Store at 4 °C until analyzed (*see* Fig. 2a, b).

4 Notes

1. Matrigel is a solubilized basement membrane preparation extracted from the Engelbreth-Holm-Swarm (EHS) mouse sarcoma, a tumor rich in extracellular matrix proteins, including laminin (a major component), collagen IV, heparin sulfate proteoglycans, entactin/nidogen and a number of growth factors, which occur naturally in the EHS tumor. Defrost the Matrigel at +4 °C overnight, aliquot it in chill Eppendorf, and freeze again. On the day of your experiment, defrost the

Matrigel at +4 °C for 4 h. Just before use, dilute it at 1/10 in cold DMEM/F-12 and keep on ice.

2. To dissolve Ultroser™ G (Pall Corporation, #15950-017), add 20 ml of sterile H_2O on the top of the powder without shaking. After 20 min of incubation at RT, vigorously shake and wait until complete dissolution. Pass it through a 0.22 μm filter. Add to the media or froze it until further use.
3. As concentration of the Ki67 antibody can differ between batches, titration should be performed.
4. The stock solution is 2 mM (w/v) in water. Dilute the stock solution in 1× PBS to obtain a solution at 2 nM (v/v), and keep it at +4 °C for 1 week only.
5. Use one 30 ml container and one petri dish *per* mouse. If the amount of muscle is less than the whole hind limbs (*e.g.*, two *tibialis anterior*), the use of 4 ml polypropylene FACS tubes for the digestion step is recommended.
6. Mice have to be dissected in <5 min after death. If the time of dissection is longer, the number of viable cells will decrease.
7. A too long incubation in the digestion buffer (more than 1 h) will result in an increase of leaking labeling and of death cell.
8. Be careful the mixture is very dense and the cell strainer can be blocked. Change the filter every time it is required.
9. For 1 ml of sample, take off 50 μl to perform control tubes (non-labeled, single labeling, and CD34-FITC FMO). Adjust the volume in function of your sample.
10. Quantity of antibody is for one entire mouse. For the single tubes (single labeling and FMO), use 100 μl of the antibody mix.
11. Viable cells do not incorporate the DAPI and are so negative for it.
12. Due to side effect of the border that could perturb MuSC fate, avoid the use of 96-well plate.
13. Plate the cells in a high volume (400–500 μl/well) to avoid side effect of the meniscus.
14. In this assay we do not make the distinction between Ki67 and MyoD expression. To do so, change one of the two antibodies for a goat-made antibody, for example.
15. Fusion is evaluated as the percentage of nuclei into myotubes among the total number of nuclei.
16. For all the washes, carefully discard supernatant with a needle, and put 1× PBS with another needle on a 2.5 ml syringe. All the volumes here are for 48-well plate.

References

1. Mounier R, Chretien F, Chazaud B (2011) Blood vessels and the satellite cell niche. Curr Top Dev Biol 96:121–138
2. Kuang S, Kuroda K, Le Grand F, Rudnicki MA (2007) Asymmetric self-renewal and commitment of satellite stem cells in muscle. Cell 129:999–1010
3. Yin H, Price F, Rudnicki MA (2013) Satellite cells and the muscle stem cell niche. Physiol Rev 93:23–67
4. Theret M, Gsaier L, Schaffer B, Juban G, Ben Larbi S, Weiss-Gayet M, Bultot L, Caterina C, Foretz M, Desplanches D, Sanz P, Zang Z, Yang L, Vial G, Viollet B, Sakamoto K, Brunet A, Chazaud B, Mounier R (2017) AMPKalpha1-LDH pathway regulates muscle stem cell self-renewal by controlling metabolic homeostasis. EMBO J 36:1946
5. Joe AW, Yi L, Natarajan A, Le Grand F, So L, Wang J, Rudnicki MA, Rossi FM (2010) Muscle injury activates resident fibro/adipogenic progenitors that facilitate myogenesis. Nat Cell Biol 12:153–163

Chapter 35

Evaluating the Role of Host AMPK in *Leishmania* Burden

Diana Moreira, Jérôme Estaquier, Anabela Cordeiro-da-Silva, and Ricardo Silvestre

Abstract

The study of host AMP-activated protein kinase (AMPK) activation during *Leishmania* infection imposes distinct types of techniques to measure protein expression and activation, as well as to quantify, at transcription and translational levels, its downstream targets. The investigation of host AMPK protein modulation during *Leishmania* infection should primarily be assessed during in vitro infections using as a host murine bone marrow-derived macrophages (BMMos). The infection outcome is assessed measuring the percentage of infected cells in the context of BMMos. To evaluate AMPK activity during infection, the expression of AMPK phosphorylated at Thr172 as well as the transcription and translational levels of its downstream targets are evaluated by quantitative PCR and immunoblotting. The modulation of AMPK activity in vivo is determined specifically in sorted splenic macrophages harboring *Leishmania* parasites recovered from infected mice using fluorescent-labeled parasites in the infectious inocolum. The modulation of AMPK activity was assessed by AMPK activators and inhibitors and also using AMPK, SIRT1, or LKB1 KO mice models. The infection outcome in BMMos and in vivo was further determined using these two different approaches. To finally understand the metabolic impact of AMPK during infection, in vitro metabolic assays in infected BMMos were measured in the bioenergetic profile using an extracellular flux analyzer.

Key words Leishmania, AMPK, Bioenergetic profile, Extracellular flux analyzer, AMPK activators and inhibitors, SIRT1, Mitochondria, Cell metabolism, Macrophages

1 Introduction

Leishmania spp. is the causative agent of leishmaniasis, a neglected tropical disease transmitted by the bite of an infected female sand fly [1]. These parasites are mainly phagocyted by macrophages being able to subvert their intracellular signaling pathways and compete for similar resources [2–4]. A key question in the context of host-pathogen interactions is how pathogens survive in a hostile environment and how they hijack host machinery for their own benefit.

To address AMPK signaling during *Leishmania* infection, bone marrow precursors are differentiated in vitro with macrophage colony-stimulating factor (M-CSF) and used as a target cell for

Dietbert Neumann and Benoit Viollet (eds.), *AMPK: Methods and Protocols*, Methods in Molecular Biology, vol. 1732, https://doi.org/10.1007/978-1-4939-7598-3_35,

infection (Subheading 3.1). This differentiation procedure leads to a higher yield and reproducibility, being these bone marrow-derived macrophages (BMMos) commonly considered as a model for the role of resident macrophages [5]. The infection is performed at early (6 h post-infection) and at later time points of infection (18 h post-infection) to acquire a dynamic profile of the infection process. The level of infected cells was obtained through the infection of BMMos with CFSE-labeled parasites being the percentage of $CFSE^+$ or $eFluor670^+$ cells, obtained by FACS analysis, a direct measurement of parasites internalization [6, 7] (Subheading 3.1). A direct analysis of AMPK activation in a context of infection is addressed through immunoblotting of total and phosphorylated Thr172 both in infected BMMos (Subheading 3.1) and in sorted infected splenic macrophages (Subheading 3.2). The modulation of AMPK activity during infection can be obtained establishing a pharmacological approach where an AMPK activator (AICAR) and/or inhibitor (compound C) can be used isolated or in combination, as was described by us and by other authors in different contexts of infection [7–9]. The establishment on an in vivo infection (Subheading 3.2) using myeloid-restricted (Mac)-AMPK, SIRT1, or LKB1 KO mice (Subheading 3.3) is imperative to evaluate the impact of AMPK for the infection outcome in *Leishmania*-parasitized organs. SIRT1 has been investigated in different contexts as a potential modulator of AMPK activation. On one hand SIRT1 protein has been described as an upstream activator of AMPK through LKB1 deacetylation and on the other hand has been considered a downstream target of AMPK, becoming activated by the increase levels of NAD^+ [10–13]. The parasite load in *Leishmania*-parasitized organs is determined ultimately by real-time quantitative PCR (qRT-PCR) (Subheading 3.2) [7, 14]. The metabolic impact of AMPK during *Leishmania* infection can be finally addressed using the extracellular flux analyzer in infected BMMos. Host bioenergetic profile at real time is traced at basal conditions and in response to distinct pharmacological agents, which allow the quantification of metabolic parameters as extracellular acidification rate (ECAR), oxygen consumption rate (OCR), spare respiratory capacity (SRC), and glycolytic capacity (Subheading 3.3). Overall, with these techniques we could trace the activation of host AMPK network during *Leishmania* infection and the impact on parasite survival.

2 Materials

2.1 Animals and Parasites

1. Myeloid cell-specific (Mac)-Sirt1 KO mice, Mac-AMPKα1 KO mice, Mac-LKB1 KO mice on C57BL/6 genetic background, and the respective littermate lox control (Lysozyme

M-Cre^{neg} Sirt1$^{flox/flox}$) mice. All animals used in experiments are aged from 6 to 12 weeks.

2. *L. infantum* (MHOM/MA/67/ITMAP-263) promastigotes.

2.2 Culture Reagents

1. Macrophage medium: DMEM, 4.5 g/L glucose, 20 mM HEPES, 10% (v/v) heat-inactivated fetal bovine serum (FBS), 2 mM L-glutamine, 100 U/ml penicillin, 100 mg/ml streptomycin.
2. *Leishmania* medium: RPMI 1640, 20 mM HEPES, 10% (v/v) heat-inactivated FBS, 2 mM L-glutamine, 100 U/ml penicillin, 100 mg/ml streptomycin.
3. Macrophage growth factor: 100 μg/ml M-CSF.
4. XF medium: unbuffered DMEM, 4.5 g/L glucose, 2% (v/v) FBS, 2 mM L-glutamine, 100 U/ml penicillin, 100 mg/ml streptomycin.
5. Carboxyfluorescein succinimidyl ester (CFSE, FITC) and eFluor670 (APC): 5 mM stock solution.
6. AICAR (5-Aminoimidazole-4-carboxamide ribonucleotide).
7. Compound C (also known as Dorsomorphin).
8. SRT1720.

2.3 FACS Staining

1. DMEM-EDTA: DMEM, 50 mM EDTA.
2. Phosphate buffer saline (PBS): 145 mM NaCl, 2.7 mM KCl, 1.5 mM KH_2PO_4, 8 mM $Na_2HPO_4 \cdot 2H_2O$, pH 7.
3. PBS-FBS: PBS, 2% (v/v) FBS.
4. Probes: 14.6 mM 2-[N-(7-nitrobenz-2-oxa-1,3-diazol-4-yl) amino]-2-deoxy-D-glucose (2-NBDG) and 1 mg/ml 7-Aminoactinomycin D (7-AAD).

2.4 Antibodies

1. FACS: anti-mouse monoclonal antibodies—anti-CD11b-PE (M1/70), anti-Ly6C-PerCP/Cy5.5 (HK1.4), anti-Ly6G-Pacific Blue (1A8), and anti-F4/80-PerCP-Cy5.5 (BM8).
2. Cell magnetic separation: CD3ε and CD19 microbeads.
3. PBS-EDTA buffer: PBS, 0.5% (w/v) BSA (bovine serum albumin), 2 mM EDTA, pH 7.2.
4. Immunoblot: total AMPKα (23A3), AMPKα phosphorylated at Thr172, total SIRT1 (H-300), total PGC1β (E-9), β-actin (C4), total PGC1α (4C1.3), and horseradish peroxidase-coupled secondary reagents.

2.5 Quantitative PCR Analysis

1. TRIzol reagent.
2. Chloroform.
3. Isopropanol.

Table 1
List of primers used for real-time quantitative PCR (qRT-PCR)

Genes	Forward sequence	Reverse sequence	Accession number
Ppargc1a	AGCCGTGACCACTGACAACGAG	GCTGCATGGTTCTGAGTGCTAAG	NM_008904
Slc2a4	ACATACCTGACAGGGCAAGG	CGCCCTTAGTTGGTCAGAAG	NM_009204
RPS29	CACCCAGCAGACAGACAAACTG	GCACTCATCGTAGCGTTCCA	NM_009093

4. Ethanol 75% (c/v) in H_2O.
5. H_2O RNase free.
6. RNeasy micro kit.
7. QIAmp DNA micro kit.
8. cDNA synthesis Kit.
9. SYBR Green Supermix.
10. Primers: R221 and R332 primers parasite load quantification and primers for real-time quantitative PCR listed in Table 1.
11. DNazol.

2.6 Immunoblot

1. Lysis buffer: 50 mM Tris-HCL, pH 7.4, 1% (v/v) Triton X-100, 150 mM NaCl, 10% (v/v) glycerol, 50 mM NaF, 5 mM sodium pyrophosphate, 1 mM Na_3VO_4, 25 mM sodium-β-glycerophosphate, 1 mM DTT, 0.5 mM PMSF, protease and phosphatase inhibitor cocktails.
2. Dc protein assay with reagent S (Bio-Rad).
3. SDS polyacrylamide gel 10% resolving gel buffer (4.5 mL): 1.9 mL H_2O, 1.7 mL 30% (w/v) acrylamide, 1.3 mL Tris-HCL pH 8.8, 50 μL of 10% (w/v) SDS, 50 μL of 10% (w/v) APS, 2 μL of TEMED. Stacking gel (3 mL): 2.1 mL of H_2O, 500 μL of 30% (w/v) acrylamide, 380 μL of 0.5 M Tris-HCL pH 6.8, 30 μL of 10% (w/v) SDS, 30 μL of 10% (w/v) APS, 3 μL of TEMED.
4. Transfer pack with nitrocellulose membrane.
5. Western blot transfer system.
6. Ponceau S.
7. Block/diluent solutions: 10% (w/v) BSA, 0.05% (v/v) Tween 20.
8. SuperSignal West Pico or West Dura chemiluminescent substrate.
9. Striping solution I: 0.2 M glycine, 0.5 M NaCl, pH 2.8.
10. Striping solution II: 0.5 M Acetic acid, 0.5 M NaCl, pH 2.5.

2.7 Equipment

1. Gamma irradiator.
2. Flow cytometer.
3. Western blot transfer system.
4. Microplate reader.
5. Western blot detection system.
6. Protein expression quantification software.
7. Spectrophotometer.
8. Real-time PCR thermal cycler.
9. Magnetic cell separator system.
10. Extracellular flux analyzer.

3 Methods

3.1 Infection of Bone Marrow-Derived Macrophages with L. infantum

3.1.1 Isolation and Culture of Mouse Bone Marrow-Derived Macrophages

1. Anesthetize mice through isoflurane inhalation and euthanize by cervical dislocation.
2. Isolate the femurs and tibias of each mouse with a sterile scalp and scissor from the hind legs (*see* **Note 1**).
3. Holding the femurs and the tibias with the help of a scissor, cut off with a scalpel each tip of the bones. Recover bone marrow precursors by flushing the bone marrow with 3–5 mL of ice-cold complete macrophage medium (per femur or tibia) with the help of a syringe and a 26 G needle.
4. Centrifuge bone marrow cells at 300 × *g* for 10 min at 4 °C and resuspend in complete macrophage medium.
5. Plate the bone marrow precursor cells without counting in a 75 cm^2 culture flask in a volume of 15 mL of complete macrophage medium. Incubate at 37 °C with 5% CO_2 for 4–6 h.
6. Discard the adherent cells (differentiated macrophages from the stroma), and recover the bone marrow precursors present in the supernatant. Count with trypan blue and seed the bone marrow precursors in macrophage medium with 20 ng/ml of M-CSF at a proportion of 1×10^5 cells in 200 µL of medium in 96-well plates, 2×10^5 cells in 400 µL of medium in 24-well plates, and 1×10^6 cells in 2 mL of medium in 6-well plates.
7. Renew M-CSF growth factor at day 4 of culture in each well by adding 20 ng/ml of M-CSF. Macrophages acquired a definitive differentiation status at day 7 of culture, being defined as BMMos (*see* **Note 2**).

3.1.2 Labeling of Promastigotes and Infection Assay

1. Start a 5 mL culture of *L. infantum* promastigotes at a concentration of 1×10^6 promastigotes/ml of *Leishmania* medium (*see* **Note 3**).

2. At day 5 of growth, wash *L. infantum* promastigotes twice with 5 mL of PBS and resuspend the parasites in 1 mL of PBS. Count the parasites by diluting 1/10 in 2% (v/v) glutaraldehyde that fix the parasites. Dilute the *Leishmania* culture to 6×10^7 promastigotes in 1 mL of PBS.
3. Label with 5 μM CFSE for 10 min or 1 μM eFluor670 for 5 min at 37 °C followed by 5 min incubation at 4 °C to stop the reaction (*see* **Note 4**).
4. Wash the parasites twice with 5 mL of PBS, and resuspend in 1 mL of *Leishmania* medium before proceeding to infections.
5. Count the parasites by diluting 1/10 in 2% (v/v) glutaraldehyde and infect 7-day differentiated BMMos with labeled and unlabeled *L. infantum* promastigotes at a 1:10 ratio.
6. Irradiate 6×10^7 promastigotes suspended in 1 mL of *Leishmania* culture medium at 3000 Gy. Perform control experiments with those irradiated parasites using the previous co-culture ratio.
7. After 4 h of incubation, remove the medium of each well. Wash the cells, at least twice, with macrophage culture medium pipetting up and down several times.
8. For each round of washing, observe under the microscope if the parasites are still present in the supernatant. Repeat the washing procedure until the complete removal of non-internalized parasites.
9. Detach BMMos after 6 and 18 h post-infection. Remove the macrophage medium and add an equivalent volume of DMEM-EDTA solution. Wait 5 min at room temperature, and recover the BMMos by pipetting up and down several times.
10. Centrifuge at $300 \times g$ for 10 min at room temperature.
11. Resuspend BMMos in 200 μL of PBS-2%FBS solution, and incubate for 15 min at room temperature with 7-AAD at 1 μg/ml.
12. Transfer the cells to the cytometer tubes. Acquire the samples in a flow cytometer.
13. In the cytometer adopt the following gate strategy: exclude the death cells that are stained positively to 7-AAD. In the viable population (7-AAD$^-$), gate the cells that stained positively to eFluor670 (eFluor670$^+$) or CFSE (CFSE$^+$).
14. Obtain the percentage of infected cells by the % of CFSE$^+$ or eFluor670$^+$ cells. Determine the cell viability by the percentage of negative 7-AAD stained cells (*see* **Note 5**).

3.2 Infection of Mice with *L. infantum* and Sorting of Infected Splenic Macrophages

3.2.1 In Vivo Infection

1. Infect mice intraperitoneally, using a 26 G needle, with 1×10^8 CFSE-labeled *L. infantum* promastigotes resuspended in 200 μL of sterile PBS.

3.2.2 Parasite Load Quantification

1. At 10 days post-infection, anesthetize mice through isoflurane inhalation and euthanize by cervical dislocation. Remove and weigh spleen and liver. Transfer both organs to a 70 μm mesh cell strainer, within a small petri dish, and use the syringe plunger to process the organs to generate a single cell suspension. Centrifuge at 300 × *g* for 10 min at 4 °C, and resuspend in 5 mL of complete macrophage medium.
2. Extract DNA from 10 mg of spleen and liver (single cell suspensions) or 3×10^6 bone marrow cells by DNazol, according to the manufacturer instructions. Dissolve DNA in 100 μL of nuclease-free water. Quantify the total DNA in a NanoDrop spectrophotometer and prepare a twofold serial concentrations dilution adjusted for each tissue.
3. Quantify *Leishmania infantum* DNA by qPCR using 1000 nM of R223 and 500 nM of R333 primers for the small subunit rRNA (SSUrRNA) [15]. As a template use 400 ng of total DNA in 20 μL of reaction with SYBR Green Supermix, according to the manufacturer's instructions.
4. Perform a touchdown qPCR in Bio-Rad My Cycler iQ5, with a final annealing temperature of 65 °C [16]. The denaturation temperature is at 94 °C (5 s) and synthesis at 72 °C (10 s) with 30 cycles (*see* **Note 6**).
5. Extrapolate CTs from a standard curve constructed previously with a serial dilutions of *L. infantum* DNA (strain MHOM/MA/67/ITMAP-263) diluted in host DNA (from spleen of naïve mice). Calculate then *Leishmania* content expressed by parasites/μg of DNA (*see* **Note 7**).

3.2.3 Sorting of Infected Splenic Macrophages

1. Euthanize naïve and CFSE-*L. infantum* promastigote infected mice at 18 or 48 h post-infection. Collect the spleens into a falcon with 5 mL of macrophage culture medium.
2. Process the organs as **step 2** in Subheading 3.2.1. Determine the cell number.
3. Wash the cells twice with 5 mL PBS. Pipette off supernatant completely and resuspend cell pellet in 80 μL of PBS-EDTA buffer per 10^7 cells.
4. Deplete splenic T and B lymphocytes using CD3ε and CD19 microbeads coupled with depletion columns using a magnetic cell isolation separator.

5. Label the remaining cell suspension with 2 μg/ml anti-CD11b-PE, anti-Ly6C-PerCP/Cy5.5 and anti-Ly6G-Pacific Blue diluted in 25 μL of PBS-FBS solution for 30 min at 4 °C in the dark.
6. Wash the cells twice with 200 μL of PBS-FBS solution, and resuspend the cell pellet in 200 μL of PBS-FBS solution. Transfer the cell suspension to the cytometer tubes.
7. Sort the cells according to the surface expression of $CD11b^{+}Ly6C^{int/high}Ly6G^{low}$ and CFSE expression gated on infected ($CFSE^{+}CD11b^{+}Ly6C^{int/high}Ly6G^{low}$) or bystander ($CFSE^{-}CD11b^{+}Ly6C^{int/high}Ly6G^{low}$) splenic macrophages. As a control, sort $CD11b^{+}Ly6C^{int/high}Ly6G^{low}$ cells from the spleen of non-infected mice. The purity of the separation should be higher than 90%.
8. Count the cells obtained after the sorting assay using trypan blue to exclude dead cells.
9. Sorted splenic macrophages are rinse with PBS by centrifugation at 300 × *g* for 10 min at 4 °C.
10. Resuspend 1×10^5 sorted macrophages in 350 μL of RLT buffer with 7 μL of 2-mercaptoethanol, and isolate RNA according to RNeasy micro kit manufacturer's instructions.
11. Analyze the transcription levels of Ppargc1a (PGC-1α) and Slc2a4 (GLUT4) by qPCR using RPS29 as housekeeping gene.
12. Resuspend 1×10^6 sorted macrophages in ice-cold lysis buffer for 30 min at 4 °C with shaking. The supernatant is recovered after centrifugation at 17,000 × *g* during 20 min at 4 °C.
13. Analyze AMPK activation by immunoblot using the experimental procedure described in Chapter 27 (*see* **Note 8**).

3.3 Modulation of AMPK in a Context of Host-L. infantum interaction

1. Infect KO mouse models (Mac-Sirt1 KO, Mac-AMPKα1 KO, and Mac-LKB1 KO mice) and the respective littermate lox controls, as described in Subheading 3.2.
2. Evaluate the parasite load by qPCR as described in Subheading 3.2.

3.3.1 Modulation of AMPK Activity During In Vivo L. infantum Infection

3.3.2 Modulation of AMPK Activity in In Vitro L. infantum-Infected BMMos

1. Treat BMMos, from WT, Mac-SIRT1 KO, Mac-AMPK KO, and Mac-LKB1 KO mice, previously infected with CFSE or eFluor670-*L. infantum* promastigotes, at 6 h post-infection with 440 μM AICAR, 440 μM AICAR + 5 μM compound C, 1 μM SRT1720 or left untreated (*see* **Note 9**).

2. After 24 h of infection, detach BMMos by using the DMEM-EDTA solution and centrifuge at 300 × *g* for 10 min at room temperature.
3. Resuspend cells in 200 μL of PBS-2%FBS solution and incubate for 15 min at room temperature with 7-AAD at 1 μg/ml.
4. Evaluate the infection rate as described in the Subheading 3.1.

3.3.3 In Vitro Metabolic Assays of Infected Bone Marrow Macrophages

1. Collect bone marrow precursors as described in the Subheading 3.1. Perform the 7-day differentiation process in 75 cm^2 culture flasks.
2. After 7 days in culture, scrap the cells and seed BMMos at 2×10^5 cells/well in 400 μL of complete macrophage medium in XF-24 cell culture plates. Let the cells to adhere during an overnight period (*see* **Note 10**).
3. This procedure warrants a homogeneous distribution of the cells under the XF-24 plate surface, decreasing the variability among wells.
4. After an overnight period, infect the cells with irradiated or not *L. infantum* promastigotes at a 1:10 ratio, during 6 and 18 h.
5. One hour before the defined times of infection, wash the cells with pre-warmed XF medium. In the final wash, add 200 μL of XF medium to each well, and incubate for an hour at 37 °C without CO_2.
6. Determine the real-time measurement of bioenergetic profile (eight wells per condition), oxygen consumption rate (OCR), and extracellular acidification rate (ECAR), under basal conditions and in response to oligomycin (1 μM), fluoro-carbonyl cyanide phenylhydrazone (FCCP—1 μM), rotenone (1 μM), and antimycin A (1 μM), using an extracellular flux analyzer, at 6 and 18 h post-infection (Fig. 1).

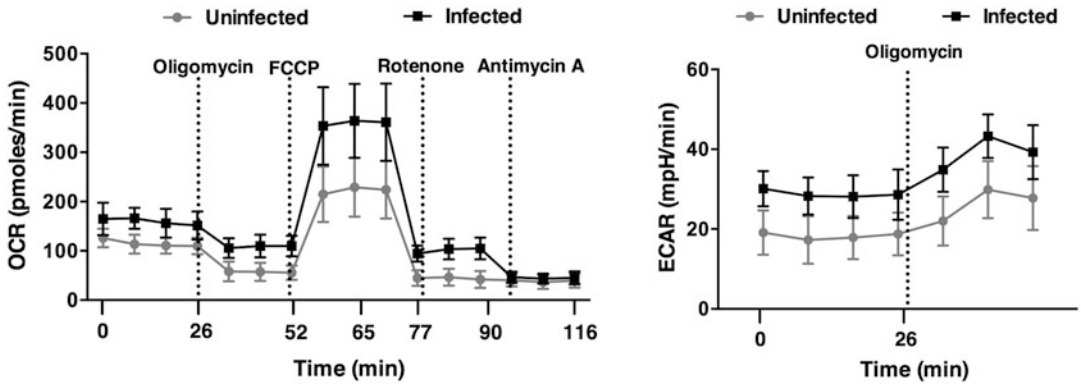

Fig. 1 A representative image of the real-time measurement of oxygen consumption rate (OCR) and the extracellular acidification rate (ECAR) in uninfected and infected BMMo. The different bioenergetic profiles are obtained under basal conditions and in response to oligomycin (1 μM), fluoro-carbonyl cyanide phenylhydrazone (FCCP—1 μM), rotenone (1 μM), and antimycin A (1 μM), using an XF-24 Extracellular Flux Analyzer

7. Obtain the non-mitochondrial respiration by subtracting the rotenone/antimycin A values. Calculate the spare respiratory capacity (SRC) by subtracting FCCP from basal OCR values, and define the glycolytic capacity as the variation between oligomycin and basal ECAR values. Normalize the values for all the conditions in relation to the protein content.

4 Notes

1. To maintain aseptic conditions and to easily remove the surrounding tissue, collect the femurs and tibias into alcohol solution for few seconds transferring afterward to DMEM medium.
2. Determine the purity of the macrophage culture by quantifying by flow cytometry the percentage of the cells expressing simultaneously the two surface markers CD11b and F4/80, which should be superior to 90%.
3. Maintain a cloned line of virulent *L. infantum* (MHOM/MA/67/ITMAP-263) by weekly subpassages at 26 °C in *Leishmania* medium. Use *L. infantum* promastigotes under four to ten passages in all the experiments.
4. eFluor 670 has a peak emission at 670 nm being detected with a 660/20 band-pass filter (equivalent to APC, Alexa Fluor™ 647, or eFluor™ 660) while CFSE peak emission of 521 nm being detected with a 530/30 nm band-pass emission filter (equivalent to GFP or FITC). Given that both dyes display similar results, the choice of labeling dye relates to the disponibility of the flow cytometry detectors and possibility to multicolor flow cytometry.
5. Giemsa staining is an alternative procedure to determine the percentage of infected cells. Upon **step 8**, Subheading 3.1.2, remove the macrophage medium and wash BMMos with 1 mL of PBS. Add 1 mL of 1% (v/v) of paraformaldehyde for 20 min. Rinse twice with 1 mL of PBS and add 1 mL of Giemsa stain previously diluted 1:20 in deionized water. Incubate for 30 min and rinse with deionized water. Air dry and count the infected cells and the number of intracellular parasites in a microscope at a 400× magnification. Cell nucleus and the parasites acquire a purple coloration. The volumes given consider an infection protocol for 2×10^5 BMMos in 400 μL of medium in 24-well plates. Up or downscale accordingly to the chosen infection protocol.
6. Whenever the qPCR gave a positive (with the expected melting curve) but unquantifiable value or a doubtable specific product (aberrant melting curve), perform a nested PCR [17] that has a

higher sensitivity (0.01 parasites) than the qPCR (0.6 parasites) to confirm the positivity of the quantitative result. For the first amplification reaction, use 300 nM of R221 and R332 primers [17]. For the second reaction, use 10 μL of the first PCR product diluted 1:40, which will serve as a template with the same R223 and R333 primers (300 nM and 150 nM, respectively) used for the qPCR.

7. As alternatives, the detection and quantification of *L. infantum* kinetoplastid DNA can be performed by TaqMan-based qPCR assay [18] or the parasite burden determined by limiting dilution assay [19]. For the former, reaction mixtures are composed of ABI TaqMan PCR 2× (Applied Biosystems), 375 nM of direct primer (CTTTTCTGGTCCTCCGGGTAGG), 375 nM of reverse primer (CCACCCGGCCCTATTTTACACCAA), 250 nM of hydrolysis probe (5′FAM-TTTTCGCAGAACGCCCCTACCCGC-3′TAMRA), and 100 ng of sample DNA. Thermocycling settings consist of one hold of 10 min at 95 °C followed by a two-step temperature (95 °C for 15 s and 60 °C for 60 s) over 40 cycles. A standard curve is established corresponding to a range of 50,000–0.01 parasites. Sample normalization is performed by quantifying a host gene (murine albumin), in 10 μL parallel reactions consisting of SYBR Green ROX Mix 2×, 100 nM of forward primer (CCATTGGTGAGACCAGAGGT), 100 nM of reverse primer (GAGGCAGGCAGCTTTATCAG), 100 ng of DNA, and the same thermal profile used for parasite quantification. A calibration curve ranging from 10,000 to 0.1 cells is established and parasite load expressed as the number of parasites per million of host cells. For the parasite burden, remove the organs from the mice (spleen and liver), weight and homogenize in RPMI medium. After cell counting, perform a subsequent twofold dilutions, in quadruplicate, in 96-well plates, and then incubate at 26 °C for 15 days. Record the presence or absence of motile promastigotes in each well. Calculate the number of parasites per gram of organ (parasite burden) as follows: parasite burden = [(geometric mean of reciprocal titer from each quadruplicate cell culture/weight of homogenized organ) reciprocal fraction of the homogenized organ inoculated into the first well].
8. AICAR is an AMPK activator, compound c is an AMPK inhibitor, and SRT1720 is an activator of SIRT1. BMMos from Mac-SIRT1 KO mice are treated with AICAR and AICAR + compound c, and BMMos from Mac-AMPK KO and Mac-LKB1 KO mice are treated with SRT1720, respectively.
9. In the immunoblot assays, use as a readout the expression of total AMPK, phosphorylated AMPK-Thr172, and PGC-1α.

10. The procedure warrants a homogeneous distribution of the cells under the XF-24 plate surface, decreasing the variability among wells.

Acknowledgments

This work was supported by the Northern Portugal Regional Operational Programme (NORTE 2020), under the Portugal 2020 Partnership Agreement, through the European Regional Development Fund (FEDER) (NORTE-01-0145-FEDER-000013) and the Fundação para a Ciência e Tecnologia (FCT) (contract IF/00021/2014 to R.S.), by FEDER funds through the Operational Competitiveness Programme (COMPETE), and by national funds through FCT (Fundação para a Ciência e a Tecnologia) under the project FCOMP-01-0124-FEDER-011054 (PTDC/SAU-FCF/100749/2008) and PTDC/BIA-MIC/118644/2010. The research leading to these results has also received funding from the European community's Seventh Framework Programme under grant agreement No.602773 to JE and ACS (Project KINDRED). DM was supported by SFRH/BD/91543/2012. JE thanks the Canada Research Chair program for their supports.

References

1. Murray HW, Berman JD, Davies CR, Saravia NG (2005) Advances in leishmaniasis. Lancet 366:1561–1577
2. Estaquier J, Vallette F, Vayssiere JL, Mignotte B (2012) The mitochondrial pathways of apoptosis. Adv Exp Med Biol 942:157–183
3. Rodrigues V, Cordeiro-da-Silva A, Laforge M, Ouaissi A, Silvestre R, Estaquier J (2012) Modulation of mammalian apoptotic pathways by intracellular protozoan parasites. Cell Microbiol 14:325–333
4. Rodrigues V, Cordeiro-da-Silva A, Laforge M, Ouaissi A, Akharid K, Silvestre R, Estaquier J (2014) Impairment of T cell function in parasitic infections. PLoS Negl Trop Dis 8:e2567
5. Manzanero S (2012) Generation of mouse bone marrow-derived macrophages. Methods Mol Biol 844:177–181
6. Resende M, Moreira D, Augusto J, Cunha J, Neves B, Cruz MT, Estaquier J, Cordeiro-da-Silva A, Silvestre R (2013) *Leishmania*-infected MHC class II high dendritic cells polarize CD4+ T cells toward a nonprotective T-bet+ IFN-gamma+ IL-10+ phenotype. J Immunol 191:262–273
7. Moreira D, Rodrigues V, Abengozar M, Rivas L, Rial E, Laforge M, Li X, Foretz M, Viollet B, Estaquier J, Cordeiro da Silva A, Silvestre R (2015) *Leishmania infantum* modulates host macrophage mitochondrial metabolism by hijacking the SIRT1-AMPK axis. PLoS Pathog 11:e1004684
8. Bulusu V, Thakur SS, Venkatachala R, Balaram H (2011) Mechanism of growth inhibition of intraerythrocytic stages of *Plasmodium falciparum* by 5-aminoimidazole-4-carboxamide ribonucleoside (AICAR). Mol Biochem Parasitol 177:1–11
9. Kondratowicz AS, Hunt CL, Davey RA, Cherry S, Maury WJ (2013) AMP-activated protein kinase is required for the macropinocytic internalization of ebolavirus. J Virol 87:746–755
10. Fulco M, Cen Y, Zhao P, Hoffman EP, McBurney MW, Sauve AA, Sartorelli V (2008) Glucose restriction inhibits skeletal myoblast differentiation by activating SIRT1 through AMPK-mediated regulation of Nampt. Dev Cell 14:661–673
11. Hou X, Xu S, Maitland-Toolan KA, Sato K, Jiang B, Ido Y, Lan F, Walsh K, Wierzbicki M,

Verbeuren TJ, Cohen RA, Zang M (2008) SIRT1 regulates hepatocyte lipid metabolism through activating AMP-activated protein kinase. J Biol Chem 283:20015–20026

12. Lan F, Cacicedo JM, Ruderman N, Ido Y (2008) SIRT1 modulation of the acetylation status, cytosolic localization, and activity of LKB1. Possible role in AMP-activated protein kinase activation. J Biol Chem 283:27628–27635
13. Canto C, Gerhart-Hines Z, Feige JN, Lagouge M, Noriega L, Milne JC, Elliott PJ, Puigserver P, Auwerx J (2009) AMPK regulates energy expenditure by modulating NAD+ metabolism and SIRT1 activity. Nature 458:1056–1060
14. Cunha J, Carrillo E, Sanchez C, Cruz I, Moreno J, Cordeiro-da-Silva A (2013) Characterization of the biology and infectivity of Leishmania infantum viscerotropic and dermotropic strains isolated from HIV+ and HIV- patients in the murine model of visceral leishmaniasis. Parasit Vectors 6:122
15. van Eys GJ, Schoone GJ, Kroon NC, Ebeling SB (1992) Sequence analysis of small subunit ribosomal RNA genes and its use for detection and identification of *Leishmania* parasites. Mol Biochem Parasitol 51:133–142
16. Miro G, Oliva G, Cruz I, Canavate C, Mortarino M, Vischer C, Bianciardi P (2009) Multicentric, controlled clinical study to evaluate effectiveness and safety of miltefosine and allopurinol for canine leishmaniosis. Vet Dermatol 20:397–404
17. Cruz I, Chicharro C, Nieto J, Bailo B, Canavate C, Figueras MC, Alvar J (2006) Comparison of new diagnostic tools for management of pediatric Mediterranean visceral leishmaniasis. J Clin Microbiol 44:2343–2347
18. Rodrigues V, Laforge M, Campillo-Gimenez L, Soundaramourty C, Correia-de-Oliveira A, Dinis-Oliveira RJ, Ouaissi A, Cordeiro-da-Silva A, Silvestre R, Estaquier J (2014) Abortive T follicular helper development is associated with a defective humoral response in *Leishmania infantum*-infected macaques. PLoS Pathog 10:e1004096
19. Silvestre R, Cordeiro-Da-Silva A, Santarem N, Vergnes B, Sereno D, Ouaissi A (2007) SIR2-deficient *Leishmania infantum* induces a defined IFN-gamma/IL-10 pattern that correlates with protection. J Immunol 179:3161–3170

Chapter 36

Analysis of Transgenerational Phenotypes Following Acute Starvation in AMPK-Deficient *C. elegans*

Emilie Demoinet and Richard Roy

Abstract

Environmental variation experienced early in life can result in long-term reproductive consequences. We have recently identified an important role for AMPK in the prevention of transgenerational defects following starvation of L1 stage larvae in *C. elegans*. Here we describe a means of analyzing these transgenerational defects following a single exposure to energy stress during early larval development. We also provide methods to quantify the histone modifications that are affected by this stress, along with the resulting reproductive defects that arise in later generations.

Key words C. elegans, AMPK, L1 starvation, Transgenerational defects, Epigenetics, Chromatin, Immunostaining

1 Introduction

Throughout evolution, the ability of organisms to adjust to environmental challenges has been critical in the selection of adaptations that enhance survival and/or fitness. Some of these adaptations result in evolutionary trade-offs that nevertheless improve survival in the generations of animals that were subjected to a given challenge. Others fall into a class of short-term modifications of gene expression that affect survival of subsequent generations through epigenetic mechanisms.

These epigenetic changes have been observed downstream of multiple developmental/physiological contexts and can have lasting multigenerational effects on gene expression affecting diverse processes. In mammalian organisms these transgenerational epigenetic phenomena can be correlated with changes that affect the methylation state of the DNA and also in modifications of the unstructured histone tails that comprise the overall chromatin landscape [1–4]. Changes in DNA methylation have been identified between siblings born during periods of famine versus abundance suggesting that these changes reflect epigenetic marks that

Dietbert Neumann and Benoit Viollet (eds.), *AMPK: Methods and Protocols*, Methods in Molecular Biology, vol. 1732, https://doi.org/10.1007/978-1-4939-7598-3_36,

impinge on gene expression of the affected individuals [5–8]. Moreover, these changes were further correlated with an increased frequency of various disorders that were not observed in siblings that were conceived during periods when adequate nutrition was accessible [5, 9, 10].

Although the small free-living nematode *C. elegans* does not possess the enzymes required for cytosine methylation, changes in histone modification have been linked to heritable transgenerational phenotypes [2, 11–14]. Recently, our group described a requirement for the AMP-activated protein kinase (AMPK) in blocking specific histone modifications during periods of acute starvation [15]. In its absence, a critical histone modification is aberrantly written onto the chromatin, thereby earmarking these regions of the genome as genes that should be, albeit inappropriately, actively expressed. This dysregulation of gene expression ultimately disrupts the integrity of the germ cells, which transmit this information to successive generations, often becoming progressively worse with each subsequent generation.

To assess this multigenerational effect of reducing AMPK function in the early L1 larval stage, we designed a means of tracking animals throughout several generations to assess any reproductive defects that arise following the initial period of starvation. We describe here how we use three different methods of tracking to test different patterns of inheritance following the starvation during the L1 diapause. The following sections describe an adaptable means of assessing transgenerational phenotypes in *C. elegans* with a particular focus on the defects that arise in the germ line downstream of acute starvation using animals wherein both catalytic subunits have been disrupted and therefore lack all AMPK signaling. The same multigenerational analyses could easily be modified to determine various other parameters such as metabolic signatures and/or other physiological states of the AMPK mutant descendants by ensuring that the starting populations will provide enough animals at each generation to perform the desired assays in a statistically significant manner.

AMPK null mutants (*aak-1*; *aak-2*) are viable if they are not subjected to starvation or other stresses, and they are fertile if they are not stressed during development. Therefore, hermaphrodites can be maintained on minimal bacterial agar plates (NGM medium) seeded with a thin layer of *E. coli* (strain OP50) until they become gravid (full of embryos) adults. Gravid adult hermaphrodites can then be subjected to alkaline/hypochlorite treatment to dissolve the animals, leaving the embryos intact. The embryos are washed three times in M9 buffer and then placed in a minimum volume of M9 buffer for incubation overnight to hatch the animals (details below). These emergent first larval stage (L1) animals will survive in the absence of food for approximately 2 weeks in a developmentally quiescent state that is referred to as the L1 diapause. In this state,

metabolism is maintained at a low level, as is overall gene expression. Cell divisions do not occur, nor do L1 specific cellular movements/migrations take place while the animal has not met an appropriate food/energy contingency to trigger the onset of post-embryonic development. The initiation of development can occur at almost any point during this period by placing animals in the presence of a food source, which in the laboratory consists of a lawn of *E. coli* bacteria (here OP50, but other strains are also effective). Ingesting the food is sufficient to trigger escape from the diapause and the initiation of the larval developmental program. Animals that are maintained for longer durations in the L1 diapause can initiate development after feeding, but their progression is often irregular, and they often give rise to sterile adults. Unlike AMPK mutant animals, these starved wild-type animals do not transmit these defects in a heritable manner, suggesting that AMPK plays a critical role during the L1 diapause to adjust to the nutrient/energy challenge associated with starvation and to maintain the integrity of the primordial germ cells that will give rise to all the germ cells and consequently the gametes, in the adult.

Here we describe how to quantify the various defects that arise due to starvation in these AMPK mutant animals. We detail our methods of examining multigenerational phenotypes that may arise in animals that were subjected to acute starvation. In addition, we provide a well-established protocol to analyze and quantify chromatin modifications that occur in the germ line using commercially available antibodies. Although we focus on the germ line in *C. elegans*, our methods can be easily adapted for detailed analysis of somatic changes in gene expression or metabolism that may occur in a similar transgenerational manner.

2 Materials

The following solutions should be prepared in advance:

1. Alkaline hypochlorite (bleaching solution, 50 mL): 1.2% (v/v) sodium hypochlorite (household bleach), 0.5 M KOH. This should be prepared just prior to use in an amber 50 mL Falcon tube to minimize exposure to light and hence loss of efficiency.
2. M9 buffer: 22 mM KH_2PO_4, 42 mM Na_2HPO_4, 86 mM NaCl, 1 mM $MgSO_4$.
3. Ice-cold methanol (100% methanol kept at −20 °C).
4. Coating solution for poly-L-lysine coated slides: 0.1% (w/v) poly-L-lysine, 0.1% (w/w) gelatin, 0.01% (w/w) chromoalum, Milli-Q H_2O (prepare 1 mL).
5. 2× fixative solution: open a fresh 10 mL vial of 16% formaldehyde, and dilute to a final concentration of 4% formaldehyde

and 0.025 M phosphate ($Na_2PO_4 \cdot H_2O$, pH 7.2). Formaldehyde is toxic so prepare this and use it in a fume hood (*see* **Note 1**).

6. Washing solution (PBST): PBS with 0.1% (v/v) Triton X-100.
7. Blocking solution: PBST, 1% (w/v) BSA.
8. DAPI nuclear counterstain: DAPI 1 μg/mL dissolved in PBST.
9. Microscopy essentials: Coplin jar, metal block for freeze cracking, standard rectangular glass microscope slides (75 × 25 mm/1.1–1.2 mm thick), glass cover slips.

Other materials:

10. NGM plates (Nematode Growth Medium): mix 3 g NaCl, 17 g agar, and 2.5 g peptone in a 2 L Erlenmeyer flask. Add 975 mL H_2O. Cover mouth of flask with aluminum foil. Autoclave to sterilize, and then cool the flask in a 55 °C water bath for 15 min. For the following step, use sterile procedures to proceed: add 1 mL of 1 M $CaCl_2$, 1 mL of 5 mg/mL cholesterol (diluted in ethanol), 1 mL of 1 M $MgSO_4$, and 25 mL of 1 M KPO_4 buffer. Swirl to mix well. Dispense 11–12 mL of NGM solution into 6 cm petri plates by using a peristaltic pump. Cool plates at room temperature for 2–3 days before use in order to detect the presence of contaminants. Plates can be stored in an airtight container at 4 °C for several weeks (seeded or unseeded).
11. *E. coli* OP50 strain: defrost OP50 strain regularly, and start a culture of *E. coli* on a LB plate (10 g Bacto tryptone, 5 g Bacto yeast, 5 g NaCl, 15 g agar, H_2O to 1 L, pH 7.5). Use a single colony to start a liquid culture, and let it grow overnight at 37 °C (the bottle of liquid culture can be stored at 4 °C for several weeks and remains usable).
12. NGM seeded plates: seed plates using sterile technique with approximately 50 μL of OP50 culture. Spreading bacteria in a "Z"-shaped lawn will help to visualize and count animals, since the worms tend to spend most of the time in the bacteria. Incubate seeded plates overnight at room temperature.
13. *C. elegans* N2 and *aak-1*; *aak-2* strains. Strains can be acquired from the Caenorhabditis Genetics Center (https://cbs.umn.edu/cgc/strains). Worms were freshly thawed prior to the experiment and grown at 15 °C on NGM seeded plates as previously described [16].

3 Methods

3.1 Effects on the Parental (P_0) Generation

3.1.1 Alkaline Hypochlorite Treatment and L1 Survival

1. Defrost strains and let them grow without any period of starvation for at least three generations at 20 °C prior to starting the experiment.
2. Collect gravid adults from three 6 cm NGM (Nematode Growth Media) plates seeded with *E. coli* OP50 bacterial lawns by washing plates with M9 or water and transferring the solution to a 15 mL polystyrene conical test tube (*see* **Note 2**).
3. Pellet the animals by centrifuging at low speed for 1 min (~1500 rpm on a standard tabletop centrifuge, 400 × *g*) at room temperature, and gently aspirate the supernatant taking care not to remove the animals in the pellet.
4. Perform 1–3 washes by filling the tube with M9 and repeating the aspiration step until the wash buffer is clear of bacteria.
5. Add 1 volume of alkaline hypochlorite solution for every volume of larvae collected in M9 buffer. Vortex and invert the tubes during the incubation period until the cuticle of the adult animals is fully dissolved and there are no traces of animal debris (*see* **Note 3**).
6. When there is no visible remaining debris in the tube, stop the reaction by dilution by adding M9 buffer to fill the tube (*see* **Note 4**).
7. Speed is critical, so quickly centrifuge for 1 min at 400 × *g*, and discard the supernatant. Repeat this twice to remove all the diluted alkaline hypochlorite solution, carefully aspirating the wash buffer at each step to avoid taking up the isolated embryos.
8. Add 2–3 mL of sterile M9 buffer to the pellet, and incubate overnight at the desired temperature with gentle agitation.
9. All embryos should have hatched by the next morning, and only live L1 larvae should be present in the buffer.
10. Adjust the titer so that it is 6–10 L1 larvae/μL. L1 larvae are very fragile and should be manipulated with care at all times. Some animals may die due to the procedure, and this number can be determined after the L1 larvae crawl out of the drop onto the bacteria (*see* **Note 5**).
11. The emergent L1 larvae can be maintained in this starved state (L1 diapause) for varying durations to test the effects of starvation on various parameters (*see* **Note 6**).
12. After the selected durations in the diapause, animals can be aliquoted onto plates containing OP50 to initiate

postembryonic development. L1 larvae are very small and fragile and are often best manipulated in liquid.

13. Every 48 h, deposit 10 μL aliquots onto freshly seeded NGM plates (with OP50). Make at least two duplicates per condition and strain.
14. Allow time for the liquid to disappear, and then count the number of L1 larvae per plate (initial) (*see* **Note 7**).
15. The following day, count the number of moving animals as viable (those that are moving or those that made a trail in the bacterial lawn).
16. The survival rate can be calculated as the number of viable animals/initial number seeded.

3.1.2 Post-diapause Recovery Defects and Determination of Adult Survival

1. To monitor for growth defects induced by L1 starvation, keep the plates at 20 °C, and let the animals develop.
2. It is important to monitor the animals periodically throughout postembryonic development for various growth or developmental phenotypes (i.e., 24 h, 48 h after being placed on food and then at the L4, L4 + 1d, L4 + 2d, and L4 + 3d).
3. To calculate adult survival, transfer 50–100 L4 stage larvae onto 2–3 OP50-seeded plates (*see* **Note 8**).
4. Count the initial number of animals at L4 stage (day 0).
5. Record the number of adult animals that are present on the plate every 2 days from day 0 (L4 + 2d to L4 + 8d) (*see* **Note 9**).
6. Compare with the initial number of animals transferred onto the plate.

3.1.3 Fertility Phenotyping: Sterility and Brood Size

- Adult sterility: adult hermaphrodites that were subjected to varying durations of starvation during the early L1 stage (L1 diapause) demonstrate a substantially high frequency of sterility. We use the following method to quantify the defects in fertility that arise after acute starvation (Fig. 1):

  1. Transfer 100–150 μL of L1 stage larvae that were subjected to varying durations of L1 diapause onto OP50-seeded plates.
  2. Allow them to grow and develop for 2–3 days at 20 °C, until they reach the L4 larval stage (*see* **Note 10**).
  3. Single 50–100 L4 stage larvae that were subjected to varying durations in the L1 diapause to individual bacteria-seeded plates (*see* **Note 11**).
  4. Let them grow so they can eventually self-fertilize and generate an F_1 generation of progeny.

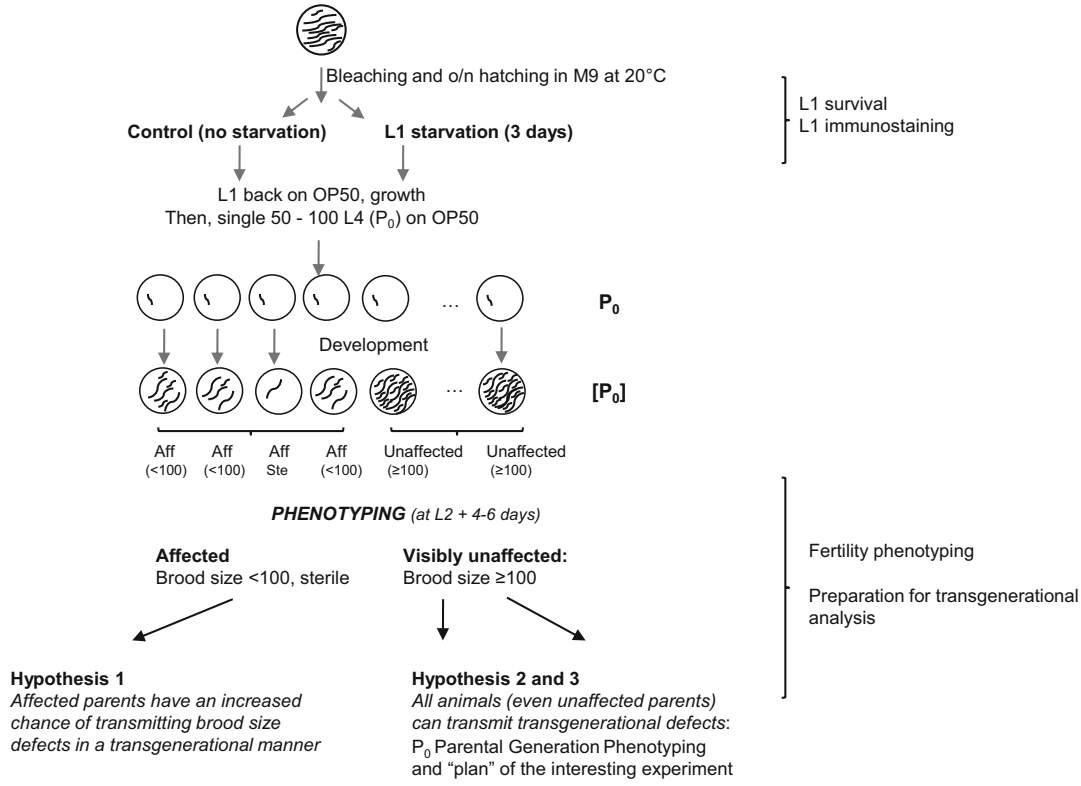

Fig. 1 Determination of the P_0 parental phenotypes through inference from the subsequent filial generation. Parents (P_0) are grown to adulthood and subjected to alkaline hypochlorite treatment to recover embryos. The embryos are hatched overnight to yield emergent L1 stage larvae. These animals are then allowed to grow and are counted to confirm whether the reproductive fitness of the parents is "affected (Aff)" or "Unaffected" by the initial starvation based on brood size; Ste is sterile

5. Record the number of plates that still contain single animals 96 h after being transferred as L4: these animals can be considered as sterile. Plates that generate progeny will have several smaller larvae on the bacterial lawn.

- Quantification of brood size: by counting the number of animals on each plate, the brood size can be determined for each individual parent (P_0) that had been subjected to the initial diapause.

6. Fertile animals are allowed to reproduce and are then transferred daily to a new seeded OP50 plate throughout their entire reproductive period (3–4 days) (*see* **Note 12**).
7. Count the number of F_1 offspring that were present on each plate when they reach the L4/young adult stage (*see* **Note 13**).

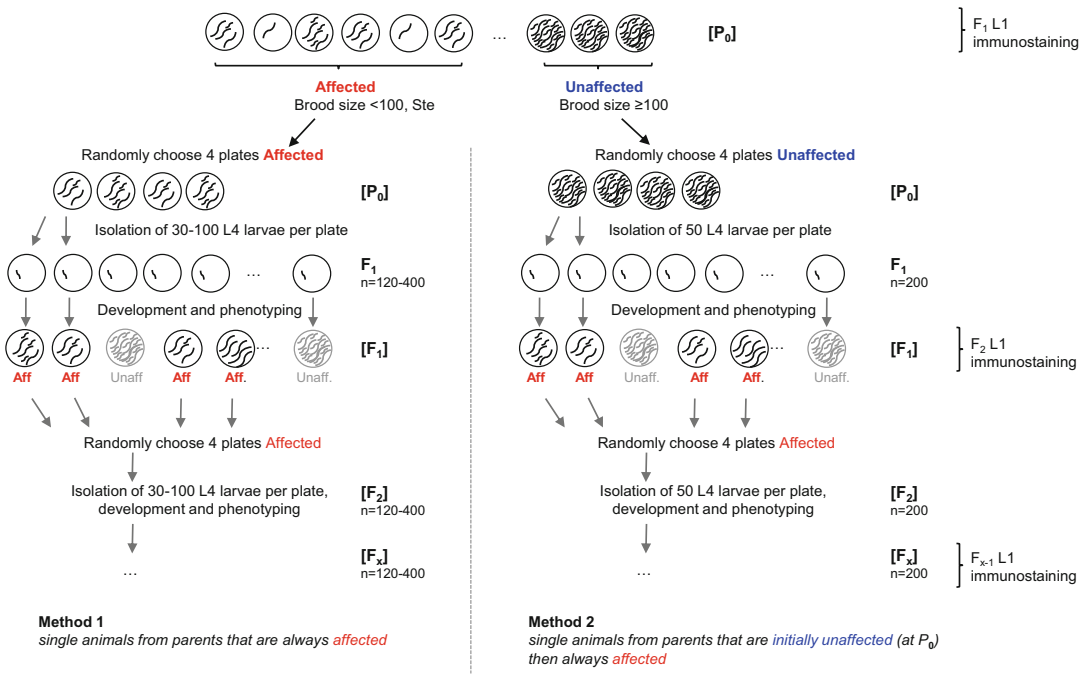

Fig. 2 Transgenerational analysis of animals subjected to acute starvation in the L1 diapause stage. We use three distinct methods to test the degree of transgenerational impact following 3 days of starvation. Methods 1 and 2 differ in the reproductive phenotypes of the parents to be analyzed. Method 3 is only different from Method 2 through continuous selection of L4 progeny that arises from unaffected parents at each generation. Any generation of interest can be tested for histone modifications or other biological parameters by performing alkaline hypochlorite treatment (bleaching) followed by immunostaining of the emergent L1 larvae. Reproductive fitness based on brood size of the parents is used to classify them as "affected (Aff)" or "unaffected" by the initial starvation. F_x refers to filial generation; Ste is sterile

3.2 Transgenerational Defects

3.2.1 Multigenerational Analysis of Brood Size

Both sterility and brood size can be assessed at every generation following the initial L1 diapause. It requires that the investigator maintains an orderly array of plates that represent the progeny of individual parents that were subjected to starvation at the L1 stage. In our analysis of AMPK in the regulation of germ cell integrity, we noted that fertile P_0 animals fell into two classes: those that generated a normal brood size and those that appeared compromised (smaller brood size than wild type). Curiously, even if the parents appeared normal, the next generation often had a reduced brood size even when they were never subjected to starvation, as the initial event is documented through epigenetic changes mediated through histone modifications. We therefore monitored phenotypic defects in the AMPK mutants that were subjected to the L1 diapause in successive generations according to three different methods of multigenerational analysis (Fig. 2).

- Method 1: assuming that the animals that were most affected by the acute starvation will always segregate the most affected

progeny, in this first selection, we assessed brood size in descendants from AMPK mutant parents that had a reduced number of progeny (<100 progeny), and although they were not the most severely affected (dead or sterile), they were among the most affected by the acute starvation during the L1 diapause that were able to reproduce. In each subsequent generation, we selected descendants for analysis that, like their parents, also had a reduced brood size.

1. Follow the previously described Subheading 3.1.1: bleach healthy gravid AMPK null mutants (*aak-1*; *aak-2*), and maintain them 3 days without food in the L1 diapause.
2. Place 3-day-starved L1 larvae on OP50-seeded plates, and allow them to grow at 20 °C.
3. Once most of the larvae reach the L4 stage, single out 50–100 larvae onto fresh OP50-seeded plates, and let them develop in order to evaluate both fertility and brood size as described above. This will allow you to determine if the parents generated a normal brood size or whether the reproduction/brood size was compromised.
4. Select four plates from the affected parental plates, i.e., those that produce small broods (<100 F_1 progeny), and single out between 30 and 100 F_1 L4 larvae from each of these four plates to individual plates seeded with OP50.
5. Incubate these plates at 20 °C, and allow them to reproduce (120–400 individual animals from 4 initial F_1 isolates) (*see* **Note 14**).
6. 4–6 days after the isolation, count the number of F_2 progeny generated by each F_1 descendant to determine its brood size phenotype: affected or unaffected.
7. Continue the experiment into the next generation by repeating the steps described above: randomly select four affected plates (<100 F_2 progeny).
8. From each of these plates, single out 30–100 F_2 L4 larvae in individual plates and allow them to reproduce (120–400 individual animals from 4 F_2 isolates) an F_3 brood.
9. Estimate the brood size when the F_3 progeny reaches the L4/young adult stage as described above. These steps were repeated successively such that the brood size of ~120–400 individual animals can be assessed and used for downstream analyses.

- Method 2: alternatively, we could not rule out that animals may be initially fertile, producing a brood of normal size, but the effects of the acute starvation are recorded and worsen with each successive generation. To test this possibility, we chose to select

visibly unaffected parents (those that generated more than 100 F_1 progeny), and then using the same type of multigenerational analysis described above, we then select the affected progeny (born from an F_1 parent that produced a <100 progeny), as described below:

1. Allow P_0 parents to self-fertilize (as described in **step 3** Subheading 3.2.1).
2. Randomly select four plates not affected (more than 100 F_1), and single out 50 F_1 L4 larvae to individual plates seeded with OP50.
3. Incubate these plates at 20 °C, and allow them to reproduce (200 individual animals from 4 initial F_1 isolates), and estimate the brood size of each of the F_1 parents as affected or unaffected plates. Some of these parents have a low brood size, while others are almost normal.
4. Randomly select four affected plates (that produced a low brood size), and we redo this selection at every subsequent generation.
5. Single out 50 F_1 L4 larvae to individual plates seeded with OP50 from each of these four affected plates, let them develop, and estimate their brood size as affected or unaffected.
6. For every subsequent generation, select progeny from four affected plates, let them develop, and estimate their brood size.

- Method 3: it is also possible that the animals that are born from normal parents and themselves produce a normal brood might eventually demonstrate the brood size defect only in later generations. This would be typical of a progressive loss of reproductive fitness over multiple generations. If we constantly select animals from parents that produce normal brood sizes and evaluate their brood size, we could potentially determine if this epigenetic phenomenon is recapitulated even in animals that appear to be reproductively normal.

  1. Derive the transgenerational analysis from the four randomly selected unaffected P_0 plates, as we described above in Method 2.
  2. Single out 50 L4 F_1 larvae from each of these four plates that harbored the parents that had normal brood sizes and appeared unaffected based on the above criteria.

3. Allow these animals to reproduce, and evaluate their brood size by counting the number of F_2 animals.
4. Once again, randomly select four unaffected plates, single out 50 L4 F_2 larvae, let them reproduce, and evaluate their brood size.
5. For all downstream analyses, we repeat these steps while continuously selecting animals that are born from parents that produce normal-sized broods.

3.3 Histone Modifications Identification by L1 Immunostaining Using the Freeze/Crack Method

Because of the epigenetic nature of the effect of acute starvation in AMPK mutants, it may be of interest to assess the levels of various histone marks at successive generations following the initial period of starvation. If you choose to examine the levels of such modifications in the actual population that you have assessed for brood size defects, it is important that your starting population is large enough so that at each generation you obtain a minimum number of *C. elegans* hermaphrodites to stain. The staining parameters are well described in several standard immunostaining in *C. elegans* procedures that make use of a typical freeze/crack step. For each generation of interest, it will be essential to first collect gravid adult hermaphrodites for treatment with alkaline hypochlorite (bleaching) to obtain embryos and subsequently L1 larvae of generation of interest.

To quantify the levels of various histone marks in the primordial germ cells of L1 larvae or even in the germ cells of later stage larvae at each generation, we use a standard *C. elegans* immunostaining procedure coupled with commercially available antibodies, or antibodies that have been generously provided by our *C. elegans* colleagues or from the *C. elegans* Genetic Center (CGC) at the University of Minnesota. The following steps will permit investigators to carry out the permeabilization and fixation procedures followed by primary and secondary antibody binding steps.

3.3.1 Preparing Slides for Compound Microscopy

1. Wipe pre-cleaned frosted edge slides with a lint-free tissue so that they are very clean.
2. Spread a thin layer of the coating solution on the slides with a cell rake, and let the slide dry for 10 min at 95 °C. Repeat the operation twice.

3.3.2 Freezing Worms: Preparing L1 Larvae for Staining

1. Prepare the L1 stock by performing alkaline hypochlorite treatment (bleaching) as described above, and then let them develop in M9 at 20 °C overnight.
2. The following day, wash the recovered L1 larvae two times with water, and centrifuge the larvae at 400 × *g* for 2–3 min (*see* **Note 15**).

3. Deposit 5–10 μL of resuspended L1 larvae in water on to the coated slides (3–4 slides per condition, 2 spots containing L1 larvae per slide).
4. Add 5 μL of 2× fixation solution directly on the spot containing the L1 larvae, and allow them to fix in a glass dish for 5 min at room temperature. Be sure the dish is humidified if longer incubations are used (alternatively this fixation step can be performed directly after the freeze/crack step with similar staining efficiencies). Place a metal block on dry ice during this period.
5. Gently place a coverslip over the spot of L1 larvae so that that the edge of the coverslip extends over the edge of the slide. Gently compress the two together, and remove any excess liquid with Whatman filter paper.
6. Without allowing the slide/coverslip to move or shift, carefully place the slides on the piece of chilled metal/metal block that is on dry ice. The slides should appear frozen within 1 min. Keep them on the metal block/dry ice for 5 min until they are thoroughly frozen (*see* **Note 16**).

3.3.3 Freeze/Crack and Fixation

1. For a better cracking result, remove the slides that were kept at −80 °C, allow to warm up on dry ice, and submerge them in a liquid nitrogen back just prior to the cracking step.
2. Crack the slide sandwich by swiftly separating the coverslip from the slide, and then immediately submerge the slide in a Coplin jar or a similar vessel filled with ice-cold methanol for 1 min.
3. Air-dry the slides for 30 s to 1 min, and then submerge the slides in a Coplin jar filled with PBS for 5 min to rinse off the fixative. Wash two times with PBST, and proceed to the staining procedure.

3.3.4 Immunostaining

The antibody staining protocol is similar to standard *C. elegans* protocols for any tissue [17].

1. Add 150 μL of blocking solution per sample on the slides (two slots per slide), and allow 15 min–1 h in a humidified chamber.
2. Incubate each sample with 40 μL of primary antibody (here rabbit anti-H3H4me3) solution diluted 1:1000 in blocking solution. Cover the sample in the depression in the slide with a piece of Parafilm, and leave it overnight in a moist chamber.
3. The following day, wash the slides three times in a jar containing PBST, allowing at least 5 min between each wash.
4. Incubate the slide with secondary antibody diluted in blocking solution for 2–3 h. Add 40 μL per sample, cover them with a

piece of Parafilm as above, and leave them in a dark humid chamber for 2–3 h at room temperature.

5. Wash the slides three times in a jar containing PBST allowing at least 5 min between each wash.
6. Add DAPI (1 μg/mL in PBST) to the slide to counterstain the nuclei, incubate 2 min, and rinse quickly. Alternatively, DAPI can be added to the mounting solution.
7. Remove most of the liquid, and add the mounting solution (i.e., Vectashield or ProLong antifade). Seal the edges with nail polish if you need to maintain the slide for future analysis.
8. The samples can then be imaged using a compound or a confocal microscope equipped with the appropriate filters and wavelengths. Following the imaging the slides can be maintained at −80 °C for an extended period of time.

Although at present we can conclude that functional AMPK is required to ensure that such epigenetic modifications that are typical of activating gene expression in the germ line do not occur during periods of acute starvation, i.e., during the L1 diapause, we believe that AMPK may also have other critical roles in adjustment that contribute to these transgenerational defects in brood size. By performing simple, well-organized multigenerational lineages, investigators that are interested in identifying novel AMPK targets can pinpoint the key processes that may be affected in the progressive deterioration in reproductive fitness that we observe in these mutant animals following a brief period of starvation. We envisage that these may include effectors of small RNA biosynthesis, other histone modifying enzymes, and/or metabolic enzymes or precursors required to generate critical substrates for all these AMPK-regulated processes.

4 Notes

1. Prepare the 2× fixative solution, and use as soon as chilled or later the same day. Discard any unused fixative in the appropriate disposal.
2. Be careful when you start your experiment: animals need to be freshly thawed and grown at least three generations at 20 °C without being starved at any time.
3. This typically takes between 7 and 9 min, but the duration will depend on the starting volume of pellet, temperature, and the efficiency of the hypochlorite solution.
4. The embryos are more resistant to this treatment, but don't let the reaction go too long, or all the embryos will die as well.

5. Therefore, it is suggested that the L1 larvae be diluted in sterile M9 buffer with a density of 6–10 L1 larvae/μL and constant titer for all downstream procedures [18].
6. The larvae must be therefore maintained in sterile conditions in M9, free of any carcasses or debris that might act as a nutrient source.
7. At this step, you should have around 60–100 L1 per plates, do not hesitate to count following each period of starvation, and readjust the volume in M9 to maintain the L1 titer.
8. To simplify the counting, use plates seeded with OP50 in a "Z" shape instead of a spot. Larvae will be everywhere on the Z shape, and this will simplify the counting.
9. Since *C. elegans* is hermaphroditic, it is important to transfer the mother onto new OP50 plates to prevent self-progeny that could potentially skew the survivability values.
10. With prolonged durations of starvation, post-diapause larvae will recover slowly and will develop with some heterogeneity. Vulval defects can often be seen at the L4 stage.
11. L4 larvae are very simple to distinguish by the crescent-like pattern that appears in the medio-ventral region around the developing vulva (Christmas tree stage) [19]. The animals are slightly smaller than adult animals and never possess adult alae (cuticular ridges on the lateral side visible with a compound microscope) or oocytes, although later L4 stages may contain developing sperm.
12. To simplify the counting, use, as before, NGM plates bacteria seeded with a "Z" shape.
13. Brood size can also been determined by visual observation (Fig. 1) and plates recorded as affected (reduced brood size, <100 progeny) or unaffected (normal brood size, more than 100 progeny). Brood size is a critical measure of fecundity, and it contributes to overall reproductive fitness if assessed over generations.
14. It is important to keep the parental plates, where the P_0 mother is still alive 3 days post-L4 stage, to be sure that the reduced brood size phenotype does not derive from somatic defects (bagging, bursting, etc.).
15. Water is preferred when washing the L1 larvae because salt interferes with the adherence of the animals to the poly-L-lysine coated slides.
16. At this point, slides may be stored in a labeled box at −80 °C for several days, although they should not be kept more than a few days at −80 °C, as the water will start to evaporate through sublimation and the larvae will not stain as well. If the slides were stored at −80 °C, let them "warm up" on dry ice for 10 min just before cracking them.

References

1. Feil R, Fraga MF (2012) Epigenetics and the environment: emerging patterns and implications. Nat Rev Genet 13:97. https://doi.org/10.1038/nrg3142. nrg3142 [pii]
2. Heard E, Martienssen RA (2014) Transgenerational epigenetic inheritance: myths and mechanisms. Cell 157(1):95–109. https://doi.org/10.1016/j.cell.2014.02.045
3. Gapp K, von Ziegler L, Tweedie-Cullen RY, Mansuy IM (2014) Early life epigenetic programming and transmission of stress-induced traits in mammals: How and when can environmental factors influence traits and their transgenerational inheritance? Bioessays 36 (5):491–502. https://doi.org/10.1002/bies.201300116
4. Grossniklaus U, Kelly WG, Kelly B, Ferguson-Smith AC, Pembrey M, Lindquist S (2013) Transgenerational epigenetic inheritance: how important is it? Nat Rev Genet 14(3):228–235. https://doi.org/10.1038/nrg3435
5. Ahmed F (2010) Epigenetics: Tales of adversity. Nature 468(7327):S20. https://doi.org/10.1038/468S20a. 468S20a [pii]
6. Heijmans BT, Tobi EW, Stein AD, Putter H, Blauw GJ, Susser ES, Slagboom PE, Lumey LH (2008) Persistent epigenetic differences associated with prenatal exposure to famine in humans. Proc Natl Acad Sci U S A 105 (44):17046–17049. https://doi.org/pnas.080/pnas.0806560105,0806560105 [pii]
7. Lumey LH, Stein AD, Susser E (2011) Prenatal famine and adult health. Annu Rev Public Health 32:237–262. https://doi.org/10.1146/annurev-publhealth-031210-101230
8. Tobi EW, Slagboom PE, van Dongen J, Kremer D, Stein AD, Putter H, Heijmans BT, Lumey LH (2012) Prenatal famine and genetic variation are independently and additively associated with DNA methylation at regulatory loci within IGF2/H19. PLoS One 7(5):e37933. https://doi.org/10.1371/journal.pone.0037933,PONE-D-12-01997 [pii]
9. Stein AD, Zybert PA, van de Bor M, Lumey LH (2004) Intrauterine famine exposure and body proportions at birth: the Dutch Hunger Winter. Int J Epidemiol 33(4):831–836. https://doi.org/10.1093/ije/dyh083,dyh083 [pii]
10. Roseboom T, de Rooij S, Painter R (2006) The Dutch famine and its long-term consequences for adult health. Early Hum Dev 82 (8):485–491. https://doi.org/10.1016/j.earlhumdev.2006.07.001,S0378-3782(06)00184-8 [pii]
11. Kelly WG (2014) Transgenerational epigenetics in the germline cycle of Caenorhabditis elegans. Epigenetics Chromatin 7(1):6. https://doi.org/10.1186/1756-8935-7-6
12. Greer EL, Beese-Sims SE, Brookes E, Spadafora R, Zhu Y, Rothbart SB, Aristizabal-Corrales D, Chen S, Badeaux AI, Jin Q, Wang W, Strahl BD, Colaiacovo MP, Shi Y (2014) A histone methylation network regulates transgenerational epigenetic memory in C. elegans. Cell Rep 7(1):113–126. https://doi.org/10.1016/j.celrep.2014.02.044,S2211-1247(14)00158-2 [pii]
13. Greer EL, Maures TJ, Ucar D, Hauswirth AG, Mancini E, Lim JP, Benayoun BA, Shi Y, Brunet A (2011) Transgenerational epigenetic inheritance of longevity in Caenorhabditis elegans. Nature 479:365. https://doi.org/10.1038/nature10572. nature10572 [pii]
14. Lim JP, Brunet A (2013) Bridging the transgenerational gap with epigenetic memory. Trends Genet 29(3):176–186. https://doi.org/10.1016/j.tig.2012.12.008,S0168-9525(12)00212-0 [pii]
15. Demoinet E, Li S, Roy R (2017) AMPK blocks starvation-inducible transgenerational defects in Caenorhabditis elegans. Proc Natl Acad Sci U S A 114(13):E2689–E2698. https://doi.org/10.1073/pnas.1616171114
16. Brenner S (1974) The genetics of Caenorhabditis elegans. Genetics 77(1):71–94
17. Goodyer W, Kaitna S, Couteau F, Ward JD, Boulton SJ, Zetka M (2008) HTP-3 links DSB formation with homolog pairing and crossing over during C. elegans meiosis. Dev Cell 14(2):263–274. https://doi.org/10.1016/j.devcel.2007.11.016,S1534-5807(07)00438-8 [pii]
18. Artyukhin AB, Schroeder FC, Avery L (2013) Density dependence in Caenorhabditis larval starvation. Sci Rep 3:2777. https://doi.org/10.1038/srep02777,srep02777 [pii]
19. Mok DZ, Sternberg PW, Inoue T (2015) Morphologically defined sub-stages of C. elegans vulval development in the fourth larval stage. BMC Dev Biol 15:26. https://doi.org/10.1186/s12861-015-0076-7

Chapter 37

Human γ2-AMPK Mutations

Arash Yavari, Dhruv Sarma, and Eduardo B. Sternick

Abstract

In humans, dominant mutations in the gene encoding the regulatory γ2-subunit of AMP-activated protein kinase (*PRKAG2*) result in a highly penetrant phenotype dominated by cardiac features: left ventricular hypertrophy, ventricular pre-excitation, atrial tachyarrhythmia, cardiac conduction disease, and myocardial glycogen storage. The discovery of a link between the cell's fundamental energy sensor, AMPK, and inherited cardiac disease catalyzed intense interest into the biological role of AMPK in the heart. In this chapter, we provide an introduction to the spectrum of human disease resulting from pathogenic variants in *PRKAG2*, outlining its discovery, clinical genetics, and current perspectives on its pathogenesis and highlighting mechanistic insights derived through the evaluation of disease models. We also present a clinical perspective on the major components of the cardiomyopathy associated with mutations in *PRKAG2*, together with less commonly described extracardiac features, its prognosis, and principles of management.

Key words AMPK, Cardiac conduction disease, Cardiac hypertrophy, Cardiomyopathy, Glycogen storage, LVH, Pre-excitation, *PRKAG2*, Wolff-Parkinson-White syndrome

1 Discovery of Mutations in *PRKAG2* as a Cause of Hypertrophic Cardiomyopathy

Hypertrophic cardiomyopathy (HCM) is the commonest inherited cardiac disease (with a prevalence of ~1 in 500 individuals) segregating as an autosomal dominant trait. HCM is defined clinically by the presence of left ventricular hypertrophy (LVH, i.e., increased thickening of the left ventricular wall) which is not solely explained by abnormal cardiac loading conditions [1, 2]. While the majority of HCM cases are recognized to be asymptomatic, its most dramatic clinical complication—and one which has gained widespread public recognition in the context of competitive athletes—is sudden cardiac death (SCD) [3]. Pathologically, HCM is characterized by ventricular hypertrophy (often primarily affecting the interventricular septum), cardiomyocyte disarray, and cardiac fibrosis. While the genetics of HCM are complex, with significant genetic and allelic heterogeneity, the majority of the ~500 causal mutations described reside in components of the sarcomere—the fundamental

Dietbert Neumann and Benoit Viollet (eds.), *AMPK: Methods and Protocols*, Methods in Molecular Biology, vol. 1732, https://doi.org/10.1007/978-1-4939-7598-3_37,

contractile unit of myocytes—prompting the conceptualization of HCM as a "disease of the sarcomere" [4, 5].

Comprehensive genetic screening identifies sarcomeric mutations in only up to ~60% of individuals with the HCM phenotype, suggesting additional non-sarcomeric etiologies [2]. Early clinical reports of rare kindreds exhibiting features of HCM in conjunction with unusual cardiac electrophysiological disturbances, such as ventricular pre-excitation (apparent on the surface ECG) with supraventricular arrhythmia (together termed the Wolff-Parkinson-White syndrome, WPW), and/or advanced atrioventricular (AV) block, reinforced the notion that non-sarcomeric genes might account for some of this genetic shortfall [6–8]. In 1995, a single disease locus for an inherited form of ventricular pre-excitation and HCM was mapped to chromosome 7q3 using genetic linkage analysis [9]. The subsequent mapping in 2000 of the gene *PRKAG2* encoding the energy-sensing γ2-regulatory subunit of AMP-activated protein kinase (AMPK) to the same locus (7q36), in conjunction with biochemical and biophysical evidence suggesting myocardial energetic compromise as a unifying mechanistic basis for HCM, led to the examination of *PRKAG2* as a candidate HCM gene [10, 11]. Examination of two families with a phenotype of HCM and ventricular pre-excitation in whom sarcomeric mutations had not been identified led to the discovery of two causal mutations of *PRKAG2*—one a missense substitution, His383Arg (His142Arg), in the second cystathionine β-synthase domain (CBS2) and the other an in-frame codon insertion between CBS1 and CBS2 (Arg350_Glu351insLeu) [10]. In parallel, genetic linkage analysis led to the identification of a missense mutation (Arg302Gln) in CBS1 in two separate families where WPW segregated as an autosomal dominant trait [12]. This genetic transmission pattern is illustrated for another *PRKAG2* mutation (Arg531Gly) in Fig. 1.

Both initial clinical reports linking mutations in highly conserved regions of *PRKAG2* to human disease noted a specific but variable cardiac phenotype encompassing LVH, ventricular pre-excitation, atrial arrhythmia, progressive atrioventricular conduction disease, progression to ventricular dilatation with heart failure requiring transplantation, and sudden death [10, 12]. A subsequent genetic study screening *PRKAG2* from families with either HCM or WPW, or isolated familial WPW, identified two further pathogenic variants (Thr400Asn and Asn488Ile) and delineated the pathological features distinguishing cardiomyopathy associated with *PRKAG2* mutations from typical sarcomeric HCM, namely an absence of significant myocyte disarray and relatively little interstitial fibrosis, but striking cardiomyocyte cytosolic vacuolation containing PAS-positive inclusions consistent with glycogen [13]. More broadly, in addition to elucidating the molecular genetic basis of familial HCM with pre-excitation—since then

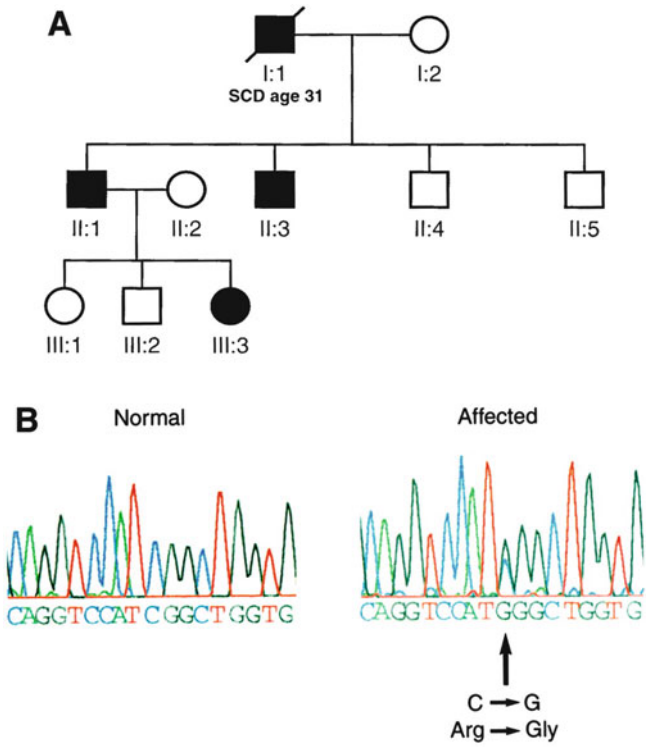

Fig. 1 Pedigree of a family with PRKAG2 cardiomyopathy and causal missense mutation. Upper panel, pedigree of a family with a *PRKAG2* mutation (in this case Arg531Gly) illustrating autosomal dominant transmission. Affected members are denoted by solid symbols, square symbols indicate males, and circles indicate females. Crossed through symbols denote individuals who suffered premature sudden cardiac death. Lower panel, identification of the causal *PRKAG2* mutation by DNA sequencing (Reproduced from ref. 30 with permission from Wolters Kluwer Health, Inc.)

variably styled *PRKAG2* cardiac syndrome, *PRKAG2* cardiomyopathy, or *PRKAG2* disease—these seminal reports fuelled intense scientific interest into the cardiac functions of AMPK [14–16].

2 Clinical Genetics of *PRKAG2* Mutations

Multiple distinct heterozygous variants in *PRKAG2* have been described in association with a highly penetrant cardiac phenotype (Table 1), most frequently Arg302Gln and Asn488Ile which constitute ~57% and ~21% of cases, respectively [17]. The great majority of these variants are missense substitutions located in the adenine nucleotide binding CBS domains [18]. Moreover, the Arg302Gln mutation is homologous in location to a naturally occurring dominant mutation (Arg200Gln) in CBS1 of γ3 in

Table 1
Reported human *PRKAG2* variants linked to a cardiomyopathy phenotype

Variant	Onset	Number of families/ patients	Key features	Reference
p.Arg302Gln	Adult	Commonest described *PRKAG2* mutation—~135 patients	**Common**: short PR interval, ventricular pre-excitation (VPE), and frequent episodes of supraventricular tachycardia (SVT); bradycardia due to sinus node dysfunction; conduction abnormalities including RBBB and AV block; high incidence of permanent pacemaker implantation **Variable**: LVH ranges from absent [29] to severe [56] **Infrequent/rarely described**: cardiac transplantation, SCD	[12, 13, 24, 27, 28, 29, 56, 57, 65, 66, 67, 76, 78, 87]
p.Asn488Ile	Pediatric-adult	Second commonest described—~40 patients	**Common**: moderate, progressive LVH (70% of patients) and VPE (58%) **Variable**: SVT (30%) and pacemaker implantation (30%), seven patients (15%) with extracardiac features including myalgia, proximal myopathy, and poorly controlled seizures **Infrequent/rarely described**: SCD, thromboembolic stroke	[13, 24]
p.Gly100Ser	Adult	Single family of 12	Severe AV block, sinus node dysfunction, VPE, and SVT; LVH (8/12) progressing to end-stage heart failure in 4/12 patients	[88]
p.Ser333Pro	Adult	Family of three	VPE (2/3 cases); conduction system disease with LBBB and AV block (2/3 cases) Moderate asymmetric LVH Muscle pain and exercise intolerance, with skeletal muscle glycogenosis	[67]
p.Val336Ala	Pediatric-Adult	Family of four	Severe conduction system disease (AV block and LBBB) VPE and paroxysmal AF (atrial fibrillation), with one SCD Progressive LVH with end-stage heart failure by middle age	[67]

(continued)

Table 1
(continued)

Variant	Onset	Number of families/ patients	Key features	Reference
p.His344Pro	Adult	Family of two	LVH and heart failure, VPE and conduction system disease	[76]
p.Arg350_ Glu351insLeu	Adult	Family of five	Severe LVH and LV dysfunction requiring cardiac transplant High incidence of SVT and SCD	[10]
p.His383Arg	Pediatric	Family of three	LVH and early cardiac dilation, short PR interval and bizarre QRS complex	[10]
p.Arg384Thr	Neonatal	Single patient	Biventricular hypertrophy, severe atrial wall thickening; short PR interval and fetal bradycardia; cardiac and skeletal muscle glycogenosis; death at 5 months	[25]
p.Thr400Asn	Adult	Single patient	VPE, SVT, sinus node dysfunction, required pacemaker implantation, LVH	[13]
p.Lys485Glu	Adult	Single patient	Sinus bradycardia, VPE, episodes of AF with rapid ventricular conduction, LVH Early LV dilatation requiring transplantation	[74]
p.Tyr487His	Pediatric	Family of three	Modest LVH, extremely short PR, sudden cardiac death	[89]
p.Glu506Gln	Infancy	Family of three	Severe biventricular and septal hypertrophy, requiring eventual cardiac transplant; short PR interval and ventricular pre-excitation Normal glycogen content and absence of glycogen deposits on histology and EM of endomyocardial biopsy	[55, 67]
p.Glu506Lys	Adult	Family of eight	Severe biventricular hypertrophy and short PR interval in all patients One patient with sinus node dysfunction requiring pacemaker implantation	[72]
p.His530Arg	Adult	Nine patients (family of four, family of three, and two individuals)	LVH (8/9 patients), cardiac transplant in one patient VPE, SVT with SCD in two patients, progressive conduction system disease	[67, 68, 75, 90]

(continued)

Table 1
(continued)

Variant	Onset	Number of families/ patients	Key features	Reference
p.Arg531Gly	Pediatric	Family of four	VPE, short PR interval, SVT; sinus node dysfunction and conduction block LVH absent; early onset, persistent hypertension	[30]
p.Arg531Gln	Neonatal	Three patients (separate families)	Massive biventricular hypertrophy, short PR interval, fetal bradycardia and death by 3 months; macroglossia, dysmorphic kidneys, skeletal muscle glycogenosis (2)	[26]
p.Ser548Pro	Adult	Single patient	Severe sinus bradycardia requiring pacemaker, mild-moderate LVH Muscle stiffness, raised plasma creatine kinase and skeletal muscle glycogenosis	[67, 80]

AF atrial fibrillation, *AV* atrioventricular, *LVH* left ventricular hypertrophy, *RBBB* right bundle branch block, *SCD* sudden cardiac death, *SVT* supraventricular tachycardia, *VPE* ventricular pre-excitation
p. refers to position numbering in relation to the first amino acid of the protein sequence in accordance with HGVS recommendations on nomenclature [91]
Note 1: Variants—While the variants listed are those which have been reported to date in the published literature as causal for *PRKAG2* cardiomyopathy, not all of these necessarily meet current standards for interpretation of a sequence variant as pathogenic or even likely pathogenic [21]. In particular, nonrecurrent variants reported as pathogenic should be interpreted with care in the context of broader genetic evidence, including publically available datasets on variant frequency (e.g., gnomAD [22], http://gnomad.broadinstitute.org/)
Note 2: Number of families/patients—In some cases, particularly with more frequently described variants, some overlap may exist in reporting of individual cases

purebred Hampshire pigs (denoted RN^{-}) [19] and the first described naturally occurring human γ3 mutation (Arg225Trp) [20], both of which are associated with increased skeletal muscle glycogen content.

Notably in the setting of growing awareness of the disease, not all of the *PRKAG2* variants described necessarily robustly satisfy contemporary proposed criteria for classification of Mendelian variants as pathogenic [21]. Findings in favor of interpretation of a variant as pathogenic include de novo mutations (with confirmation of both maternity and paternity) in an individual with the disease but no family history, well-defined functional in vitro and/or in vivo studies indicative of a deleterious effect of the

gene product, absence of the variant from control population databases (e.g., Exome Sequencing Project, 1000 Genomes Project, Exome Aggregation Consortium, or gnomAD [22]), and a new missense substitution at an amino acid residue where a different substitution has been previously identified as pathogenic [21]. Other supporting criteria include co-segregation with disease in multiple affected family members and the presence of multiple lines of computational evidence (e.g., with regard to residue conservation) to support an adverse impact of the variant on the gene product, although use of in silico prediction algorithms is not without limitation [21]. In contrast, criteria in favor of classification as a benign variant include the presence of a high allele frequency for the variant in population databases (>5% in Exome Sequencing Project, 1000 Genomes Project, or Exome Aggregation Consortium), observation in healthy (heterozygous) adults where full penetrance is anticipated at a young age, lack of segregation in affected family members, or several lines of in silico evidence arguing against a deleterious impact of the variant on the gene product. By allocating a different weighting to these (and other) pathogenic and benign criteria, variants relevant to Mendelian disease can be classified as "pathogenic," "likely pathogenic," of "uncertain significance," "likely benign," or "benign" [21]. While not disease-specific, such a framework structures the process of reliable rare variant interpretation, aiding categorization as causal in disease or likely innocent bystander, a growing and important challenge given the increasing clinical and research application of high-throughput DNA sequencing, and use of more extensive gene panels [23].

PRKAG2 mutations display autosomal dominant transmission and largely present in late adolescence or early adult life (mean age 24 years in one case series) [24]. A minority of sporadic cases present in infancy, likely reflecting de novo mutation, typically with profound impact on kinase activity and florid clinical sequelae [25, 26]. While penetrance is close to 100%, there is, in common with sarcomeric HCM, evidence of significant variability in disease expressivity, including within families, some of whom carry effectively unique "private" mutations [2]. Thus, while pre-excitation appears to be highly prevalent in Arg302Gln mutation carriers [17], families with a high incidence of right bundle branch block and short PR interval, but no LVH or pre-excitation, and others with no demonstrable glycogen excess have all been described [27–29]. Notwithstanding the rarity of the syndrome (with ~200 patients reported in the literature), attempts at genotype-phenotype correlation have been made, with findings of a higher frequency of LVH but lower rate of electronic pacemaker implantation, with the Asn488Ile compared to Arg302Gln variant [17]. At the extreme end of the disease spectrum, mutations at the Arg531 residue in CBS4 are notable for their association with early presentation or fulminant phenotype: paroxysmal atrial

fibrillation and atrial flutter have been described from the age of 2 years (but with no LVH even up to age of 41 years) in association with the Arg531Gly variant [30], while the Arg531Gln mutation results in a rapidly fatal syndrome presenting in prenatal or neonatal life with massive cardiomegaly, bradycardia in utero, ventricular pre-excitation, and profound non-lysosomal glycogen accumulation [26].

3 *PRKAG2* Disease Mechanisms: Insights from Murine Models

To elucidate the pathophysiological mechanisms underlying the cardiac phenotype associated with *PRKAG2* mutations, a number of murine disease models have been developed. With the exception of a recently described gene targeted model [31], these share a similar design, namely, cardiac-restricted overexpression of human mutant or WT *PRKAG2* cDNA under the control of a powerful, cardiac-specific promoter (α-myosin heavy chain, α-MHC) resulting in primarily fetal atria and postnatal ventricular expression [32–35]. These overexpressing transgenic (TG) models near uniformly recapitulate the more severe end of the human disease spectrum, including severe LVH (Fig. 2), ventricular pre-excitation, profound cardiac glycogen accumulation, ventricular dysfunction, and early mortality (Table 2).

3.1 Basis of PRKAG2-Associated Ventricular Pre-excitation

Surface ECG recordings of all four TG mouse models overexpressing mutant *PRKAG2* have identified mice with apparent ventricular pre-excitation (i.e., short PR interval and widening of the QRS complex) (Fig. 3). Multiple patterns of ventricular activation have been described in the same mice [32], suggesting multiple accessory connections, as have been observed in the human disease [36]. Importantly, cardiac-restricted overexpression of WT *PRKAG2* appears insufficient to induce ventricular pre-excitation [37]. Consistent with the temporal expression profile of the transgene promoter, surface ECG recordings are normal at birth, with subsequent evidence of ventricular pre-excitation emerging in the majority of TG mice overexpressing mutant *PRKAG2* by 4 weeks, i.e., postnatal manifestation [37]; loss of pre-excitation in adult TG mice, confirmed by electrophysiological study (EPS), has also been documented. In addition to pre-excitation, older mice up to 15 months of age display spontaneous supraventricular tachycardia and sinus bradycardia and pauses [37].

In the case of the TG^{N488I} and TG^{R302Q} models, the presence of functional accessory pathways has been confirmed using detailed in vivo EPS combined with pharmacological challenge. These have revealed procainamide-sensitive, adenosine-resistant functioning accessory pathways permitting atrioventricular (AV) conduction outside the AV node-His pathway [33, 37]. Moreover, in the case

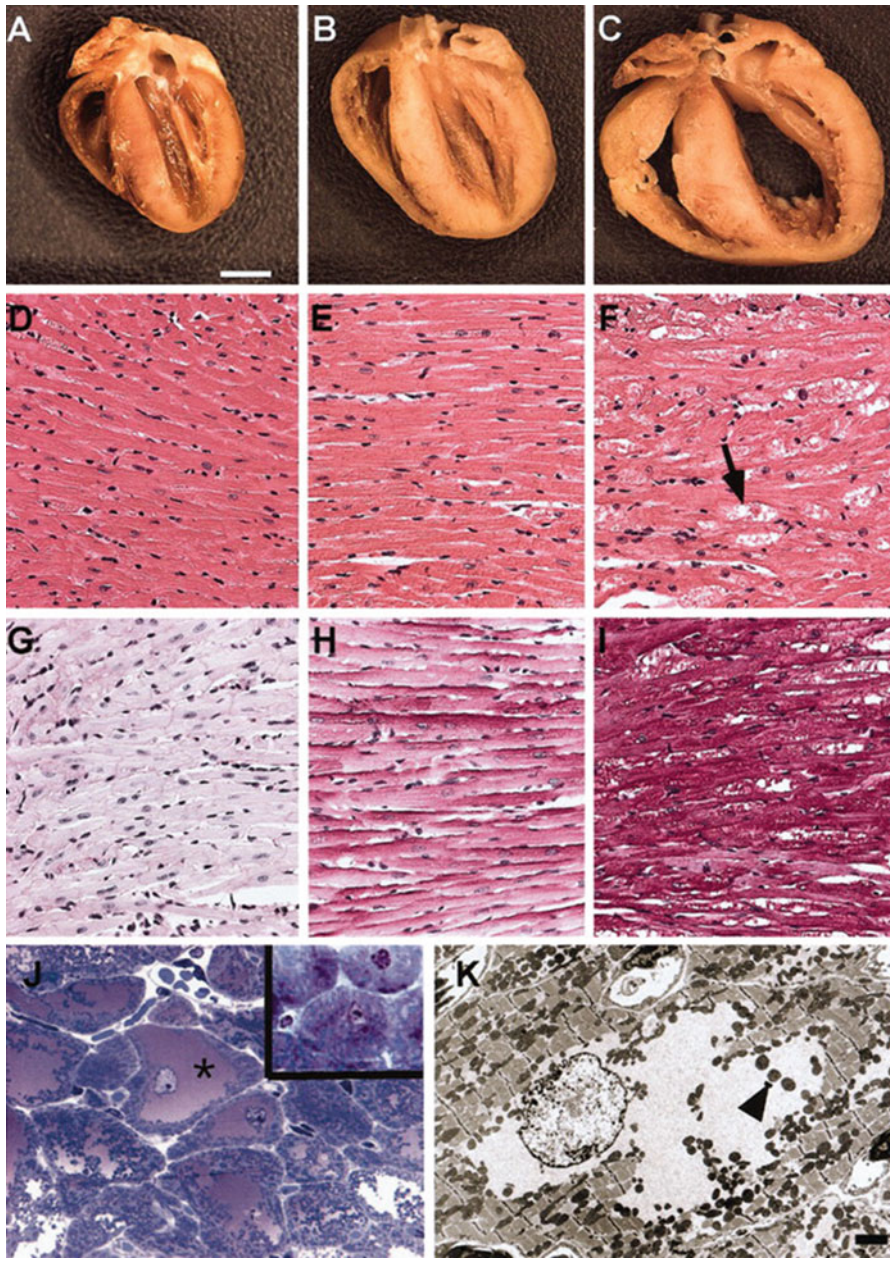

Fig. 2 Transgenic mice with cardiac-restricted overexpression of mutant *PRKAG2* recapitulate the severe end of the human PRKAG2 cardiomyopathy phenotypic spectrum. Upper row, long-axis sections of hearts from non-transgenic wild-type (**a**), TG^{WT} (**b**), and TG^{N488I} (**c**) mice, demonstrating marked cardiac hypertrophy resulting from cardiac-restricted overexpression of an Asn488Ile mutated *PRKAG2* transgene (i.e., TG^{N488I}) and milder hypertrophy resulting from overexpression of WT *PRKAG2* alone (TG^{WT}); scale bar 2 mm. Second row, hematoxylin and eosin-stained sections from WT (**d**), TG^{WT} (**e**), and TG^{N488I} (**f**) mice illustrating cardiomyocyte vacuolation. Third row, PAS-stained sections from WT (**g**), TG^{WT} (**h**), and TG^{N488I} (**i**) mice. Lower row, cardiac section stained with toluidine blue illustrating large glycogen pools in cardiomyocytes from TG^{N488I} mice but normal appearances (inset) from WT mice, (**j**) and transmission electron micrograph of an TG^{N488I} cardiomyocyte demonstrating free cytosolic glycogen and myofibrillar disruption (**k**); scale bar 3 μm (Reproduced from ref. 32 with permission from Wolters Kluwer Health, Inc.)

Table 2
Murine models of PRKAG2 cardiomyopathy

Model and *PRKAG2* mutation	Main observations	Measured effect on AMPK activity	Reference
TG^{N488I} (Asn488Ile)	Both TG^{WT} and TG^{N488I}—20-fold greater cardiac *PRKAG2* RNA and γ2-protein expression than non-TG mice TG^{WT}—cardiac hypertrophy (1.5-fold increased HW:BW over non-TG) and cardiac glycogen accumulation (sixfold increased glycogen:HW over non-TG). No decline in cardiac function by 20 weeks TG^{N488I}—severe cardiac hypertrophy (2.4-fold increased HW:BW over non-TG) and profound cardiac glycogen accumulation (33-fold increased glycogen:HW over non-TG). Overt pre-excitation (short PR/δ wave) in ~50% with EP study evidence of accessory AV connections. Thinning and disruption of the annulus fibrosus with multiple vacuolated, glycogen-loaded myocytes. Cardiac conduction system disease. Severe LV dysfunction by 20 weeks on echo. Stress-induced syncope and sudden death (20–40 weeks)	Elevated cardiac basal α1- and α2-associated AMPK activity in TG^{N488I} versus TG^{WT}	[32, 37]
TG^{R302Q} (Arg302Gln)	TG^{WT}—cardiac hypertrophy (HW 140 mg vs non-TG 117 mg) TG^{R302Q}—severe cardiac hypertrophy (~3-fold increased HW over non-TG). Twofold increased expression of B-type natriuretic peptide over TG^{WT} and non-TG. Cardiomyocyte vacuolation and glycogen retention. Muscle bundles extending from the atrium to the ventricle in the region of the fibrous body. Ventricular dilatation and reduced systolic function on echo. Overt ventricular pre-excitation on surface ECG. Increased sinus cycle length and functioning procainamide-sensitive accessory pathways. Inducible orthodromic atrioventricular reentrant tachycardia with atrial programmed electrical stimulation	Reduced cardiac γ2-specific and total AMPK activity in adult TG^{R302Q} versus non-TG. No significant response of TG^{R302Q} to AMP Increased cardiac AMPK activity in neonatal (7-day-old) TG^{R302Q} versus non-TG	[33, 49]
TG^{R531G} (Arg531Gly)	TG^{WT}—cardiac hypertrophy (1.3-fold increased LV mass over non-TG), significant from 4 weeks. Fivefold increased cardiac glycogen content over non-TG at 8 weeks. Normal ventricular volumes and function TG^{R531G}—severe cardiac hypertrophy (2.5-fold increased LV mass over non-TG). Profound	Cardiac γ2-associated AMPK activity near-undetectable in 4- and 8-week-old TG^{R531G} mice but comparable to non-TG at 1 week of age	[34]

(continued)

Table 2
(continued)

Model and *PRKAG2* mutation	Main observations	Measured effect on AMPK activity	Reference
	cardiac glycogen accumulation (80-fold and 15-fold greater than non-TG and TG^{WT}, respectively). Overt ventricular pre-excitation. Marked ventricular dilatation and severely impaired function (EF = 26% versus 58% in non-TG). Increased spontaneous mortality, more prominent in males		
TG^{T400N} (Thr400Asn)	TG^{WT} control not employed TG^{T400N}—cardiac hypertrophy apparent by 1 week of age (~4-fold increased HW:BW over non-TG by age 4 weeks). Marked myocyte vacuolization and glycogen retention (~100-fold greater than WT at 4 weeks). Later emergence of ventricular remodelling with dilatation and dysfunction (8–12 weeks). Partial phenotypic rescue of TG^{T400N} by crossbreeding with $TG^{\alpha 2DN}$	Initial increase in AMPK activity from 2 days to 2 weeks followed by decreased below TG^{WT} levels	[35]
N485I and R528G knock-in (KI) lines (Asn488I and Arg531Gly)	No significant differences in cardiac expression of γ2-AMPK or α1-/α2-subunit mRNA expression between WT and knock-in mice KI—small but significant increase in absolute cardiac mass in both lines at age 24 weeks. Increased cardiac glycogen in R528G KI only at age 26 weeks. Increased sinus cycle length in both KI lines. Significant small reduction in PR interval in R528G KI (13%) with no discernible differences in QRS duration from WT controls	Elevated pACC in cardiac and skeletal muscle in KI lines	[31]

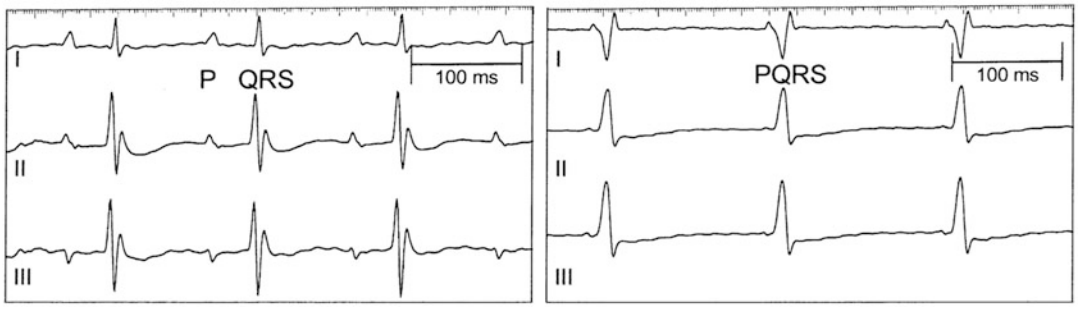

Fig. 3 Ventricular pre-excitation in transgenic mice overexpressing mutant *PRKAG2*. Surface ECG recordings of TG^{WT} (left) and TG^{R302Q} (right) mice, illustrating a shortened PR interval and widened QRS complex in TG^{R302Q} mice consistent with ventricular pre-excitation (Reproduced from ref. 33 with permission from Wolters Kluwer Health, Inc.)

of the TG^{R302Q} model, atrial electrical stimulation induced orthodromic AV reentrant tachycardia, consistent with anterograde AV nodal conduction and retrograde conduction via the accessory pathway [33].

Detailed histological evaluation of serial sections from TG^{N488I} mice with ventricular pre-excitation has identified its anatomic basis in this model: myocardial connections are observed to disrupt the annulus fibrosus (which acts in health to electrically insulate the ventricles from the atria outside the specialized conducting tissue axis) and are apparent by 2.5 weeks of age and largely located in the anteroseptal region close to the His-Purkinje system [32, 37, 38]. These connections appear to represent ventricular muscle formed of vacuolated, glycogen-engorged cardiomyocytes (Fig. 4) [32].

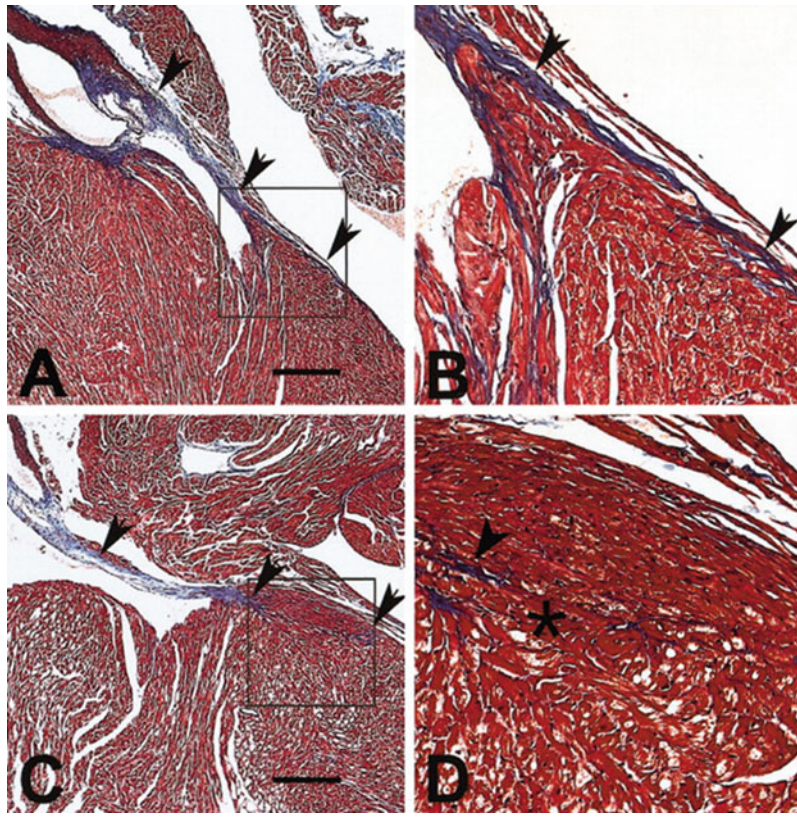

Fig. 4 Anatomical substrate for ventricular pre-excitation—disruption of annulus fibrosus integrity in a murine transgenic model of *PRKAG2* cardiomyopathy. Masson's trichrome stained sections through AV junction myocardium in TG^{WT} (upper panels, **a**, **b**) and TG^{N488I} (lower panels, **c**, **d**) mice in the region of the right paraseptal area demonstrating an intact annulus fibrosus (blue staining, arrowheads) in TG^{WT} hearts but an interrupted annulus with direct contact between atrial and vacuolated ventricular cardiomyocytes (**d**, asterisk) in TG^{N488I} mice; scale bar 200 μm (Reproduced from ref. 32 with permission from Wolters Kluwer Health, Inc.)

The reversibility of ventricular pre-excitation and other manifestations of *PRKAG2* disease has been investigated in a series of elegant experiments using a tetracycline-controlled binary α-MHC-driven system of Asn488Ile transgene expression in mice. Early transgene suppression (using oral doxycycline administration) from prenatal up to 8 weeks of adult life ($TG^{OFF(E\text{-}8\ weeks)}$) was sufficient to prevent ventricular pre-excitation—even with subsequent expression of the mutant transgene for 12 weeks—and associated with a histologically intact annulus fibrosus [16]. In contrast, Asn488Ile transgene suppression commencing after 4 weeks ($TG^{OFF(4–16\ weeks)}$) reduced the frequency of overt pre-excitation from ~50% to 11%, while mutant transgene suppression beyond 8 weeks of life ($TG^{OFF(8–20\ weeks)}$) was found to have no effect on the development or persistence of pre-excitation [16]. Early transgene suppression ($TG^{OFF(E\text{-}8\ weeks)}$) was also associated with a reduction in myocardial glycogen level and delayed, but did not prevent, LVH and LV chamber dilatation or reduced ventricular systolic function [16]. However, $TG^{OFF(8–20\ weeks)}$ mice had similar rates of sinoatrial and AV block to mice (TG^{ON}) which had not undergone any mutant transgene suppression, indicating that early suppression of mutant *PRKAG2* transgene expression, and associated glycogen reduction, could prevent pre-excitation but did not favorably impact upon cardiac conduction system disease or prevent eventual adverse ventricular remodelling and heart failure.

While the murine studies suggest accumulation of a critical mass of glycogen to be a prerequisite for development of ventricular pre-excitation, this does not exclude other potential AMPK-mediated, glycogen-independent contributors to accessory pathway formation, such as abnormal AV canal development [39], particularly in the setting of a relatively hypomorphic annulus fibrosus. Recent findings of reduced TGFβ signalling in human induced pluripotent stem cell (iPSC)-derived cardiomyocytes expressing a *PRKAG2* mutation have suggested a molecular substrate for this [40].

3.2 The Role of Glycogen and Glycogen-Independent Disease Mechanisms

Multiple lines of evidence highlight glycogen excess as an important contributor to the pathogenesis of *PRKAG2* cardiomyopathy: prominent cardiac glycogen accumulation in human *PRKAG2* mutation carriers and murine transgenic models [13, 32]; cardiac phenotypic overlap with inherited disorders of glycogen metabolism (e.g., infantile Pompe disease), including the presence of ventricular pre-excitation; amelioration of the disease phenotype in parallel with change in myocardial glycogen content in experimental models [16]; the well-established role of AMPK in regulating cellular glucose uptake and glycogen metabolism [41–43], with evidence of enhanced glucose uptake and reduced glycolytic flux in isolated TG^{N488I} hearts [44]; and the observation of increased

skeletal muscle glycogen content in association with a γ3 mutation homologous to a pathogenic γ2-variant [19].

These observations have led to the conceptualization of *PRKAG2* cardiomyopathy as a glycogen storage disorder, with its disease manifestations proposed as being largely attributable to bulk glycogen accumulation, including glycogen-associated alteration in electrophysiological conduction properties [13, 45]. However, passive cellular engorgement by glycogen is unlikely sufficient to fully account for the magnitude of cardiac hypertrophy observed in the transgenic murine models. Exemplifying this, in the TG^{T400N} model, glycogen is estimated to account for only ~4% of the increase in cardiac mass [46], suggesting a substantial contribution from true cellular hypertrophy [34].

Findings from the inducible Asn488Ile murine transgenic model (*see* Subheading 3.1), where a period of early mutant transgene suppression was sufficient to prevent ventricular pre-excitation, suggest an important role for glycogen excess in its pathogenesis [16] and, by inference, in traditional glycogen storage diseases [32]. More direct evidence to a support a causal role for glycogen in the development of pre-excitation comes from a study of TG^{N488I} mice designed to co-harbor a homozygous knock-in mutation (Arg582Ala) in muscle glycogen synthase 1 (*Gys1*), rendering the latter insensitive to normal allosteric stimulation by glucose-6-phosphate (G6P) [47], a metabolic intermediary found elevated in hearts from mutant *PRKAG2* transgenic mice [44]. Substantiating inferences from metabolic flux analysis suggesting a key role for G6P-mediated glycogen synthase activation in mutant *PRKAG2*-associated cardiac glycogen accumulation [44], these mice ($TG^{N488I}/GS^{R582A/R582A}$) have substantially reduced (~6-fold) myocardial glycogen content [48]. Strikingly this was associated with normalization of the PR interval (Fig. 5), consistent with elimination of ventricular pre-excitation, and a corresponding improvement in annulus fibrosus appearance [48]. However, genetic inhibition of G6P-stimulated glycogen synthase activity had no significant effect on cardiac hypertrophy—suggesting a glycogen storage-independent mechanism for LVH—and only partly rescued cardiac function (mean echocardiography-derived LV fractional shortening 32%, 42%, and 58%, in TG^{N488I}, $TG^{N488I}/GS^{R582A/R582A}$, and non-TG mice, respectively) [48]. Further investigation of myocardial signalling in TG^{N488I} and $TG^{N488I}/GS^{R582A/R582A}$ mice has identified enhanced insulin sensitivity (including increased P-AKT^{Ser473}) in conjunction with mTOR pathway activation [48], the latter finding also observed in TG^{T400N} mice as early as 2 weeks of age [46]. As a corollary, inhibition of mTOR in TG^{N488I} mice, using rapamycin from age 2–6 weeks, substantially (~45%) ameliorates their cardiac hypertrophy [48]. A further consequence of AKT hyperactivity identified was that of forkhead box O (FoxO) transcription factor pathway

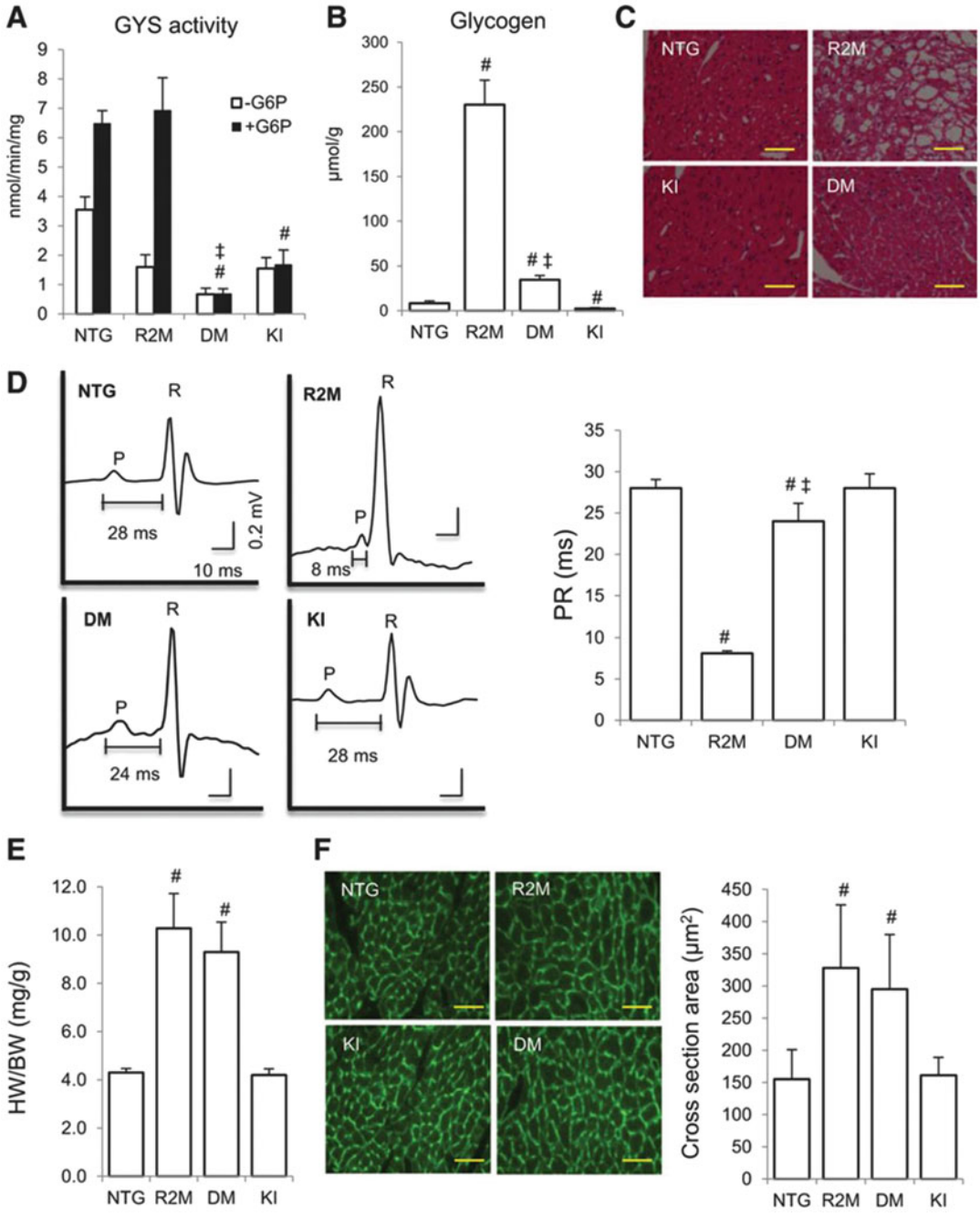

Fig. 5 Genetic targeting of GYS1 to abrogate glucose-6-phosphate induced activation in transgenic mice expressing mutant *PRKAG2* ameliorates glycogen storage, eliminating ventricular pre-excitation, but does not impact upon cardiac hypertrophy. Rescue of ventricular pre-excitation, but not LVH, of TG^{N488I} mice through genetic inhibition of glucose-6-phosphate (G6P)-stimulated glycogen synthase activity. (**a**) Cardiac glycogen synthase activity in the presence (+) or absence (−) of G6P in non-transgenic (NTG), TG^{N488I} (R2M), double transgenic $TG^{N488I}/GS^{R582A/R582A}$ (DM), and homozygous knock-in $GS^{R582A/R582A}$ (KI) mice. (**b**) Cardiac glycogen level. (**c**) Hematoxylin and eosin staining of cardiac sections illustrating absence of vacuoles in double

inactivation. Confirming the importance of this mechanistically, TG^{N488I} mice crossed with mice overexpressing FoxO1 in the heart display marked improvement in LVH, with full rescue of hypertrophy when combined with rapamycin treatment [48]. These observations highlight altered myocardial mTOR and FoxO signalling as sufficient to account for LVH in the TG^{N488I} model. In addition, analysis of proliferation markers, Ki67 and phosphohistone H3, in hearts from 2-week-old TG^{N488I} mice has revealed evidence of contributory cardiomyocyte proliferation at this early stage [48].

Recently, prompted in part by concerns relating to the presence of a phenotype in transgenic mice overexpressing WT *PRKAG2* alone [49], knock-in (KI) mice designed to express more physiological levels of cardiac γ2-expression have been developed and their cardiac phenotype described [31]. The latter mice—bearing a single mutation in either of two γ2-residues corresponding to human Asn488Ile or Arg531Gly (murine Asn485Ile and Arg528Gly, respectively)—exhibit a more subtle phenotype than the cardiomyocyte-restricted TG mouse lines, characterized by modest increases in cardiac mass (by age 24 weeks), upregulation in cardiac markers of hypertrophy, and (in the case of the Arg528Gly KI) significantly increased cardiac glycogen levels [31]. ECG assessment revealed a small reduction in the PR interval (~13%) of Arg528Gly KI mice but no significant change in QRS duration in either KI line compared to WT control, suggesting no overt ventricular pre-excitation. Taken together, these findings suggest the presence of interspecies differences such that, in the mouse, a genetic overexpression strategy may be required to fully recapitulate the more extreme cardiac phenotypes observed in humans bearing *PRKAG2* mutations, particularly ventricular pre-excitation which may be contingent on a critical mass of glycogen driven by a threshold level of mutant holoenzyme complexes.

4 Impact of *PRKAG2* Mutations on AMPK Activity

4.1 Insights from In Vitro Studies

The identification of a functional role for tandem CBS motifs as allosteric binding domains for adenine nucleotides whose mutation could result in inherited disease [18], including *PRKAG2* cardiomyopathy, suggested that γ2-mutations may directly impact upon AMPK energy sensor function by disrupting its interaction with

Fig. 5 (continued) transgenic mice (DM); scale bar 40 μm. (**d**) Ventricular pre-excitation is present in TG^{N488I} (R2M) mice, but not in double transgenic (DM) mice. (**e**) Heart weight/body weight ratio and (**f**) cardiomyocyte cross-sectional area determined by wheat germ agglutinin staining illustrating persistence of cardiac hypertrophy in double transgenic mice (DM); scale bar 40 μm (Reproduced from ref. 48 with permission from Wolters Kluwer Health, Inc.)

adenyl nucleotides. Structural support for this emerged from the mapping of pathogenic γ2-mutations onto equivalent residues in a mammalian γ1-containing core AMPK complex. This revealed that almost all the mutations examined involved amino acids with side chains close to the adenyl binding site, the majority in direct contact with AMP/ATP phosphate groups [50].

Early biochemical studies explored the effect of such CBS domain mutations on AMPK activity using a variety of experimental approaches, including transient or stable expression of a γ1-mutation (Arg70Gln, equivalent to Arg302Gln in γ2 or Arg200Gln in γ3) in COS cells or pulmonary fibroblasts, respectively [51]; introduction of the Thr400Asn and Asn488Ile γ2-mutations into the yeast γ-subunit homologue (Snf4) with analysis of interaction with Snf1 (α-subunit homologue) [13]; and transient transfection of WT or mutant γ3 (Arg225Gln) into COS cells [52]. These reports suggested the primary consequence of γ2-mutations to be that of enhanced basal activation of AMPK complexes. Other studies transfecting CCL13 cells with a series of mutant γ2-variants noted defective activation of AMPK by AMP in vitro but without evidence for a significant effect on holoenzyme activity under basal conditions [18, 53]. A subsequent report characterizing the biochemical impact of an Arg531Gln missense mutation in γ2—identified as a sporadic mutation in three neonates with a fulminant and ultimately fatal clinical course—noted a profound (>100-fold) reduction in mutant AMPK binding affinity for both AMP and ATP [26]. When expressed in HEK-293 cells, the Arg531Gln mutation (together with the identically situated but biochemically and clinically less severe Arg531Gly mutation) was found to enhance basal AMPK activation. Critically and in contrast to studies employing CCL13 cells, this latter study employed a cell line expressing the major AMPK upstream kinase, LKB1 [26]. Accordingly, these data suggested that while associated with a reduction or complete loss of sensitivity to AMP and ATP (whose degree is dependent upon the individual mutation), in the basal state and in the presence of adequate upstream LKB1, γ2-mutations act to *enhance* AMPK activity. Notably this mechanism more readily reconciles with the observed dominant inheritance pattern, unlike that of a purported loss of function of one allele of a minority γ-isoform in the setting of an intact WT allele (i.e., haploinsufficiency).

4.2 Insights from In Vivo Models

In parallel with these studies, generation of transgenic mice bearing human *PRKAG2* mutations enabled AMPK activity to be directly assayed from cardiac tissue extracts. Initially, these also revealed apparently discrepant findings, with reports of elevated α1- and α2-AMPK-associated basal activity in TG^{N488I} mice [32], contrasting with descriptions of reduced total and γ2-specific AMPK activity in TG^{R302Q} [33] and TG^{R531G} [34] models (the latter with no difference at age 1 week) (Table 2).

An important observation in this regard was the apparent association of age with AMPK activity, peaking early on (~2 weeks) but subsequently falling below TG^{WT} levels (after ~4 weeks). This, coupled with the finding that reduction in AMPK activity extended to involve γ1-containing AMPK complexes in older mice, highlighted the critical role of an extrinsic factor in modulating the primary effect of mutations in γ2 [34]. The inverse correlation between myocardial glycogen levels (which steadily accumulate with age) and AMPK activity in TG mice overexpressing mutant *PRKAG2* provided a clear substrate for this (Fig. 6) [35]. Substantiating the primary impact of γ2-mutations on the holoenzyme,

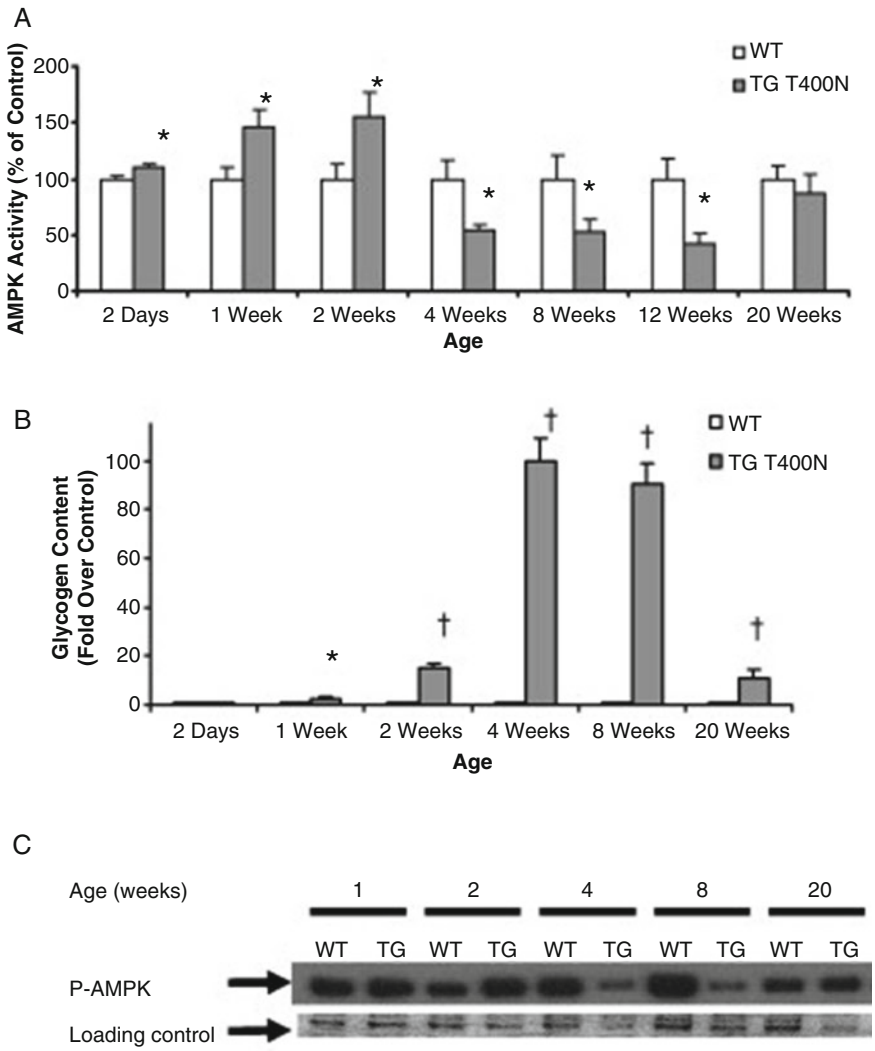

Fig. 6 Inverse association between myocardial AMPK activity and glycogen content in TG^{T400N} mice. Temporal change in cardiac AMPK activity (**a**), glycogen content (**b**), and pan α-Thr172 phosphorylation (P-AMPK) (**c**) in TG^{T400N} mice (Reproduced from ref. 35 with permission from Elsevier)

activity assays from both rat neonatal cardiomyocytes acutely transduced with Arg302Gln γ2-expressing adenovirus and cardiac extracts from 1-week-old TG^{R302Q} mice—experimental settings expected to be devoid of significant glycogen accumulation—revealed increased AMPK activity, contrasting with adult mice [49]. Verifying the role of enhanced basal AMPK activity as the driver of cardiomyopathy, double transgenic TG^{N488I} mice overexpressing a dominant negative α2-mutant ($TG\alpha2^{DN}$) exhibit marked amelioration in cardiac hypertrophy, glycogen levels, and PR interval shortening, together with normalization of contractile function, compared to TG^{N488I} mice alone [15].

In addition to the dynamic relationship between cardiac glycogenosis and AMPK activity, ex vivo cardiac perfusion studies using the TG^{N488I} model highlight the importance of ambient nucleotide concentrations on AMPK activity [54]. Determination of AMPK activity from excised cardiac tissue has potential limitations in determining the γ2-mutation's true in situ effect, largely due to the inherent organ anoxia and attendant ATP depletion accompanying postmortem tissue harvesting. Perfusion of isolated TG^{N488I}, TG^{WT}, and non-TG WT hearts followed by assessment of myocardial energetic status after a period of stabilization revealed no differences in phosphocreatine, ATP, or free AMP levels determined by ^{31}P NMR spectroscopy, suggesting normal energetic status under these conditions [54]. Assays of freeze-clamped cardiac tissue in this metabolically equilibrated state revealed increased α2-associated AMPK activity—and a corresponding ~4-fold increase in pan α-Thr172 phosphorylation, reflecting total AMPK activity—in TG^{N488I} mice over both TG^{WT} and non-TG controls. In contrast, assessment of AMPK activity after a period of no-flow global cardiac ischemia, which resulted in a ~15-fold rise in the AMP/ATP ratio, revealed a sevenfold increase in pan α-Thr172 phosphorylation in WT but no corresponding increase in TG^{N488I} hearts (Fig. 7). These findings, in conjunction with other studies [26, 50], point to a more nuanced view of the activity consequences of γ2-mutations beyond a simple "gain of function." Thus, under conditions of replete cellular ATP, lack of (appropriate) inhibition of mutant γ2-AMPK complexes leads to enhanced activity. In contrast, mutant γ2-AMPK is less responsive to activation under conditions of cellular stress where ATP is depleted and AMP levels rise.

5 Clinical Phenotype Associated with *PRKAG2* Mutations

5.1 Typical Presentation

The cardiac phenotype associated with *PRKAG2* mutations includes left ventricular hypertrophy (LVH, varying from absent to massive), ventricular pre-excitation, sinus node dysfunction including chronotropic incompetence, atrial tachyarrhythmia,

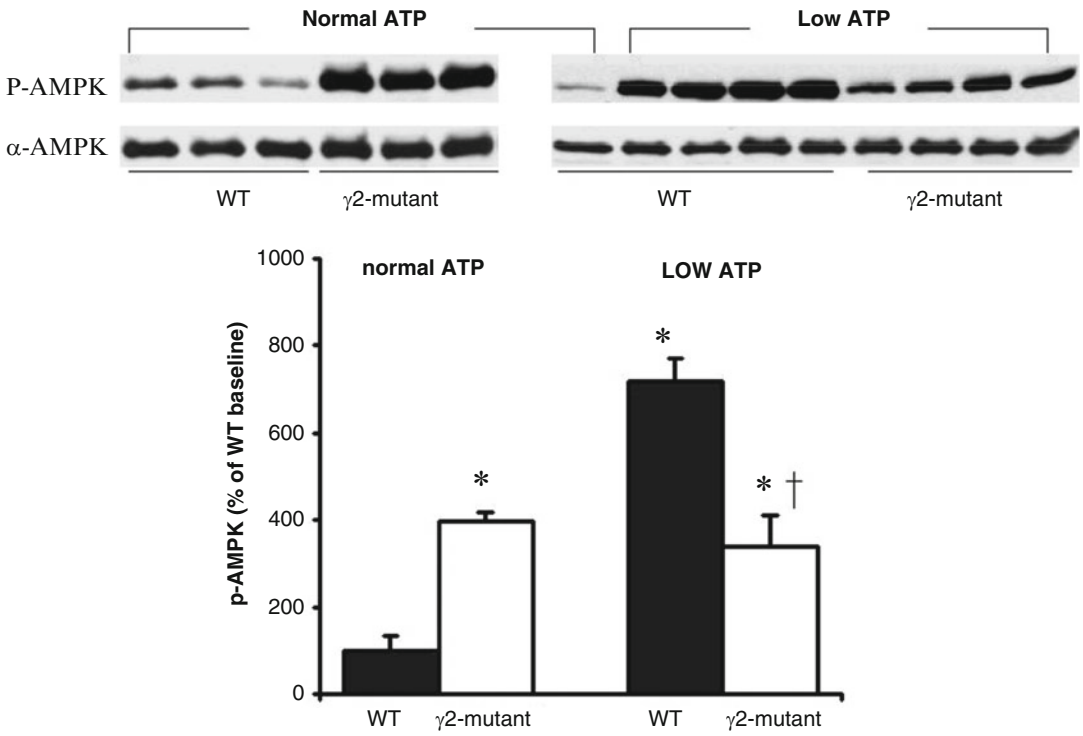

Fig. 7 Ambient ATP concentration influences the impact of mutant *PRKAG2* on AMPK Thr172 α-AMPK phosphorylation. Pan α-Thr172 phosphorylation immunoblots (upper row) and associated densitometry (lower row) from freeze-clamped WT and TG^{N488I} ex vivo perfused hearts under conditions of normal and depleted ATP (Reproduced from ref. 54 with permission from Wolters Kluwer Health, Inc.)

progressive cardiac conduction system disease, cardiomyocyte glycogen excess, and propensity to SCD.

Individuals bearing a *PRKAG2* mutation typically present with palpitations, pre-syncope, syncope, chest pain, features of heart failure (e.g., exertional dyspnea), or sudden death. They may also be identified after identification of an abnormal ECG (Fig. 8), unexplained LVH or, rarely (contrasting with sarcomeric HCM) through the presence of a cardiac murmur [55, 56]. The age of presentation, severity of symptoms, and natural history may be influenced by the specific mutation inherited. It has been suggested that the course of the disease for the same mutation may have interfamilial variability and, occasionally, even intrafamilial heterogeneity [24]. The overall mean age at diagnosis for all reported mutations is ~30 years [17]. For the two most commonly reported mutations, mean age at diagnosis ranges from 19 years (Asn488Ile variant) to 36 years (Arg302Gln variant) [17]. Pediatric or even antenatal (de novo) presentation has been reported in association with a number of variants, including His383Arg [10], Arg384Thr [25], Arg531Gly [30], and Arg531Gln [26], and has been linked to a more severe clinical phenotype.

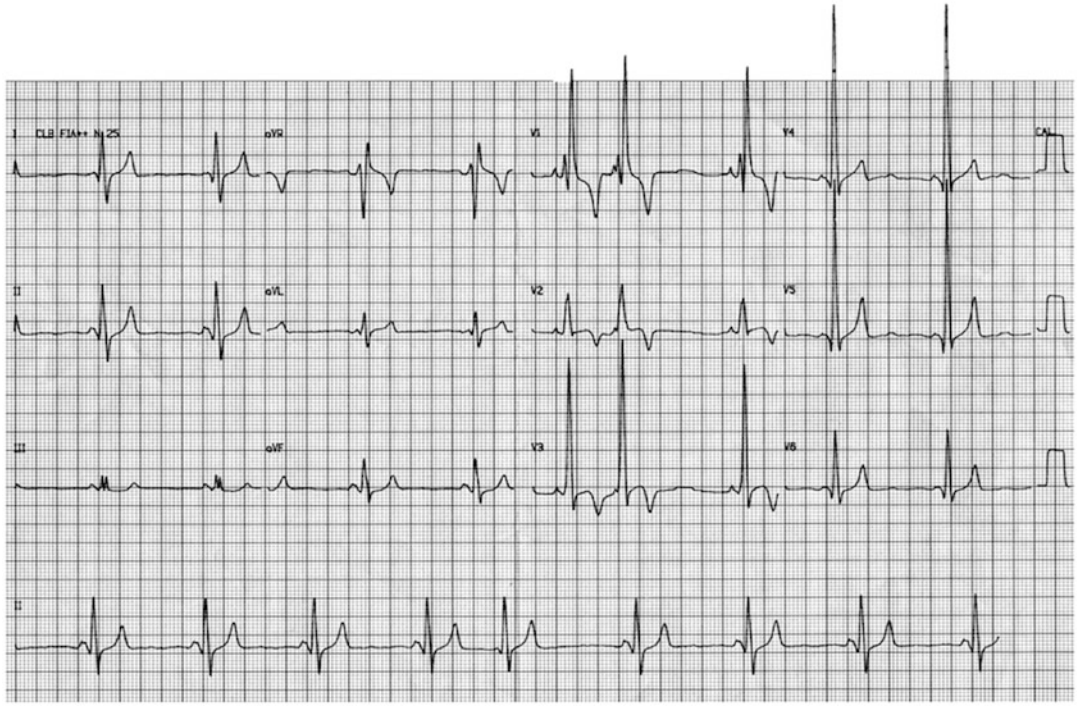

Fig. 8 Typical presenting ECG features associated with a pathogenic mutation in *PRKAG2*. 12-lead ECG of a 26-year-old male Arg302Gln *PRKAG2* mutation carrier with a history of paroxysmal atrial fibrillation and syncope. It demonstrates sinus bradycardia, atrial ectopy, and ventricular pre-excitation with a pattern suggestive of a left-sided accessory pathway with a very short PR interval which does not increase during the atrial extrasystole

In younger patients (below 35 years), SCD usually arises due to very rapid anterograde conduction of a supraventricular arrhythmia (e.g., atrial fibrillation) directly over an accessory pathway—i.e., pre-excited supraventricular arrhythmia—which may degenerate into a lethal ventricular arrhythmia [29]. In older patients (over 35–40 years), SCD is thought to more frequently reflect the sudden onset of complete heart block or asystole resulting in hemodynamic collapse. It is possible that other pathogenic mechanisms may be involved in cases with particularly massive cardiac hypertrophy [24].

5.2 Clinical Electrophysiology

5.2.1 Atrial Arrhythmia

Symptoms caused by atrial tachyarrhythmias usually commence between the end of adolescence and the third decade of life. Indeed, paroxysmal atrial flutter and fibrillation are responsible for most symptomatic cases among young adults. The resulting ventricular heart rate may be very rapid in the setting of conduction over an associated accessory pathway with short refractory period and can result in SCD (Fig. 9). Fatal thromboembolic stroke in

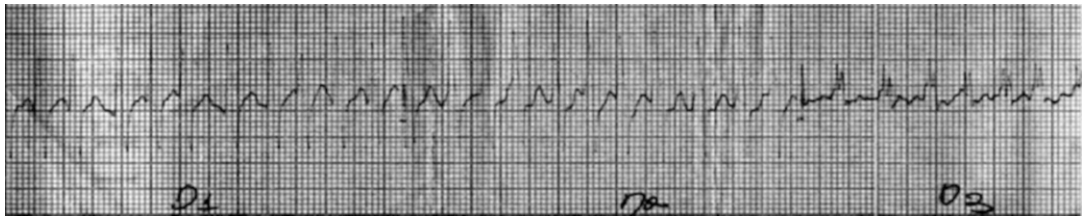

Fig. 9 Atrial fibrillation with extremely rapid ventricular conduction associated with *PRKAG2* cardiomyopathy. Rhythm strip of the same patient as in Fig. 8 demonstrating atrial fibrillation with a very rapid ventricular rate of ~280 beats/min. The patient died suddenly several months after this ECG was obtained

association with atrial fibrillation has also been reported in one case series as the most frequent cause of death [24].

The prevalence of atrial tachyarrhythmia (specifically atrial fibrillation and/or atrial flutter) progressively increases with age and, based on some patient series, may exceed 80% by ~50 years of age [57]. The incidence of atrial fibrillation is much higher in *PRKAG2* mutation carriers than in patients with otherwise sporadic isolated Wolff-Parkinson-White syndrome [58]. It has been suggested that in the absence of significant atrial fibrosis, atrial hypertrophy in conjunction with ion channel dysfunction [59]—either through a direct modulatory effect on channel function or due to an acidic pH resulting from substantial intracellular glycogen accumulation—may in part explain the strong susceptibility to atrial fibrillation (Fig. 10) [60].

5.2.2 Sinus Bradycardia and Chronotropic Incompetence

Individuals bearing a mutant *PRKAG2* gene, particularly those with the Arg302Gln variant, may develop progressive, symptomatic sinus bradycardia, often with resting heart rates below 40 beats per minute. Bradycardia during infancy or fetal development appears to be rare but has been reported prenatally with both the Arg531Gln and Arg384Thr mutations and may prompt urgent Caesarean section [25, 26]. In adult mutation carriers, the true incidence of sinus node disease may be underestimated given the large proportion who develop concomitant AV conduction block and undergo pacemaker implantation before potential symptoms arising from sinus bradycardia become manifest [17]. A further manifestation of sinus node disease in *PRKAG2* cardiomyopathy is an inadequate heart rate increment on exercise (chronotropic incompetence). The latter can be associated with exercise limitation and may symptomatically benefit from pacemaker implantation [12, 24].

5.2.3 Atrioventricular Conduction Abnormalities

AV conduction disturbances of primary genetic origin, despite being increasingly recognized in a number of conditions, are still considered rare. Atrioventricular conduction block may occur as a single abnormality, such as in Lenègre's disease caused by a mutation in the sodium channel *SCN5A* [61], or in association with

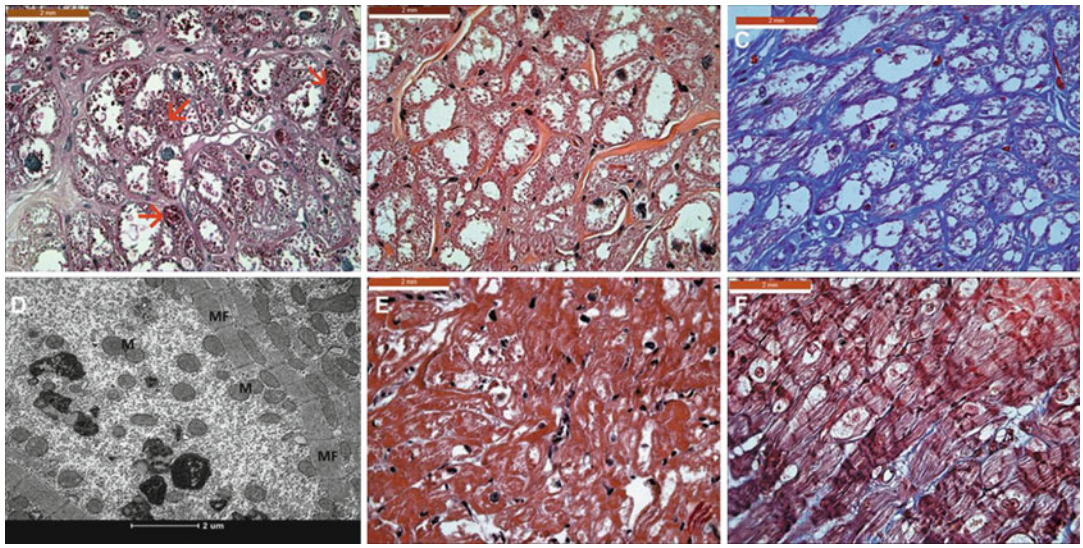

Fig. 10 Cardiac histological findings in an individual with the Arg302Gln *PRKAG2* mutation. Cardiac histology from a 52-year-old male with the Arg302Gln mutation, permanent atrial fibrillation, and LVH. Upper row illustrates right atrial appendage sections stained with PAS (**a**), hematoxylin and eosin (**b**), and Masson trichrome staining (**c**), illustrating severe cardiomyocyte vacuolization and granular inclusions consistent with glycogen (arrows) but no significant fibrosis. Lower row demonstrates similar findings in the same patient from the RV septum, including transmission electron microscopy (**d**), with ventricular cardiomyocyte vacuolization, abundant glycogen accumulation (**e**), and, in contrast to familial HCM, a conspicuous absence of myocardial disarray (**f**) (Reproduced from ref. 60 with permission from Wolters Kluwer Health, Inc.)

cardiomyopathies, such as dilated cardiomyopathy due to mutations of the *LMNA* gene, or cardiomyopathies associated with hypertrophy such as that due to mutations in *LAMP2* or *PRKAG2* [62–64]. In *PRKAG2* cardiomyopathy, progression to symptomatic AV block is a common event between the third and fourth decades. Concurrent with AV block is loss of ventricular preexcitation. This is an expected event in the setting of a fasciculoventricular pathway since its proximal end connects to the AV conduction axis, usually in the bundle branches (Fig. 11). Advanced AV block can present abruptly and represents an important cause of SCD in patients with *PRKAG2* mutations. The incidence of heart block and pacemaker implantation can vary dependent upon the mutation carried. Thus, a 55% pacemaker implantation rate has been reported for patients with the Arg302Gln mutation, as compared to 30% of those with the Asn488Ile mutation [17]. Notably conduction system disturbances—reflecting conduction delay—can occur at multiple levels, including intra-atrial, intrahisian, infrahisian, and intraventricular. Reflecting the latter, reports of bundle branch block, most frequently complete or incomplete right bundle branch block but also left bundle branch block or left anterior hemiblock, have been made in association with *PRKAG2* mutations [27, 57, 65, 66].

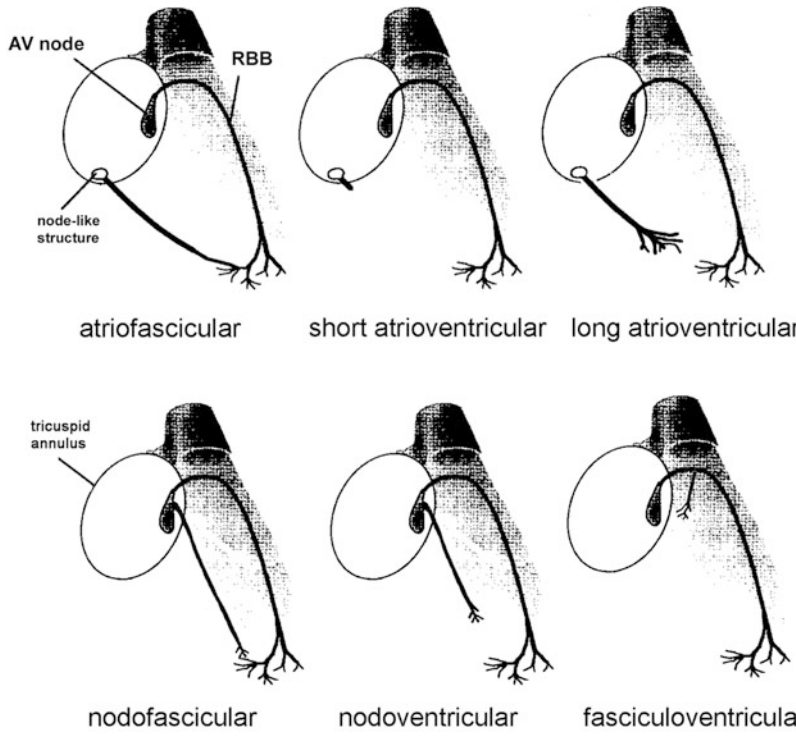

Fig. 11 Schematic illustrating the course of different anatomical variants of ventricular pre-excitation. Note the course and proximal ends of fasciculoventricular and nodoventricular pathways representing the substrate for most ventricular pre-excitation associated with *PRKAG2* mutations (Reproduced from ref. 69 with permission from Blackwell Futura)

5.2.4 Ventricular Pre-excitation

Ventricular pre-excitation is an extremely common, although not invariable, finding in *PRKAG2* cardiomyopathy, being reported in 77% of patients in a recent case series [67]. The underlying accessory pathways are frequently multiple and with bidirectional conduction [36, 68]. Notably this finding of multiple patterns of ventricular activation (consistent with several accessory pathways) has also been observed in transgenic mouse models of the disease [32]. Preclinical experiments have suggested ventricular pre-excitation in the setting of *PRKAG2* mutations to be linked to disruption of the normal electrical insulation function of the annulus fibrosus between the atria and the ventricles (Fig. 4) [32]. Structural damage to the annulus due to glycogenosis has been proposed to allow electrical conduction to bypass normal conduction via the AV node. Several authors have reported accessory pathways with atypical decremental conduction properties in patients with *PRKAG2* mutations, with a prevalence of between 50 and 100% [12, 27]. The majority of patients with the Arg302Gln mutation with ventricular pre-excitation who have undergone invasive electrophysiological assessment have a pre-excitation variant occurring over fasciculoventricular pathways

[69–71], although nodoventricular fibers have also been reported (Fig. 11) [28]. Fasciculoventricular fibers are not a substrate for reentrant tachycardia, and due to the small incidence of a truly atrioventricular accessory pathway, circus movement tachycardia is rarely reported. If catheter ablation is attempted in this setting, it is very important to correctly identify the type of accessory pathway in order to avoid iatrogenic damage to the conduction system axis, as can occur if a fasciculoventricular pathway is not distinguished from a superior paraseptal accessory pathway [57, 69–71]. An isolated short PR interval in the absence of a delta wave (abnormal slurred initial QRS vector) or QRS prolongation (i.e., without the Wolff-Parkinson-White ECG pattern and with exclusion of rarer variants of accessory pathway at EPS in some) has also been reported [27, 65, 67].

5.3 Heart Failure

Symptoms of heart failure can occur in the setting of preserved ventricular systolic function, usually in the presence of severe LVH (suggesting significant diastolic dysfunction) as in the case of a Turkish family carrying the Glu506Lys mutation [72]. This may be associated with biochemical evidence supporting a diagnosis of heart failure, as in the case of the 19-year-old proband with the latter mutation who exhibited severe biventricular hypertrophy and a profound elevation in plasma N-terminal pro-B-type natriuretic peptide to 32,822 pg/ml (normal range in the non-acute setting <125 pg/ml) [72, 73]. Progression to frank systolic heart failure appears to be more frequent in the setting of a *PRKAG2* mutation than that encountered in classical sarcomeric HCM, being reported in the former in ~12% of all patients [17] and even higher (up to 25%) in some cohorts [67]. When considering the incidence of progression to ventricular dilatation with severe systolic dysfunction and potential requirement for cardiac transplantation, published reports suggest the existence of genotype-phenotype correlations. Thus, progression from HCM to end-stage cardiac failure has been described in three carriers of the Val336Ala variant from a single family [67], while a de novo Lys485Glu mutation was identified in a single patient diagnosed with HCM and WPW at age 15 years who subsequently progressed to severe cardiac enlargement and symptomatic heart failure by his early 20s [74]. Marked propensity toward early transition to cardiac dilatation with systolic failure has been noted in patients harboring other mutations, such as His383Arg [10], His530Arg [67, 75], and Arg350_Glu351insLeu [10], with individuals undergoing cardiac transplantation between 19 and 42 years of age. Fulminant onset of ultimately fatal infantile heart failure in the setting of severe HCM has been reported with de novo Arg531Gln mutations, mirroring the profound biochemical impact of this mutation on adenine nucleotide binding and basal activation of AMPK [26]. In contrast to these variants, the frequency of progression of hypertrophy to a dilated

phase with left ventricular dysfunction appears lower with the two most commonly described *PRKAG2* mutations (Arg302Gln and Asn488Ile), with transplantation reported in one case at age 42 years [12, 24, 65].

5.4 Sudden Death

A recent summary of published cases estimated sudden death to affect ~9% of mutation carriers, with a mean age of death at 33.4 years [17]. A more recent case series ($n = 34$) reported sudden death in as many as 32% of individuals, with a mean age of 44 years [67]. Given the high rate of permanent pacemaker implantation (reported as ~43% [17]), frequently in the age range of 30–40 years, it is likely that timely pacemaker implantation prevents sudden death in many mutation carriers. The majority of cases in this age group are thought to reflect the occurrence of pre-excited atrial fibrillation triggering ventricular fibrillation or perhaps even primary ventricular fibrillation (the latter more likely in the setting of severe cardiac hypertrophy or progression to a dilated hypokinetic ventricular phenotype), rather than high-grade AV conduction block [27].

While runs of non-sustained ventricular tachycardia have been identified using Holter ambulatory ECG monitoring in a small proportion of *PRKAG2* mutation carriers (largely with severe LVH) [24], there are no data regarding aborted episodes of SCD in patients with *PRKAG2* mutations who have received an implantable cardioverter defibrillator (ICD), although analysis of such events could yield mechanistic insights. In our own experience, many *PRKAG2* mutation carriers who have received an ICD were initially misdiagnosed with (classical) familial HCM and received it for primary prevention purposes. One of our three patients with an ICD has experienced inappropriate therapies that were triggered by atrial fibrillation and a consequent fast ventricular rate beyond the programmed rate cutoff for device therapy. In a series of patients carrying the Arg302Gln mutation who underwent electrophysiological study, none had inducible sustained ventricular tachycardia on programmed ventricular stimulation [27], an observation mirrored during study of TG^{R302Q} mice [33]. These findings may reflect the relatively lower degree of myocardial fibrosis encountered in *PRKAG2* cardiomyopathy compared to familial HCM (Fig. 10)—indeed, a recent cardiovascular magnetic resonance study identified late gadolinium enhancement, a marker of focal fibrosis, in only two of six mutation carriers analyzed, both of whom displayed severe LVH (Fig. 12) [76]. The molecular substrate for this is unclear, but recent findings from human iPS cell-derived cardiomyocyte models bearing the Asn488Ile mutation suggest that this may involve attenuated TGFβ signalling [40].

5.5 Ventricular Hypertrophy

Together, LVH and ventricular pre-excitation represent the most common clinical features in patients with *PRKAG2* mutations, with a frequency of LVH of 78% ($n = 41$) in one large patient

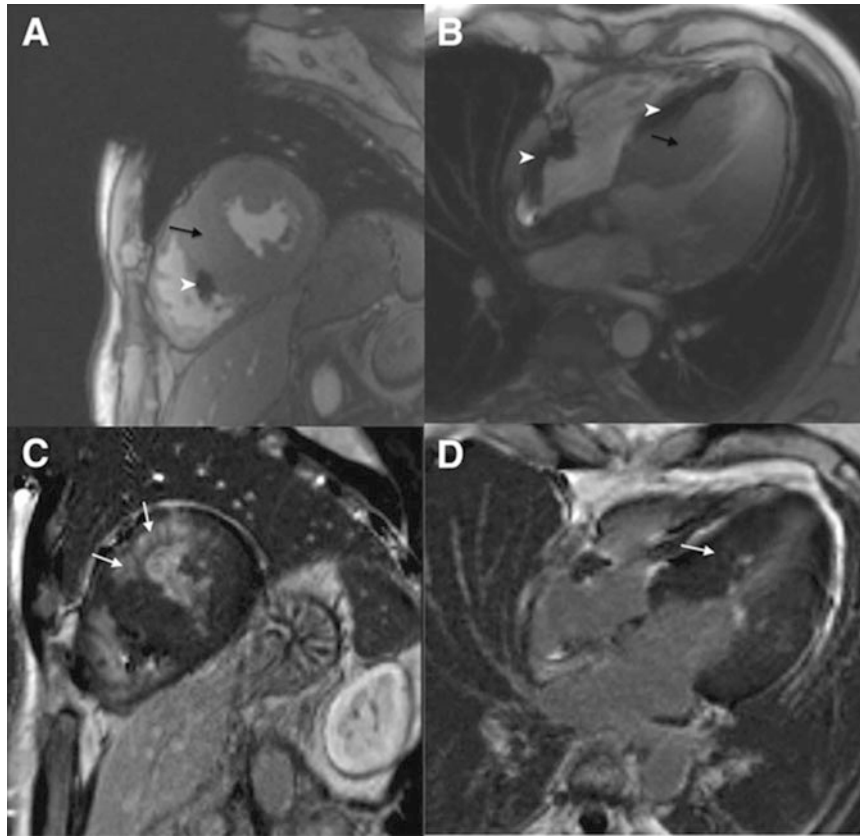

Fig. 12 Cardiovascular magnetic resonance images from a 48-year-old male *PRKAG2* mutation carrier with a pacemaker. Upper row depicts the heart in short-axis (**a**) and horizontal long-axis (**b**) views, demonstrating severe (up to 31 mm) interventricular septal hypertrophy (black arrows) and image artefact due to a pacemaker lead (white arrow heads). Lower row (**c**, **d**) depicts late gadolinium-enhanced images in the same imaging planes which show patchy enhancement in the anteroseptal hypertrophied regions (white arrows) likely to reflect focal myocardial fibrosis (Reproduced from Pöyhönen et al. Journal of Cardiovascular Magnetic Resonance 2015; 17:89 [76] with permission via the CC-BY 4.0 licence. The original article is an open access article distributed under the terms of the Creative Commons Attribution 4.0 International License (http:/creativecommons.org/licenses/by/4.0/), which permits unrestricted use, distribution, and reproduction in any medium, provided the original work is properly cited)

series [24]. A greater propensity for carriers of the Asn488Ile mutation to express LVH has been noted than those with the Arg302Gln variant (70% versus 42%, respectively) [17]. Cardiac hypertrophy typically involves the left ventricle but may also involve the right, can be massive in extent, and may be associated with left ventricular outflow tract obstruction potentially requiring relief by surgical septal myectomy or alcohol septal ablation [55, 56, 72, 77]. In sporadic cases bearing fatal infantile mutations, hypertrophy involving the atrial walls has also been described, measuring over 1 cm in one case [26]. The pattern of LVH may be concentric or, phenocopying sarcomeric HCM, preferentially involve the septum

(asymmetric septal hypertrophy) (Fig. 12) and can vary within families [24, 25, 56]. Massive septal hypertrophy (44 mm thickness) has been associated with myocardial infarction of the septum in the setting of unobstructed coronary arteries and speculated to reflect extreme blood supply-demand mismatch [78]. The use of cardiovascular magnetic resonance in a cohort of six patients has revealed other patterns of LVH, including asymmetric hypertrophy involving the mid-inferolateral left ventricle [76].

Reflecting the complexity of the *PRKAG2* mutation-associated phenotype, multiple reports also document the existence of otherwise phenotypically positive mutation carriers who do not have LVH [27, 29, 30, 65]. Whether some of these individuals with reported normal overall LV mass may in fact express more subtle manifestations of LVH, such as wall thickening affecting only one or a few isolated LV segments and more reliably identified by segmental analysis by CMR [76], or represent the impact of genetic, epigenetic, or environmental modifiers [79] is unclear.

5.6 Reported Extracardiac Features

Notwithstanding systemic expression of *PRKAG2* across tissues and in marked contrast to other disorders associated with cardiac glycogen storage (e.g., Pompe or Danon disease), cardiomyopathy is frequently the sole clinical manifestation of a *PRKAG2* mutation.

5.6.1 Skeletal Myopathy

Initial reports of extracardiac disease involving skeletal muscle [24, 80]—resulting in myalgia (muscle pain) or stiffness during or after exercise and sometimes associated with proximal muscle weakness, elevation in serum creatine kinase level or progression in weakness—highlighted the potential deleterious impact of mutant *PRKAG2* expression on other organ systems. Underlining their rarity, skeletal muscle manifestations have only been described in carriers of the Asn488Ile mutation [24] and one carrier with the Ser548Pro variant [80]. This paucity may reflect the relatively modest contribution of γ2-containing complexes to total AMPK activity in the skeletal muscle [81]. It may also indicate a lack of systematic evaluation for skeletal muscle-related pathology (including subclinical involvement) or an attribution of symptoms of effort intolerance primarily to cardiac disease. Where undertaken in symptomatic cases, histopathology and ultrastructural assessment of the skeletal muscle have revealed subsarcolemmal vacuolation of some muscle fibers with associated non-lysosomal glycogen accumulation [80], although reports differ on the presence of mitochondrial changes such as ragged red fibers [24].

5.6.2 Other Features

Early onset of systemic arterial hypertension has been reported in Arg531Gly and Lys485Gln mutation carriers, the latter presenting with hypertension at age 15 years [30, 74]. Assuming a direct link, the mechanism(s) underlying hypertension in *PRKAG2* mutation carriers are unclear but may conceivably involve perturbed AMPK-related signalling in vascular endothelial and/or smooth muscle cells [82] and/or reflect a renal contribution [83].

Mirroring metabolic findings from a novel gene-targeted mouse model (R299Q γ2-AMPK knock-in) bearing the equivalent mutation, human Arg302Gln mutation carriers have been identified to exhibit increased adiposity, greater fasting glucose, and higher levels of glycated adult hemoglobin (HbA_{1c}), together with reduced estimates of pancreatic islet β-cell function [84]. Evaluation of R299Q γ2-AMPK knock-in mice suggests ghrelin signalling-dependent hyperphagia and intrinsic impairment of insulin secretion as major mechanisms underlying this metabolic phenotype [84].

There are clinical reports of rarer features occurring in association with *PRKAG2* mutations although, given their infrequency, causal inference is not clearly established for all of them. These include epilepsy presenting with generalized tonic-clonic seizures, frequently in conjunction with myalgia [24] and, in the case of the infantile fatal Arg531Gln mutation, a case with macroglossia, enlarged dysmorphic kidneys, and increased number of pancreatic islets [26].

Reflecting the presence of extracardiac features that occur in some patients, the term PRKAG2 syndrome or PRKAG2 disease is increasingly used.

6 Prognosis

The high prevalence of arrhythmic and myocardial complications associated with *PRKAG2* mutations has been highlighted in a recent large case series of 34 patients from nine families, with a survival rate of 67% at age 60 years [67]. While specific indications for ICD implantation in *PRKAG2* mutation carriers are unclear, given the high incidence of progression to complete heart block and its often abrupt onset, timely permanent pacemaker implantation—e.g., in the setting of unexplained syncope—is critical and, arguably, represents the most important prognostic therapeutic intervention for the disease. Given that fasciculoventricular pathways have been shown to represent the substrate for ventricular preexcitation in many patients, catheter ablation in these circumstances carries a high risk of inducing iatrogenic AV conduction block and precipitating the requirement for permanent pacing.

7 Management

A key initial step in the clinical management of *PRKAG2* disease is its prompt identification, facilitated by a high index of clinical suspicion in cases of unexplained familial LVH. While the pattern of LVH evident on echocardiographic and/or CMR imaging is

indistinguishable from that of the more common familial sarcomeric HCM, the identification of an isolated short PR interval and/or frank ventricular pre-excitation pattern on ECG is a strong diagnostic clue. However, the occurrence of shortened PR interval on ECG in conjunction with a phenotype of HCM is not uniquely associated with *PRKAG2* syndrome. Its differential diagnosis includes, but is not limited to, other inherited disorders including lysosomal and/or other storage disorders. The latter include Pompe, Anderson-Fabry, or Danon disease, in addition to primary mitochondrial diseases with cardiac involvement (e.g., MERRF, myoclonic epilepsy with ragged red fibers, syndrome or MELAS—mitochondrial myopathy, encephalopathy, lactic acidosis, and stroke-like episodes), although these frequently co-feature a variety of prominent extracardiac symptoms and signs that aid in their identification [17]. Ultimately, *PRKAG2* genotyping is required for a definitive diagnosis [17]. In addition to facilitating clinical management and prognostication of the index case, positive genetic identification enables cascade screening of at-risk family members, both to identify (potentially subclinical) carriers for further assessment and long-term follow-up and to provide reassurance and discharge, as appropriate [85].

In certain clinical scenarios, endomyocardial biopsy (EMB) has been used as part of the investigative workup [56, 74], typically revealing the presence of characteristic histological features (cardiomyocyte hypertrophy with prominent cytosolic vacuolation, vacuolar and intracellular glycogen excess, and absence of significant myocyte disarray) [13, 24]. However, given its invasive nature with attendant procedural risks, current international guidelines on the use of EMB recommend it to be considered in a minority of cases where careful noninvasive assessment (including clinical assessment, pedigree analysis, noninvasive cardiac imaging, and laboratory and molecular genetic testing) has failed to reveal the cause, particularly if storage or infiltrative disorders are suspected or in cases of acute unexplained heart failure [1, 86]. Notably, rare reports describe symptomatic, genotype-positive patients without histological evidence of cardiac glycogen excess [28, 55]. Such observations may reflect true heterogeneity in phenotypic expression (and, by inference, the existence of glycogen-independent disease mechanisms), allelic differences, sampling differences in the setting of nonuniform cardiac disease involvement (as in the case of EMB where the right interventricular septum is typically sampled, as opposed to postmortem evaluation of the whole heart), or variations in tissue extraction times and processing techniques.

Given the rarity of *PRKAG2* mutations and the associated challenges of conducting clinical trials for such disorders, there are at present no evidence-based consensus statements to guide its specific treatment; however, a recent summary of published cases has outlined broad treatment guidelines, including suggestions on

Table 3
Proposed guidelines for treating patients with the PRKAG2 syndrome

Clinical feature	Diagnosis	Proposed treatment
Cardiomyopathy	ECG at least every 1 year Echocardiography at baseline and every 1–2 years (depending on morphological changes or clinical progression) Exercise stress testing with O2 consumption for effort inducible arrhythmias and for prognostic assessment Serum BNP at baseline and for clinical progression Holter ECG monitoring/event monitor to stratify the risk for sudden cardiac death or symptomatic patients Consider individual risk factors for SCD and specific EPS patterns Electrophysiological assessment Dynamic arterial pressure monitoring for patients with hypertension	Standard heart failure treatment and specifically Appropriate fluid management avoiding dehydration especially when hypertrophy is more severe Prompt consideration for cardiac transplantation in those patients with clinical progression or end-stage heart failure Standard antiarrhythmic treatment Early consideration for PM implantation ICD implantation AV accessory pathway ablation Hypertension treatment avoiding dehydrating drugs if systolic and diastolic functions preserved
Skeletal myopathy	Specialist neuromuscular evaluation Muscle biopsy may be performed for diagnostic workup	Physical therapy and rehabilitation
Genetic	Accurate familial history and PRKAG2 genetic testing for probands and for at-risk relatives	Genetic and reproductive risk counselling

AV Atrioventricular, *BNP* brain natriuretic peptide, *EPS* electrophysiological study, *ICD* implantable cardioverter defibrillator, *PM* pacemaker, *SCD* sudden cardiac death
Reproduced from Table 5 of ref. 17 with permission from Wolters Kluwer Health, Inc. http://circep.ahajournals.org/content/9/1/e003121.long

follow-up frequency (Table 3) [17]. Clinical care of individuals with *PRKAG2* mutation-related disease requires expertise from multiple disciplines (specialists in inherited cardiac conditions, cardiac electrophysiology, cardiac imaging, heart failure, clinical genetics, genetics counselling, and potentially cardiothoracic and transplantation surgery). Management is currently based largely on the principles and experience of supportive care used to treat patients with more common familial HCM [1] and carefully tailored to individual presentation, mindful of the specific family history (e.g. of SCD), and entailing long-term clinical follow-up. Particular attention is paid to managing the complex spectrum of cardiac electrophysiological manifestations (including sinoatrial disease, atrial tachyarrhythmia, ventricular pre-excitation, and AV block), risk stratification for sudden arrhythmic death, and surveillance for potential progression to frank systolic heart failure.

8 Conclusion and Perspectives

Since the molecular cloning and mapping of the gene encoding the γ2-regulatory energy-sensing subunit of AMPK in 2000 [11], followed soon after by its causal link to a human inherited cardiomyopathy with distinctive electrophysiological and histological features, the literature pertaining to *PRKAG2* and AMPK's function in the heart has greatly increased. Reflecting the collective research efforts of numerous scientists examining the AMPK pathway and clinicians managing individuals with the *PRKAG2* syndrome, knowledge of disease mechanisms underlying the associated cardiomyopathy has significantly advanced. These insights and future studies hold promise not only to foster the development of specific therapeutics for this monogenic disorder but more broadly to inform understanding of the fundamental biology of the eukaryotic cellular energy sensor and the potential for its targeting to treat more prevalent, complex cardiac and metabolic diseases.

Acknowledgments

The authors gratefully acknowledge Dr Kate Thomson and Karen McGuire (Oxford Medical Genetics Laboratories) for their insightful comments on the manuscript. This work was supported by Starter Grants for Clinical Lecturers (supported by the Academy of Medical Sciences, Wellcome Trust, Medical Research Council, British Heart Foundation, Arthritis Research UK, and the Royal College of Physicians and Diabetes UK) and an academic clinical lectureship by the National Institute of Health Research to A.Y.

References

1. Elliott PM, Anastasakis A, Borger MA, Borggrefe M, Cecchi F, Charron P, Hagege AA, Lafont A, Limongelli G, Mahrholdt H, McKenna WJ, Mogensen J, Nihoyannopoulos P, Nistri S, Pieper PG, Pieske B, Rapezzi C, Rutten FH, Tillmanns C, Watkins H (2014) 2014 ESC Guidelines on diagnosis and management of hypertrophic cardiomyopathy: the Task Force for the Diagnosis and Management of Hypertrophic Cardiomyopathy of the European Society of Cardiology (ESC). Eur Heart J 35 (39):2733–2779. https://doi.org/10.1093/eurheartj/ehu284
2. Watkins H, Ashrafian H, Redwood C (2011) Inherited cardiomyopathies. N Engl J Med 364(17):1643–1656. https://doi.org/10.1056/NEJMra0902923
3. Maron BJ (2015) Historical perspectives on sudden deaths in young athletes with evolution over 35 years. Am J Cardiol 116 (9):1461–1468. https://doi.org/10.1016/j.amjcard.2015.07.072
4. Thierfelder L, Watkins H, MacRae C, Lamas R, McKenna W, Vosberg HP, Seidman JG, Seidman CE (1994) Alpha-tropomyosin and cardiac troponin T mutations cause familial hypertrophic cardiomyopathy: a disease of the sarcomere. Cell 77(5):701–712
5. Ashrafian H, Watkins H (2007) Reviews of translational medicine and genomics in cardiovascular disease: new disease taxonomy and therapeutic implications cardiomyopathies: therapeutics based on molecular phenotype. J Am Coll Cardiol 49(12):1251–1264. https://

doi.org/10.1016/j.jacc.2006.10.073. S0735-1097(07)00130-1 [pii]

6. Massumi RA (1967) Familial Wolff-Parkinson-White syndrome with cardiomyopathy. Am J Med 43(6):951–955
7. Westlake RE, Cohen W, Willis WH (1962) Wolff-Parkinson-White syndrome and familial cardiomegaly. Am Heart J 64:314–320
8. Braunwald E, Morrow AG, Cornell WP, Aygen MM, Hilbish TF (1960) Idiopathic hypertrophic subaortic stenosis. Am J Med 29 (6):924–945. https://doi.org/10.1016/0002-9343(60)90074-7
9. MacRae CA, Ghaisas N, Kass S, Donnelly S, Basson CT, Watkins HC, Anan R, Thierfelder LH, McGarry K, Rowland E et al (1995) Familial Hypertrophic cardiomyopathy with Wolff-Parkinson-White syndrome maps to a locus on chromosome 7q3. J Clin Invest 96 (3):1216–1220. https://doi.org/10.1172/JCI118154
10. Blair E, Redwood C, Ashrafian H, Oliveira M, Broxholme J, Kerr B, Salmon A, Ostman-Smith I, Watkins H (2001) Mutations in the gamma(2) subunit of AMP-activated protein kinase cause familial hypertrophic cardiomyopathy: evidence for the central role of energy compromise in disease pathogenesis. Hum Mol Genet 10(11):1215–1220
11. Lang T, Yu L, Tu Q, Jiang J, Chen Z, Xin Y, Liu G, Zhao S (2000) Molecular cloning, genomic organization, and mapping of PRKAG2, a heart abundant gamma2 subunit of 5′-AMP-activated protein kinase, to human chromosome 7q36. Genomics 70 (2):258–263. https://doi.org/10.1006/geno.2000.6376. S0888-7543(00)96376-6 [pii]
12. Gollob MH, Green MS, Tang AS, Gollob T, Karibe A, Ali Hassan AS, Ahmad F, Lozado R, Shah G, Fananapazir L, Bachinski LL, Roberts R (2001) Identification of a gene responsible for familial Wolff-Parkinson-White syndrome. N Engl J Med 344(24):1823–1831. https://doi.org/10.1056/NEJM200106143442403
13. Arad M, Benson DW, Perez-Atayde AR, McKenna WJ, Sparks EA, Kanter RJ, McGarry K, Seidman JG, Seidman CE (2002) Constitutively active AMP kinase mutations cause glycogen storage disease mimicking hypertrophic cardiomyopathy. J Clin Invest 109(3):357–362. https://doi.org/10.1172/JCI14571
14. Gollob MH, Green MS, Tang AS, Roberts R (2002) PRKAG2 cardiac syndrome: familial ventricular preexcitation, conduction system disease, and cardiac hypertrophy. Curr Opin Cardiol 17(3):229–234
15. Ahmad F, Arad M, Musi N, He H, Wolf C, Branco D, Perez-Atayde AR, Stapleton D, Bali D, Xing Y, Tian R, Goodyear LJ, Berul CI, Ingwall JS, Seidman CE, Seidman JG (2005) Increased alpha2 subunit-associated AMPK activity and PRKAG2 cardiomyopathy. Circulation 112(20):3140–3148. https://doi.org/10.1161/CIRCULATIONAHA.105.550806. CIRCULATIONAHA.105.550806 [pii]
16. Wolf CM, Arad M, Ahmad F, Sanbe A, Bernstein SA, Toka O, Konno T, Morley G, Robbins J, Seidman JG, Seidman CE, Berul CI (2008) Reversibility of PRKAG2 glycogen-storage cardiomyopathy and electrophysiological manifestations. Circulation 117 (2):144–154. https://doi.org/10.1161/CIRCULATIONAHA.107.726752. CIRCULATIONAHA.107.726752 [pii]
17. Porto AG, Brun F, Severini GM, Losurdo P, Fabris E, Taylor MR, Mestroni L, Sinagra G (2016) Clinical spectrum of PRKAG2 syndrome. Circ Arrhythm Electrophysiol 9(1): e003121. https://doi.org/10.1161/circep.115.003121
18. Scott JW, Hawley SA, Green KA, Anis M, Stewart G, Scullion GA, Norman DG, Hardie DG (2004) CBS domains form energy-sensing modules whose binding of adenosine ligands is disrupted by disease mutations. J Clin Invest 113(2):274–284. https://doi.org/10.1172/JCI19874
19. Milan D, Jeon JT, Looft C, Amarger V, Robic A, Thelander M, Rogel-Gaillard C, Paul S, Iannuccelli N, Rask L, Ronne H, Lundstrom K, Reinsch N, Gellin J, Kalm E, Roy PL, Chardon P, Andersson L (2000) A mutation in PRKAG3 associated with excess glycogen content in pig skeletal muscle. Science 288(5469):1248–1251
20. Costford SR, Kavaslar N, Ahituv N, Chaudhry SN, Schackwitz WS, Dent R, Pennacchio LA, McPherson R, Harper ME (2007) Gain-of-function R225W mutation in human AMPK-gamma(3) causing increased glycogen and decreased triglyceride in skeletal muscle. PLoS One 2(9):e903. https://doi.org/10.1371/journal.pone.0000903
21. Richards S, Aziz N, Bale S, Bick D, Das S, Gastier-Foster J, Grody WW, Hegde M, Lyon E, Spector E, Voelkerding K, Rehm HL (2015) Standards and guidelines for the interpretation of sequence variants: a joint consensus recommendation of the American College of Medical Genetics and Genomics and the Association for Molecular Pathology. Genet Med 17(5):405–424. https://doi.org/10.1038/gim.2015.30

22. Lek M, Karczewski KJ, Minikel EV, Samocha KE, Banks E, Fennell T, O'Donnell-Luria AH, Ware JS, Hill AJ, Cummings BB, Tukiainen T, Birnbaum DP, Kosmicki JA, Duncan LE, Estrada K, Zhao F, Zou J, Pierce-Hoffman E, Berghout J, Cooper DN, Deflaux N, DePristo M, Do R, Flannick J, Fromer M, Gauthier L, Goldstein J, Gupta N, Howrigan D, Kiezun A, Kurki MI, Moonshine AL, Natarajan P, Orozco L, Peloso GM, Poplin R, Rivas MA, Ruano-Rubio V, Rose SA, Ruderfer DM, Shakir K, Stenson PD, Stevens C, Thomas BP, Tiao G, Tusie-Luna MT, Weisburd B, Won HH, Yu D, Altshuler DM, Ardissino D, Boehnke M, Danesh J, Donnelly S, Elosua R, Florez JC, Gabriel SB, Getz G, Glatt SJ, Hultman CM, Kathiresan S, Laakso M, McCarroll S, McCarthy MI, McGovern D, McPherson R, Neale BM, Palotie A, Purcell SM, Saleheen D, Scharf JM, Sklar P, Sullivan PF, Tuomilehto J, Tsuang MT, Watkins HC, Wilson JG, Daly MJ, MacArthur DG (2016) Analysis of protein-coding genetic variation in 60,706 humans. Nature 536 (7616):285–291. https://doi.org/10.1038/nature19057

23. Walsh R, Thomson KL, Ware JS, Funke BH, Woodley J, McGuire KJ, Mazzarotto F, Blair E, Seller A, Taylor JC, Minikel EV, Exome Aggregation C, MacArthur DG, Farrall M, Cook SA, Watkins H (2017) Reassessment of Mendelian gene pathogenicity using 7,855 cardiomyopathy cases and 60,706 reference samples. Genet Med 19(2):192–203. https://doi.org/10.1038/gim.2016.90

24. Murphy RT, Mogensen J, McGarry K, Bahl A, Evans A, Osman E, Syrris P, Gorman G, Farrell M, Holton JL, Hanna MG, Hughes S, Elliott PM, Macrae CA, McKenna WJ (2005) Adenosine monophosphate-activated protein kinase disease mimicks hypertrophic cardiomyopathy and Wolff-Parkinson-White syndrome: natural history. J Am Coll Cardiol 45 (6):922–930. https://doi.org/10.1016/j.jacc.2004.11.053. S0735-1097(04)02500-8 [pii]

25. Akman HO, Sampayo JN, Ross FA, Scott JW, Wilson G, Benson L, Bruno C, Shanske S, Hardie DG, Dimauro S (2007) Fatal infantile cardiac glycogenosis with phosphorylase kinase deficiency and a mutation in the gamma2-subunit of AMP-activated protein kinase. Pediatr Res 62(4):499–504. https://doi.org/10.1203/PDR.0b013e3181462b86. 00006450-200710000-00022 [pii]

26. Burwinkel B, Scott JW, Buhrer C, van Landeghem FK, Cox GF, Wilson CJ, Grahame Hardie D, Kilimann MW (2005) Fatal congenital heart glycogenosis caused by a recurrent activating R531Q mutation in the gamma 2-subunit of AMP-activated protein kinase (PRKAG2), not by phosphorylase kinase deficiency. Am J Hum Genet 76(6):1034–1049. https://doi.org/10.1086/430840. S0002-9297(07)62898-5 [pii]

27. Sternick EB, Oliva A, Magalhaes LP, Gerken LM, Hong K, Santana O, Brugada P, Brugada J, Brugada R (2006) Familial pseudo-Wolff-Parkinson-White syndrome. J Cardiovasc Electrophysiol 17(7):724–732. https://doi.org/10.1111/j.1540-8167.2006.00485.x. JCE485 [pii]

28. Tan HL, van der Wal AC, Campian ME, Kruyswijk HH, ten Hove Jansen B, van Doorn DJ, Oskam HJ, Becker AE, Wilde AA (2008) Nodoventricular accessory pathways in PRKAG2-dependent familial preexcitation syndrome reveal a disorder in cardiac development. Circ Arrhythm Electrophysiol 1 (4):276–281. https://doi.org/10.1161/CIRCEP.108.782862. CIRCEP.108.782862 [pii]

29. Zhang LP, Hui B, Gao BR (2011) High risk of sudden death associated with a PRKAG2-related familial Wolff-Parkinson-White syndrome. J Electrocardiol 44(4):483–486. https://doi.org/10.1016/j.jelectrocard.2010.02.009

30. Gollob MH, Seger JJ, Gollob TN, Tapscott T, Gonzales O, Bachinski L, Roberts R (2001) Novel PRKAG2 mutation responsible for the genetic syndrome of ventricular preexcitation and conduction system disease with childhood onset and absence of cardiac hypertrophy. Circulation 104(25):3030–3033

31. Yang X, Mudgett J, Bou-About G, Champy MF, Jacobs H, Monassier L, Pavlovic G, Sorg T, Herault Y, Petit-Demouliere B, Lu K, Feng W, Wang H, Ma LJ, Askew R, Erion MD, Kelley DE, Myers RW, Li C, Guan HP (2016) Physiological expression of AMPKgamma2RG mutation causes Wolff-Parkinson-White syndrome and induces kidney injury in mice. J Biol Chem 291:23428. https://doi.org/10.1074/jbc.M116.738591

32. Arad M, Moskowitz IP, Patel VV, Ahmad F, Perez-Atayde AR, Sawyer DB, Walter M, Li GH, Burgon PG, Maguire CT, Stapleton D, Schmitt JP, Guo XX, Pizard A, Kupershmidt S, Roden DM, Berul CI, Seidman CE, Seidman JG (2003) Transgenic mice overexpressing mutant PRKAG2 define the cause of Wolff-Parkinson-White syndrome in glycogen storage cardiomyopathy. Circulation 107(22):2850–2856. https://doi.org/10.1161/01.CIR.0000075270.13497.2B. 01.CIR.0000075270.13497.2B [pii]

33. Sidhu JS, Rajawat YS, Rami TG, Gollob MH, Wang Z, Yuan R, Marian AJ, DeMayo FJ, Weilbacher D, Taffet GE, Davies JK, Carling D, Khoury DS, Roberts R (2005) Transgenic mouse model of ventricular preexcitation and atrioventricular reentrant tachycardia induced by an AMP-activated protein kinase loss-of-function mutation responsible for Wolff-Parkinson-White syndrome. Circulation 111(1):21–29. https://doi.org/10.1161/01.CIR.0000151291.32974.D5. 01.CIR.0000151291.32974.D5 [pii]
34. Davies JK, Wells DJ, Liu K, Whitrow HR, Daniel TD, Grignani R, Lygate CA, Schneider JE, Noel G, Watkins H, Carling D (2006) Characterization of the role of gamma2 R531G mutation in AMP-activated protein kinase in cardiac hypertrophy and Wolff-Parkinson-White syndrome. Am J Physiol Heart Circ Physiol 290(5):H1942–H1951. https://doi.org/10.1152/ajpheart.01020.2005. 01020.2005 [pii]
35. Banerjee SK, Ramani R, Saba S, Rager J, Tian R, Mathier MA, Ahmad F (2007) A PRKAG2 mutation causes biphasic changes in myocardial AMPK activity and does not protect against ischemia. Biochem Biophys Res Commun 360(2):381–387. https://doi.org/10.1016/j.bbrc.2007.06.067. S0006-291X(07)01292-2 [pii]
36. Mehdirad AA, Fatkin D, DiMarco JP, MacRae CA, Wase A, Seidman JG, Seidman CE, Benson DW (1999) Electrophysiologic characteristics of accessory atrioventricular connections in an inherited form of Wolff-Parkinson-White syndrome. J Cardiovasc Electrophysiol 10(5):629–635
37. Patel VV, Arad M, Moskowitz IP, Maguire CT, Branco D, Seidman JG, Seidman CE, Berul CI (2003) Electrophysiologic characterization and postnatal development of ventricular pre-excitation in a mouse model of cardiac hypertrophy and Wolff-Parkinson-White syndrome. J Am Coll Cardiol 42(5):942–951
38. Becker AE, Anderson RH (1981) The Wolff-Parkinson-White syndrome and its anatomical substrates. Anat Rec 201(1):169–177. https://doi.org/10.1002/ar.1092010118
39. Aanhaanen WT, Boukens BJ, Sizarov A, Wakker V, de Gier-de Vries C, van Ginneken AC, Moorman AF, Coronel R, Christoffels VM (2011) Defective Tbx2-dependent patterning of the atrioventricular canal myocardium causes accessory pathway formation in mice. J Clin Invest 121(2):534–544. https://doi.org/10.1172/jci44350
40. Hinson JT, Chopra A, Lowe A, Sheng CC, Gupta RM, Kuppusamy R, O'Sullivan J, Rowe G, Wakimoto H, Gorham J, Zhang K, Musunuru K, Gerszten RE, SM W, Chen CS, Seidman JG, Seidman CE (2016) Integrative analysis of PRKAG2 cardiomyopathy iPS and microtissue models identifies AMPK as a regulator of metabolism, survival, and fibrosis. Cell Rep 17(12):3292–3304. https://doi.org/10.1016/j.celrep.2016.11.066
41. Hudson ER, Pan DA, James J, Lucocq JM, Hawley SA, Green KA, Baba O, Terashima T, Hardie DG (2003) A novel domain in AMP-activated protein kinase causes glycogen storage bodies similar to those seen in hereditary cardiac arrhythmias. Curr Biol 13(10):861–866
42. Polekhina G, Gupta A, Michell BJ, van Denderen B, Murthy S, Feil SC, Jennings IG, Campbell DJ, Witters LA, Parker MW, Kemp BE, Stapleton D (2003) AMPK beta subunit targets metabolic stress sensing to glycogen. Curr Biol 13(10):867–871
43. McBride A, Ghilagaber S, Nikolaev A, Hardie DG (2009) The glycogen-binding domain on the AMPK beta subunit allows the kinase to act as a glycogen sensor. Cell Metab 9(1):23–34. https://doi.org/10.1016/j.cmet.2008.11.008. S1550-4131(08)00360-4 [pii]
44. Luptak I, Shen M, He H, Hirshman MF, Musi N, Goodyear LJ, Yan J, Wakimoto H, Morita H, Arad M, Seidman CE, Seidman JG, Ingwall JS, Balschi JA, Tian R (2007) Aberrant activation of AMP-activated protein kinase remodels metabolic network in favor of cardiac glycogen storage. J Clin Invest 117(5):1432–1439. https://doi.org/10.1172/JCI30658
45. Gollob MH (2003) Glycogen storage disease as a unifying mechanism of disease in the PRKAG2 cardiac syndrome. Biochem Soc Trans 31(Pt 1):228–231. https://doi.org/10.1042/bst0310228
46. Banerjee SK, McGaffin KR, Huang XN, Ahmad F (2010) Activation of cardiac hypertrophic signaling pathways in a transgenic mouse with the human PRKAG2 Thr400Asn mutation. Biochim Biophys Acta 1802(2):284–291. https://doi.org/10.1016/j.bbadis.2009.12.001. S0925-4439(09)00294-4 [pii]
47. Bouskila M, Hunter RW, Ibrahim AF, Delattre L, Peggie M, van Diepen JA, Voshol PJ, Jensen J, Sakamoto K (2010) Allosteric regulation of glycogen synthase controls glycogen synthesis in muscle. Cell Metab 12(5):456–466. https://doi.org/10.1016/j.cmet.2010.10.006
48. Kim M, Hunter RW, Garcia-Menendez L, Gong G, Yang YY, Kolwicz SC Jr, Xu J,

Sakamoto K, Wang W, Tian R (2014) Mutation in the gamma2-subunit of AMP-activated protein kinase stimulates cardiomyocyte proliferation and hypertrophy independent of glycogen storage. Circ Res 114(6):966–975. https://doi.org/10.1161/circresaha.114.302364

49. Folmes KD, Chan AY, Koonen DP, Pulinilkunnil TC, Baczko I, Hunter BE, Thorn S, Allard MF, Roberts R, Gollob MH, Light PE, Dyck JR (2009) Distinct early signaling events resulting from the expression of the PRKAG2 R302Q mutant of AMPK contribute to increased myocardial glycogen. Circ Cardiovasc Genet 2(5):457–466. https://doi.org/10.1161/CIRCGENETICS.108.834564. CIRCGENETICS.108.834564 [pii]
50. Xiao B, Heath R, Saiu P, Leiper FC, Leone P, Jing C, Walker PA, Haire L, Eccleston JF, Davis CT, Martin SR, Carling D, Gamblin SJ (2007) Structural basis for AMP binding to mammalian AMP-activated protein kinase. Nature 449 (7161):496–500. https://doi.org/10.1038/nature06161. nature06161 [pii]
51. Hamilton SR, Stapleton D, O'Donnell JB Jr, Kung JT, Dalal SR, Kemp BE, Witters LA (2001) An activating mutation in the gamma1 subunit of the AMP-activated protein kinase. FEBS Lett 500(3):163–168
52. Barnes BR, Marklund S, Steiler TL, Walter M, Hjalm G, Amarger V, Mahlapuu M, Leng Y, Johansson C, Galuska D, Lindgren K, Abrink M, Stapleton D, Zierath JR, Andersson L (2004) The 5′-AMP-activated protein kinase gamma3 isoform has a key role in carbohydrate and lipid metabolism in glycolytic skeletal muscle. J Biol Chem 279(37):38441–38447. https://doi.org/10.1074/jbc.M405533200. M405533200 [pii]
53. Daniel T, Carling D (2002) Functional analysis of mutations in the gamma 2 subunit of AMP-activated protein kinase associated with cardiac hypertrophy and Wolff-Parkinson-White syndrome. J Biol Chem 277 (52):51017–51024. https://doi.org/10.1074/jbc.M207093200. M207093200 [pii]
54. Zou L, Shen M, Arad M, He H, Lofgren B, Ingwall JS, Seidman CE, Seidman JG, Tian R (2005) N488I mutation of the gamma2-subunit results in bidirectional changes in AMP-activated protein kinase activity. Circ Res 97(4):323–328. https://doi.org/10.1161/01.RES.0000179035.20319.c2. 01.RES.0000179035.20319.c2 [pii]
55. Kelly BP, Russell MW, Hennessy JR, Ensing GJ (2009) Severe hypertrophic cardiomyopathy in an infant with a novel PRKAG2 gene mutation: potential differences between infantile and adult onset presentation. Pediatr Cardiol 30 (8):1176–1179. https://doi.org/10.1007/s00246-009-9521-3
56. Yogasundaram H, Paterson ID, Graham M, Sergi C, Oudit GY (2016) Glycogen storage disease because of a PRKAG2 mutation causing severe biventricular hypertrophy and high-grade atrio-ventricular block. Circ Heart Fail 9(8):pii: e003367. https://doi.org/10.1161/circheartfailure.116.003367
57. Sternick EB, Oliva A, Gerken LM, Magalhaes L, Scarpelli R, Correia FS, Rego S, Santana O, Brugada R, Wellens HJ (2011) Clinical, electrocardiographic, and electrophysiologic characteristics of patients with a fasciculoventricular pathway: the role of PRKAG2 mutation. Heart Rhythm 8(1):58–64. https://doi.org/10.1016/j.hrthm.2010.09.081. S1547-5271(10)01024-6 [pii]
58. Vaughan CJ, Hom Y, Okin DA, McDermott DA, Lerman BB, Basson CT (2003) Molecular genetic analysis of PRKAG2 in sporadic Wolff-Parkinson-White syndrome. J Cardiovasc Electrophysiol 14(3):263–268
59. Light PE, Wallace CH, Dyck JR (2003) Constitutively active adenosine monophosphate-activated protein kinase regulates voltage-gated sodium channels in ventricular myocytes. Circulation 107(15):1962–1965. https://doi.org/10.1161/01.CIR.0000069269.60167.02. 01.CIR.0000069269.60167.02 [pii]
60. Back Sternick E, de Almeida Araujo S, Ribeiro da Silva Camargos E, Brasileiro Filho G (2016) Atrial pathology findings in a patient with PRKAG2 cardiomyopathy and persistent atrial fibrillation. Circ Arrhythm Electrophysiol 9 (12):e004455. https://doi.org/10.1161/circep.116.004455
61. Schott JJ, Alshinawi C, Kyndt F, Probst V, Hoorntje TM, Hulsbeek M, Wilde AA, Escande D, Mannens MM, Le Marec H (1999) Cardiac conduction defects associate with mutations in SCN5A. Nat Genet 23 (1):20–21. https://doi.org/10.1038/12618
62. McNair WP, Ku L, Taylor MR, Fain PR, Dao D, Wolfel E, Mestroni L (2004) SCN5A mutation associated with dilated cardiomyopathy, conduction disorder, and arrhythmia. Circulation 110(15):2163–2167. https://doi.org/10.1161/01.cir.0000144458.58660.bb
63. Fatkin D, MacRae C, Sasaki T, Wolff MR, Porcu M, Frenneaux M, Atherton J, Vidaillet HJ Jr, Spudich S, De Girolami U, Seidman JG, Seidman C, Muntoni F, Muehle G, Johnson W, McDonough B (1999) Missense mutations in the rod domain of the lamin A/C gene as causes of dilated cardiomyopathy and conduction-system disease. N Engl J Med

341(23):1715–1724. https://doi.org/10.1056/nejm199912023412302

64. Arad M, Maron BJ, Gorham JM, Johnson WH Jr, Saul JP, Perez-Atayde AR, Spirito P, Wright GB, Kanter RJ, Seidman CE, Seidman JG (2005) Glycogen storage diseases presenting as hypertrophic cardiomyopathy. N Engl J Med 352(4):362–372. https://doi.org/10.1056/NEJMoa033349. 352/4/362 [pii]
65. Charron P, Genest M, Richard P, Komajda M, Pochmalicki G (2007) A familial form of conduction defect related to a mutation in the PRKAG2 gene. Europace 9(8):597–600. https://doi.org/10.1093/europace/eum071. eum071 [pii]
66. Govindan M, Ward D, Behr E (2010) A rare connection: fasciculoventricular pathway in PRKAG2 disease. J Cardiovasc Electrophysiol 21(3):329–332. https://doi.org/10.1111/j.1540-8167.2009.01578.x. JCE1578 [pii]
67. Thevenon J, Laurent G, Ader F, Laforet P, Klug D, Duva Pentiah A, Gouya L, Maurage CA, Kacet S, Eicher JC, Albuisson J, Desnos M, Bieth E, Duboc D, Martin L, Reant P, Picard F, Bonithon-Kopp C, Gautier E, Binquet C, Thauvin-Robinet C, Faivre L, Bouvagnet P, Charron P, Richard P (2017) High prevalence of arrhythmic and myocardial complications in patients with cardiac glycogenosis due to PRKAG2 mutations. Europace 19(4):651–659. https://doi.org/10.1093/europace/euw067
68. Aggarwal V, Dobrolet N, Fishberger S, Zablah J, Jayakar P, Ammous Z (2015) PRKAG2 mutation: an easily missed cardiac specific non-lysosomal glycogenosis. Ann Pediatr Cardiol 8(2):153–156. https://doi.org/10.4103/0974-2069.154149
69. Sternick EB, Wellens HJJ (2006) Historical notes and classification of the variants of ventricular preexcitation. Variants of ventricular preexcitation: recognition and treatment. Blackwell Futura, Malden, MA
70. Sternick EB, Gerken LM, Vrandecic MO, Wellens HJ (2003) Fasciculoventricular pathways: clinical and electrophysiologic characteristics of a variant of preexcitation. J Cardiovasc Electrophysiol 14(10):1057–1063
71. Sternick EB, Rodriguez LM, Gerken LM, Wellens HJ (2005) Electrocardiogram in patients with fasciculoventricular pathways: a comparative study with anteroseptal and midseptal accessory pathways. Heart Rhythm 2(1):1–6. https://doi.org/10.1016/j.hrthm.2004.10.009
72. Bayrak F, Komurcu-Bayrak E, Mutlu B, Kahveci G, Basaran Y, Erginel-Unaltuna N (2006) Ventricular pre-excitation and cardiac hypertrophy mimicking hypertrophic cardiomyopathy in a Turkish family with a novel PRKAG2 mutation. Eur J Heart Fail 8(7):712–715. https://doi.org/10.1016/j.ejheart.2006.03.006. S1388-9842(06)00072-9 [pii]
73. Ponikowski P, Voors AA, Anker SD, Bueno H, Cleland JG, Coats AJ, Falk V, Gonzalez-Juanatey JR, Harjola VP, Jankowska EA, Jessup M, Linde C, Nihoyannopoulos P, Parissis JT, Pieske B, Riley JP, Rosano GM, Ruilope LM, Ruschitzka F, Rutten FH, van der Meer P (2016) 2016 ESC Guidelines for the diagnosis and treatment of acute and chronic heart failure: the Task Force for the diagnosis and treatment of acute and chronic heart failure of the European Society of Cardiology (ESC) Developed with the special contribution of the Heart Failure Association (HFA) of the ESC. Eur Heart J 37(27):2129–2200. https://doi.org/10.1093/eurheartj/ehw128
74. Liu Y, Bai R, Wang L, Zhang C, Zhao R, Wan D, Chen X, Caceres G, Barr D, Barajas-Martinez H, Antzelevitch C, Hu D (2013) Identification of a novel de novo mutation associated with PRKAG2 cardiac syndrome and early onset of heart failure. PLoS One 8(5):e64603. https://doi.org/10.1371/journal.pone.0064603
75. Morita H, Rehm HL, Menesses A, McDonough B, Roberts AE, Kucherlapati R, Towbin JA, Seidman JG, Seidman CE (2008) Shared genetic causes of cardiac hypertrophy in children and adults. N Engl J Med 358(18):1899–1908. https://doi.org/10.1056/NEJMoa075463. NEJMoa075463 [pii]
76. Poyhonen P, Hiippala A, Ollila L, Kaasalainen T, Hanninen H, Helio T, Tallila J, Vasilescu C, Kivisto S, Ojala T, Holmstrom M (2015) Cardiovascular magnetic resonance findings in patients with PRKAG2 gene mutations. J Cardiovasc Magn Reson 17:89. https://doi.org/10.1186/s12968-015-0192-3
77. Tong KL, Brown C, Ports TA, McGlothlin D, De Marco T (2010) Alcohol septal ablation to treat heart failure due to dynamic left ventricular outflow tract obstruction in a patient with glycogen storage disease related to the *prkag2* gene mutation. J Card Fail 16(8):S110. https://doi.org/10.1016/j.cardfail.2010.06.384
78. Sternick EB, de Almeida Araujo S, Rocha C, Gollob M (2014) Myocardial infarction in a teenager. Eur Heart J 35(23):1558. https://doi.org/10.1093/eurheartj/ehu015
79. Ho CY, Charron P, Richard P, Girolami F, Van Spaendonck-Zwarts KY, Pinto Y (2015)

Genetic advances in sarcomeric cardiomyopathies: state of the art. Cardiovasc Res 105 (4):397–408. https://doi.org/10.1093/cvr/cvv025

80. Laforet P, Richard P, Said MA, Romero NB, Lacene E, Leroy JP, Baussan C, Hogrel JY, Lavergne T, Wahbi K, Hainque B, Duboc D (2006) A new mutation in PRKAG2 gene causing hypertrophic cardiomyopathy with conduction system disease and muscular glycogenosis. Neuromuscul Disord 16 (3):178–182. https://doi.org/10.1016/j.nmd.2005.12.004. S0960-8966(05)00354-8 [pii]
81. Cheung PC, Salt IP, Davies SP, Hardie DG, Carling D (2000) Characterization of AMP-activated protein kinase gamma-subunit isoforms and their role in AMP binding. Biochem J 346(Pt 3):659–669
82. Nagata D, Hirata Y (2010) The role of AMP-activated protein kinase in the cardiovascular system. Hypertens Res 33(1):22–28. https://doi.org/10.1038/hr.2009.187
83. Kottgen A, Pattaro C, Boger CA, Fuchsberger C, Olden M, Glazer NL, Parsa A, Gao X, Yang Q, Smith AV, O'Connell JR, Li M, Schmidt H, Tanaka T, Isaacs A, Ketkar S, Hwang SJ, Johnson AD, Dehghan A, Teumer A, Pare G, Atkinson EJ, Zeller T, Lohman K, Cornelis MC, Probst-Hensch NM, Kronenberg F, Tonjes A, Hayward C, Aspelund T, Eiriksdottir G, Launer LJ, Harris TB, Rampersaud E, Mitchell BD, Arking DE, Boerwinkle E, Struchalin M, Cavalieri M, Singleton A, Giallauria F, Metter J, de Boer IH, Haritunians T, Lumley T, Siscovick D, Psaty BM, Zillikens MC, Oostra BA, Feitosa M, Province M, de Andrade M, Turner ST, Schillert A, Ziegler A, Wild PS, Schnabel RB, Wilde S, Munzel TF, Leak TS, Illig T, Klopp N, Meisinger C, Wichmann HE, Koenig W, Zgaga L, Zemunik T, Kolcic I, Minelli C, FB H, Johansson A, Igl W, Zaboli G, Wild SH, Wright AF, Campbell H, Ellinghaus D, Schreiber S, Aulchenko YS, Felix JF, Rivadeneira F, Uitterlinden AG, Hofman A, Imboden M, Nitsch D, Brandstatter A, Kollerits B, Kedenko L, Magi R, Stumvoll M, Kovacs P, Boban M, Campbell S, Endlich K, Volzke H, Kroemer HK, Nauck M, Volker U, Polasek O, Vitart V, Badola S, Parker AN, Ridker PM, Kardia SL, Blankenberg S, Liu Y, Curhan GC, Franke A, Rochat T, Paulweber B, Prokopenko I, Wang W, Gudnason V, Shuldiner AR, Coresh J, Schmidt R, Ferrucci L, Shlipak MG, van Duijn CM, Borecki I, Kramer BK, Rudan I, Gyllensten U, Wilson JF, Witteman JC, Pramstaller PP, Rettig R, Hastie N, Chasman DI, Kao WH, Heid IM, Fox CS (2010) New loci associated with kidney function and chronic kidney disease. Nat Genet 42 (5):376–384. https://doi.org/10.1038/ng.568. ng.568 [pii]
84. Yavari A, Stocker CJ, Ghaffari S, Wargent ET, Steeples V, Czibik G, Pinter K, Bellahcene M, Woods A, Martinez de Morentin PB, Cansell C, Lam BY, Chuster A, Petkevicius K, Nguyen-Tu MS, Martinez-Sanchez A, Pullen TJ, Oliver PL, Stockenhuber A, Nguyen C, Lazdam M, O'Dowd JF, Harikumar P, Toth M, Beall C, Kyriakou T, Parnis J, Sarma D, Katritsis G, Wortmann DD, Harper AR, Brown LA, Willows R, Gandra S, Poncio V, de Oliveira Figueiredo MJ, Qi NR, Peirson SN, McCrimmon RJ, Gereben B, Tretter L, Fekete C, Redwood C, Yeo GS, Heisler LK, Rutter GA, Smith MA, Withers DJ, Carling D, Sternick EB, Arch JR, Cawthorne MA, Watkins H, Ashrafian H (2016) Chronic activation of gamma2 AMPK induces obesity and reduces beta cell function. Cell Metab 23(5):821–836. https://doi.org/10.1016/j.cmet.2016.04.003
85. Yavari A, Ashrafian H (2010) Inherited cardiac disease. Medicine 38(9):496–501
86. Cooper LT, Baughman KL, Feldman AM, Frustaci A, Jessup M, Kuhl U, Levine GN, Narula J, Starling RC, Towbin J, Virmani R (2007) The role of endomyocardial biopsy in the management of cardiovascular disease: a scientific statement from the American Heart Association, the American College of Cardiology, and the European Society of Cardiology Endorsed by the Heart Failure Society of America and the Heart Failure Association of the European Society of Cardiology. Eur Heart J 28(24):3076–3093. https://doi.org/10.1093/eurheartj/ehm456
87. Fabris E, Brun F, Porto AG, Losurdo P, Vitali Serdoz L, Zecchin M, Severini GM, Mestroni L, Di Chiara A, Sinagra G (2013) Cardiac hypertrophy, accessory pathway, and conduction system disease in an adolescent: the PRKAG2 cardiac syndrome. J Am Coll Cardiol 62(9):e17. https://doi.org/10.1016/j.jacc.2013.02.099
88. Zhang BL, RL X, Zhang J, Zhao XX, Wu H, Ma LP, JQ H, Zhang JL, Ye Z, Zheng X, Qin YW (2013) Identification and functional analysis of a novel PRKAG2 mutation responsible for Chinese PRKAG2 cardiac syndrome reveal an important role of non-CBS domains in regulating the AMPK pathway. J Cardiol 62 (4):241–248. https://doi.org/10.1016/j.jjcc.2013.04.010
89. Arad M, Penas-Lado M, Monserrat L, Maron BJ, Sherrid M, Ho CY, Barr S, Karim A, Olson

TM, Kamisago M, Seidman JG, Seidman CE (2005) Gene mutations in apical hypertrophic cardiomyopathy. Circulation 112 (18):2805–2811. https://doi.org/10.1161/CIRCULATIONAHA.105.547448. 112/18/2805 [pii]

90. Xie C, Zhang YP, Song L, Luo J, Qi W, Hu J, Lu D, Yang Z, Zhang J, Xiao J, Zhou B, JL D, Jing N, Liu Y, Wang Y, Li BL, Song BL, Yan Y (2016) Genome editing with CRISPR/Cas9 in postnatal mice corrects PRKAG2 cardiac syndrome. Cell Res 26(10):1099–1111. https://doi.org/10.1038/cr.2016.101
91. den Dunnen JT, Dalgleish R, Maglott DR, Hart RK, Greenblatt MS, McGowan-Jordan J, Roux AF, Smith T, Antonarakis SE, Taschner PE (2016) HGVS recommendations for the description of sequence variants: 2016 update. Hum Mutat 37(6):564–569. https://doi.org/10.1002/humu.22981

INDEX

Dietbert Neumann and Benoit Viollet (eds.), *AMPK: Methods and Protocols*, Methods in Molecular Biology, vol. 1732, https://doi.org/10.1007/978-1-4939-7598-3,

D

E

F

G

H

I

K

L

M

N

O

P

Q

R

S

T

V

U

W

X

Y

Z